Report Prepared by:
Francisco J. Presuel-Moreno
With
Francisco Gutierrez
James Zielske
Valeria Casas
Yu-You Wu

Final Report

Analysis and Estimation of Service Life of Corrosion Prevention Materials Using Diffusion, Resistivity and Accelerated Curing for New Bridge Structures -
Volume 1: Corrosion Prevention Materials (Monitoring and Forensic Examination)
(BDK79-977-02)

submitted to

Florida Department of Transportation Research Center
605 Suwannee Street
Tallahassee, Florida 32399

submitted by

Francisco Presuel-Moreno
Center for Marine Materials
Department of Ocean and Mechanical Engineering
Florida Atlantic University – Sea Tech
101 North Beach Road
Dania Beach, Florida 33004

December 2013

Disclaimer

The opinions, findings, and conclusions expressed in this publication are those of the author and not necessarily those of the State of Florida Department of Transportation.

SI* (MODERN METRIC) CONVERSION FACTORS

APPROXIMATE CONVERSIONS TO SI UNITS

Symbol	When You Know	Multiply By	To Find	Symbol
		LENGTH		
in	inches	25.4	millimeters	mm
ft	feet	0.305	meters	m
yd	yards	0.914	meters	m
mi	miles	1.61	kilometers	km
		AREA		
in^2	square inches	645.2	square millimeters	mm^2
ft^2	square feet	0.093	square meters	m^2
yd^2	square yard	0.836	square meters	m^2
ac	acres	0.405	hectares	ha
mi^2	square miles	2.59	square kilometers	km^2
		VOLUME		
fl oz	fluid ounces	29.57	milliliters	mL
gal	gallons	3.785	liters	L
ft^3	cubic feet	0.028	cubic meters	m^3
yd^3	cubic yards	0.765	cubic meters	m^3
	NOTE: volumes greater than 1000 L shall be shown in m^3			
		MASS		
oz	ounces	28.35	grams	g
lb	pounds	0.454	kilograms	kg
T	short tons (2000 lb)	0.907	megagrams (or "metric ton")	Mg (or "t")
		TEMPERATURE (exact degrees)		
°F	Fahrenheit	5 (F-32)/9 or (F-32)/1.8	Celsius	°C
		ILLUMINATION		
fc	foot-candles	10.76	lux	lx
fl	foot-Lamberts	3.426	$candela/m^2$	cd/m^2
		FORCE and PRESSURE or STRESS		
lbf	poundforce	4.45	newtons	N
lbf/in^2	poundforce per square inch	6.89	kilopascals	kPa

APPROXIMATE CONVERSIONS FROM SI UNITS

Symbol	When You Know	Multiply By	To Find	Symbol
		LENGTH		
mm	millimeters	0.039	inches	in
m	meters	3.28	feet	ft
m	meters	1.09	yards	yd
km	kilometers	0.621	miles	mi
		AREA		
mm^2	square millimeters	0.0016	square inches	in^2
m^2	square meters	10.764	square feet	ft^2
m^2	square meters	1.195	square yards	yd^2
ha	hectares	2.47	acres	ac
km^2	square kilometers	0.386	square miles	mi^2
		VOLUME		
mL	milliliters	0.034	fluid ounces	fl oz
L	liters	0.264	gallons	gal
m^3	cubic meters	35.314	cubic feet	ft^3
m^3	cubic meters	1.307	cubic yards	yd^3
		MASS		
g	grams	0.035	ounces	oz
kg	kilograms	2.202	pounds	lb
Mg (or "t")	megagrams (or "metric ton")	1.103	short tons (2000 lb)	T
		TEMPERATURE (exact degrees)		
°C	Celsius	1.8C+32	Fahrenheit	°F
		ILLUMINATION		
lx	lux	0.0929	foot-candles	fc
cd/m^2	$candela/m^2$	0.2919	foot-Lamberts	fl
		FORCE and PRESSURE or STRESS		
N	newtons	0.225	poundforce	lbf
kPa	kilopascals	0.145	poundforce per square inch	lbf/in^2

*SI is the symbol for the International System of Units. Appropriate rounding should be made to comply with Section 4 of ASTM E380.
(Revised March 2003)

Technical Report Documentation Page

1. Report No.	2. Government Accession No.	3. Recipient's Catalog No.	
4. Title and Subtitle Analysis and Estimation of Service Life of Corrosion Prevention Materials Using Diffusion, Resistivity and Accelerated Curing for New Bridge Structures - Volume 1: Corrosion Prevention Materials (Monitoring and Forensic Examination)		5. Report Date December, 2013 6. Performing Organization Code FAU-OE-CMM-08-3	
7. Author(s) Francisco Presuel-Moreno, Francisco Gutierrez, James Zielske, Valeria Casas, Yu-You Wu		8. Performing Organization Report No. BDK-79-977-02	
9. Performing Organization Name and Address Center for Marine Materials Florida Atlantic University – SeaTech 101 North Beach Road Dania Beach, Florida 33004		10. Work Unit No. (TRAIS) 11. Contract or Grant No. BDK79-977-02	
12. Sponsoring Agency Name and Address Florida Department of Transportation 605 Suwannee Street, MS 30 Tallahassee, FL 32399		13. Type of Report and Period Covered Final Report May 18 2010 – December 30, 2013 14. Sponsoring Agency Code	
15. Supplementary Notes			

16. Abstract

This investigation compiles the results describing the performance of: a) reinforced concrete specimens cast with 0.37 water to cementitious (w/cm) and binary blends of high performance concrete; the specimens have been exposed to seawater wet/dry weekly cycles for over 18 years; b) diffusivity and resistivity of concrete after 5 years at the Key Royale Bridge (from cores); c) high corrosion-resistant alloys (316, 304, 2304, and other alloys) cast in 0.5 water to cement ratio (w/c) concrete exposed outdoors to wet/dry cycles with 15% NaCl solution exposed for seven to ten years; d) accelerated transport method to investigate corrosion initiation and propagation of duplex stainless steel embedded in concrete (2101 and 2304); e) effect of mill scale on corrosion initiation of corrosion-resistant alloys embedded in mortar and exposed to simulated pore solution with incremental chloride additions; f) follow-up of elongation (concrete prisms) due to alkali silica reaction (ASR) and the resistivity (cylinders) of concrete with 19% Fly Ash (FA), high alkalinity, seven different coarse aggregates, and, in some cases, Li additions; g) chloride threshold as a function of elevation of carbon-steel-reinforced mortar piles simulating partially immersed concrete substructures. A number of specimens were terminated for forensic analysis. Resistivity, diffusivity (obtained from chloride profiles), and LPR were some of the tests used to assess the performance of the above-described materials. In the case of the concrete prism of the ASR investigation, selected specimens were terminated for petrographic examination of lapped surfaces and thin sections. It was found that FL2 coarse aggregate and both coarse aggregate granites might be prone to ASR for situations in which the pH of the concrete is increased. Further evidence was found that concrete with 50% FA has low apparent diffusion coefficiennt, but the chloride threshold is lowered compared to only ordinary Portland cement (OPC) concrete (as a result of lower pH in the pore solution). This caused corrosion to initiate on more rebars on specimens with 50% FA than on specimens with OPC only. Stainless steel 316 and 304 rebars, when properly pickled in the as received condition, show no sign of corrosion. However, 316 and 304 rebars that were wire brushed before embedding them in concrete, initiated corrosion after several years of exposure. From tests on reinforced mortar specimens, duplex stainless steels investigated appear to have a chloride threshold similar to that of 304.

17. Key Word	18. Distribution Statement		
Bridge substructures, bulk diffusion, resistivity, chloride at the rebar trace, corrosion-resistant alloys, binary mixes, alkali silica reaction	No restrictions. This document is available to the public through NTIS, Springfield, VA 22161		
19. Security Classif. (of this report) Unclassified	20. Security Classif. (of this page) Unclassified	21. No. of Pages 485	22. Price

Form DOT F 1700.7 (8-72) Reproduction of completed page authorized

ACKNOWLEDGMENTS

The authors are indebted to the FDOT State Materials Office for assisting in preparing the different concrete specimens and conducting several tests and initial curing at SMO for this study and, in particular, Mr. Mario Paredes, Mr. Ronald Simmons, and several SMO Technicians (Dennis Baldi, Richard Delorenzo, Pat Carlton, Thomas Frank, Jason Burchfield). The assistance of several students that work as graduate/undergraduate research assistants (Taylor Reeves, Andrew Sajban, Nicholas Agostinelli, Yohan Miglis, Scott Shill, Yali Sun) is also acknowledged. The authors also acknowledge materials provided by Outokumpu Stainless AB (Sweeden) used for tests described in Chapter 5 and Chapter 6.

Executive Summary

This investigation compiles the results describing the performance of: a) reinforced concrete specimens cast with 0.37 water to cementitious (w/cm) and binary blends of high performance concrete; the specimens were exposed to seawater wet/dry cycles for over 18 years; b) diffusivity and resistivity after 5 years at the Key Royale Bridge; c) high corrosion-resistant alloys (316, 304, 2304, and other alloys) cast in 0.5 water to cement ratio (w/c) concrete exposed outdoors to wet/dry cycles with 15% NaCl solution exposed for seven to ten years; d) accelerated transport method to investigate corrosion initiation and propagation of duplex stainless steel embedded in concrete (2101 and 2304); e) effect of mill scale on corrosion initiation of corrosion-resistant alloys embedded in mortar and exposed to simulated pore solution with incremental chloride additions; f) follow-up of elongation (prisms) due to alkali silica reaction (ASR) and the resistivity (cylinders) of concrete with 19% Fly Ash (FA), high alkalinity, seven different coarse aggregates, and, in some cases, Li additions; g) chloride threshold as a function of elevation of carbon-steel-reinforced mortar piles simulating partially immersed concrete sub-structures. A number of specimens were terminated for forensic analysis. Resistivity, diffusivity (obtained from chloride profiles), Linear Polarization Resistance (LPR) were some of the tests used to assess the performance of the above described materials. In the case of the concrete prism of the ASR investigation selected specimens were terminated for lapped surfaces and thin sections. It was found that FL2 coarse aggregate, and both coarse aggregate granites might be prone to ASR for situations in which the pH of the concrete is increased. Further evidence was found that concrete with 50% FA has low apparent diffusion coefficient (D_{app}), but the chloride threshold is lowered compared to only ordinary Portland cement (OPC) concrete. This caused corrosion to initiate on more rebars on specimens with 50% FA than on specimens with OPC only. Stainless steel 316 and 304 rebars when properly pickled in the as received condition, show no sign of corrosion. However, rebars with these alloys that were wire brushed before embedding them initiated corrosion after several years. From tests performed on reinforced mortar specimens; the duplex stainless steels investigated appear to have a chloride threshold similar to that of 304. The chloride profiles obtained from cores obtained at KRB (fender piles) suggest that surface concentration (C_s) is a function of elevation and that the diffusivity decreases as a function of elevation (possibly due in part to a lower moisture content at higher elevations). No much difference was found when comparing the D_{app} from the lower elevations obtained now, with those measured as part of a previous project (BD546-08 “Characterization of New and Old Concrete Structures Using Surface Resistivity Measurements”).

TABLE OF CONTENTS

DISCLAIMER ii

CONVERSION FACTOR TABLE iii

TECHNICAL REPORT DOCUMENTATION PAGE iv

ACKNOWLEDGEMENTS v

EXECUTIVE SUMMARY vi

TABLE OF CONTENTS vii

LIST OF FIGURES xii

LIST OF TABLES xviii

1 BACKGROUND 1

2 D_{app} AND ρ_{WET} OF HPC LABORATORY SPECIMENS 5

2.1 ABSTRACT 5

2.2 INTRODUCTION 5

2.3 EXPERIMENTAL 6

2.3.1 Specimens 6

2.3.2 Potential Measurements 9

2.3.3 pH 9

2.3.4 Terminated Specimens: Diffusivity, Resistivity and Visual Examination 10

2.4 RESULTS AND DISCUSSION 11

2.4.1 Potential vs. Time 11

2.4.2 Visual Inspection of Terminated Samples 16

2.4.3 Chloride Profiles and Concentration above the Rebar Trace 17

2.4.4 Diffusion Coefficient 20

2.4.5 Resistivity and Diffusion Coefficient - D_{app} 21

2.4.6 D_{app}, pH and Cl^- at the Rebar Trace 23

2.5 CONCLUSIONS 24

2.6 ACKNOWLEDGMENTS 24

3 D_{app} AND ρ_{WET} OF HPC FIELD SPECIMENS 25
3.1 INTRODUCTION 25
3.2 EXPERIMENTAL 25
3.3 RESULTS 27
3.3.1 Porosity 27
3.3.2 Chloride Profiles 27
3.3.3 Resistivity vs. Time 29
3.3.4 D_{nssm} vs. Resistivity 31
3.3.5 D_{app} vs. Elevation and D_{nssm} vs. Elevation 33
3.4 CONCLUSIONS 35
4 CORROSION RESISTANT ALLOYS (CRAS) EMBEDDED IN CONCRETE EXPOSED OUTDOORS 36
4.1 INTRODUCTION 36
4.2 EXPERIMENTAL 36
4.2.1 Materials 36
4.2.2 Concrete Mix Designs 37
4.2.3 Simulated Deck Slab (SDS) Specimens 38
4.2.4 Specimen Terminations and Dissections 43
4.2.5 Chloride Analysis 44
4.2.6 Linear Polarization Resistance and Solution Resistance 45
4.3 RESULTS AND DISCUSSION 45
4.3.1 Potential vs. Time 45
4.3.2 Linear Polarization 49
4.3.3 Chloride Analyses 51
4.3.4 Visual Inspection of Terminated Specimens 54
4.3.5 Outdoor Specimens 62
4.3.6 Discussion 63
4.4 CONCLUSIONS 64

5 ACCELERATED CHLORIDE TRANSPORT TO INVESTIGATE CORROSION INITIATION AND PROPAGATION OF DUPLEX STAINLESS STEEL EMBEDDED IN CONCRETE 65
5.1 ABSTRACT 65
5.2 INTRODUCTION 65
5.3 EXPERIMENTAL PROCEDURE 66
5.3.1 Accelerated Chloride Transport Methods 68
5.3.2 Linear Polarization Resistance (LPR) and Electrochemical Impedance Spectroscopy (EIS) 69
5.3.3 Autopsy Procedure for Terminated Specimens 70
5.3.4 Chloride Analysis 71
5.4 RESULTS 71
5.4.1 Phase I 71
5.4.2 Phase II 72
5.5 CONCLUSIONS 97
6 EFFECT OF CRA INITIAL SURFACE CONDITION ON CORROSION INITIATION 99
6.1 SPECIMENS IMMERSED IN SIMULATED PORE SOLUTION 99
6.1.1 ABSTRACT 99
6.1.2 INTRODUCTION 99
6.1.3 EXPERIMENTAL PROCEDURE 100
6.1.4 RESULTS 102
6.1.5 CONCLUSIONS 111
6.2 CRAs EMBEDDED IN MORTAR WITH REDUCED COVER 112
6.2.1 ABSTRACT 112
6.2.2 INTRODUCTION 112
6.2.3 EXPERIMENTAL PROCEDURE 113
6.2.4 RESULTS 115
6.2.5 CONCLUSIONS 126
7 HIGH ALKALINITY CEMENTS EFFECT ON THE CONTROL OF ALKALI-SILICA REACTION 128

7.1 ABSTRACT 128
7.2 INTRODUCTION 128
7.3 EXPERIMENTAL 129
7.3.1 Concrete Mixtures 129
7.3.2 Length Changes 131
7.3.3 Resistivity 131
7.3.4 Non-Steady-State Diffusion 132
7.3.5 Bulk Diffusion 132
7.3.6 Visual Observation 132
7.4 RESULTS AND DISCUSSION 133
7.4.1 Length Change 133
7.4.2 Specimens with Florida Limestone 134
7.4.3 Specimens with Granite Aggregate 136
7.4.4 Specimens with ASR-Prone Aggregates 138
7.4.5 Resistivity vs. Time 140
7.4.6 Selection of Terminated Specimens 143
7.4.7 Visual Inspection 144
7.4.8 Petrography 146
7.4.9 Thin Section and Polarizing Microscope 148
7.5 CONCLUSIONS 152
7.6 ACKNOWLEDGMENTS 152
8 EFFECT OF POLARIZATION ON STEEL IN SIMULATED REINFORCED CONCRETE BRIDGE SUBSTRUCTURES EXPOSED TO MARINE ENVIRONMENTS 153
8.1 ABSTRACT 153
8.2 INTRODUCTION 153
8.3 EXPERIMENTAL PROCEDURES 155
8.3.1 Materials 155
8.3.2 Specimens 156
8.3.3 Experimental Setup 157

8.3.4 Measurement, Monitoring and Chloride Analysis....159
8.3.5 Age at Which Specimens Were Terminated....160
8.4 RESULTS....161
8.4.1 Potential Evolution vs. Time....161
8.4.2 Comparison of Experimental Measurement with Field Results....170
8.4.3 Depolarization Test....172
8.4.4 Visual Inspection and Chloride Analysis....184
8.4.5 Chloride Concentration....187
8.5 DISCUSSION....192
8.5.1 Development of Testing Method....192
8.5.2 Potentials and Corrosion Initiation....193
8.5.3 Chloride Concentration of Active Sites and Potentials....193
8.6 CONCLUSIONS....195
9 CONCLUSIONS....196
REFERENCES....199
APPENDIX A: Pictures of Terminated Specimens (Chapter 2)....204
APPENDIX B: Rebar Potential vs. Time (Chapter 2)....227
APPENDIX C: Applied Electric Field on Specimens of Chapter-5....244
APPENDIX D: Potential vs. time and Forensic Examination for specimens in Chapter-5....245
APPENDIX E: Petrographic and Polarizing Micrographs of Terminated ASR Specimens (Chapter 7)....279
APPENDIX F: Potential/Depolarization/24-off E vs. Time for Specimens in Chapter 8....450

LIST OF FIGURES

Figure 2.1: Schematic illustration of the specimen geometry 7
Figure 2.2: Typical potential evolution on AO specimens (1.9 cm cover)....11
Figure 2.3: Typical potential evolution on AO specimen with 3.2 cm concrete cover 12
Figure 2.4: Typical potential evolution on CO specimens. (1.8 cm Cover) 12
Figure 2.5: Typical potential evolution on specimens with FA and 1.9 cm cover 13
Figure 2.6: Typical potential evolution on specimens with FA and 3.2 cm cover 14
Figure 2.7: Typical potential evolution on specimens with SF 15
Figure 2.8: Example of terminated rebars undergoing corrosion 16
Figure 2.9: Chloride profiles and chloride concentration at the rebar trace, AO and CO specimens. (Obtained after 5700 days of exposure)....18
Figure 2.10: Chloride profiles and chloride concentration at the rebar trace, FA specimens. (Obtained after 5700 days of exposure)....18
Figure 2.11: Chloride profiles and chloride concentration at the rebar trace, SF specimens. (Obtained after 5700 days of exposure)....19
Figure 2.12: Resistivity vs. D_{app} 23
Figure 3.1: Location at which the cores were obtained at each cored fender pile....26
Figure 3.2: Chloride profiles obtained after 5 years of exposure (cores) 28
Figure 3.3: Chloride profiles obtained after bulk diffusion test (4 inch diameter slice)....29
Figure 3.4: Moisture vs. time 30
Figure 3.5: Resistivity vs. time while expose in high humidity and then immersed in water. (FP1-OPC, FP2-FA+UFA, FP3-FA, FP4-FA+SF, FP5-FA+BFS,FP6-FA+MK) 30
Figure 3.6: Resistivity vs. wt% change (FP1-OPC, FP2-FA+UFA, FP3-FA, FP4-FA+SF, FP5-FA+BFS,FP6-FA+MK)....31
Figure 3.7: D_{nssm} vs. Resistivity, and correlation obtained from tests on 4 inch cores 32
Figure 3.8: D_{nssm} vs. Resistivity: a) Grouped by core diameter, b) grouped by mix 32
Figure 3.9: D_{app} vs. elevation....33
Figure 3.10: D_{nssm} vs. elevation 34
Figure 4.1: Specimen Nomenclature 39
Figure 4.2: Sample schematic....40
Figure 4.3: Schematic illustration of the CREV type simulated deck slab specimens....41
Figure 4.4: View of a mold for a CCRV-SMI specimen prior to concrete pouring 42
Figure 4.5: Photograph of two SDS specimens under exposure 42

Figure 4.6: Photograph of SDS specimens under exposure in the outdoor test yard 43
Figure 4.7: Schematic illustration of the concrete sectioning as listed in dissection steps 2 and 3 above 44
Figure 4.8: Schematic illustration of the of the milling process above the rebar trace 44
Figure 4.9: Potential evolution for 316(A) embedded in STD1 or STD2 concrete 45
Figure 4.10: Potential evolution for 316(B) embedded in STD1 or STD2 concrete 46
Figure 4.11: Potential evolution on specimens with Stelax in STD1 or STD2 concrete 47
Figure 4.12: Potential evolution on specimens with 304SS in STD1 or STD2 concrete 47
Figure 4.13: Potential evolution on specimens with 2304 rebar in STD1 concrete 48
Figure 4.14: Potential evolution on specimens with WB-316 and WB-304 in STD1 concrete 48
Figure 4.15: Average Rc, minimum Rc and Ecorr 51
Figure 4.16: plots the average [Cl^-] versus depth for the cores from Set 4, 5 and 6 52
Figure 4.17: [Cl^-] versus depth for the cores on STD1-2304 specimen 52
Figure 4.18: [Cl^-] versus depth for the cores (2-WB-316-1) 53
Figure 4.19: [Cl^-] versus depth for the cores on 5-STD1-2304-3 specimen 53
Figure 4.20: Photographs of specimen and top rebars and bar trace of specimen 4-CCRV-3Cr12-1 subsequent to dissection 55
Figure 4.21: Photographs of top rebars and bar trace of specimen 3-CCRV-316-1 subsequent to dissection 56
Figure 4.22: Photographs of specimen and top rebars and bar trace of specimen 4-CCR-SMI-3 subsequent to dissection 56
Figure 4.23: Photographs of top rebars and bar trace of specimen 6-WB-304-1 subsequent to dissection 57
Figure 4.24: Photographs of top rebars and bar trace of specimen 2-WB-316-1 subsequent to dissection. The figure also shows close-ups of the larger corrosion spot before and after cleaning it 58
Figure 4.25: Photographs of top rebars and bar trace of specimen 5-STD1-2304-1 subsequent to dissection 59
Figure 4.26: Photographs of top rebars and bar trace of specimen 5-STD1-2304-1 subsequent to dissection 60
Figure 4.27: Photographs of two bottom rebars and bar trace of specimen 5-STD1-2304-3 subsequent to dissection. Close-up or large corrosion site before and after cleaning is also included 61
Figure 4.28: Current state for specimens 2-BCAT-316-2 and 6-BCAT-304-1 62
Figure 4.29: Pictures of the surface cracks on 3-CCRV-3Cr12 specimens 63
Figure 4.30: Pictures of the corrosion spots on the surface of 4-BCCD-SMI (left) and 6-CVNC-SMI-3 (right) 63
Figure 5.1: Sample schematic, dimensions and specifications 67
Figure 5.2: Picture of the specimen 67
Figure 5.3: Batch 1 & batch 2 potential measurements over time during Phase I 72
Figure 5.4: Plots symbols clarification 73
Figure 5.5: OCP measurements over time for Phase II plots of samples Batch 1-1 and 2-1 73

Figure 5.6: Rp_meas-Rs over time for Phase II plots of samples Batch 1-1 and 2-1 75
Figure 5.7: Diagram of the crack evolution over time for specimen batch 1-1 76
Figure 5.8: Lateral cracks pictures for specimen Batch 1-1 77
Figure 5.9: Diagram of the crack evolution over time for specimen batch 2-1 78
Figure 5.10: Picture of final crack pattern for specimen batch 1-2 79
Figure 5.11: Picture of final crack pattern for specimen batch 2-2 80
Figure 5.12: Autopsy and visual examination of rebars of specimen batch 1-1 81
Figure 5.13: Autopsy and visual examination of rebars of specimen batch 1-2 82
Figure 5.14: Autopsy and visual examination of rebars of specimen batch 1-1 83
Figure 5.15: Close-up picture of sample batch 1-1B rebar before and after cleaning 84
Figure 5.16: Autopsy and visual examination of batch 2-1 85
Figure 5.17: Autopsy and visual examination of top row rebars on specimen batch 2-2 86
Figure 5.18: Autopsy and visual examination of top row rebars on specimen batch 2-4 87
Figure 5.19: Close-up picture of sample batch 2-1B after cleaning 88
Figure 5.20: Chloride profiles for specimens batch 1-1 and 2-1 and at the rebar trace 88
Figure 5.21: Observed length L and value explanation process for specimen 1-1 rebar C 94
Figure 5.22: Observed length L and value explanation process for specimen 2-2 rebar B 95
Figure 5.23: Plot of the Xcrit values for equations (1), (2) and experimental results as a function of C/L ratio 97
Figure 6.1: Rebar immersed in SPS 102
Figure 6.2: Potential vs. time on UNS S32304 and UNS S30400 (C, H and S surface conditions) NaCl% series stepwise additions of Sodium Chloride 104
Figure 6.3: Potential vs. time on S32101 (C, H and S surface conditions) 105
Figure 6.4: Rc as measured on UNS S32101 rebar samples for the 3 surface conditions 106
Figure 6.5: Rc vs. time measured on UNS S30400 and UNS S2304 samples (C, H, S surface conditions) 107
Figure 6.6: Terminated UNS S32101 specimens. Upon removal from solution, after removing mortar and finally after cleaning 108
Figure 6.7: Visual inspection on UNS S32304 terminated specimens; top pictures are shortly after removing from solution, middle pictures after removing mortar, bottom pictures after cleaning surface 109
Figure 6.8: Visual inspection on UNS S30400 terminated specimen. Upon removal of the solution, after removing mortar and after removing corrosion products, bottom pictures after cleaning surface 109
Figure 6.9: Visual inspection on UNS S32101 terminated specimens after removal from solution 110
Figure 6.10: Visual inspection on UNS S32304 terminated specimens after removing from solution 110
Figure 6.11: Visual inspection on UNS S30400 terminated specimens after removing from solution 111
Figure 6.12:CRA reinforced mortars 114

Figure 6.13: Potential evolution on mortar samples with UNS S32304 and UNS S30400 upon exposure to 15% NaCl solution. Wet/dry cycles began on the day indicated by the vertical dash line 116
Figure 6.14: Potential vs. time for UNS S32101 embedded in mortar. Wet/dry cycles (4 days wet/ 3 days dry) began on the day 40 indicated by the vertical dash line 117
Figure 6.15: Rc vs. time (bottom) on UNS S32101 embedded in mortar. Wet/dry cycles (4 days wet/ 3 days dry) began on the day indicated by the vertical dash line 118
Figure 6.16: Rc measured on UNS S32304 and UNS S30400 embedded in mortar with w/c=0.5. Wet/dry cycles (4 days wet/ 3 days dry) began on the day indicated by the vertical dash line 119
Figure 6.17: Ecorr and Rc measured on UNS S32304 and SSC rebar embedded in mortar with w/c=0.42. Wet/dry cycles (4 days wet/ 3 days dry) began on the day indicated by the vertical dash line 120
Figure 6.18: As received (C) specimens for the different CRA alloys embedded in mortar w/c=0.5 122
Figure 6.19: Visual examination after exposing rebar for H and S surface condition for the three CRA types 123
Figure 6.20: As received (C) specimens for the different CRA alloys embedded in mortar w/c=0.41 124
Figure 6.21: Cracks observed on S32101-H and S32101-S 125
Figure 7.1: Length change (%) for concrete prisms prepared with Florida aggregates 134
Figure 7.2: Length change (%) for concrete prisms prepared with Georgia(GG) and Nova (NG) granites coarse aggregates 136
Figure 7.3: Length change (%) for concrete prisms prepared with H1(Spratt) and H2 (Sudbury) coarse aggregates known to be moderate and highly ASR reactive 138
Figure 7.4: Length change for prisms with no fly ash, prepare with FL1, H1 and H2 coarse aggregates 140
Figure 7.5: Typical evolution of resistivity with time. Concrete mixes prepared with Florida aggregates and various EqA and Li contents 141
Figure 7.6: Typical evolution of resistivity with time. Concrete mixes prepared with granite, H1 and H2 aggregates and various EqA and Li contents 143
Figure 7.7: Example of specimens with not bleeding products 144
Figure 7.8: Example of specimens with significant ASR products that have bled 145
Figure 7.9: Specimens with FL2 aggregate selected to be terminated 145
Figure 7.10: Photograph of a lapped surface and two close-ups on specimen 29B 146
Figure 7.11: Typical cracks patterns observed on specimens with NG, H1 and H2 147
Figure 7.12: Length Change vs. time on specimens with different coarse aggregate 149
Figure 7.13: Evidence of ASR gel on thin section of specimen 27A 150
Figure 7.14: Evidence of ASR gel on thin section of specimen 02-C with NG 150
Figure 7.15: Evidence of ASR gel on thin section of specimens with H1 coarse aggregate 151
Figure 7.16: Evidence of ASR gel on thin section of specimen 39B with H2 coarse aggregate 151

Figure 8.1: Photograph of a coastal bridge spalled piling 154
Figure 8.2: Simulated Piling Specimen (units: mm) 157
Figure 8.3: Photograph with four simulated pile specimens 158
Figure 8.4: Photograph of the tank assembly for affecting polarization of the lower portion of the specimens....160
Figure 8.5: Potential of the left and right bars at eight elevations and macro-cell current in specimen M1as a function of exposure time (measurement elevations in cm relative to the waterline). 162
Figure 8.6: Potential of the left and right bars at eight elevations and macro-cell current in specimen K2 as a function of exposure time (measurement elevations in cm relative to the waterline) 163
Figure 8.7: Potential of the left and right bars at eight elevations and macro-cell current in specimen K3 as a function of exposure time (measurement elevations in cm relative to the waterline). 165
Figure 8.8: Potential of the left and right bars at eight elevations and macro-cell current in specimen K4 as a function of exposure time (measurement elevations in cm relative to the waterline) 167
Figure 8.9: Potential versus elevation data (a) piling C of bent 4 of the Hurricane Pass Bridge (elevation referenced to mean high tide, and data at -100 m refers to measurements with the reference electrode in the water) and (b) left bar of specimen M1 171
Figure 8.10: Typical depolarization plots of the left bar of Specimen M1 and left bar of Specimen N1 at different elevations as a function of depolarization time for test performed in May 2010 (measurement elevations in inches relative to the waterline). 172
Figure 8.11: 24-hr off potential plots of the M1 left bar and right bar at different elevations as a function of exposure time (measurement elevations in cm relative to the waterline).....174
Figure 8.12: 24-hr off potential plots of the K2 left bar and right bar at different elevations as a function of exposure time (measurement elevations in cm relative to the waterline).....175
Figure 8.13: 24-hr off potential plots of the K3 left bar and right bar at different elevations as a function of exposure time (measurement elevations in cm relative to the waterline).....176
Figure 8.14: 24-hr-off potential plots of the L1 left bar and right bar at different elevations as a function of exposure time (measurement elevations in cm relative to the waterline).....177
Figure 8.15: Net depolarization (mV) after 24-hr plots of the M1 left bar and right bar at different elevations as a function of exposure time (measurement elevations in cm relative to the waterline). 180
Figure 8.16: Net depolarization (mV) after 24-hr plots of the K2 left bar and right bar at different elevations as a function of exposure time (measurement elevations in cm relative to the waterline). 181
Figure 8.17: Net depolarization (mV) after 24-hr plots of the L1 left bar and right bar at different elevations as a function of exposure time (measurement elevations in cm relative to the waterline). 182
Figure 8.18: M1 right rebar - corrosion spots on right rebar at 13.00 cm, 14.80 cm and 16.20 from the bottom of specimen (7.00cm, 9.80cm and 11.20cm from the water line).....184

Figure 8.19: K1 right rebar low portion–corrosion spots at level 17.5cm from the bottom of specimen (12.5cm from the water line) 185
Figure 8.20 K2 right rebar–corrosion spots on rebar.....186
Figure 8.21: K3 left rebar–corrosion spots at 16.5cm and 28.3cm from the bottom of specimen (11.5cm and 23.3cm from the water line) 186
Figure 8.22: K3 right rebar–corrosion spots from 14cm to 18.25cm from the bottom of specimen (9.0cm to13.25cm from the water line) 187
Figure 8.23: Chloride profile of specimen K1.....191
Figure 8.24: Chloride profile of specimen K3.....191
Figure 8.25: Chloride profile of specimen M1 192
Figure 8.26: Values of E_p vs C_T obtained from present work and reported by other investigators 195

LIST OF TABLES

Table 2-1: Mix design and admixture content* 6
Table 2-2: Mix design AO and CO 8
Table 2-3: Mix design FA1, FA2, FA3, FA4 8
Table 2-4: Mix design SF1, SF2, SF3, SF4 9
Table 2-5: Number of samples with reinforcements per mix and height/cover 9
Table 2-6: Chloride concentrations at the rebar trace (kg/m^3) 19
Table 2-7: Minimum and average [Cl^-] kg/m^3 at the rebar trace on those corroding 20
Table 2-8: D_{app} calculated for each sliced core 21
Table 2-9: Diffusivity after 3.3 and >15 years and ρ_{wet} after 15 years 22
Table 2-10: pH values measured at day 1200 [1] 24
Table 3-1: Dates at which the fender piles were deployed and cored 27
Table 3-2: Porosity calculations 27
Table 3-3: List of D_{nssm} and Resistivity 31
Table 3-4: Comparison of D_{app} and D_{nssm} on 10 cm diameter core slices 34
Table 4-1: Alloys investigated 37
Table 4-2: Alloys composition 37
Table 4-3: Concrete batch mix design 38
Table 4-4: Listing of the various specimen types, variables, and the nomenclature for each 40
Table 4-5: R_c (KOhms) values and correspond E_{corr} measured on selected specimens 49
Table 4-6: R_c (KOhms) values and correspond E_{corr} measured on selected specimens 50
Table 4-7: Chloride concentration at the rebar trace 54
Table 5-1: Chloride concentration at rebar trace (kg/m^3) and chloride by weight cementitious percentage (WC%) for Batch 1-1 and Batch 1-2 90
Table 5-2: Chloride concentration at rebar trace (kg/m^3) and chloride by weight cementitious percentage (WC%) for Batch 2-1 and Batch 2-2 90
Table 5-3: Critical chloride threshold value for different steels in percent weight of cement (WC) % 90
Table 5-4: Mass loss approximation and parameters 93
Table 5-5: X_{crit} and $X/(c/\phi)$ values for different equations and parameters 96
Table 6-1: CRA chemical compositions determined via XRF. 100
Table 6-2: CRA chemical compositions determined via XRF. 113
Table 6-3: Chloride concentration measured at the rebar trace on terminated specimens 126

Table 7-1: Chemical composition of cements and FA used (weight percent) 130
Table 7-2: Aggregate Properties 130
Table 7-3: List of mixes 130
Table 7-4: Listing of concrete series with FPL-1 coarse aggregate and length change after one, two and eight years 135
Table 7-5: Listing of concrete series with FPL-2 coarse aggregate and length change after one, two and eight years 135
Table 7-6: Listing of concrete series with FPL-3 coarse aggregate and length change after one, two and eight years 136
Table 7-7: Listing of concrete series with GG coarse aggregate and length change after one, two and eight years 137
Table 7-8: Listing of concrete series with NG coarse aggregate and length change after one, two and eight years 138
Table 7-9: Listing of concrete series with H1 coarse aggregate and length change after one, two and eight years 139
Table 7-10: Listing of concrete series with H2 coarse aggregate and length change after one, two and eight years 139
Table 7-11: List of specimens terminated (indicating specimen ID) 144
Table 8-1: Details of concrete mixes 155
Table 8-2: Compositions of Cement and Fly Ash (unit: % mass) 156
Table 8-3: Listing of specimens and resistor 158
Table 8-4: Exposure Age in Days at which each Rebar was terminated 160
Table 8-5: Current data for polarized specimens* 169
Table 8-6: Potential data at lowest and highest elevations for polarized specimens* 170
Table 8-7: 24-hour off-potentials of rebar in specimens K1, K2, K3 and L1 (unit: mV vs. SCE) 178
Table 8-8: 24-hour off-potentials of rebar in specimens M1, M2, N1 and N2 (unit: mV vs. SCE) 178
Table 8-9: Net depolarized potentials of rebar in specimens K1, K2, K3 and L1 (unit: mV) 183
Table 8-10: Net depolarized potentials of rebar in specimens M1, M2, N1 and N2 (unit: mV) 183
Table 8-11: Locations of corrosion spots on rebars 187
Table 8-12: Chloride concentration of K1, K2, K3 and L1 at rebar trace 189
Table 8-13: Chloride concentration of M1, M2, N1 and N2 at rebar trace 190

1 BACKGROUND

There are multiple materials that are currently being used to extend the durability of new bridge structures: e.g., high performance concrete (HPC), stainless steel reinforcements, corrosion inhibiting chemical admixtures, high alkalinity cements, etc. FDOT has made a large investment identifying those materials that have proven to increase the service life of concrete structures. However, more detailed information is required to optimize the use some of these materials in FDOT specifications.

At the beginning of this project, there were still a larger number of samples prepared with some of these different materials at Florida Atlantic University (FAU). These samples were prepared as part of past FDOT-funded projects, but due to their excellent performance had not reached significant damage or failure. As part of this project additional monitoring took place, and selected specimens were terminated for forensic analysis. These terminated specimens were selected either because corrosion had initiated or to assess the rebar surface condition in time to be included in the final report. Other terminated specimens were selected to monitor other properties (e.g., visual inspection upon exposing the rebar, petrography of lapped surfaces, resistivity on cores, chloride profiles from cores, chloride at the rebar trace, etc.).

Additionally, there is interest in determining the service life using variables such as concrete resistivity (ρ_{wet}), apparent chloride diffusion coefficient (D_{app}), and chloride threshold. Additional information and insight regarding these parameters was gained. The following chapters describe the project objectives and selected significant findings. Each chapter has been written as a self-contained paper. For some of the chapter additional details can be found in the included appendices.

The objectives of this research were to:

1) Determine chloride diffusivity and resistivity of 15-yr outdoor-exposed samples (currently 18.8+ years old).
This objective was met. The approach and results are the content of chapter 2. A brief description follows. Several specimens were selected for forensic examination. Samples were terminated at three different times (15.5, 16.5, and 17 years). The first set of terminated specimens included at least a specimen from each mix prepared. Not all terminated specimens contained corroding rebars. Most terminated specimens were cored. Some of the cores were then used for resistivity and others for chloride profiles so that D_{app} could be calculated. A good correlation was found between D_{app} vs. ρ_{wet}. It was found that concrete with the largest fly ash (50%) replacement had the lowest

D_{app}, the corrosion of the rebars initiated about the same time that some of the specimens with OPC only due to the lower pH in the pore solution. This then translates into a lower critical chloride concentration (C_T). Specimens with only SF had somewhat higher D_{app} than FA mixes. The potential evolution for some of the HPC samples not always followed the traditional passive to active transition. There was usually a monotonic decay from positive (e.g. +100 mVsce) values towards more negative values (e.g. -50 or even -100 mVsce). Once the potential of the reinforcement reached these more negative values an additional downward transient usually took place, but was not always abrupt. In some cases a recovery (shift) to more positive potential values took place and remained there for quite some time, eventually a potential drop was found once corrosion initiated and progressed.

2) Determine chloride diffusivity and ρ_{wet} of 5-6 years Key Royale HPC mixes.

Chapter 3 describes the findings for this objective. Cores were obtained from a fender piles for each mix. Nine cores were obtained per selected fender pile. One core was obtained from the top face (nominal 4 inches diameter) of the fender piles and the other cores (nominal 2 inches in diameter) were obtained from one of the lateral faces at four different elevations (two per elevations). The resistivity vs. time was first monitored from the 4 inches diameter cores. Apparent porosity was determined, but the test was modified as to not affect the microstructure: e.g. cores were dried at 50ºC and then the moisture was increased by placing these cores in high humidity for several weeks followed by several days immersed in water. The boiling in water step was not performed. Chloride profiles were determined and D_{app} calculated from the cores obtained at four elevations. D_{nssm} tests were performed on remainder of the 2 inches cores that were longer than 5 cm long and on a 5 cm slice from the 4 inches diameter core.

3) Determine chloride threshold on piles made with mortar fly ash simulating partially immersed structures.

Chapter 8 details the findings for this objective. All reinforced mortar piles were terminated for forensic examination. Not all rebars initiated corrosion along the exposed face. In some cases corrosion took place under the shrinkage wrap. Off potential as a function of elevation at 24 hours of depolarization and net-depolarization after 24 hours at these elevations were used as indicators of when corrosion began. It was confirmed that polarization increases the chloride threshold. However, corrosion might have initiated as a result of the periodic depolarization tests. Additionally, on some cases the prolonged exposure allowed chlorides to move under the shrinkage wrap causing crevice corrosion.

4) Determine the elongation of five year samples exposed (currently > 7 years old) in high humidity and high temperature room.

Chapter 7 describes the results after 7 years of exposure in high humidity and elevated temperature room. Specimens that contained the two investigated granite coarse aggregates and high alkalinity appear to be prone to

ASR as well as FL2 coarse aggregate Florida limestone. Additional confirmation might be needed to verify that ASR took place on the other two Florida limestone coarse aggregates as the elongation did not exceed the threshold even after 7 years of exposure and polarizing micrographs were not conclusive.

5) Obtain chloride concentration at the rebar trace of samples with high performance corrosion resistant alloys.
Chapter 4 contains the results of this objective. Seven specimens were terminated to accomplish this objective. Corrosion sites were observed on the specimens in which the 304 or 316 CRA rebars were wired brushed before embedding them into the concrete. These rebars were wire brushed with a stainless steel brush before casting the specimen. Corrosion initiated in at least one specimen out of three, for both 304 and 316 rebars that had the surface wire brushed. Corrosion initiated on the reinforcement of two specimens with 2304 rebars in the as received condition and STD1 configuration. On one of these two specimens, the corrosion took place on the top layer rebars (only one rebar). On the second (the most recent terminated) specimen, the corrosion took place on the bottom layer rebars (only one rebar). However, in this latter specimen the chloride profile did not follow normal diffusion shape, i.e. the chloride at the level of the second row of rebars was higher than at the depth of the first row of rebars. In addition, LPR tests were performed on selected specimens multiple times. The specimens selected for LPR testing were momentarily brought into laboratory and returned outdoors after the LPR tests.

6) Determine if pickling is needed for high performance CRAs thru laboratory experiments.
Chapter 6 is divided into two sections. Section 6.1 describes rebars immersed in pore solution, and section 6.1 describes the results of rebars embedded in mortar with a reduced cover. The mill scale was re-created on as received rebars for three types of alloys: 304, 2304 and 2101. The implemented process produces a mill scale that is worst (i.e. thicker and removed more Cr from the surface) than what is usually obtained at an industrial setting. It was found that corrosion initiated on rebars with the mill scale upon adding 5% NaCl for 304 and 2304 and 2% NaCl for 2101 rebars. However, after almost two years of exposure the specimens were removed and corrosion appears to propagate at a slow to very modest rate. Test for rebars embedded in mortar appear to confirm this observation. Corrosion initiated on rebars milled+sandblasted after adding 10% NaCl for 304 and 2304 and 6.5% NaCl for 2101 rebars. The chloride threshold for as received rebars embedded in mortars (w/c>= 0.5) and exposed for more than 500 days to 15% NaCl (permanent and cyclic – see chapter for details) was > 6 wt% cement for 304, 2304 and 2101 based on chloride concentrations determined from the mortar above the rebar trace. A set of reinforced mortar specimens with 2304 prepared with lower w/cm and exposed for >1300 days initiated corrosion at chloride levels between 7 and 9 wt% of cement (based on chloride concentration at the rebar trace).

Chapter 5 contains the summary of results for tests on specimens reinforced with duplex rebars (2304 and 2101) on which chloride transport was accelerated via a migration cell approach. The geometry selected is the simulated

deck slab. This additional task was performed towards determining the chloride threshold on these alloys. It is important to note that corrosion initiated at a lower concentration due to possible removal of the passive layer as a result of anodic polarization caused by stray current that resulted from the electric field application. Hence, placing stainless steel rebars on systems (e.g. rail) where stray currents might be present and the reinforced concrete exposed to chlorides might require additional monitoring. Corrosion usually initiated on one rebar, and additional electric field was applied to transport additional chlorides as to initiate corrosion on the other two rebars on the top row. This usually caused that the rebar where corrosion had initiated to corrode at a high rate which shorten the corrosion propagation, i.e. it caused cracks to be visible (this is due again stray currents) after a few weeks. As a result of this observation additional insight was obtained regarding how much corrosion products would produce a crack on specimens with duplex stainless steel. Corrosion did not initiate on the rebars of one of the specimens with 2304. Additionally, in most instances after activation there was a tendency of the corrosion potential to drift towards more noble values on multiple rebars per specimen, i.e. there is a tendency to re-passivate. (This was not observed in cases in which the potential reached potential < -550 mVsce, for these cases a more modest drift took place)

2 D_{app} AND ρ_{WET} OF HPC LABORATORY SPECIMENS

2.1 ABSTRACT

The reported research was performed for the purpose of determining the chloride threshold concentration for high performance concrete under exposure conditions relevant to coastal bridge substructures in Florida. The experiments were based upon a series of reinforced and non-reinforced concrete specimens that contained 1) 20, 35 and 50 percent replacement by fly ash, 2) 6, 15 and 27 percent replacement by silica fume, and 3) control specimens (no pozzolanic admixture). The specimens have now been exposed to one week wet - one week dry ponding cycle with natural sea water since January, 1995. Most of the exposure took place outdoors, but for a couple years the specimens were stored inside the laboratory. The rebar potential of the reinforced concrete slabs were monitored with time in order to determine when active corrosion commenced. Some of the specimens have activated. After ~15.6, 16.5 and 17 years' of exposure, selected specimens were terminated for forensic examination. The corrosion extent was determined from visual examinations. Cores were also taken from the terminated specimens to determine the extent of chloride ingress and to determine the concrete resistivity. The chloride concentration above the rebar trace was also measured on the terminated samples. From the measured chloride concentration profiles, the diffusion coefficient of the different concrete mixes was determined and correlated against the corresponding measured wet resistivity. Specimens with 50 percent FA had the lowest D_{app}, but also the lowest chloride threshold, likely due to a reduction of pH.

2.2 INTRODUCTION

It is well-known that concrete is one of the most used materials in construction. However, the deterioration of reinforced concrete structures has been a constant concern for years, and corrosion of the reinforcing steel is the main cause of this deterioration. Once corrosion has initiated, cracks in concrete form and propagate due to tension stress forces produced by corrosion products accumulated during the propagation stage. The corrosion products occupy a larger volume when compared to the volume of a non-corroding rebar. A critical area in a partially-immersed reinforced concrete structure exposed to severe weather conditions (i.e., direct exposure to sea water) is the splash zone, where the most severe corrosion conditions usually develops with time.

Many publications have reported the chloride resistance of concrete made with binary or ternary concrete mixes. In the present effort an additional set of results are reported. But in addition to the corrosion potential, time to corrosion, and D_{app}; the chloride above the rebar trace and the resistivity of saturated concrete were also measured. In here, a correlation between wet resistivity (ρ_{wet}) and D_{app} has been fitted to the values obtained from tests performed on cores obtained from terminated samples that were exposed outdoors for over 15 years.

Most modern structures are built with concrete that have low water-to-cementitious ratio (w/cm). However, many of the published experimental results use relatively high water to cement ratio as a way to reduce the time to corrosion initiation. This paper reports results on concrete specimens prepared with relative low water-to-cementitious ratio of ~0.37. The concrete diffusivity was measured from chloride profiles after 1200 days and after more than 5700 days (i.e., cores obtained after 15.6, 16.5 and 17 years). The D_{CL} obtained at both instances were compared and it was found that D_{app} of concrete with FA significantly decreased with time. A more modest reduction in D_{app} was observed when comparing D_{app} of concretes with silica fume.

2.3 EXPERIMENTAL

2.3.1 Specimens

A set of 72 specimens was made based upon concrete mix designs with different fly ash, silica fume and calcium nitrite contents, as listed in Table 2-1

Table 2-1: Mix design and admixture content*

Mix Design Designation	Fly Ash percent	Silica Fume Percent	Calcium Nitrate l/m^3
AO	0	0	0
CO	0	0	19.8
FA1	20	0	0
FA2	35	0	0
FA3	50	0	0
FA4	35	0	19.8
SF1	0	6	0
SF2	0	15	0
SF3	0	27	0
SF4	0	15	9.9

* %FA and %SF content are % of FA/(c+FA) and SF/(c+SF) respectively

All mixes were made with Holnam Type H Portland cement and a water-to-cementitious ratio of 0.37. The sources for the coarse and fine aggregates were Brooksville and Kueka, respectively. The slabs were cast at the FDOT Materials Laboratory in Gainesville, Florida, in October, 1994 and were subsequently delivered to the Marine Corrosion Laboratory at Florida Atlantic University. The different mix designs and concrete properties are listed in Tables 2-2 through 2-4.

The specimens were of two types — reinforced and non-reinforced, where the former contained five number three (9.5 mm diameter) steel bars and the latter contained no embedded steel. The reinforced specimens comprised the corrosion test program, per se. Most of the reinforced specimens were 12.7 cm high with 1.9 cm cover over the

top bars, while a limited number of specimens were 15.2 cm thick with 3.2 cm cover. Table 2-5 lists the number of reinforced samples casted for each mix and height/cover. The slab geometry is as illustrated in Figure 2.1.

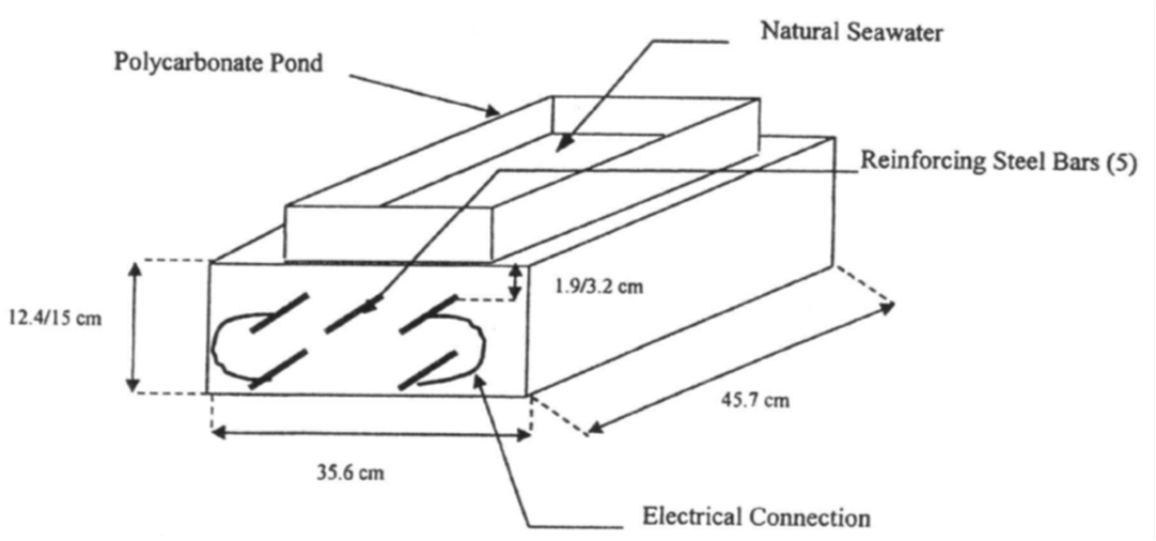

Figure 2.1: Schematic illustration of the specimen geometry

Prior to exposure testing, the specimens were inverted (as-cast face down); and a polycarbonate bath was mounted on what became the top surface. A one week wet — one week dry ponding cycle was instituted in January, 1995 using fresh natural sea water. The typical conductivity of seawater measured at our site is ~ 50 mS/cm. A rectangular plastic plate is placed on top of the specimens to prevent rainfall or minimize evaporation during the rainy/dry seasons respectively. As shown in Figure 2.1, each of the bottom bars were electrically connected to one of the top bars so that a macro-cell resulted between the two. An electrical switch (not shown) between these bar pairs permitted measurement of macro-cell current. The top-middle bar was left electrically-isolated to obtain data independent of any macro-cell action. Macrocell measurements were performed up to day 3000, and results from these measurements will not be presented in here.

Table 2-2: Mix design AO and CO

	AO	CO
Cement, kgs	113.5	56.7
Fly Ash, kgs	0	0
Silica Fume, kgs	0	0
Calcium Nitrite, kgs	0	2.6
Water, kgs	33.3	14.3
Coarse Aggregates, kgs	286.8	143.4
Coarse Aggregates, % excess moisture	2.06	2.5
Fine Aggregates, kgs	215.6	107.8
Fine Aggregates, % excess moisture	1.3	1.5
Unit Weight, kgs/m^3	2,292.5	2,276.4
w/cm ratio	0.37	0.367
RCP Avg. 91 Days	4896 (High)	6285 (High)
WP Avg.	2.6E-11	3.3E-11
Strength Avg. 28 days (psi)	6407	6983

Table 2-3: Mix design FA1, FA2, FA3, FA4

	FA1	FA2	FA3	FA4
Cement, kgs	90.8	73.8	56.7	36.9
Fly Ash, kgs	22.7	39.7	56.7	19.9
Silica Fume, kgs	0	0	0	0
Calcium Nitrite, kgs	0	0	0	2.6
Water, kgs	27.6	27.8	28.0	12.2
Coarse Aggregates, kgs	287.4	287.4	287.4	144.2
Coarse Aggregates, % excess moisture	2.96	2.3	2.3	2.9
Fine Aggregates, kgs	212.4	206.0	199.6	101.9
Fine Aggregates, % excess moisture	2.68	3.68	3.68	3.0
Unit Weight, kgs/m^3	2,263.6	2,247.6	2,231.6	2,231.6
w/cm ratio	0.367	0.37	0.37	0.363
RCP Avg. 91 Days	989	713	731	NA
WP Avg. 91 Days	2.9E-12	3.9E-12	4.71E-12	NA
Strength Avg. 28 days (psi)	6604	6190	5267	4964
Strength Avg. 91 days (psi)	7715	7673	6621	6452

Table 2-4: Mix design SF1, SF2, SF3, SF4

	SF1	SF2	SF3	SF4
Cement, kgs	55.1	52.2	48.3	52.2
Fly Ash, kgs	0	0	0	0
Silica Fume, kgs	3.6	9.5	17.8	9.5
Calcium Nitrite, kgs	0	0	0	1.34
Water, kgs	12.5	9.4	5.1	8.3
Coarse Aggregates, kgs	144.2	144.2	144.2	144.2
Coarse Aggregates, % excess moisture	2.65	2.7	2.9	2.9
Fine Aggregates, kgs	108.7	107.6	106.1	107.6
Fine Aggregates, % excess moisture	2.680	2.68	2.68	2.7
Unit Weight, kgs/m^3	2,279.6	2,273.2	2,262.0	*2,265.2*
w/cm Ratio	0.37	0.367	0.368	0.365
RCP Avg. 91 Days	2061	720	598	868
WP Avg. 91 Days	9.8E-12	NA	NA	2.6E-12
Strength Avg. 28 days (psi)	7065	7374	7624	7071
Strength Avg. 91 days (psi)	7624	7571	7681	7495

Table 2-5: Number of samples with reinforcements per mix and height/cover

Height/ Cover	AO	CO	FA1	FA2	FA3	FA4	SF1	SF2	SF3	SF4
12.7 /1.9 cm	5	4	4	4	4	3	3	3	3	3
15.2 /3.2 cm	3		3	3	3					

2.3.2 Potential Measurements

Corrosion state of the reinforcement, i.e., determination whether the embedded steel was passively or actively corroding, was assessed as a function of time by macro-cell current (first 3000 days) and corrosion potential (half-cell potential) measurements, the latter being measured in general accord with standard practice during the wet cycle. In the present experiments, potentials were recorded using a high resistance voltmeter that measured the rebar against a saturated calomel electrode (SCE) with a pre-wetted sponge being used as an electrical junction between the concrete surface and the reference electrode. The electrode was placed above the rebar at the center of the rebar length.

2.3.3 pH

Selected non-reinforced concrete specimens were cored and the pH measured via a leaching technique. These measurements were performed when the concrete was ~1100 days. The pH was measured as during phase I of this project. A description of the method used and additional details for the testing conditions can be found in

reference [1]. The pH was measured both under laboratory conditions and also under a nitrogen gas atmosphere to prevent carbonation of the leached solution.

2.3.4 Terminated Specimens: Diffusivity, Resistivity and Visual Examination

Some of the non-reinforced specimens served as companion specimens from which cores were extracted at various times so that the ingress of chlorides could be monitored without destructively altering the reinforced specimens. Concrete cores from non-reinforced specimens were drilled after 1200 days and the chloride profiles and D_{app} obtained [1]. After 5700, 6000, 6250 days of exposure it was decided to terminate selected reinforced specimens. On day 5700, at least one specimen per mix type was terminated and not necessarily undergoing corrosion. Before cutting the specimens open, these specimens were also cored. Four cores were typically drilled from each specimen, with two cores sliced for chloride profiles and the other two cores were used to measure the concrete resistivity. After segmenting the concrete sample along the rebar length, the rebars at the top row were exposed and the surface condition documented. The pieces of concrete above the rebar were milled to collect concrete powder (1 to 2 mm depth) along the rebar trace. Caution was used to prevent milling over rust spots. These concrete samplings were then used to measure the chloride concentration representative of the concentration above the rebar trace. The chloride concentration determination was performed using FDOT method [2] or a modified approach that used a smaller amount of concrete powder when necessary. This method measures the total chlorides.

As indicated in the previous paragraph, two (or one) concrete cores per terminated specimen were selected to assess the resistivity (ρ_{wet}) of the concrete (water saturated concrete). The resistivity measurements follow a FDOT method [3]. This ρ_{wet} was achieved by placing the cores in a high humidity chamber (~95% RH). Two different measurements were taken on these 4.5 cm cores: 1) resistivity measurements along the longitudinal direction of the concrete core ρ vs. time (eight readings 90 degrees apart two times around), and 2) weight percent change vs. time (from initial recorded weight). Both measurements were performed at laboratory conditions with temperature ~21 ±2 ºC. These two sets of measurements started about a week after being cored which might have allowed the cores to get drier when compared to outdoor exposure conditions; on the other hand, the cores were obtained using a wet-coring procedure.

2.4 RESULTS AND DISCUSSION

2.4.1 Potential vs. Time

Figure 2.2 to Figure 2.7 show measured potential vs. time plots. Each plot has 3 series. 'E1 on' and 'E3 on' correspond to the measured potential of the coupled rebars on the left and on the right on each specimen, respectively. E2 corresponds to the measured potential on the center rebar. Figure 2.2 shows the potential evolution on specimens AO2 and AO3. Both of these specimens were terminated around day 5700. It can be observed that corrosion initiated on the three rebars on specimen AO3. But based on the terminal potential values, none of the rebars on specimen AO2 appear active. However, at around day 4500, there was a momentary potential drop; the potential of all rebars recovered (shifted to more positive potential values) soon after this event. Upon opening specimen AO2, the three rebars showed some red rust spots (rather than black/ dark green corrosion products). For AO specimen with 1.9 cm concrete cover, seven out of 12 rebars became active of those terminated, and 1 of 3 rebars from the non-terminated specimen appear active. Figure 2.3 shows the potential evolution on specimen AO5, which is one of the specimens with a cover of 3.2-cm; the other two specimens show similar behavior. A potential transient has been taking place over the last 2000 days, and excursions to values more negative than -100 mVsce have been observed. No rebar has become active on AO specimens with 3.2 cm concrete cover. The appendix corresponding to this chapter contains additional potential vs. time plots for all specimens.

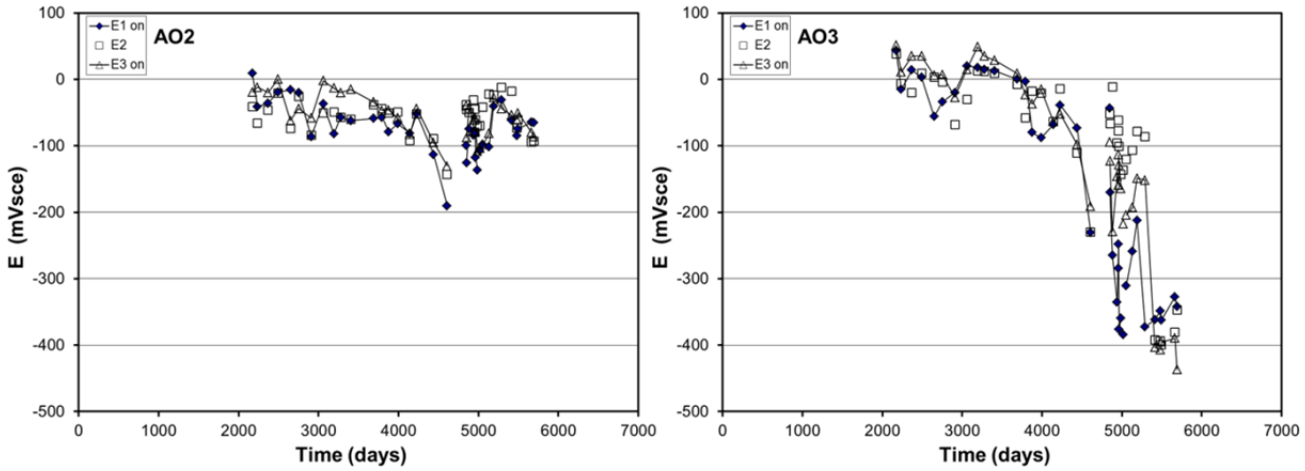

Figure 2.2: Typical potential evolution on AO specimens (1.9 cm cover)

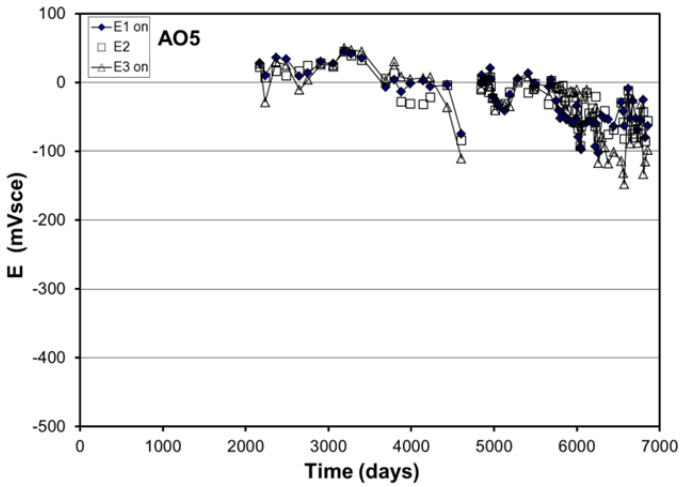

Figure 2.3: Typical potential evolution on AO specimen with 3.2 cm concrete cover

Figure 2.4 shows the potential evolution on specimens CO-2 and CO-3 from the CO group. In CO-3, 'E1 on', i.e., the potential of the left-coupled rebars reached ~-500 mVsce. The other two ('E2' and 'E3 on') showed a more modest potential drop, 'E3 on' approached -200 mVsce, whereas E2 reached a value of -110 mVsce. CO-3 specimen was terminated and all rebars showed corrosion spots. All CO specimens have 1.9 cm cover. With respect to rebars in specimen CO-2, two rebars (E2 and 'E3-on') have become active, but specimen CO-2 has not been terminated. One other CO specimen was terminated but no rebars were active, and the fourth specimen has not been terminated and none of the rebars have experienced the potential decay.

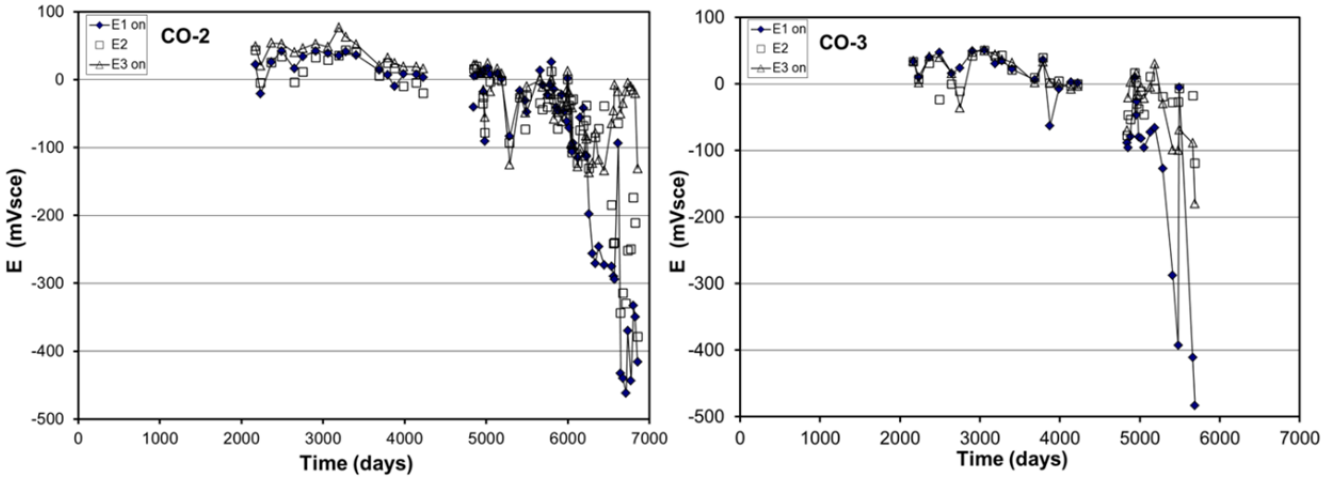

Figure 2.4: Typical potential evolution on CO specimens. (1.8 cm Cover)

Figure 2.5 shows typical potential evolution on FA specimens with 1.9 cm cover and Figure 2.6 shows typical potential evolution on FA specimens with 3.2 cm cover. Figure 2.5 shows the potential evolution for FA1-3, FA2-6, FA3-5 and FA4-1. The potential of the three rebars in FA1-3 have shifted towards more negative values. Two

rebars on FA2-6 (right rebar section terminated ~ day 6250) had initiated corrosion based on the measured potential. The potential of all rebars from specimen FA3-5 had shifted to more negative values, indicating that corrosion likely initiated. On FA4-1, all rebars also experience a negative potential shift. Moreover, the left and right rebar pairs monotonically decayed to values more negative than -300 mVsce. No significant potential shift was observed on specimens with 3.2 cm cover for groups FA1 (e.g. FA1-5) and FA2 (e.g. FA2-6). Using the potential criteria, several rebars from the FA3 group have become active, three out of nine rebars with 3.2 cm concrete cover (e.g., FA3-1 in Figure 2.6) and eight out of twelve rebars with 1.9 cm concrete cover. Similarly, seven out of nine rebars prepared with FA4 mix have become active. For the FA4 group no specimen was prepared with 3.2 concrete cover.

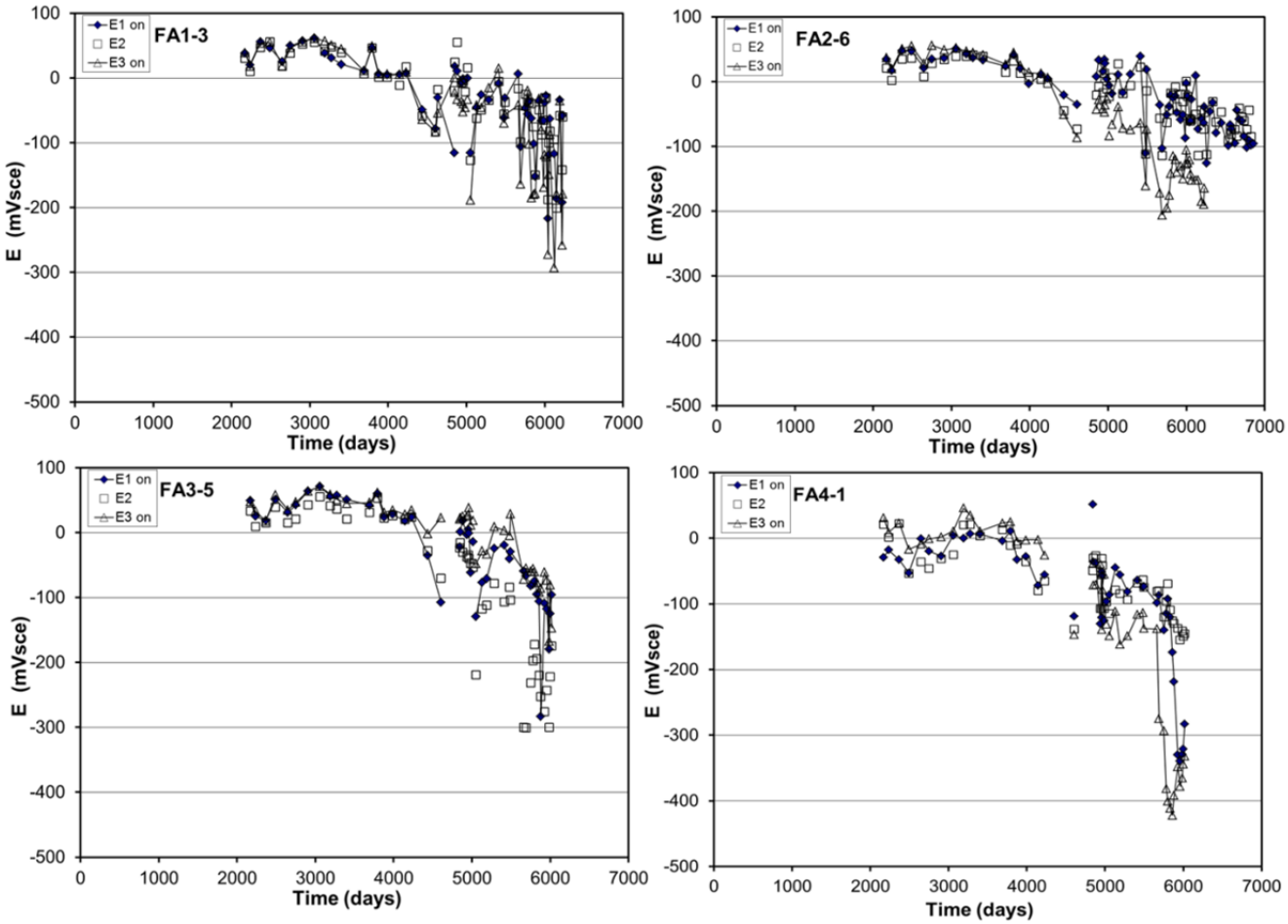

Figure 2.5: Typical potential evolution on specimens with FA and 1.9 cm cover

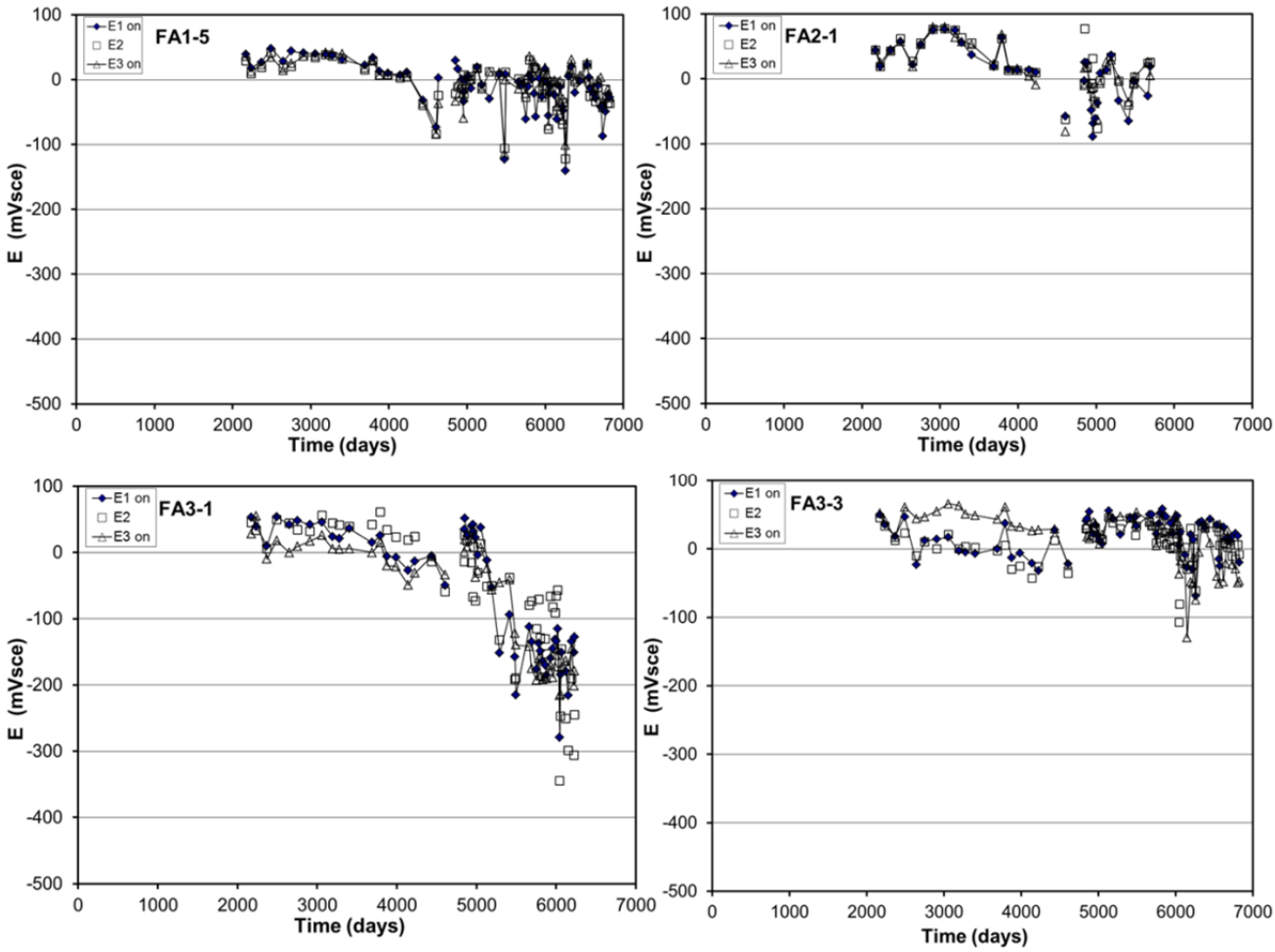

Figure 2.6: Typical potential evolution on specimens with FA and 3.2 cm cover

Figure 2.7 shows the potential evolution on selected SF specimens (one per concrete mix). Four rebars out of nine became active from the SF1 specimens by day 7000. Six rebars out of nine became active by day 7000 for the specimens of group SF2, three are from a specimens not yet terminated. The non-corroding rebars correspond to a specimen that was terminated on day 5700. Although the last set of potential values measured on specimen SF2-1 ranged between -150 and -180 mVsce, the top rebars on the left and right side showed black/dark green rust spots upon visual inspection. One out of nine rebars on SF3 specimens and no rebar from those in the SF4 group have become active based on potential transients. All specimens for SF1, SF2, SF3 and SF4 have a concrete cover of 1.9 cm.

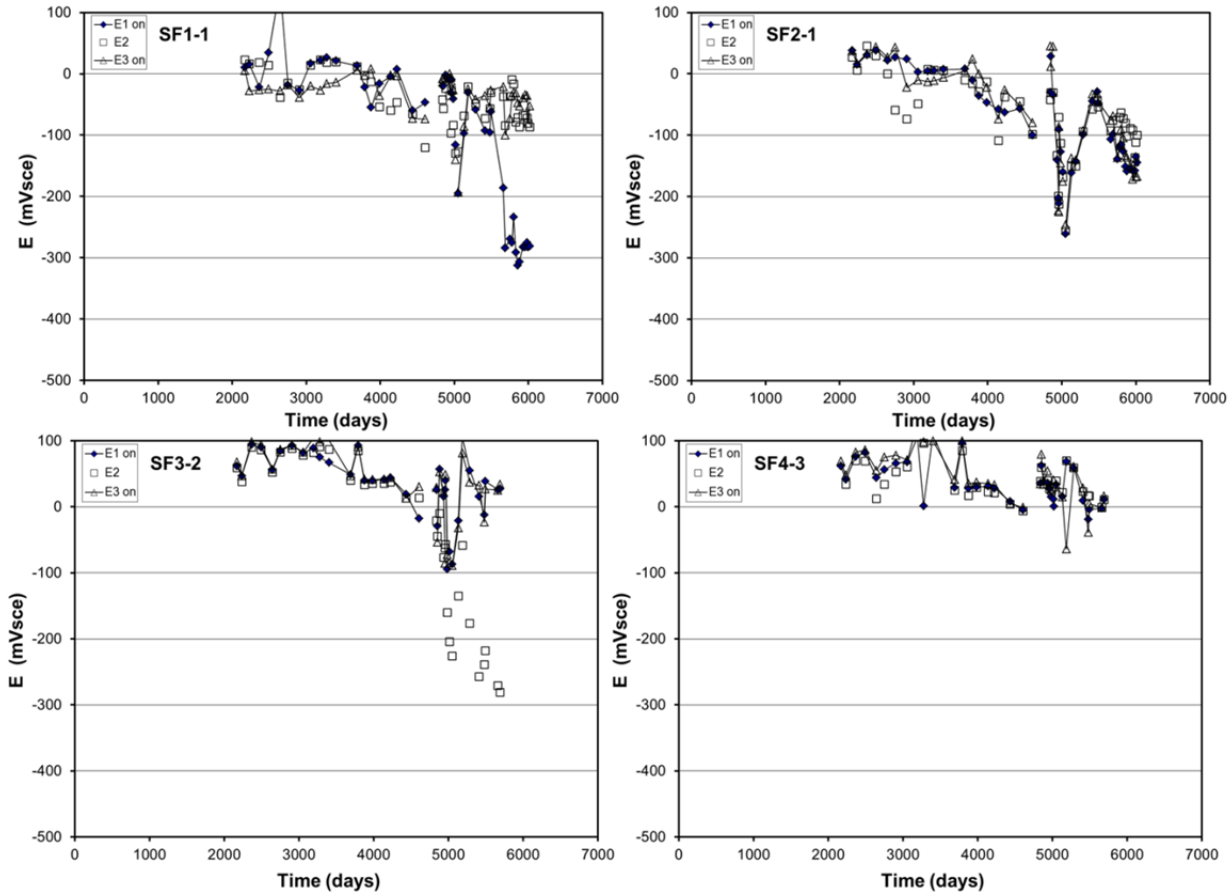

Figure 2.7: Typical potential evolution on specimens with SF

In the passive potential state, the potential ranged from 50 to -100 mVsce for AO and CO groups, and tended to range between 100 and -50 mVse i.e., even nobler (more positive potential) values for those with admixtures. These ranges of values correspond to readings taken after 2000 days of exposure. Angst [4], Hartt [1] and others have reported that an asymptotic potential increase occurs during the first 400 to 600 days and is most likely due to passive layer growth and the associated reduction in passive current, but could be also influenced by the change in resistivity as the concrete hydrates. The lower pH (see section below) for concrete with admixtures (FA or SF) might have contributed to an additional potential increase. In the plots shown above, a saturation value was usually observed by day 3000. In several instances the potential remained at the saturation value for some additional time, but in many a gradual potential decay was observed (with the slope being as little as 20 mV in 1000 days). After this initial decay the rebars experienced a potential drop. In some cases the rebar potential returned to more positive values (repassivation). Angst [4] suggests that this might occur in instances in which the chloride concentration at the rebar can be sufficiently high to initiate pitting, but might not necessarily be able to sustain pit growth. Such events can be observed on Figures 2.2, 2.3, 2.5 and 2.7. Interestingly, the duration of the repassivation lasted from a few months (e.g., AO3, CO3, SF1-1 in Figures 2.2, 2.4 and 2.7 respectively) to a few

years (e.g. FA1-3 and FA2-6 in Figure 2.5). The potential of the rebars continue to decay and usually with a steeper slope. Eventually a significant and abrupt potential drop is observed with the rebar potential value remaining or shifting to even more negative values. This large potential drop is what is typically associated with time to initiation. Angst [4] suggests identifying: the time to corrosion initiation and the time to stable corrosion to determine when corrosion is propagating at a stable rate. In this investigation, no abrupt potential drop was observed from a relative stable passive potential value. In several instances only one rebar experience a stable potential drop that can be identified indicative of corrosion initiation and with maintenance of this condition. In several instances it was decided to terminate the specimen upon one of the rebars reaching potential values approx. -160 to -180 mVsce and with potential oscillation (for some of the specimens terminated at day 6000 or 6250) and corrosion confirmed via visual inspection. Not all rebars that experience corrosion had a single transition from passive to active. In several cases momentary drops were observed with the potential recovered (i.e. shifted to more positive values) after sometime. The reason for the recovery to more positive potential values is likely a combination of environmental (Temp, Season high/low humidity) and electrochemical conditions.

2.4.2 Visual Inspection of Terminated Samples

All rebars from the terminated samples were subjected to visual inspection. Figure 2.8 show typical photos for four instances in which corrosion was actively taking place. The pictures correspond to rebars from samples AO-3, CO-3, FA3-4, FA4-3, SF1-3 and SF2-1 and showcase worst case scenarios (i.e. some of the larger corrosion spots). Only one of the terminated specimens suffered from delamination AO3. The Appendix corresponding to this chapter contains photographs for all terminated specimens grouped per specimen mix composition. In some cases either no corrosion was found or only red-rust, and in others dark gray spots (but not similar to those associated with on-going corrosion).

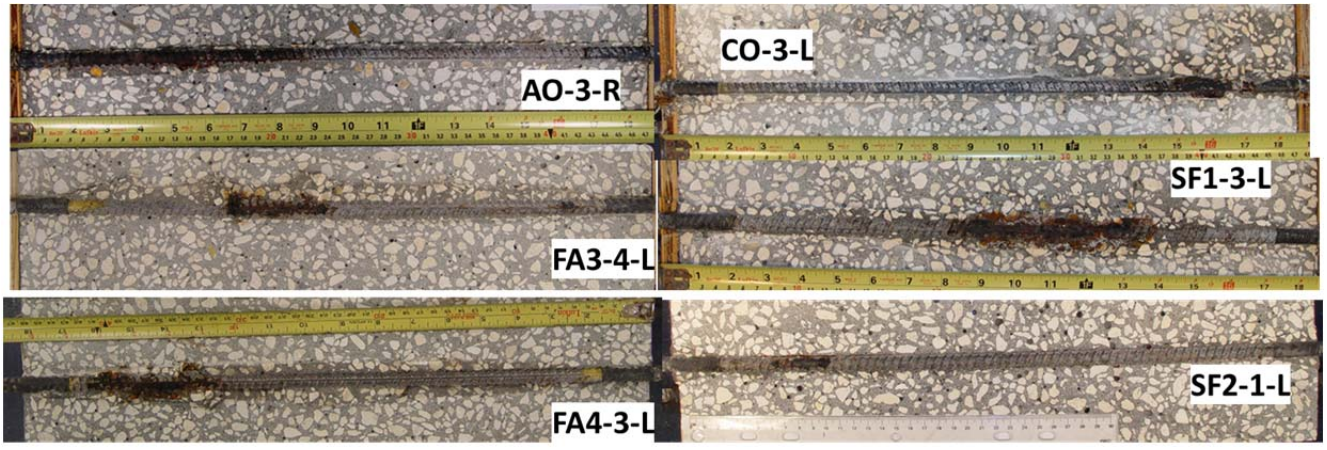

Figure 2.8: Example of terminated rebars undergoing corrosion

Four AO specimens were terminated and showed different amounts of corrosion AO3 and AO8 showed significantly larger corrosion spots as shown in Figure 2.8. Corrosion spots on rebars of AO1 and AO2 specimens were manly red rust of various sizes. Terminated FA1 and FA2 specimens only showed red-rust or dark gray spots, not typically associated with on-going corrosion.

2.4.3 Chloride Profiles and Concentration above the Rebar Trace

This section presents selected chloride concentration profiles obtained from slicing the cores selected for chloride analysis. Results are also presented for chloride concentration just above the rebar trace. The chloride concentration shown per slice is the average concentration from triplicate measurements and the average of two measurements for the concentrations corresponding to locations above the rebar trace. The build-up effect due to rebar presence has been reported before by Sagues [5] and Hartt [6] from modeling and experimental results. The rebar interrupts the pathway for chloride transport. The rebar is impervious to the passage of chlorides, which in turn, causes the chloride concentration to build-up faster in the region adjacent to the rebar closest to the exposed surface. Figure 2.9 shows the chloride concentration profiles for AO and CO specimens. Chloride concentrations corresponding to concrete locations just above the rebar trace ranged from 5 to 11.5 kg/m^3 and are inside a drawn ellipse. Figure 2.10 and Figure 2.11 show the chloride profiles obtained from FA specimens and SF specimens, respectively. The results shown in here provide further evidence that for some geometries the rebar presence effect on chloride build up should not be neglected. The derating factor for the tested geometry ranges from 0.57 (C_T/C_S=0.5 e.g. as for AO) to 0.65 (C_T/C_S=0.3 e.g. as for FA3) for a ~0.5 ratio corresponding to the rebar diameter to the smaller cover. Two of the FA specimens terminated shown in Figure 2.10 were 15 cm thick with 3.2 cm cover; all other terminated specimens had 1.9 cm concrete cover.

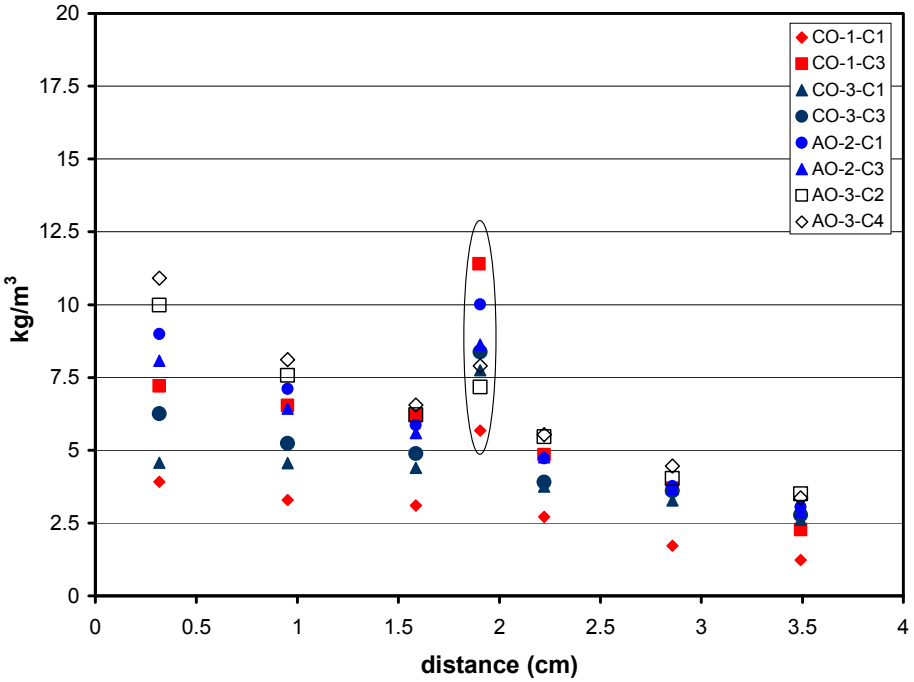

Figure 2.9: Chloride profiles and chloride concentration at the rebar trace, AO and CO specimens. (Obtained after 5700 days of exposure)

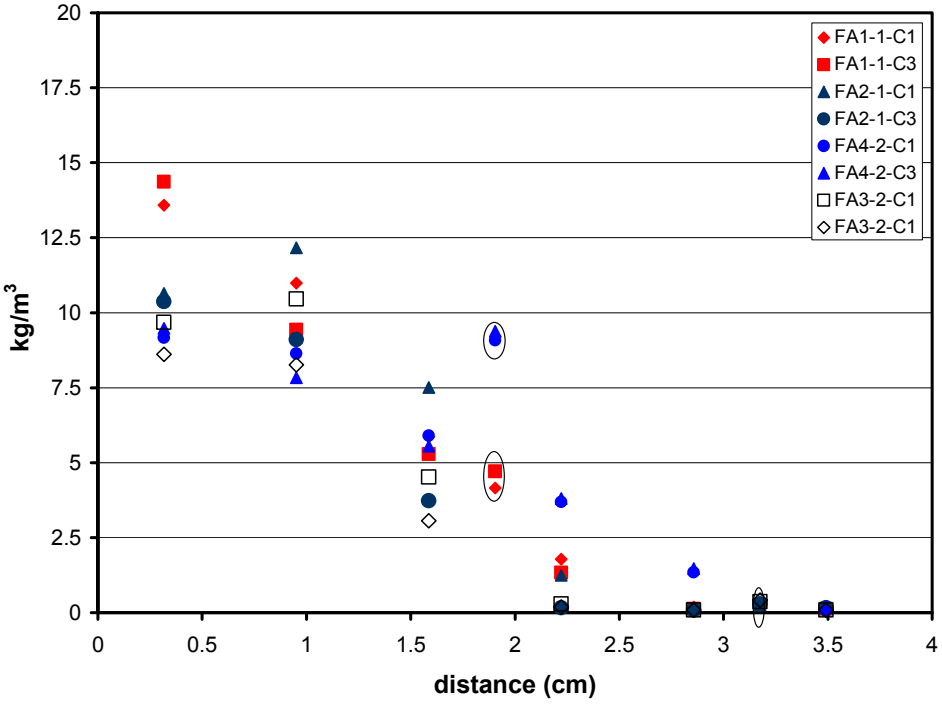

Figure 2.10: Chloride profiles and chloride concentration at the rebar trace, FA specimens. (Obtained after 5700 days of exposure)

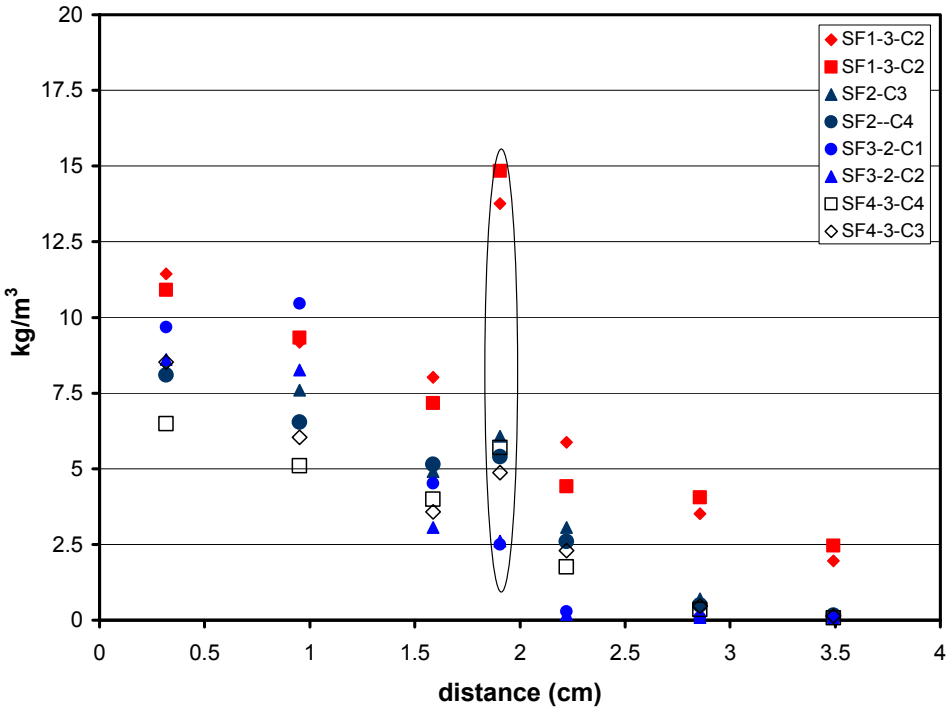

Figure 2.11: Chloride profiles and chloride concentration at the rebar trace, SF specimens. (Obtained after 5700 days of exposure)

Table 2-6: Chloride concentrations at the rebar trace (kg/m^3)

	L		Ce		R			L		Ce		R	
AO1	NA	Y	NA	-	NA	Y	FA1-1	4.3	N	3.4	N	4.7	N
AO2	8.0	Y	7.9	Y	10.0	Y	FA1-3	6.4	Y	2.9	Y	3.3	Y
AO3	6.9	Y	7.9	Y	6.7	Y	FA2-1	0.3	N	0.3	N	0.2	N
AO8	5.8	Y	7.4	Y	8.9	Y	FA2-6	C	-	C	-	5.5	Y
CO1	6.8	N	4.8	N	5.4	N	FA3-1	1.2	Y	NA	Y	1.4	Y
CO3	6.4	Y	8.4	Y	8.4	Y	FA3-2	0.4	N	0.4	N	0.3	N
SF1-1	7.2	Y	8.1	N	6.4	N	FA3-4	3.1	Y	C	-	C	-
SF1-3	14.8	Y	14.9	Y	11.6	Y	FA3-5	2.2	Y	1.6	Y	1.9	Y
SF2-1	8.2	Y	7.9	Y	6.8	Y	FA3-7	3.5	Y	1.3	Y	3.3	Y
SF2-2	6.1	Y	5.0	Y	5.2	Y	FA4-1	8.9	Y	7.6	Y	6.9	Y
SF3-2	2.6	N	2.4	Y	2.5	N	FA4-2	9.0	Y	8.9	Y	9.4	Y
SF4-3	4.1	N	5.7	N	NA	N	FA4-3	9.9	Y	C	-	C	-

Y- Corrosion was confirmed. N – No corrosion observed. NA – Not Available,
C – Continues to be exposed. L- Left, Ce – Center, R- Right

Table 2-6 shows the chloride concentration measured at the rebar trace for those forensically analyzed. Table 2-7 shows the minimum and average chloride concentration at the rebar trace for each concrete mix. The values shown on were obtained from those where corrosion was visually confirmed.

Table 2-7: Minimum and average $[Cl^-]$ kg/m^3 at the rebar trace on those corroding

	Min	Average
AO	5.8	7.7
FA1	2.9	4.2
FA2	5.5	5.5
FA3	1.4	2.2
FA4	6.9	8.7

	Min	Average
CO	6.4	7.7
SF1	7.2	12.1
SF2	5.0	6.5
SF3	2.4	2.4
SF4	>5.7	>5.7

The chloride concentrations displayed in Table 2-6 and Table 2-7 are not chloride thresholds, per se, as some specimens were terminated sometime after the negative potential shift occurred. However, these values are used here to compare between groups. For cases in which the specimen was terminated shortly after activation, the measured values could be considered representative of C_T. Eleven rebars from AO group showed corrosion with 5.8 kg/m^3 as the minimum chloride measured at the rebar trace ($[Cl^-]_{tmin}$). For the CO group, $[Cl^-]_{tmin}$= 6.4 kg/m^3, and was just slightly higher than for the AO group. Hence, not much benefit was achieved by the calcium nitrate admixture. $[Cl^-]_{tmin}$ values suggest that the chloride threshold for rebars embedded in FA3 is lower than for those in FA1 and FA2. Actually, the $[Cl^-]_{tmin}$ measured on FA1 and FA3 specimens is lower than that observed on AO or CO specimens. Rebars from each FA-group showed corrosion: ten rebars from FA3; seven rebars from FA4; three from FA1; and one from group FA2. (Some other specimens were terminated, but the rebars did not display corrosion, see Table 2-6 for details) The chloride concentration that caused corrosion for those embedded in FA4 seems to be higher than for the other FA groups, then again, a higher concentration was reached in the same amount of time. The $[Cl^-]_{tmin}$ was ~7.2 kg/m^3 for the SF1 group and four of the terminated rebars have displayed corrosion, $[Cl^-]_{tmin}$=5 kg/m^3 for SF2, and six rebars have shown corrosion. For SF3, $[Cl^-]_{tmin}$=~2.4 kg/m^3, and only one rebar displayed corrosion. Finally, for SF4 $[Cl^-]_{tmin}$ = 5.7 kg/m^3, and no rebar displayed corrosion.

2.4.4 Diffusion Coefficient

Table 2-8 shows the diffusion coefficients calculated for each sliced core grouped per mix-design. Fit column indicates if any values were removed to obtain a better fit. The table also includes the age at which the specimen was terminated, and this was the age used to calculate D_{app}. The calculated Cs is also included. The average D_{app} for mixes AO and CO were slightly greater than 1×10^{-12} m^2/s. The average D_{app} for SF mixes ranged between ~2×10^{-13} (SF3) and 7×10^{-13} (SF1) m^2/s. The average D_{app} were even smaller for FA mixes, ranging from 9×10^{-14} (FA3) and 2.9×10^{-13} (FA4) m^2/s, i.e. the mix with 50% FA (FA3) had the lower D_{app}. The relatively low D_{app} are in part due to the fact that seawater was used as the solution. Justnes [7] and others have reported that seawater components (e.g. magnesium) can interact with the pore solution and form other compound which slows down further the chloride penetration.

Table 2-8: D_{app} calculated for each sliced core

ID	Fit	Age yrs	Cs Calc	Dapp m^2/s	Dapp Average
AO2-C1	1-Re	15.6	15.0	1.3E-12	1.5E-12
AO2-C3	1-Re	15.6	13.7	1.5E-12	
AO3-C1	1-Re	15.6	15.8	1.5E-12	
AO3-C2	1-Re	15.6	17.1	1.3E-12	
AO8-C1	No-R	16.5	15.3	1.5E-12	
AO8-C2	No-R	16.5	16.4	1.7E-12	
CO-1-C1	2Re	15.6	9.3	8.4E-13	1.4E-12
CO-1-C3	2Re	15.6	10.8	8.3E-13	
CO3-C1	2Re	15.6	10.3	2.0E-12	
CO3-C2	No-R	15.6	11.0	2.0E-12	
SF1-3-C1	N-R	15.6	21.8	7.3E-13	7.1E-13
SF1-3-C4	1R	15.6	21.7	6.9E-13	
SF1-1-C1	No-R	16.5	21.8	6.9E-13	
SF1-1-C2	No-R	16.5	20.6	7.2E-13	
SF2-2-C3	1R	15.6	23.9	2.6E-13	2.4E-13
SF2-2-C4	1R	15.6	21.4	2.7E-13	
SF2-1-C1	1R	16.5	26.5	2.2E-13	
SF2-1-C2	1R	16.5	23.9	2.1E-13	
SF3-2-C1	1R	15.6	31.6	2.1E-13	1.9E-13
SF3-2-C2	1R	15.6	13.5	1.7E-13	
SF4-3-C3	No-R	15.6	17.3	2.7E-13	2.6E-13
SF4-3-C4	No-R	15.6	17.1	2.4E-13	

ID	Fit	Age yrs	Cs Calc	Dapp m^2/s	Dapp Average
FA1-1-C1	1R	15.6	42.6	1.5E-13	1.2E-13
FA1-1-C3	1R	15.6	37.1	1.5E-13	
FA1-3-C1	1R	17	22.3	1.1E-13	
FA1-3-C2	1R	17	23.0	9.9E-14	
FA1-3-C3	1R	17	23.1	1.0E-13	
FA2-1-C1	1R	15.6	37.1	1.5E-13	1.3E-13
FA2-1-C3	1R	15.6	44.1	1.0E-13	
FA3-1-C1	1R	17	30.9	7.4E-14	9.0E-14
FA3-1-C2	1R	17	35.2	6.3E-14	
FA3-1-C3	1R	17	36.9	5.6E-14	
FA3-2-C1	1R	15.6	50.2	1.0E-13	
FA3-2-C2	1R	15.6	41.5	9.5E-14	
FA3-5-C2	1R	16.5	31.3	1.6E-13	
FA3-5-C1	No-R	16.5	20.3	1.6E-13	
FA3-7-C1	1R	17	36.0	6.5E-14	
FA3-7-C2	1R	17	31.9	7.8E-14	
FA3-7-C3	1R	17	39.6	4.9E-14	
FA4-2-C1	2R	15.6	35.8	2.3E-13	2.9E-13
FA4-2-C3	1R	15.6	23.0	3.3E-13	
FA4-1-C1	1R	16.5	34.0	3.2E-13	
FA4-1-C2	1R	16.5	29.1	2.8E-13	

2.4.5 Resistivity and Diffusion Coefficient - D_{app}

Table 2-9 shows the average chloride diffusivity calculated from the profiles after 1200 and after more than 5700 days of exposure. D_{app} values after 1200 were reported earlier by Hartt [2]. For the profiles obtained after more than 5700 days (see Figures 2.10 and Figure 2.11) of exposure there were cases in which the maximum concentration did not correspond to the slice closest to the surface. For those cases the first layer (lower values) were omitted when performing the fit. The values shown in the table are the average D_{app} obtained from at least two cores. No D_{app} was measured at 1200 days on CO specimens. At 5700 days, the largest D_{app} was measured on AO and CO specimens. Followed by D_{app} values measured on SF1. FA1 and FA2 showed very similar D_{app}. The smallest D_{CL} value corresponded to FA3 concrete mixture. Table 2-9 also includes the average ρ_{wet} measured (average of the values measured on at least two cores) after more than 15 years of outdoor exposure.

Table 2-9: Diffusivity after 3.3 and >15 years and ρ_{wet} after 15 years

	D (m^2/s)		ρ_{wet} 15 yr
Mix design	3.3 years	15 years	kohm-cm
AO	3.48E-12	1.50E-12	4.6
CO	N/A	1.40E-12	4.8
FA1	8.02E-13	1.20E-13	19.5
FA2	7.35E-13	1.30E-13	36.0
FA3	5.73E-13	9.00E-14	62.0
FA4	7.35E-13	2.90E-13	18.0
SF1	1.96E-12	7.10E-13	8.8
SF2	2.29E-12	2.40E-13	16.0
SF3	1.01E-12	1.90E-13	20.0
SF4	9.97E-13	2.60E-13	13.5

Figure 2.12 shows two series of data that relate ρ_{wet} (wet resistivity) vs. D_{app}. Both series are shown with the same resistivity values, although it is likely that the resistivity values at three years were somewhat smaller than those recorded after more than 15.6 years. All D_{app} values were lower after 15 years of exposure when compared to those measured after 3.3 years. Adding calcium nitrate appears to lower the resistivity and increases the D_{app} for both SF and FA when compared to corresponding SF or FA concrete mixtures that contained comparable SF or FA amounts in the concrete mix. There appears to be an outlayer at 3.3 years, but not at 15 years. For the series after 3.3 years, the outlayer corresponds to SF2. After 3.3 years the D_{app} is lower for those measured on FA concretes. After more than 15.6 years of exposure the D_{app} for SF3 was as low as the average D_{app} for FA1. The observed D_{app} values at 15 years are likely influenced by not fully saturated concrete and that exposed surface did not contain solution all the time. Additionally, Justnes [7] and others have reported that Seawater components (e.g. magnesium) can interact with the pore solution and form other compound which slows down further the chloride penetration.

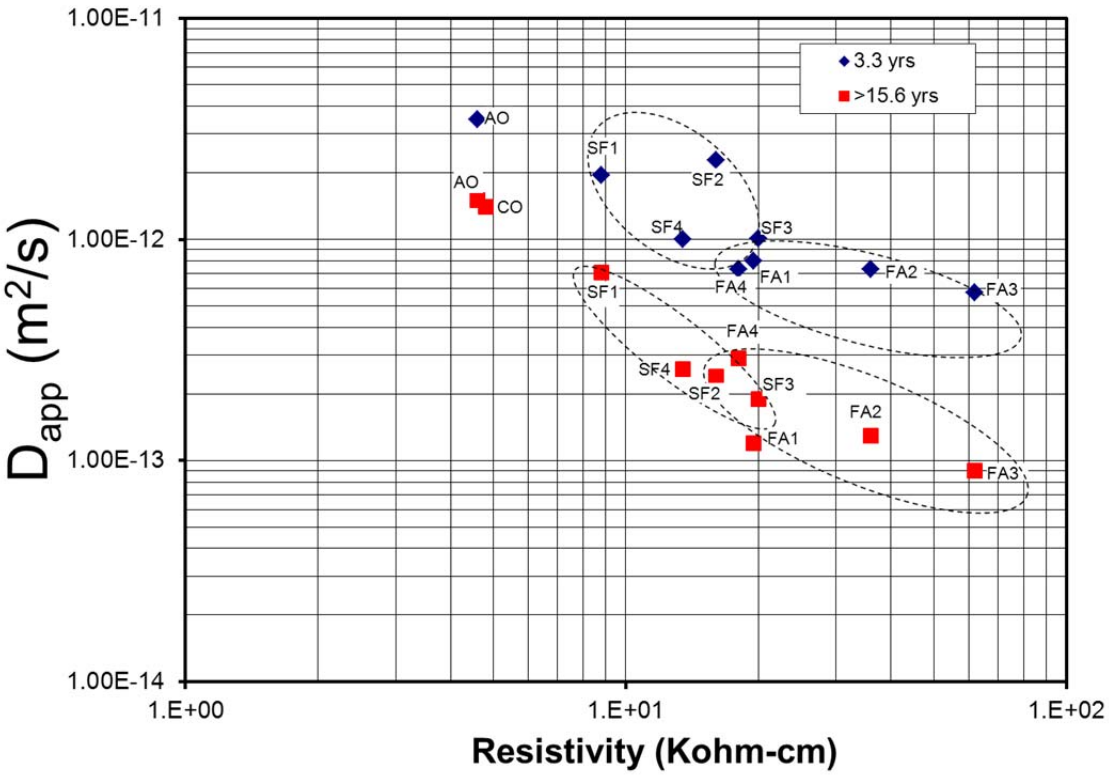

Figure 2.12: Resistivity vs. D_{app}

2.4.6 D_{app}, pH and Cl^- at the Rebar Trace

Table 2-10 shows pH values measured on cored specimens from each concrete mix at 1200 days. The values are somewhat higher than those reported by others. Comparing only how much the pH was reduced by different amounts of admixtures and remembering that a 0.1 change in pH corresponds to a factor of two variations in OH^- activity. This might explain why corrosion initiated at significantly lower concentration on specimens with 50% FA; even though these specimens have the lower chloride diffusivity. Thus the lower C_T needs to be kept in mind when estimating service life of structures that contain high admixture replacement ratios even though these mixes usually have a lower D_{app}.

Table 2-10: pH values measured at day 1200 [1]

	Laboratory	Admixture	N_2 glove box	Admixture
Specimen	pH	pH reduction	pH	pH reduction
AO	13.7		13.84	
FA1	13.46	0.24	13.57	0.27
FA2	13.27	0.43	13.39	0.45
FA3	12.57	1.13	13.18	0.66
FA4	13.27	0.43	13.36	0.48
SF1	13.3	0.4	13.7	0.14
SF2	13.51	0.19	13.51	0.33
SF3	13.27	0.43	13.47	0.37
SF4	13.42	0.28	13.59	0.25

2.5 CONCLUSIONS

1. The D_{app} of concrete mixture prepared with FA decreased close to one order of magnitude (at least 5X) from 1200 days to 5700 days, with the largest reduction observed on those with higher FA. A more modest reduction in D_{CL} was observed on samples with SF. The observed D_{app} is likely influenced by not fully saturated concrete and that exposed surface did not contain solution all the time.

2. The $[Cl^-]_{tmin}$ (measured on rebars corroding) suggest that the chloride threshold for samples of concrete mixtures with 50% FA appear to be lower than those observed on the other FA admixture amounts. Corrosion initiated on more rebars from specimens with 50% FA, than with OPC only due to the lower chloride threshold.

3. A good correlation was observed between ρ_{wet} (wet resistivity) and D_{app}.

4. Further evidence was found that the rebar presence increases the chloride concentration compared to the concentration measured at the same depth

2.6 ACKNOWLEDGMENTS

The authors are indebted to the Florida Department of Transportation (FDOT) for financial support of this research and to Mr. Mario Paredes and Mr Ron Simmons of the FDOT State Materials Office. In addition, the authors appreciated the assistance with laboratory work and measurements provided by Mr. A. Sajban, Mr. J. Zielske, Mr. B. Seo, Mr. F. Gutierrez and several undergraduate students of the Marine Materials Lab at FAU. The authors also acknowledge Dr. Hartt and Dr. Lee whom were in charge of phase I of this project. The opinions expressed in this paper are those of the authors and not necessarily of the FDOT.

3 D_{app} AND ρ_{WET} OF HPC FIELD SPECIMENS

3.1 INTRODUCTION

D_{app} measured from field specimens usually differs from D_{app} measured on laboratory accelerated sample testing. As part of this project a second visit to the Key Royale Bridge took place. This allowed to monitor the evolution of the D_{app} and ρ_{wet} by coring fender piles of the research Key Royale bridge (KRB) at Anna Maria Island, FL. The fender piles (and the bridge piles) were prepared with five HPC mixes and a concrete mix made only with ordinary Portland cement (OPC), the latter only for the fender piles. The new determined values are compared to those recently obtained in project BD546-08 [15]. In addition RMT were performed on 4 inch diameter cored cylinders obtained from the topside of the fender piles. These cored cylinders were used to monitor wet resistivity and for D_{nssm}. Eight cores per selected fender pile were obtained at four different elevations. The sections closer to the surface were sliced and pulverized to obtain chloride profiles, and from these D_{app} values. Some of these cores were long enough that a modified D_{nssm} as per NT 492[16] was performed on the remaining section. Additional details about the location of the bridge and other details can be found in [15].

3.2 EXPERIMENTAL

The visit to the KRB was made in collaboration with UF and USF. During the field visit nine cores were obtained per fender pile selected. One core was 4 inch diameter and was obtained from the top side. The other eight cores were obtained as depicted in Figure 3.1.

In here we report the D_{app} values calculated from the obtained profiles and compare these with the D_{app} values obtained during a previous visit. Some of the cores obtained during this visit were long enough to obtain the profiles and have a section long enough that a modified NT492 test was performed on 5 cm long slices. The modification consisted in obtaining covers that fitted two inch diameter of the cores and adjust the equation to allow for smaller cross-section. D_{nssm} was also calculated from NT492 tests on 4 inch diameter and 2 inch thick slice obtained from the larger diameter cores. However, not all 2 inch diameter cores were long enough to perform the NT492 modified test.

Resistivity vs. moisture content was monitored, the concrete porosity (via a modified ASTM in which each cylinder was dried at 50°C as to prevent modifying the microstructure, the boiling step was also not performed) was determined.

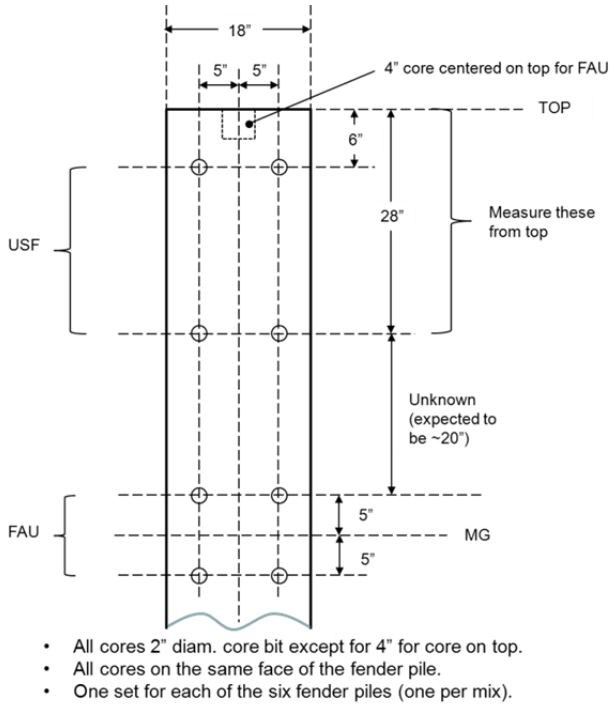

Figure 3.1: Location at which the cores were obtained at each cored fender pile

For each 10 cm diameter core a five cm thick slice was sent back to SMO for chloride bulk diffusion. Table 3-1 presents the date at which each fender pile is believed to had been driven on site, each pile was a few months old by that time. The table also shows the dates at which the fender piles were cored. The four inch diameter core was obtained on 12/1/2011 for the fender pile with OPC, however the other eight cores were obtained on a later trip on 4/4/2012. The table also indicates the assumed exposure time in years and the label ID used in the figures in the results section. On some figures the mix composition is also included.

Table 3-1: Dates at which the fender piles were deployed and cored

	Exposure times		Note OPCtop	Coring 1	Coring 2		
			12/1/2011	Exposure	Exposure	Trip1	Trip 2
	Driven	Cored-Earlier	Cored2nd	Years	Years	Label	Label
OPC	9/7/2006	4/15/2009	4/4/2012	2.61	5.58	45	FP1
FA+UFA	9/7/2006	4/15/2009	12/1/2011	2.61	5.24	44	FP2
FA	9/7/2006	4/15/2009	12/1/2011	2.61	5.24	43	FP3
FA+SF	1/15/2007	4/15/2009	11/30/2011	2.25	4.88	42	FP4
FA+BFS	1/15/2007	4/15/2009	11/30/2011	2.25	4.88	41	FP5
FA+MET	1/15/2007	4/15/2009	11/30/2011	2.25	4.88	40	FP6

3.3 RESULTS

3.3.1 Porosity

Table 3-2: Porosity calculations

weight in g	OPC	UFA	FA	SF	BFS	MET
	KYB1	KYB2	KYB3	KYB4	KYB5	KYB6
W_{app} (D)	2145.8	2150.1	2163.9	2171.4	1838.5	2077.5
W_{dry} (A)	3586.1	3675.5	3670.3	3699.5	3129.3	3566.4
$W_{saturaed}$ (C)	3668.3	3700.2	3709.1	3733.3	3151.6	3602.6
$Porosity_{boil****}$	**5.40%**	**1.59%**	**2.51%**	**2.16%**	**1.70%**	**2.37%**
$Porosity_{saturated}$ = (C-A)/(C-D)						

Table 3-2 shows the porosity results obtained from a modified ASTM test. No boiling took place on these specimens. Only the OPC mix had a porosity larger than 5%. The specimens with FA+UFA and FA+Slag (BFS in table 3-2) had the smallest porosities, less than 2%. The other three compositions had a porosity larger than 2%, but smaller than 2.52%. The ranking is OPC > FA > FA+MK > FA+SF > FA+Slag > FA+UFA. Had the test followed the standard is likely that slight larger porosity values might have been obtained. Also, the ranking might have followed a different sequence.

3.3.2 Chloride Profiles

The cores were sliced at FAU. A layer of 0.08 inches (0.2 cm) was milled before slicing the cores. Each layer afterwards was 0.25 inches (0.635 cm). The titrations were made at SMO. Figure 3.2: Chloride profiles obtained after 5 years of exposureshows the chloride profiles obtained at each elevation. On each fender pile the lowest C_s corresponded to those cores obtained at the highest location. The C_s for the second highest location was usually 5 lb/cyd larger than that observed at the highest location. However, this difference was smaller for FA+MK mix

(about 2 lb/cyd) and larger for the mix with FA+UFA (close to 10 lb/cyd). Skin effect was observed at some elevations on cores from fenders piles with FA+MK and FA+SF.

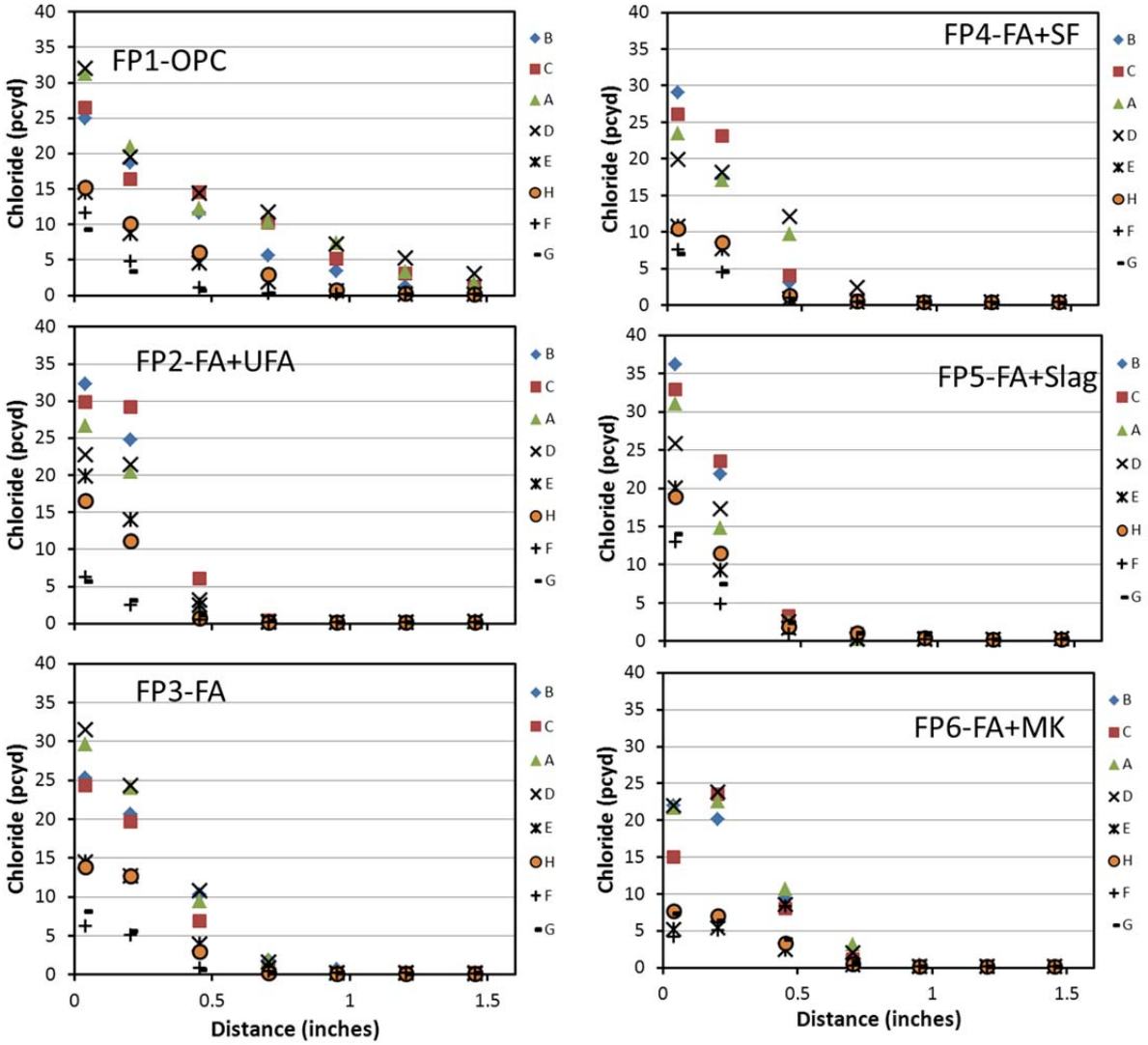

Figure 3.2: Chloride profiles obtained after 5 years of exposure (cores)

Chloride profiles shown in Figure 3.3 were obtained after performing bulk diffusion test similar to NT-443 but for 1 year of exposure. In this case each slice was 0.635 cm, and hence not direct comparison can be made of the concentration values for the first layer of the profiles shown in Figure 3.2 and Figure 3.3.

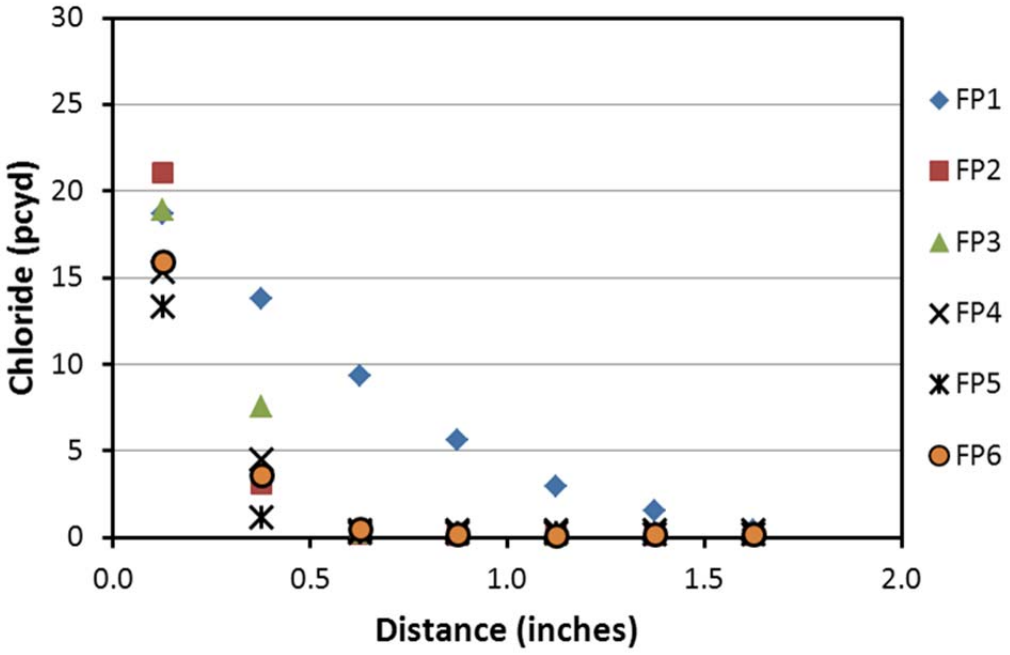

Figure 3.3: Chloride profiles obtained after bulk diffusion test (4 inch diameter slice)

3.3.3 Resistivity vs. Time

After the specimens were placed in the oven at 50°C, the specimens were then placed in a high humidity environment for 44 days and then immersed in water. Figure 3.4 shows how the weight percent change, i.e, how the moisture increased with respect to the dry weight. Figure 3.5 shows how the resistivity evolved with time during this same period of time. Figure 3.66 shows the measured resistivity vs. wt% change for the data shown in Figure 3.4 and Figure 3.55. It is evident that the lower resistivity and larger wt% change was observed for the OPC specimen.

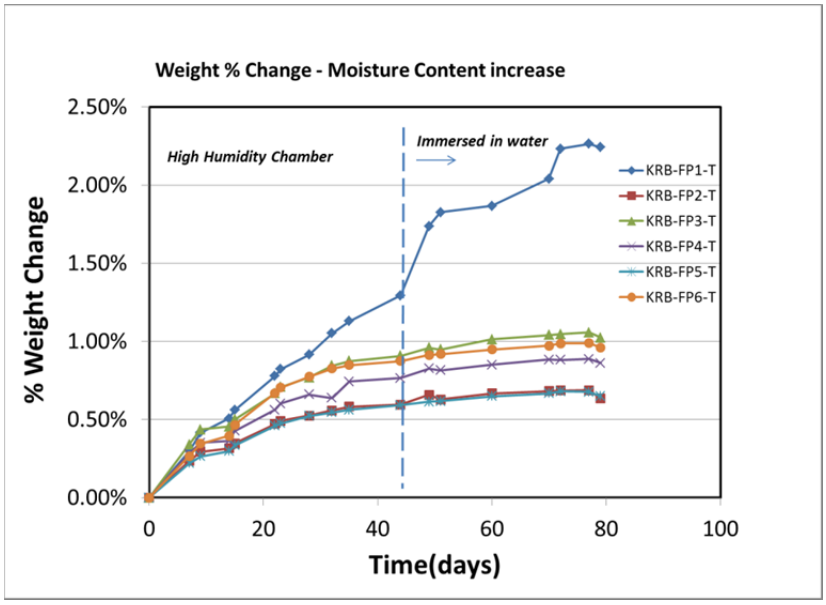

Figure 3.4: Moisture vs. time

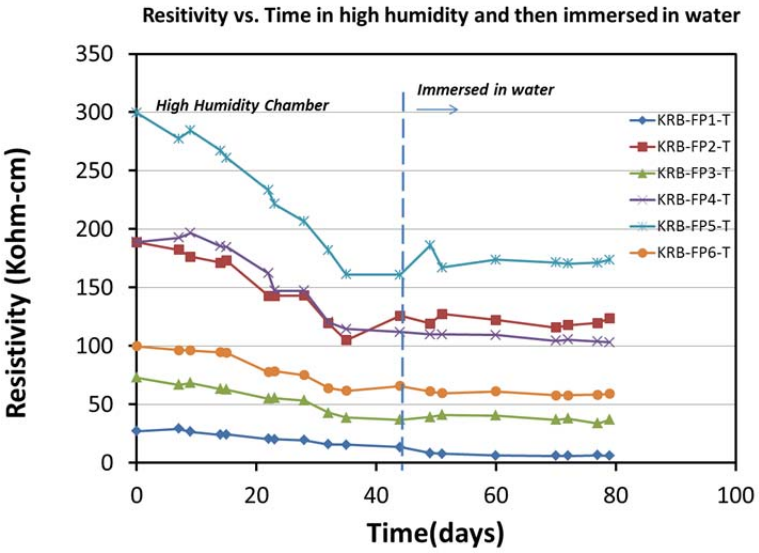

Figure 3.5: Resistivity vs. time while expose in high humidity and then immersed in water. (FP1-OPC, FP2-FA+UFA, FP3-FA, FP4-FA+SF, FP5-FA+BFS,FP6-FA+MK)

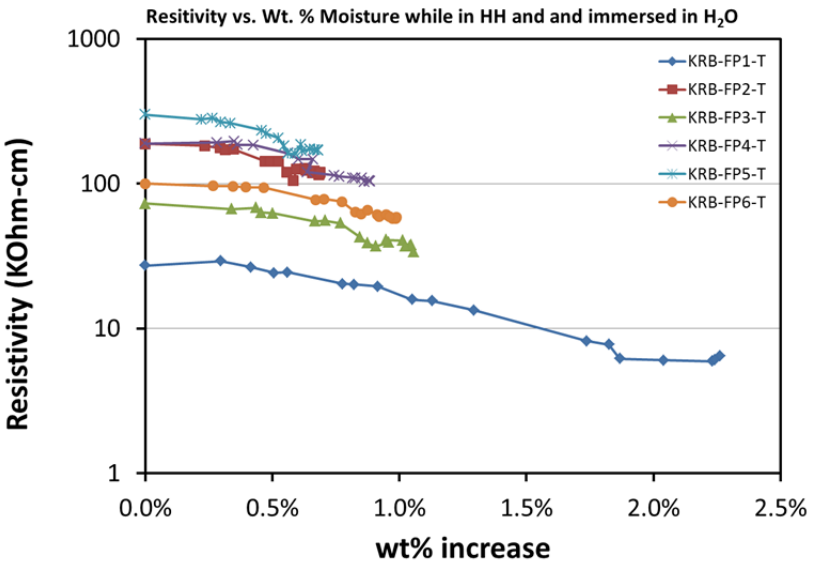

Figure 3.6: Resistivity vs. wt% change (FP1-OPC, FP2-FA+UFA, FP3-FA, FP4-FA+SF, FP5-FA+BFS,FP6-FA+MK)

3.3.4 D_{nssm} vs. Resistivity

Table 3-3 shows the measured values for resistivity (normalized for geometry and temperature) and also the migration coefficients for each of the tested cores. The resistivity measured on the two inches cores (different elevations) were larger than that obtained from the four inch core (obtained from the top). One possibility is that the tidal and splash allowed for further curing on the sides than at the top due to additional wetting at these elevations. Another variable that could have influenced the results is that better concrete compaction occurred on the sides than at the top.

Table 3-3: List of D_{nssm} and Resistivity

4 inch Cores

		Resistivity (Kohm-cm)	Dnss x10^{-12} (m^2/s)
OPC	KYB-FP1	7.7	10.27
FA+UFA	KYB-FP2	127.3	0.59
FA	KYB-FP3	40.9	1.54
FA+SF	KYB-FP4	109.9	0.81
FA+Slag	KYB-FP5	167.2	0.54
FA+MK	KYB-FP6	59.5	0.99

2 inch Cores

		Resistivity (Kohm-cm)	Dnss x10^{-12} (m^2/s)
FA+UFA	FP2-A	141.0	0.32
FA+UFA	FP2-B	153.4	0.29
FA+UFA	FP2-D	132.6	0.28
FA	FP3-B	40.5	0.9
FA	FP3-F	62.1	0.84
FA	FP3-H	45.9	0.78
FA+SF	FP4-B	139.8	0.55
FA+SF	FP4-E	124.7	0.6
FA+SF	FP4-F	131.2	0.43
FA+SF	FP4-H	119.2	0.94
FA+Slag	FP5-C	186.2	0.41
FA+Slag	FP5-D	206.8	0.32
FA+Slag	FP5-E	212.0	0.29
FA+MK	FP6-A	83.5	0.53
FA+MK	FP6-E	104.1	0.43
FA+MK	FP6-H	108.3	0.43

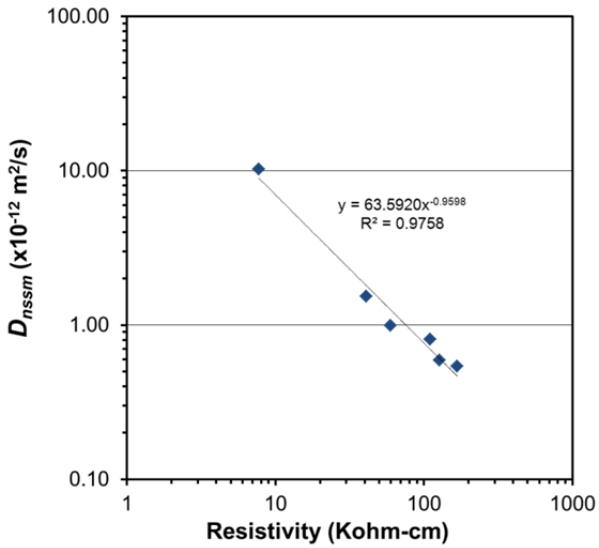

Figure 3.7: D_{nssm} vs. Resistivity, and correlation obtained from tests on 4-inch cores

Figure 3.7 and Figure 3.8 show plots of D_{nssm} vs. resistivity measured from the cores obtained during the current visit to KRB. Figure 3.7 shows only the migration coefficient values obtained on the four inches slices. This figure also shows a correlation obtained for the shown values using a power type of equation. The exponent is not quite one, but close (0.9598), and the constant gave a value of 63.6, which is somewhat lower than is reported in the D_{nssm} chapter of the accelerated curing in Volume 2 of this report.

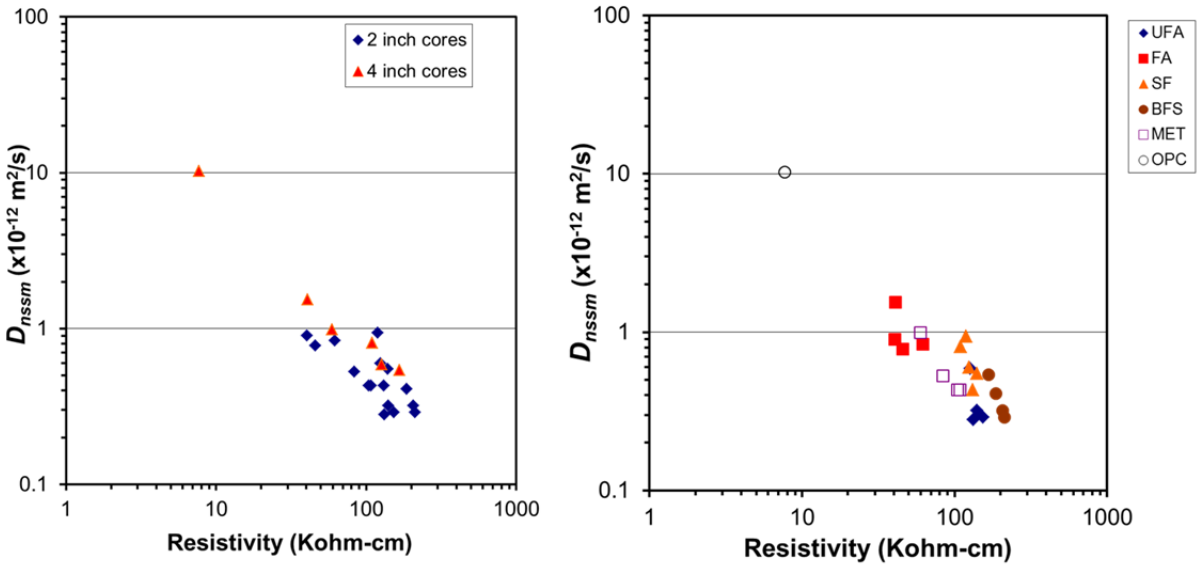

Figure 3.8: D_{nssm} vs. Resistivity: a) Grouped by core diameter, b) grouped by mix

Figure 3.8 shows that the larger diffusivity and lower resistivity corresponded to the OPC specimens as it was expected. Most of the migration coefficients were less than 1 $\times 10^{-12}$ m^2/s. The D_{nssm} values also suggest that the

concrete of the two inch cores were better hydrated/cured as the D_{nssm} from 4 inch diameter were about twice the D_{nssm} values measured on 2 inch cores with the same composition. There is a little more scatter when considering only the D_{nssm} from the 2 inch cores.

3.3.5 D_{app} vs. Elevation and D_{nssm} vs. Elevation

Figure 3.9 shows the D_{app} calculated values vs. elevation. These elevations reflect the elevations at which the cores were obtained. D_{app} values are shown for both the currently reported visit and from a previous visit. The values obtained at higher elevations appear to suggest lower D_{app} values at these locations. However, at these higher elevations the moisture content is likely lower. Moreover, the chloride at the surface was lower for the D_{app} corresponding to the higher elevations.

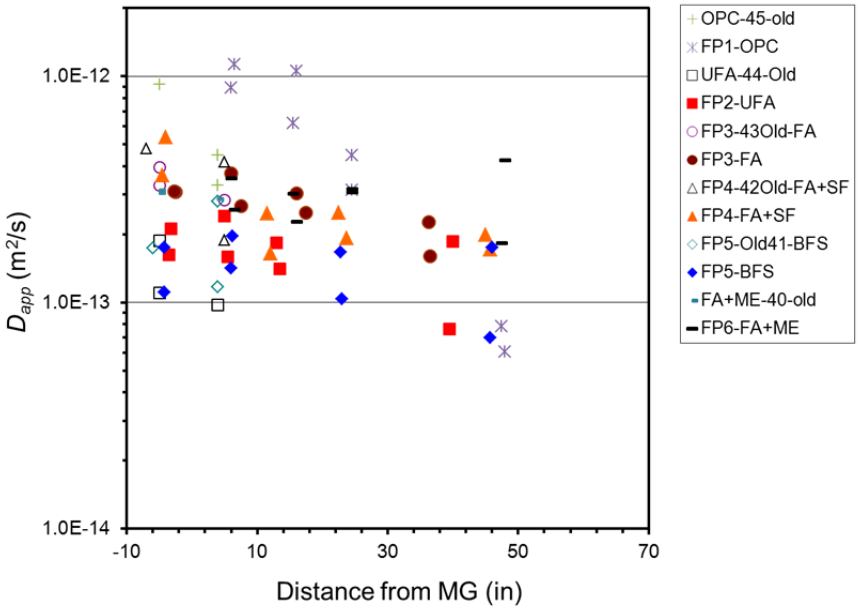

Figure 3.9: D_{app} vs. elevation

Figure 3.10 shows the D_{nssm} vs. elevation. The figure shows the D_{nssm} values for cores that were long enough to measure D_{nssm}. It also shows that the D_{nssm} did not change as a function of elevation within a given mix, this might be due to the fact that the cores were water saturated prior to the test. The values within the ellipse correspond to D_{nssm} values measured on the 10 cm diameter core 5 cm long slice (core obtained from the top). Prior to performing NT492 the specimens are water saturated and during the test the specimens are exposed to the same C_s. This suggest that if the concrete at the higher elevations were saturated, then a similar apparent diffusion coefficient would be expect assuming exposure to similar C_s. Incidentally, when comparing D_{app} values shown in Figure 3.9: the larger D_{app} reduction at the higher elevation was observed for the OPC samples and this is likely influenced by a lower moisture content at these elevations. This might be due to more interconnected pore

structure of the OPC mix when compared to the other concrete compositions (as suggested by the resistivity values). With time the pore interconnectivity and pore percentage likely is lower on those concrete with FA as the pozzolanic reaction progresses. Additionally the observed D_{nssm} values were in general somewhat larger than the D_{app} measured on the corresponding cores, but differed by less than a factor of two. Moreover, for most compositions the values were lower than 1×10^{-12} m^2/s for both D_{app} and D_{nssm}, indicating low to extremely low permeability concrete.

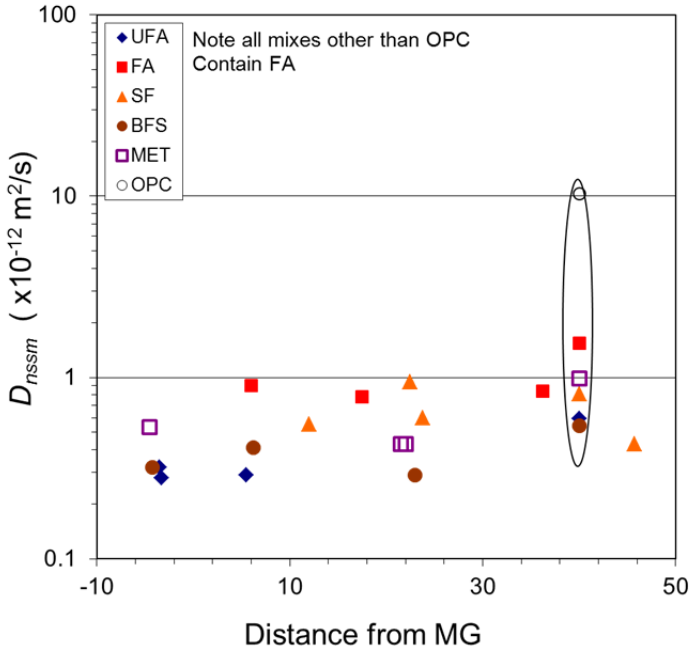

Figure 3.10: D_{nssm} vs. elevation

Incidentally, there was no significant reduction on the D_{app} values when comparing the D_{app} obtained after 2 and 5 years of exposure, for the D_{app} calculated values from cores obtained at the lower elevations.

Table 3-4: Comparison of D_{app} and D_{nssm} on 10 cm diameter core slices

Mix	Pile ID	D_{app} x10^{-12} m^2/s	D_{nssm} x10^{-12} m^2/s
OPC	FP1	5.85	10.27
FA+UFA	FP2	0.4	0.59
FA	FP3	0.98	1.54
FA+SF	FP4	0.76	0.81
FA+Slag	FP5	0.26	0.54
FA+MK	FP6	0.59	0.99

Table 3.4 compares the D_{app} and D_{nssm} obtained on 10 cm diameter concrete slices from the cores taken at the top side of each of the fender pile. The D_{app} after exposing the slices for one year to 16.5% NaCl and includes the binding component, whereas the D_{nssm} does not (or only a small contribution due to the short duration of the RMT test). Similar ranking can be observed for the two set of diffusivity values. Piles with OPC only had the larger values, as expected. Interestingly, for OPC mix the D_{app} value from bulk diffusion test (i.e. 10 cm diameter and 5 cm slice) was at least 5 times larger than the D_{app} calculated values from profiles obtained from cores (5 cm diameter) after 5 years of exposure at the two lower elevations.

Work in Progress and Possible Future-Work

A few slices remain from the cores obtained at the top of each fender pile. These concrete slices could be used for additional D_{app}, D_{nssm}, or to conduct chloride diffusion under controlled non-saturated conditions, or exposed outdoors (e.g. at Florida Atlantic University Dania Beach site and on the eastern side for natural chloride deposition for various exposure durations). Either of these approaches might be worth considered as part of future research.

3.4 CONCLUSIONS

Chlorides profiles were obtained from sliced cores. These profiles were used to calculate D_{app} values after approximately 5 years of exposure. The diffusivity values measured after the first visit (approx. 2.5 years of exposure) were similar to those obtained during the second visit (approx. 5 years of exposure) for each corresponding mix.

The chloride diffusivity smaller at the higher elevation for each mix, but the diffusivities were of the same order of magnitude. However, the chloride penetration from the chloride profile was significantly smaller at this higher elevation and a corresponding smaller C_s was observed. C_s values were not the same for all mixes at the same elevations.

D_{nssm} were obtained from NT492 tests and correlated to the wet resistivity. Except for OPC mixture, all concrete are of low to extremely low chloride permeability. Comparable magnitude of values were obtained for each mix when comparing D_{app} values after bulk diffusion for 1 year (i.e. modified NT443) and D_{nssm} values after NT492 test.

4 CORROSION RESISTANT ALLOYS (CRAS) EMBEDDED IN CONCRETE EXPOSED OUTDOORS

4.1 INTRODUCTION

This chapter describes the follow-up of the outdoor exposure specimens that were part of Project BD228[8]. Currently the group-1 specimens (oldest SDS) are slightly over ten years old whereas group 6 specimens are slightly over seven years old. These Simulated deck slabs (SDS) specimens were prepared as part of project BD228 [8]. These samples were prepared at SMO and then transported to FAU-SeaTech for exposure (one week wet with 15% NaCl and one week dry). The remaining specimens continue to be subjected to weekly wet and dry cycles with 15% NaCl. In this chapter the focus is on selected groups of specimens that contain: 316.18, 316.16, 304, 2304 and 3Cr12. Additional background for preparing these specimens and previously terminated specimens with intermediate alloys can be found in BD228 [8]. A brief description of the materials and experimental procedure follows. The results and discussion is then presented.

4.2 EXPERIMENTAL

4.2.1 Materials

Reinforcing Steels

Table 4-1 lists the various steels that were employed in the original study. These are the same as addressed in project BD228. Composition for all bars is shown in Table 4-2 Bar size in all cases was #5 (nominally 16 mm diameter) except for Type 304 SS which was #4 (12.7 mm diameter). The two types of clad bars (designated as STAX and SMI) were fabricated by two distinct processes, the former by packing a stainless steel tube with steel scrap followed by rolling and the latter by plasma spray application of stainless steel to a carbon steel billet and then rolling. Unless noted otherwise, bars were tested in the as-received surface condition. All specimens with Black bar, MMFX2 and 2201 and most of those with 3Cr12 were terminated during the previous phase of the project as part of BD228. Additionally, the two clad bars are currently not commercially available and thus would not be the main focus of this report.

Table 4-1: Alloys investigated

Designation./Spec.	Common Design.	As-Rec'd. Cond.	Microstructure	PREN[1]	Supplier
UNS-S31603	Type 316LSS	Pickled[2]	Austenite	26.4 [3]	Slater Steels Corporation
				25.1 [4]	Dunkirk Specialty Steel
UNS-S30400	Type 304SS	Pickled[2]	Austenite	19.6	Dunkirk Specialty Steel
UNS-S32304	Type 2304SS	Pickled	Duplex (Austenite plus Ferrite)	24.9	UGITECH
ASTM A955-98	Type 2101LDXSS	As-Rolled	Lean Duplex (Austenite plus Ferrite)	25.1	Gerdau AmeriSteel Corp.
ASTM A1035	MMFX 2	As-Rolled	Microcomposite austenite-martensite	9.4	MMFX Corporation
AASHTO MP 13M/MP 13-04	Nouvinox	Pickled	316 Clad/Carbon Steel Core	-	Stelax Industries, Ltd.
	SMI	Pickled	316 Clad/Carbon Steel Core	-	CMC Steel Group
UNS-S41003	Type 3Cr12SS	Pickled	Ferritic	12	American Utility Metals
ASTM A615	Black Bar	As-Rolled	Ferrite/Pearlite	0.3	Gerdau AmeriSteel Corp.

[1] PREN (Pitting Resistance Equivalent Number) where PREN = %Cr + 3.3·%Mo + 16·%N

[2] Pickled with HF and nitric acid per ASTM A380.

[3] Subsequently designated as 316.16.

[4] Subsequently designated as 316.18.

Table 4-2: Alloys composition

Alloy	C	Mn	P	S	Si	Cr	Ni	Mo	Cu	N	Fe
Type 316.16	0.03	1.55	0.025	0.001	0.59	18.43	10.06	2.08	0.42	0.068	Bal.
Type 316.18	0.03	1.66	0.026	0.005	0.42	16.97	10.07	2.15	0.85	0.065	Bal.
Type 304SS	0.07	0.94	0.020	0.001	0.58	18.25	8.12	0.40	0.30	-	Bal.
Type 2205SS	0.029	1.68	0.028	0.004	0.63	21.58	4.80	2.64	-	0.15	Bal.
Type 2304SS	0.03	1.16	0.026	0.002	0.45	22.33	4.16	0.25	0.30	0.11	Bal.
Type 2101SS	0.04	4.70	0.019	0.001	0.80	22.47	1.68	0.24	0.38	0.117	Bal.
A1035	0.05	0.45	0.012	0.015	0.23	9.30	0.10	0.03	0.12	-	Bal.
Type 3Cr12SS	0.04	0.38	0.018	0.024	0.71	11.69	0.50	0.09	0.02	-	Bal.
A615	0.30	1.22	0.013	0.032	0.26	0.21	0.19	0.04	-	-	Bal.

4.2.2 Concrete Mix Designs

Two concrete mix designs were employed when preparing the specimens. These are designated: STD1 (5 bags cement and 0.50 water-to-cement ratio (w/c)) which yields a very-high permeability concrete, and STD2 (7 bags of cement and 0.41 w/c) which results in moderate permeability. Target mix designs for each of these are listed in Table 4-3. The various corrosion resistant alloy types, in addition to black bar (Table 4-1), were used as reinforcement but as indicated above specimens with MMFX2, 2201 and most 3Cr12 were terminated during as part of the BD228 project. A set of specimens with 3Cr12 remained for one of the configurations and relevant findings will be discussed in here.

Table 4-3: Concrete batch mix design

Material	STD1	STD2
Cement (Bags)	5	7
Cement, kg	213	300
Water, kg	107	122
Water/Cement	0.50	0.41
Fine Aggregate (silica sand), kg	652	540
Coarse Aggregate (limestone), kg	753	753

4.2.3 Simulated Deck Slab (SDS) Specimens

The standard specimen (STD) consisted of all straight bars in the as-received condition in concrete compacted according to ASTM C192. However, other specimens employed variations of this according to the description and nomenclature listed in Table 4-4.

Prior to casting, the reinforcement was degreased by cleaning with hexane, followed by the application of heat shrink tubing at the bar ends to provide an electrical barrier at the concrete-reinforcement interface leaving only the center portion of the reinforcement to within approximately 25 mm of the concrete surface exposed (groups 4, 5 and 6). The casting procedure was similar for all specimen types. This involved placement of freshly mixed concrete in the specimen molds in two lifts followed by consolidation of each lift for 20 to 30 seconds on a vibration table. The first lift filled the specimen mold approximately half full, and the second lift completely filled the mold. The surface of the specimens was troweled smooth using a wooden or metal float. After 24 hours, the molds were dissembled; and the specimens were removed, placed in sealed plastic bags, and stored for six months. The design of each of the four specimen types is provided below.

The simulated deck slab (SDS) specimens were fabricated with six bars, three of which comprised a top and three a bottom layer, as illustrated schematically in Figure 4.2. Concrete cover for all bars was 25 mm, and triplicate specimens were prepared for each bar type and specimen variable (described below). Because of the large inventory of specimens, fabrication and delivery to FAU occurred at six different times. The Interim Report and BD228 final report provided results for exposure of the six specimens lots, and data for these has been updated and is discussed for selected sets in this report. A distinction between the initial and final three lots is that heat shrink end sleeves were not installed on bar ends of Lots 1-3 specimens. Because of concern that absence of sleeves on bars of the initial three lots may have resulted in premature corrosion initiation where rebars exited the concrete, replicates of black bar (BB), 3Cr12, MMFX-2, and 2201 reinforced specimens (these were the only STD type specimens that initiated corrosion) were included in Lot 5. Otherwise, specimens of Lots 4-6 consisted

of reinforcement types/specimen configurations that were not present in Lots 1-3. The following example (Figure 4.1) illustrates the nomenclature that was adapted to identify a standard specimen:

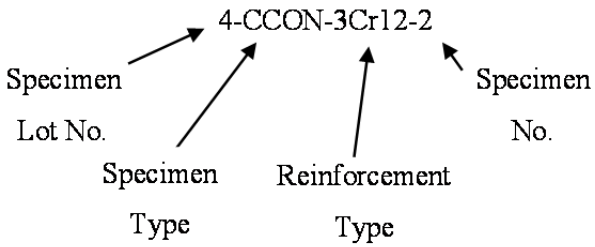

Figure 4.1: Specimen Nomenclature

Thus, the last digit identifies this as simulated deck slab specimen no. 2. The reinforcement is 3Cr12 with a simulated crack from Lot 4. The default mix design (no indication) is STD1. Concrete mix designs STD1 and STD2 were employed for Type 316.16, 316.18, 304SS, Stelax and SMI bars but with most specimens being prepared using the former. Ten different modifications to the above standard SDS specimen configuration were prepared and exposed, as listed and described below.

1. Slabs with a corrosion resistant bar type for the top layer and black bars in the bottom (designated BCAT). All specimens of this type, except for those reinforced with Type 304SS, were included in the first three lots; and results were provided in the Interim Report.[19] Results for Type 304SS BCAT specimens are presented here.

2. Slabs with a simulated concrete crack (designated CCON). In fabrication of these specimens, a 1.6 mm thick stainless steel shim was placed vertically in the form on top of and perpendicular to the upper bars at the mid span. The shim was removed subsequent to initial concrete set. Reinforcement types in Lots 4-6 SDS specimens that employed this configuration were Type 304SS and SMI and from Lots 1-3 SDS were Type 316SS and 3Cr12.

3. Slabs with a bar splice that formed a crevice (designated CREV). In this case, two bars that overlapped for a portion of their embedded length replaced each of the three single top bars in the standard specimen. Hence, the top reinforcement layer consisted of six rebars instead of three, as was the case for the other specimen types. Cover for each of the bar pairs was maintained at 25 mm. Figure 4.3 illustrates this specimen type schematically. Reinforcement types in Lots 4-6 SDS specimens that employed this configuration were Type 304SS and SMI.

4. Slabs with a bar crevice (splice) per the above configuration but also with a simulated concrete crack (designated CCRV). Reinforcement types in Lots 4-6 SDS specimens that employed this configuration were 3Cr12, Type 304SS, and SMI and Type 316SS from Lot 3.

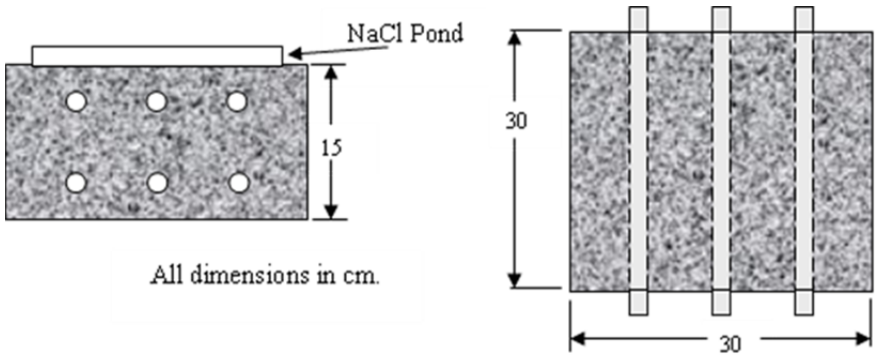

Figure 4.2: Sample schematic

5. Slabs with a simulated concrete crack and black bar cathode (designated CCNB). Specimens that employed this configuration was Type 304SS and Type316SS.

6. Slabs with wire brushed bars (designated WB). Only specimens with Type 304SS bars in Lot 6 employed this condition.

7. Slabs with a simulated concrete crack and 3 mm holes drilled through the cladding on the top of upper bars at 25 mm spacing (designated CSDB). Only specimens with SMI bars were employed in this condition.

8. Slabs with 3 mm holes drilled through the cladding of upper bars at 25 mm spacing (USDB).

9. Slabs with 3 mm holes drilled through the cladding of upper bars at 25 mm spacing and and black bar cathode (BCCD).

10. Slabs with with a bar crevice (splice) per configuration 3 (above), with no end caps for SS Clad rebars. (CVNC)

Table 4-4: Listing of the various specimen types, variables, and the nomenclature for each

STD1	STD1 concrete mix
STD2	STD2 concrete mix
BCAT	STD1 concrete. Bottom mat black steel.
CCON	STD1 concrete mix, simulated concrete crack
CCNB	STD1 concrete mix, bottom mat (cathode) black bar, simulated crack
CREV	STD1 concrete mix,top bar crevice.
CCRV	STD1 concrete mix, simulated concrete crack, top bar crevice.
WB	STD1 concrete mix, top bars wire brushed.
USDB	STD1 concrete mix, 3 mm diameter clad holes 25 mm apart on top bars.
CSDB	STD1 concrete mix, simulated concrete crack, 3 mm diameter clad
BCCD	STD1 concrete mix, 3 mm diameter clad holes 25 mm apart on top bars,bottom black steel
CVNC	STD1 concrete mix, top bar crevice, no end caps.

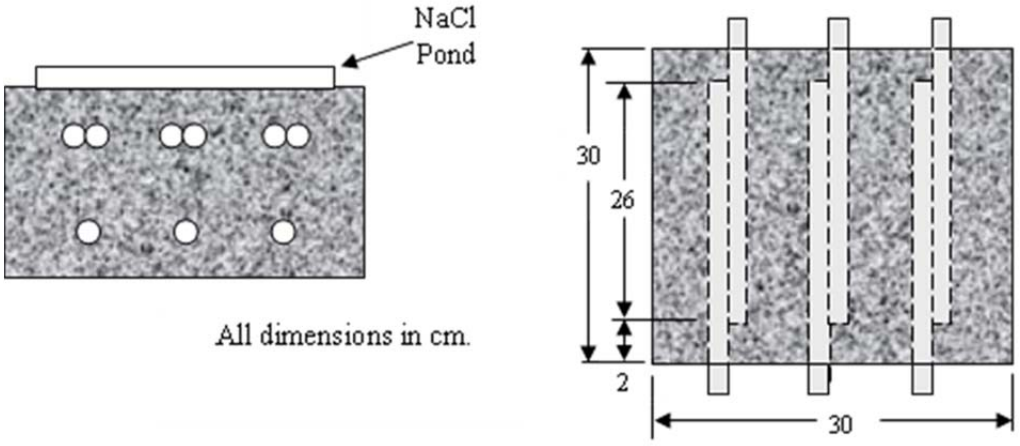

Figure 4.3: Schematic illustration of the CREV-type simulated deck slab specimens

Upon delivery to FAU, an electrical connection was established between bars in each of the two layers of each slab using a stainless steel wire in conjunction with a drilled hole and connection screw at one end of each bar. The specimen sides were coated with a UV resistant paint, inverted relative to their orientation at casting, and a plastic bath with a vented lid was mounted on what was the bottom formed face. Prior to ponding, the specimens were stored outdoors in a covered location for two months at the FAU Sea Tech Campus which is approximately 300 m inland from the Atlantic Ocean southeast of Ft. Lauderdale. For lots 4, 5 and 6; the initial week of ponding was with potable water to promote saturation or a high humidity pore structure so that, upon ponding, diffusion and not sorption would be the primary Cl- ingress mechanism. This was followed by cyclic one week wet – one week dry ponding with 15 wt% NaCl. The salt water pondings commenced on July 26, 2005, August 10, 2005, and December 11, 2006, respectively, for Lots 4, 5, and 6. For Lots 1, 2 and 3 the primary initial chloride transport was sorption as 15 wt% NaCl commenced after the three months outdoors exposure.

Figure 4.4: View of a mold for a CCRV-SMI specimen prior to concrete pouring

Figure 4.4 is a photograph of a mold with CCRV-SMI reinforcement prior to concrete pouring. Figure 4.5 shows two specimens under test, and Figure 4.6 is a perspective view of the test site.

Figure 4.5: Photograph of two SDS specimens under exposure

Monitoring of potential of electrically connected bars of individual specimens and of voltage drop between bar layers was performed every other week and subsequently once a month (towards the end of the wet period). The onset of active corrosion was defined as having occurred if a measureable voltage drop was detected for two consecutive measurement periods.

Figure 4.6: Photograph of SDS specimens under exposure in the outdoor test yard

4.2.4 Specimen Terminations and Dissections

Selected specimens were designated for dissection. At least four of the selected specimens were cored to obtain chloride profiles. The specimens were then opened and evaluated according to the following procedure:

1. Testing/exposure was terminated and the ponding bath removed, (coring was performed if specimen chosen)

2. Two saw cuts were then made, each of which was perpendicular to the top surface and parallel to and at mid-spacing between the center and each of the two outer bars of each layer.

3. For each of the three resultant specimen parts, a further saw cut was made on each of the previous saw cut faces and on what had been the two specimen side faces opposite and parallel to the top rebars to a depth approximately 10 mm from each rebar. In some cases where corrosion of bottom layer black bars was thought to have occurred, this procedure was performed at the level of these bars also.

4. Each specimen section was split open by placing a chisel in one of the saw cuts from step 3 and tapping gently with a hammer until fracture occurred. This exposed both the rebar and its trace, which were then examined for corrosion and photographed.

5. The concrete rebar trace (above the rebar) was then milled and chloride content determined.

Figure 4.7 schematically illustrates the location of concrete cuts as listed in steps 2 and 3 above.

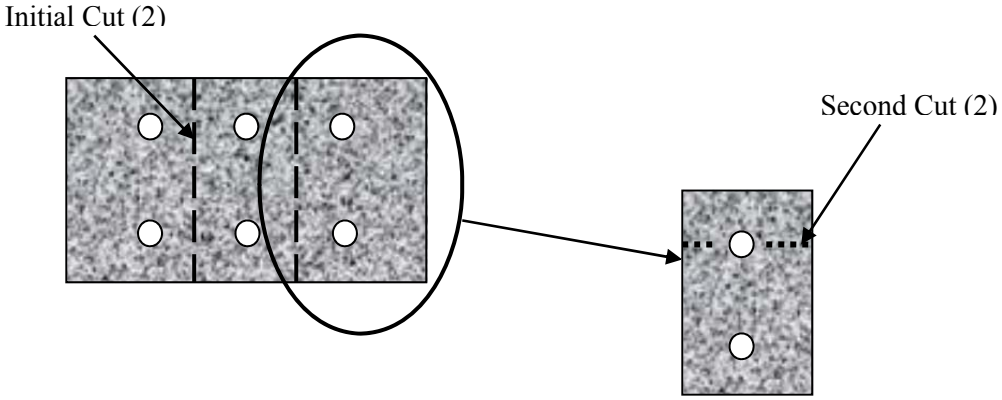

Figure 4.7: Schematic illustration of the concrete sectioning as listed in dissection steps 2 and 3 above

4.2.5 Chloride Analysis

Concrete samples for [Cl-] determinations were acquired from SDS specimens according to two methods. The first method involved acquiring a 35 mm diameter core from the top concrete surface at the mid spacing between two adjacent top layer bars. This was then sliced parallel to the top surface at 6.4 mm intervals and separately grinding the individual slices to powder. The second involved individually mounting the concrete sections from the top portion of each specimen on a mill and milling a cut approximately 0.8 mm deep along that portion of the rebar trace that was void of corrosion products using a 10 mm diameter square end mill. Figure 4.8 **Error! Reference source not found.**illustrates this process schematically. For both methods (coring and milling), the powder samples were analyzed for [Cl-] using the FDOT wet chemistry method.

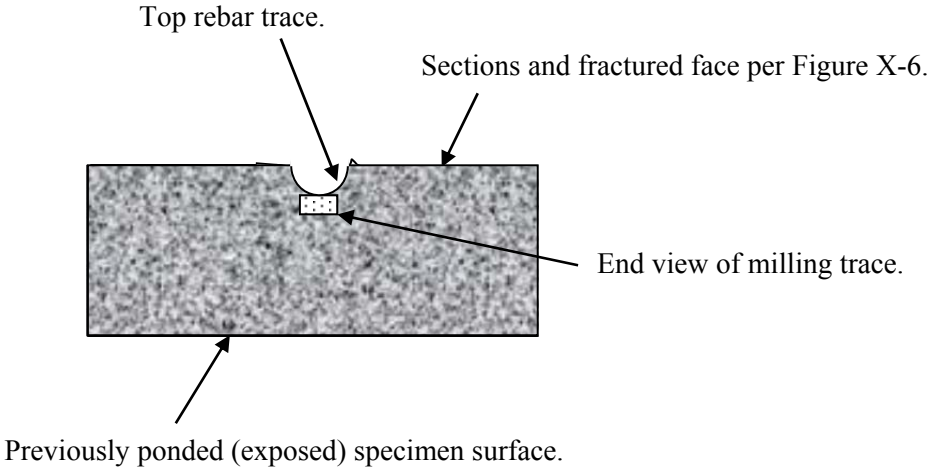

Figure 4.8: Schematic illustration of the of the milling process above the rebar trace

4.2.6 Linear Polarization Resistance and Solution Resistance

Selected specimens were brought into the lab to perform linear polarization resistance over the duration of the project. LPR tests were performed only on rebars on the top row, by momentarily disconnecting the bottom rebars and the interconnection between each rebar on the top row. A saturated calomel electrode was used as a reference electrode and at titanium activated mix metal oxide mesh was used as the counter electrode. Both the counter electrode and reference electrode were position above the rebar that was being tested. The linear polarization test was performed at a scan rate of 0.1 mV/sec, from 12 mV below the open circuit potential (OCP) to OCP. Electrochemical Impedance Spectroscopy was use to estimate the solution resistance by taken the magnitude of the impedance measured at ~60 Hz. Below Rc values are reported by subtracting from (Rp-Rs – LPR test) the measured Rs (EIS test). After completing the LPR measurements on each rebar; the rebars were reconnected and the specimen taken back outdoors.

4.3 RESULTS AND DISCUSSION

4.3.1 Potential vs. Time

Specimens made of STD1 and STD2 were prepared with 316.16 (identified in here as 316(B)), 316.18 (ID here as 316(A)), 304, and one of the stainless steel clads. Figure 4.9 shows the potential evolution for specimens prepared with rebar 316(A). The coupled potential measured for all specimens are more positive than -200 mVsce, suggesting that corrosion has not initiated. Momentary drifts to more negative values were periodically observed.

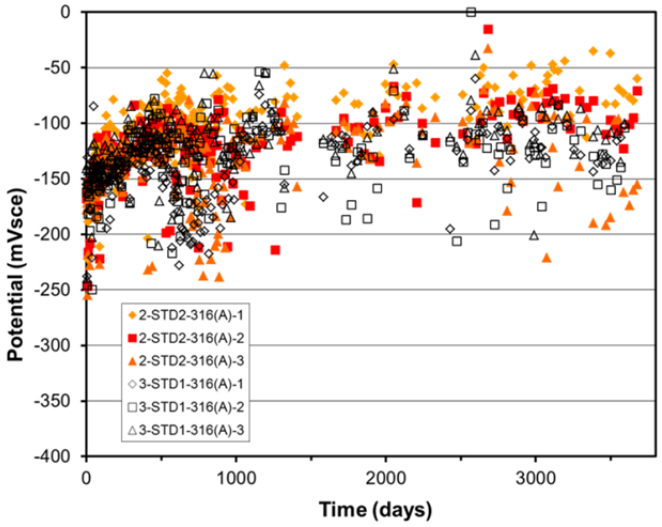

Figure 4.9: Potential evolution for 316(A) embedded in STD1 or STD2 concrete

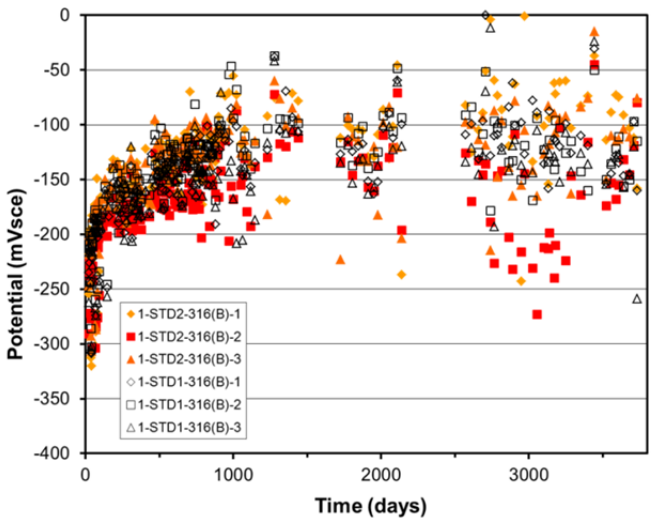

Figure 4.10: Potential evolution for 316(B) embedded in STD1 or STD2 concrete

Figure 4.10 shows similar potential transients for specimens with rebar 316(B). In this case the coupled potential on two specimens cast in STD2 concrete momentarily reached values as negative as -250 mVsce (i.e. approx. -320 mVcse), but then recovered and all potential values are currently mostly more positive than -150 mVsce. Figure 4.11 shows the potential evolution for specimens prepared with Stelax clad rebar. The scatter of the potential values after day 2500 is quite pronounced. Potentials values more negative than -300 mVsce were observed on STD1-2, STD1-3 and STD2-3. However the last set of measurements ranged between -250 mVsce and -100 mVsec. Some of these specimens were selected for LPR testing and the results are discussed below. Finally, Figure 4.12 shows the potential evolution on specimens prepared with 304SS rebars, and the potential values have been monitored up-to 2500 days. In general, the potential values on all specimens were more positive than -200 mVsce, suggesting that corrosion has not initiated. (A few excursions to somewhat more negative values were measured in a few instances)

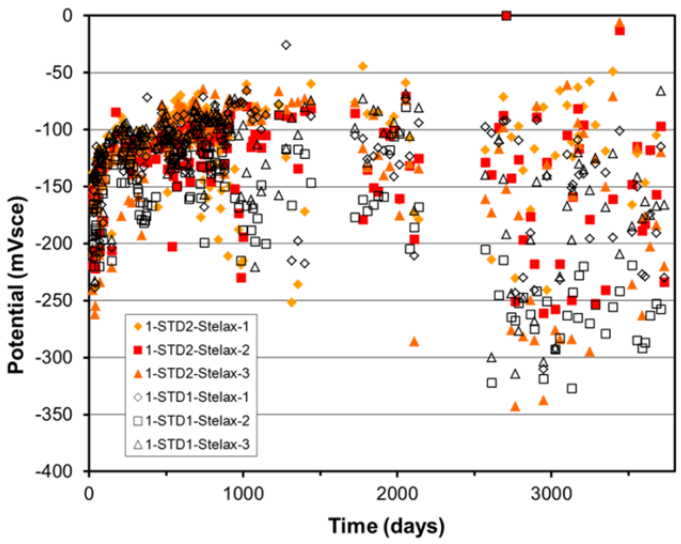

Figure 4.11: Potential evolution on specimens with Stelax in STD1 or STD2 concrete

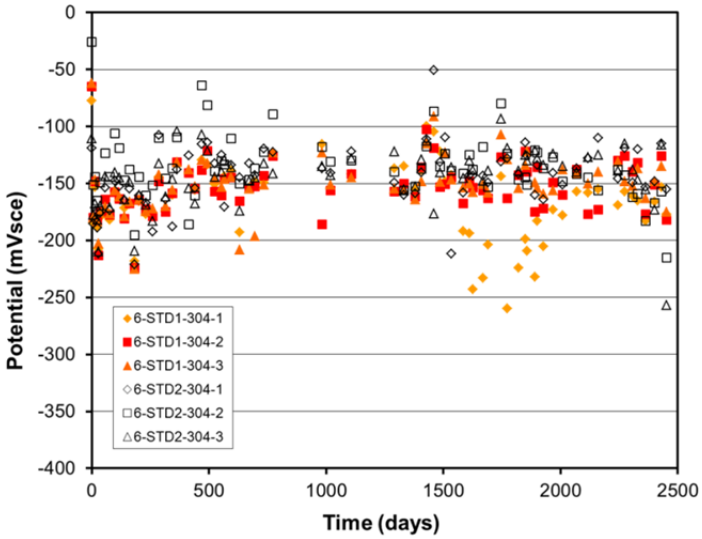

Figure 4.12: Potential evolution on specimens with 304SS in STD1 or STD2 concrete

Based on the potential values measured over time as an indicator; no corrosion has initiated on specimens with rebars: 316(A), 316(B), 304, and the two clads in the as received condition. Even when crevice (exception are clad rebars with not caps), intentional cracks were present or combination of both (specimens with both crack and crevice configuration were terminated and are described below). Potential vs. time suggest that corrosion initiated on two 5-STD1-2304 specimens (i.e. contained 2304 rebars) as can be observed on Figure 4.13. These two specimens were terminated at the ages indicated by the circled symbols. Upon forensic examination (details

shown below): a)Corrosion initiated on two or three top row rebars of one of specimen 5-STD-2304-1; b) On specimen 5-STD1-2304-3 corrosion initiated, but not on a top row rebar, rather on a rebar on the second row.

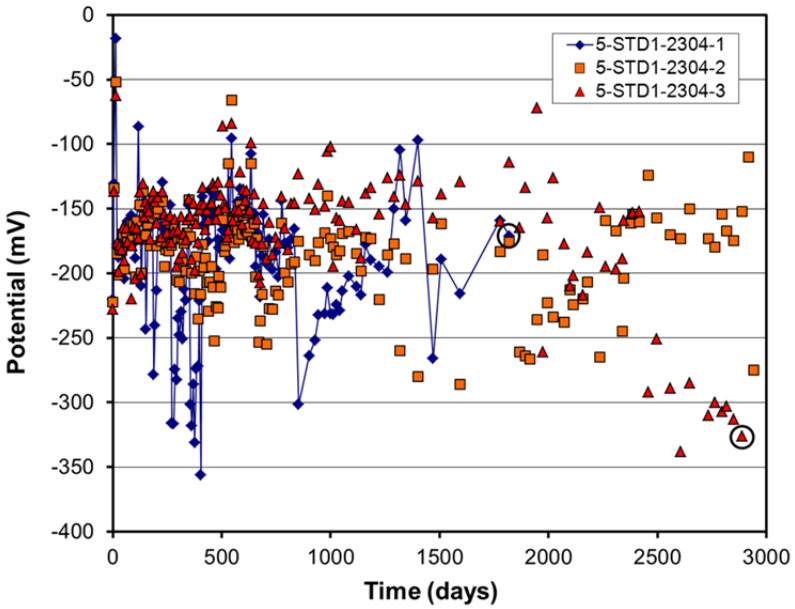

Figure 4.13: Potential evolution on specimens with 2304 rebar in STD1 concrete

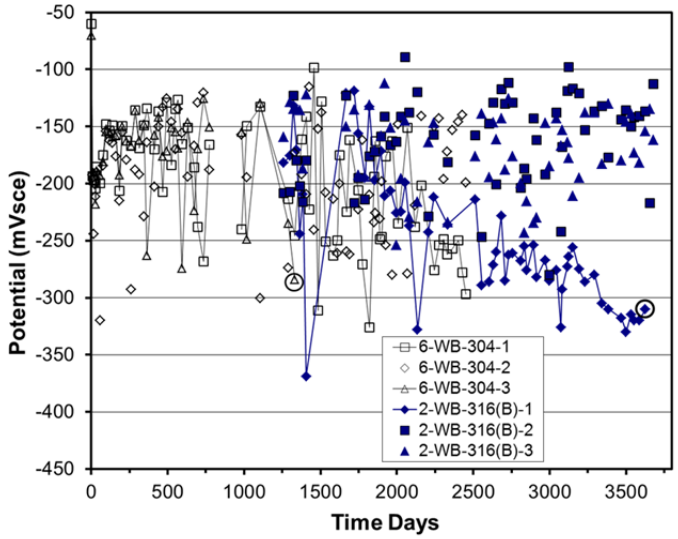

Figure 4.14: Potential evolution on specimens with WB-316 and WB-304 in STD1 concrete

The rebars for two sets of specimens were wire brushed before concrete casting: one contained 316(B) rebars and the other 304 rebars. The potential evolution of the measured coupled values are shown in Figure 4.14. Based on potential drops observed, one WB-316 specimen and one WB-304 specimen experienced corrosion initiation.

Specimen 6-WB-304-3 was terminated ~200 days after the potential drop, whereas 2-WB-316(B)-1 was terminated on day 3600 about 600 days after the potential was stable at values more negative than -300 mVsce. Specimen 6-WB-304-1 recently experience momentary potential drift to values as negative as -300 mVsce, but was not terminated. In the past, the potential drifted back to more positive values. The other remaining specimens show potential values of ~-200 mVsce. Additional detail will be given below for those specimens that were terminated.

Not shown in here are potential evolution for specimens that contained BB on the bottom row. In those specimens the potential indicate that corrosion initiated. However, upon visual inspection the rebar that is corroding is the BB and not the stainless steel.

4.3.2 Linear Polarization

Linear Polarization measurements were performed on selected specimens at four different times during the duration of the project. May 2011, Dec 2011, July 2012, June/July 2013. No attempt was made to calculate apparent corrosion rates. Rather the Rc values are reported in here (i.e. measured LPR (Rc+Rs) but with the Rs subtracted by the Rs values measured via EIS). The area assumed when running the experiments was 1 cm^2, and the values shown below are not corrected for nominal rebar area. The specimens were selected from the high performance CRA. Table 4-5 shows the Rc and corresponding corrosion potentials measured for each top rebar momentarily isolated for 1-STD2-316, 1-STD1-Stelax and 1-STD2-Stelax. The smallest Rc value recorded was 7.7 Kohms on STD2-316 specimens, 1.3 Kohms on STD2-Stelax specimens and the minimum Rc was 0.3 KOhms (although the most recent Rc values was 1.4 Kohms) on 1-STD1-Stelax specimens.

Table 4-5: R_c (KOhms) values and correspond E_{corr} measured on selected specimens

	1-STD2-316		1-STD2-STELAX		1-STD1-Stelax			
	E	Rc	E	Rc	E	Rc	E	Rc
May-11	-290	17.4	-185	21.3	-115	10.8		
	-163	88.0	-139	4.4	-116	16.3		
	-154	94.0	-168	13.3	-117	12.4		
Dec-11			-66	12.3	-113	7.0		
			-65	2.7	-121	12.0		
			-67	12.3	-114	8.0		
Jul-12	-175	81.3	-182	7.4	-327	1.3	-350	0.3
	-163	91.6	-155	2.3	-216	3.4	-237	1.7
	-179	13.0	-164	13.1	-166	2.6	-487	0.5
June/July 2013	-210	7.7	-214	8.6			-269	1.4
	-144	62.0	-283	1.3			-255	13.7
	-202	16.6	-196	4.7			-150	6.7
Max	-154	94.0	-185	21.3	-116	16.3		
Min	-210	7.7	-283	1.3	-350	0.3		

None of the specimens in Table 4-5 were terminated. Table 4-6 shows the Rc and corresponding corrosion potentials measured for each top rebar momentarily isolated for groups 2-WB-316, 5-STD1-2304, and 6-WB-304. The smallest Rc value recorded was 4.6 Kohms on 2-WB-316 specimen, 17.2 Kohms on 5-STD1-2304 specimen, and Rc was 0.6 KOhms (although the most recent Rc was 4 Kohms) on 6-WB-304 specimen. One of the 2-WB-316 and one of the 5-STD1-2304 were terminated in July 2013 included in Table 4-5. Values of Rc smaller than 5 Kohms accompanied with potential more negative than -300 mVsce appear to be indicative that corrosion had initiated or that an electrochemical process is taking place at a fast rate. Figure 4.15 shows average Rc values measured over the first three periods on selected specimens described above. The minimum Rc and Ecorr values are also shown in Figure 4.15.

Table 4-6: R_c (KOhms) values and correspond E_{corr} measured on selected specimens

	2-WB-316						5-STD1-2304				6-WB-304			
	E	Rc	E	Rc	E	Rc	E	Rc	E	Rc	E	Rc	E	Rc
May-11	-334	8.7	-225	10.5	-246	13.7	-225	23.7	-191	33.9	-358	0.6	-227	7.6
	-308	6.5	-275	5.2	-207	24.6	-215	29.9	-186	31.3	-230	12.8	-200	10.2
	-227	19.6	-186	21.0	-197	36.0	-217	36.8	-187	31.5	-223	16.2	-191	16.8
Dec-11	-292	11.8	-147	9.1	-147	17.9	-182	21.7	-182	23.7	-271	4.9	-284	6.4
	-321	4.8	-159	10.7	-150	15.4	-180	20.7	-179	19.6	-234	12.4	-233	10.9
	-290	12.5	-146	15.6	-147	30.0	-183	24.8	-180	24.7	-280	7.6	-228	15.3
Jul-12	-206	18.6	-161	7.8			-171	20.3	-192	22.1	-181	8.2	-179	8.9
	-319	4.6	-193	11.8			-169	20.5	-185	17.2	-173	10.7	-169	8.3
	-239	8.9	-161	17.1			-175	24.3	-192	18.5	-216	11.2	-163	12.0
June/July	-315	13.1			-152	18.0	-186	21.8	-265	20.4	-250	10.1		
2013	-351	6.4			-152	15.9	-189	47.6	-202	19.1	-310	4.0		
	-294	15.6			-152	38.8	-185	26.8	-203	20.7	-260	12.9		
Max	-152	38.8					-189	47.6			-191	16.8		
Min	-319	4.6					-185	17.2			-358	0.6		

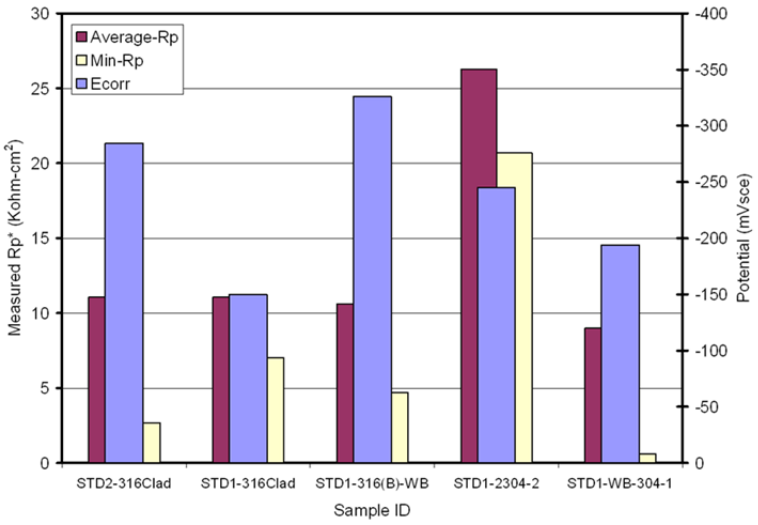

Figure 4.15: Average Rc, minimum Rc and Ecorr

4.3.3 Chloride Analyses

Figure 4.16 to Figure 4.19 show the [Cl^-] analysis results for samples acquired both by coring and milling of SDS specimens. In all cases, [Cl^-] determined from milled samples was from locations along the bar trace where the reinforcement remained passive. Figure 4.16 plots the average [Cl^-] versus depth for the cores obtained in August 2010. Figure 4.16 also shows the age of the specimens upon coring. Due to the high water to cement ratio and prolonged exposure time; the chloride concentration measured on the opposite end of the core was as large (8 to 9.2 kg/m3 – 2.89 to 3.32 wt/o cement) on cores terminated on August 2010. The specimen age ranged from 1300 to 2000 days. The chloride concentration data for cores from lot 4 and lot 5 generally indicate decreasing [Cl^-] with depth into (when omitting the first layer) concrete as expected. The profile on lot 6 core shows that the concentration profile is almost flat at about 8.5 kg/m^3. Figure 4.17 show that differences in individual profiles were observed presumably as a consequence of spatial concrete inhomogeneity. Figure 4.18 and Figure 4.19 show individual [Cl^-] versus depth data for both cores (cored August 2013) and millings for 2-WB-316 and 5-STD-2304 specimens respectively, for which these determinations were made. One of the profiles shown in Figure 4.19 (core left) is similar to the trend observed for the profile of Lot 6 core shown in Figure 4.16, however the concentration is almost uniform 15.25 kg/m^3 or 5.5 wt/o cement. The profile for core-right shows that the concentration at 6 inches is ~17 kg/m^3 but the concentration at 4 cm depth is approx. 11 kg/m^3. As the specimens become older, leaks develop over time on the ponding reservoir that might have caused the concentration at the surface not to be the desired 15% NaCl for the whole wet period. Figure 4.19 shows that an even more bizarre profile trend was observed on specimen 5-STD1-2304-3 which explains why corrosion initiated at one of the rebars on the bottom layer and not the top row of rebars. Similar to what was observed in Figure 4.18 the concentration at the opposite end of the core was between 14 and 16 kg/m^3. Based on the concentrations at the

rebar trace it appears that C_T is greater than 12 kg/m3 (4.4 wt/o cement) but smaller than 16 kg/m3 (5.9 wt/o cement) Trends are apparent from these data that suggest differences in concrete age at the time of coring was a factor. Table 4-7 shows the average chloride concentration measured at the rebar trace (in some cases traces at selected rebars are shown)

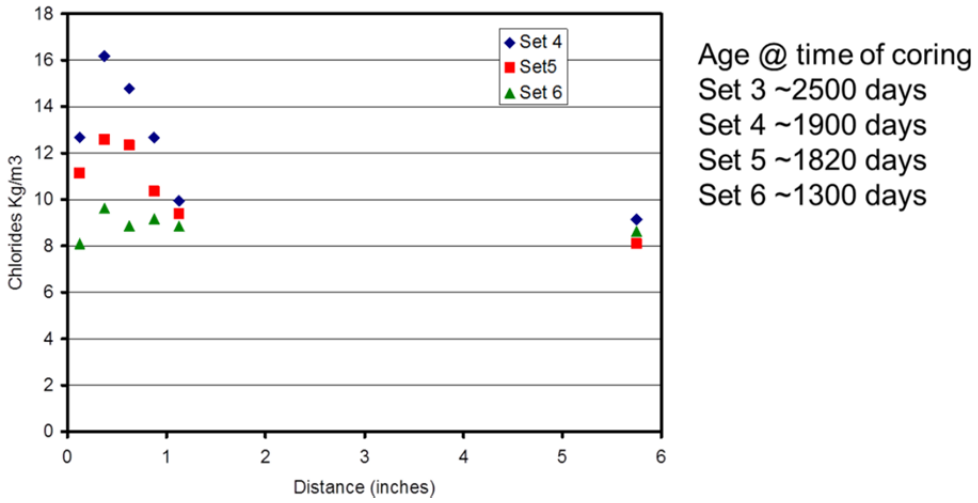

Figure 4.16: plots the average [Cl^-] versus depth for the cores from Set 4, 5 and 6

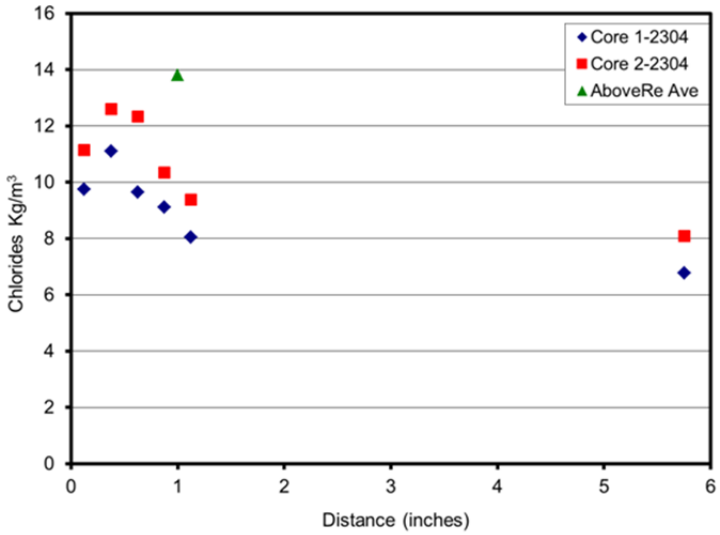

Figure 4.17: [Cl^-] versus depth for the cores on STD1-2304 specimen

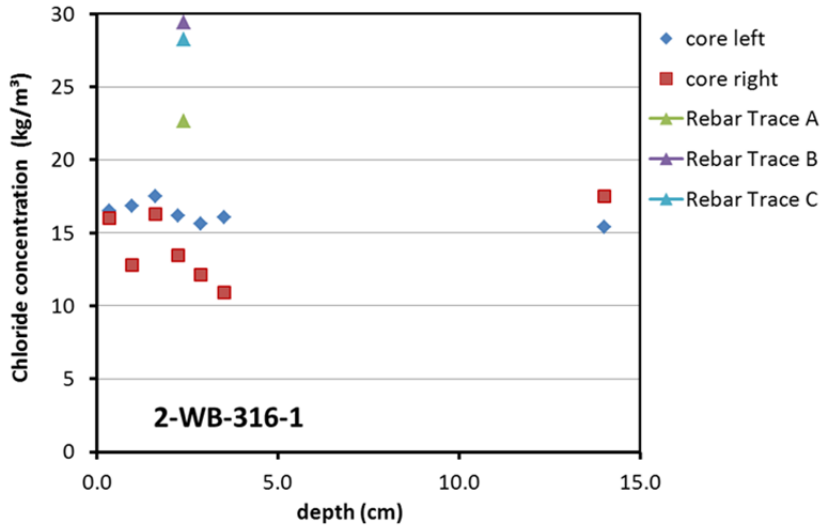

Figure 4.18: [Cl^-] versus depth for the cores (2-WB-316-1)

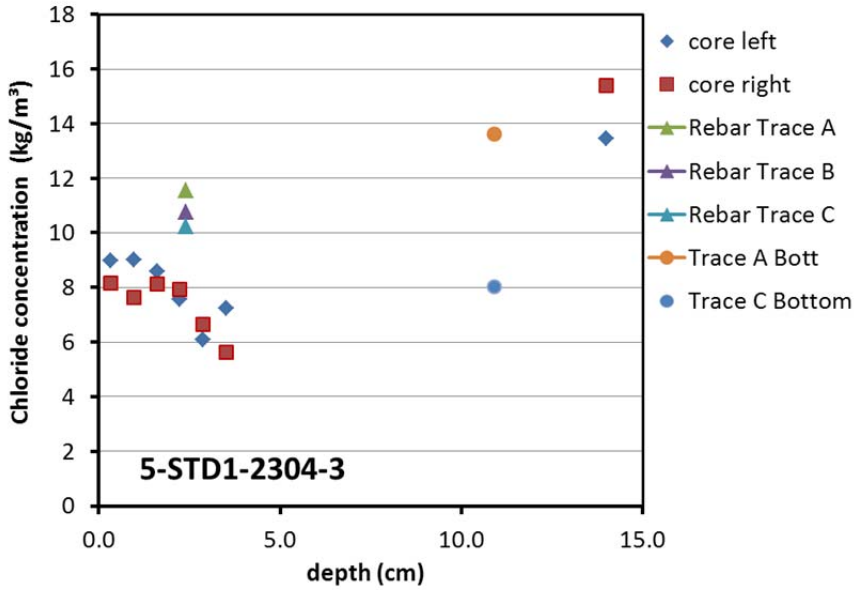

Figure 4.19: [Cl^-] versus depth for the cores on 5-STD1-2304-3 specimen

Table 4-7: Chloride concentration at the rebar trace

	kg/m^3	%wt Concrete	%wt Cement
2-WB-316-1-Avetop	26.8	1.20	9.67
2-WB-316-1-Bott_C	20.1	0.90	7.27
3-CCRV-316	21.4	0.96	7.73
4-CCRV-SMI	22.7	1.02	8.19
4-CCRV-3Cr12-1	15.8	0.71	5.70
6-WB-304-1-L	13.7	0.61	4.95
6-WB-304-1-R	6.5	0.29	2.35
5-STD1-2304-1	13.8	0.62	4.98
5-STD1-2304-3	10.9	0.49	3.92
5-STD1-2304-3-B-L	13.6	0.61	4.91
5-STD1-2304-3-B-R	8.0	0.36	2.90

4.3.4 Visual Inspection of Terminated Specimens

Specimens were terminated on August 2010 and two more on July 2013. Terminated on August 2010: 3-CCRV-316(B)-1, 4-CCRV-SMI-3, 4-CCRV-3Cr12-1, 5-STD1-2304-1, 6-WB-304-3. Terminated on July 2013: 2-WB-316(B)-1, 5-STD1-2304-3.

Three specimens of type CCRV were terminated, one with 3Cr12, one with SMI SS clad and the third with 316SS. Recall that CCRV are slabs with a bar splice that formed a crevice (two overlapped rebars) but also with a simulated concrete crack. Figure 4.20 to Figure 4.26 show the surface condition upon exposure. Only the specimen with 3CR2 showed significant buildup of corrosion products. The picture on the left shows that a crack has appeared above the left rebar by the time the specimen was terminated. Below in another section; pictures are shown of the top surface for the other two specimens with 3Cr12. The specimens with SMI and 316 showed no corrosion, rather a pristine surface condition was observed for both. CCRV terminated specimens with SMI and 3Cr12 rebars had been exposed to NaCl cycles for 1900 days and CCRV-316 for 2500 days.

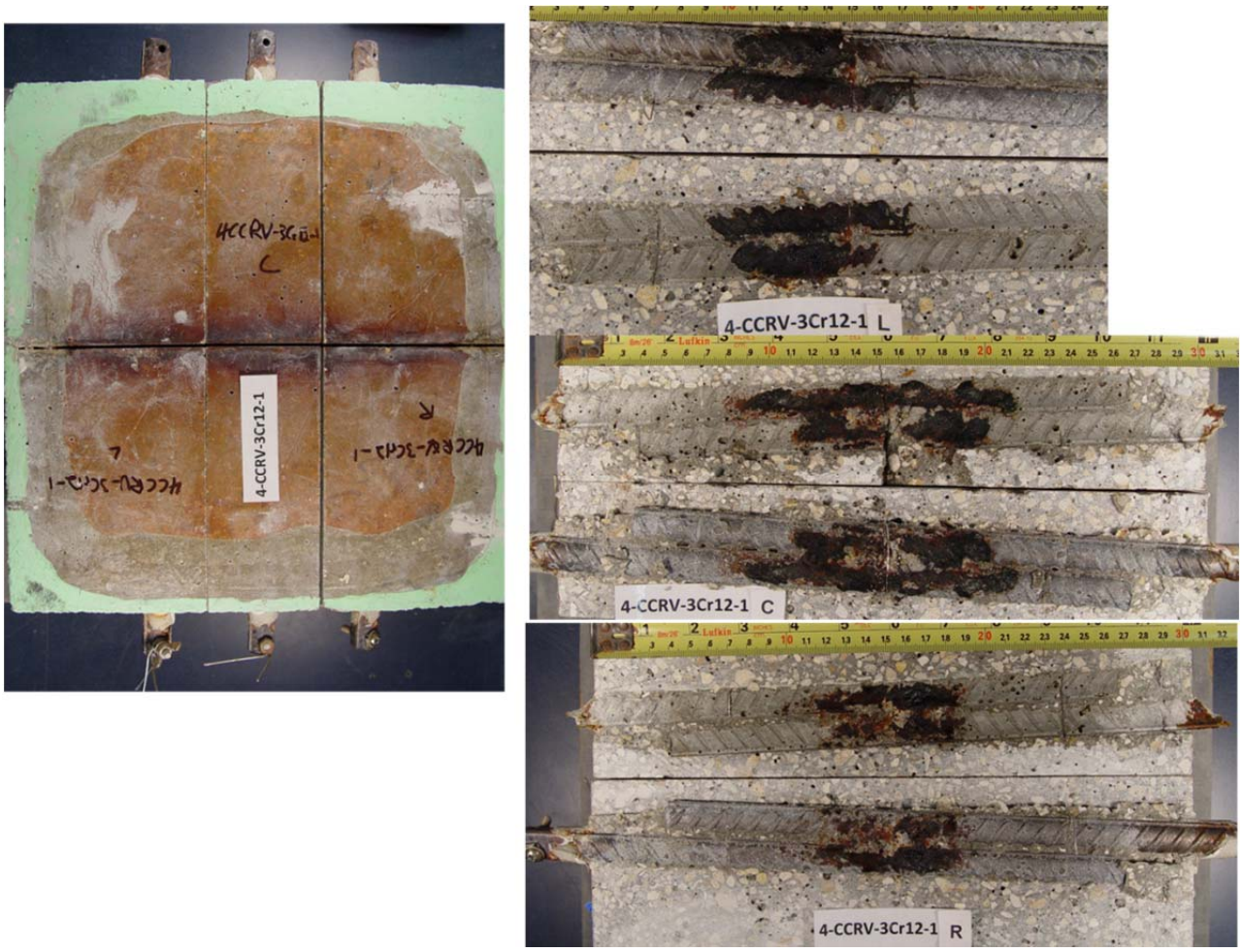

Figure 4.20: Photographs of specimen and top rebars and bar trace of specimen 4-CCRV-3Cr12-1 subsequent to dissection

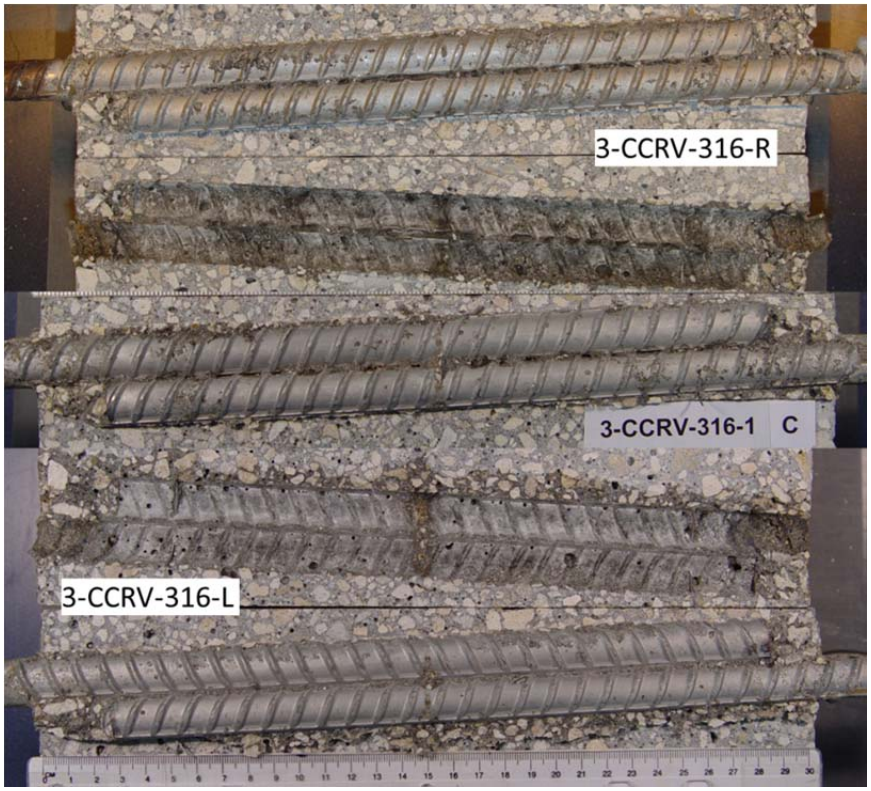

Figure 4.21: Photographs of top rebars and bar trace of specimen 3-CCRV-316-1 subsequent to dissection

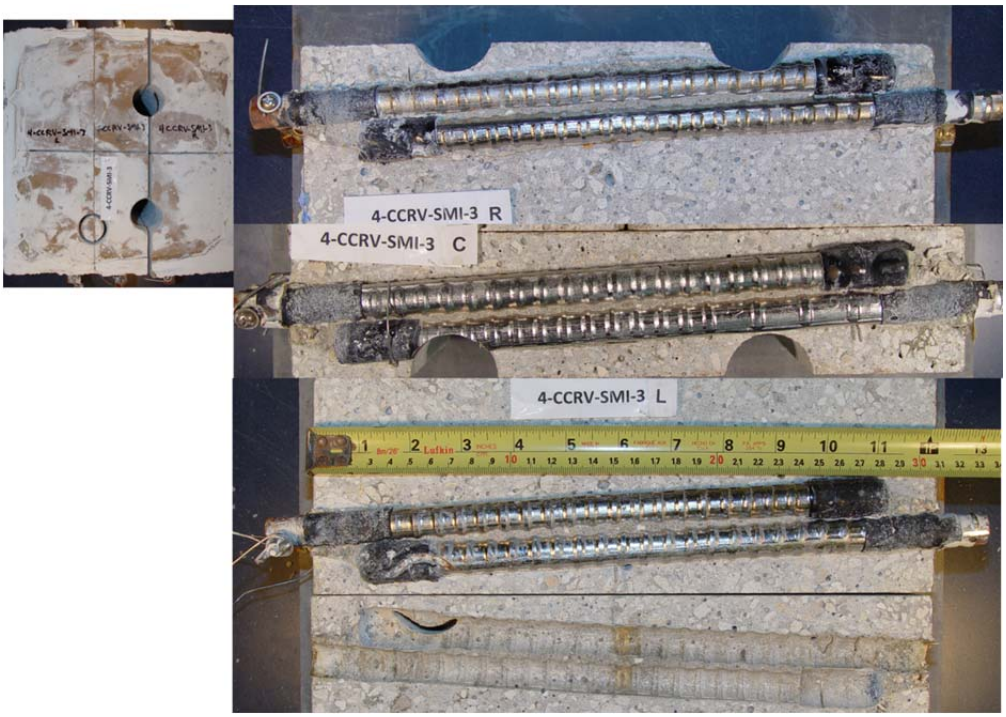

Figure 4.22: Photographs of specimen and top rebars and bar trace of specimen 4-CCR-SMI-3 subsequent to dissection

Two specimens of type WB were terminated, one contained 304 rebars and the other 316 rebars. Figure 4.23 shows photographs after cutting and subsequent to the dissection that took place for 6-WB-304-3. This specimen had been exposed outdoors to NaCl solution cycles for ~1300 days by the type the specimen was terminated. All three rebars show small corrosion spots, most of the spots were superficial and the corrosion products had turned red by the time the specimens were opened.

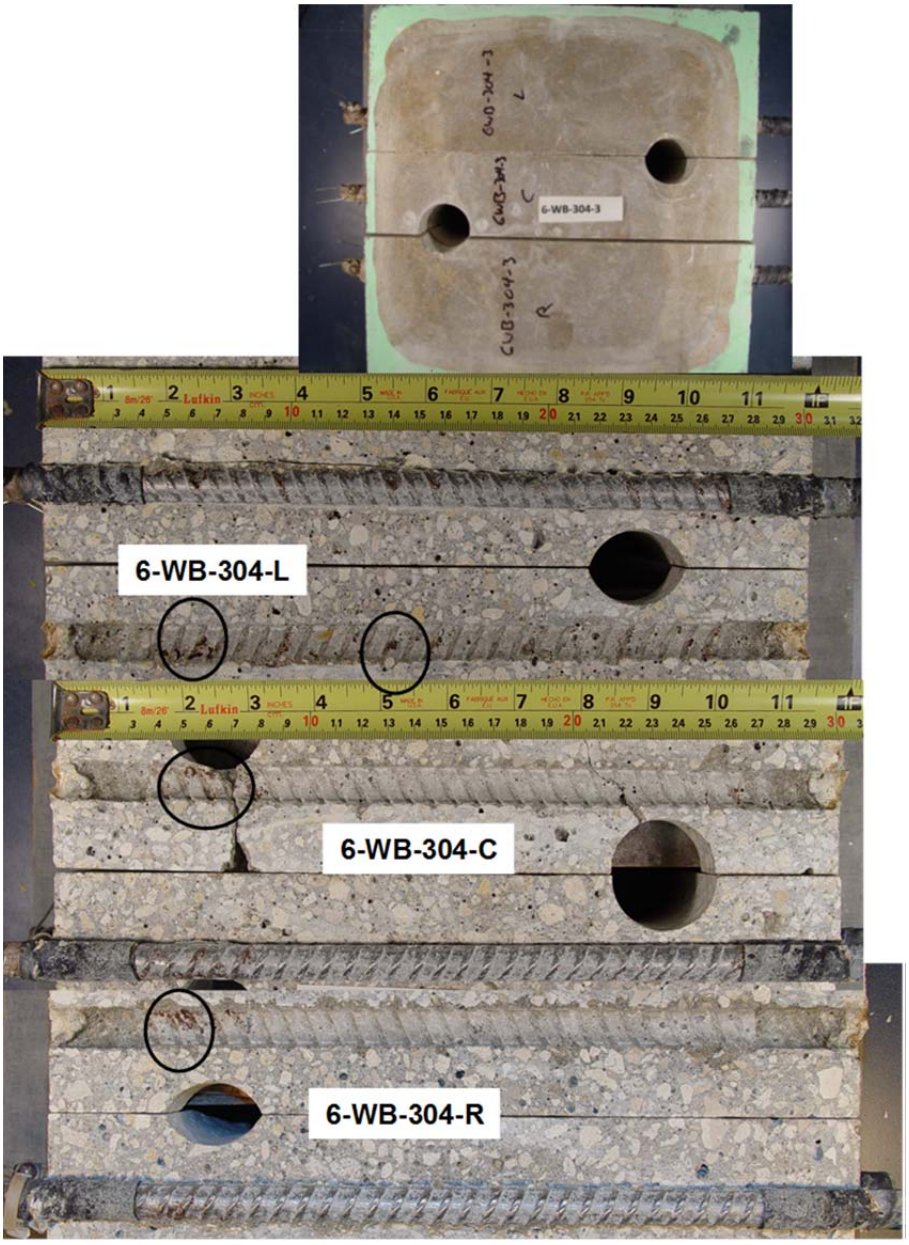

Figure 4.23: Photographs of top rebars and bar trace of specimen 6-WB-304-1 subsequent to dissection

Figure 4.24 shows photographs after cutting and subsequent to the dissection that took place for 2-WB-316-1. This specimen had been exposed outdoors to NaCl solution cycles for 3600 days by the time the specimen was terminated. All three rebars show corrosion, however the corrosion spots were found along the ribs of the rebars. With rebar A (left) and B (center) rebar having a greater coverage compared to rebar C (right rebar). Similar to what was discussed for WB-304 specimen, the corrosion products had turned red by the time the specimens were open. Rebar B (center) also had a large corrosion spot close to edge and it is believed that a differential aeration cell (easier access to oxygen) might have contributed for more aggressive corrosion at this site. For this spot, the corrosion products were black/dark green and were easy to observe on the rebar trace. Upon removing the rebar, dark corrosion products were visible at the rebar surface. On the left column are close-ups before cleaning and after cleaning. In this case the corrosion had penetrated a couple of millimeters.

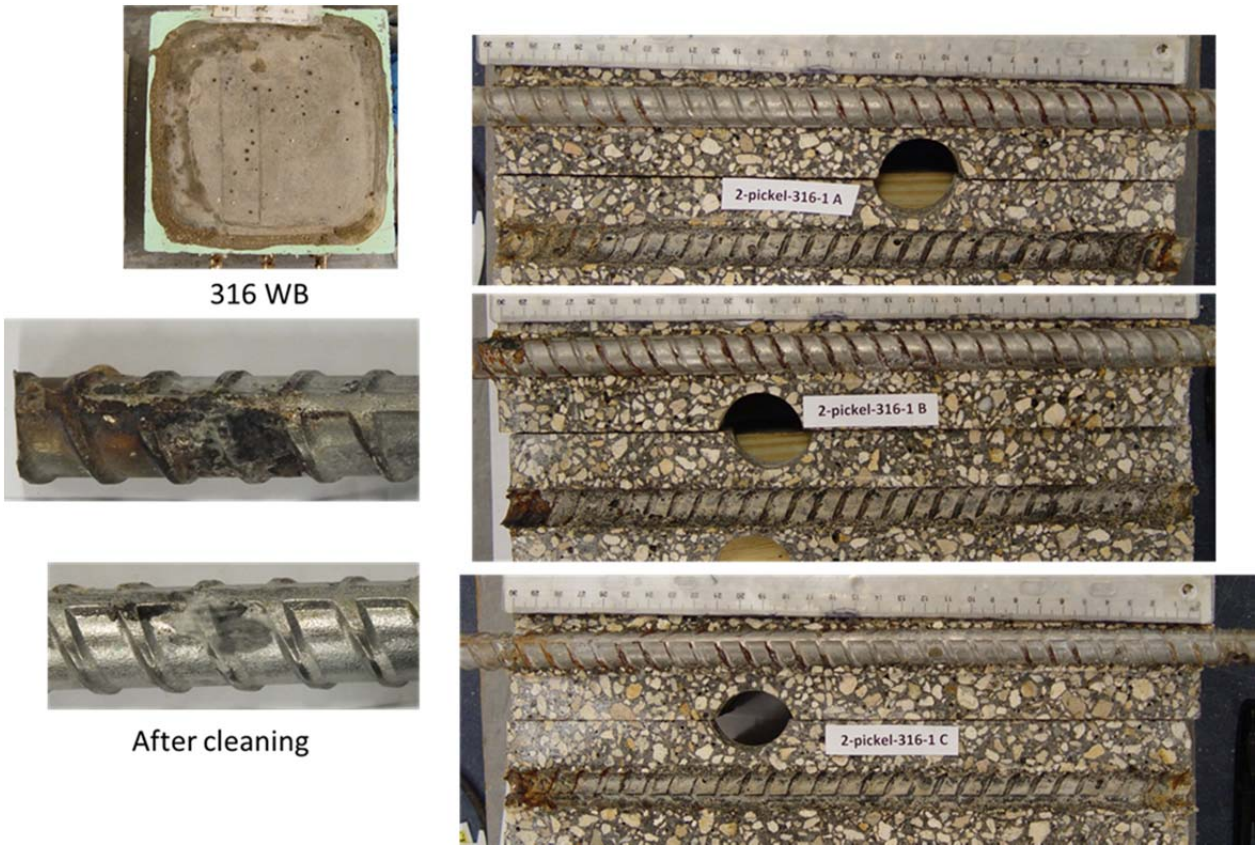

Figure 4.24: Photographs of top rebars and bar trace of specimen 2-WB-316-1 subsequent to dissection. The figure also shows close-ups of the larger corrosion spot before and after cleaning it

Two specimens with 2304 rebars were terminated. One was terminated after approx. 1700 days (specimen 5-STD1-2304-1) and the other specimen (5-STD1-2304-3) was terminated after ~2900 days of outdoor exposure to cyclic ponding with NaCl solution. Figure 4.25 shows photographs subsequent to dissection on 5-STD1-2304-1, only the right rebar show a corrosion spot. Figure 4.26 and Figure 4.27 shows photographs subsequent to

dissection on 5-STD1-2304-3, no corrosion spots were observed on the top row rebar as can be observe on Figure 4.25. However, one of the bottom row rebar shows a large corrosion spot close to the edge. No corrosion was observed underneath the shrinkage wrap. It is believed that a differential aeration was present at this location. By day 2900 the chloride concentration was as high or higher at the bottom rebar level than was observed at the top rebar depths at day 1700. It is not clear why corrosion initiated at this rebar and not at one of the rebars on the top layer.

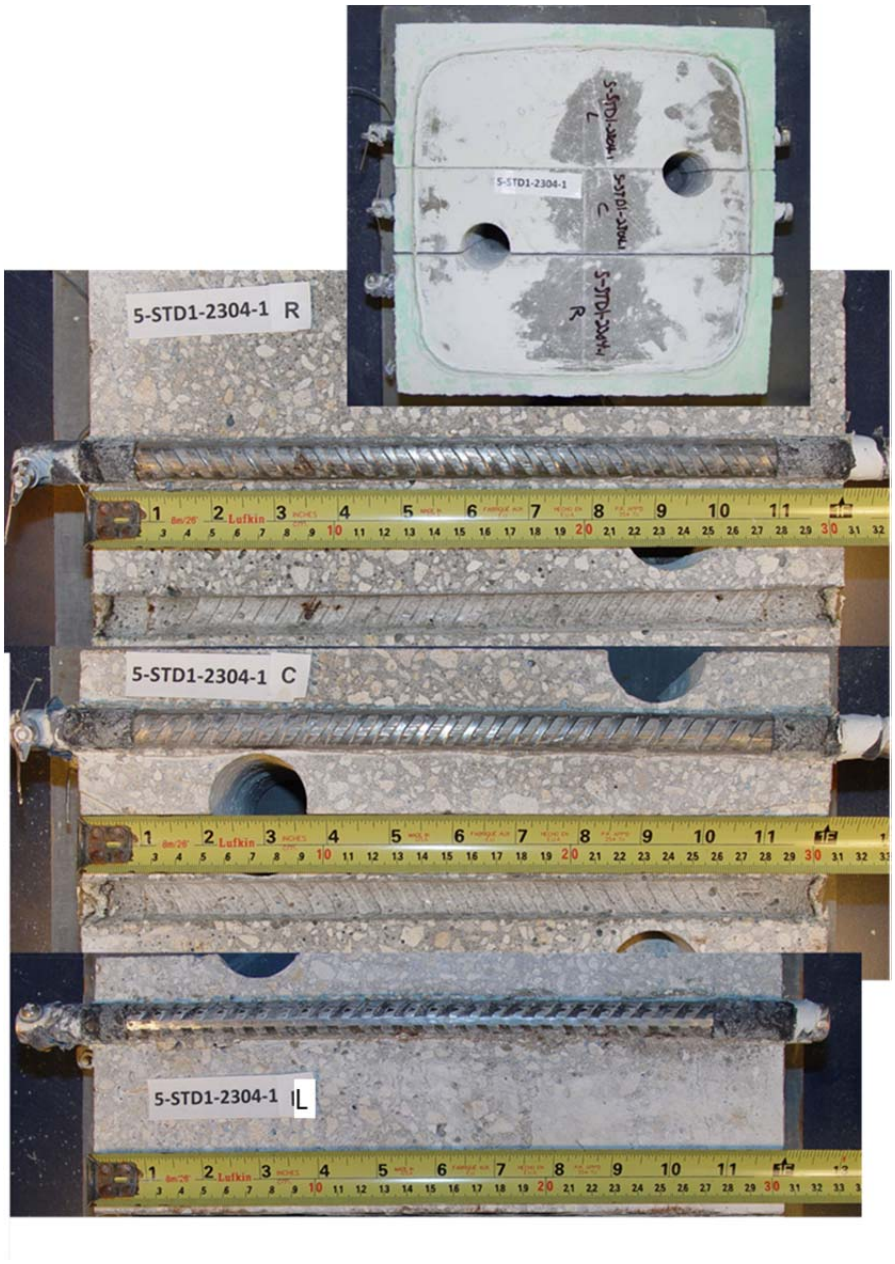

Figure 4.25: Photographs of top rebars and bar trace of specimen 5-STD1-2304-1 subsequent to dissection

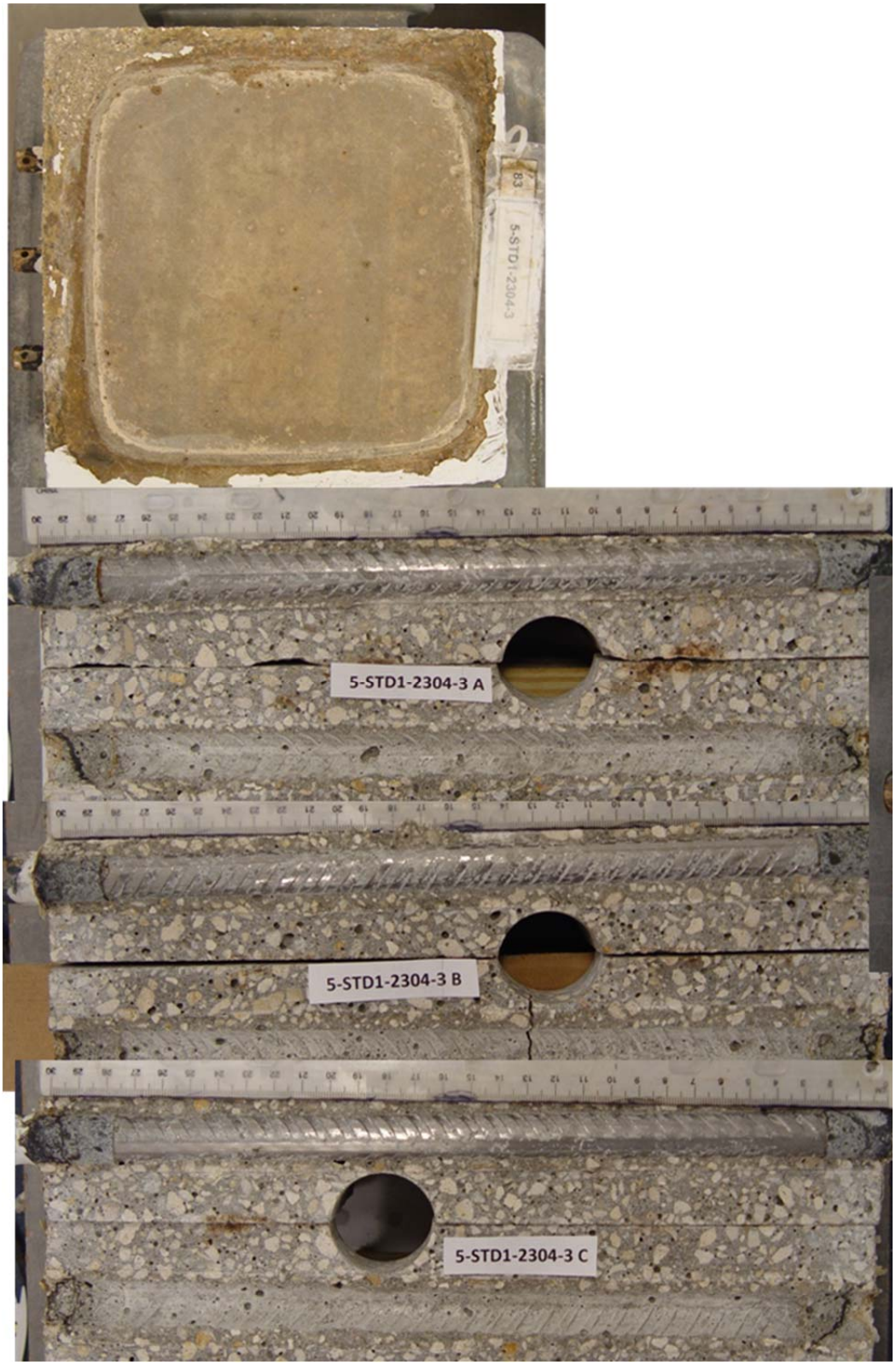

Figure 4.26: Photographs of top rebars and bar trace of specimen 5-STD1-2304-1 subsequent to dissection

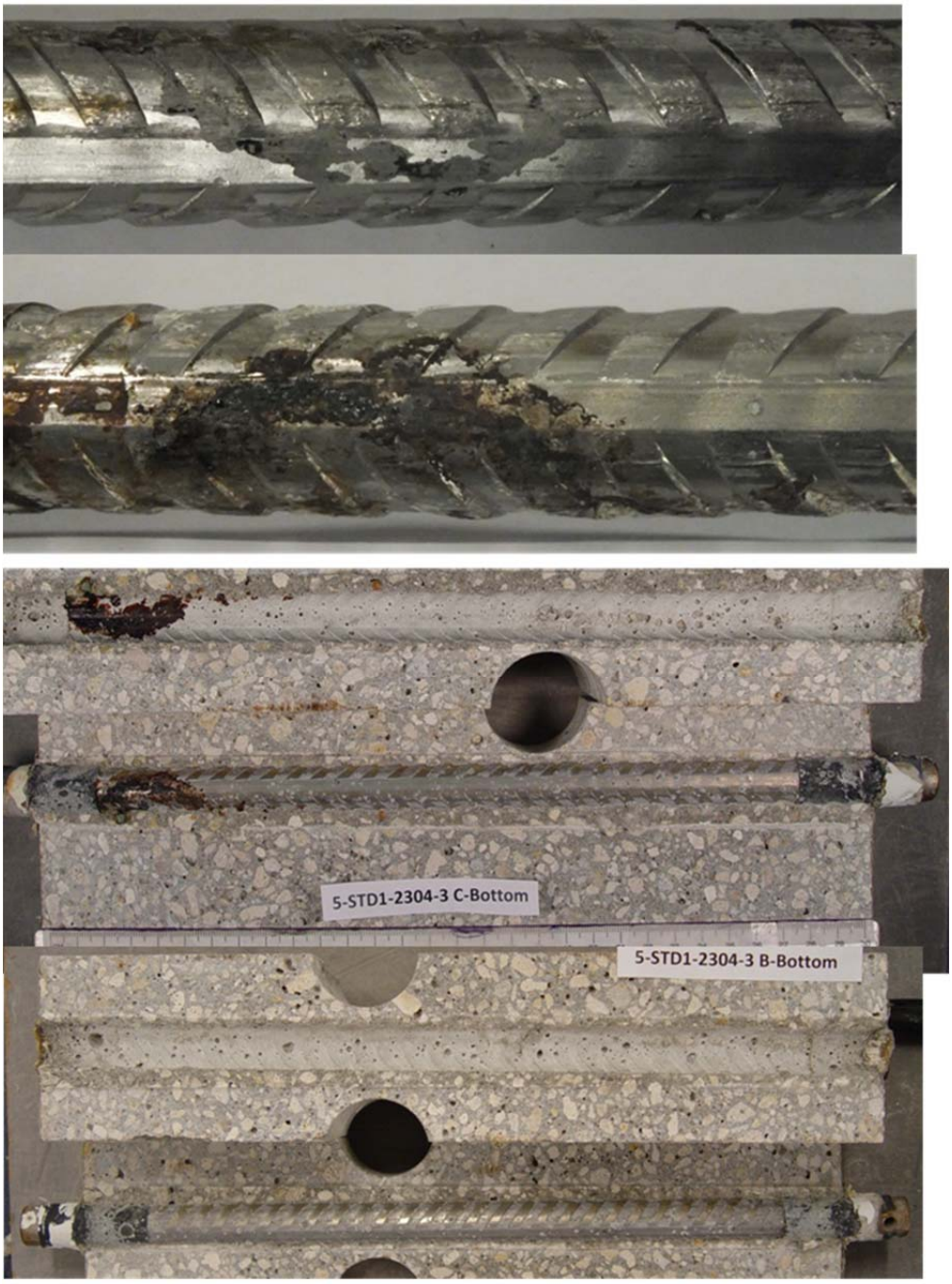

Figure 4.27: Photographs of two bottom rebars and bar trace of specimen 5-STD1-2304-3 subsequent to dissection. Close-up or large corrosion site before and after cleaning is also included

4.3.5 Outdoor Specimens

This section presents photographs on selected specimens that continue to be exposed.

4.3.5.1 BCAT specimens.

Specimens of type BCAT are shown in Figure 4.28. It is evident that the corrosion of the BB rebars on the bottom layer have progressed to such extend that crack have reached the top layer rebars on both shown specimens. The condition is worst for the specimen with 316, as it has been exposed for 10 years compared to 7 years of exposure for the specimen with 304 rebars. These photographs are a reminder that when the design of a structure calls for a high performance corrosion resistant alloy (e.g. 316 or 304 or comparable) on the outer layer only and BB on the interior layers, the concrete used in structure should still be of good enough quality to prevent corrosion of the BB on the inner layers.

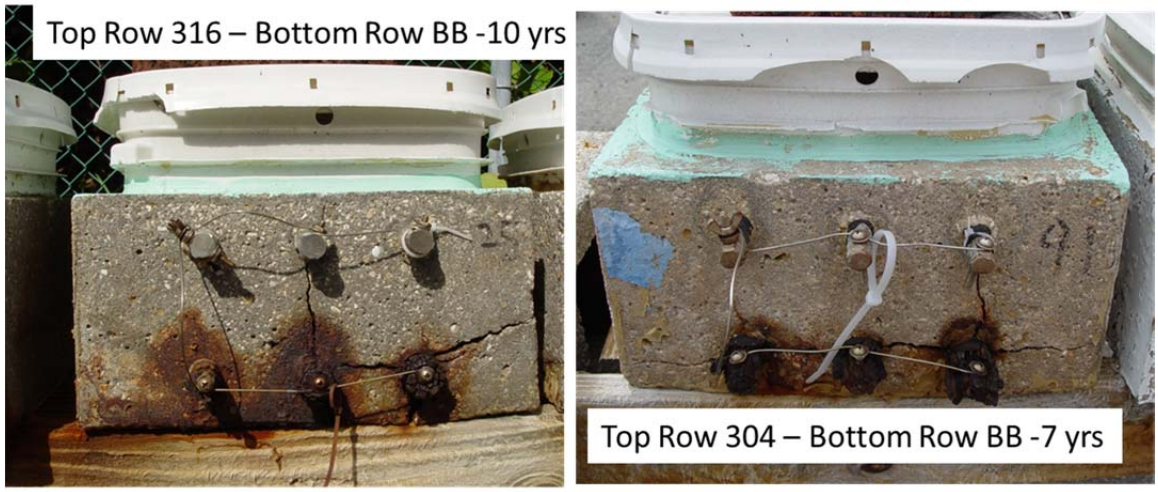

Figure 4.28: Current state for specimens 2-BCAT-316-2 and 6-BCAT-304-1

4.3.5.2 Selected cases in which specimens show corrosion spots on the surface.

These are cases in which the clad rebar was intentionally damaged and the specimen 3-CCRV-3Cr12-2&3. Figure 4.29 shows the current state of the surface condition for both remaining 3-CCRV-3Cr12. Both photographs show surface cracks, the picture on the left column shows the left rebar with a longitudinal crack (along the rebar) that then curved perpendicularly, and might have contributions from the corrosion products of the other two rebars. The picture on the right shows that the left and right rebars have thin longitudinal cracks parallel to the rebar. Figure 4.30 shows a 4-BCCD-SMI specimen on the picture on the left column and a 6-CVNC-SMI-3 specimen on the picture on the right. Specimen 4-BCCD-SMI show three corrosion spots at the rebar surface due to the intentional damaged done to the clad (3 mm perforations), whereas 6-CVNC-SMI is a specimen with crevice, but

with the cut surface of the clad rebar (under the pond) with no end-cap. Three distinctive spots are visible and next to the rebar on the right a small crack has appeared.

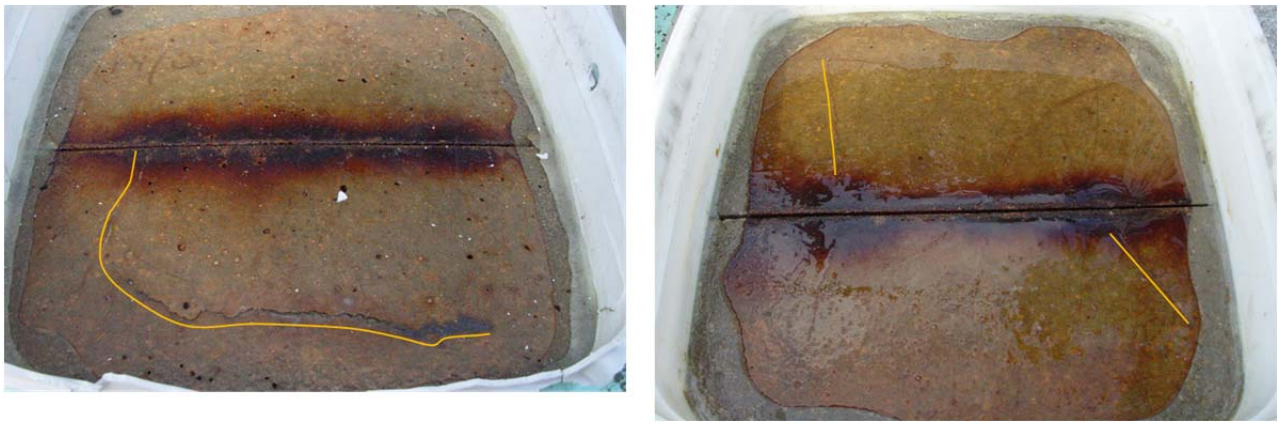

Figure 4.29: Pictures of the surface cracks on 3-CCRV-3Cr12 specimens

Figure 4.30: Pictures of the corrosion spots on the surface of 4-BCCD-SMI (left) and 6-CVNC-SMI-3 (right)

4.3.6 Discussion

So far no corrosion has initiated on specimens with 316 or 304 rebar in the as received condition even if crevice and crack were present (CCRV type). Specimens that were WB (304 or 316) appear to initiate corrosion at a lower chloride concentration than those in the as received condition. Specimens with clad and damage show some signs of corrosion also those with CREV with not end caps. Specimens with 2304 rebars appear to have a chloride threshold of approximately 6 wt/o cement. This chloride threshold is comparable to what others have reported for this alloy and it is also in agreement to the values reported in the CRA embedded in mortar chapter of this report. It might be desirable to continue the exposure and monitoring of the remaining specimens. Of particular interest

would be to not terminate any specimens on which corrosion initiates, but rather continue exposure until cracks are visible on the top surface. As the samples age the solution reservoir might need replacement and fresh layer of paint might also be in order.

4.4 CONCLUSIONS

Specimens with 304 and 316 rebars appear to be viable rebar candidates when a long service life is desired.

Specimens with 304 and/or 316 that experienced wire brushing before embedding them into the concrete experienced corrosion after more than five years of exposure, but the corrosion appears to be propagating at a slow rate.

When considering placing high performance corrosion resistant alloys on the outer layer and carbon steel in the inner portion, concrete quality should be such that the permeability is low. Otherwise, situations as shown above might occur.

Intermediate CRA as 3CR12 produced cracks at the rebar surface due to corrosion products build up. The cover was small on these specimens due to simulated crack and also crevice condition was present. Specimens with similar geometry that contained 316 show no signs of corrosion.

Specimens with 2304 rebar appear to initiated corrosion at 5 wt% cement, but propagate at a slow rate.

5 ACCELERATED CHLORIDE TRANSPORT TO INVESTIGATE CORROSION INITIATION AND PROPAGATION OF DUPLEX STAINLESS STEEL EMBEDDED IN CONCRETE

5.1 ABSTRACT

Two duplex stainless steels rebars: UNS32304SS and UNS32101SS were selected to investigate the corrosion initiation and propagation in reinforced concrete specimens. No chlorides were added to the concrete mix. Three of six embedded rebars had one inch concrete cover. A methodology was implemented to accelerate the chloride transport. The solution used was 20% NaCl by weight. First, cyclic ponding in a moderate elevated temperature (37°C) curing room took place, followed by a migration cell approach at laboratory room temperature. This methodology allowed corrosion to initiate in a relative short period of time (months rather than years). After corrosion had initiated and propagated for some time; selected specimens were terminated for visual examination. On specimens selected for autopsy, the rebars in the top row showed corrosion to various degrees. Corrosion had propagated to such extent on the terminated specimens that cracks had appeared at the concrete surface. Stray current likely caused accelerated corrosion on rebars where corrosion had initiated first. Based on chloride concentrations measured at the rebar trace, corrosion initiated: on UNS32101 rebars on average at 7.9 kg/m^3, and UNS32304 rebars on average at 6.0 kg/m^3. The findings also suggest that UNS32304 rebars corroded at a slower rate than UNS32101.

5.2 INTRODUCTION

Corrosion of the reinforcing steel due to chloride ions is a major concern that bridges and other structures face when exposed to marine environments. There are two periods that typically model the service life of a reinforced concrete structures: 1) time to corrosion initiation, (once a critical chloride threshold concentration (C_T) is exceeded) and 2) corrosion propagation stage [8] [9] [10]. The time to corrosion initiation of corrosion resistant alloys (CRAs) reinforcements embedded in concrete is expected to be significantly longer than for carbon steel rebars. The longer time to corrosion initiation is due to the higher C_T of these alloys [8] [9]. Once C_T is exceeded at the rebar trace corrosion initiates and the corrosion propagation stage begins.

Corrosion propagation stage is usually assumed to last a few years (typically five years). This duration applies to carbon steel rebar embedded in concrete of moderate durability. Corrosion is assumed to propagate at a slower rate on CRAs. However, it is unknown how long would the propagation stage would be for CRAs or how corrosion would spread during the propagation stage. Most experimental work has been done to determine the time to corrosion initiation and chloride threshold with the specimens terminated shortly after corrosion has initiated. Several authors have investigated corrosion of the CRAs as an alternative to carbon steel reinforcement

as an approach to achieve bridge repair-free service life in excess of 75 years. Currently a couple of US state DOTs (Virginia and Oregon) require CRAs rebars be used in new bridge construction exposed to aggressive chlorides environments. Previous studies [8] [9] [11] have identified duplex stainless steel and austenitic stainless steel (with high PREN and with Ni and Mo) as alloys with a high chloride threshold. One of the methods developed to determine the chloride threshold concentration was to do an anodic potential hold (+200 mVsce) on the studied alloys while exposed to simulated pore solution with chlorides [12] [13]. Tests in solution provided comparable ranking of the different alloys. However, not enough time was usually allowed during initial immersion in simulated pore solution for a mature/thick passive layer to form before adding the chlorides. A mature passive layer is expected to be present on CRAs embedded in concrete when the chlorides ions arrive. Based on previous studies, that reported chloride thresholds, a relative high chloride concentration was usually first added to the solution when the more corrosion resistant alloys were exposed. In recent years the use of corrosion resistant alloys (e.g. duplex stainless steels) has been suggested as a way to achieve a long maintenance-free service life [11]. Two corrosion resistance alloys (CRA) duplex stainless steels rebars: UNS32304 and UNS32101 embedded in concrete were selected in this study to investigate corrosion initiation and corrosion propagation stages.

5.3 EXPERIMENTAL PROCEDURE

The selected reinforced concrete specimen geometry simulates a bridge deck. The simulated deck slab specimens are 30cm wide, 30cm long and 15cm high as shown in Figure 5.1. The specimens were made in two batches with the same procedure and mixture composition: 390.4 kg/m^{3}cementitious content and the concrete unit weight 2230 kg/m^3, #89 limestone gravel as coarse aggregate, standard Florida's river sand, 10% fly ash as cementitious replacement and 0.42 water/cementitious (w/cm) ratio. Six specimens per batch were casted, which consisted of five specimens with reinforcement and one blank specimen (i.e. with no rebar). Each specimen with reinforcement was fabricated with six embedded bars, three of which are located in a top row and the other three are located in a bottom row (see Figure 5.1 and Figure 5.2 for dimensions and a nomenclature of the specimen).

Stainless steel UNS32101 rebars were embedded in batch-1 samples and UNS32304 rebars were embedded in batch-2 samples. The rebars were in the as received condition and according to the manufacturer these had been properly pickled. The rebars on the top layer (were facing the bottom during casting) are 2.5 cm below from the concrete top surface (concrete cover). Each rebar is approximately 1.65 cm in diameter (#5) and approx. 35 cm long. It can be observed from Figure 5.1 and Figure 5.2 that the rebars project out approximately 2.5 cm from the concrete block on both sides. The rebar section outside and about 2 cm inside of the concrete block was wrapped at both ends with a plastic heat shrink tubing. An activated titanium mesh was placed on the top side of the concrete (embedded into the concrete by a few mm) when the specimens were casted (see Figure 5.1 dotted line

on front view, depth not to scale). This top side at cast is the bottom surface during exposure. No chlorides were added to the concrete at casting.

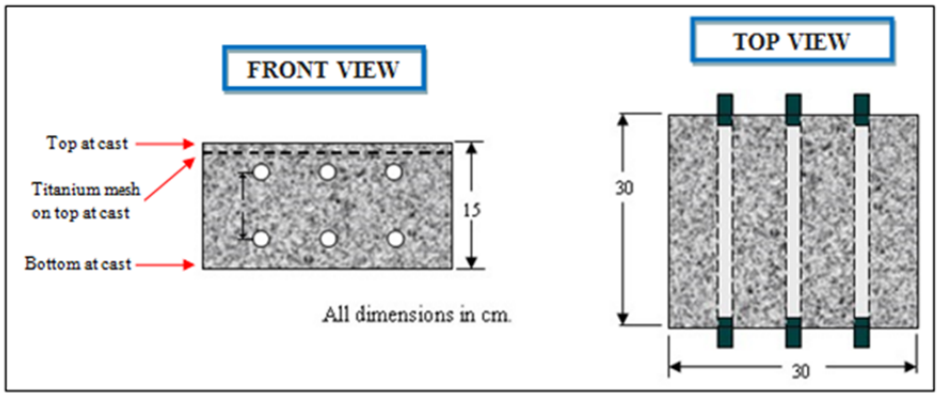

Figure 5.1: Sample schematic, dimensions and specifications

The specimens were prepared at the FDOT state materials office (SMO). The molds were removed 24 hours after casting. Then specimens were placed in a high moisture environment (fog curing room) for about 45 days at SMO-FDOT. The specimens were then transported to Florida Atlantic University (FAU) laboratories at SeaTech. The specimens were exposed for 15 days to laboratory humidity and temperature (65-70% RH and 22°C). Once at SeaTech, the samples were inverted (i.e. bottom at cast is now top of the specimen). During these 15 days, a reservoir was made of acrylic, and was attached with a marine contact adhesive and sealant (See Figure 5.2) on the top face of the specimen. Each rebar was drilled and tapped on one end to accommodate stainless steel machine screws that were then used as electrical contacts (See Figure 5.2). Stainless steel screws were installed and adjusted with two washers, a nut and butterfly nut on each rebar to ensure good electrical connection. These connections were used during the electrochemical measurements.

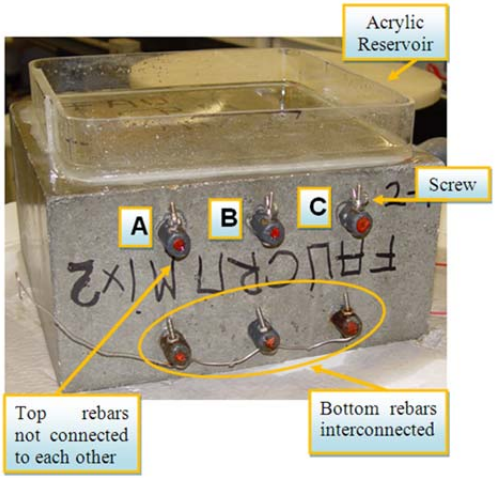

Figure 5.2: Picture of the specimen

5.3.1 Accelerated Chloride Transport Methods

A methodology was implemented to accelerate the chloride transport and it is divided into two phases: Phase I (wet and dry cycles) and Phase II (application of electric field).

Method during Phase I: Phase I took place when the specimens reached 60 days of age (45 day fog room + 15 laboratory room temperature) During these initial 60 days the passive layer likely formed naturally on the rebar surface and continued to grow during phase I. The specimens were exposed in an elevated temperature room (37.8 °C) for 120 days. The elevated temperature room has a system of three heaters; each one is connected to a digital temperature controller to ensure that the room is at the desired temperature; it also has two fans to circulate the air around the room. Specimens were exposed to dry and wet cycles: three days dry and four days wet. The solution was 20% sodium chloride reagent grade (percentage by mass) and was added to the reservoir during the wet exposure days. This method allows the chloride to be transported through concrete faster due to the higher temperature (hence higher diffusivity) but similar to what is typically done in the laboratory under room temperature. Also, it is likely that the passive layer continue to form, as the chlorides might have not reached the rebar surface within the 120 days of exposure or a low chloride concentration might be present at the rebar depth of those on the top row. In the wet part of the cycle, the NaCl solution is transported by diffusion and capillary suction. During phase I, open circuit potential (OCP) measurements were taken twice per week for each rebar on the top row named A, B, C and for the three bottom interconnected-rebars. The readings were made with a high impedance voltmeter and a saturated calomel electrode. Linear polarization was performed only once during this period on selected specimens and on selected rebars.

Method during Phase II: The specimens were placed back in the laboratory room temperature (22ºC), in high humidity chambers. Each high humidity chamber was made of a prismatic plastic container of 62 cm width, 90 cm length and 20 cm height. The bottom 2 cm of each chamber was filled with fresh water. Then, three white plastic (HDPE) square pieces of about 4 cm height, 4 cm width and 70 cm length were placed on the bottom surface to support the samples and also to prevent the water at the bottom from directly wetting the specimens. Two specimens were placed on every chamber. Once transferred from the elevated temperature room, the side faces of the specimens were sprayed with water every day for 7 days to increase the moisture content of the concrete. This wetting continued during phase II as required (usually twice per week). It is very important that the specimens are as water saturated as possible prior the application of the electric field method in order to have an efficient chloride transport via migration [14].

A second activated titanium mesh was placed on the solution reservoir. The 20% sodium chloride solution remained in the reservoir all the time and was periodically changed (every three to four weeks). An electric field was then applied periodically to accelerate the chloride transport via migration. A 20 V potential difference was applied between the two activated Ti MMO meshes and was provided by a power supply (initial and later applications were done at 15 V). The positive pole was connected to the bottom mesh, which was already embedded into the concrete, and the negative pole was connected to the top mesh placed on the solution reservoir. With this set-up the electric field accelerate the chloride transport down through the concrete by migration. The voltage applied to the specimens with the electric field was removed periodically to monitor the rebars off potential evolution and to identify when corrosion might have initiated. See the appendix of this chapter for the applied voltage schedule showing the days when the electric field was applied for each specimen.

Batch 1 samples were transported to the RT high humidity chamber on day 120 of Phase I and Batch 2 samples were transported one week later. The electric field was applied first on Batch 1 samples with 15 Volts, but after the initial two periods the potential difference was set up to 20 Volts between the two activated Ti MMO meshes for all samples. This voltage adjustment was made to accelerate the chloride transport. A numerical model was implemented and the computed potential difference between the top surface and the top of a rebar with 2.5 cm concrete cover is 2.48 V when applying 15V and 3.25 V when applying 20 V between the two activated Ti MMO meshes. These two values were obtained by assuming that the rebar were conductive, if the rebars are assumed to be insulators (due to passive layer) the potential difference at the rebar surface are lower: 1.78 V (15V) and 2.38 V (20V). The actual potential difference between the reservoir and the rebar top (2.5 cm concrete cover) likely is somewhere in between. While the electric field was removed, LPR and EIS were measured on rebars: A, B, C and the three interconnected-rebars (those on interconnected-rebars, only after day 24 and on selected specimens). These measurements were made one day or more after electric field removal. The rebar potential was measured a few seconds after removing the electric field, one hour, 24 hours and every other day if the specimen was left disconnected. The specimens were left disconnected for various durations (see below) of time. For cases in which the specimens were left disconnected for more than 20 days; subsequent potential measurements were performed weekly.

5.3.2 Linear Polarization Resistance (LPR) and Electrochemical Impedance Spectroscopy (EIS)

The solution resistance Rs was measured via EIS. The impedance magnitude measured at a frequency of approx. 60 Hz was assumed to be the Rs of the system. The linear polarization value measured is labeled on the axis as “Rp_meas”. The Rp_meas contains the solution resistance of the system. The linear polarization test was performed from 15 mV below OCP to OCP at a scan rate of 0.1 mV/sec. The values shown in the results section are the Rp_meas minus Rs also known as Rc. An area of 1 cm was assumed during the test, but the actual area

under the ponding section is approx. 42 cm^2 for each rebar. For the bottom 3 interconnected-rebars as they are interconnected the measured area is 126 cm^2. The performed measurements were divided in two different sub-stages on each sample; one to five days of electric field disconnection was the time to allow the rebars to depolarize similar to what is done on an extended depolarization test; sub-stage two corresponds to test performed after five days of electric field disconnection and assumes that rebar potentials have no or very little residual polarization from the electric field.

5.3.3 Autopsy Procedure for Terminated Specimens

Three specimen(s) for each batch (Batch-1-1, Batcht-1-2, Batch-1-5, Batch-2-1, Batch-2-2, and Batch-2-4) that became active were designated for autopsy. These specimens were sectioned, the rebars of both layers exposed and evaluated according to the following procedure:

1. Testing/exposure was terminated, the solution in the reservoir removed, and the acrylic reservoir removed,
2. Four (or two) cores were obtained from in between the rebars on the clear space where no rebars are on the way. Each core is drilled from the top surface all through the bottom surface of the specimen. The obtained cores were 3 cm in diameter.
3. Two of the cores (one per each side) were sliced for chloride profiles. Six slices were obtained with a wet saw. Each slice was marked every 0.635 cm (actual slice is thinner due to thickness of the blade). Then each slice was pulverized to perform chloride analysis.
4. After coring, two saw cuts were then made on each specimen. Each cut was made parallel to the rebar length. These cuts were made at equi-space between the center rebar and each of the two outer bars.
5. For each of the three resultant concrete sections, additional secondary saw cuts were made on each of the new exposed cut faces and on the side faces. The cuts were made parallel to the top surface such that the top and bottom rebars could be exposed. The cut was made to a depth approximately 10 mm from each rebar. This procedure was performed at both rebar depths.
6. Each specimen section was split open by placing a chisel in one of the secondary saw cuts from step 5 and tapping gently with a hammer until fracture occurred. This exposed both the rebar and its trace, which were then examined for corrosion products and photographed.
7. The rebars surface condition (with corrosion products if already corroding) was captured in pictures as seen just after opening them. Then, a plastic brush was used to remove as much of the corrosion products from these rebars. After this partial cleaning, close up pictures were taken on selected rebars with a stereo microscopy. This was done to appreciate in more detail the corrosion extent. Finally, the corrosion product was removed from each rebar segment per ASTM G-01. This was achieved by repeatedly conducting a

procedure of immersion in cleaning solution (93.5 wt% HCl + 0.7 wt% Sb_2O_3 + 4.7 wt% $SnCl_2$) and then brushed to remove any remaining corrosion products (multiple times if needed until the rebar weight stopped changing). After this additional clean-up, additional close up pictures were taken with a stereo microscope to document and appreciate in more detailed the corrosion extent (once the corrosion products have been removed) into the rebar (i.e. to identify how much rebar section was lost).

8. The concrete section above the rebar trace of the top-row rebars was milled and collected to obtain the chloride concentration above the rebar trace. (Portions with corrosion products if present were avoided)

5.3.4 Chloride Analysis

The chloride concentration was determined via a slightly modified FDOT method [2] at the rebar trace and at the different concrete depths (sliced cores). This method measures the total amount of chlorides.

5.4 RESULTS

5.4.1 Phase I

The plots on Figure 5.3 show typical potential evolution vs. time for samples batch 1-5 and batch 2-1. The potential evolution during phase I for the other samples from batch I and II are included in reference [10] and in the appendix of this chapter. Initially the measured potential of the rebars embedded in batch 1 specimens ranged between ~-50 and ~-200 mVsce. The potential of rebars embedded in specimens of batch 2, initially ranged from ~-100 to ~-240 mVsce. The potential values of UNS32304 (batch 2) rebars are more negative than the potential values of UNS32101 (batch 1) rebars. Over the first 80 days the potential values of all rebars tend to shift slightly more positive values. Towards the end of phase I (last two sets of measurements) some of the rebar potentials dropped slightly (by ~ approx. 25 mV). The observed potential values suggest that corrosion did not take place on neither of the CRA rebars during phase I. The average of the last five potential measurements in phase I for UNS32101 rebars was -121 mVsce while the average of the last five measurements potential value for UNS32304 rebars was -179 mVsce.

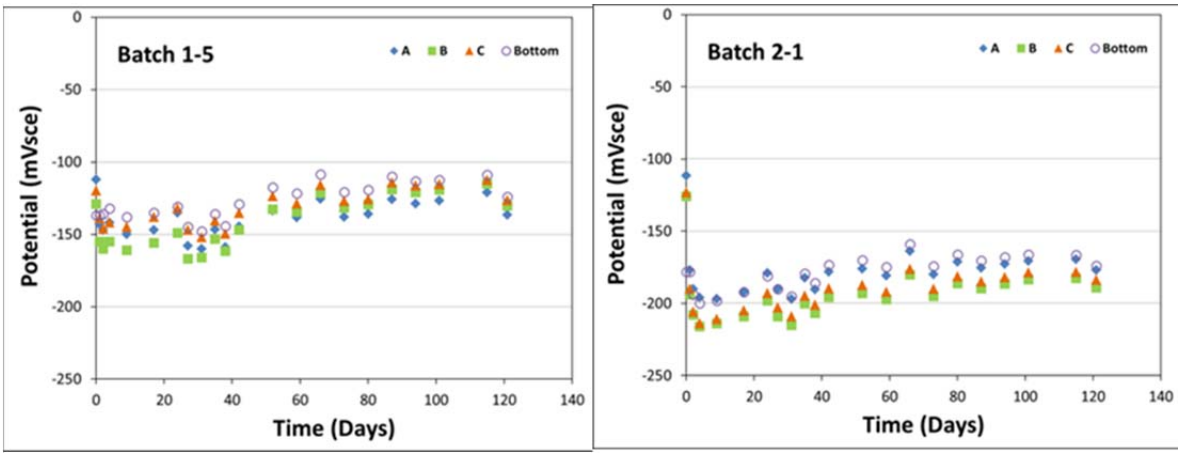

Figure 5.3: Batch 1 & batch 2 potential measurements over time during Phase I

5.4.2 Phase II

The number of days shown in the plots is counted with respect to day one of phase II. (i.e., for batch-1 specimens day 1 is 12/14/2012, and for batch-2 specimens day 1 is 12/20/2012). Figure 5.5 shows plots of the potential evolution vs. time measured during phase II on rebars of batch 1-1 (S32101) and batch 2-1 (S32304) specimens measured while the electric field has been removed. Here the filled symbols correspond to measurements taken between one and five days after the electric field has been disconnected; empty symbols correspond to measurements taken after more than five days of the system being disconnected. Figure 5.4 shows a graphic explanation of this labeling arrangement. This methodology allows to observe the rebar potential drift (due to depolarization) after each electric field application.

As indicated above Figure 5.5 on the left side shows the potential evolution of the reinforcement during phase II measured on specimen batch 1-1. The initial measured potential values ranged from ~-96 mVsce to ~-126 mVsce before applying any electric field. After spraying water on the samples in the high humidity chamber and the initial electric field application for one week, the potential values of the rebars became slightly more positive (compared to the initial values). Then, upon subsequent application of additional electric field periods, the measured potential values dropped considerably. By day 61, and four days after removing the electric field, the rebar OCP values ranged from ~-277 mVsce (Rebar A) to ~-357 mVsce (Rebars B and C). Later, by day 98 (after 38 day of the electric field being disconnected), the potential of rebars A and B had shifted to more positive potential values and remained stable at ~-83 mVsce and ~-136 mVsce respectively; but, rebar C only recovered slightly and the potential remained at ~-320 mVsce. Finally, after additional periods of electric field application, on day 166 four days after removing electric field the potential of the top row rebars ranged from ~-440 mVsce to ~-484 mVsce. The potential of the top row rebars ranged between ~-341 mVsce and ~-572 mVsce by day 188 (~46 days after this last disconnection), suggesting that corrosion might have initiated. Batch-1-1 specimen was

terminated on day 189. The potential evolution of the rebar in the other four specimens batch-1-2, 1-3, 1-4, and 1-5 have similar behavior than that described above for Batch-1-1 specimen and the plots can be seen on [10]. After several applications of the electric field (i.e. chloride have been transported to the rebar surface) the potential values measured on the top row rebars dropped significantly. The rebar potential values < -300 mVsce were observed on: By day 157 on two rebars of Batch-1-2 specimen (this specimen was terminated on day 158); and by day 188, on two rebars of Batch-1-3 specimen, three rebars on Batch-1-4, and two rebars on Batch-1-5 (all rebars on the top layer).

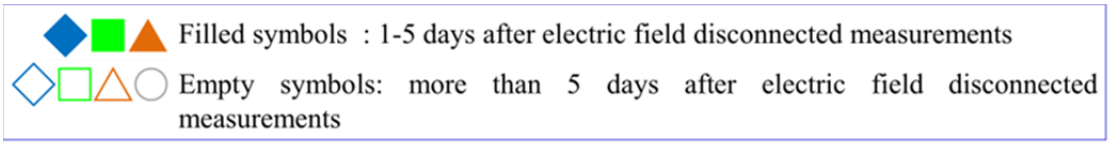

Figure 5.4: Plots symbols clarification

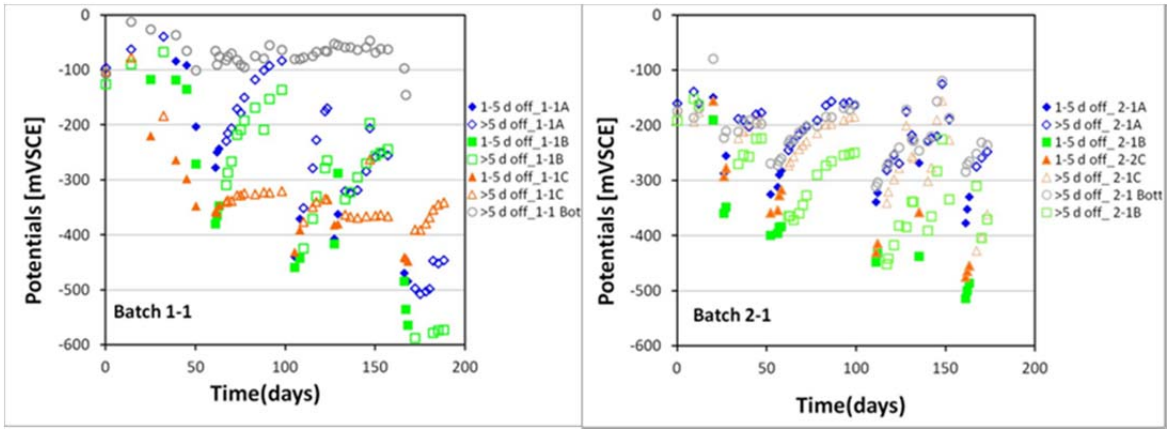

Figure 5.5: OCP measurements over time for Phase II plots of samples Batch 1-1 and 2-1

Figure 5.5 on the right side shows that the initial potential values measured on the rebars of batch-2-1 specimen ranged from ~-160 mVsce to ~-192 mVsce. Upon applying electric field a few times the measured potential values dropped considerably. On day 61 the potential values ranged from ~-252 mVsce to ~-399 mVsce (four days after the electric field had been disconnected). After 38 days of no electric field application (i.e. by day 100), the potential values of the rebars shifted to more positive values and then remained stable at potential values that ranged from ~-163 mVsce to ~-249 mVsce. After additional periods of electric field were applied the rebar potential values ranged from ~-440 mVsce to ~-484 mVsce by day 162. By day 183, after the electric field had been disconnected for 21 days the potential value of rebar A was ~-203 mVsce and rebars B and C potential values were ~-301 mVsce and ~-305 mVsce, respectively, suggesting that corrosion might have initiated on rebars B and C. Batch-2-1 specimen was terminated on day 184. The potential evolution of the rebar in the other

four specimens batch-2-2, 2-3, 2-4, and 2-5 have similar behavior than that described above for Batch-2-1 specimen; the plots can be seen in [10] and in the appendix of this chapter. After several applications of the electric field (i.e. chlorides have been transported to the rebar surface) the OCP values had dropped significantly. Rebar potential values < -300 mVsce were observed on: by day 153 on two rebars of Batch-2-2 specimen (this specimen was terminated on day 154); and by day 188 two rebars of Batch-2-3 specimen, one rebars on Batch-2-4specimen, and no rebars on Batch-2-5 specimen.

Figure 5.6 shows the effective Rc evolution measured on the specimens of batch 1-1 and 2-1 during phase II. The Rc (Rp_{meas}-Rs) values shown has the solution resistance subtracted but the shown values are not corrected for area. The initial Rc measured values were performed on day 39 for batch 1-1 (Days counted from the beginning of phase II and three days after disconnection of the electric field application). The plot on the left in Figure 5.6 shows that the initial values of Rc measured on rebars of batch 1-1 specimen. The Rc ranged between 3.7 KΩ and 10.4 KΩ by day 39, after three days of the electric field being disconnected. Then, after additional electric field application the measured Rc values dropped considerably. By day 108, the Rc values ranged from 0.8 KΩ to 1.1 KΩ - three days after disconnecting the electric field. On day 157, i.e., after 28 days of the electric field being disconnected the Rc values increased to values that ranged from 3.5 KΩ to 4.6 KΩ. Upon additional electric field application, the Rc values dropped again considerably. On day 168 the Rc values of rebars were very small, ranging from 0.2 KΩ to 0.7 KΩ - one day after the last electric field application. Then, after 20 days (i.e., by day 188) of the electric field being disconnected, the Rc values slightly increased and were stable at a range of Rc values between 0.4 KΩ and 1.5 KΩ. This suggests that by then corrosion or other electrochemical reactions were taking place at a high rate. The lower potential values and smaller Rc values are believed to be due to the presence of chlorides at the rebar's surface exceeding the critical concentration, which is likely at a concentration high enough to initiate corrosion. The application of the electric field polarizes anodically the rebars (due to the ionic current); this polarization might have caused corrosion to initiate at a lower chloride concentration than would be observed under natural exposure. The large exposed surface area (when compared to that usually used when this alloy is tested in simulated pore solution) might have increased the chance of corrosion initiating at a lower concentration. The smaller Rc values measured during the propagation (once corrosion has initiated) are also influenced by the residual effects of the additional electric field applications and any remaining ionic current present (i.e., stray current on those where corrosion had initiated), this likely caused a faster rate of corrosion which in turn produced corrosion products at a higher rate than if corrosion had initiated and progressed naturally. The Rc evolution of other samples (batch 1-2, 1-3, 1-4, and 1-5), also have similar behavior as described for batch 1-1 specimens and the plots can be seen in [10] and in the appendix of this chapter. After several applications of the electric field, the Rc values dropped. Rc values measured on rebars B and C were < 4 kΩ by day 158 on

specimen 1-2. Similarly the Rc values measured on rebars B and C on specimens 1-3 and 1-4 were < 4 kΩ by day 188. For specimen 1-5, only the Rc value measured on rebar B was < 4 kΩ by day 188.

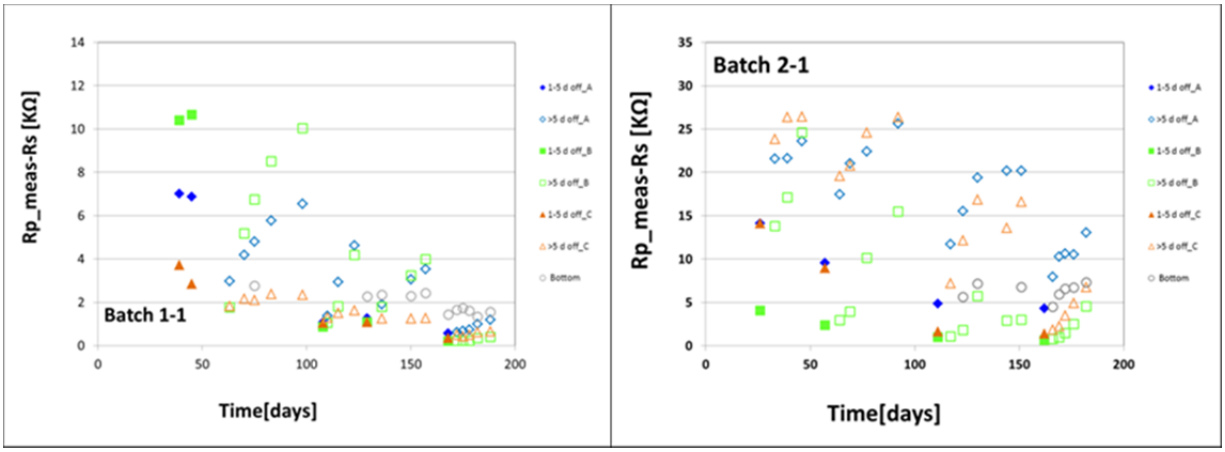

Figure 5.6: Rp_meas-Rs over time for Phase II plots of samples Batch 1-1 and 2-1

The plot on the right in Figure 5.6 shows that the initial Rc values measured on rebar of sample batch 2-1 ranged between 4 KΩ and 14.1 KΩ on day 26 (3 days after the electric field has been disconnected) and shifted to 25 KΩ while disconnected. Then after an additional period of electric field application the Rc value measured were were somewhat smaller than those measured on day 26. On day 57 the Rc values ranged from 2.4 KΩ to 9.5 KΩ. These measurements were performed one day after the electric field had been disconnected. Subsequently, the measured Rc values increased and ranged from 15 KΩ to 26 KΩ by day 92, after the electric field had been off for 35 days. Upon two additional electric field applications; the measured values of the Rcs dropped considerately. On this specimen, day 165 was the last day when the electric field was applied. The measured Rc - three days after electric field had been disconnected (day 168) - values were smaller than 5 KΩ and that measured for rebars B and C < 1 KΩ. Then the values of rebars B and C recovered and became stable at 4.5 KΩ and 6.7 KΩ respectively by day 188 (46 days after the last disconnection). For rebar A the Rc value reached a value of 13 kΩ by day 188. Rebars B and C showed a negative potential (<-300mVsce) on day 188, and a Rc values < 7 kΩ. This set of values might suggest that corrosion might have initiated on these two rebars. The Rc evolution of the rebars on the other specimens (batch 2-2, 2-3, 2-4, and 2-5) also shows similar behavior as described above and the plots can be found in the appendix of this chapter. The Rc values measured on rebars A and B in sample 2-2 were below 5 kΩ on day 153 (this specimen was terminated on day 154). By day 188 the Rc values measured were < 5 kΩ: on all top row rebars in sample 2-3 and on rebars B and C in sample 2-4. However, the Rc values of all rebars in sample 2-5 were > 9 kΩ on day 188.

5.4.2.1 Observed Surface Cracks

Several days to several weeks after corrosion had initiated on one or more rebars, the top concrete surface (i.e., reservoir face) of some specimens of both batch-1 and batch-2 started to show cracks. The propagation of the crack(s) was recorded and mapped in drawings. Each drawing was made in an engineering paper with 1.00:3.75 scale. The reported lengths are based on measurements made on the specimen and crack(s).

Figure 5.7 shows the propagation of the crack(s) on the top surface of specimen batch1-1 at the indicated dates. The red line(s) in the drawings represents the new crack length which was identified on the day of the inspection and the black line represents the crack lengths recorded on the previous inspection. No cracks were observed on day 168 on specimen batch-1-1. Then, during the next inspection on day 177, there was a crack as shown in Figure 5.7 by the red line. This was a very thin crack less than 0.01 cm. By day 185; the crack had propagated to other directions and the previously recorded crack became wider than before, but still less than 0.01 cm wide. The new crack branches can be seen by the red line. Finally, this specimen was terminated on day 186.

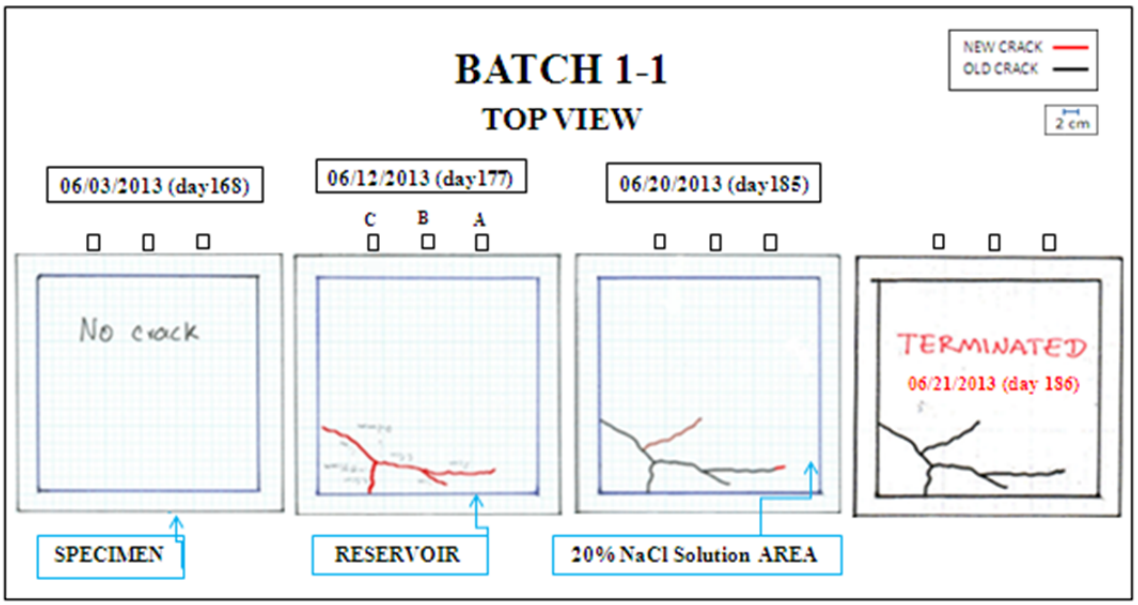

Figure 5.7: Diagram of the crack evolution over time for specimen batch 1-1

Figure 5.8 shows pictures of lateral sides for specimen batch 1-1 after performing the secondary saw-cuts. As shown in the figure, a crack was observed that was about 11 cm long and was observed on each of the three shown cuts corresponding to each top three rebars. It is not clear if the corrosion products from more than one rebar contributed to these observed cracks. According with the visual observation after autopsy (see following section); it is possible that the lateral crack might have initiated from the corrosion products of rebar B or rebar C. The crack was observed on both sides of the transversal faces (i.e. the crack was all across segment that contains rebar B) and extended to the other segments that contain rebars A and C.

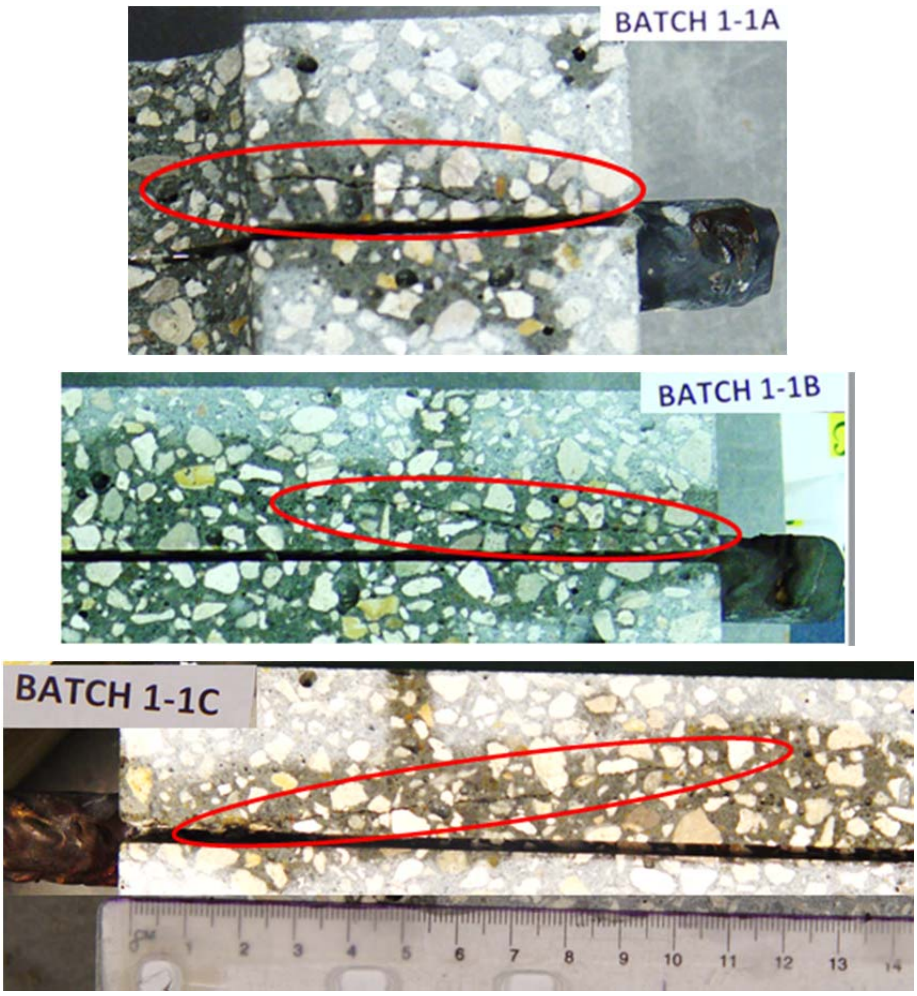

Figure 5.8: Lateral cracks pictures for specimen Batch 1-1

Figure 5.9 shows the propagation of the crack(s) observed on the top surface of specimen batch 2-1 at the indicated dates. The red line indicates the new crack length which was identified in the day of the inspection and the black line indicates the crack(s) length recorded on the previous inspection. For this sample by day 168 there were two cracks on both ends above rebar B (center rebar on top). Each crack length was about 4 centimeters (cm) long and less than 0.01 cm width. Then, during the next inspection on day 177 the cracks length did not change. Finally, by day 186 the cracks length still remained the same.

When comparing the crack evolution observed on batch 1-1 (Figure 5.7) and batch 2-1 (Figure 5.9) specimens, it is relevant to mention that the crack observed on specimen batch 1-1 grew up significantly from day 162 to day 179. On the other hand, the recorded cracks on batch 2-1 specimen did not change during the different inspections. The way the cracks evolved suggest that when the rebars on batch-1 (S32101) specimens corrode, the corrosion rate is faster than the corrosion rate observed on corroding rebars (S32304) from batch-2 specimens.

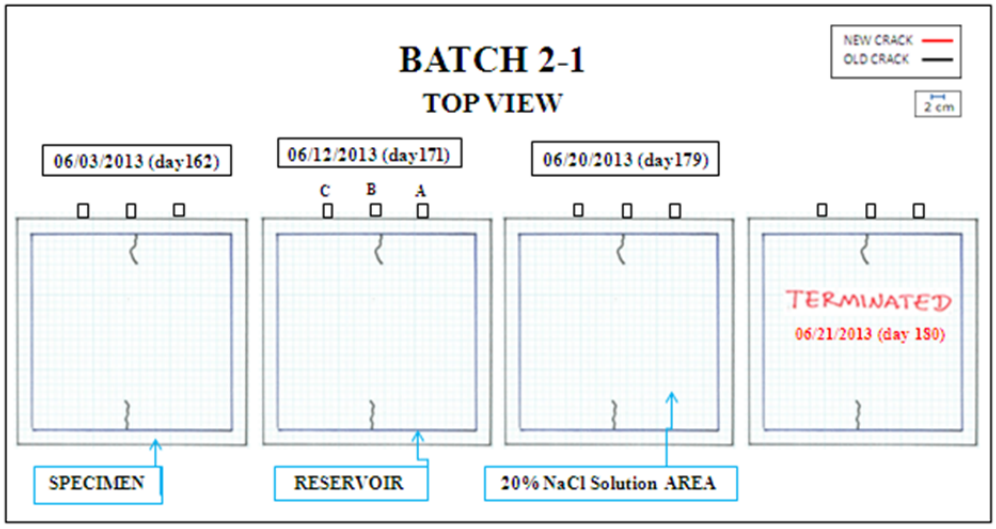

Figure 5.9: Diagram of the crack evolution over time for specimen batch 2-1

Figure 5.10 shows a picture of the top view of Batch-1-2 specimen. The picture also contains a highlighted view of the observed cracks (red lines drawn for emphasis). This specimen has a crack on each side of the middle rebar. Based on potential and Rc values, it is speculated that corrosion initiated on rebar B first and due to the additional electric field applied to attempt to initiate corrosion on rebars A and C, this caused corrosion to proceed at a high rate (due to stray current) which eventually lead to a crack(s) to be visible on the top surface of the sample.

All the other specimens of batch-1 (1-3, 1-4, 1-5) have visible crack(s) when inspected on day 162. During the inspection performed on day 200 all of the visible cracks observed on day 162 have grown over time. The Appendix for chapter 5 shows how the crack maps evolved with time for every batch-1 specimens (except for batch-1-2 specimen which was terminated on day 158).

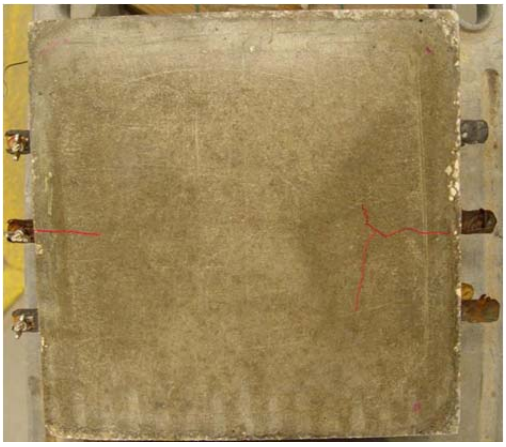

Figure 5.10: Picture of final crack pattern for specimen batch 1-2

Figure 5.11 shows a picture of the top view of Batch-2-2 specimen taken on day 152. The picture also contains a highlighted view of the observed cracks (red lines). The specimen has a crack on one side above the center rebar B. This crack extents parallel to the rebar approximately 7 cm long; about 3 cm of the specimen edge two crack branches expand perpendicularly to the left and to the right (each one approximately 6 cm long). Similar to what was described above for Batch-1-2 specimen, it is speculated that corrosion initiated on rebar B first and due to the additional electric field applied to attempt to initiate corrosion on rebars A and C, this accelerated corrosion on rebar B (due to stray current) which eventually lead to a crack to be visible on the top surface of the sample.

As indicated above, specimen Batch-2-1 showed one crack on each side (approximately 4 cm long each one) above and along rebar B (center rebar – Figure 5.9). These cracks were visible during the inspection performed on day 162; during subsequent inspections (up to day 185) the cracks lengths remained the same. Specimen Batch-2-3 showed no cracks during the initial inspection (day 162) nor after the inspection done on day 186. Sample 2-4 showed one crack on rebar B, approximately 7 cm long on the inspection done on day 162; after inspection done on day 185 the crack remained the same length. Sample 2-5 showed no cracking at the initial inspection (day 162); but during the inspection on day 185, it showed a crack approximately 5 cm long. The Appendix for Chapter 5 shows diagrams of the crack propagation for every specimen per inspection day for batch-2 (except for specimen Batch-2-2 shown in Figure 5.11).

Figure 5.11: Picture of final crack pattern for specimen batch 2-2

5.4.2.2 Specimens Terminated and Dissected

Specimens Batch-1-1, Batch-1-2 and Batch-1-5 were terminated. These specimens were selected for autopsy because the measured values of OCP and Rc suggested that corrosion had initiated. Figure 5.12 shows pictures of the top-layer of rebars and corresponding rebar trace taken within a few minutes after opening Batch 1-1 specimen. These pictures capture the corrosion extent.

Figure 5.12a shows a top view of rebar A. The picture shows the corrosion products observed upon exposure of the top rebar surface. The corrosion products have a dark brown and black color. Spots of corrosion products are observed almost all along the rebar; but, it has three midsize spots: on the left (largest of the three), on the middle, and on the right. Rebar B corrosion extent is shown in Figure 5.12b. The corrosion products have a dark brown and black color. The corrosion on this rebar extents from the left side all the way to the middle of the rebar and covers all the top surface about (11 cm long and 1 cm width). This rebar is the one that has the most corrosion products and likely the rebar that caused the crack that was observed on the surface. Corrosion products observed on Rebar C are shown in Figure 5.12c. The corrosion products have a dark brown and black color. The corrosion is almost all along the rebar. However, except for a large corrosion spot on the left, the other corrosion sites consisted of smaller spots than those observed for Rebars A and B. The biggest corrosion spot is on the left side of the rebar (about 5 cm long and 1 cm width). The back side of each rebars A, B, and C showed no corrosion. No corrosion products were observed on the three bottom rebars. It is suggested that the chloride concentration above the bottom rebars did not exceed C_T; hence, corrosion did not initiate at this depth (concrete cover about 10.5 cm). Figure 5.13 shows the rebar and rebar trace for the top row rebars on Batch 1-2 Specimen and Figure 5.14 shows the rebar and rebar trace for the top row rebars on Bach 1-5 specimen.

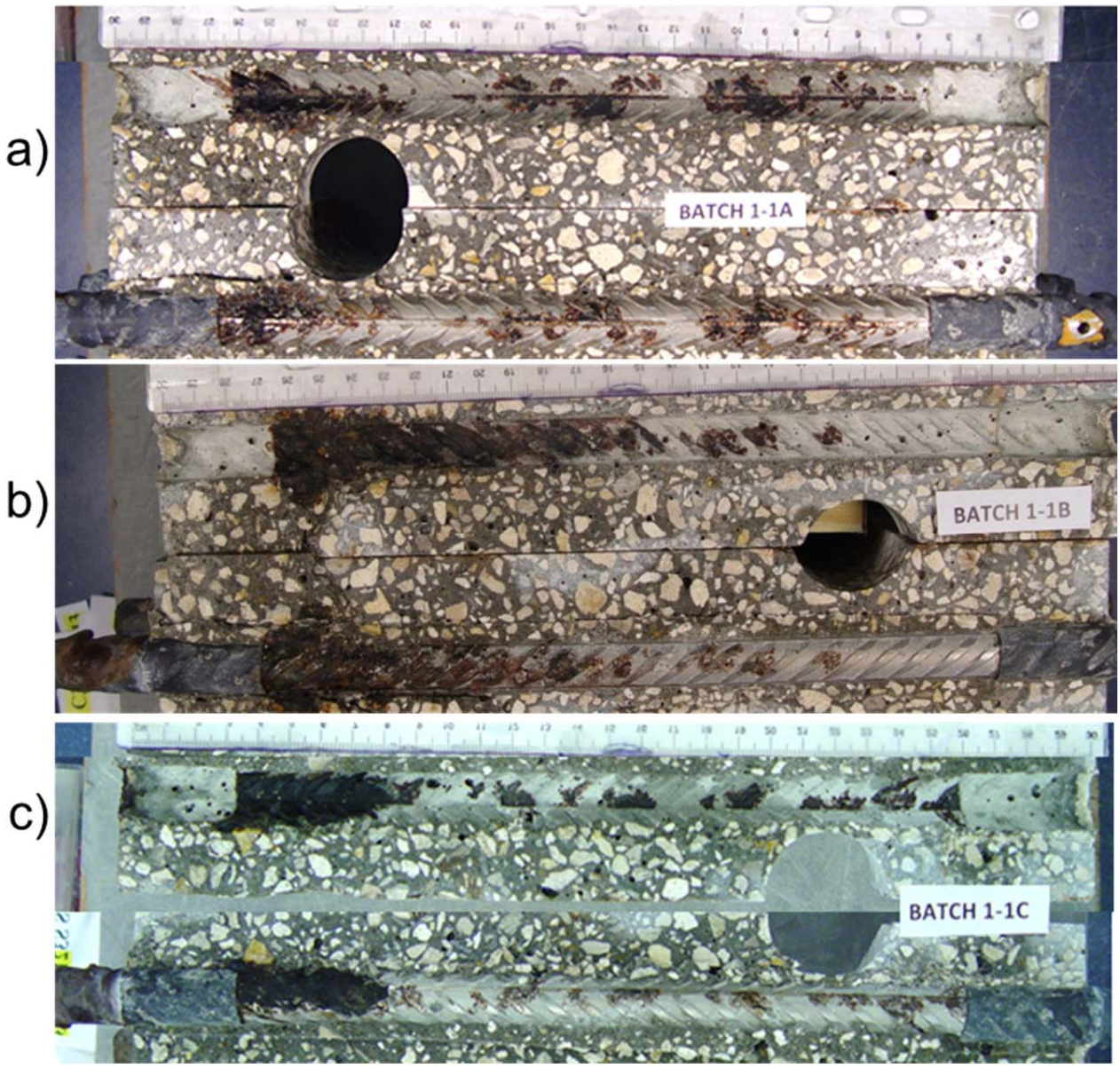

Figure 5.12: Autopsy and visual examination of rebars of specimen batch 1-1

Figure 5.13: Autopsy and visual examination of rebars of specimen batch 1-2

Specimen batch 1-2 was terminated first, and thus the coverage of corrosion products was smaller than that observed on Specimen batch 1-1. Rebar 1-2-BT showed the largest amount of corrosion products and likely was the one that caused the observed crack. Figure 13 shows the rebar surface for specimen batch 1-5. The corrosion coverage was somewhat similar to that observed on specimens 1-2 than what was observed on specimen 1-1. The center rebar were the one that corroded the most on all specimens.

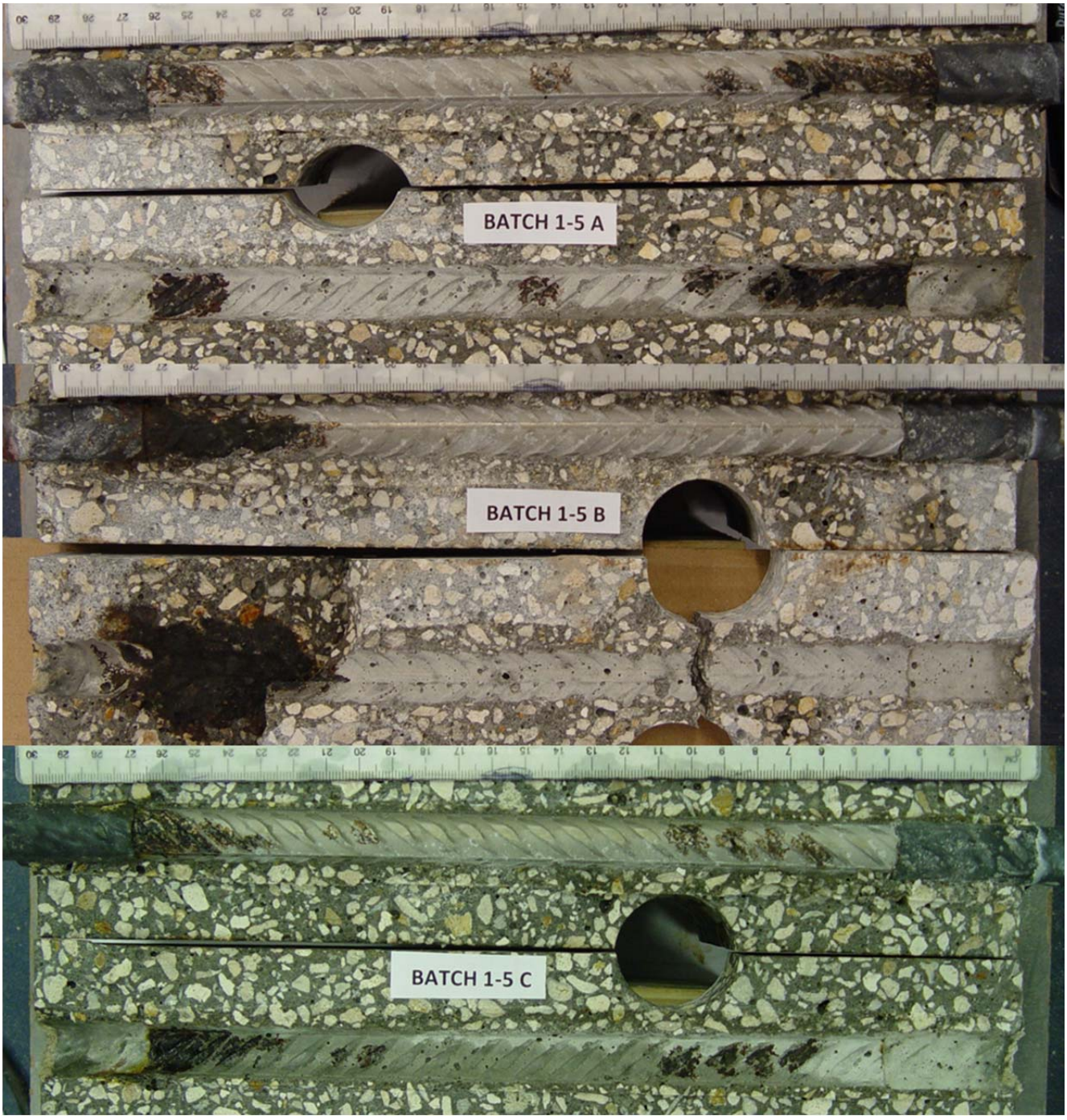

Figure 5.14: Autopsy and visual examination of rebars of specimen batch 1-1

The corrosion products on the rebars were partially cleaned with a plastic brush and then cleaned as per ASTM G-01. Figure 5.15 shows the surface of rebar B (batch 1-1 specimen) after acid cleaning. From the photos the degree of pitting corrosion on the rebar surface was observed. The pits were of various sizes and depths (Figure 5.15). Here we can see that the larger pits looked like craters on sites with largest amount of corrosion. Close-up

pictures after cleaning for rebars A and C respectively of batch 1-1 sample can be found in the appendix of this chapter; similar form of corrosion was observed for these rebars, but to a lesser extent.

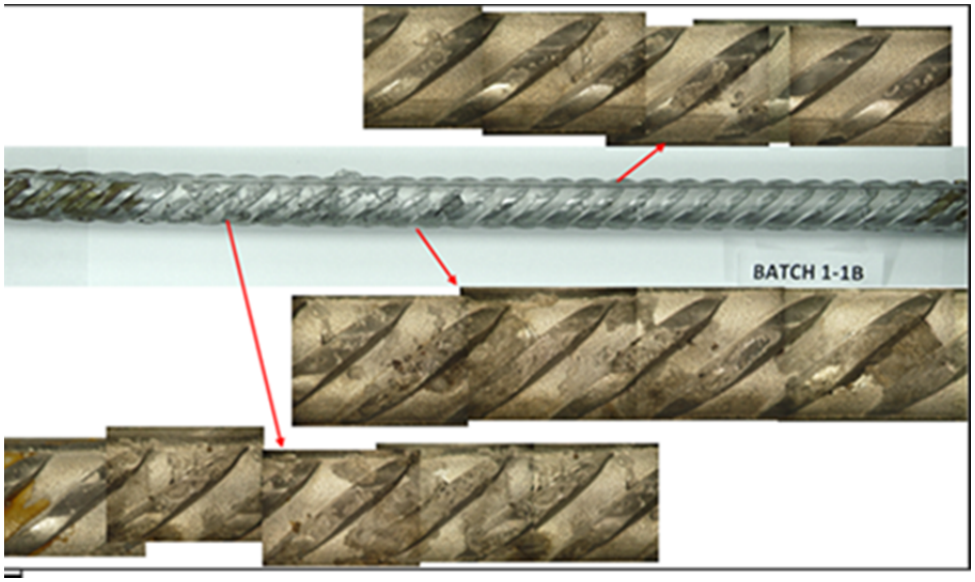

Figure 5.15: Close-up picture of sample batch 1-1B rebar before and after cleaning

Specimen batch 2-1 was selected for autopsy because the measured values of OCP and Rc suggested that corrosion had initiated. Figure 5.16 shows pictures of the rebars taken within a few minutes after opening the sample. These pictures capture the extent of corrosion. Figure 5.16a shows a top view of rebar A. The picture shows the corrosion products observed upon exposure of the top surface of this rebar. The corrosion products have a dark brown and black color. Rebar A has a few small corrosion spots on the left side of the rebar. Rebar B corrosion extent is shown in Figure 5.16b. The corrosion products have a dark brown and black color. This rebar have corrosion products in both sides but the right side is the largest (about 4 cm long and 1 cm width). Rebar C corrosion extent is shown in Figure 5.16c. The corrosion products have a dark brown and black color. The corrosion spots are found almost all along the rebar length. The biggest corrosion spot is on the left side of the rebar (about 6 cm long and 1 cm width). No corrosion products were observed on the three bottom rebars. It is suggested that the chloride concentration above the bottom rebars did not exceed C_T; so, corrosion did not initiate at this depth (about 10.5 cm). Figure 5.17 shows the rebar and rebar trace for the top row rebars on Batch 2-2 Specimen and Figure 18 shows the rebar and rebar trace for the top row rebars on Bach 2-4 specimen. Rebar 2-2-AT had just a very small corrosion spot. The largest corrosion was observed on Rebar 2-2-BT (i.e. center rebar), with corrosion spots at both ends. Corrosion on rebars 2-2-CT was more spread with smaller corrosion spots.

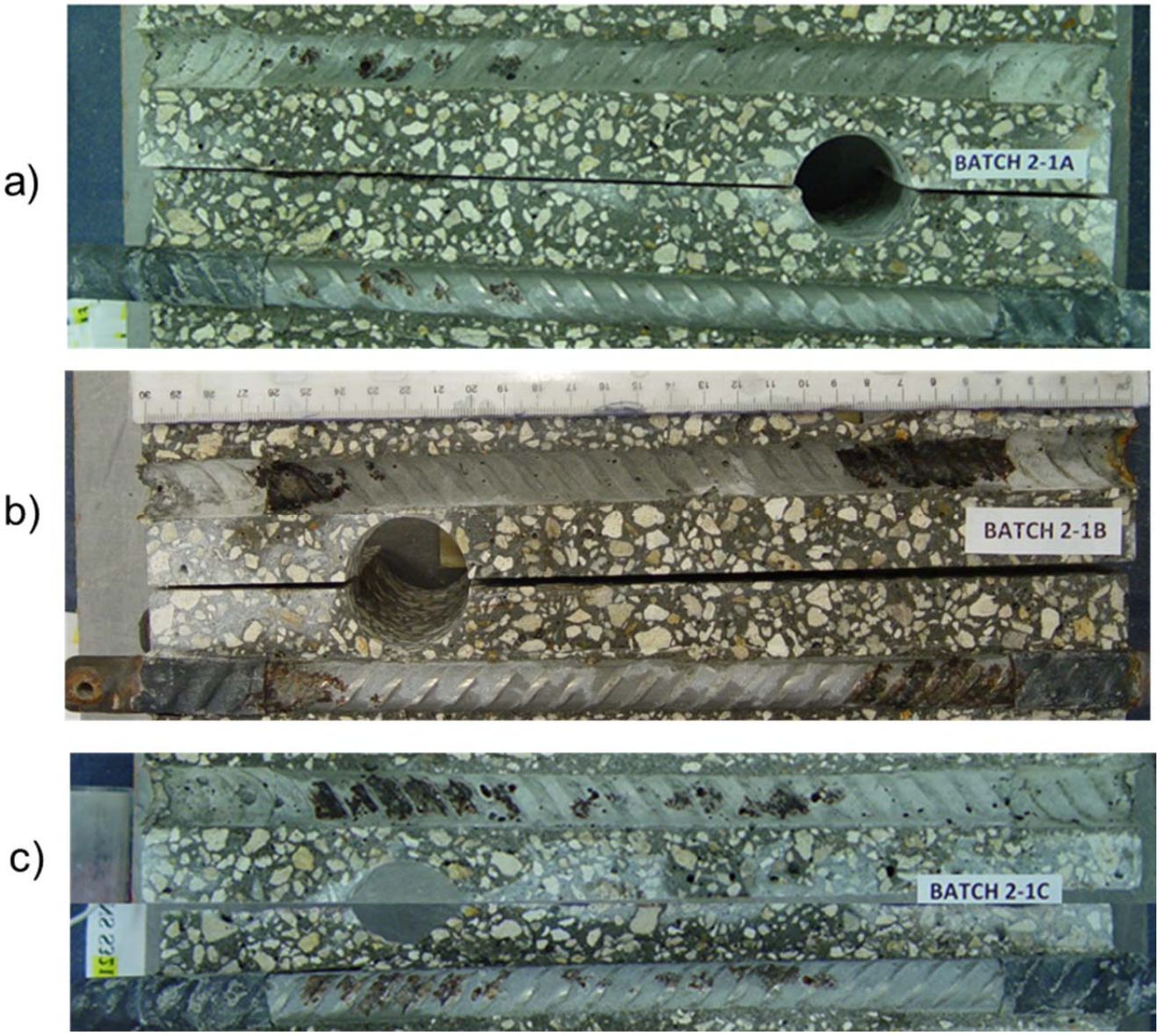

Figure 5.16: Autopsy and visual examination of batch 2-1

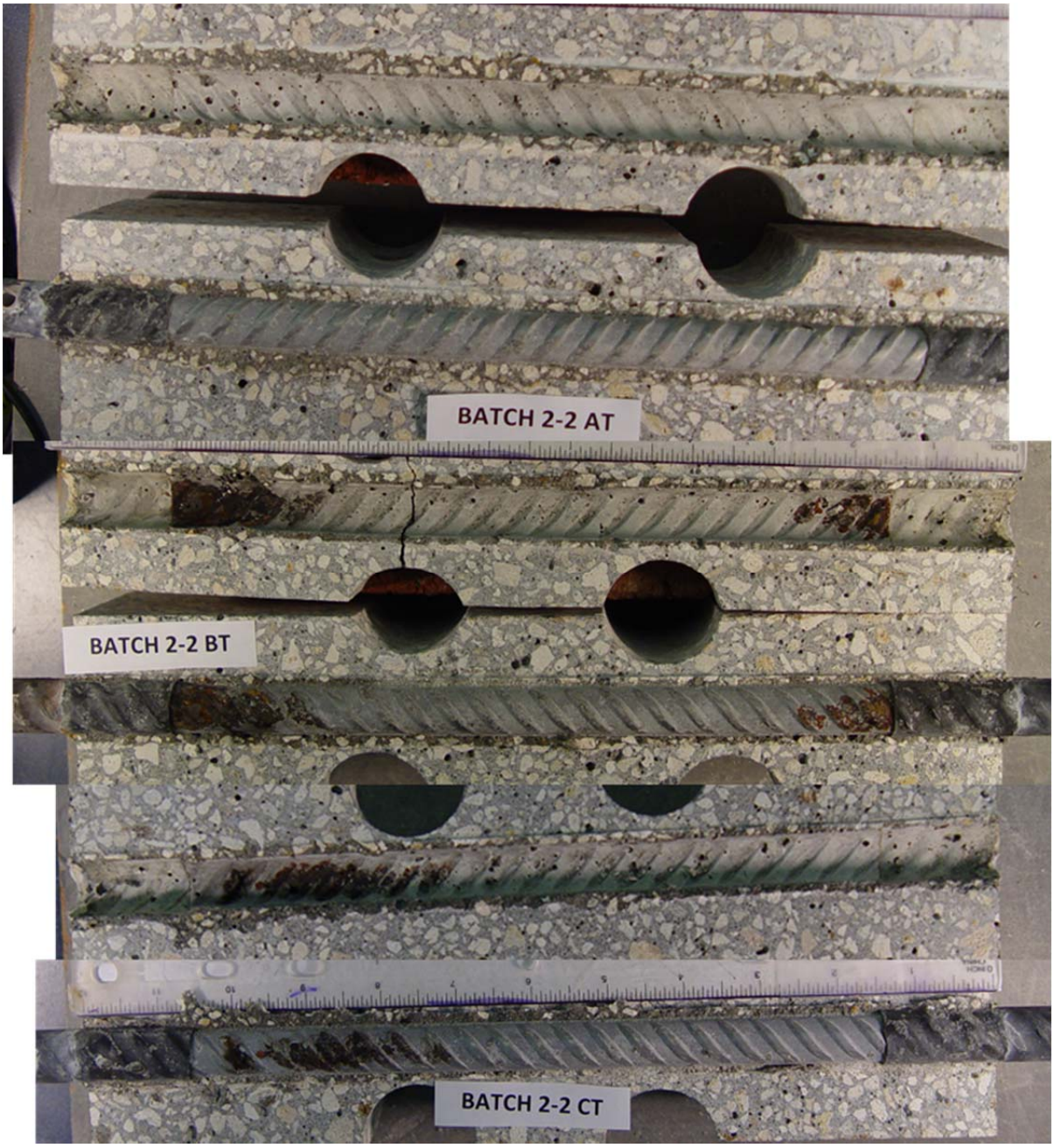

Figure 5.17: Autopsy and visual examination of top row rebars on specimen batch 2-2

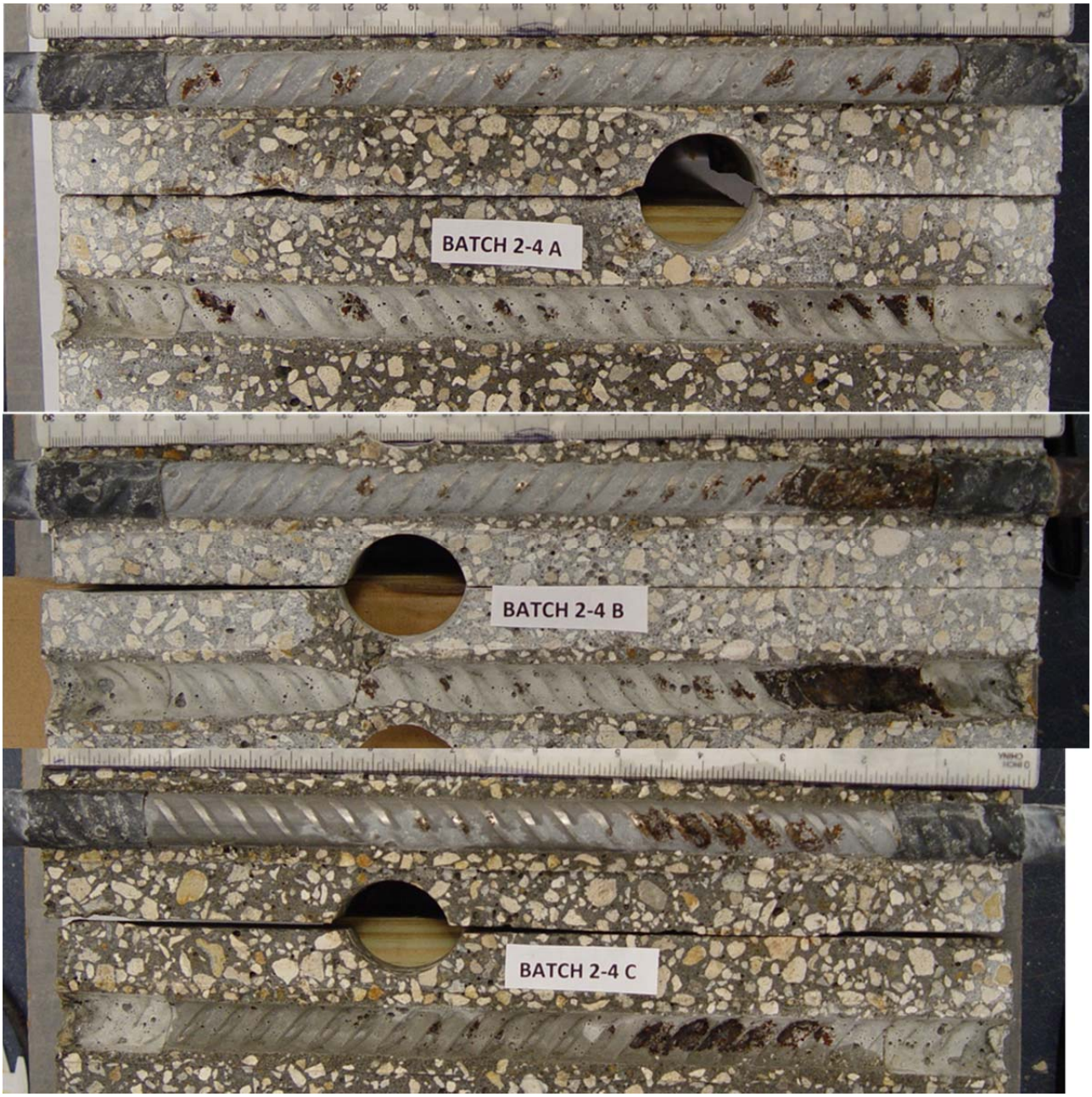

Figure 5.18: Autopsy and visual examination of top row rebars on specimen batch 2-4

The rebars surface with corrosion products were cleaned with a plastic brush and then cleaned as per ASTM G-01. Figure 5.19 shows the surface of batch 2-1B after acid cleaning. Here we can see the depth and size of the pits. The corrosion on 2-1B was less than that observed on rebar 1-1B

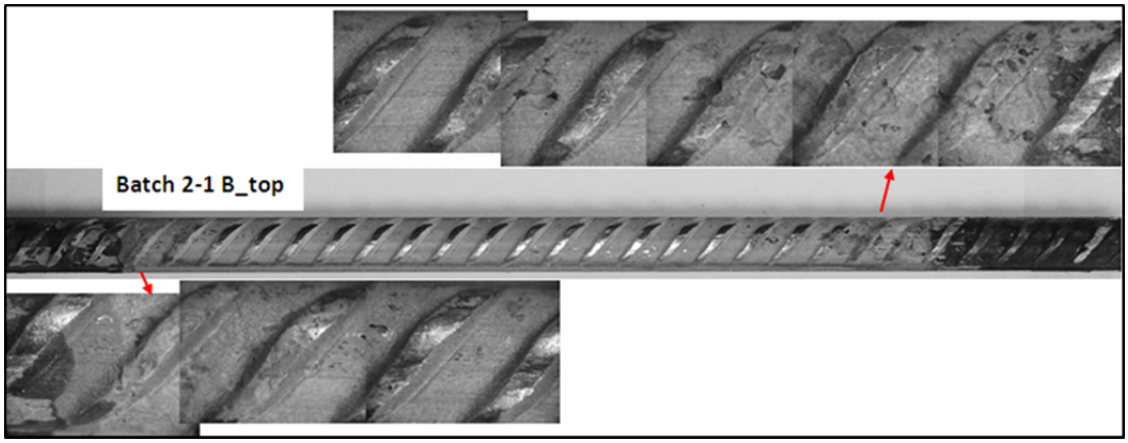

Figure 5.19: Close-up picture of sample batch 2-1B after cleaning

5.4.2.3 Chloride Analysis

Figure 5.20 shows a plot on the left column that corresponds to the chloride profile and the chloride concentration at the rebar trace for batch 1-1 specimen. The chloride concentrations are shown as percent with respect to the cementitious mass (390 kg/m^3). As expected the chloride content of the profiles decreases as a function of depth. The chloride content at the rebar trace for rebar A and C was higher compared to the concentration measured on the slice at the same depth; but the chloride concentration measured at the trace of rebar B was slightly lower. This can be caused by the fact that the concrete powder collected on this rebar trace was less than for the other two rebar traces. It is important to point out that the transport of the chloride is not quite uniform and depends on the pore structure and tortuosity. Also a certain amount of chlorides might have been consumed at the corrosion sites due to the autocatalytic nature of pitting corrosion (corrosion was greatest on rebar B).

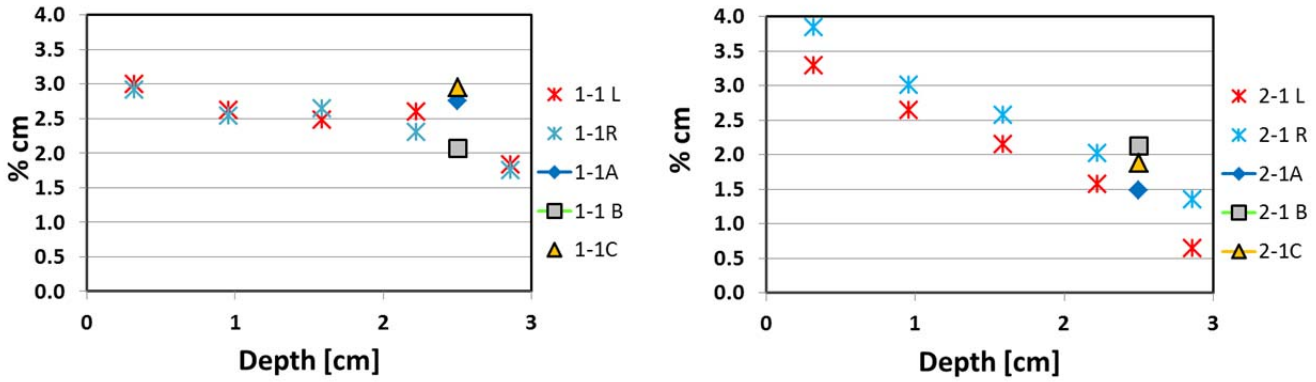

Figure 5.20: Chloride profiles for specimens batch 1-1 and 2-1 and at the rebar trace

Figure 5.20 on the right side shows a plot of the chloride profile and the chloride concentration at the rebar trace for batch 2-1 specimen. The concentration at the rebar depth from the profiles is lower than that observed on batch

1-1 specimen. The chloride content measured at the trace of rebar A and C was higher compared (as suggested by previous research [5] to the concentration measured from the core at the same depth (2.5cm). The chloride concentration measured at the trace of rebar A was slightly lower. This could have been caused by the concrete heterogeneity and also the chloride migration reached higher concentrations at some areas of the concrete than others (due to the meshes shape). It is important to point out that chloride transport also depend on the pore structure and tortuosity. Chloride profiles were also measured on the other two specimens per batch type.

5.4.2.4 Approximated Chloride Threshold of Austenitic and Duplex Stainless Steels

Table 5-1 and Table 5-2 shows the chloride concentration obtained from the concrete powder milled at the rebar trace of each rebar on the top row. According to the chloride concentrations in these tables, it is clear that the specimen that were open first (i.e., specimens batch 1-2 and batch 2-2) have lower chloride concentration at the rebar trace than specimens that were open 30 and >60 days later. It is important to point out that during this additional period of time one additional cycle of electric field potential was applied for 8 days with a potential difference of 15 volts. On Table 2 the chloride average for specimen batch 2-2 was taken from rebars A and B only because rebar C showed only a very small corrosion spot. Each table contains the concentration in kg/m^3 units and in weight percent with respect to the total cementitious amount (WC%). The average WC% on specimen Batch 1-1 was 2.6 percent, for Batch 1-2 it was 1.24 percent and for Batch 1-5 it was 1.74 suggesting that the electric field application was not as effective on specimens Batch 1-5 or additional re-distribution of chlorides took place. Whereas, for Batch 2-1 specimen WC% was 1.84 percent, for Batch 2-2 the WC% was 1.22 percent and for Batch 2-4 WC% was 2.59 (additional diffusion might allowed the chloride to reach a higher concentration). These values might be larger than the actual chloride concentration that allowed corrosion to initiate and then to progress. Based on results reported by Trejo [21], the anodic polarization likely lowered the chloride concentration at which corrosion initiates. This is likely due to the electrochemical reduction of the protective Chromium oxide layer (Hanson [14]) as a result of the ionic current and polarization. Additionally, the set-up appears to produce more uniform electric field above Rebar B (center top rebar), and that might be why in most cases corrosion initiated on these rebar first. A concentration cell might have also occurred via oxygen having a path of less resistance over the shrinkage wrap. The range of chloride concentration found on UNS32101 rebar trace was between 0.95 and 2.95 WC%, whereas for UNS32304 the range was between 1.06 and 2.63 WC% (not including the concentration corresponding to the rebar with the small corrosion spot).

Table 5-1: Chloride concentration at rebar trace (kg/m^3) and chloride by weight cementitious percentage (WC%) for Batch 1-1 and Batch 1-2

alloy	Specimen Rebar	kg/m^3	WC %
S32101	1-1 A	10.77	2.76
	1-1 B	8.10	2.08
	1-1 C	11.52	2.95
	1-1 (average)	**10.13**	**2.60**

alloy	Specimen Rebar	kg/m^3	WC %
S32101	1-2 A	4.31	1.10
	1-2 B	6.57	1.68
	1-2 C	3.69	0.95
	1-2 (average)	**4.86**	**1.24**

alloy	Specimen Rebar	kg/m^3	WC %
S32101	1-5 A	5.98	1.53
	1-5 B	7.91	2.03
	1-5 C	6.46	1.66
	1-5 (average)	**6.78**	**1.74**

Table 5-2: Chloride concentration at rebar trace (kg/m^3) and chloride by weight cementitious percentage (WC%) for Batch 2-1 and Batch 2-2

alloy	Specimen Rebar	kg/m^3	WC %
S32304	2-1 A	5.80	1.49
	2-1 B	8.35	2.14
	2-1 C	7.35	1.88
	2-1 (average)	**7.17**	**1.84**

alloy	Specimen Rebar	kg/m^3	WC %
S32304	2-2 A	4.15	1.06
	2-2 B	5.41	1.39
	2-2 C*	1.93	0.49
	2-2 (average)	**4.78**	**1.22**

alloy	Specimen Rebar	kg/m^3	WC %
S32304	2-4 A	10.25	2.63
	2-4 B	9.95	2.55
	2-4 C	6.90	1.77
	2-4 (average)	**10.10**	**2.59**

Table 5-3: Critical chloride threshold value for different steels in percent weight of cement (WC) %

Author	alloy	kg/m^3	WC %	w/c or w/cm	Corroded Y/N	Note
Trejo	carbon steel	0.5	0.1	0.5	Y	mortar geometry
[10]	microcomposite	4.5	0.8	0.5	Y	
	S30400	5.0	1.2	0.5	Y	migration Cl penetration method
	S31600	10.8	1.9	0.4	Y	Counter at rebar depth - XX potential
Castellote [11]	carbon steel		1.1	0.4	Y	mortar geometry, migration cell, 12V
Bertolini [12]	S32101		3 to 5		Y	mortar geometry
	S32304		3 to 5		Y	Cl added to the mix
	S31600		8.0		Y	
Schonning & Randstrom [6]	S30400		>4		N	mortar geometry
	S31600		>4		N	Cl added to the mi:
	S32101		>4		N	
	S32304		>4		N	
[F. Presuel, F. Gutierrez, personal communication]	C2 S32304	25.0	3.9	0.5	N	mortar geometry
	C4 S32304	31.1	4.9	0.5	Y	dry/ wet -15% NaCl Solution
	C4 S32101	30.9	4.9	0.6	Y	
	C3 S30400	25.6	4.0	0.5	N	
	C1 S30400	24.1	3.8	0.5	N	
	S03-S32304	32.8	5.2	0.4	Y	
Presuel [13]	S32304	13.9	6.5	0.5	Y	SDS Geometry/ Concrete
	S30400	13.9	6.5	0.5	Y*	Outdoor exposure
	S31600	16.1	7.7	0.5	N	weekly dry/wet 15% NaCl solution
This Investigation	S32101	4.9 - 10.1	1.3 - 2.6	0.4	Y	SDS Geometry / Concrete 10%FA as cementitious
	S32304	4.8 - 10.1	1.2 - 2.6	0.4	Y	dry/wet & migration Cl penetration method

Table 5-3: Critical chloride threshold value for different steels in percent weight of cement (WC) % shows a comparison of the critical chloride threshold concentration (C_T), chloride added to the concrete, or chloride concentration measured at the rebar trace corresponding to different steels (including austenitic and duplex) as reported by several authors. In a few instances corrosion did not initiate; for those cases the values shown are lower bound values, i.e., C_T is greater than the value shown. This data is compared with the results of this research and parallel ongoing research being conducted at FAU. It is important to point it out that the C_T values may vary from author to author because the experiments were performed with different specimen geometry (small and large specimens), with different total surface area exposed, and different methods of chloride transport (i.e. dry/wet cycles, electric field application, chlorides cast during mix preparation). However, all rebars were embedded in mortar or concrete specimens in the as received condition. Trejo [21] reports values of C_T by weight cement % that are lower compared with the values reported by the others authors' (Table 5-3: Critical chloride threshold value for different steels in percent weight of cement (WC) %). This lower C_T values can be caused from the way in which the experiment was performed; small mortar geometry was used (7.5 cm X 15 cm cylinder specimens). The experiment used a migration cell to accelerate the chloride transport. An electric field was applied at periodic intervals by setting a potential difference of 20 V between a cathode in a reservoir with Cl^- solution and an anode embedded at the depth of the reinforcement. The electric field applied by Trejo was considerably larger than the one employed in this investigation between top surface and rebar surface. Table 5-3: Critical chloride threshold value for different steels in percent weight of cement (WC) % also shows the C_T values reported by Castellote [18] for carbon steel. The WC% reported by Castellote is close to 1%: a migration cell approach was used but the anode electrode was not at the rebar depth, and the potential difference was 12 V across a mortar specimen 7 cm thick. The rebar was embedded centered in mortar (7cm X 7 cm). The electric field was applied between the NaCl reservoir and plate bottom (electrical connected, wet sponge, to the sample). Periodic intervals of potential difference were applied. The w/c was 0.37 for the mortars. Table 5-3 also shows the C_T values reported by Bertolini [19] for 316, 2101 and 2304 stainless steel. Bertolini reports that the C_T values for duplex range from 3 to 5 % by weight of cement. In Bertolini's experiment, the rebars were embedded in mortar (25cm x 15cm x 5cm) and chloride was added by mass of cement upon casting for those that caused corrosion initiation.

Table 5-3: Critical chloride threshold value for different steels in percent weight of cement (WC) % also shows the C_T values reported by Presuel [20] (See Chapters 4 and 6); the C_T values were measured on mortar specimens and also on concrete specimens, for UNS32304 the values is close to 5%. The chloride concentration at the rebar trace from this investigation, ranged between 0.95 and 2.95 WC% for UNS32101, whereas for UNS32304 the range was between 1.06 and 2.63. These values are larger than those reported by Trejo's but lower than Bertolini's or Presuel's with the rebar not polarized. This observation confirms that the migration approach

polarizes the steel due to the ionic current flowing and as indicated above Hanson [14] and other suggest that CrO2 could be reduced as a result of this. A lower C_T was observed even if a mature passive layer was originally present. Specimens tested at an early (28 days to 2 months) age appear to have even lower C_T values (Trejo's [21]). Chlorides casted into the concrete as for specimens tested by Bertolini might have prevented or modified the passive layer formation within the concrete pore solution, thus these C_T might need to be considered as lower bound values. An additional comment is that the rebar potential upon removing the electric field on rebars A or C generally tended to more positive values suggesting that most of the surface was re-passivating and it is confirmed by the observed upward trends of the Rc values.

5.4.2.5 Localized corrosion built-up that caused concrete cover to cracks

In this investigation additional application of the electric field while trying to initiate the corrosion of non-corroding top rebars produce stray current that accelerated the corrosion rate of the rebar where corrosion initiated first. Even after removing the electric field the corrosion continue at a high rate in some rebars which produced the visible cracks described above. Corrosion of the reinforcing steel causes the concrete cover (C) to crack, when the metal loss reaches a critical penetration depth X_{crit}. This value is very important for predictive models of the corrosion propagation stage. Previous investigations [22] [23] found that the values of X_{crit} increased when corrosion becomes more localized. This investigation compares X_{crit} values calculated from the results of this investigation (assumptions given below) with models based on empirical equations proposed in [22] and [23] by Sagues research group.

Table 5-4: Mass loss approximation and parameters shows the mass loss obtained from the terminated rebars that showed corrosion (UNS S32101 and S32304 top row) and the different parameter used to calculate it. This investigation did not have the initial weight of the rebars. In order to obtain the mass loss of the corroded rebars the following procedure was performed:

- After opening the specimens, the corrosion product was removed from each rebar segment as per ASTM G-01. This was achieved by repeatedly conducting a procedure of immersion in cleaning solution (93.5 wt% HCl + 0.7 wt% Sb_2O_3 + 4.7 wt% $SnCl_2$) and then brushed to remove any remaining corrosion products (multiple times if needed until the rebar weight stopped changing).
- After the clean up the weight on the rebars were measured (see Table 5-4: Mass loss approximation and parameters for the results).
- Then, the approximate volume of each rebar was calculated based on the rebar length (see Table 5-4 for the results).

- Since the bottom rebars did not corrode; they were used as reference to find out the density of each rebar type (S32101 and S32304). The average density for each alloy was calculated (see Table 5-4: Mass loss approximation and parameters for the results). These values assumed cylinder shape for the rebar.
- Then, with each rebar volume and the average density per alloy type, the apparent initial weight of each rebar was calculated (see Table 5-4: Mass loss approximation and parameters for the results).
- Finally, the mass loss for each rebar was calculated by subtracting from the apparent initial weight the measured weight after cleaning (see Table 5-4: Mass loss approximation and parameters for the results).

Table 5-4: Mass loss approximation and parameters

		final measured mass g	total length cm	volume cm^3	density g/cm^3	mean density g/cm^3	apparent calculated initial mass g	mass loss g
Bottom Rebars	1-1A	562.2	37.3	79.76	7.05	**7.04**		
	1-1B	558.8	37.2	79.54	7.03			
	1-1C	542.2	36	76.98	7.04			
	2-1A	556.3	35.7	76.34	7.29	**7.28**		
	2-1B	555.7	35.8	76.55	7.26			
	2-1C	555.5	35.6	76.12	7.30			
Top Rebars	1-1A	529.4	35.2	75.27			529.82	0.419
	1-1B	559.7	37.2	79.54			559.92	0.222
	1-1C	550.5	36.7	78.47			552.40	1.896
	1-2A	555.8	36.9	78.90			555.41	
	1-2B	549.4	36.6	78.26			550.89	1.491
	1-2C	538.7	35.8	76.55			538.85	0.150
	1-5A	546.1	36.3	77.62			546.38	0.276
	1-5B	546.3	36.4	77.83			547.88	1.581
	1-5C	561.5	37.4	79.86			562.18	0.680
	2-1A	555.2	35.7	76.34			555.84	0.636
	2-1B	553.2	35.6	76.12			554.28	1.079
	2-1C	556.4	35.7	76.34			555.84	
	2-2A	554.9	35.6	76.12			554.28	
	2-2B	553.9	35.6	76.12			554.28	0.379
	2-2C	554.7	35.6	76.12			554.28	
	2-4A	556.1	35.8	76.44			556.61	0.515
	2-4B	552.3	35.6	76.12			554.28	1.979
	2-4C	553.1	35.6	76.12			554.28	1.179

In Table 5-4: Mass loss approximation and parameters the highlighted cell in yellow are the rebars that likely caused the crack(s) for each specimen. These are the rebars that had the largest mass loss per each specimen.

Some rebars mass loss are not shown; as a negative value would have been reported because the mass loss was small and due also to the simplified approach used to calculate the original mass.

A previous investigation [23] proposed a relationship between X_{crit} and the length of the localize corrosion. When the length is short the amount of X_{crit} is greater compared to the case of more uniform corrosion [22]. Based on experiments from an investigation [23] where corrosion was approximately approaching uniform states (around the anode area):

$$X_{crit} = 0.0111\left(\frac{C}{\emptyset}\right)\left(\frac{C}{L}+1\right)^2$$

Equation (5-1)

Where C is the concrete cover depth, Ø is the rebar diameter assuming cylinder shape of the rebar, and L is the length of the corroding segment. For our investigation the L value was obtained from measurements on the rebar side where the crack was observed, and from the sum of the different lengths of each small pitting corrosion spots that were observed to be deep enough to contribute to the crack formation. An illustration of how L value was obtained for specimen 1-1 rebar C (46 mm) is shown in Figure 5.21: Observed length L and value explanation process for specimen 1-1 rebar C The top picture shows the corrosion spots circled in red and the bottom picture is the same image without the circled spots.

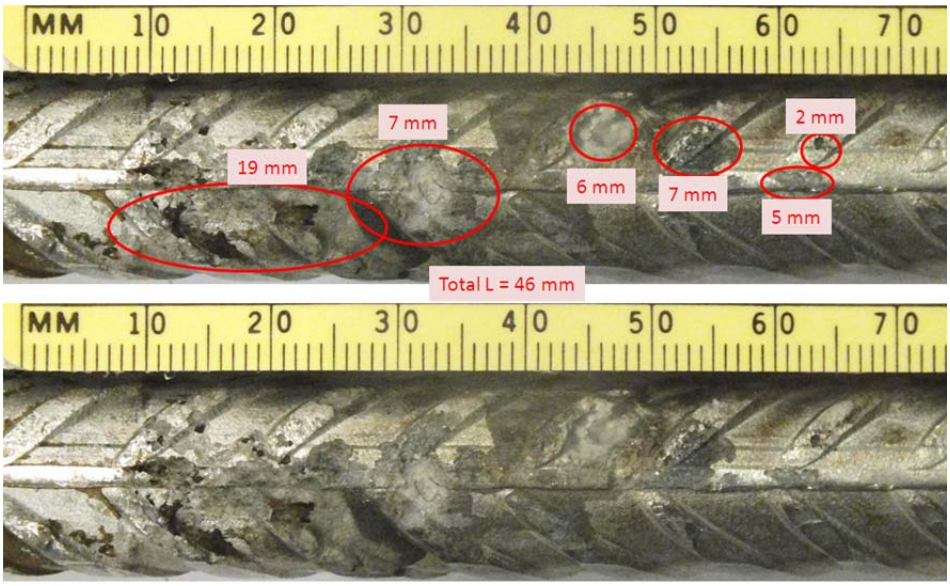

Figure 5.21: Observed length L and value explanation process for specimen 1-1 rebar C

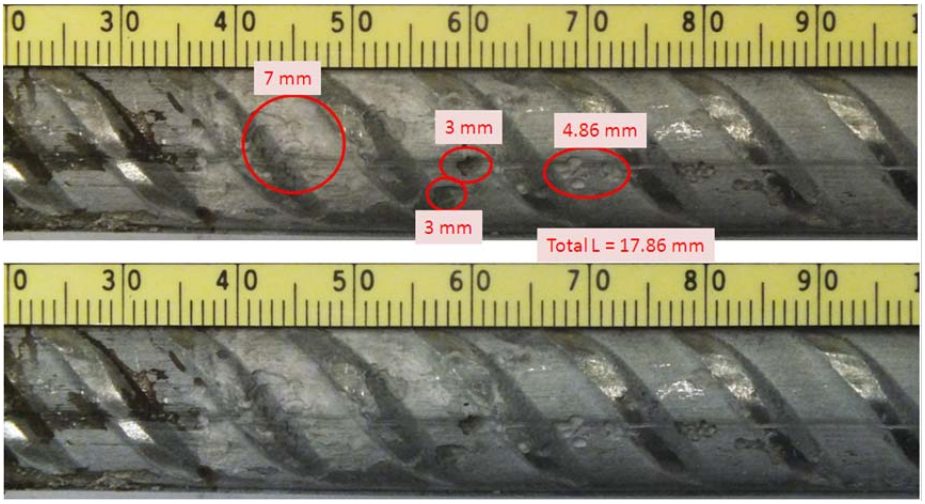

Figure 5.22: Observed length L and value explanation process for specimen 2-2 rebar B

Figure 5.22: Observed length L and value explanation process for specimen 2-2 rebar B shows an illustration of the area were the measurement for L was obtained for rebar 2-2 B (17.86 mm). The top picture shows the corrosion spots circled in red and the bottom picture is the same image without the circled spots.

A more recent investigation [22], proposed equation (1) be modified. Investigation [22] replaced the exponential 2 of the term $\left(\frac{C}{L}+1\right)$ of equation (1) and replaced it by 1.48 that was obtained by an exponent of 1.48. This new exponent was obtained by a fit to previous reported values Busba [22] and Torres [23] reported their results. Thus:

$$\text{Xcrit} = \ 0.0111\left(\frac{C}{\emptyset}\right)\left(\frac{C}{L}+1\right)^{1.48}$$

Equation (5-2)

Table 5-5: X_{crit} and X/(c/ϕ) values for different equations and parameters shows the predicted X_{crit} values for $\left(\frac{C}{L}+1\right)$ and (C/ Ø) pairs relevant to our experiment using empirical equations (5-1) and (5-2). Two different approaches were used to calculate L, with and without overlap as indicated. Table 5-5: X_{crit} and X/(c/ϕ) values for different equations and parameters also shows X_{crit} values. Calculated X_{crit} were obtained using the mass loss (ΔW) from Table 5-4: Mass loss approximation and parameters for those rebars that likely caused the cracks and the following equation [23]:

$$\text{Xcrit} = \frac{\Delta W \ x \ 10^3}{\pi \emptyset L \rho_{Fe}}$$

Equation (5-3)

Table 5-5: X_{crit} and $X/(c/\phi)$ values for different equations and parameters

overlap															
	ΔW (g)	ϕ (mm)	ρ(FE)	L (mm) corrode	X_{crit} equ 3	C (mm)	X_{crit} equ 1 n=2	X_{crit} equ 2 n=1.48		c/ϕ	C/L	1+C/L	X/(c/ϕ) n=2	X/(c/ϕ) n=1.48	X/(c/ϕ) eq 3.3
1-1C	1.896	16.5	7.86	46	0.1012	23	0.03481	0.02820		1.39	0.50	1.50	0.0250	0.0202	0.0726
1-2B	1.491	16.5	7.86	41	0.0893	23	0.03770	0.02991		1.39	0.56	1.56	0.0270	0.0215	0.0640
2-1B_T	1.079	16.5	7.86	31	0.0854	23	0.04695	0.03518		1.39	0.74	1.74	0.0337	0.0252	0.0613
2-2B	0.379	16.5	7.86	17.86	0.0521	23	0.08098	0.05266		1.39	1.29	2.29	0.0581	0.0378	0.0374
1-5B	1.581	16.5	7.86	23	0.1687	23	0.061891	0.043161		1.39	1.00	2.00	0.0444	0.0310	0.1210
2-4B	1.979	16.5	7.86	18	0.2698	23	0.080277	0.052322		1.39	1.28	2.28	0.0576	0.0375	0.1936

no-overlap															
	ΔW (g)	ϕ (mm)	ρ(FE)	L (mm) corrode	X_{crit} equ 3	C (mm)	X_{crit} equ 1 n=2	X_{crit} equ 2 n=1.48		c/ϕ	C/L	1+C/L	X/(c/ϕ) n=2	X/(c/ϕ) n=1.48	X/(c/ϕ) eq 3.3
1-1C	1.896	16.5	7.86	43	0.1082	23	0.03645	0.02917		1.39	0.53	1.53	0.0262	0.0209	0.0776
1-2B	1.491	16.5	7.86	34	0.1076	23	0.04349	0.03324		1.39	0.68	1.68	0.0312	0.0238	0.0772
2-1B_T	1.079	16.5	7.86	27	0.0981	23	0.05306	0.03851		1.39	0.85	1.85	0.0381	0.0276	0.0704
2-2B	0.379	16.5	7.86	15.86	0.0587	23	0.09289	0.05829		1.39	1.45	2.45	0.0666	0.0418	0.0421
1-5B	1.581	16.5	7.86	19	0.2042	23	0.075606	0.050052		1.39	1.21	2.21	0.0542	0.0359	0.1465
2-4B	1.979	16.5	7.86	16	0.3036	23	0.09193	0.057842		1.39	1.44	2.44	0.0659	0.0415	0.2178

Although the rebars investigated here are CRAs; we assumed the density of iron in Equation 5.3. Figure 5.23 shows the estimated critical penetration X_{crit}, calculated for the rebars that likely caused the crack(s) for both approaches used to calculate L (i.e. overlapped and no-overlap). Recall, that in here L is the sum of the lengths of the spots affected by corrosion as explained above. Here the continuous lines are calculated from equations (1), (2) and the triangle symbols are the calculated X_{crit} values using the length and mass obtained from this research. In both plots, the calculated X_{crit} values from this research are larger than those from both models when the C/L ratio is between 1 and 2 (1 to 1.8 when considering overlap); but for values of C/L greater than 2 (1.8 for those assuming overlap) the X_{crit} is similar to the values suggested by equation (2). The larger X_{crit} values can be caused because in our experiments the corrosion was more localized (corrosion was observed only on one side of the rebar and in most cases it did not cover all the top rebar surface width) whereas the empirical equations assume that corrosion is uniform along L (i.e. around all the rebar).

Comparing the plots of the results assuming no overlap corrosion length and overlap corrosion length (different corrosion spots in the same longitudinal area) it shows that the overlap corrosion have lower Xcrit values than the not overlap values. Five out of six points were significantly above the expected values from both models. Hence, it appears that additional correction might need to be included in the equations to account for partial coverage of the rebar surface.

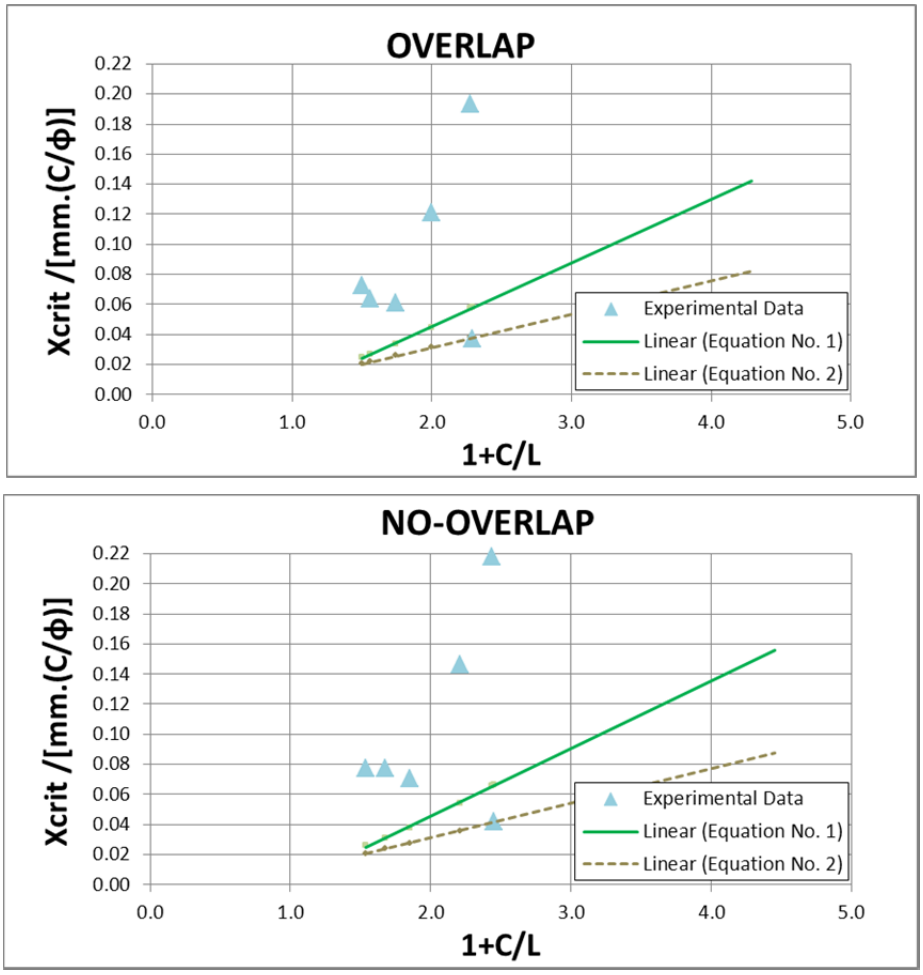

Figure 5.23: Plot of the Xcrit values for equations (1), (2) and experimental results as a function of C/L ratio

5.4.2.6 Final Comments

A lower applied potential (e.g. 2 V across the two counter electrodes) is recommended, if a similar approach is to be used again to investigate chloride threshold for these CRA rebars. This lower potential difference would likely prevent polarizing the steel via stray currents to values where the CrO_2 layer might be reduced. It is likely that the test would take longer. However, a closer value to a critical chloride threshold would be obtained.

5.5 CONCLUSIONS

- Developed a methodology that allows for corrosion to initiate and propagate on concrete specimens embedded with CRAs and initially chloride free.
- Stray current might have caused an accelerated corrosion rate (due to additional electric field application once corrosion had initiated) on reinforcing bar(s) where corrosion had initiated.

- The results from this investigation suggest that UNS S32304 rebars corrode at a slower rate than UNS S32101 rebars (once corrosion has initiated).
- The average CT for UNS S32101 rebars was found to range between 0.95 and 2.95 WC%, whereas for UNS32304 the range was between 1.05 and 2.6 WC% (i.e. % by cementitious).
- The results of chloride concentration at the rebar trace from this investigation, of UNS S32101 rebars and UNS S32304, are found to be lower compared to reported C_T values on specimens under non-accelerated chloride transport. As indicated in the discussion this likely was due to stray currents.
- On several rebars corrosion propagation caused the concrete to crack. The corrosion propagated at a fast rate due to stray currents (on rebars where corrosion initiated first) present while trying to initiate corrosion on the other rebars.
- Mass loss as little as 0.65 gr caused a surface crack on specimens with UNS32304. The smallest mass loss observed on UNS32101 was ~1.4 gr, but it is likely that a crack appeared with smaller corrosion mass loss.

6 EFFECT OF CRA INITIAL SURFACE CONDITION ON CORROSION INITIATION

6.1 SPECIMENS IMMERSED IN SIMULATED PORE SOLUTION

6.1.1 ABSTRACT

Most corrosion experiments conducted on reinforced concrete are terminated upon corrosion initiation. This paper presents preliminary results on corrosion initiation and propagation on three corrosion resistant alloys (CRAs). The experiments were conducted with the CRAs exposed to simulated pore solution (with chloride concentration gradually increased via NaCl additions). Three surface conditions were tested on each CRA type: as received, with mill scale, with mill scale then sandblasted. The open circuit potential was monitored over time. Linear polarization resistance and solution resistance were measured periodically. In this research the experiments were not terminated upon corrosion initiation, rather exposure continued to gain a better understand how corrosion propagates. Some specimens were terminated after 200 days of exposure and the rest of specimens after more than 550 days of exposure.

6.1.2 INTRODUCTION

Several authors have investigated corrosion resistant alloys as an alternative to carbon steel reinforcement as an approach to achieve bridge repair-free service life in excess of 75 years. Currently a couple of US state DOTs (Virginia and Oregon) require CRAs rebars be used in new bridge construction exposed to chlorides. Previous studies [9] [24] have identified duplex stainless steel and austenitic stainless (with high Pitting Resistance Equivalent Number (PREN) and with Ni and Mo) as the alloys with the higher chloride threshold. Most of the research reported[2-5] aimed to determine the chloride threshold was performed in calcium hydroxide solution with chlorides added to this solution; in most instances concurrently. One of the methods developed is to do an anodic potential hold on the studied alloy while exposed to the chloride solutions [12] [13] Tests in solution provide comparable ranking of the different alloys. However, not enough time is usually allowed during initial immersion in solution for a mature/thick passive layer to form before adding chlorides, as is expected to be present on CRAs embedded in concrete. Based on previous studies that have reported chloride thresholds, a relative high chloride concentration is usually added to the solution when the more corrosion resistant alloys are exposed.

Current procedures of stainless steel (austenitic, ferritic or duplex) rebar include the removal of the mill scale via a process called pickling. The presence of the mill scale in stainless steel has been reported to reduce the chloride threshold [12][31]. Some of the initial testing in the US [25] [26] [27] was performed on CRAs where the mill scale was not properly removed. Hanson [24] has reported that mill scale is not too detrimental on higher end stainless steels (UNS S32205, UNS S31600) based on samples immersed in solution and mortar reinforced samples casted with chlorides. Scully and Hurley [12] reported significant reduction in the chloride threshold with the mill scale present (but in their case the mill scale was produced in the laboratory). Based on conversations with producers of stainless steel rebars, improper pickling (or presence of mill scale) is no longer an issue. Pickling is now integrated on the stainless steel rebar production. Several papers report performance of CRAs embedded in concrete. Tests of intermediate CRAs rebars embedded in concrete usually are terminated upon corrosion initiation [8] [28] [29] [30]. Corrosion does not initiate on the more corrosion resistant CRAs embedded in concrete, even if the concrete is poor (i.e. high w/c ratio) and with reduced cover (e.g. 2.5 cm) [30]. Within the literature review performed no results were found describing the propagation stage on CRAs. Some authors venture to indicate that corrosion rate would be slower and hence a longer propagation time (T_p) should be given for CRAs. Hurley and Scully [9] [12] proposed a propagation model to determine the propagation stage for CRAs. In here, three different CRA rebars and three surface conditions were investigated: as received or pickled, lab produced mill-scale and sandblasted to remove lab produced mill-scale. Corrosion initiated and propagated on the latter two type of surface condition on the three different alloys, but the chloride threshold was different depending on alloy composition.

6.1.3 EXPERIMENTAL PROCEDURE

The alloys investigated in here are: UNS S30400, UNS S32304 and UNS S32101. Table 6-1 contains measured chemical composition on the tested alloys via x-ray fluorescence (XRF). UNS S30400 was recovered from terminated reinforced concrete samples part of a previous research program [8]. The UNS S32304 was from old stock from the same program. Alloy UNS S32101 was provided by a manufacturer during the fall of 2011.

Table 6-1: CRA chemical compositions determined via XRF.

	Mo	Cu	Ni	Fe	Mn	Cr
UNS S30400	0.41	0.42	8.57	71.50	1.08	17.86
UNS S32101	0.16	0.24	1.54	72.03	4.78	20.91
UNS S32304	0.27	0.30	4.09	71.67	1.25	21.90

The length of the segments ranged from 10 cm (UNS S30400) to 12 cm long (typical length for the other two alloys). All tested CRA's were received pickled. Three surface conditions were investigated: pickled (as received), with mill scale, mill scale and then sandblasted. The mill scale was re-created by placing the CRA rebar segments into a high temperature oven at 1050°C for 1 hour and air cooling (after Scully method). This method creates a scale worst that would have been obtained if the rebar segments would have been quenched as is customary in the industrial production line. Some of the segments with mill scale were then sandblasted to prepare the third surface condition group. The as received rebar segments are named here C condition, those with mill scale are named here H condition and those with mill scale then sandblasted are identified in here as S condition.

The rebar segments were then drilled on one of the ends to accommodate a Cu wire used as electrical contact. The drilled hole was of a slightly smaller diameter than the Cu wire. The Cu wire was then pushed into the drilled hole. A polymeric mortar cover was added to both rebar ends as to delay/prevent corrosion of the electrical connection (Cu wire and CRA interface). Cylindrical plastic shape molds were used for casting the polymeric mortar. An activated titanium mix metal oxide mesh surface was used as a counter electrode. The composition of the simulated pore solution in grams per liter is: 3.7 gr Na(OH) + 10.5 gr K(OH) + 3 gr $Ca(OH)_2$. The nominal pH of this solution is ~ 13.3, and is based on Li's SPS [32]. A 15 liters plastic container was used to immerse both UNS S32304 and UNS S30400 segments. Nine specimens (3 per surface condition) per CRA type were exposed. A second container (8 liters) was set-up to place the UNS S32101 samples, due to the expected lower chloride threshold of this alloy. Additionally, UNS S32101 segments were prepared at a later date than the other two groups. UNS S32304 and UNS S30400 specimens were immersed for three weeks in simulated pore solution before chloride additions began. Similarly UNS S32101 samples were immersed in simulated pore solution for two weeks before chloride additions began. Sodium chloride was periodically added and is reported by wt% in the results section. On the larger container the chloride addition started at 5% NaCl and eventually reached 23% NaCl, whereas for the smaller the initial concentration was 1% and eventually reached 11%. The chlorides eventually reached the electrical contact on some samples immersed in solution with the measurements not being reliable thereafter. Additionally, selected segments were terminated after 360 days of exposure for UNS30400 and UNS S32304. Selected UNS S32101 specimens were terminated after 260 days of exposure. All remaining specimens were terminated after 700 days for UNS32304 and UNS30400 and after 550 days for UNS32101. Forensic visual inspection was conducted upon specimen termination. The first set of terminated specimens was chosen from those that did not have good electrical contact anymore. Figure 6.1 shows the 15 liters container where UNS S30400 and UNS S32304 segments were immersed (The blue tape contains the samples ID)

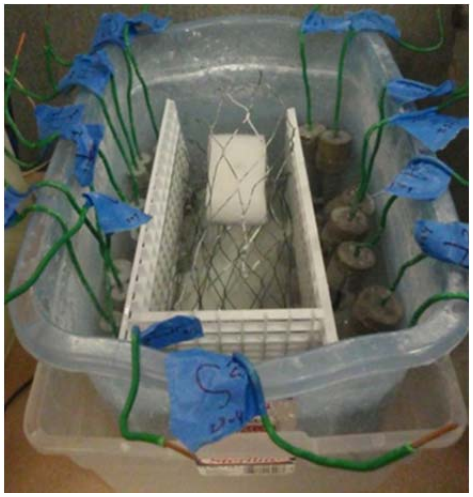

Figure 6.1: Rebar immersed in SPS

The OCP was measured at least once a week using a saturated calomel electrode (SCE) as a reference electrode. The OCP measurements were more frequent during the early exposure period. All reported values are in the SCE scale. Occasionally, The solution resistance (Rs) was measured via EIS. The solution resistance in here is the impedance modulus measured at 56 Hz. The LPR was performed every week at the beginning, and after ~60 days every 2 weeks. The LPR tests were carried out from 15 mV cathodic from OCP (i.e. 15 mV below OCP) to the OCP at a rate of 0.1 mV/s. In this investigation, linear polarization resistance (LPR) and open circuit potentials (OCP) were used as techniques to monitor corrosion evolution, not necessarily corrosion rate, as the actual active area would not be known (localized corrosion usually occurs on CRAs).

6.1.4 RESULTS

6.1.4.1 Samples immersed in simulated pore solution + Sodium Chloride

The rebars were momentarily removed from the solution before transferring into new solution for the initial two sodium chloride additions. This transfer likely allowed some additional oxygen to reach the rebar surface and interact with the passive layer, than if the rebars would have not been removed. Subsequent sodium chloride additions were performed without removing the rebars, and mixing was achieved by using a plastic rectangular bar to manually stir the solution. Every other week water level was checked and water was added when needed to keep the same solution volume.

6.1.4.2 Potential vs. Time

Figure 6.2 and Figure 6.3 shows the potential evolution vs. time for the CRA's immersed in solution. Each figure shows several plots. The x-axis indicates time in days that the rebar samples have been immersed in the solution. The right y-axis (secondary axis) of each plot indicates sodium chloride additions in percentage by weight in the

solution. The black continuous line indicates when and to what concentration was the sodium chloride added to the solution. Figure 6.3 shows the potential evolution vs. time for both UNS S32304 and UNS S30400 alloys for each of the three surface conditions investigated each in a different subplot. The rebar specimens were immersed in simulated pore solution for 3 weeks before any sodium chloride was added. The top two plots correspond to the C (as-received) condition, the second row to those with H surface condition and the bottom row for those with S surface condition. The initial measured potential for both alloys under C and S surface condition started at ~-300 mVsce and increased during the time with no chlorides, whereas the potential for rebar specimens with H surface condition ranged from -100 to -200 mVsce likely due to the presence of the mill scale. Upon adding 5% NaCl to the simulated pore solution there was a distinctive potential drop for UNS S30400-H specimens similar to what is observed on carbon steel rebars once the chloride threshold is exceeded. A similar trend was observed on UNS S32304-H specimens. For UNS S30400-S specimens a potential drop was observed once the solution contained 10% NaCl, whereas for UNS S32304-S the potential drop took place on two rebars while the solution contained 12.5% but the potential drop of the last S rebar occurred with 19% NaCl. For both, UNS S30400 and S32304 rebars with C surface condition the potential drop occurred with the solution having 17% or > NaCl. However, the potential drop of the latter group might be influenced by chlorides reaching the surface of the electrical contact under the mortar. Large potential shift to more positive or oscillations in potential values might be indicative of poor electrical contact. Figure 6.3 shows the potential vs. time on UNS S32101 specimens. In the case of UNS S32101, corrosion initiation (potential drop) began at 6.5% NaCl on one specimen with C surface condition, at 2% NaCl on those with H (mill scale) and between 3% and 4 % NaCl on S specimens. The above values are estimates based on the potential vs. time.

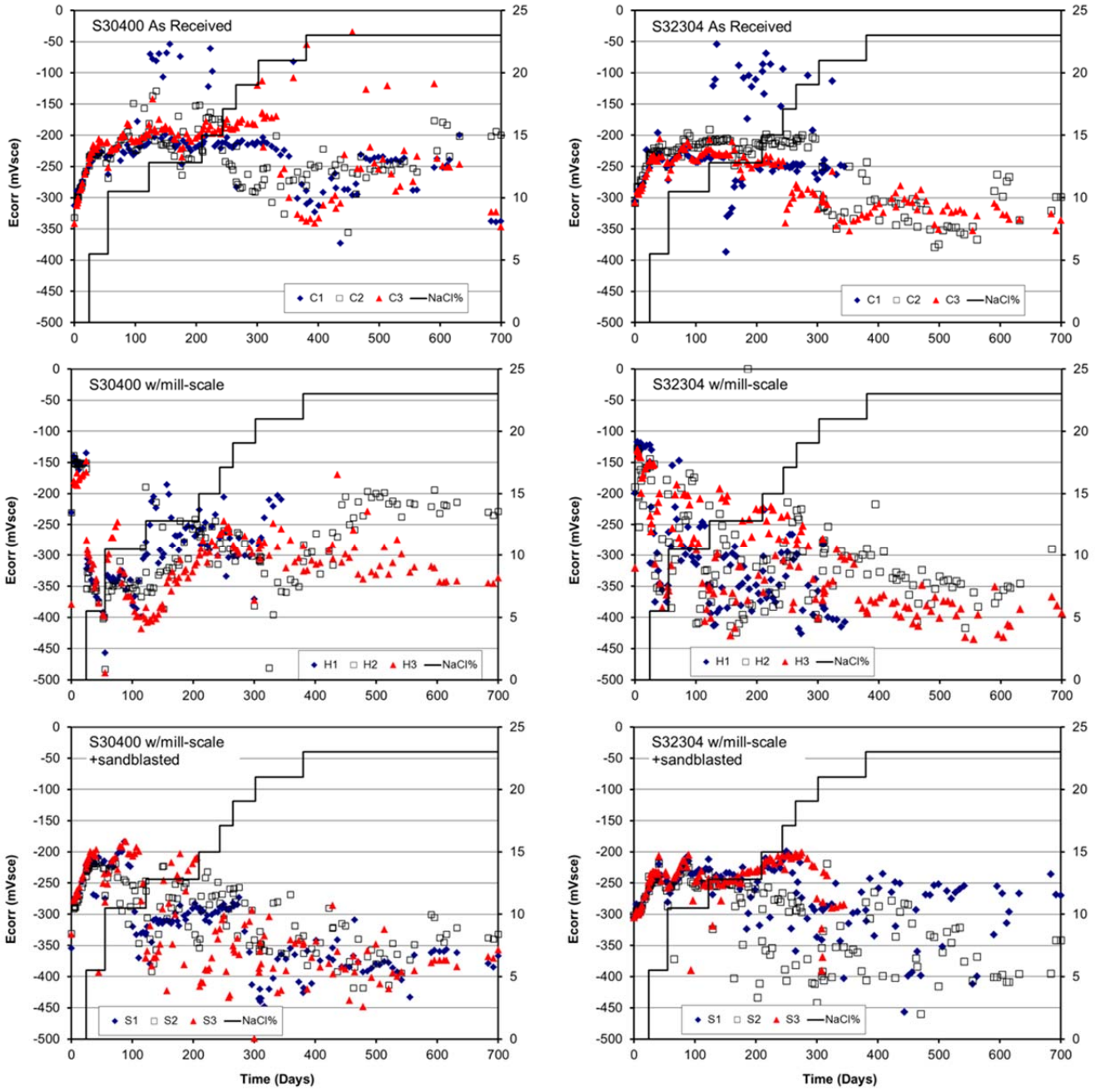

Figure 6.2: Potential vs. time on UNS S32304 and UNS S30400 (C, H and S surface conditions) NaCl% series stepwise additions of Sodium Chloride

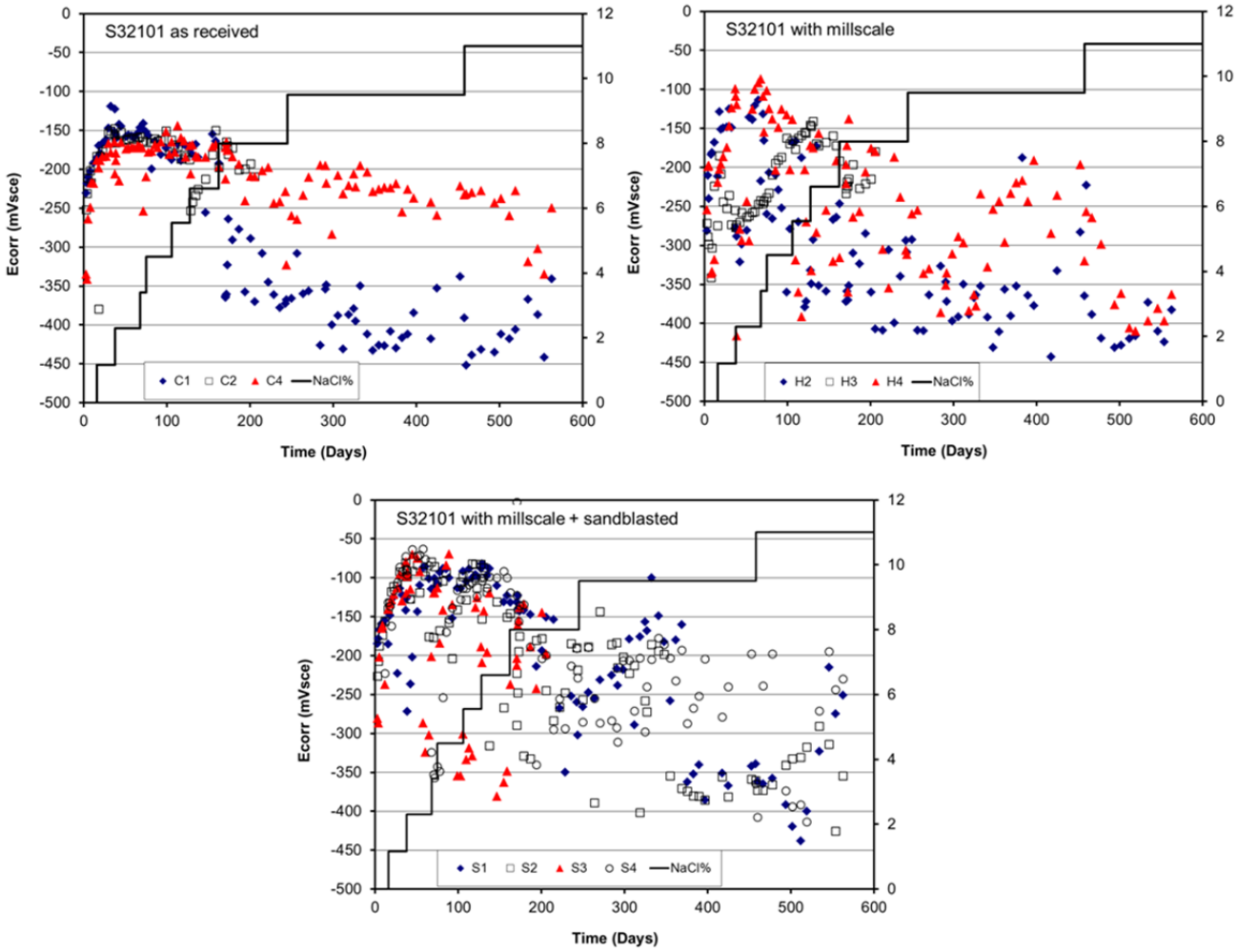

Figure 6.3: Potential vs. time on S32101 (C, H and S surface conditions)

Similar trends are observed from Figure 6.4 and Figure 6.5 corresponding to the measured Rc vs. time. In some cases the magnitude of the Rc measured exceeded 100 KOhm; those values were truncated from the plots. These large Rc values are sometimes indicators that the electrical contact was no longer good. The values are more scattered in the plots shown in in both Figure 6.4 and Figure 6.5. Figure 6.4 shows plots for UNS S32101. In the case of UNS S32101-C specimens, the measured Rc ranged between 30-50 KOhm before a potential drop occurred. After a significant potential drop occurred an accompanying reduction on the Rc measured was observed. The Rc measured on UNS S32101-H and UNS S32102-S ranged between 10-25 Kohm and 5-15 Kohms respectively. Only a modest reduction on Rc was observed after a significant potential drop. This suggests that the reaction rates were similar before and after corrosion initiated, or that the corrosion sites are small. Figure 6.5 shows the Rc measured on UNS S30400 and UNS S32304 specimens. The Rc values measured on C and S samples are plotted with the same scale. Rc magnitudes larger than 40 Kohms were measured on C and S non-corroding specimens, upon corrosion initiation the Rc measured on S specimens ranged between 10 and 30

Kohms, and continue to drop as additional chloride was added to values smaller than 5 KOhm. Smaller Rcs were measured on UNS S30400-S rebars than on UNS S32304-S rebars. The transition to corrosion is more evident on H specimens for both UNS S32304 and UNS S30400 alloys. Before corrosion the Rc ranged between 10 and 25 Kohm and upon corrosion initiation the Rc was typically less than 5 Kohms. Similar to what was observed on S rebars, the Rc values were smaller for UNS S30400.

The longer the samples are exposed to high chloride concentration the more likely is that the electrical contact can be damaged due to corrosion or to handling of the copper wire. These specimens might require better sealing of the mortar placed on both ends if samples are to be exposed for a prolonged period of time. Once the NaCl exceeded 5%, it likely reduced the dissolved oxygen concentration in the water and that might have played some role in the observed potential negative shifts in pore water exposure. Moreover, the high Cr content in these alloys has been reported to lower the oxygen reduction that can take at the metal electrolyte interface.

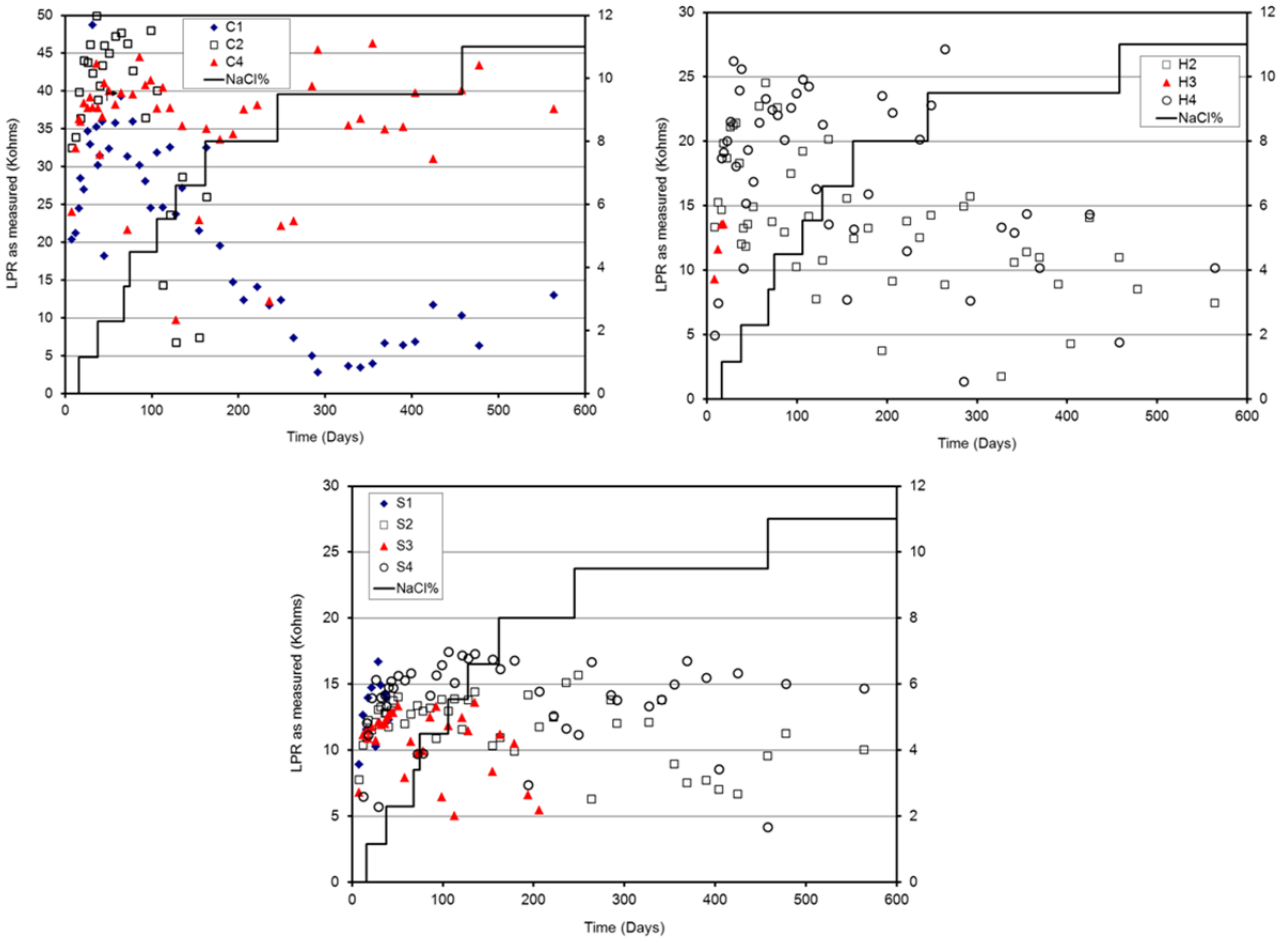

Figure 6.4: Rc as measured on UNS S32101 rebar samples for the 3 surface conditions

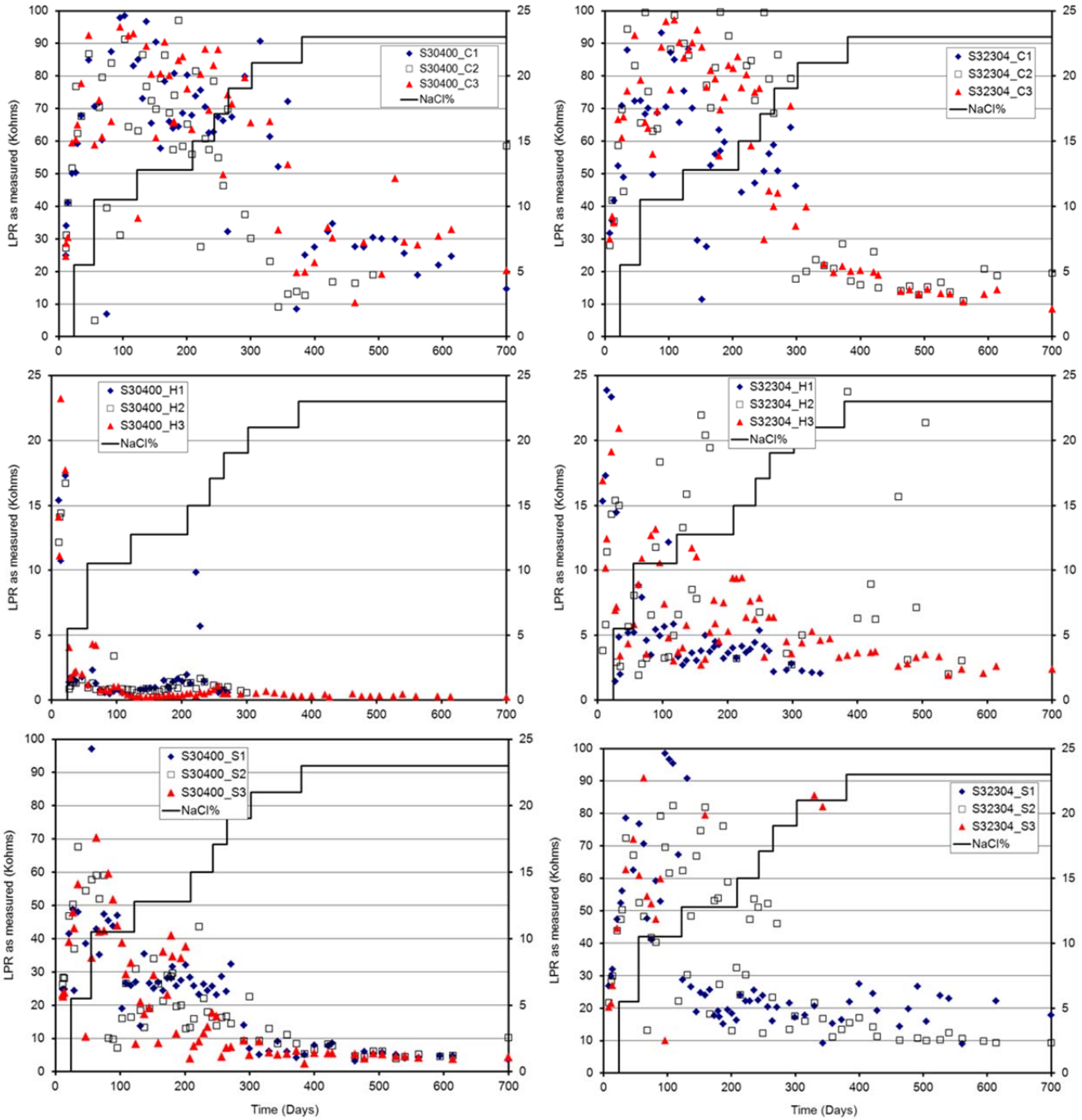

Figure 6.5: Rc vs. time measured on UNS S30400 and UNS S2304 samples (C, H, S surface conditions)

6.1.4.3 Visual Forensic Analysis.

Figure 6.6 to Figure 6.8 show pictures of selected terminated specimens for the various alloys and surface conditions after 200 to 300 days of exposure. Those segments showing corrosion were cleaned as per ASTM G1-03[33]. No record was available of the initial weight; hence the removal of the corrosion products was performed to qualitatively assess the corrosion depth and extent. Figure 6.6 shows rebar segments for alloys UNS S32101. The C segment showed no corrosion, and it is likely that the electrical contact corroded. The H segment showed a small corrosion spot. S terminated specimen showed a thin longitudinal corrosion spot. Upon cleaning it was determined that the corrosion had not penetrated significantly. Figure 6.7 shows the amount of corrosion observed on UNS S32304 terminated segments. All segments showed corrosion spots. Two small spots were observed on C specimen and one spot on S specimen. The corrosion extent on UNS S32304-H1 was significantly larger. Still the depth was similar to the thickness of the mill scale. Figure 6.8 shows the UNS S30400-H1, this was the only one terminated for this alloy. UNS S30400-H1 showed the largest coverage of corrosion from all those terminated. Upon cleaning it was found that corrosion had not consumed all the mill scale.

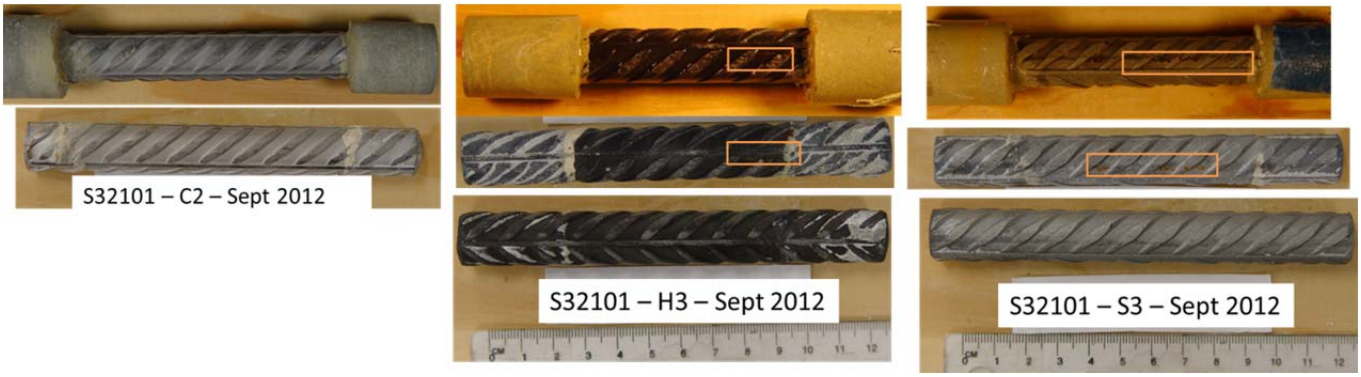

Figure 6.6: Terminated UNS S32101 specimens. Upon removal from solution, after removing mortar and finally after cleaning

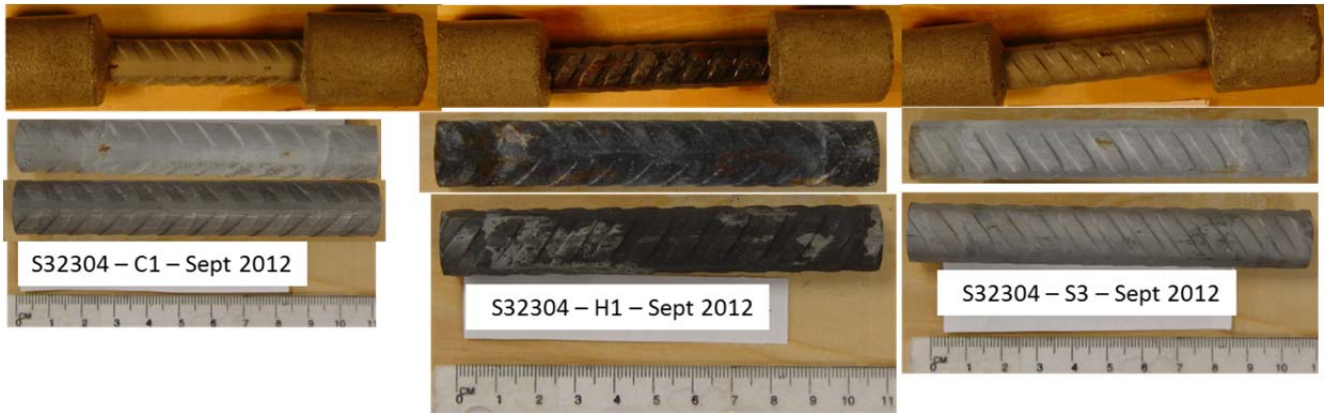

Figure 6.7: Visual inspection on UNS S32304 terminated specimens; top pictures are shortly after removing from solution, middle pictures after removing mortar, bottom pictures after cleaning surface

Figure 6.8: Visual inspection on UNS S30400 terminated specimen. Upon removal of the solution, after removing mortar and after removing corrosion products, bottom pictures after cleaning surface

Figure 6.9 to Figure 6.11 show pictures of selected terminated specimens upon exposure completion for the various alloys and surface conditions after 600 to 700 days of exposure. For these terminated samples the pictures show the surface condition upon removal from the chloride rich simulated pore solution. It is evident that the corrosion spots on C type of surface condition is very small or non-present regardless of the type of alloy.

Figure 6.9: Visual inspection on UNS S32101 terminated specimens after removal from solution

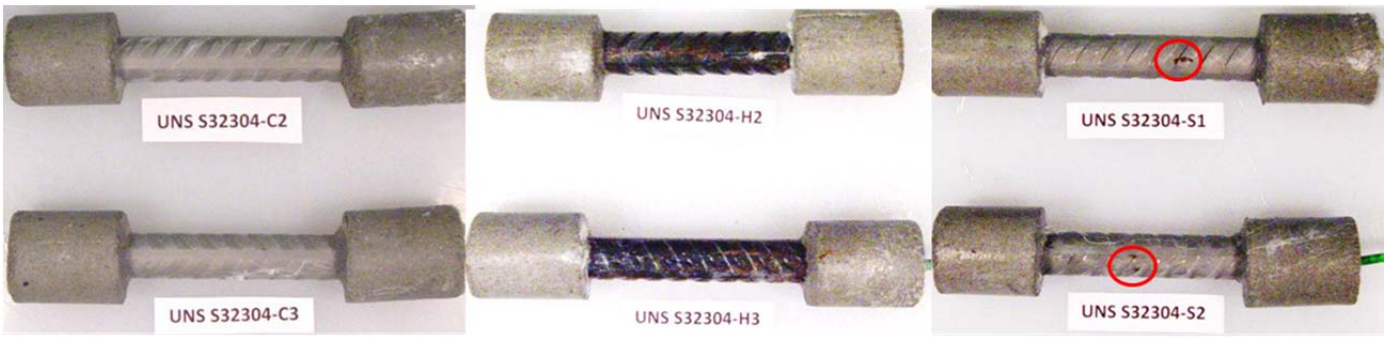

Figure 6.10: Visual inspection on UNS S32304 terminated specimens after removing from solution

All H and S type of specimens showed various degrees of corrosion coverage. Due to the dark red color those with H surface condition are difficult to identify. Usually, H type of specimens had the larger coverage with corrosion products. This agrees with corrosion initiating on these specimens because of low Cr at the surface due to the mill-scale. The S specimens showed small corrosion spots. Interestingly, UNS30400 had the larger corrosion spots on this type of surface condition, followed by UNS32101 and the least number of corrosion spots corresponded to UNS32304. Not shown in here are corrosion spots that took place sometimes at the connection site. This affected the electrochemical measurements. Rebars with surface type C (as receive) either did no show corrosion or it was very small spot, regardless of the alloy type.

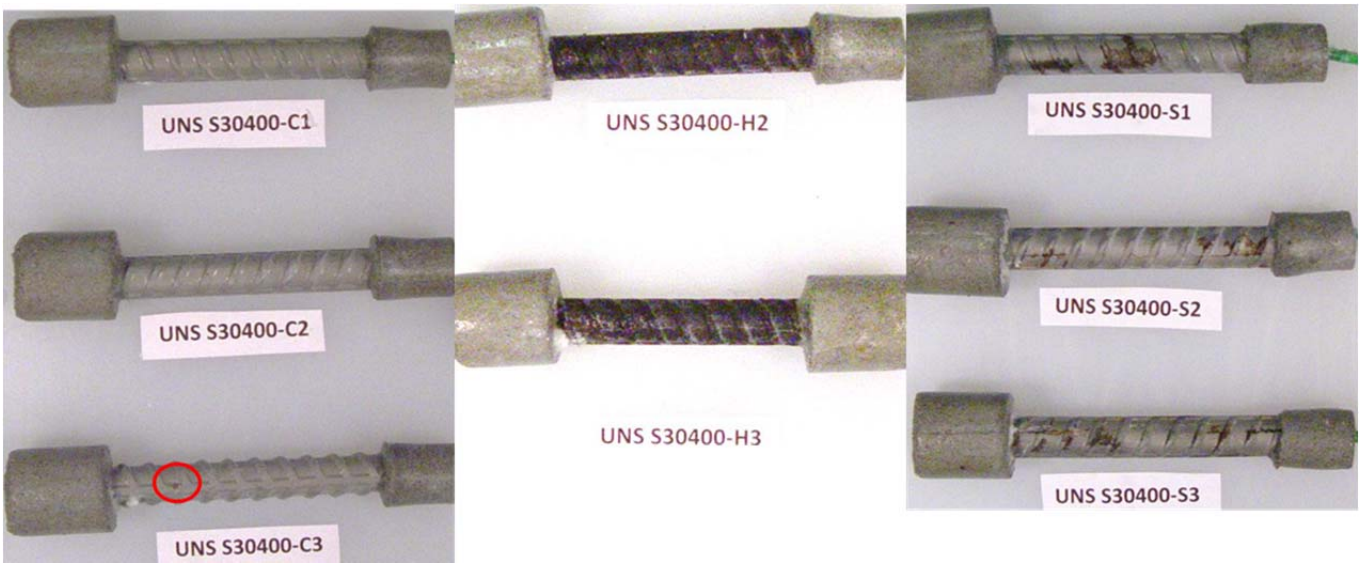

Figure 6.11: Visual inspection on UNS S30400 terminated specimens after removing from solution

The above results suggest that starting with simulated pores solution and incrementally adding chlorides to the solution better resemble how the chloride build up might occur in reinforced concrete structures. The drawback is that this method is quite time consuming and prone to corrosion from the side where the electrical contact is made. Nevertheless, all three alloys seem to perform well in the as received condition. The results suggest that UNS32304 and UNS30400 if properly pickled have a chloride threshold larger than 23.5% NaCl, whereas UNS32101 has a C_T > 11% (largest concentration used in the experiment). It is suggested that a coating by applied to the mortar as a way to prevent corrosion from taking place at the contact site.

6.1.5 CONCLUSIONS

Mill scale presence is detrimental to the chloride threshold of CRA. Removal of mill scale via sandblasting still produces a material with lower chloride threshold than properly pickled rebar.

Rebars segments immersed in SPS for a few weeks followed by NaCl additions over time appears to provide a methodology to follow-up corrosion propagation.

6.2 CRAs EMBEDDED IN MORTAR WITH REDUCED COVER

6.2.1 ABSTRACT

Most corrosion experiments conducted on reinforced concrete are terminated upon corrosion initiation. This paper presents results on corrosion initiation and propagation on three corrosion resistant alloys (CRAs). CRAs embedded in mortar specimens (most with 0.5 w/c ratio) with a reduced cover (~10 mm) exposed to 15% (m/m%) NaCl (initially permanent ponding and later alternate ponding). Three surface conditions were tested on each CRA type: as received, with mill scale, with mill scale then sandblasted. The open circuit potential was monitored over time. Linear polarization resistance and solution resistance were measured periodically. In this research the experiments were not terminated upon corrosion initiation, rather exposure continued to gain a better understand how corrosion propagates. Selected specimens were terminated and visual inspections performed. Cracks appeared only on one type of CRA with millscale or sandblasted surface condition after actively corroding for more than 200 days. However, differential aeration cell might have been responsible for these cracks.

6.2.2 INTRODUCTION

Several authors have investigated corrosion resistant alloys as an alternative to carbon steel reinforcement as an approach to achieve bridge repair-free service life in excess of 75 years. Currently a couple of US state DOTs (Virginia and Oregon) require CRAs rebars be used in new bridge construction exposed to chlorides. Previous studies [9] [24] have identified duplex stainless steel and austenitic stainless (with high Pitting Resistance Equivalent Number (PREN) and with Ni and Mo) as the alloys with the higher chloride threshold. Most of the research reported [12] [13] aimed to determine the chloride threshold was performed in calcium hydroxide solution with chlorides added to this solution; in most instances concurrently. One of the methods developed is to do an anodic potential hold on the studied alloy while exposed to the chloride solutions [12] [13]. Tests in solution provide comparable ranking of the different alloys. However, not enough time is usually allowed during initial immersion in solution for a mature/thick passive layer to form before adding chlorides, as is expected to be present on CRAs embedded in concrete. Based on previous studies that have reported chloride thresholds, a relatively high chloride concentration was first added to the solution when the more corrosion resistant alloys were exposed. In this investigation, linear polarization resistance (LPR) and open circuit potentials (OCP) were used as techniques to monitor corrosion evolution, not necessarily corrosion rate, as the actual active area would not be known (localized corrosion usually occurs on CRAs).

Current procedures of stainless steel (austenitic, ferritic or duplex) rebar include the removal of the mill scale via a process called pickling. The presence of the mill scale in stainless steel has been reported to reduce the chloride

threshold. Some of the initial testing in the US [8] [12] [25] was performed on CRAs where the mill scale was not properly removed. Hanson [24] has reported that mill scale is not too detrimental on higher end stainless steels (UNS S32205, UNS S31600) based on samples immersed in solution and mortar reinforced samples casted with chlorides. Scully and Hurley [12] reported significant reduction in the chloride threshold with the mill scale present (but in their case the mill scale was produced in the laboratory). Based on conversations with stainless steel producers of rebars, improper pickling (or presence of mill scale) is no longer an issue. Pickling is now integrated on the stainless steel rebar production. Several papers report performance of CRAs embedded in concrete. Tests of intermediate CRAs rebars embedded in concrete usually are terminated upon corrosion initiation [8] [28] [29] [30]. Corrosion does not initiate on the more corrosion resistant CRAs embedded in concrete, even if the concrete is poor (i.e. high w/c ratio) and with reduced cover (e.g. 2.5 cm)[8]. Within the literature review performed no results were found describing the propagation stage on CRAs. Some authors venture to indicate that corrosion rate would be slower and hence a longer propagation time (T_p) should be given for CRAs. Hurley and Scully[9] [12] proposed a propagation model to determine the propagation stage.

6.2.3 EXPERIMENTAL PROCEDURE

The alloys investigated in here are: UNS S30400, UNS S32304 and UNS S32101. Table 6-2 contains measured chemical composition on the tested alloys via x-ray fluorescence (XRF). UNS S30400 was recovered from terminated reinforced concrete samples part of a previous research program [8]. The UNS S32304 was from old stock from the same program. Alloy UNS S32101 was provided by a producer during the fall of 2011.

Table 6-2: CRA chemical compositions determined via XRF.

	Mo	Cu	Ni	Fe	Mn	Cr
UNS S30400	0.41	0.42	8.57	71.50	1.08	17.86
UNS S32101	0.16	0.24	1.54	72.03	4.78	20.91
UNS S32304	0.27	0.30	4.09	71.67	1.25	21.90

CRA rebars were segmented into 16 cm long pieces. All tested CRA's were received pickled. Three surface conditions were investigated: pickled (as received), with mill scale, mill scale and then sandblasted. The mill scale was re-created by placing the CRA rebar segments into a high temperature oven at 1050°C for 1 hour and air cooling (after Scully method [12]). This method creates a scale worst that would have been obtained if the rebar segments would have been quenched as is customary in the industrial production line. Selected segments with mill scale were then sandblasted to prepare the third surface condition group. The as received rebar segments are named here C condition, those with mill scale are named here H condition and those with mill scale then sandblasted are identified in here as S condition.

Figure 6.12: CRA reinforced mortars

The CRA reinforced mortar specimens were 7.5 cm tall, 12.5 cm wide and 13.5 cm long (direction of the rebar). Figure 6.12 shows a couple of the specimens during exposure. The rebar was centered along the 12.5 cm x 7.5 cm faces. Each rebar was drilled and tapped on one end to accommodate machine screws that were then used as electrical contacts (See Figure 6.13). The average mortar cover was: 1.05 cm for UNS S30400 (#4 Rebar), 0.91 cm for UNS S32304 and 0.94 cm for UNS S32101 (#5 Rebar). The target w/c was 0.5, but for samples embedded with UNS S32101 the w/c was slightly higher (~0.52 w/c). Silica sand from Florida was used in saturated surface dry condition before adding it to the mix. The proportion of the mortar mix was 2.7/1/0.5 for sand/cement/water respectively. A vibration table was used to properly compact the mortar, the molds were filled in three layers. The rebars were placed at the bottom of the mold. The molds were removed after 24 hrs, and then placed in a high humidity environment for 7 days. The samples were then moved to laboratory humidity and temperature (65-70% RH and 72F). Once the samples were dry enough, the samples were inverted (i.e. rebar closer to the top) and a plastic cylinder (2.5 cm tall, 9.5 cm internal diameter and 11.2 cm outside diameter) glued using a marine grade epoxy. The samples remained with no solution for the rest of the second week. Thereafter a 15% NaCl solution was placed in the reservoir. Alternate immersion began on day 165 for mortar specimens embedded with UNS S30400 and UNS S32304 and on day 40 on specimens with UNS S32101. The schedule for alternate immersion was 4 days wet and 3 days dry. Six mortar specimens with similar cover than those described above but with 0.42 w/c were cast with as received UNS S32304 and Stainless Steel Clad Rebars (3 specimens per rebar type). These specimens were prepared a few years back (currently ~1600 days of exposure). These samples also had a water reservoir installed and 15% NaCl solution. Continuous ponding took place for ~1000 days before starting an alternate immersion schedule.

The OCP was measured at least once a week using a saturated calomel electrode (SCE) as a reference electrode. The OCP measurements were more frequent during the early exposure period. All reported values are in the SCE scale. The solution resistance (Rs) was measured via electrochemical impedance spectroscopy (EIS) and was measured before performing the LPR tests. The solution resistance in here is the impedance modulus measured at 56 Hz. The LPR was performed every week at the beginning, and after ~60 days every 2 weeks or at other frequencies. The LPR tests were carried out from 15 mV cathodic from OCP (i.e. 15 mV below OCP) to the OCP at a rate of 0.1 mV/s. During the alternate immersion period, these tests were performed the last day wet in the cycle. In the results sections Rc values are reported with the Rs subtracted but no area corrected.

Two specimens per surface condition for each CRA type were terminated for mortar specimens with w/c=0.5. Three specimens (2 with UNS S32304 and 1 of the SSC) were terminated from those prepared with w/c=0.41. Visual inspection was performed. Chloride concentration were obtained at the rebar trace away from any observed corrosion sites.

6.2.4 RESULTS

6.2.4.1 Results for CRAs embedded in mortar w/c=0.5

Figure 6.13 shows the potential vs. time measured on UNS S32304 and UNS S30400 rebars embedded in mortar and with three different surface conditions. Two of the UNS S30400-C specimens (C1 and C2) experienced a potential drop by day 50 and might be due to the presence of a higher chloride concentration and C3 specimen experienced a similar potential drop around day 300. Only specimen UNS S32304-C2 experienced a significant potential drop around day 400.

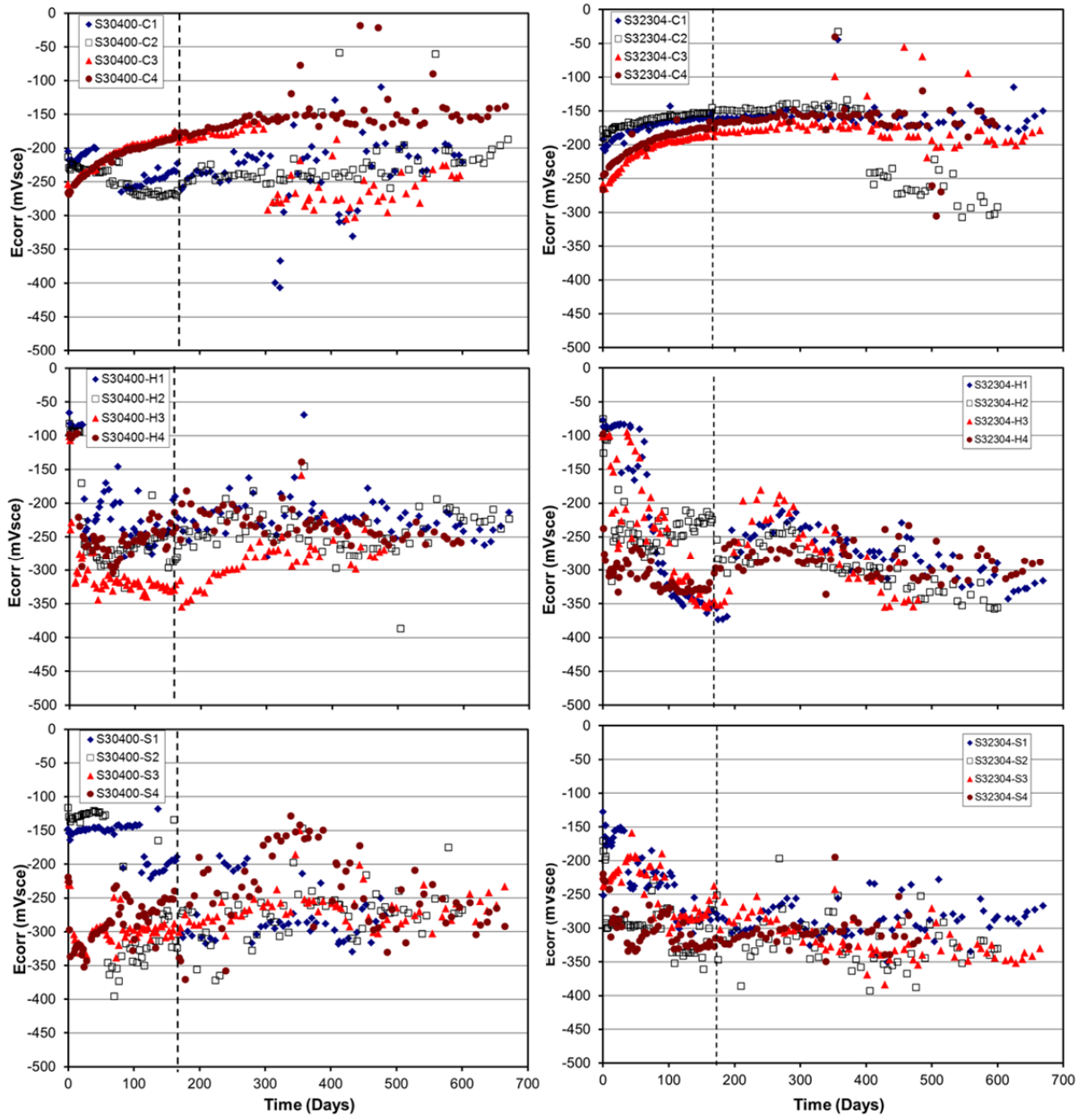

Figure 6.13: Potential evolution on mortar samples with UNS S32304 and UNS S30400 upon exposure to 15% NaCl solution. Wet/dry cycles began on the day indicated by the vertical dash line

A significant potential drop took place on all H and S specimens when compared to initial observed potential values. The potential drop took place at later times on UNS S32304-H specimens than on UNS S30400-H specimens. Two of the UNS S30400-S and two of the UNS S32304-S specimens showed a potential drop almost immediately after filling the reservoir with NaCl solution, the other two showed a potential drop at later times, but before day 200. On several specimens the rebar potential experiences either oscillations or shifted to more positive potential values over time. Figure 6.14 shows potential vs. time for the 3 surface conditions for alloy UNS S32101 and Figure 6.15 shows the corresponding Rc values vs. time obtained on specimens reinforced with

UNS S32101. The potential drop and accompanying decrease in Rc values is even more dramatic on UNS S32101 specimens for all surface conditions. Three of the specimens with C surface condition experienced a potential drop after a relative short period of exposure (within 60 days). The rebar of the fourth specimen showed an initial transition at ~ day 210, but reached potential values as negative as those observed on the other three around day 250. The specimens with UNS S32101-C rebars settle at potentials of -300 to -400 mVsce. More negative potential were observed for UNS S32101-H and UNS S32101-S samples (-320 to -450 mVsce). Figure 6.15 shows the Rc values measured on UNS S32101 specimens. Before the decay in Rc value took place on C specimens the Rc value ranged between 20 and 45 Kohms, and decayed to values ranging between 5 and 10 KOhms. The Rc values measured on H and S specimens range between 10 and 1 Kohms. Not all specimens registered a clear transition/drop in Rc values measured observed before and after the potential drop.

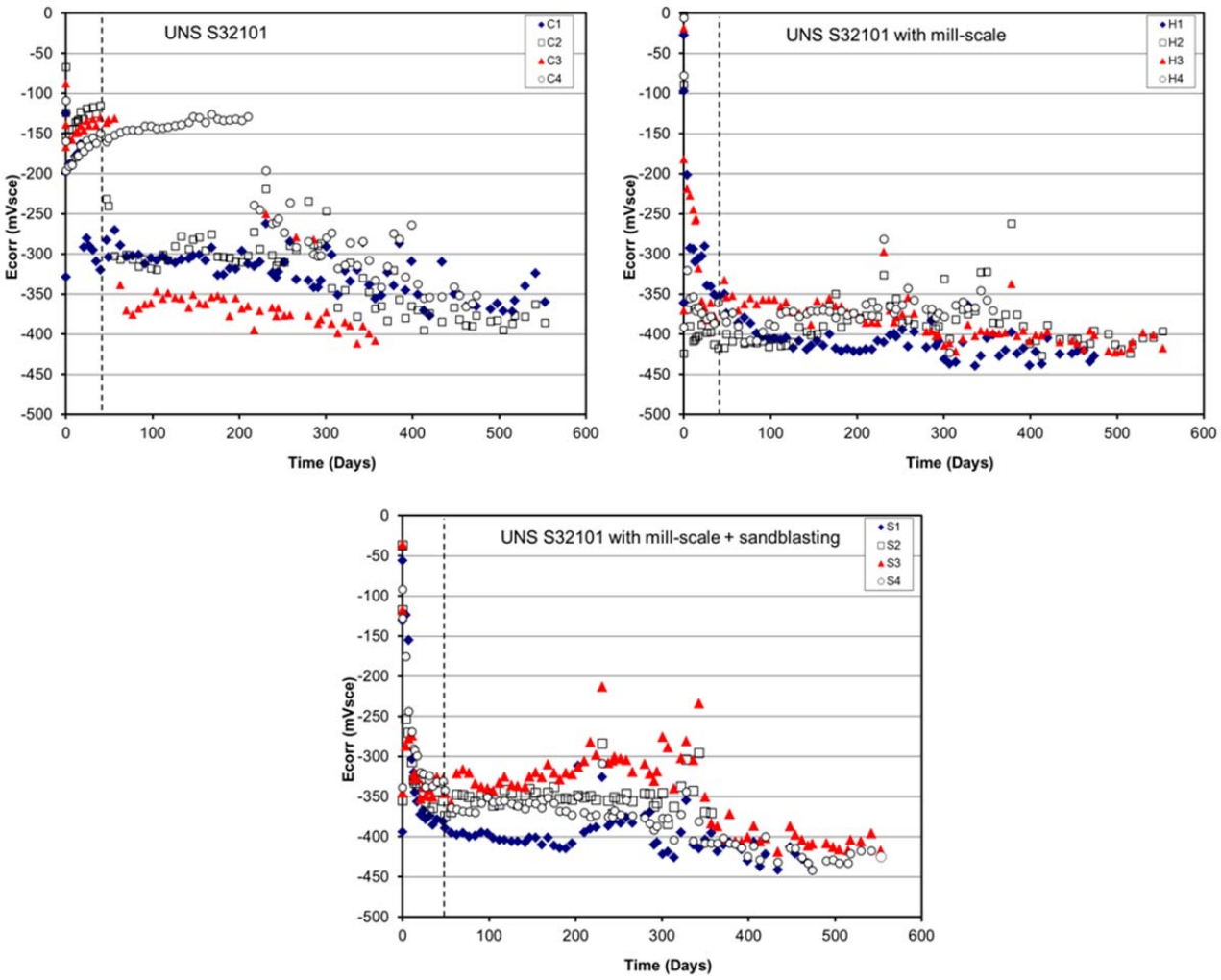

Figure 6.14: Potential vs. time for UNS S32101 embedded in mortar. Wet/dry cycles (4 days wet/ 3 days dry) began on the day 40 indicated by the vertical dash line

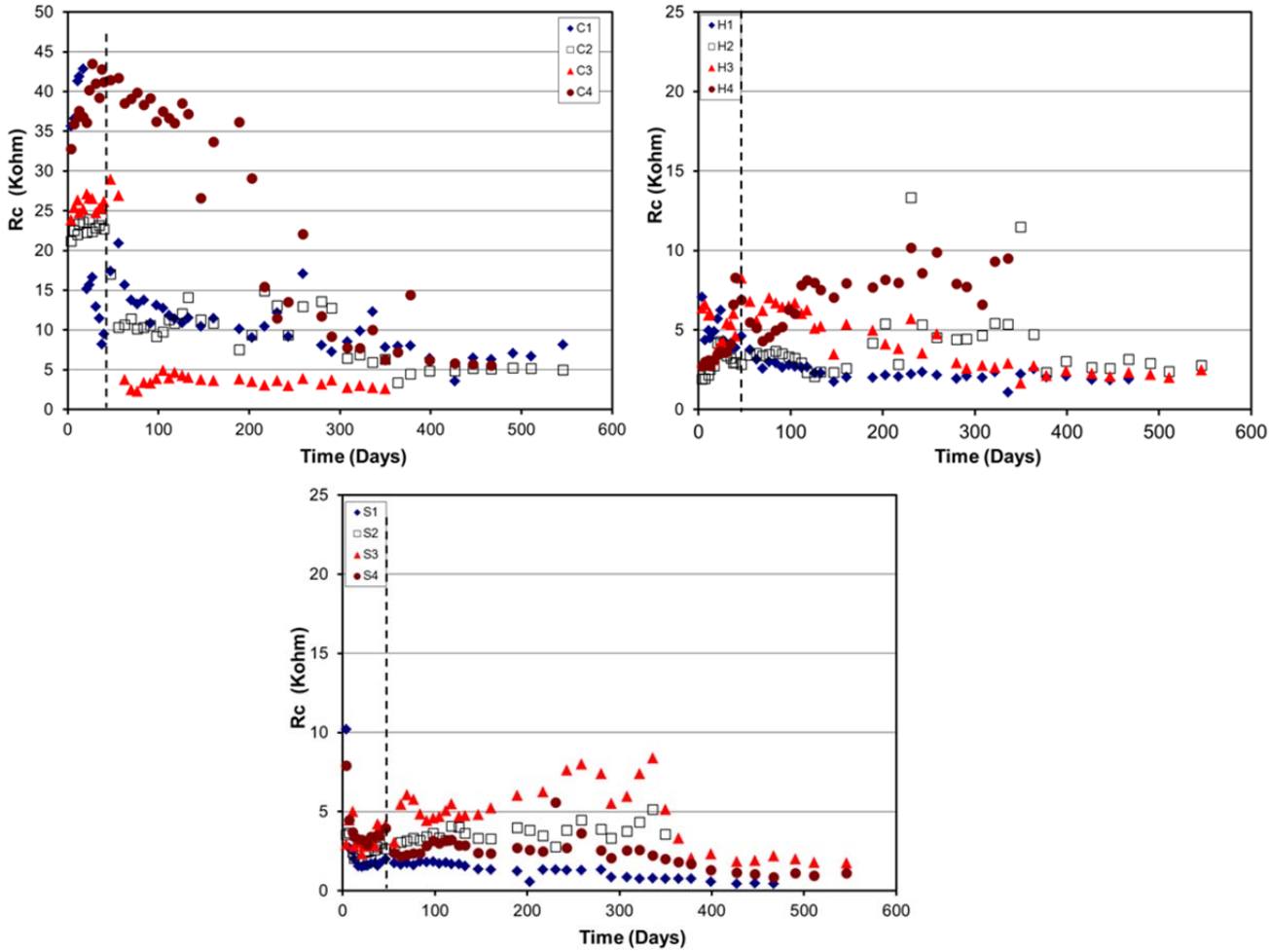

Figure 6.15: Rc vs. time (bottom) on UNS S32101 embedded in mortar. Wet/dry cycles (4 days wet/ 3 days dry) began on the day indicated by the vertical dash line

Figure 6.16 shows Rc vs. time measured on UNS S32304 and UNS S30400 specimens. During the 700 days monitored, the magnitude of the Rc on specimens with C type rebars ranged between 50-90 Kohm on those with UNS S32304 and between 40 and 90 Kohms for those with UNS S30400. Two of the UNS S30400-C (C1 and C3) two of the UNS S32304-C (C2 and C4) have experience a significant reduction of measured Rc to values ranging between 10 and 30 Kohms. After the drop in Rc values, the Rc measured on H type rebars ranged between 1 to 5 Kohms. The mortar specimens with UNS S32304-S type rebars showed Rc values between 25 and 50 Kohms (specimens S1 and S3) before transitioning to lower Rc values (5 to 20 KOhm). In the case of UNS S30400-S specimens the measured Rc values ranged between 5 and 20 KOhm. Two specimens per surface condition and rebar type have been terminated. The remaining mortar specimens will continue to be exposed to alternate immersion and periodic visual inspections are planned to detect for either corrosion spots at the surface or the appearance of cracks. Based on Rc and E measured values it could be argued that all UNS S32101

specimens (i.e. C, H and S specimens) are undergoing corrosion and all S and H type rebar specimens for the other two alloys.

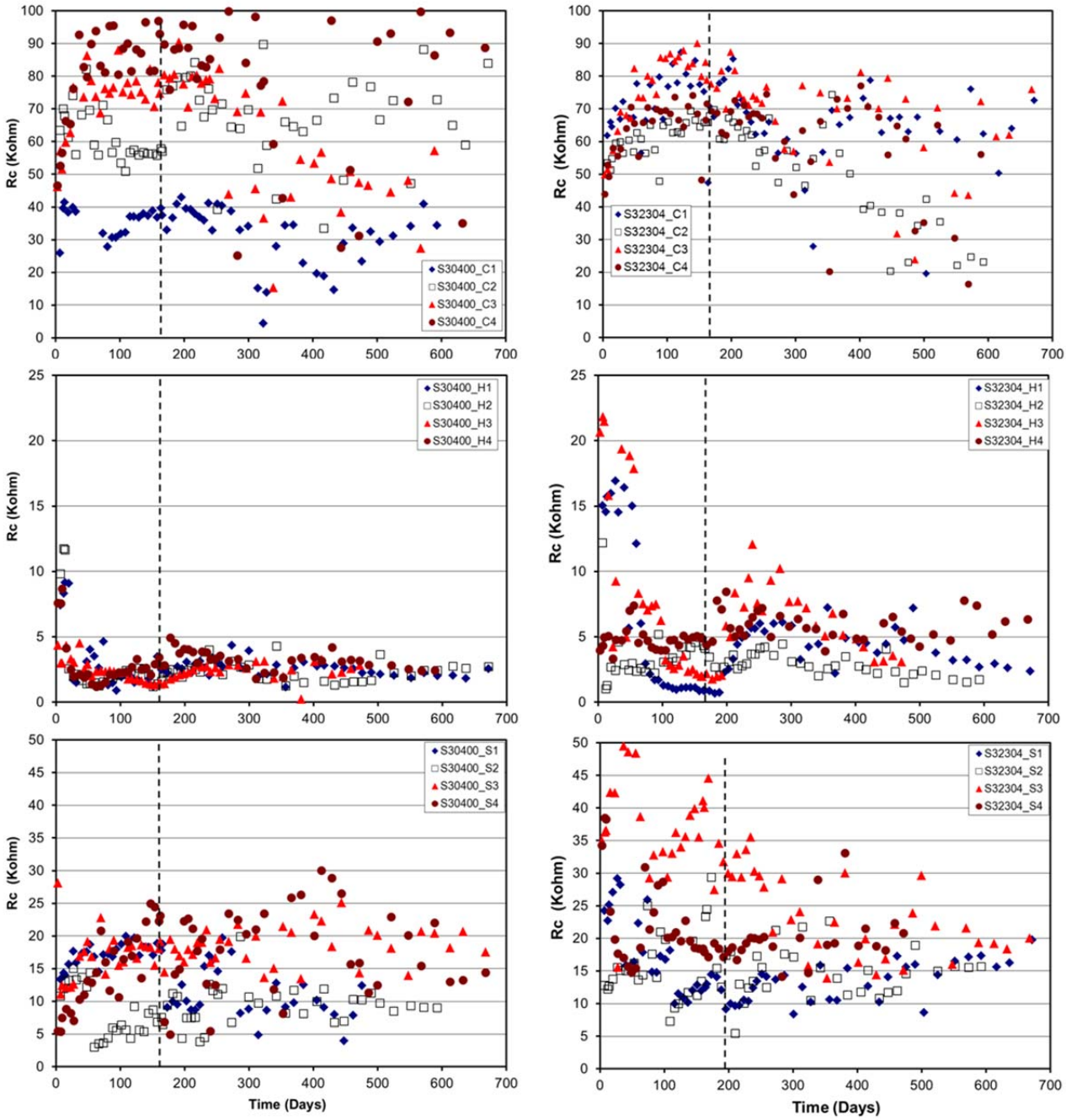

Figure 6.16: Rc measured on UNS S32304 and UNS S30400 embedded in mortar with w/c=0.5. Wet/dry cycles (4 days wet/ 3 days dry) began on the day indicated by the vertical dash line

6.2.4.2 Results for samples in mortar with lower w/c ratio

Figure 6.17 shows both potential vs. time and Rc vs. time on the two sets of reinforced mortar samples prepared with lower w/cm (~0.41 ratio). On the left side are the two potential plots and on the right side the two plots for Rc values vs. time. The potential measured on specimens with UNS S32304 remain between -150 and -100 mVsce for the first 1000 days, during this period the Rc ranged from 20 to 40 KOhm settling at values around 20 KOhm by day 1000. Shortly after starting the wet/dry cycles; specimen A with UNS S32304 experienced both a potential drop (now ~-350 mVsce) and a reduction on measured Rc (to 8-9 KOhms) to about half of the value before the decay (~18 KOhms). The combination of these two values suggest that corrosion has initiated on UNS S32304-A. Rc and potential measured on stainless steel clad (SCC-316) type of specimens experienced a larger scatter with excursions in potential to values as negative as -260 mVsce and corresponding decay in measured Rc (Sample SCC-A).

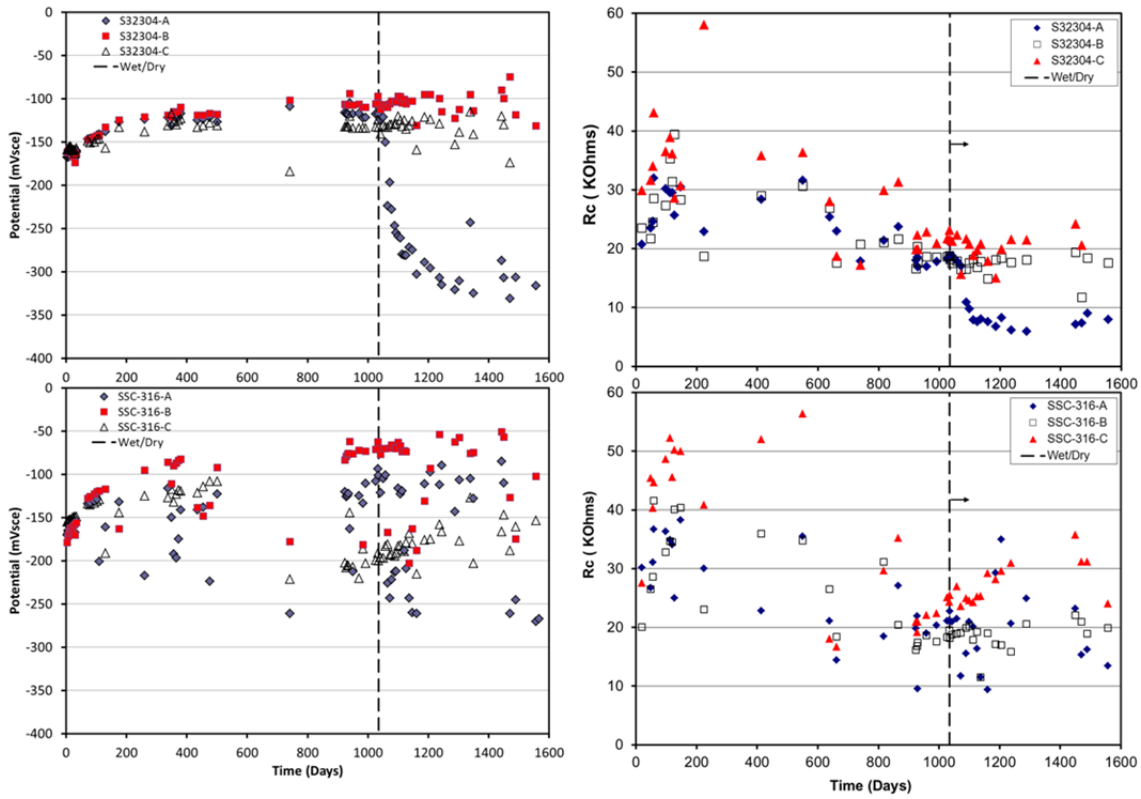

Figure 6.17: Ecorr and Rc measured on UNS S32304 and SSC rebar embedded in mortar with w/c=0.42. Wet/dry cycles (4 days wet/ 3 days dry) began on the day indicated by the vertical dash line

6.2.4.3 Visual inspection of terminated specimens

Figure 6.18 shows the exposed rebar for the rebars embedded as received i.e., type C. One of the two UNS S32304-C specimens showed corrosion and this was a very small site on the top side. No corrosion was observed

on the exposed bottom side. Both UNS S30400-C rebars showed corrosion sites close to the edge on the top side and might be due to a more pronounced differential aeration cell, one of the rebars also showed a corrosion site at the center (circled). The back side of both S30400-C rebars had no corrosion. A similar observation was seen from the pictures obtained on UNS S32101-C rebars, in the sense that corrosion took place on the top side close to the ends of the embedded rebar and one of the two rebars there was a small corrosion spot. Figure 6.19 shows the exposed rebars for both type H and S surface condition. All rebars showed corrosion sites. On H type of specimens and due to the wetting and drying some of the corrosion sites had turned into red rust spots. Both S32304-H and S30400-H rebars had black corrosion spots suggesting on-going active corrosion close to the embedded ends, and on S32304-H3 another spot was found at the center. The corrosion spots on S32101-H rebars were smaller and only small red spots were observed in the area close to the embedded ends. The corrosion extent observed on S type surface condition was less on S32304-S and S30400-S compare to corresponding H type surface condition. Both S32101-S rebar surfaces had corrosion spots with that of specimen S1 being significantly larger and caused a crack on the mortar surface.

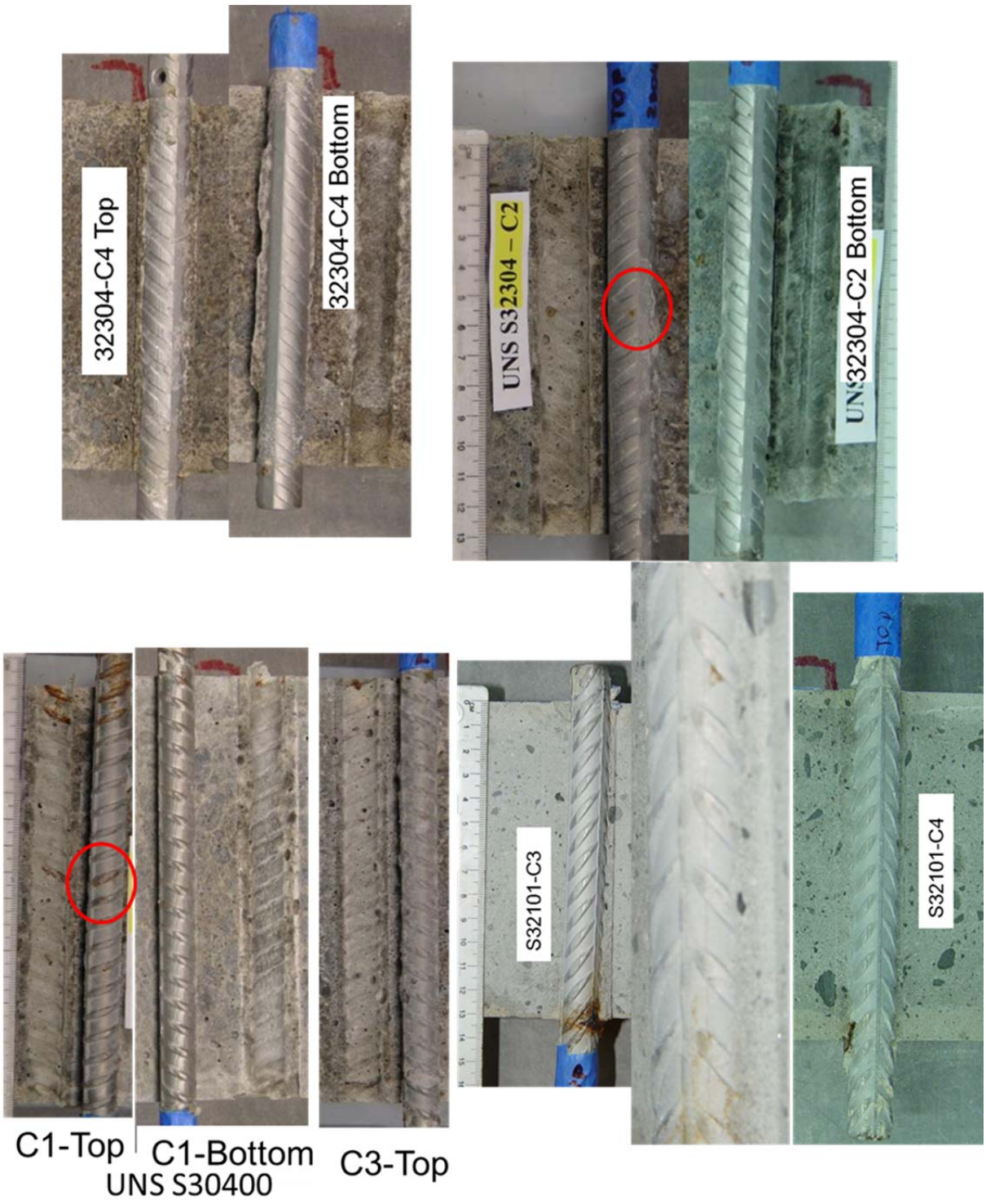

Figure 6.18: As received (C) specimens for the different CRA alloys embedded in mortar w/c=0.5

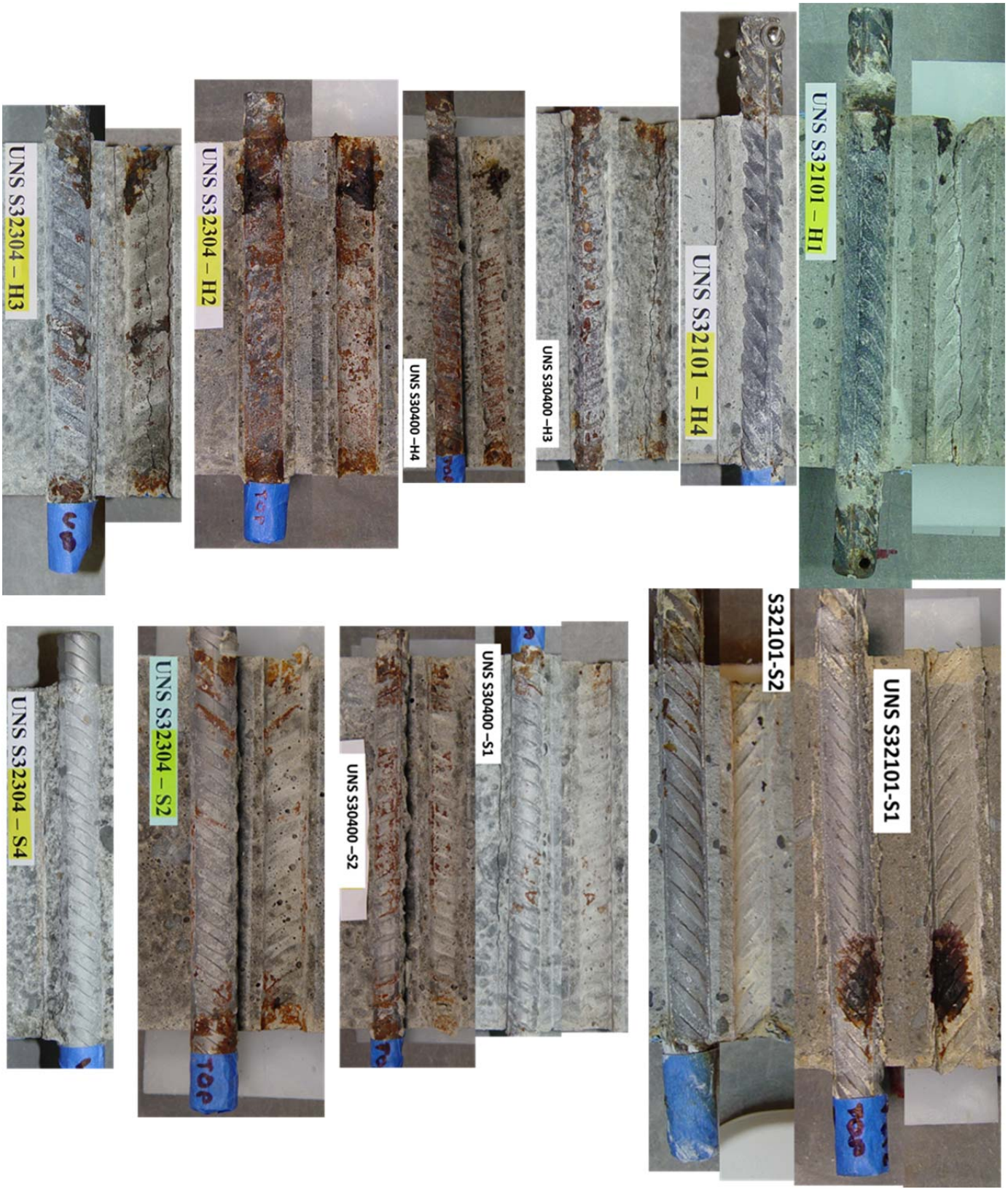

Figure 6.19: Visual examination after exposing rebar for H and S surface condition for the three CRA types

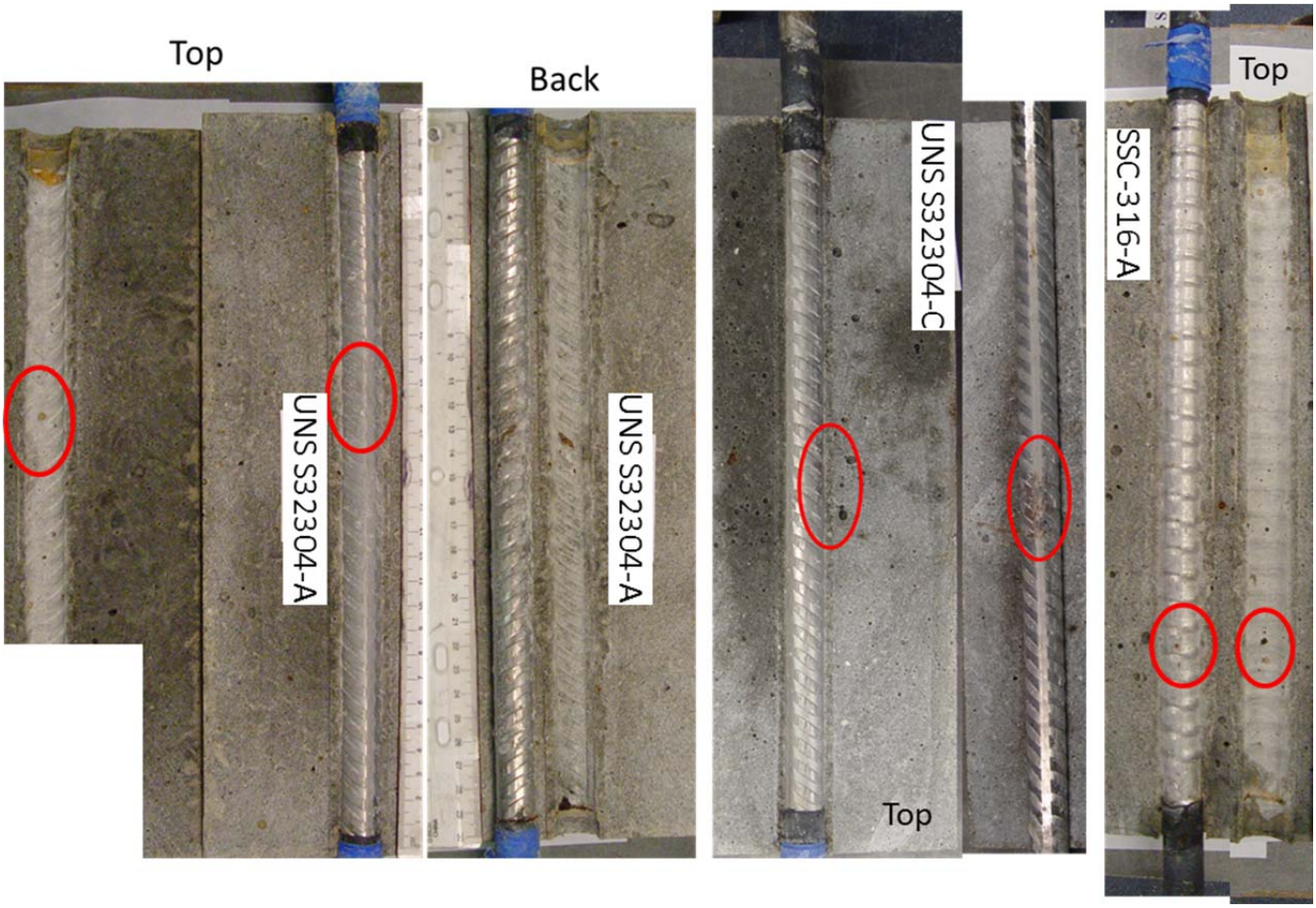

Figure 6.20: As received (C) specimens for the different CRA alloys embedded in mortar w/c=0.41

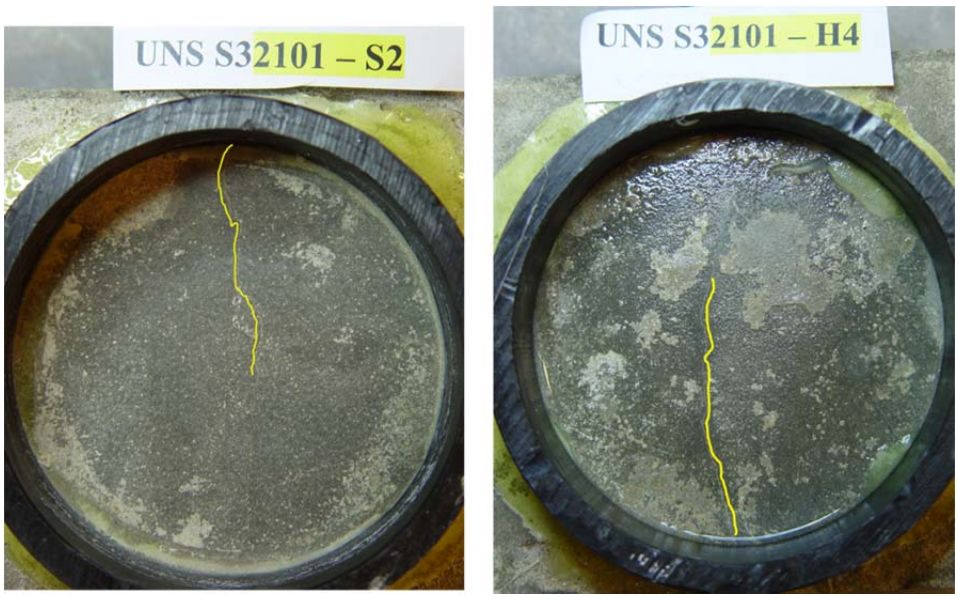

Figure 6.21: Cracks observed on S32101-H and S32101-S

Figure 6.20 shows the rebars surface of the two terminated S32304-C specimens with lower w/c ratio and on SSC rebar. The corrosion spots were significantly smaller even though specimens had been exposed almost three times longer than specimens with higher w/c ratio. On S32304-A rebar a corrosion spot was observed close to the center on the top side and another at the center on the bottoms side, plus a third spot on the bottom side close to the specimen edge. Specimen 32304-C a larger site was observed, but was not quite on the top side, rather 30/45 degrees rotation shows the corrosion site, it appears to be superficial and not to be actively ongoing. This site might have initiated during the negative potential excursion, and re-passivated shortly after. Rebar SSC-A showed a small corrosion spot. The next section discusses the chloride concentration at the rebar trace for these specimens and those described in the previous paragraph.

Another interesting observation is the appearance of crack on a couple of S32101-S and S32101-H specimens. Figure 6.21 shows two pictures of cracks that appeared at the mortar surface after approx. 300 days of exposure. No cracks have appeared on any of the other specimens regardless of surface condition or alloy type.

6.2.4.4 Chloride concentration at the rebar trace

Table 6-3 contains the chloride concentration that was obtained at the rebar trace. Concrete powder was milled on the mortar above the rebar to a depth of 1 to 2 mm maximum. The table reports the values in kg/m3, with respect to mortar unit weight (TW% - mortar unit wt assumed to be 2200 kg/m^3) and as percent of the cement weight (WC% - the cement was 530 kg/m^3, i.e. high cement amount). The chloride concentration ranged from 1.1 TW% to more than 2.4 TW%. No concrete was milled on those specimens in which the corrosion products covered most

of the mortar surface above the rebar trace. Considering only as received condition and the small spots observed it is possible to suggest that the chloride threshold for S30400-C > 1.1 TW%, for S32304-C and S32101-C >= 1.4 TW%. The specimens embedded in lower w/c ratio mortar is in agreement with the above from the values in Table 2 the C_T for S3230A-C low w/c is approx. 1.5 TW%. The cracks shown in Figure 10 might explain why the measured chloride concentration along the rebar trace on S32101-S and S32101-H were significantly larger than on C specimens or for the other two rebar types.

Table 6-3: Chloride concentration measured at the rebar trace on terminated specimens

Specimen	Average Chloride (kg/m3)	TW %	WC %
S30400-C1	24.1	1.1	4.6
S30400-C3	25.6	1.2	4.8
S30400-H3	43.6	2.0	8.2
S30400-S1	44.9	2.0	8.5
S32304-C2	25.0	1.1	4.7
S32304-C4	31.1	1.4	5.9
S32304-H3	38.6	1.8	7.3
S32304-S4	> 53	> 2.4	> 10
S32101-C3	49.2	2.2	9.3
S32101-C4	30.9	1.4	5.8
S32101-H4	> 53	> 2.4	> 10
S32101-S1	> 53	> 2.4	> 10
S32101-S2	> 53	> 2.4	> 10
S32304-A	37.4	1.7	7.1
S32304-C	32.8	1.5	6.2
SSC-A	> 53	> 2.4	> 10

6.2.5 CONCLUSIONS

Mill scale presence is detrimental to the chloride threshold of CRA. Removal of mill scale via sandblasting still produces a material with lower chloride threshold than properly pickled rebar. Corrosion propagation during the monitored time did not cause cracks on the mortars by alloys UNS S30400 and S32304, whereas some of the S32101 did experienced cracks.

The implement method appears to provide a methodology to follow-up corrosion propagation. Even with a reduced mortar cover, corrosion initiation takes several months/years on higher performance CRA rebars. Improvements to the set-up as to minimize differential aeration are recommended.

The chloride threshold for as received specimens appear to be greater than 1.4 percent of the mortar unit weight (for the mortar investigated unit weight assumed was 2200 kg/m3), which corresponds to approx. ~6 percent of the cement weight used in the mix based on the observed results on specimens with w/c=0.41. The threshold appears to be somewhat lower on specimens with w/c=0.5, but might have been influenced by differential aeration cell.

7 HIGH ALKALINITY CEMENTS EFFECT ON THE CONTROL OF ALKALI-SILICA REACTION

7.1 ABSTRACT

Corrosion of reinforcing steel in concrete exposed to sea water has been documented to be as a major cause of bridge deterioration, all over the word and particularly in Florida. Previous research has indicated, however, that as much as a 10-fold in time-to-corrosion can be realized by using high alkalinity cement. Concrete cylinders 10 cm diameter x 20 cm long and concrete prisms 7.5 cm x 7.5 cm x30 cm were prepared. Experiments involved the use of three levels of equivalent alkali content of the cement (EqA - 0.5, 1.0 and 1.2), a local silica sand, and seven coarse aggregates, three of which were limestone from different Florida quarries, and two were granites. Some samples were prepared with concrete that included Spratt limestone and Sudbury gravel, which have been documented previously as being severely and moderately alkali-silica reactivity (ASR) susceptible, respectively. Most mixes were based on Florida Department of transportation Class V concrete. In addition, some concrete mixes were admixed with ASR inhibitor ($LiNO_3$), and most concrete mixes contained fly ash. Measurements of 1) length change, and 2) electrical resistivity were made periodically for times up to eight years for length changes and up to six years for resistivity. During this period of time the specimens were stored in a room at 36ºC and high humidity. At six years of age, selected prismatic specimens were selected for petrographic and thin section examination. The three different Florida limestone coarse aggregate were not found to be ASR prone, based on the length change percentage. However modest amount of ASR was observed on thin section analysis. Modest ASR was determined based on length change percent on Granite containing specimens, however ASR was evident by visual inspection of the thin sections.

7.2 INTRODUCTION

Research carried out at FAU by Hartt [34,35] and also by others [36] using cements with high alkali content (EqA 1.0-1.2) has been demonstrated to extend the corrosion initiation time of reinforcing steel in concrete. The chloride threshold is increased due to the higher [OH^-] [34-36] in high alkali content concretes. Phase 1 of the present study was carried out to determine the suitability of high alkalinity cements to improve durability without modifying physical properties and to control the risk of alkali-aggregate reaction (AAR) [37]. It was found that some of the investigated aggregates were prone to ASR [37].

Alkali-silica reactions have been documented in Portland cement concrete since around 1940. Classical ASR involves alkali cations and OH^- from concrete pore water reacting with metastable forms of SiO_2, which are present in a wide variety of igneous, sedimentary, and metamorphic aggregates used in concrete. The fundamental cause of alkali-silica attack is an elevated [OH^-] in the concrete pore solution from cements rich in Na^+ and K^+ with the reaction product being a gel. Following this, the ASR gel imbibes water which causes the gel to expand. This expansion creates stresses which, in many cases, are sufficiently large and sustained to fracture both the offending aggregate particle and cement paste in contact with the particle. During the initial stage of ASR activity, alkali-silica gel may be formed without any deleterious effects on the concrete: but subsequently, cracking may initiate within the reacting aggregate particles. The particles may be in either the coarse or fine aggregate phase in the concrete. In the early stages of ASR activity, cracks in the reacting aggregate are widest in the particle interior. Often, a darkened rim forms along the outer edge of the reacting aggregate particle, and the cement paste in contact with the particle changes color as it becomes saturated with the gel. As ASR progresses and reaches an advanced stage, the reacting particle is completely gelatinized.

There are very few laboratory long-term exposure studies for concretes prone to experience ASR. The present study describes length changes and resistivity measurements on concrete samples that have been exposed to high humidity and 36ºC for more than eight years. The concrete samples were prepared with a variety of aggregates and 19% fly ash; after six years in this curing environment it is likely these concrete samples are close to full hydration or are fully hydrated. A selected group of prismatic specimens were terminated to evaluate extent of ASR at seven years of age. The elongation change has been measured for over eight years on the remaining samples.

7.3 EXPERIMENTAL

7.3.1 Concrete Mixtures

In order to isolate the effects of alkalinity on concrete properties, concrete mixtures with the same ASTM-type II Portland cement (F1 - EqA 0.54), w/cm, and volume content of aggregates, but different additions of sodium hydroxide and lithium nitrate admixture were prepared. On a cubic meter basis the cementitious material in the prepared concrete (with a few exceptions) included 363 kg of ASTM type II Portland cement and 83 kg of Class F fly ash (FA). The fine aggregate used in the concrete mixes was quartz sand from a Florida source with no history of alkali-silica reactivity (ASR) susceptibility. Additionally, a series of specimens were prepared with as-received high alkalinity cement (HA). Three series were prepared with no FA. The chemical composition of the cements and FA used for the mixes is given in Table 7-1. As aggregates, silica sand from a local source with a fineness modulus of 2.22, and seven coarse aggregates with a maximum nominal size of 10 mm were used in the concrete

mixes. Table 7-2 lists the aggregates and their physical properties. FA was selected as supplementary cementitious material with a cement replacement level of 19%. Table 7-3 lists the different mix designs. The w/cm was 0.41. Reference [37] contains additional detail about the experimental details and properties of the concrete mixes. The mixes with labels Li1 or Li2 indicate that these had lithium nitrate ($LiNO_3$) admixed either at the manufacturer dosage (designation Li1) or at 150 percent of this recommendation (designation Li2).

Table 7-1: Chemical composition of cements and FA used (weight percent)

Designation	SiO_2	$A1_20_3$	Fe_20_3	CaO	SO_3	Na_20	K_20	EqA
F1	19.09	5.59	4.17	63.87	3.55	0.148	0.6	0.544
HA	20.08	4.95	3.05	61.98	4.2	0.278	1.15	1.037
FA	*52.82*	21.9	6.06	4.92	0.27	0.284	1.49	1.267

Table 7-2: Aggregate Properties

Aggregate	Designation	Specific Gravity	Absorption [%]	ASR Reactive
Silica sand	Sand	2.65	1.00	n/a
Florida porous limestone 1	FL1	2.46	3.26	n/a
Florida porous limestone 2	F2	2.43	3.50	n/a
Florida porous limestone 3	F3	2.24	9.00	n/a
Nova Scotia granite	NG	2.65	0.76	n/a
Georgia granite	GG	2.65	0.76	n/a
Sudbury gravel	H2	2.72	0.46	Moderate
Spratt limestone	H1	2.70	0.46	High

Table 7-3: List of mixes

Cement type and alkalinity	Coarse Aggregate						
	FL1	F2	F3	GG	NG	H1	H2
F1	X	X	X	X	X	X	X
F1-EqAl.0	X	X	X	X	X	X	X
F1-EqA1.2O	X	X	X	X	X	X	X
F1-EqA1.0-Lil	X	X	X	X	X	X	X
F1-EqA1.0-Li2	X			X	X	X	
F1-EqA1.20-Li1	X	X	X	X	X	X	X
F1-EqA1.20-Li2	X			X	X	X	
HA	X	X	X	X	X	X	X
F1-NFA	X					X	X

EqA: Equivalent Alkalinity. Li: $LiNO_3$ addition dosage NFA- No Fly Ash

Two types of specimens were prepared: prisms and cylinders. Four prisms (76mm x 76mm x 300mm) and eight cylinders (100mm diameter x 200mm) were cast per concrete mix. The specimens were de-molded after 24 hours,

the samples were thereafter cured/stored in sealed buckets at 95% relative humidity and 36ºC. Length changes were performed on concrete prisms and resistivity measurements on concrete cylinders. (Some of the concrete cylinders were also used for 28 day compressive strength [37]). In addition, petrographic analyses were performed on concrete selected specimens at the end of year one [37] and year seven. Selected cylinders were selected at an age of six year, for bulk diffusion exposure and compression strength (half cylinder), for most mixes that have EaA of 0.54.

7.3.2 Length Changes

The measurements were performed according to ASTM C1293 [38]. According to this standard, an expansion of 0.04% is designated as the threshold below which an aggregate is thought to be long term serviceable. A more detailed classification is provided by CSA A23.2-27A [39] which set moderate and highly reactive levels. The length of the concrete prisms was measured at 0, 7, 14, 28, 56, and 90 days, every month up to 600 days and more sporadically thereafter. The specimens were taken out of the hot-room and allowed to cool at laboratory ambient temperature over a period of 16-24 hrs. It was observed that this amount was not long enough in some cases, thus the exposure to ambient temperature was extended to 48 hours for the last several length measurements. The prisms were then removed from the bucket and their length measured using a pair of calipers with a resolution of 0.02mm and a length comparator with a resolution of 0.002mm.

7.3.3 Resistivity

Resistivity measurements were taken using a four point Wenner probe according to FDOT FM 5-578[3]. Measurements were performed four times during the first two years and more sporadically thereafter. The distance between electrode tips center to center was 38mm. The results shown in the plots (see the results section) correspond to the geometry normalized resistivity average of three specimens (after 2 years the average of two specimens), from each cylinder eight readings were taken. The geometry constant for the cylinders is 1.92 [15] when using a spacing a=3.8 cm, due to the cylinder finite dimensions.

While performing some of the more recent tests, it was realized that a period longer than 24 hours is sometimes needed to allow the concrete cylinders to reach room temperature. Also, the moisture content and temperature in the lab were sometimes not maintained due to periodic A/C failures or scheduled maintenance. The moisture content was also affected when a long period of time passed before checking the water level in the storage container. These conditions resulted on spikes (up- or down-wards) in the measured values on both length change and resistivity measurements. Most of these spikes are included in the plots shown in the result section, with just a few of them removed. For the cases in which the resistivity was significantly smaller, this might be due to higher concrete temperature [40,41] at the moment the measurements were performed. In the cases in which the

resistivity was larger than subsequent measurements, lower moisture content might explain these results. [42,43] Cylinders from several mixes were selected for water immersion for up to 30 days. During this time the weight gained was measured. The resistivity was monitored during this period: only those concrete with resistivity larger than 80 kohm-cm experienced some resistivity reduction with time. It was then decided to revisit the effect of temperature on resistivity reported by several researches [40] [42] [45] [46], the results of these measurements are part of a chapter in volume two of this report.

7.3.4 Non-Steady-State Diffusion

Several of the cylinders immersed in water for resistivity measurements were selected for rapid migration testing as per NT Build 492[16]. The migration tests took place after completing the resistivity and temperature effect cycles. Since each cylinder was exposed to high moisture conditions and then immersed in water, the saturation with vacuum step was not performed. The results from these tests were then added to chapter discussing the migration coefficient determination of mature concrete with FA.

7.3.5 Bulk Diffusion

Most of the series of specimens with EqA=0.5 were selected for Bulk diffusion test in 15% NaCl after completing resistivity and temperature effect cycles. The exposure time in sodium chloride solution was one year. See volume 2 for the results of these tests.

7.3.6 Visual Observation

Pictures and maps of the surface condition of each prism were recorded at approx. 6 years of age. From these images and specimen length change vs. time several series were selected for further analysis. One prism from these selected mixes was terminated for petrographic (lapped slices) and thin section characterization via a polarizing light microscope. Two slices per terminated specimens were obtained via wet-saw cuts. The cuts were made perpendicular to the longitudinal direction. These pieces were sent to a contractor to obtain the lapped surfaces and the thin sections.

Upon receiving the lapped specimens this were photograph with no magnification and then a stereomicroscope was used to photograph individual coarse aggregates.

The thin sections were analyzed using a polarizing light microscope. Collages of pictures were prepared on occasions where ASR was identified. Each thin section was divided into grids and most of the pictures identify the row and column from where the pictures were taken.

7.4 RESULTS AND DISCUSSION

In the following sections the mix designs nomenclature will be shown according to the materials and admixtures used according to the following convention:

##/XX/YY/ZZ/WW

Where,

indicates the identification number of the mix design, XX indicates the cement type according to Table 1, YY indicates the aggregate type according to Table 2, ZZ indicates the intended EqA of the mix, and WW indicates the dosage of lithium-based ASR preventing admixture.

7.4.1 Length Change

The results were organized such that mixes containing the same aggregate are presented in one plot so that differences in length change can be best compared. Figures 1 to 4 present the length change with time.

Following the procedure of ASTM C1293, data from at least three specimens were available at every early age. In the plots each point corresponds to the average of four specimens during the first 365 days and three specimens thereafter. In a few instances the average shown after 700 days correspond to values obtained from two specimens. After 2500 days a few instances the values shown represent a single specimen, but for most cases is the average of two or three specimens.

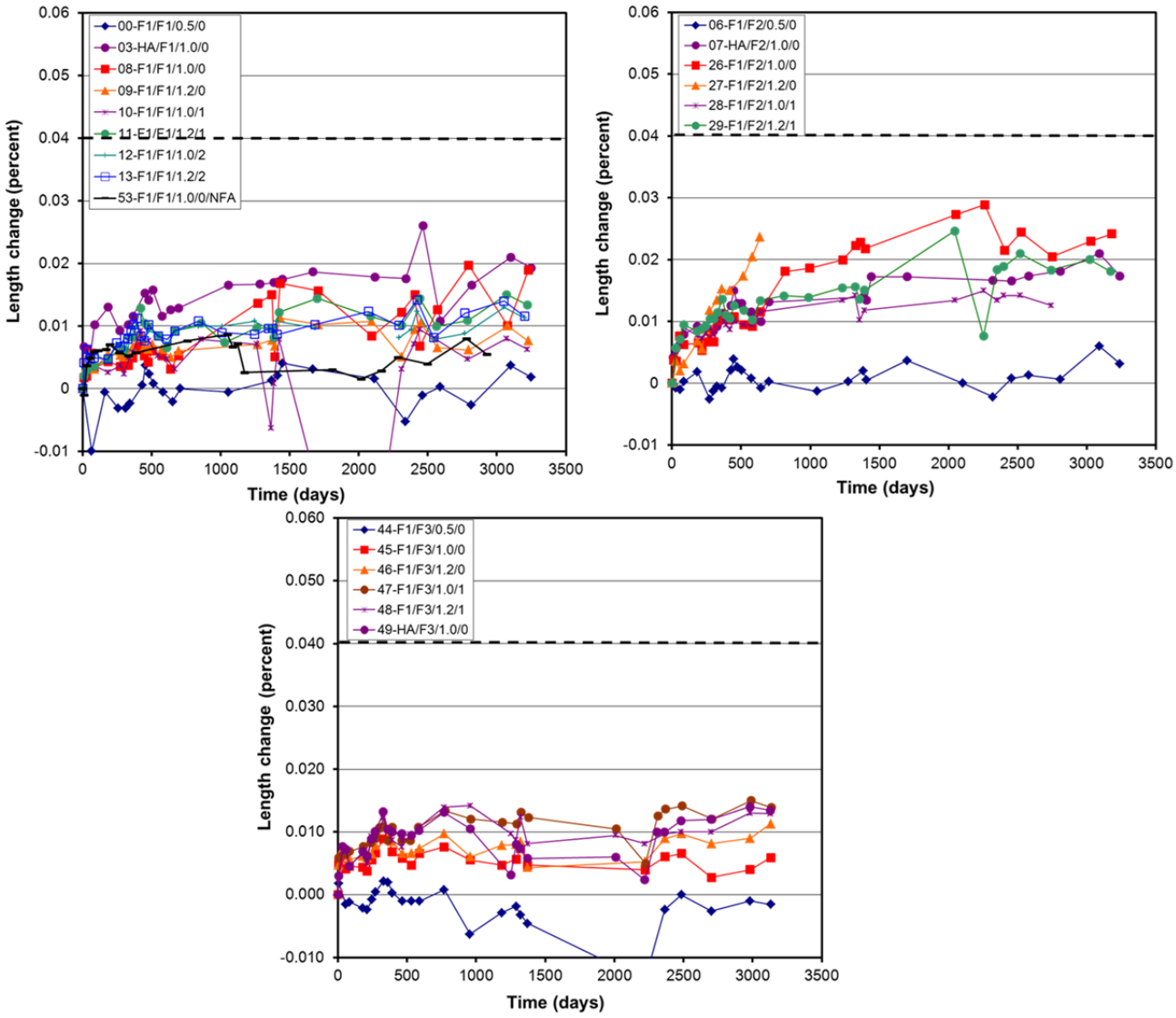

Figure 7.1: Length change (%) for concrete prisms prepared with Florida aggregates

7.4.2 Specimens with Florida Limestone

Figure 7-1 shows the plots for specimens with the three Florida aggregates and Tables 7-4, 7-5 and 7-6 lists expansions at one, two and eight years of exposure for F1, F2 and F3 coarse aggregates respectively.

Table 7-4: Listing of concrete series with FPL-1 coarse aggregate and length change after one, two and eight years

Concrete Series No.	Cement Type	Na20e, percent	LiNO3 Dosage	Expansion, percent		
				One Year	Two Years	Eight Years+
0	F1	0.5	0	-0.0024	-0.0021	0.0037
3	HA	1.0	0	0.0116	0.0129	0.0210
8	F1	1.0	0	0.0049	0.0053	0.0189
53	F1	1.0	0	0.0058	0.0076	0.0049
9	F1	1.2	0	0.0065	0.0060	0.0100
10	F1	1.0	1	0.0058	0.0047	0.0080
11	F1	1.2	1	0.0083	0.0092	0.0150
12	F1	1.0	1.5	0.0095	0.0092	0.0130
13	F1	1.2	1.5	0.0102	0.0092	0.0140

FPL1 specimens. Prisms with EqA = 0.5 exhibited contractions (average 0.0024 percent at one year and 0.0021 percent at year two, but by year eight an average expansion of 0.0037). For all other FA specimens the average two year expansion was 0.0088±0.0040 percent and the average eight year expansion was 0.0131±0.0054; this is about 60% greater value over 6 years. As such, expansions for each series were relatively modest, as were variations between the different series, the latter probably being within the range of normal measurement scatter.

Table 7-5: Listing of concrete series with FPL-2 coarse aggregate and length change after one, two and eight years

Concrete Series No.	Cement Type	Na_2O_e, percent	$LiNO_3$ Dosage	Expansion, percent		
				One Year	Two Years	Eight Years+
06	F1	0.5	0	0	0.0002	0.0007
07	HA	1.0	0	0.0102	0.0130	0.0210
26	F1	1.0	0	0.0112	0.0115	0.0244
27	F1	1.2	0	0.0152	0.0236	-
28	F1	1.0	1	0.0116	0.0116	0.0218
29	F1	1.2	1	0.0136	0.0134	0.0210

FPL2 specimens.- Expansions for the HAC cement series exceeded those with the F1 (EqA= 1.0 and no LiNO3) over the first 600 days, this trend was reversed henceforth. All shown values were below 0.03 percent length change. Most series remained well below the ASTM C1293 threshold (0.04 percent after one year). Length increases between years one and two were nil or modest except for concrete series 27 (Na2Oe = 1.2 and no LiNO3), which had a 55 percent increase and were terminated shortly after day 600.

Table 7-6: Listing of concrete series with FPL-3 coarse aggregate and length change after one, two and eight years

Concrete Series No.	Cement Type	Na_2O_e, percent	$LiNO_3$ Dosage	Expansion, percent		
				One Year	Two Years	Eight Years+
44	F1	0.5	0	0.0020	0.0008	-0.0010
45	F1	1.0	0	0.0089	0.0076	0.0066
46	F1	1.2	0	0.0089	0.0097	0.0113
47	F1	1.0	1	0.0108	0.0134	0.0150
48	F1	1.2	1	0.0100	0.0118	0.0129
49	HA	1.0	0	0.0104	0.0131	0.0140

Specimens with FPL-3 aggregate. Prisms with EqA = 0.5 exhibited a small contraction by year eight. For all other specimens the average second year expansion was 0.0105±0.0029 percent, and for the year eight the average expansion was 0.0120±0.0033, i.e., just a very modest increase in expansion. As for FPL-1 and FPL-2, expansions remained well below the ASTM C1293 threshold (0.04 percent after one year). Length increases between years two and eight, were modest which suggests that the reaction that gave rise to expansions during year one and two had subsided or ceased.

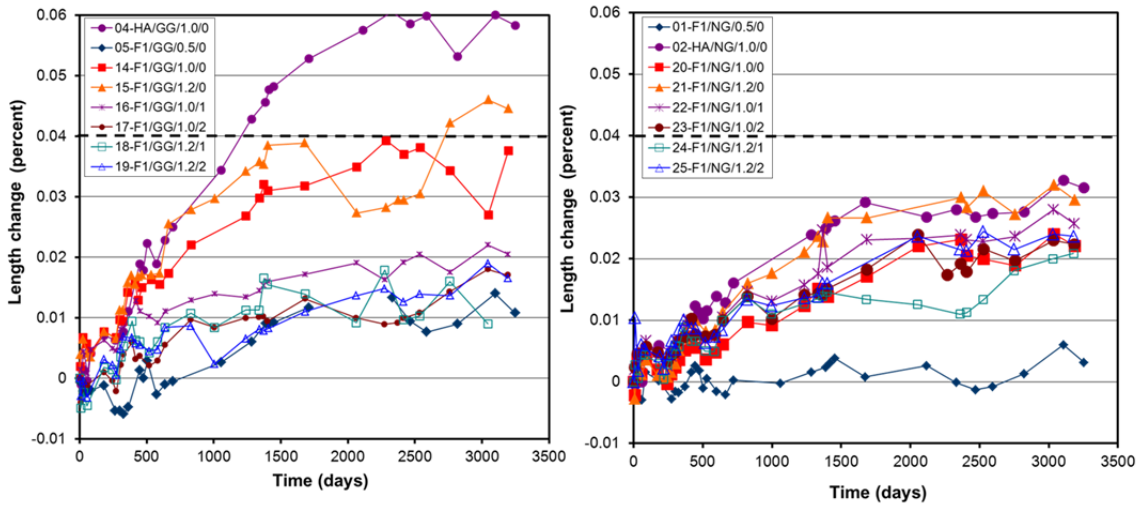

Figure 7.2: Length change (%) for concrete prisms prepared with Georgia(GG) and Nova (NG) granites coarse aggregates

7.4.3 Specimens with Granite Aggregate

Figure 7.2 shows the plots for specimens with the granite aggregates (GG or NG) and Table 7-7 and 7-8 lists expansions at one, two and eight years of exposure for specimens with GG and NG respectively.

Table 7-7: Listing of concrete series with GG coarse aggregate and length change after one, two and eight years

Concrete Series No.	Cement Type	Na_2O_e, percent	$LiNO_3$ Dosage	Expansion, percent		
				One Year	Two Years	Eight Years+
04	HA	1.0	0	0.0091	0.025	0.0599
05	F1	0.5	0	0.0047	-0.0005	0.0140
14	F1	1.0	0	0.0142	0.0252	0.0420
15	F1	1.2	0	0.0158	0.0289	0.0460
16	F1	1.0	1	0.0083	0.0152	0.0220
17	F1	1.0	1.5	0.0026	0.0089	0.0200
18	F1	1.2	1	0.0041	0.0118	0.0160
19	F1	1.2	1.5	0.0059	0.0087	0.0190

Specimens with Georgia Granite.

The 0.04 threshold length change (%) was exceeded shortly after day 1000 on mix 04 specimens (HA cement and GG aggregate) and by year eight the expansion on this series had reached 0.059 percent. Two other GG series (mixes 14 and 15 with EqA=1 and EqA=1.2 respectively) also exceeded the 0.04 % threshold by year eight, suggesting that ASR is on-going. Specimens with GG aggregate and HA cement showed the largest expansions, when compare to those with EqA=1 or EqA=1.2. All other specimens also showed a larger expansion that that observed after two years, but did not exceed 0.025 percent. Specimens containing Li solution had a reduced length change rate compared to those with high EqA and no inhibitor. A slightly larger expansion was observed on specimens with EqA=1 and Li inhibitor (1 or 1.5 dosages) than on those with EqA=1.2 and Li.

Nova Granite Aggregate Specimens.

On samples with NG and high alkalinity (HA, EqA=1 and EqA=1.2) a modest monotonic increase in length change was observed, by day 3300 the observed-length change exceeded 0.03 percent elongation on Series 02 and 21 (HA and EqA=1.2 respectively) and was slightly larger than that observed on Series 20 (EqA=1). The monotonic increase in length change was also observed on specimens with high EqA and Li. This suggests that the Li inhibitor is not as effective in stifling the ASR.

Table 7-8: Listing of concrete series with NG coarse aggregate and length change after one, two and eight years

Concrete Series No.	Cement Type	Na_2O_e, percent	$LiNO_3$ Dosage	Expansion, percent		
				One Year	Two Years	Eight Years+
01	F1	0.5	0	-0.0008	-0.0003	0.0060
02	HA	1.0	0	0.0075	0.0160	0.0327
20	F1	1.0	0	0.0051	0.0097	0.0240
21	F1	1.2	0	0.0071	0.0160	0.0320
22	F1	1.0	1	0.0085	0.0192	0.0280
23	F1	1.0	1.5	0.0073	0.0163	0.0230
24	F1	1.2	1	0.0089	0.0137	0.0209
25	F1	1.2	1.5	0.0100	0.0134	0.0244

7.4.4 Specimens with ASR-Prone Aggregates

Figure 7.3 shows plots for specimens with the two aggregates known to be prone to AAR (H1 and H2) and Table 7-9 and 7-10 lists expansions at one, two and eight years of exposure for specimens with H1 and H2 respectively. On specimens with (HA, EqA=1 and EqA=1.2) and coarse aggregate H1 or H2 the threshold was exceed by day 400 and 1200 of exposure respectively. The average prism rate of length increase and rate of increase for the HAC cement (series 02) was higher than for the other series beyond year one. The presence of Li inhibitor reduced the expansion rate, compared with those with high EqA and no Li present. The figures suggest that the expansion has stifled on specimens with high EqA and Li inhibitors for specimens with both aggregate types. It is not clear if additional exposure would produce additional expansion.

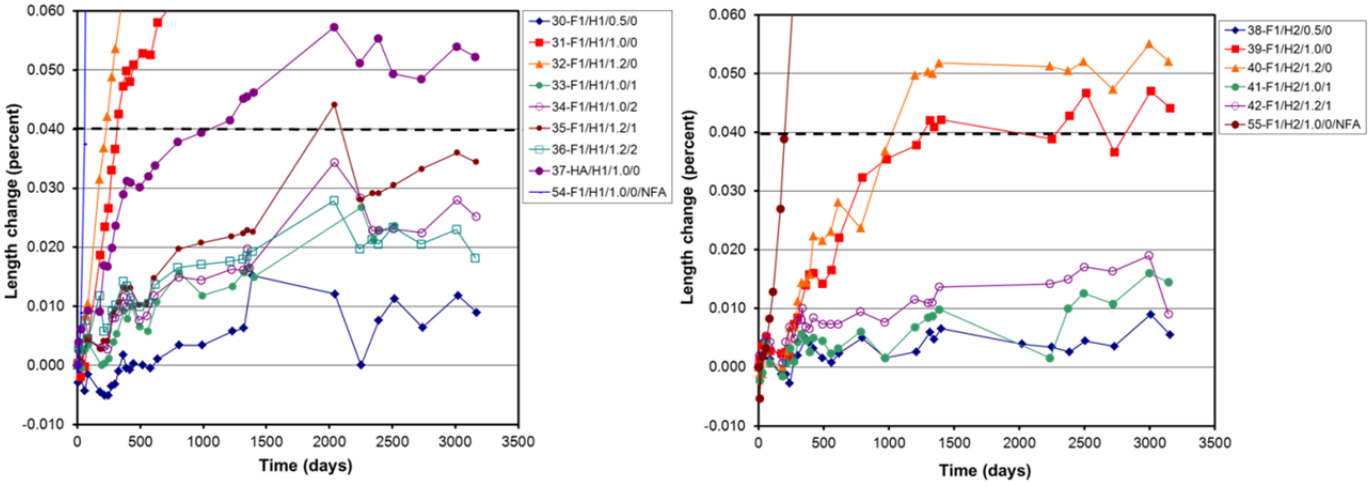

Figure 7.3: Length change (%) for concrete prisms prepared with H1(Spratt) and H2 (Sudbury) coarse aggregates known to be moderate and highly ASR reactive

Considering the variety of aggregates, alkali contents, and lithium nitrate additions, a wide range of expansions was anticipated. The largest expansion was exhibited by specimens with higher alkali content containing no lithium admixture with coarse aggregates prone to ASR, followed by mixes incorporating the latter, and finally, the plain mixes with 0.5% EqA cement which in some cases exhibited contractions and oscillations.

Table 7-9: Listing of concrete series with H1 coarse aggregate and length change after one, two and eight years

Concrete Series No.	Cement Type	Na_2O_e, percent	$LiNO_3$ Dosage	Expansion, percent		
				One Year	Two Years	Eight Years+
30	F1	0.5	0	0.0018	0.0034	0.0118
31	F1	1.0	0	0.0473	0.0688	0.0854
32	F1	1.2	0	0.0796	0.0801	0.1120
33	F1	1.0	1	0.0093	0.0157	0.0236
34	F1	1.0	1.5	0.0116	0.0149	0.0283
35	F1	1.2	1	0.0132	0.0176	0.0362
36	F1	1.2	1.5	0.0142	0.0166	0.0234
37	HA	1.0	0	0.0322	0.0389	0.0554
54*	F1	1.0	0	0.346	0.3984	0.4000

Table 7-10: Listing of concrete series with H2 coarse aggregate and length change after one, two and eight years

Concrete Series No.	Cement Type	Na_2O_e, percent	$LiNO_3$ Dosage	Expansion, percent		
				One Year	Two Years	Eight Years+
38	F1	0.5	0	0.0049	0.0050	0.0090
39	F1	1.0	0	0.0139	0.0323	0.0472
40	F1	1.2	0	0.0144	0.0240	0.0550
41	F1	1.0	1	0.0045	0.0060	0.0161
42	F1	1.2	1	0.0069	0.0095	0.0191
43	HA	1.0	0	0.0090	0.0147	0.0239
55*	F1	1.0	0	0.0852	0.1833	0.2263

Although an expansion difference between reactive and non-reactive aggregates was evident, the maximum expansion after one year was an order of magnitude less than the results found in the literature for specimens similarly exposed [47]. This difference in length change is attributed to the use of FA as cement replacement in the present specimens. Feng [48] and Thomas [49,50] among others have also reported the beneficial effects of FA and Li on reducing ASR rate. This was confirmed by casting a series of mixes with no cement replacement by FA. The results of the expansions for these mixes are presented in Figure 7-4. By day 2500 of exposure, the expansion measured on specimens with H1 and H2 was ~0.39% and ~0.22% respectively, plateaus were reached by day 1000 or shortly after.

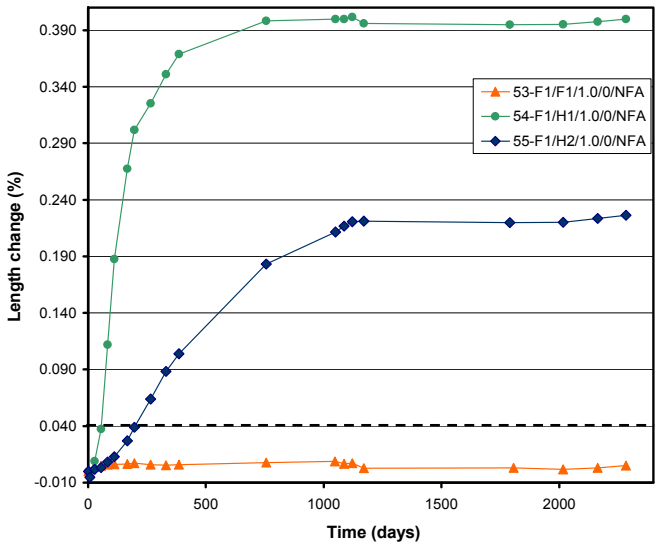

Figure 7.4: Length change for prisms with no fly ash, prepare with FL1, H1 and H2 coarse aggregates

7.4.5 Resistivity vs. Time

The results were organized such that mixes containing the same aggregate are presented in one plot, similarly to the plots showing the length changes. Figure 5 and Figure 6 show typical resistivity vs. time plots. Figure 7.5 shows the resistivity vs. time measured on the concrete cylinders prepared with Florida coarse aggregates. The later resistivity values measured for those prepared with FL1 ranged from 30 to 43 kohm-cm; those with F2 ranged from 40 to 52 kohm-cm and those with F3 aggregated ranged from 20 to 30 kohm-cm. F3 is the more porous of the three aggregates and likely contained the more water when saturated. Figure 7.6 shows the resistivity vs. time measured on concrete cylinders prepared with granite NG and GG, H1 and H2 aggregates. The resistivity for those prepared with GG aggregate ranged from 65 to 110 kohm-cm and those with NG aggregate ranged from 60 to 110 kohm-cm. Two subsets were observed on the concrete cylinders prepared with granite aggregate, those with Li inhibitor exhibited significantly larger resistivity independent of the dosage. However, this increase in resistivity due to Li presence was not observed on the samples prepared with Florida limestone aggregate. The resistivity measured on cylinders with H1 and H2 aggregates had a similar trend than those measured on cylinders with granite aggregate.

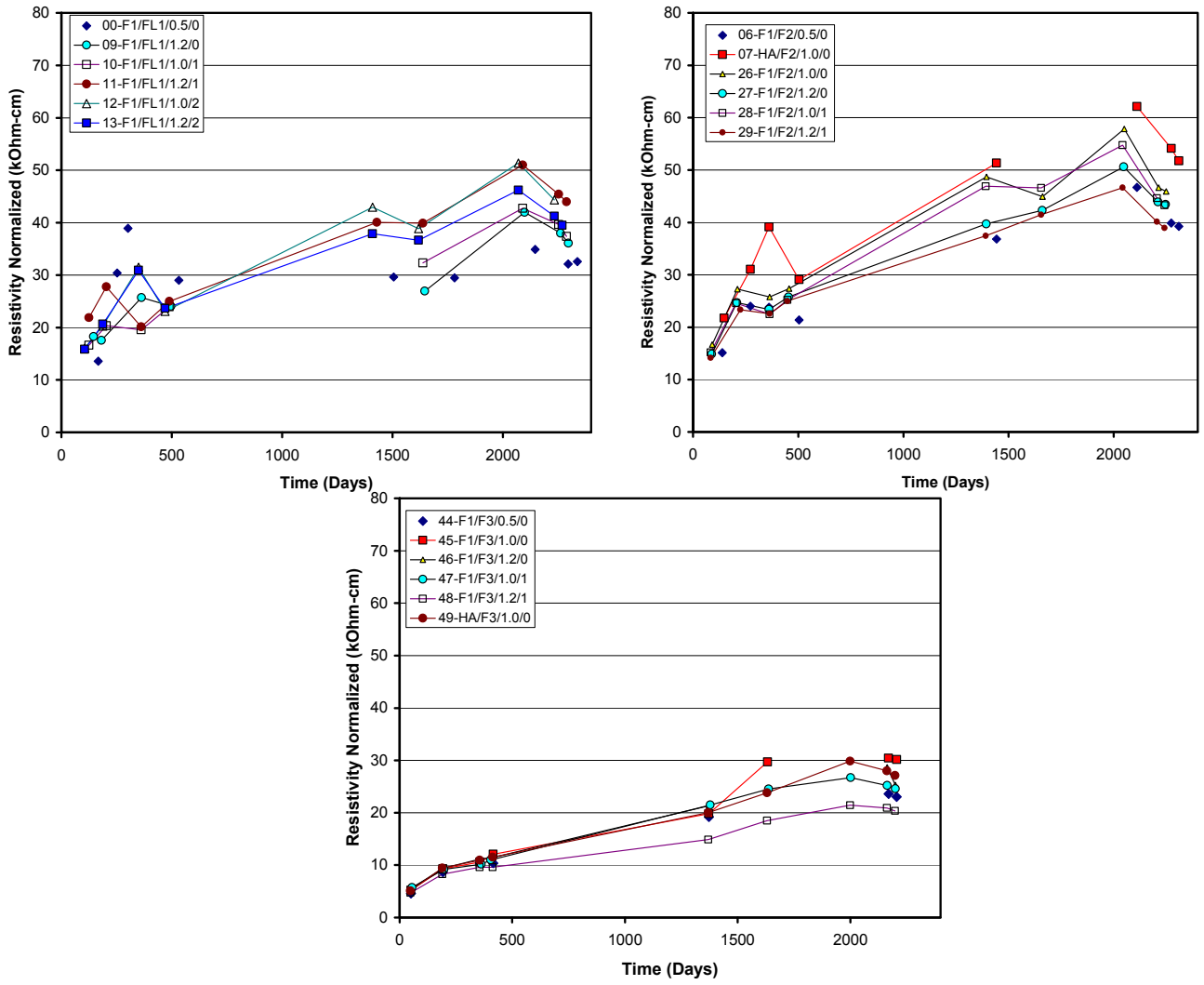

Figure 7.5: Typical evolution of resistivity with time. Concrete mixes prepared with Florida aggregates and various EqA and Li contents

Although electrical resistivity and its inverse, electrical conductivity, are thought to depend primarily on properties of the cementitious paste, the results shown above reflect an influence of the coarse aggregate as well. Fly ash pozzolanic reaction modifies both tortuosity and pore water composition (particularly at latter times when most of the hydration has taken place), therefore, is expected to have a relative large effect on concrete resistivity (and also permeability).[37] The addition of NaOH might have activated pozzolanic reaction earlier and for a longer time than on concretes with EqA=0.5 (i.e., normal OPC). Thus specimens with NaOH were observed to have larger resistivities. However, its impact depended on the concrete constituents. Except for specimens with NG coarse aggregate, resistivity was greater for EqA=1.2 than for EqA=1.0, the effect of enhanced alkalinity on resistivity was modest and probably within expected scatter. The resistivity increase for Florida coarse aggregate FL1 was greater than for F2 and F3. There was no additional effect for those specimens with admixed $LiNO_3$ on

resistivity, the measured values were similar to those that contained only NaOH for the specimens with three Florida limestone coarse aggregates. For the other coarse aggregates, a relative large resistivity increase resulted from admixed $LiNO_3$. Hartt [4] proposed that a portion of the observed resistivity changes may have been related to modified characteristics of the electrical double layer at the cement paste-pore water interface. FA hydration likely consumed some of the calcium hydroxide. Feng [48] proposed that the inhibiting effect of $LiNO_3$ against ASR in concrete can be attributed to the formation of two reaction products in the presence of lithium, these being a crystalline lithium silicate compound (Li_2SiO_3) crystal and a Li-bearing, low Ca silica gel. These two phases could serve as a diffusion barrier and protective layer to prevent/restricts the reactive silica from further attack by alkalis [48]. It is possible that these compounds also are also partially responsible of the observed increase in resistivity due to additional pore filling and more tortuous path. It was observed that if the cylinders were not cool enough the measured values were lower (as would be expected due to temperature effect) and in a couple of instances the values were higher due to not enough moisture (large peaks). It was decided to wet the interior of the storage containers more frequently and thereafter to wait up to two days before measuring the resistivity. This procedure was implemented and the last two sets of values shown per each mix reflect this. It was then decided to use some of the cylinders to investigate the temperature effect as these cylinders have been curing for close to seven years in a high moisture and elevated temperature. This is discussed in chapter three of Volume two of this report. After the resistivity/temperature testing was completed some of the cylinders with EqA=0.5 were selected for bulk diffusion (and half of the cylinder for compression) and some others were tested for RMT to calculated D_{nssm}. The results for D_{app} and D_{nssm} are included in a different chapter of this report in Volume 2

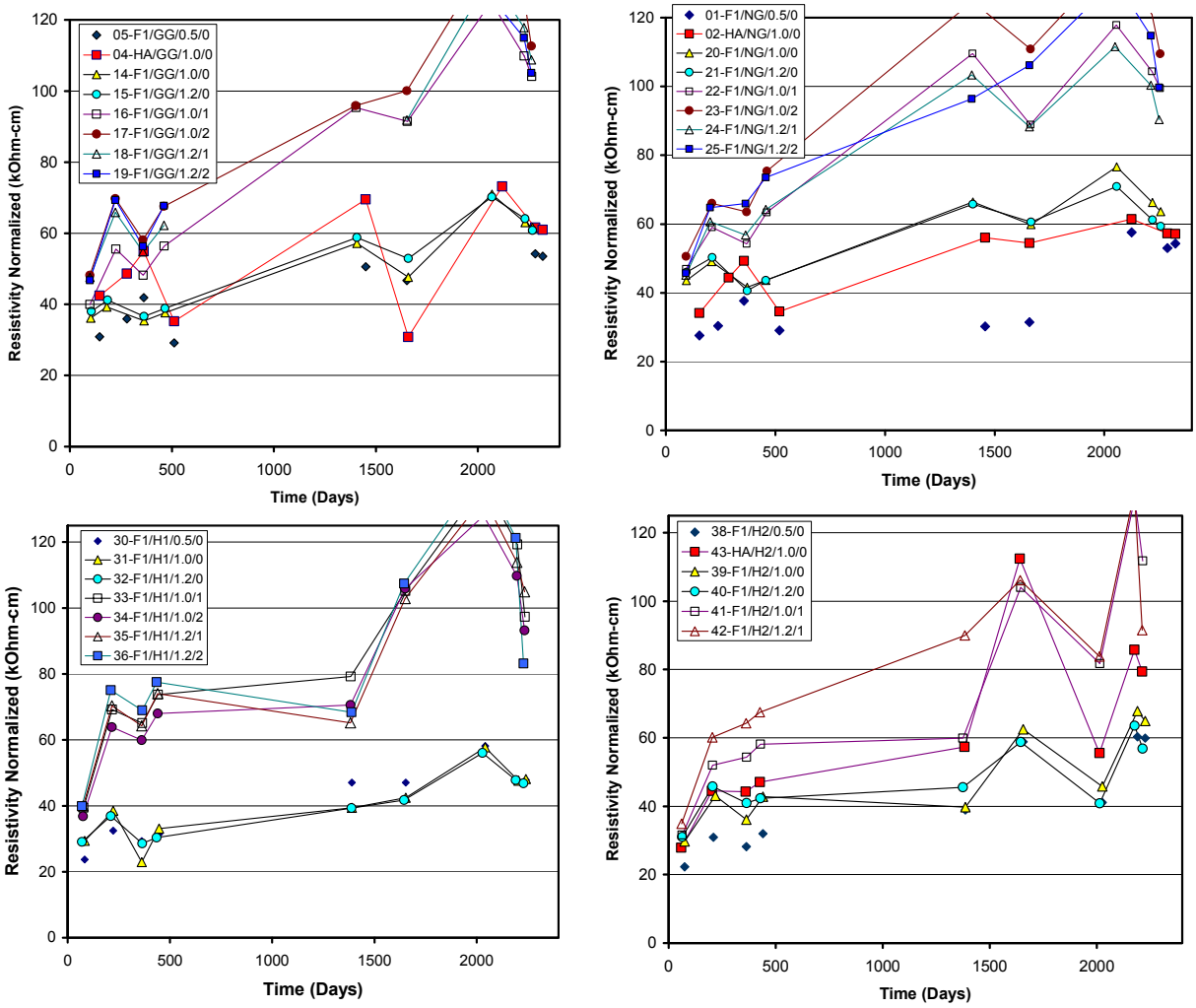

Figure 7.6: Typical evolution of resistivity with time. Concrete mixes prepared with granite, H1 and H2 aggregates and various EqA and Li contents

7.4.6 Selection of Terminated Specimens

As the expansion was small on specimens with FPL1, FPL2 and FPL3 only specimens with high alkalinity were selected (from within those with the larger expansions) to be terminated with no Li additions. Except for FLP2 in which one series with Li additions was also included. For the specimens with the other type of aggregates, specimens with high alkalinity (either HA or EqA=1.0 or EqA=1.2 via NaOH) were selected. Additionally a few specimens with high alkalinity with Li Nitrate additions were selected for further investigation. Table 7-11 contains the list of the specimens terminated in the same format as shown for Table 7-3.

Table 7-11: List of specimens terminated (indicating specimen ID)

Cement type and alkalinity	Coarse Aggregate						
	FL1	F2	F3	GG	NG	H1	H2
F1-EqAl.0	08-A		45-A		20-B	31-C	39- B
F1-EqA1.2.0		27-B		15-D	21-A		40-C
F1-EqA1.0-Lil				16-C		33-A	
F1-EqA1.0-Li2							
F1-EqA1.20-Li1		29-A			24-B		42-A
F1-EqA1.20-Li2						36-B	
HA	03-D	07-B	49-A	04-A	02-C		
F1-NFA						54-A	55-A

7.4.7 Visual Inspection

Appendices grouped per coarse aggregate type have been prepared that contain significant more detail than what is included in here and are grouped per specimen type. Each appendix contains pictures before terminating the specimen, follow by pictures of lapped cross-sections and coarse aggregate close-ups, lastly the pictures taken with the polarizing microscope are included. Figure 7.7 shows a picture for specimen 03-D (FL1) and 49-A (FL3). Figure 7.7 shows pictures taken before cutting specimens of FL1 and FL3 series. Neither specimen showed white products at the surface typically found for specimens undergoing ASR.

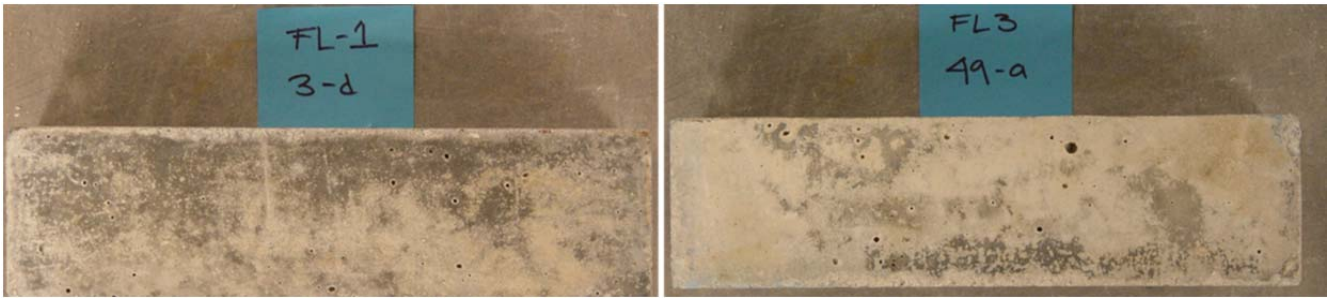

Figure 7.7: Example of specimens with not bleeding products

Pictures taken on specimens with no Fly Ash and with aggregates prone to ASR showed the opposite end of the spectra. Figure 7.8 shows a couple of pictures taken on specimens from the H1 and H2 series. Specimen 54-A shows significant coverage of white bled products, whereas specimen 55-A shows less coverage. Specimens with high alkalinity and FA with F2, H1, H2, GG or NG coarse aggregates show some white products coverage but in lesser amounts and are described below.

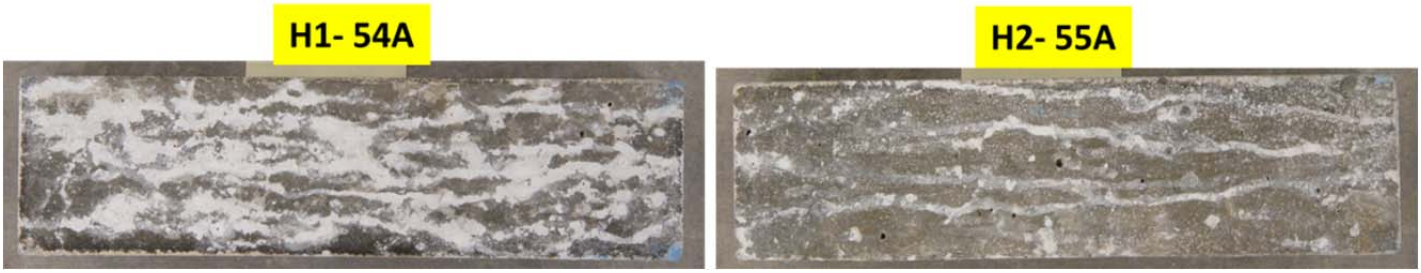

Figure 7.8: Example of specimens with significant ASR products that have bled

More modest amounts of ASR products were observed on specimens with FA and high alkalinity independent of the EqA present in the mix. Figure 7.9 shows pictures of the surface condition on specimens with FL2 aggregate. This was the worst performer of the three tested limestone aggregates. Specimen 27A showed cracks in one of the faces and intermediate coverage with ASR withe products, upon adding Li the amount of products at the surface were significantly reduced, e.g. Specimen 29B. Specimen 07B with HA cement showed less amount of ASR products than specimen 27A. Similar pictures were taken for the other terminated specimens and this can be found in the appendices. The amount of ASR products observed at the surface on specimens with high EqA and H1, H2, GG and NG coarse aggregates was usually larger than for FL2 specimen. On specimens with granite aggregates more coverage of white products was observed on those with HA cement than on specimens prepared using sodium hydroxide to elevate the pH. The presence of Li appears to reduce the amount of products observed at the surface. This above description corresponds to visual observations and pictures taken before terminating the selected specimens. Pictures taken on all specimens with the other aggregates (GG, NG, H1 and H2) showed various degrees of white leached products coverage (i.e. ASR products), for those with no Li inhibitor added. The white products were sometimes not observed on specimens with Li added or the presence of the Li inhibitor significantly reduced the amount of white ASR products observed (e.g. GG 16C and NG 24B).

Figure 7.9: Specimens with FL2 aggregate selected to be terminated

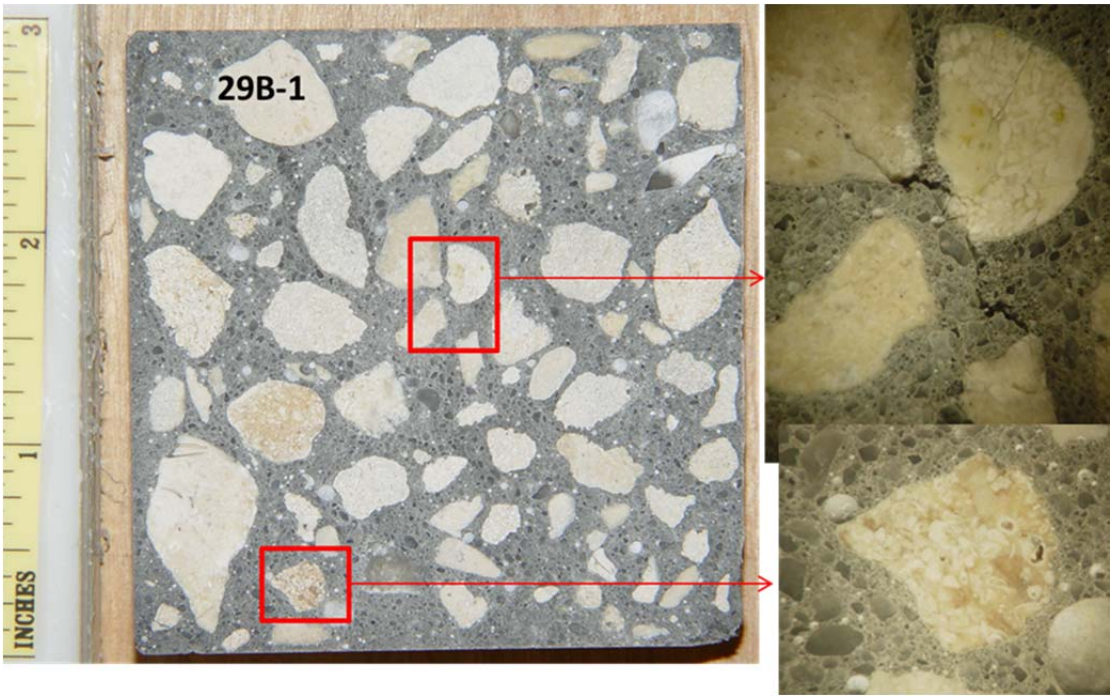

Figure 7.10: Photograph of a lapped surface and two close-ups on specimen 29B

7.4.8 Petrography

Pictures were taken for the lapped surfaces that capture the whole cross section. Additional pictures were taken of close-ups to selected sections using a stereo microscope. The close-ups usually were center on a coarse aggregate piece. FL1 and FL3 terminated specimens showed no signs of ASR. Specimens with FL2 showed various degrees of ASR. Figure 7.10 shows a photograph of one of the lapped surfaces and two close-ups obtained for specimen 29B. The larger close-up shows cracks both in the mortar and the aggregate. White spots are observed on many of the smaller pores and also on the bottom of the larger pores.

The lapped surfaces for each terminated specimens were photographed and additional close up pictures were taken using a stereo microscope for each specimen. The reader is referred to the appendix. Figure 7.11 shows that cracks were observed within the coarse aggregates on specimens with NG, H1 and H2 type of aggregates on specimens with high EqA including some that contained Li in the mix.

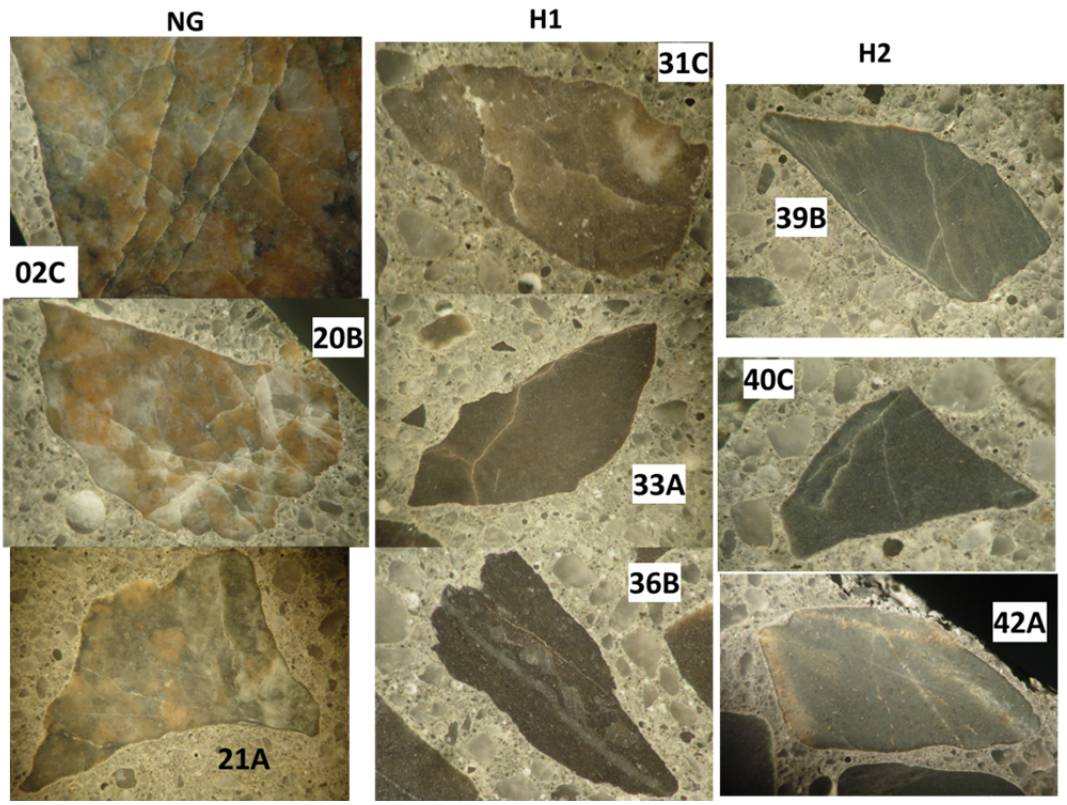

Figure 7.11: Typical cracks patterns observed on specimens with NG, H1 and H2

On specimens with no FA and H1 or H2 aggregates the ASR caused even more damage than observed above (refer to the appendix of this chapter for additional details).

7.4.8.1 Petrographic observations summary

From the specimens with limestone aggregate only those with FL2 showed cracks. Specimen 27A (with FPL2) showed cracks at the lapped surface of the concrete and an internal crack was observed on specimen 29-B lapped surface when using the stereomicroscope (Figure 7.10). As shown above, upon inspecting the lapped surfaces, several specimens with NG, H1 and H2 coarse aggregate showed cracks that were visible without magnification, but easier to visualize with it (see Figure 7.11). The worst condition was observed on H1 specimens with no Fly Ash as would be expected. Pictures taken with the stereomicroscope made easier to observe the extent of the cracks. No visible cracks were observed with the stereo microscope on specimens with GG aggregate, nor FPL1 or FPL3.

From the investigated aggregates GG, NG and FL2 coarse aggregates might be at some point considered for use in Florida. If it is decided that pH would be increased, caution and additional research might be necessary to determine the optimal amount of FA (e.g., it might be advisable to increase the FA amount from 20 percent to 30

or 40 percent). For the investigated cases, even though Li reduced the elongation rate, it does not appear to prevent cracks from occurring due to ASR upon the specimens being subjected to long term exposure. Moreover, more instances of coarse aggregates with cracks were observed on specimens with no Li than those with Li.

7.4.9 Thin Section and Polarizing Microscope

A thin section was prepared for each of the specimens that are listed in Table 7-11. The motivation to prepare these thin sections is described next. Figure VIII-12 in reference [37], Hartt and Suarez presented elongations up-to 800 days and different trends followed by several of the mixes. The length changes of these mixes were in the range of 0.007-0.013 percent. Figure 7.12 shows an updated Figure VIII-12. Specimens of mixes 14 and 27 expanded continuously and were considered ASR affected, whereas length change for mixes 03, 29, 36, and 45 appeared to have stabilized after 800 days. However, prisms of these latter four mixes exhibited cyclic behavior (periods of expansion and contraction up-to day 1000), making it unclear as to whether or not ASR would be an issue in the long-term if only elongations for one or two years were available. In the plot shown in Figure 7.12, the elongations for mixes 03, 29 and 36 eventually experience a monotonic increase and by day 3000 appear to have stabilized at a length change close to 0.02 percent, and for mix 45 the elongation percent change was less than 0.01 percent. Thus, interpretation of length change results should be complemented by not only how length change varies over time but also microscope examination, first, to determine the extent of any cracking and, second, petrographic analysis to disclose other possible ASR-related indicators. This was the motivation for selecting one specimen from each of these mixes for such analysis described in the previous section. Polarizing micrographs of thin sections were also taken. Observations on the polarizing micrographs suggest that ASR was present in all prepared thin sections. However, the area with ASR gel was small on most of those specimens with smaller elongations.

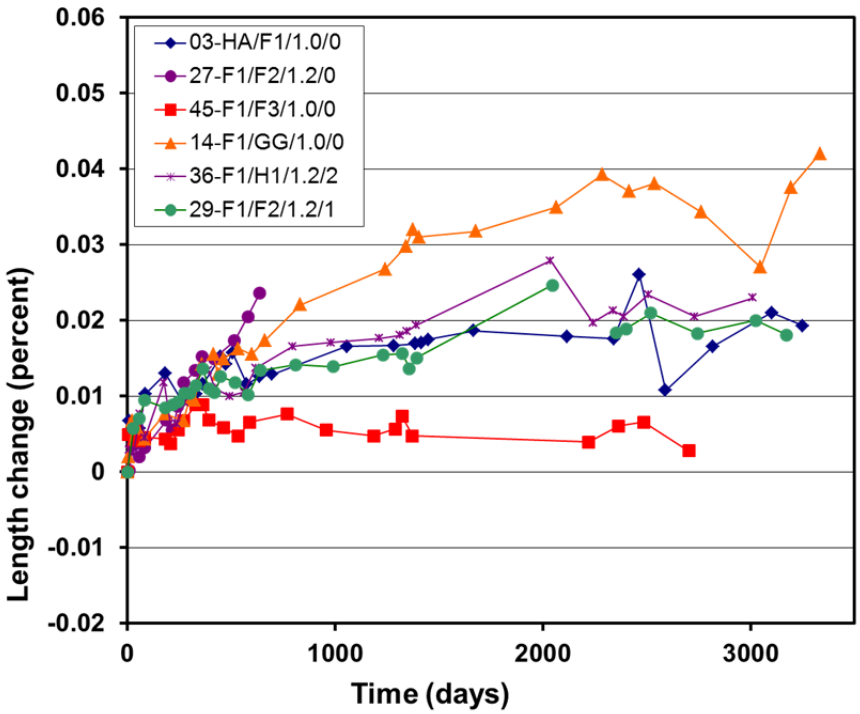

Figure 7.12: Length change vs. time on specimens with different coarse aggregate

Polarizing micrographs were taken on multiple areas of each of the thin sections. In here we report typical sections of where we believe ASR gel is visible. ASR gel was not observed everywhere; however, it appears that after 6 years (age when the specimens were terminated) of exposure there is evidence of ASR gel on all thin sections prepared. It is important to note, that further analysis of the micrographs by a geologist might be need for those specimens for which the petrography show no evidence of ASR. Specimens with FL2 coarse aggregate had the most evidence of ASR gel from specimens prepared with limestone aggregates. Figure 7.13 shows evidence of ASR gel on a specimen with FL2 and NaOH added. Specimens with NG showed considerable damage and in some cases it is hard to differentiate between cracks and presence of ASR gel. Figure 7.14 shows a typical micrograph for a region with significant damage for specimen with NG. Figure 7.15 and 7.16 show examples of ASR observed on a couple of specimens with H1 and H2 aggregates respectively, for specimens that contained FA.

The appendix for this chapter is sub-divided by aggregate type. On each sub-appendix there are pics of the specimens before being terminated. This page is followed with pictures for each terminated specimen of: 1) the lapped surface(s), 2) close-ups with stereo microscope 3) pics of the thin section using a polarizing microscope

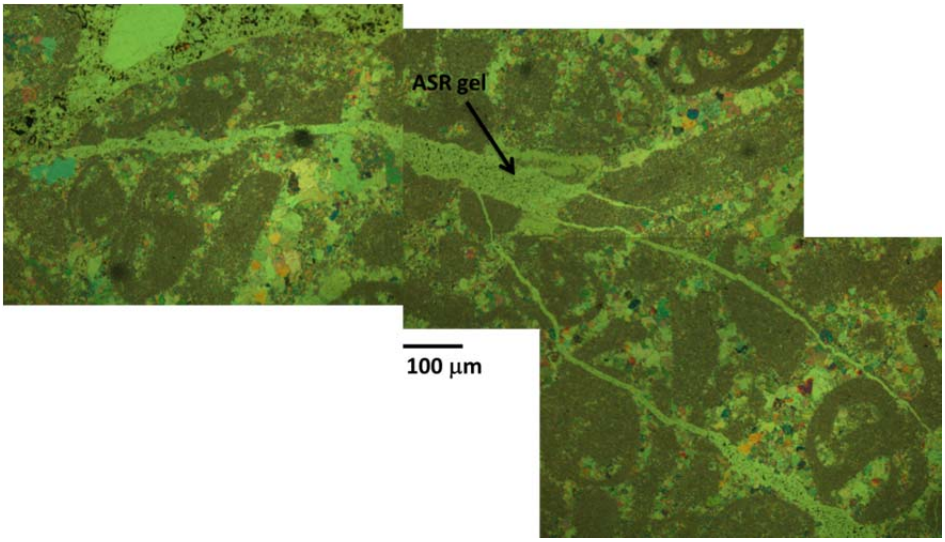

Figure 7.13: Evidence of ASR gel on thin section of specimen 27A

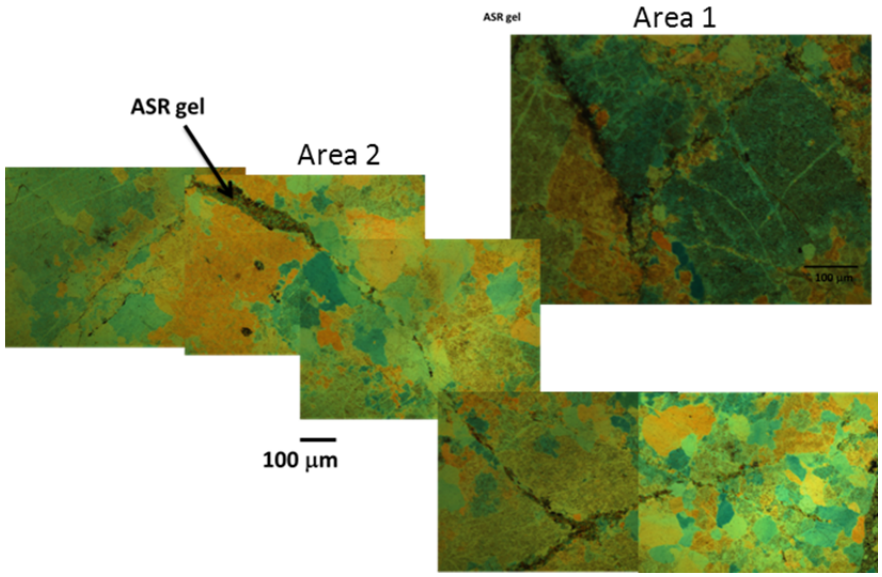

Figure 7.14: Evidence of ASR gel on thin section of specimen 02-C with NG

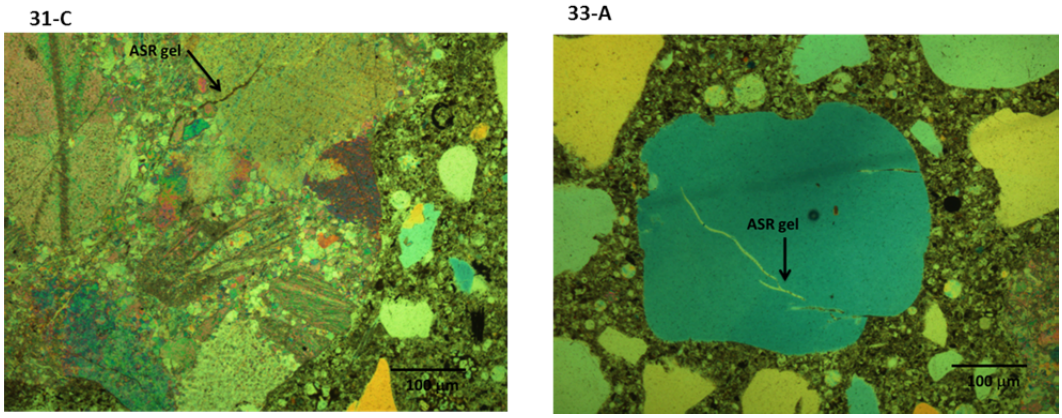

Figure 7.15: Evidence of ASR gel on thin section of specimens with H1 coarse aggregate

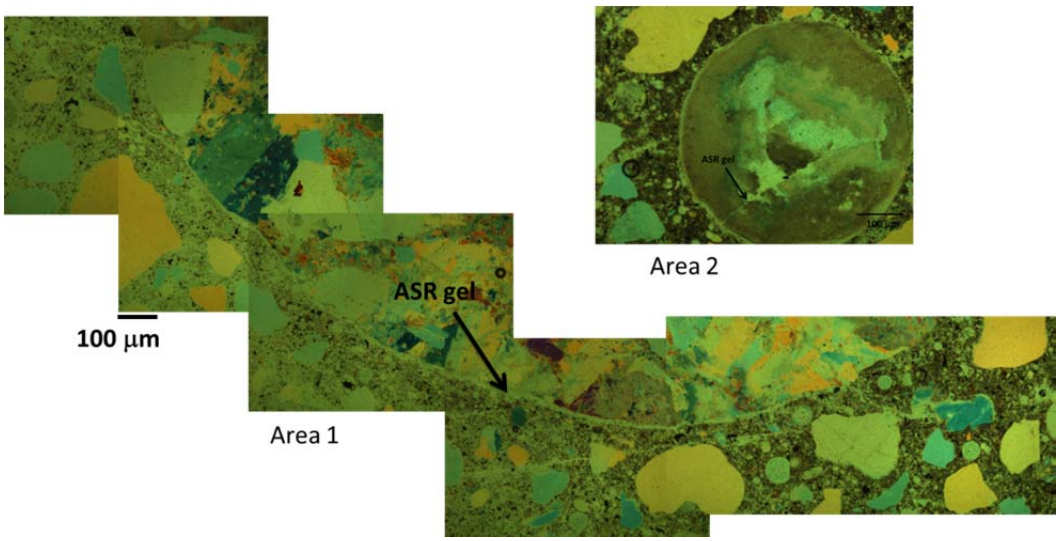

Figure 7.16: Evidence of ASR gel on thin section of specimen 39B with H2 coarse aggregate

Based on the visual observations on the thin sections, we suspect that all specimens showed ASR gel to various degrees. Specimens with NG showed the most evidence in the polarizing micrographs followed by H2 series. H1 had the largest leaching in to the surface and large cracks are observed without having to use the stereomicroscope or the thin sections. Actually, it was difficult to identify ASR gel via micrographs of thin sections on specimens with H1 aggregate. ASR gel might have transported out or the selected area chosen to obtain the thin section was not conductive to identify it. It is possible a combination of that these two phenomena took place. Specimens with NG, H1 and H2 aggregate showed cracks on both the stereomicroscope, and on the thin section micrographs this cracks look as black stream branches with no remnants of ASR gel. (In the appendices the pictures are sometimes labeled as ASR gel, but what can be seen are cracks where the gel might have been at some point in time). Many of the ASR gel observed as a thin color within a darker color aggregate corresponds to cases in which this took place on the smaller coarse aggregate (or large fine aggregates). Moreover, halos were observed in a few

occasions around small aggregate particles. For all the pictures taken on thin sections additional testing would be required to verify the presence of ASR gel by chemical methods.

Additional experiments might be needed before selecting GG, NG or FPL2 in combination with EqA=1 or EqA=1.2, the optimal Li Nitrate was not identified in this investigation. It might be possible that the maximum EqA when using this aggregates might need to be lowered (0.75 or 0.8) via a larger FA replacement (e.g. 30%) if the structure is to be exposed to elevated temperatures and high moisture conditions during field exposure. Another alternative would be to use 30-35 percent FA in combination with EqA=1.2 or EqA=1.

7.5 CONCLUSIONS

1. Concrete prisms prepared with Spratt and Sudbury aggregates showed the larger elongations. The presence of Li inhibitor and FA even with high EqA reduced significantly the amount of elongation, but did not prevent ASR. FL coarse aggregates appear to be less prone to ASR in the presence of FA and Li particularly FL1 and FL3.
2. The resistivity values measured at room temperature was found to be affected by the presence of FA, Li inhibitor and the type of aggregate. LiNO3 significantly increase the resistivity on concretes with H1, H2, GG and NG aggregates. The lowest resistivity was measured on FL3 specimens, this is believed to be due to the higher porosity of this aggregate.
3. It appears that most specimens selected for petrographic and thin section experienced some degree of ASR, except FL1 and FL2. This was not always obvious from low magnification (stereo microscope pics), but some degree of ASR as observed upon examining the thin sections.

7.6 ACKNOWLEDGMENTS

The authors are indebted to the Florida Department of Transportation (FDOT) for financial support of this research and to Mr. Mario Paredes and Ron Simmons of the FDOT State Materials Office. In addition, the authors appreciated the assistance with laboratory work and measurements given by Mr. Taylor Reeves and several undergraduate students of FAU. The authors also acknowledge Dr. Hartt and Dr. Suarez whom were in charge of phase I of this project.

8 EFFECT OF POLARIZATION ON STEEL IN SIMULATED REINFORCED CONCRETE BRIDGE SUBSTRUCTURES EXPOSED TO MARINE ENVIRONMENTS

8.1 ABSTRACT

Simulated reinforced concrete substructure element (piling) specimens were fabricated, cured for twelve months and exposed partially submerged in natural sea water. Exposure involved, first, intermittent spraying of the above waterline zone to simulate splash and spray and, second, electrically connecting the embedded reinforcement to submerged bare steel bars to affect a potential gradient from relatively negative in the submerged zone to positive in the atmospheric as occurs in actual members. Four different polarization levels were achieved by inserting resistors. On-potentials and 24 hrs depolarization tests at various elevations were used to better understand the influence of these polarizations on potential vs. elevation and how it affects time to activation. These measurements suggested when corrosion initiated, selected specimens were terminated shortly after corrosion appeared to have initiated. Upon reaching 1450 days of exposure any remaining specimens were terminated. Chlorides were determined from mortar milled at the rebar trace at various elevations (locations) avoiding corrosion spots. The chloride concentration in wt/o cement were vs. potential were compared what has been reported in the literature.

8.2 INTRODUCTION

In past studies, particular attention has focused on identification and characterization of C_T, since corrosion should not initiate as long as chloride concentration, $[Cl^-]$, at the reinforcing steel depth remains below this threshold value. Upon knowing C_T, bridge engineers can make materials selection and design choice to ensure that reinforced concrete structures are not compromised by the corrosion induced cracking and spalling during their design life. However, reported values in the literature for C_T extend over more than an order of magnitude from 0.17 % to 2.5% by weight of cement (i.e., from 0.6 to 9.7 kg/m^3 on the basis of concrete weight assuming 400 kg/m^3 cement content) for concrete test specimens and structures [49]. Variables that contribute to this range include: 1) types of raw materials and admixtures, 2) cement composition, 3) mix design, 4) concrete microstructure, 5) rebar surface condition, and 6) type of exposure [50]. Even so, laboratory and test yard experimental studies have demonstrated that C_T is variable or distributed over a range for identically designed and exposed specimens [51]. Irrespective of this, the North American concrete community generally accepts a value for C_T of 0.15~0.20% by weight of cement (0.59-0.78 kg/m^3) [52] of concrete based largely upon the laboratory

research and field evaluations in the 1960's and 1970's by the Federal Highway Administration (FHWA) and California Department of Transportation (CalTrans).

Significantly different C_T values have been reported between 1) decks and presumably for ponded slab specimens also and 2) partially submerged prisms may have resulted because exposure is macroscopically uniform for the former but not for the latter. Generally, chloride concentration is high in the submerged zone of a prism specimen or substructure element hence the reinforcing steel becomes active. However, corrosion rate and resultant damage are generally nil because of oxygen depletion in this zone. On the other hand, the chloride concentration in the atmospheric zone well above the water is relatively low with a higher oxygen concentration. Consequently, the reinforcing steel may remain passive here. However, the chloride concentration is highest in the zone immediately above the water because of splash and possibly capillary transport from below. The oxygen concentration may be low here, but proximity to the atmospheric zone above provides a macroscopic active-passive cell between the two with adequate oxygen in the region above the splash zone to drive the corrosion process. Thus, it is in the splash zone that corrosion rate is highest and cracking and spalling are most severe. Figure 8.1 shows an example of this damage in the case of a coastal bridge prestressed concrete bridge piling.

Figure 8.1: Photograph of a coastal bridge spalled piling

A resistivity gradient from low to high upon proceeding from the submerged to atmospheric zone results from the elevation dependence of moisture saturation. Consequently, macro-cells are likely to be more significant at lower elevations. Also, as noted above, the reinforcing steel in the submerged zone is expected to be active and potential is relatively negative due to low oxygen concentration here (oxygen concentration polarization). The opposite is the case in the atmospheric zone where the reinforcing steel remains passive due to low chloride concentration with a high oxygen contents so potential is relatively positive here. Thus, there is a potential

gradient from relatively negative to more positive with increasing elevation. As a result, the reinforcing steel in the submerged zone tends to cathodically polarize steel in the splash zone. This has implications with regard to defining the chloride threshold (C_T), since this parameter can increase with increasing cathodic polarization [53-57].

On partially immersed substructure elements; the reinforcing steel in the submerged zone constitute a relatively large anode surface area which should lend effectiveness to the cathodic polarization provided to the reinforcing steel in the splash zone, which is where the chloride concentration is expected to be highest and corrosion most significant, as noted above. The present research reports findings on a specimen simulating a partially immersed pile that was intended to provide a more realistic simulation of actual bridge substructure elements and thereby result in a chloride threshold (C_T). This simulation includes the polarization effect due to the submerged reinforcing portion by using an alternate method described below.

8.3 EXPERIMENTAL PROCEDURES

8.3.1 Materials

A mortar mix, designated MD1 (mix design 1), was employed to fabricate simulated piling specimens with the materials and proportions for each being listed in Table 1 and cement and fly ash compositions in Table 8-2. Table 8-1 also includes a typical mix design for Florida Department of Transportation (FDOT) Type V concrete [58] and reveals that the present mix is similar to this except that coarse aggregate was excluded. As such, the mix was intended to replicate the mortar phase (no coarse aggregates) of FDOT Type V concretes by retaining the cement content and water-to-cementitious material ratio (w/cm) of these.

Table 8-1: Details of concrete mixes

Materials	FDOT type V		Mix design 1	
	(kg/m^3)	(Vol %)	(kg/m^3)	(Vol %)
Type 1 cement	363	12	389	12.6
Fly ash	83	4	94	4.25
Water	163	18	184	18
Fine aggregate	607	23	1457	55
Coarse aggregate	1047	41	0	0
Water/Cementitious	0.37		0.38	
Sand/Cementitious	1.36		2.76	

Table 8-2: Compositions of Cement and Fly Ash (unit: % mass)

Materials	SiO_2	Al_2O_3	Fe_2O_3	CaO	SO_3	Na_2O	K_2O	EqA
Type 1 cement	23.55	6.00	3.88	60.22	2.63	0.09	0.54	0.45
Fly ash	52.82	21.90	6.06	4.92	0.27	0.28	1.49	1.27

8.3.2 Specimens

Reinforcement was as-rolled and wire brushed, 9.5 mm diameter (#3) black steel bars. A relatively low Cl^- diffusivity (D_{cl}) was projected for the selected mortar mix. This low D_{cl} would preclude corrosion initiation in a time frame acceptable for most laboratory experimentation using standardized specimen designs [59]. Thus a clear cover of 8.0 mm was selected. This cover was selected based upon calculations that assumed diffusion coefficients of 1×10^{-12} m^2/s, not including polarization of the reinforcement. Exclusion of coarse aggregate from the mix was a necessary requisite for specifying these relatively low cover.

Specimen molds were fabricated from 13 mm thick polypropylene sheet. Mortar batching employed a 57 liter mixer, and density, air content, and slump were determined for each batch according to ASTM C231 [60]. The specimens were horizontally cast in three layers for each batch and consolidated by rodding according to ASTM C192 [61]. Acceptable ranges for air content and slump were 8-12 percent and 32-64 mm, respectively. Bar positioning in the molds was such that the minimum cover face (the one with concrete cover 8 mm) from which chlorides should initially reach the reinforcement was down such that this surface had a form finish (face down during casting). The specimens were covered with plastic wrap at room temperature for the initial 24 hours subsequent to casting, after which they were removed from the molds and cured in sealed plastic containers at 100 percent relative humidity and 38°C. Curing time for the specimens was six months in this environment, and continued to cure for an additional six months at laboratory temperature and humidity.

A schematic illustration of the simulated piling specimen is shown in Figure 8.2. Each specimen consisted of two bars that were aligned and rigidly clamped in the molds prior to casting. Concrete cover was verified using a micro-covermeter subsequent to pouring and curing. More than 24 specimens were fabricated. This paper presents and discusses the results of tests performed on nine of them. The specimens were prepared as part of a recently completed project [62]

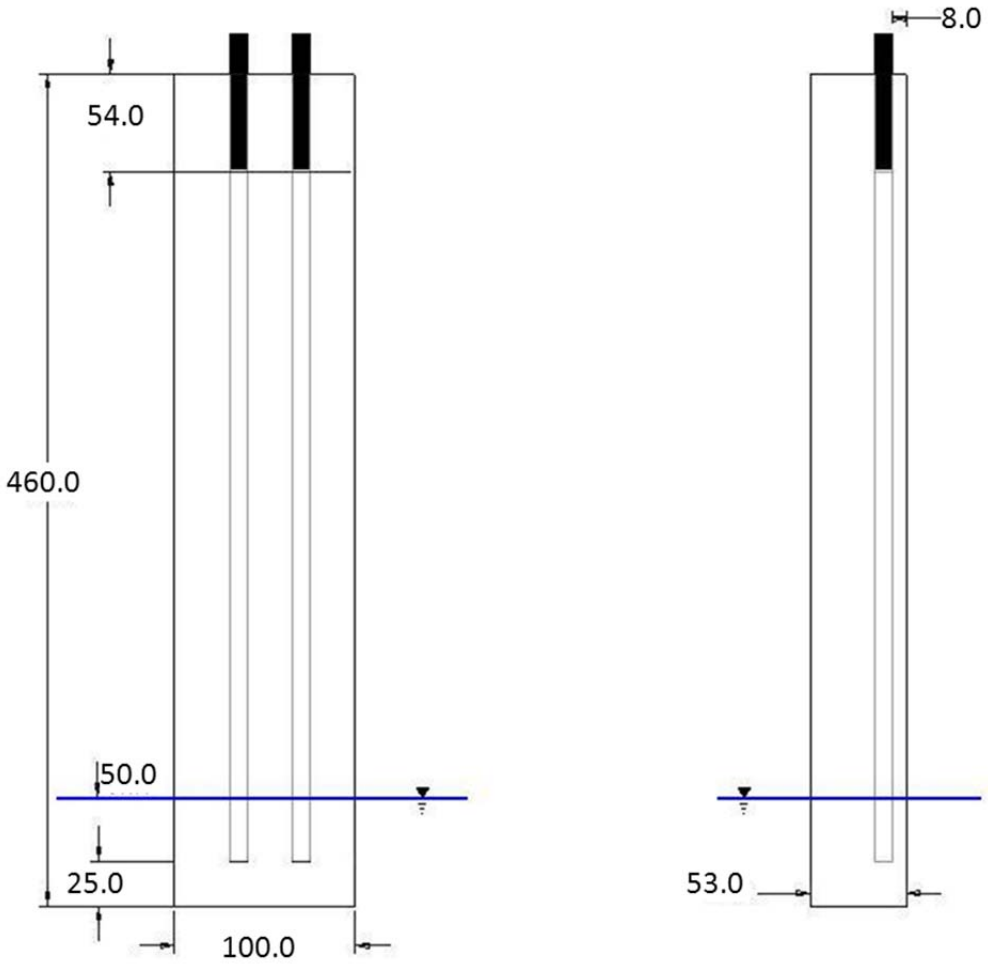

Figure 8.2: Simulated Piling Specimen (units: mm)

8.3.3 Experimental Setup

Subsequent to curing, specimens were positioned vertically in groups of four in polyethylene tanks and submerged in seawater to a depth of 5.0 cm. Additionally, the minimum cover face was sprayed each day for ten minutes every 12 hours to a height of approximately 20 cm above the waterline with the same solution. The containers were kept with the top on and the spraying allowed the relative humidity in the atmospheric zone of the specimens to be between 70 to 80 percent. The annual average relative humidity value in the Florida Bay is 74.5 percent and it is up to 95 percent during moist days. Figure 8.3 shows four specimens positioned in an exposure tank where spraying occurred. From the beginning of the exposure, each rebar was connected to an individual bare steel rebar submerged in a companion tank that was electrolytically connected to the tank in which the prism specimens were exposed via pvc piping that contained a porous filter. The procedure involved coupling both the rebar of a given specimen to the same dedicated bare submerged bar. The purpose of this was to polarize the

lower elevation of the specimen rebars and thereby simulate the potential profile that is expected to occur for actual pilings. Each rebar of simulated piling (SP) specimens that was connected to submerged bare steel (polarized specimens) was independently wired with a resistor placed between the submerged rebar and the embedded rebar.

Table 8-3 shows the four different resistor values used and the label ID given to the specimens of each group. All submerged electrical connections are sealed with a marine epoxy. Figure 8.4 provides a photograph of this arrangement where the tank with bare submerged steel bars is in the foreground and the one with SP specimens in the back. The pvc piping between the two tanks that contained the filter and provided electrolytic connection is also visible. Potential measurements between reference electrodes in the tanks containing polarized SP specimens and the tanks with the submerged bare bar indicated that the voltage drop between these was negligible. Note: Additional resistances are present due to mortar and solution resistance. Specimen L1 was polarized one week after immersion and initially immersed in 5% NaCl for 5 months.

Table 8-3: Listing of specimens and resistor

Sample Name	Resistor (Ω)
M1,M2	510
K1,K2,K3,K4	1100
N1, N2	15000
L1*	20000

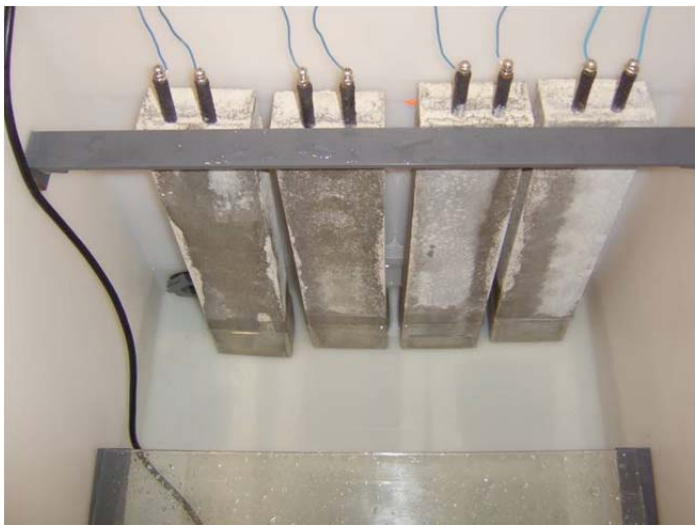

Figure 8.3: Photograph with four simulated pile specimens

8.3.4 Measurement, Monitoring and Chloride Analysis

Specimen monitoring involved routine measurement of potential as a function of elevation using a moistened-tip calomel reference electrode placed on the concrete surface directly opposite the rebar [63]. One reading was made by placing the reference in the solution and its elevation was indicated as -5 cm in the results section and represented the potential of the steel below water. Other readings were taken just above the water line (0 cm), 5, 10, 15, 20, 25, 30 cm. Also, the current between the submerged bare steel and specimen rebar was calculated from the voltage drop across the resistor.

Periodically, 24-hour depolarization tests were performed on all specimens [64]. 24-hour-off potential profiles vs. exposure time were prepared to better visualize potential transients. Plots were also prepared showing the evolution of 24-hour-net-depolarization profiles (as a function of elevation) vs. time. The potential readings were made at elevations -5, 0, 10, 20 and 30 cms.

Specimens were terminated at different age on the basis of corrosion initiation (see next section). Selected specimens were autopsied and shallow millings were then acquired shortly after corrosion initiation. This was done to minimize chloride transport as the electrical field was not longer present after removing the polarization. Monteiro, et al., noted that chloride ions migrate away from the reinforcement upon disconnection from the counter electrode when the reinforcement in the concrete or mortar specimen was cathodically polarized [65]. This action would produce a C_T lower than that which actually initiated corrosion. The time between terminating the specimen for visual inspection and milling, was usually less than a week. After a specimen is autopsied, ~ 1.0 mm millings were taken from the rebar trace in contact with the mortar. Corresponding chloride concentration was obtained by chloride titrations, which were performed on the milled powder as per the FDOT wet chemistry technique (modified to accommodate smaller mass) [2].

Figure 8.4: Photograph of the tank assembly for affecting polarization of the lower portion of the specimens

8.3.5 Age at Which Specimens Were Terminated

Polarization on the rebar in specimens was terminated at various times and the rebars were exposed for visual examination. Concrete powder was collected for chloride analysis. Table 8-4 shows the age at which each rebar was exposed.

Table 8-4: Exposure Age in Days at which each Rebar was terminated

Specimens	Rebar	End day
M1,M2	L	1451
	R	1451
K1,K2,K3	L	1442
	R	1442
K4	L	100
	R	100
N1	L	1446
	R	643
N2	L	272
	R	1066
L1	L	850
	R	850

Note: L-Left, R – Right

8.4 RESULTS

8.4.1 Potential Evolution vs. Time

Figure 8.5 shows the potential (a, b) and macro-cell current (c) versus time data for Specimen M1. Here, potential at all elevations was approximately constant prior to connection (-100 to 0 mV vs. SCE), and a potential shift to more negative values occurred upon establishing the connection to the submerged bare bar during day 1. After the connection was made, potential initially decreased linearly with time and then increased. The potentials reached pseudo-stable values after a week with potential values at high levels generally more positive than those at low levels. At each level, rebar potential values varied within a certain range before day 1218, for example, the potential values ranged -50 to -210mV at highest level (30 cm) while these were between -450 to -630 mV at the lowest level (-5 cm measured with SCE in solution). In a few instances oscillations took place, but for the most part the potential values tended towards the more noble values. A large potential drop was observed at all levels on day 1219 , which was in a range of -161 ~ -236 mV (Level 30 cm), -174 ~ -266 mV (Level 25 cm), -194~-370 mV (Level 20 cm), -312~-415 mV (Level 15 cm), -388~-528 mV (Level 10 cm), --500~-587 mV(Level 5 cm), -589~-617 mV (Level 0 cm) and -589~-617mV (Level -5 cm), with two subsequent oscillations observed (up-down-up) for each level. A gap in measurements occurred due to personnel changes, with the values measured on day 1415 being significantly more negative. It was realized that the solution had not been refreshed for a longer period than usual, consuming all or most O_2 in solution within container with the bare rebars. As such the anode (bare rebar) immersed in seawater was only able to deliver a significantly smaller macrocell current. Upon refreshing the solution, the rebar potentials at all elevations shifted to more positive values again. Figure 8.5(c) shows that the trends of macro-cell current with time on the left bar and right bar were similar from the day 22 to 1260 and the current values delivered by the left bar were generally less than those provided by the right rebar with the former in a range between 16 and 23 μA and the latter between 18.5 and 26 μA. It was also observed that the macro-cell current on the left rebar gradually decreased past day 1200 to values smaller than 10 μA. It eventually reached a value as little as 1.37 μA. This transition in the observed macro cell current might suggest that corrosion might have initiated on the embedded rebar demanding less current or that the moisture content was high at the simulated pile. The value measured by day 1440 was 4.71 μA. However, the macro-cell current measured on the right rebar past day 1260 was somewhat different from that on left rebar. The macrocell values experienced some oscillations that likely are the result of refreshing the solution. The last value measured (1440) was 25.29 μA, which showed that the macro-cell current corresponding to the right rebar returned to its original range (before 1260), this would suggest that corrosion has not initiated on the rebar on the right. The potential and macro-cell current versus time for specimen M2 can be seen in Figure 1 in the Appendix for this chapter. The trends on both rebars in specimen M2 were similar to what was observed for the left rebar on specimen M1.

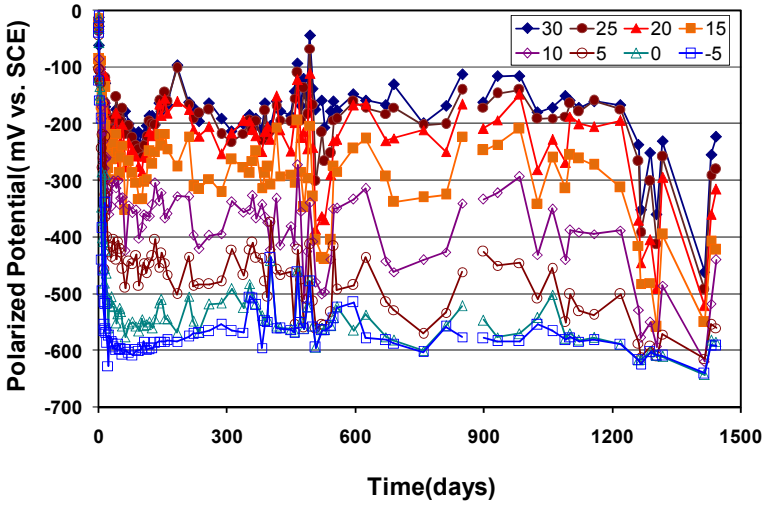

(a) Polarized potentials of left rebar in specimen M1at eight (8) levels

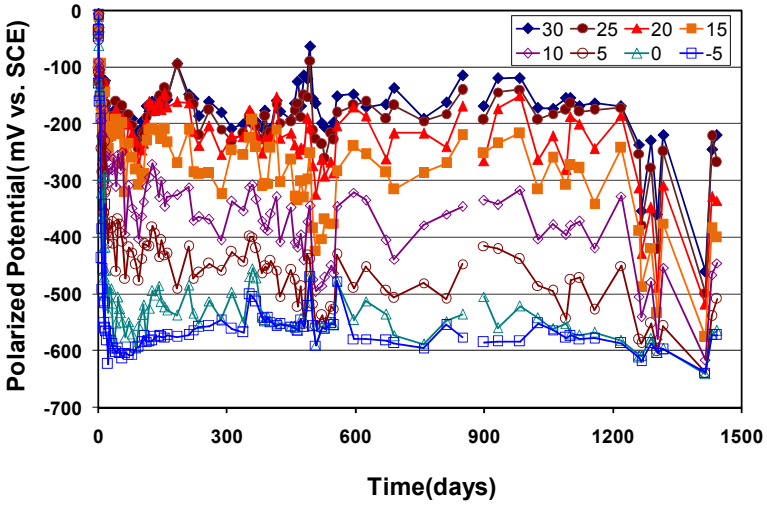

(b) Polarized potentials of right rebar in specimen M1 at eight (8) levels

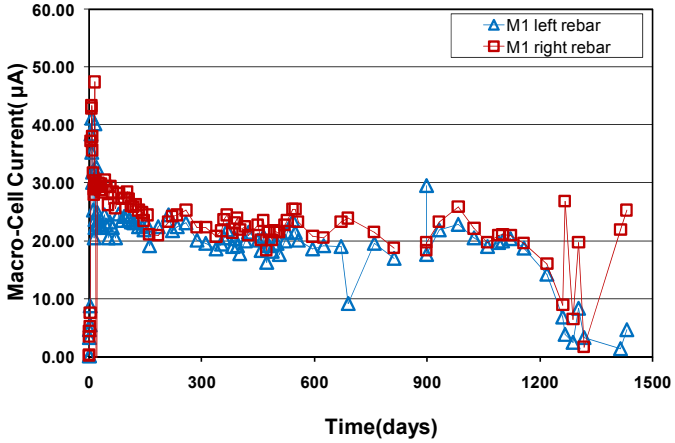

(c) Macro-cell current from left rebar and right rebar in specimen M1

Figure 8.5: Potential of the left and right bars at eight elevations and macro-cell current in specimen M1as a function of exposure time (measurement elevations in cm relative to the waterline).

Figure 8.6 shows the potential and macro-cell current versus time data for specimen K2. From Figure 8.6 (a) and Figure 8.6 (b), it can be observed that the potential transient observed for the first 1200 days was similar than that seen in Figure 8.5(a,b); however, the potential at the lowest elevation was ~40 mV nobler, and at the highest elevation, it was about ~20 to 30 mV more negative than what was observed on M1. Similarly to what was described above for M1, a potential transient took place on specimen K2 at around day 1200, the potential values shifted toward more negative values at all levels and appeared to plateau by day 1300 within a range of -350 mVsce (highest elevation) to -600 mVsce (below water). The last two sets of measurements showed and additional drop, the last set of values ranged between -450 mVsce and -600 mVsce Figure 8.6(c) shows that the trends of collected macro-cell current values with time. The measured macro-cell values for the left bar and right bar were similar and the current values on left bar were generally slightly larger than those provided to the right rebar from day 22 to day 1200. After day 1200, the macro-cell measured on each rebar gradually decreased to values smaller than 5 µA. The last macro-cell values measured were 4.5 µA (right rebar) and 2.5 µA (left), the inversion occurred approx. after day 1240. These latter on–potential values at the different elevations and macro-cell currents appear to suggest that corrosion had initiated.

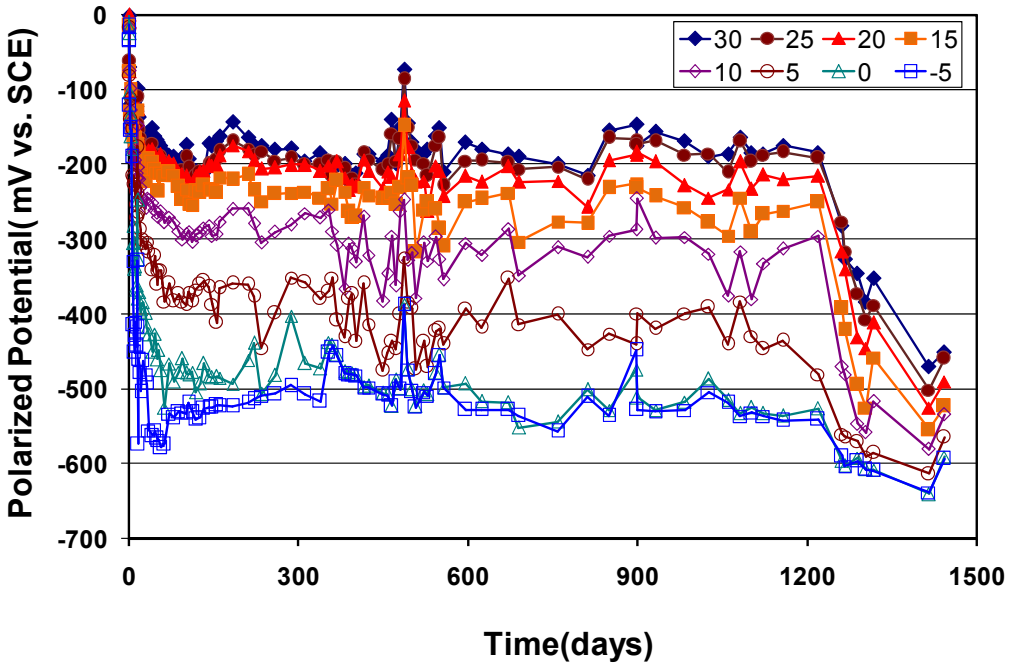

(a) Polarized potentials of left rebar in specimen K2 at eight (8) levels

Figure 8.6: Potential of the left and right bars at eight elevations and macro-cell current in specimen K2 as a function of exposure time (measurement elevations in cm relative to the waterline)

Figure 8.6 continues

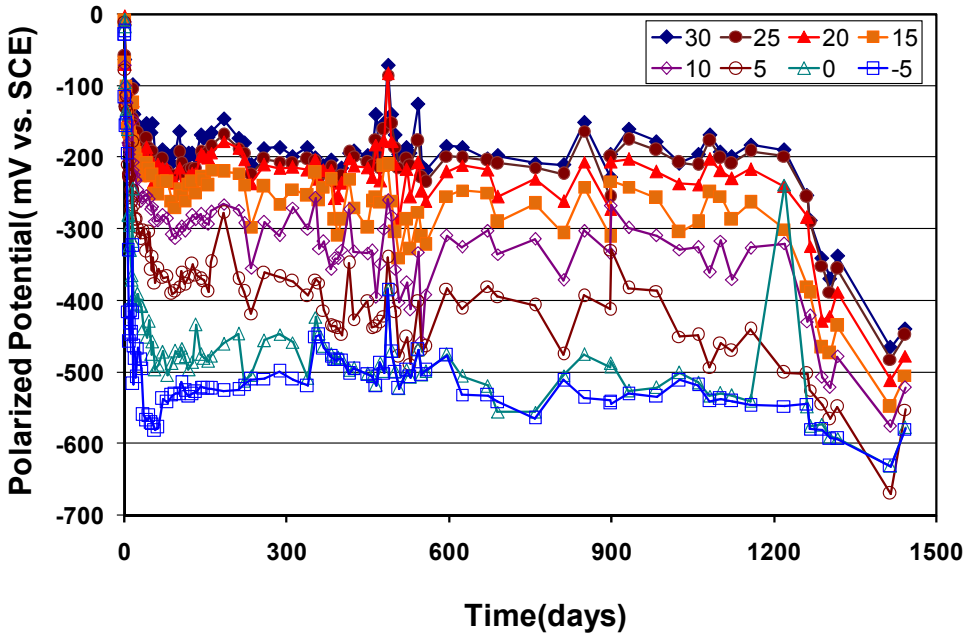

(b) Polarized potentials of right rebar in specimen K2 at eight (8)

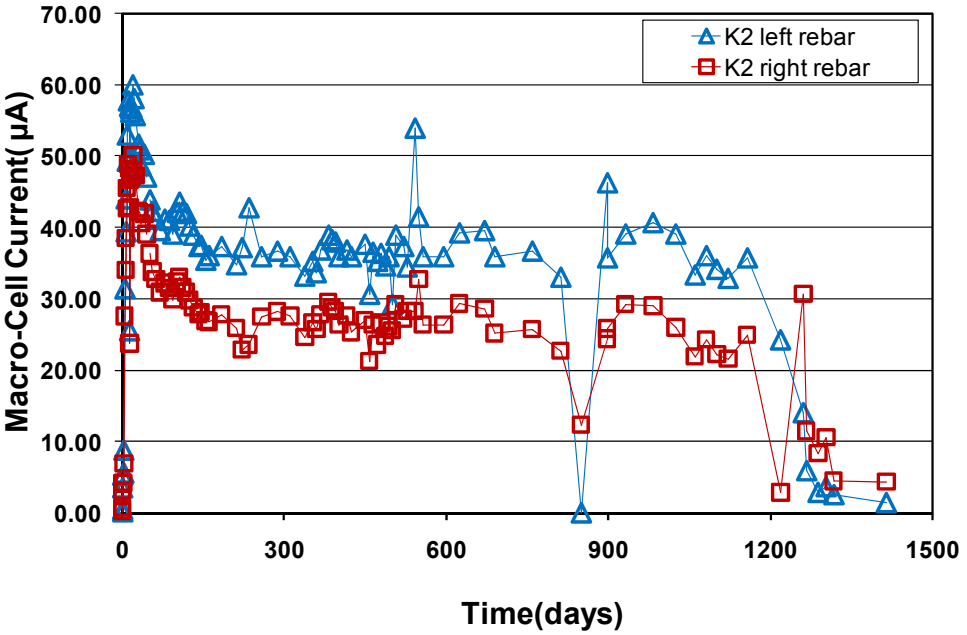

(c) Macro-cell current from left rebar and right rebar in specimen K2

Figure 8.7 shows the potential and macro-cell current versus time data for specimen K3. From Figure 8.7(a) and Figure 8.7(b), it can be seen that the trends of rebar potential with time were similar to those in specimen K2. However, after the potential transient at day 1218, the potential drop was not as pronounced on either rebar of

specimen K3. In other words, after day 1220 the potential ranges at all levels were larger than those observed on the bars in specimen K2. Figure 8.7 (c) shows that the trends of macro-cell current with time on the left bar and right bar were similar and the observed ranges of macro-cell current values were also similar. Both macro-cell current decreased with time and became stable at day 1310. At the end day 1442, the current value on the left bar was 8.23 µA and it was 8.41 µA on the right bar. Refreshing the seawater solution appears to have restored the capacity of the bare bars to delivered larger macro-cells and also the embedded rebars demanded a similar current amount than before day 1200.

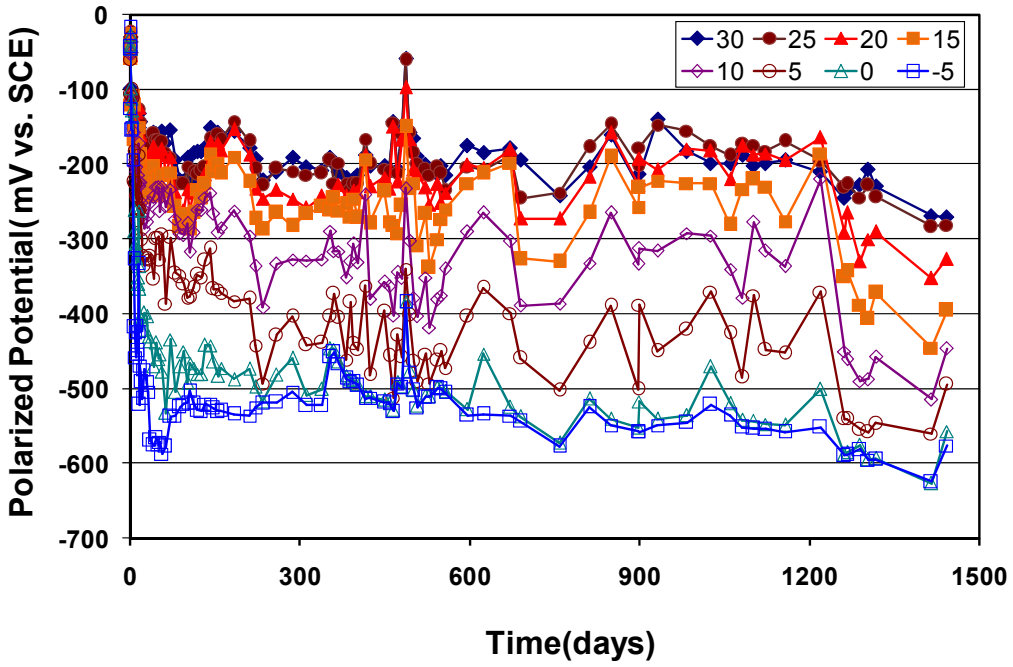

(a) Polarized potentials of left rebar in specimen K3 at eight (8) levels

Figure 8.7: Potential of the left and right bars at eight elevations and macro-cell current in specimen K3 as a function of exposure time (measurement elevations in cm relative to the waterline).

Figure 8.7 Continues

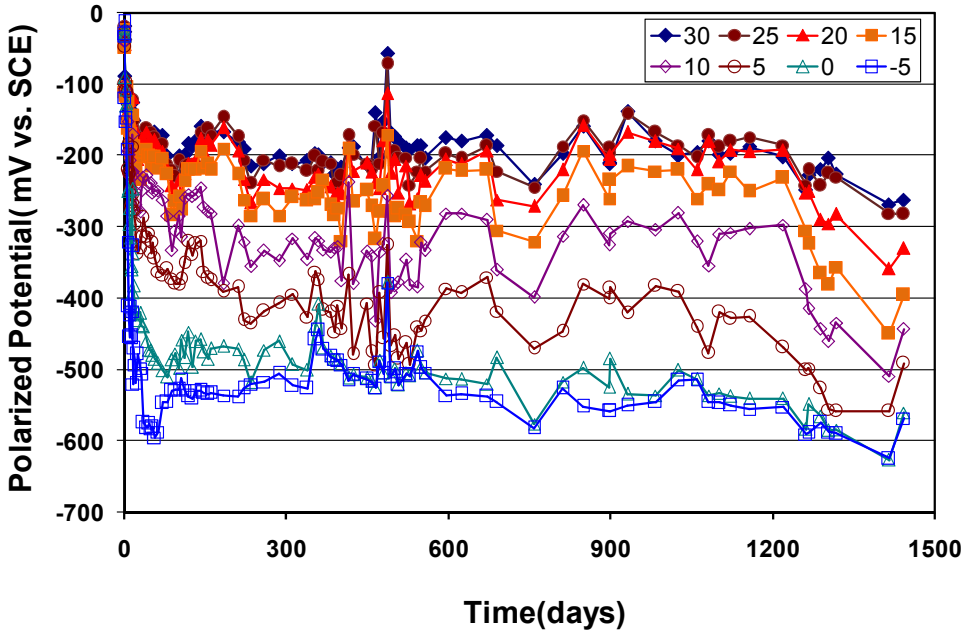

(b) Polarized potentials of right rebar in specimen K3 at eight (8)

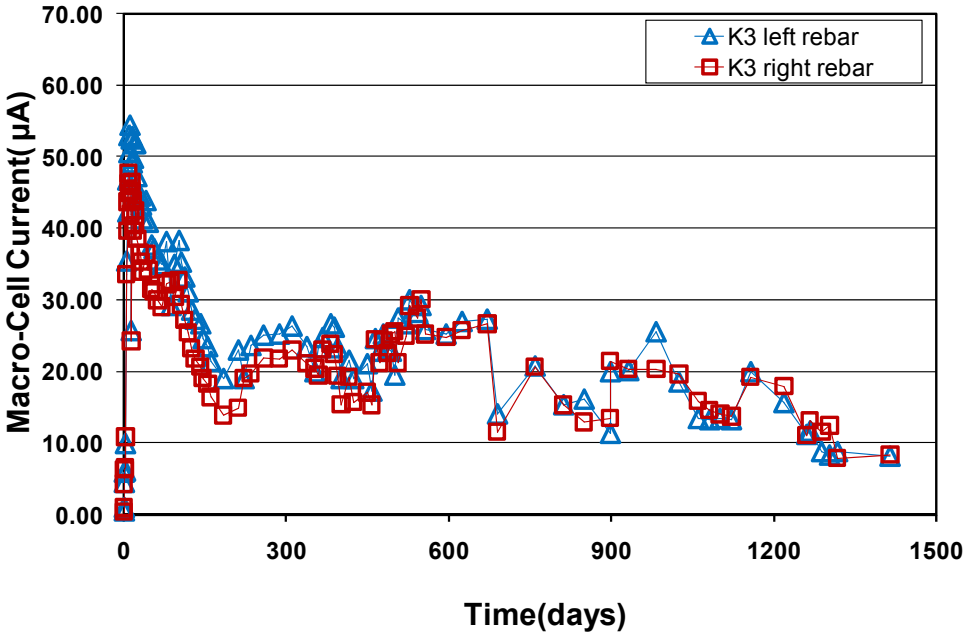

(c) Macro-cell current from left rebar and right rebar in specimen K3

Figure 8.8 shows the potential and macro-cell current versus time data for specimen K4. It indicates that the trends of potential and macro-cell were different from those in specimen K1, K2, K3. The observed potential ranges for specimen K4 are more negative and smaller. In this case the observed potential at the highest elevation was between -407 mV and -440 mV (vs. SCE) after day 70 while the potential ranged from -550 mV to -570 mV

for the lower elevation. Figure 8.8(c) shows that the macro-cell current on both left bar and right bar had similar trend after the day 20 and the former current (was generally higher than that in the latter. It was also seen that both currents increased in very slow rates and then decreased again. The current on the left bar varied between 9.3 µA and 10.9 µA and it ranged from 8.7 µA to 9.2 µA on the right bar. It is not clear why the potential distribution in specimens K4 was different from the others in group K. Specimen K4 was terminated shortly after day 100. One possible scenario is that the sprinklers that simulate the splash were defective and spray a larger amount of water and hence the concrete had a high moisture content, which resulted in larger polarization and hence more polarization was possible with a smaller macro-current.

The potential and macro-cell current versus time data for specimens M2, K1, N1 and N2 can be seen in Figure F.1, Figure F.2, Figure F.3 and Figure F.4 in Appendix F.

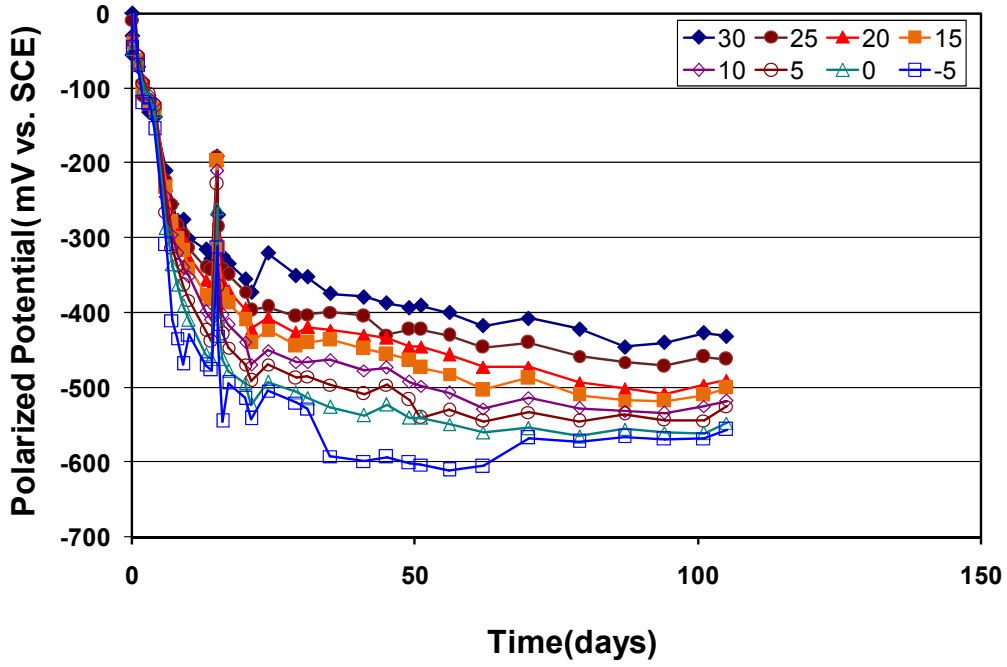

(a) Polarized potentials of left rebar in specimen K4 at eight (8) levels

Figure 8.8: Potential of the left and right bars at eight elevations and macro-cell current in specimen K4 as a function of exposure time (measurement elevations in cm relative to the waterline)

Figure 8.8: Continues

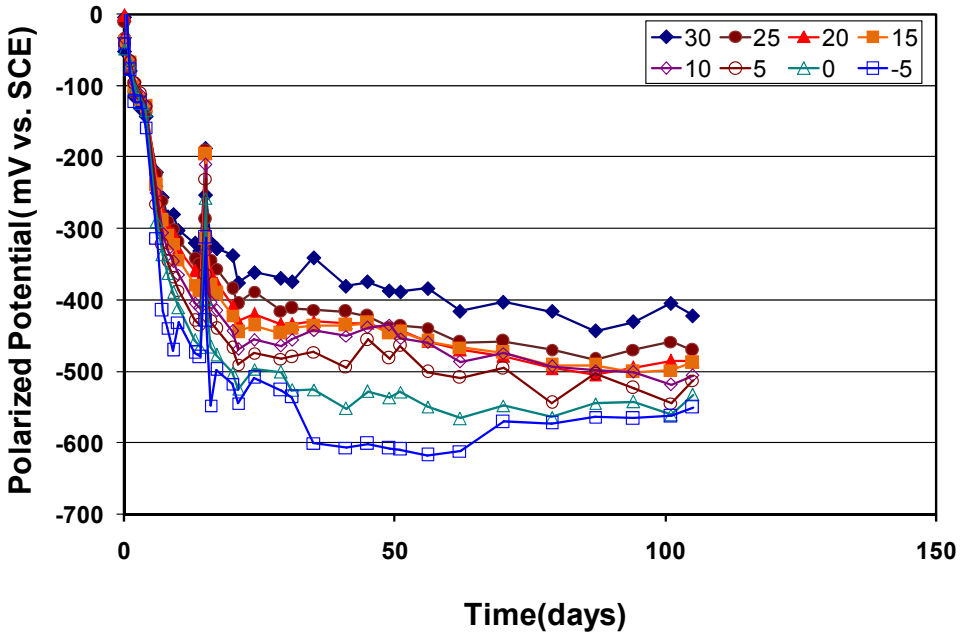

(b) Polarized potentials of right rebar in specimen K4

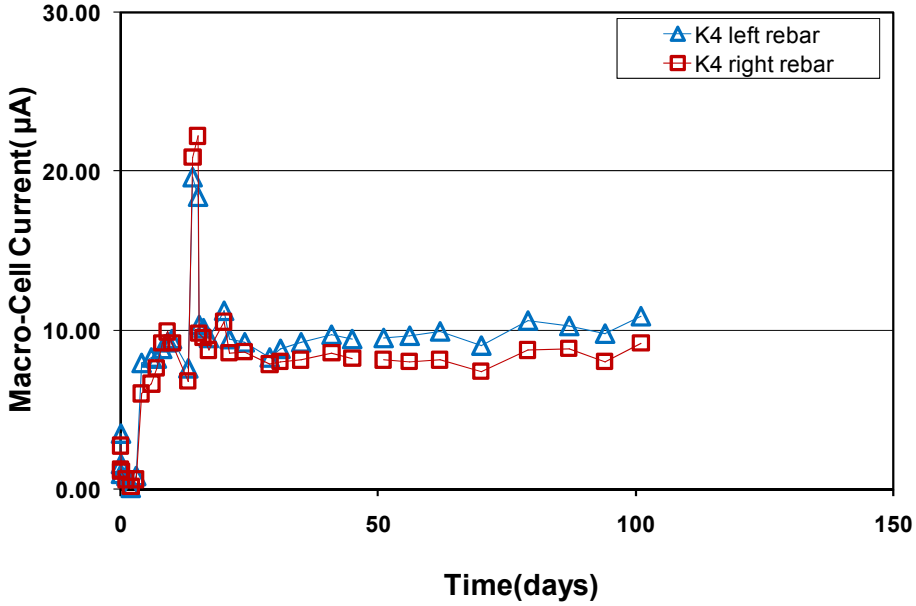

(c) Macro-cell current from left rebar and right rebar in specimen K4

Table 8-5: Current data for polarized specimens*

Specimen	Rebar location	Current (μA)		
		Max	Steady Day 60~1200	Average of last four readings
M1	L	41.2	20.82	4.46
	R	47.5	23.29	17.21
M2	L	59.8	23.15	7.35
	R	62.2	23.68	2.75
K1	L	36.5	20.65	7.41
	R	33.6	19.20	5.24
K2	L	60.0	37.25	2.72
	R	50.1	27.27	6.99
K3	L	54.4	24.47	8.56
	R	47.7	22.04	10.11
K4	L	19.6	10.03	10.40
	R	22.2	8.36	8.72
N1	L	19.3	6.24	1.92
	R	14.7	7.49	6.03
N2	L	12.0	6.34	6.14
	R	11.7	7.11	5.41
L1	L	35	21	
	R	36.5	21	

Note: Final Polarized Potential was measured at lowest and highest elevation
L- Left, R – Right

Table 8-5 shows the maximum current measured during the first 14 days, the steady current value that was eventually reached (reported values is the average between day 60 and day 1200), a third columns shows the average current value of the last four readings. Table 8-6 shows on the left column the potential range before the transient to more negative values occurred, and on the column on the right the last potential range measured at the lowest and highest location. It is evident that since each rebar is connected to a submerged bare rebar the range of values within each group indicates distinct current demands as well as how much the bare rebar was able to provide. Before day 1200, the observed steady current values on M group were relatively consistent ~ 23.68 μA, whereas for N group, it ranged from 6.24 to 7.29 μA. The largest scatter was observed on K group of specimens. K2 had the largest steady currents (27.27 and 37.25 μA), whereas K4 had the smallest at ~10.03 μA, with K1 and K3 showing values comparable to those observed on the M group.

Table 8-6: Potential data at lowest and highest elevations for polarized specimens*

Specimen	Rebar location	On potentials before transient to more negative (mV vs. SCE)		Final polarized potentials(mV vs. SCE).	
		Lowest	Highest	Lowest	Highest
M1	L	-585	-166	-591	-223
	R	-581	-167	-572	-220
M2	L	-587	-182	-586	-420
	R	-587	-184	-586	-404
K1	L	-548	-187	-577	-440
	R	-549	-224	-583	-450
K2	L	-539	-181	-593	-450
	R	-544	-189	-579	-430
K3	L			-576	-271
	R			-568	-262
K4	L			-556	-431
	R			-550	-421
N1	L			-591	-549
	R			-495	-311
N2	L			-479	-323
	R			-472	-324
L1	L			-340	-225
	R			-330	-210

Note: Final Polarized Potential was measured at lowest and highest elevation
L- Left, R - Right

8.4.2 Comparison of Experimental Measurement with Field Results

Figure 8.9(a) shows potential versus elevation data for a typical piling of the Hurricane Pass Bridge near Ft. Myers, FL, which were collected at different times [18]. While no polarization resistance measurements were made, the fact was that, first, the data was acquired at a relatively early bridge age (commissioning was in 1991) and, second, high performance concrete with silica fume was used. Hence, the rebars were passive and corrosion rate was very low (i.e. passive conditions). The data indicated that potential at a given elevation was generally similar from one measurement time to the next and was relatively negative at the lower elevations but transitioned to more positive values in the elevation range 0~0.5 m. As such, the potential profiles for the present polarized, simulated piling specimens as shown in Figure 8.9(b) were generally similar to those for an actual piling. A distinction, however, is that the potential profile for the present specimens resulted from cathodic polarization via an external source (connected submerged rebars), whereas O_2 depletion in the submerged zone concrete reinforcement was responsible for the relatively negative potentials at lower elevations in the case of the

Hurricane Pass Bridge piling, but there is a significantly larger steel surface than in the experiments described above. After sometime corrosion might initiate below water but likely would proceed at a low corrosion rate. (As indicated above O_2 depletion also took place in our experiment when the solution was not refreshed on schedule) However, in both cases, cathodic polarization of the splash/spray zone steel which is the region of interest and the source of this polarization should not be relevant.

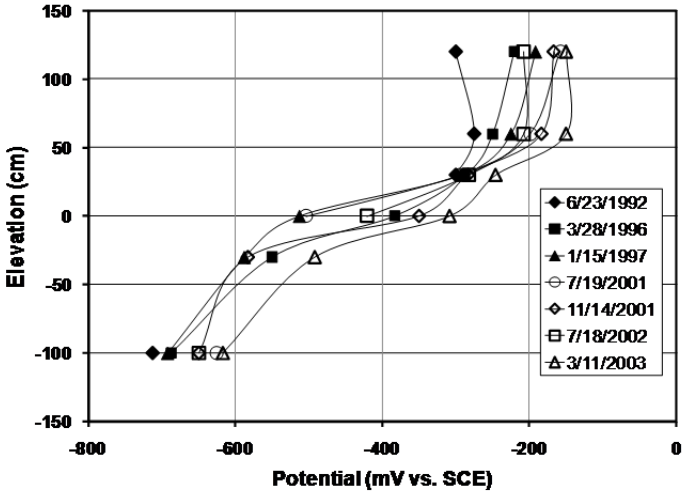

(a) Hurricane Pass Bridge at different date

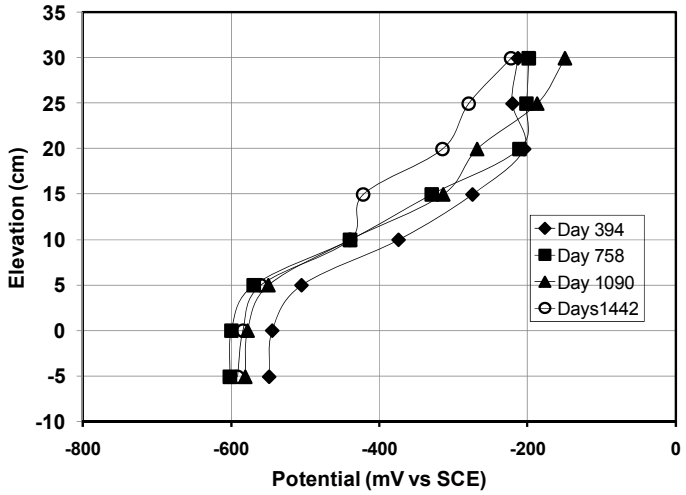

(b) Left rebar of specimen M1 at different ages

Figure 8.9: Potential versus elevation data (a) piling C of bent 4 of the Hurricane Pass Bridge (elevation referenced to mean high tide, and data at -100 m refers to measurements with the reference electrode in the water) and (b) left bar of specimen M1

8.4.3 Depolarization Test

8.4.3.1 24-hr depolarization

Figure 8.10 shows typical potential evolution for 24-hr depolarization tests performed at day 800 on M1 left rebar and N1 left rebar. The depolarization was measured at five different elevations. The negative elevation indicates measurements made with the reference electrode immersed in solution and is representative of the potential value for the reinforcement below water.

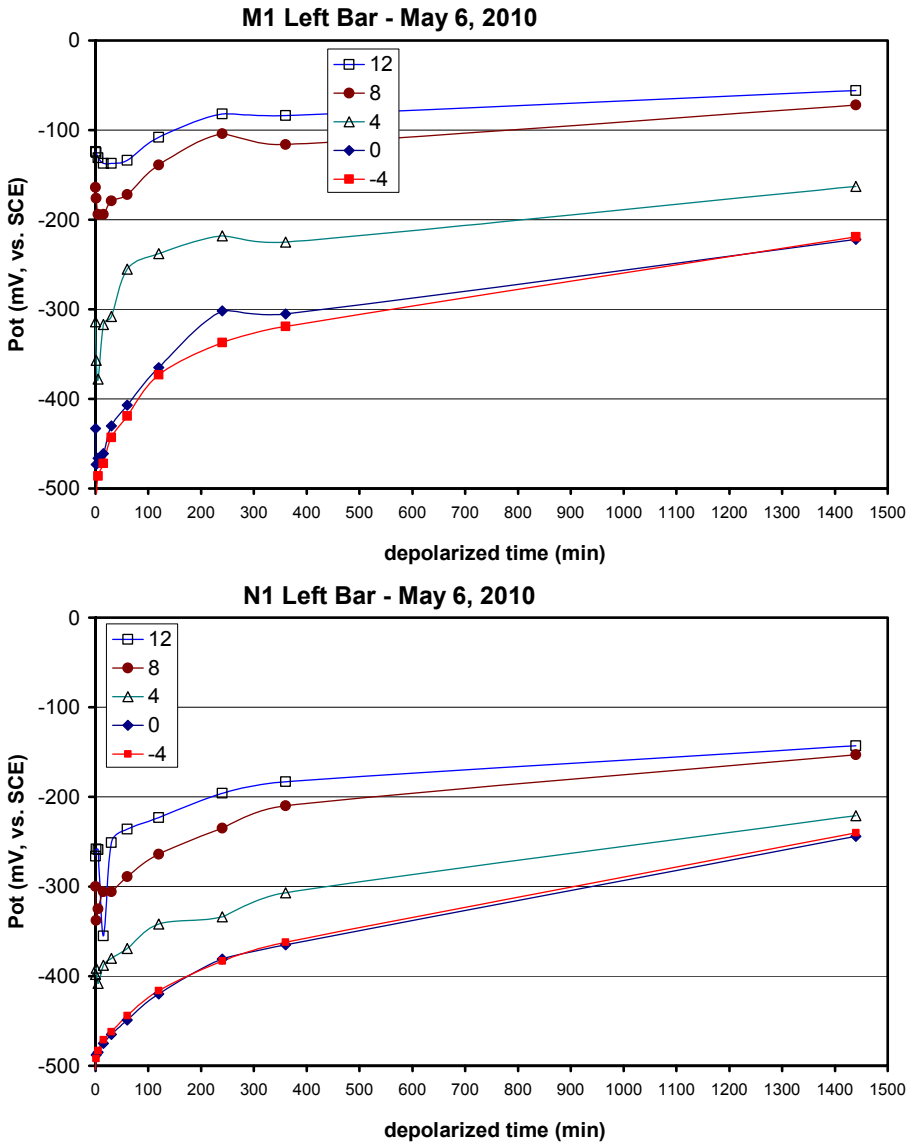

Figure 8.10: Typical depolarization plots of the left bar of Specimen M1 and left bar of Specimen N1 at different elevations as a function of depolarization time for test performed in May 2010 (measurement elevations in inches relative to the waterline).

Results from the 24-hr depolarization tests were used to prepare two types of plots: 1) the off-potential value measured after 24 hours at the different elevations; 2) the net depolarization at 24 hours at the different elevations. The net depolarization is obtained by the difference between the initial off-potential value which was measured within a few seconds of disconnecting the bare rebar and the corresponding 24-hr off potential value measured.

8.4.3.2 24-hr off-potentials

Figure 8.11 to Figure 8.14 show 24-hr off-potential profiles vs. time on the left and right bars in specimens M1, K2, K3 and L1, respectively. For the specimens M2, K1, N1 and N2, details can be seen in Figure 5 to Figure 8 in the Appendix for Chapter 8.

For specimen M1, the range of 24 –hr depolarization potential values on the left bar were generally more negative than those on the right bar as shown in Figure 8.11. The former at day 1157 was between -31 mV and -198 mV (vs. SCE) while the latter was between -3 mV and -170 mV at the same day. These values are still within the range of what is considered no corroding reinforcing steel. A potential transient took place around day 1219 at all levels and the values shifted to more negative values but with the oscillation observed (up-down-up) for each level. The most negative potentials values were between -431 mV and ~ -538 mV on the left rebar from highest to lowest levels at day 1416. These values ranged between -438 mV and ~ -588 mV on the right bar at the same day. Thereafter, the 24-hr off-potentials moved to more positive values, but did not return to the values before the potential transient at day 1219. As previous discussed, the potential transient was attributed to the solution not been refreshed for a longer period, leading to consumption of all or most O_2 in solution within the container with the bare rebars. As such the anode (bare rebar) immersed in seawater was only able to deliver a significantly smaller macrocell current. Upon refreshing the solution, the rebar potentials at all elevations shifted to more positive values again.

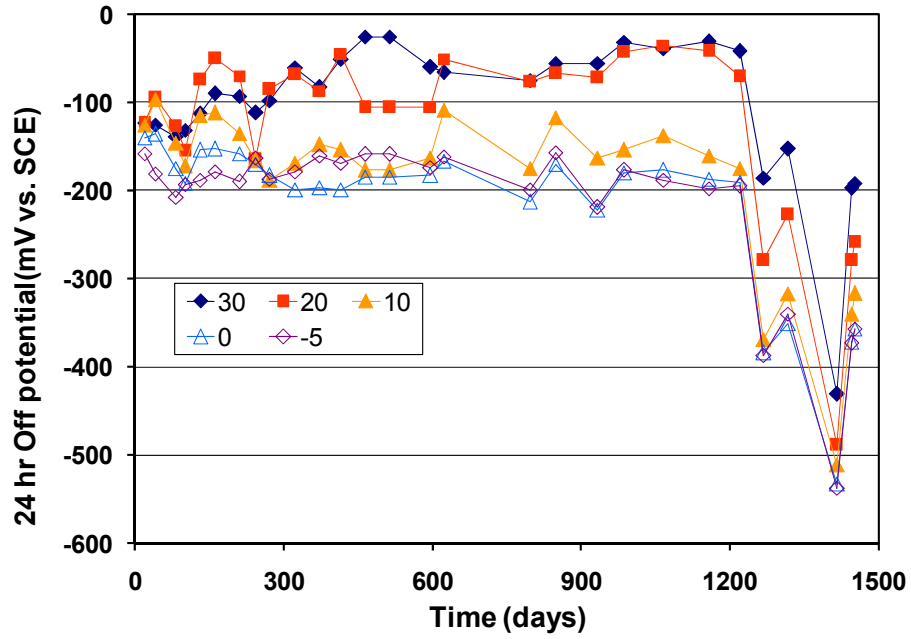

(a) 24 hr off potentials of left rebar in specimen M1

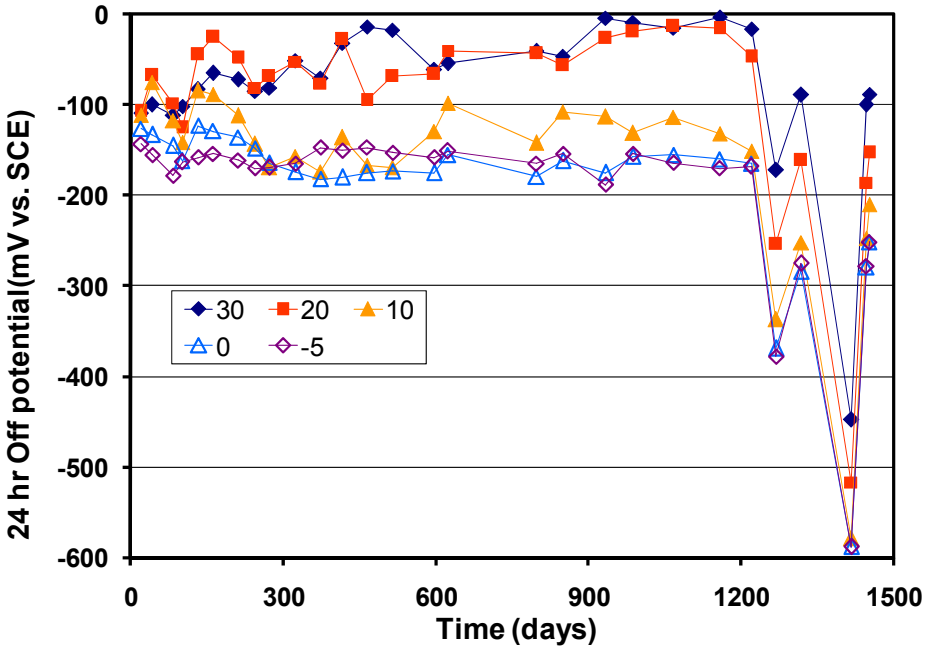

(b) 24 hr off potentials of right rebar in specimen M1

Figure 8.11: 24-hr off-potential plots of the M1 left bar and right bar at different elevations as a function of exposure time (measurement elevations in cm relative to the waterline)

For specimen K2, the ranges of 24–hr off-potential value on the left bar were generally more positive than those on the right bar as seen in Fig. 8.12, which was different from those in specimen M1. The potentials on the left

rebar at day 1157 ranged from 4 mV ~ 145 mV and these values on the right rebar were between – 83mV and -235 mV. Similar to what was observed on specimen M1, a potential transient took place on both rebars in specimen K2 around day 1200 and shifted to negative values ranging from -437 mV to -540 mV on the left bar and from -394 to -519 mV on the right bar at day 1416. The potentials slightly moved towards more positive values by the last set of measurements on day 1449. It is obvious that trends of 24-hr off-potentials in specimen K2 were clearly different from those in specimen M1 after the potential transient.

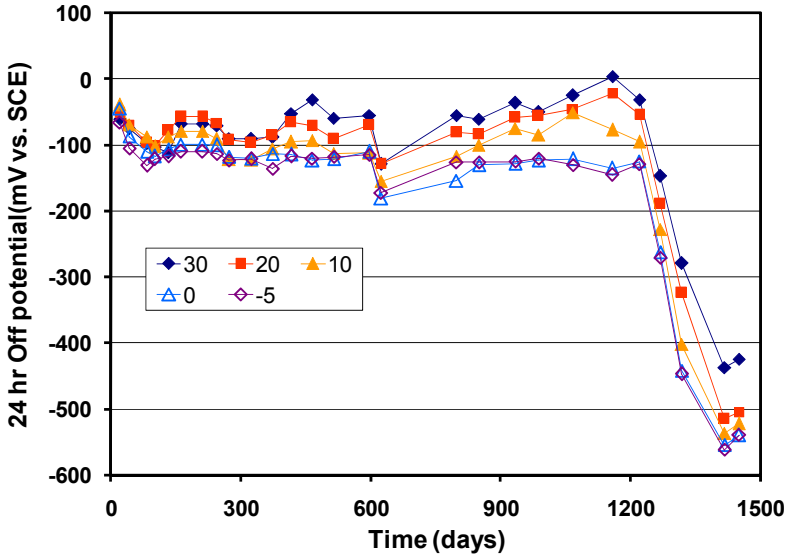

(a) 24 hr off potentials of left rebar in specimen K2

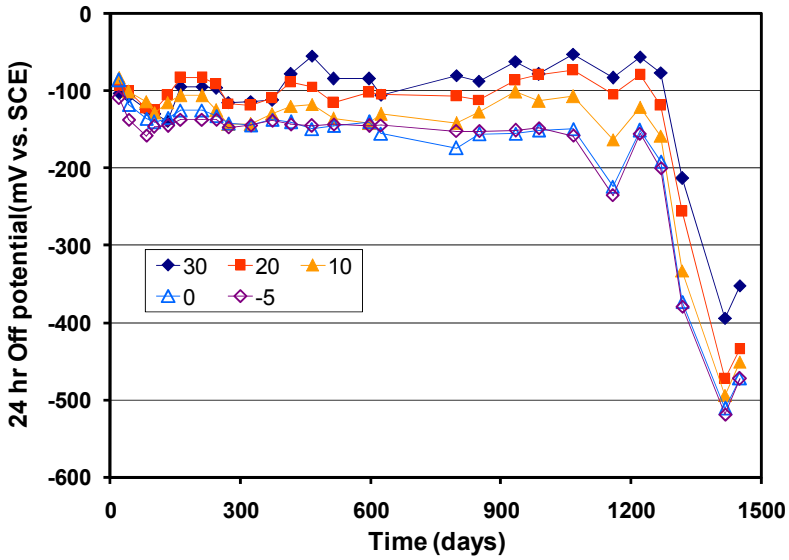

(b) 24 hr off potentials of right rebar in specimen K2

Figure 8.12: 24-hr off potential plots of the K2 left bar and right bar at different elevations as a function of exposure time (measurement elevations in cm relative to the waterline)

Figure 8.13 shows the trend of 24-hr-off-potentials on the rebars in specimen K3 before day 1219 was similar to that in specimen M1 and K2. Thereafter, the potential transient in specimen was comparable to that in specimen K2, but the potentials shifted to negative values ranging from -195 mV to -368 mV on the left bar and from -196 mV to -382 mV on the right rebar at day 1416. Obviously, the extent of potentials shift in specimen K3 was smaller than that in specimen K2. The potentials slightly moved towards more positive values after the last depolarization.

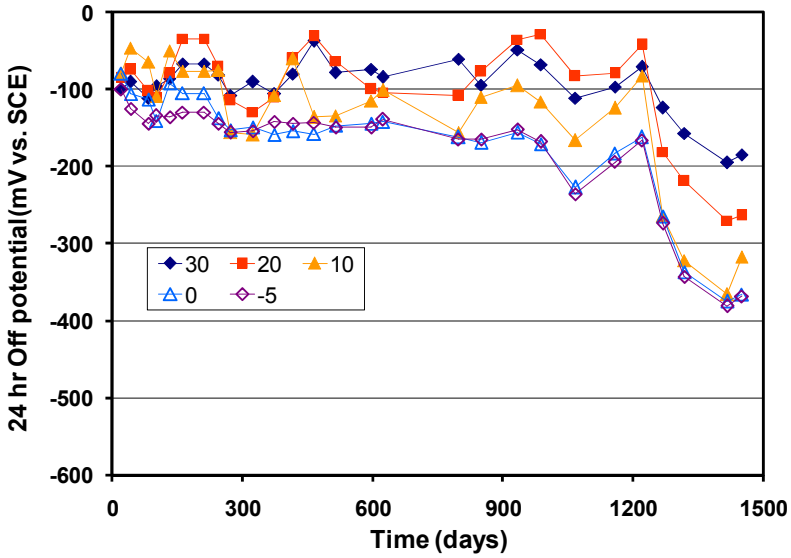

(a) 24 hr off potentials of left rebar in specimen K3

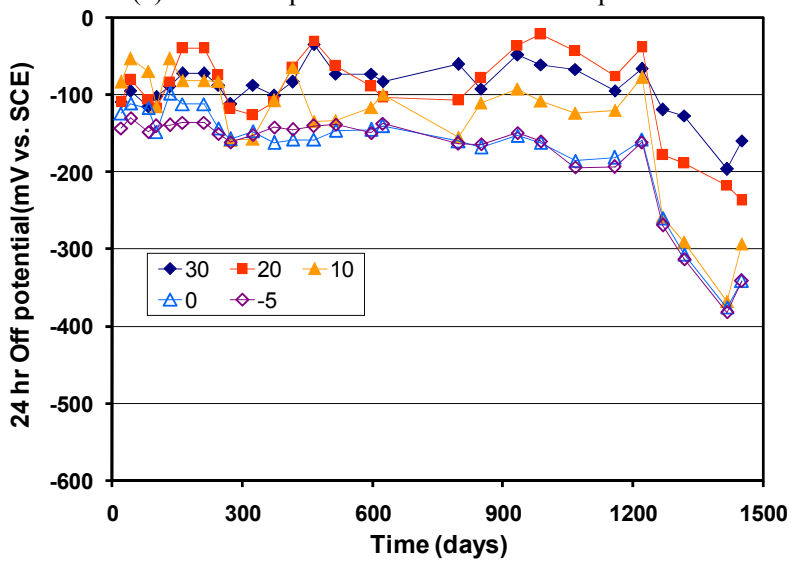

(a) 24 hr off potentials of right rebar in specimen K3

Figure 8.13: 24-hr off potential plots of the K3 left bar and right bar at different elevations as a function of exposure time (measurement elevations in cm relative to the waterline)

From Figure 8.14, it is observed that the potential transient in specimen L1 left rebar took place at day 464, which was much earlier than that in other specimens M1, K2 and K3. After day 464, the potentials moved to the more negative and then slowly shifted to the more positive values. It should be pointed out that the potentials at two high levels (20 cm & 30 cm) on the left bar and at highest level 30 cm on the right rebar returned to the original ranges by day 840. This was different from that at low levels in specimen L1 where the potentials shifted towards more positive values, but did not return to values observed before the transient for all elevations.

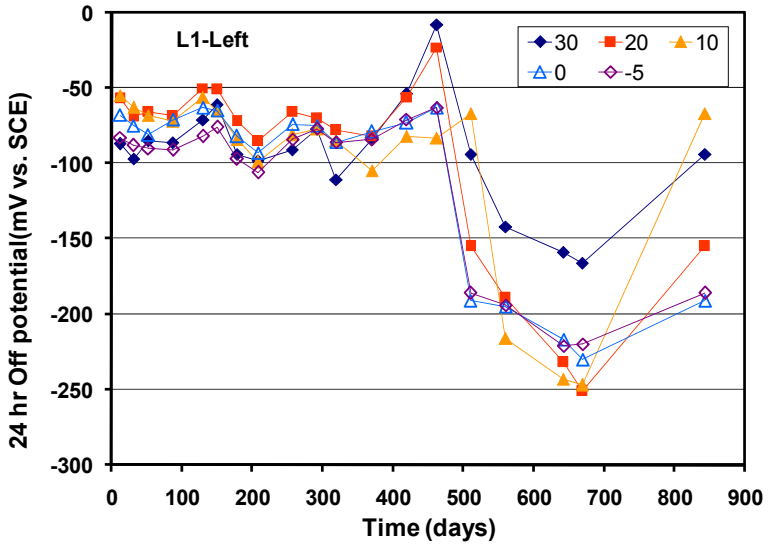

(a) 24 hr off potentials of left rebar in specimen L1

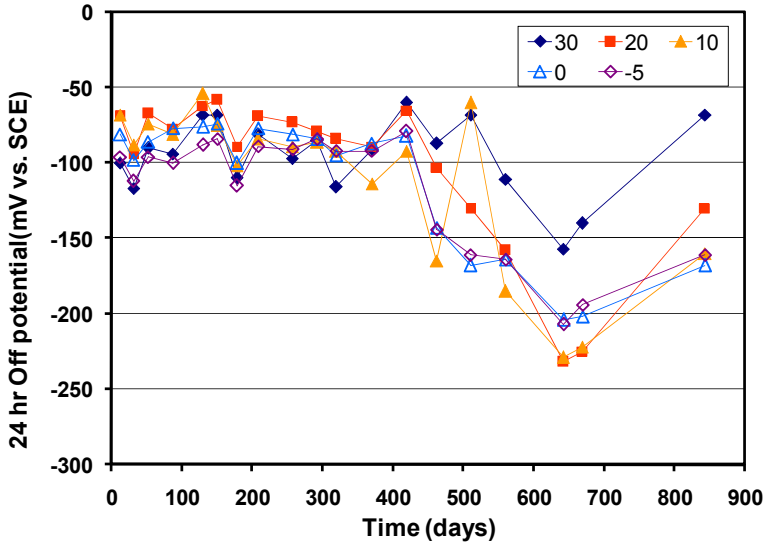

(b) 24 hr off potentials of right rebar in specimen L1

Figure 8.14: 24-hr-off potential plots of the L1 left bar and right bar at different elevations as a function of exposure time (measurement elevations in cm relative to the waterline)

Table 8-7 and Table 8-8 list the 24-hour-off potential values measured at all levels after the last 24 hr depolarization. These were performed shortly before the specimens were terminated (Table 8-4 shows the date in which each rebar was exposed).

Table 8-7: 24-hour off-potentials of rebar in specimens K1, K2, K3 and L1 (unit: mV vs. SCE)

Level	K1		K2		K3		L1	
(cm)	L	R	L	R	L	R	L	R
30	-239	-306	-424	-352	-185	-160	-94	-68
20	-342	-411	-504	-435	-263	-237	-155	-130
10	-368	-437	-522	-451	-317	-293	-67	-160
0	-391	-458	-540	-472	-366	-341	-191	-168
-5	-394	-461	-539	-472	-368	-341	-186	-161

Note 1: L-Left, R – Right; K4 was terminated at day 100 without performing 24-hour-depolarization testing
2: End days: Specimens M1, M2 = 1451 days; K1,K2,K3=1442 days;
L1=850 days.

Table 8-8: 24-hour off-potentials of rebar in specimens M1, M2, N1 and N2 (unit: mV vs. SCE)

Level	M1		M2		N1		N2	
(cm)	L	R	L	R	L	R	L	R
30	-192	-89	-231	-287	-506	-249	-246	-246
20	-259	-152	-251	-308	-556	-227	-223	-226
10	-317	-210	-318	-377	-556	-273	-280	-344
0	-357	-252	-346	-406	-556	-330	-309	-414
-5	-357	-251	-347	-405	-557	-306	-292	-423

Note 1: L-Left, R – Right
2: End day: Specimens M1, M2 = 1451 days; N1L =1446 days; N1R=643 days; N2L=272 days; N2R=1066 days

8.4.3.3 Net depolarization

Figure 8.15, Figure 8.16 and Figure 8.17 show 24 hour net depolarization values vs. time on the left bar and right bar at different elevations in specimens M1, K2 and L1 as a function of exposure time at the different elevations. Such results in specimens M2, K1, K3, N1 and N2 can be seen in Figure F.9, Figure F.10, Figure F.11, Figure F.12 and Figure F.13 in Appendix F.

The results in Figure 8.15 and Figure 8.16 show that the net depolarized potential values on the rebars in specimens M1 and K2 at the two lowest levels (-5 cm & 0 cm) were generally between 250 mV and 400 mV before day 1218. After days 1218, these net depolarized potential values ranged from 150 mV to 250 mV at level

10 cm, while the net depolarization values on these rebars at two highest levels (20 cm & 30 cm) were between 40mV to 150mV during the same period. The potential transient took place at different exposure times.

For M1 left rebar, Figure 8.15 (a) shows that the transient for net-depolarization values at the two lower levels took place after day 1219. The net depolarization values on the left rebar at level -5.0 cm decreased from 323 mV at day 1219 to 91 mV at day 1416. At level 0 cm, the net depolarization was reduced from 329 mV to 93 mV (level 30.0 cm). The potential transient at level 10cm took place at day 1317 and the net depolarized potential values went from 165 mV at day 1317 to 71 mV at day 1416. At the end day 1451, it was 135 mV. The potential transient for the two higher levels occurred at day 1268. At level 20.0cm, the net depolarization values decreased from 114 mV at day 1268 to 36 mV at day 1451. At this level, the last net-depolarization measured on day 1451 was 63 mV. At level 30.0 cm, the net depolarization values reduced from 159 mV at day 1268 to 36.0 mV at day 1451. For M1 right rebar, Figure 8.15 (b) shows that the day in which the potential transient occurred for the right rebar at the two lower levels was the same as that on M1 left rebar (day 1219). The net depolarized potential values at -5.0 cm varied from 348 mV at day 1219 to 40 mV at day 1416. It was 278 mV on day 1451. At level 0.0 cm, the net depolarized potentials value decreased from 348 mV at 1219 to 33 mV at day 1416. This value was 276 mV on day 1451. The potential transient at 10.0 cm took place at day 1317 and its net polarization values was reduced from 208 mV at day 1317 to 1 mV at day 1416, but the net-depolarization value was 220 mV on day 1451. At highest two levels, the potential transient at day 1268. At level 20.0 cm, the net polarization value varied from 134 mV at 1268 to 6 mV at 1416 while this value at level 30.0 cm decreased from 169 mV to 24 mV at the same period. The net depolarization obtained on day 1415 for levels 20.0cm and 30.0cm were 147 mV and 115 mV, respectively..

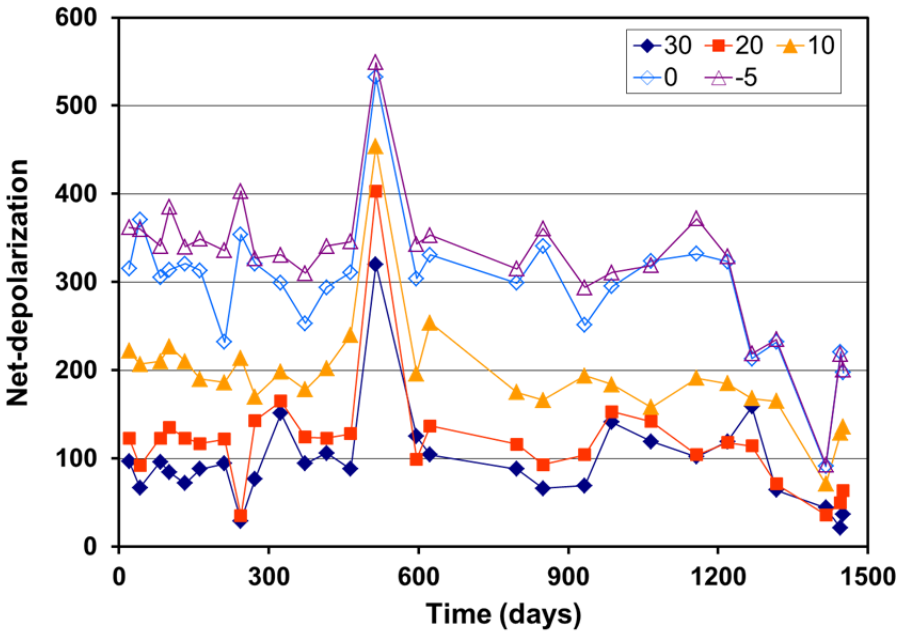

(a) Net depolarization (mV) after 24-hr plots of the M1 left bar

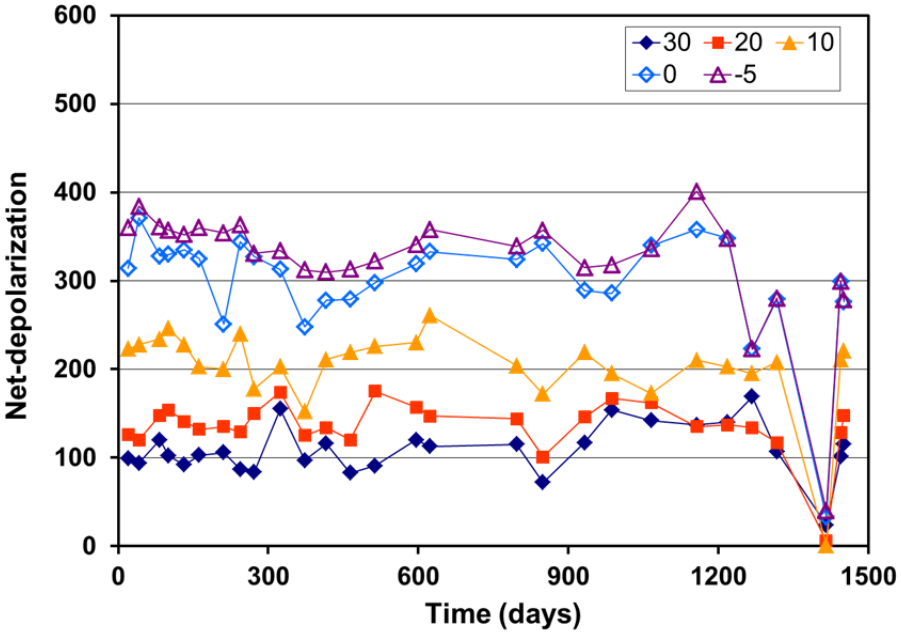

(b) Net depolarization (mV) after 24-hr plots of the M1 right bar

Figure 8.15: Net depolarization (mV) after 24-hr plots of the M1 left bar and right bar at different elevations as a function of exposure time (measurement elevations in cm relative to the waterline).

Figure 8.16 shows that the potential transient occurred on K2 left rebar and right rebar at all levels on day 1268. Figure 8.16 (a) also shows that the net depolarized potential measured on day 1449 (last) ranged from 12 mV to

60 mV on K2 left rebar at all levels; i.e., the net depolarization values were less than 100 mV. Figure 8.16 (b) shows that the net polarization values recorded after the last depolarization (day 1449) on the right rebar at levels -5 cm, 0 cm and 10 cm were 113 mV, 111 mV and 105 mV respectively. However, the net depolarized values at levels 20cm and 30 cm at the same day were 73 mV and 68 mV, i.e., both were less than 100 mV.

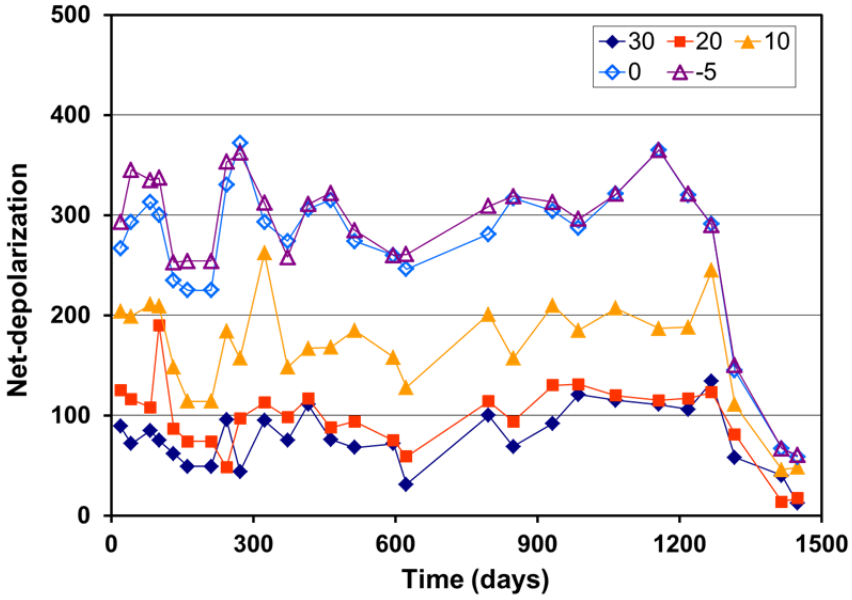

(a) Net depolarization (mV) after 24-hr plots of the K2 left bar

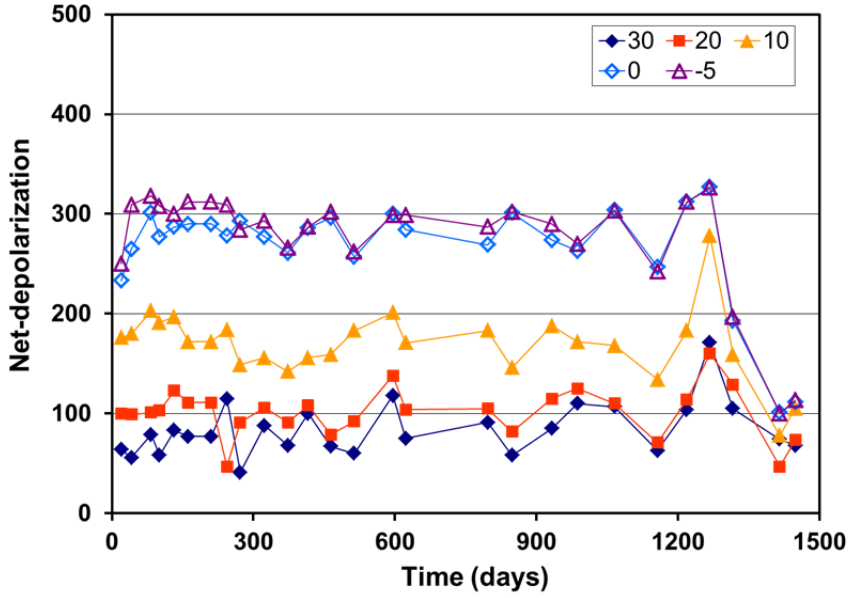

(b) Net depolarization (mV) after 24-hr plots of the K2 right bar

Figure 8.16: Net depolarization (mV) after 24-hr plots of the K2 left bar and right bar at different elevations as a function of exposure time (measurement elevations in cm relative to the waterline).

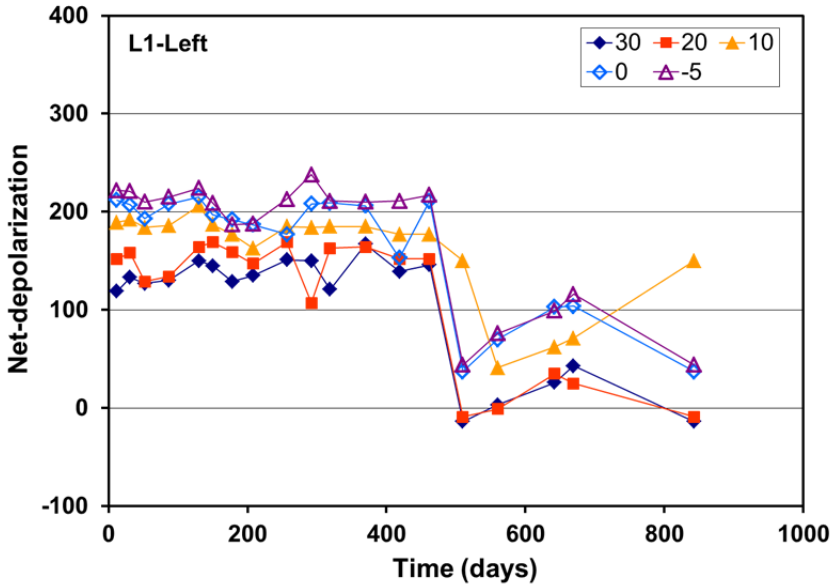

(a) Net depolarization (mV) after 24-hr plots of the L1 left bar

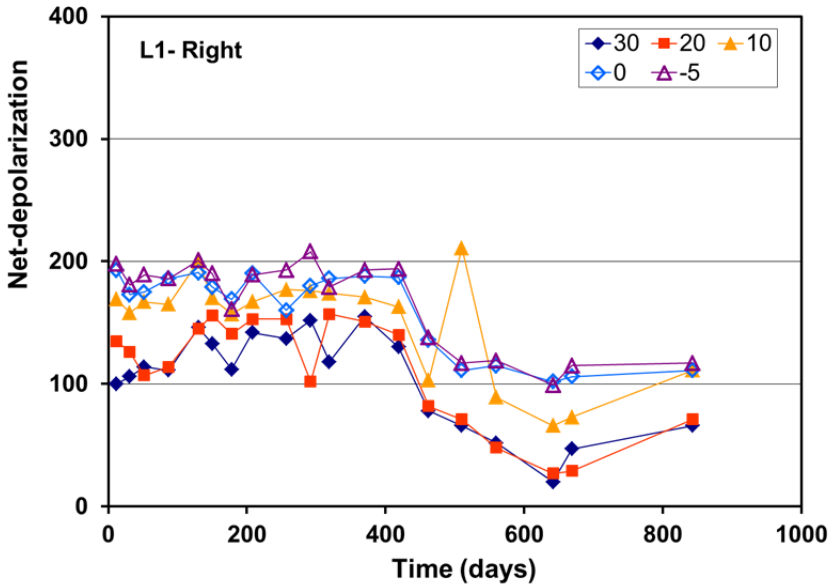

(b) Net depolarization (mV) after 24-hr plots of the L1 right bar

Figure 8.17: Net depolarization (mV) after 24-hr plots of the L1 left bar and right bar at different elevations as a function of exposure time (measurement elevations in cm relative to the waterline).

Figure 8.17 shows net depolarization plots for L1 left rebar and L1 right rebar. For L1 left rebar, the first potential transient started at day 450 mV at all levels. The second potential transient for two lowest levels (-5 cm & 0 cm) and two highest levels (20 cm & 30 cm) took place at day 660. The net-depolarization values observed at the two lowest levels and two highest levels on day 850 (last) were generally less than 50 mV, whereas it was 150 mV at

the middle level 10.0 cm. For L1 right rebar, the potential transient likely took place at day 415 at all levels. The net depolarization values at the two lowest levels (20 cm & 30 cm) and middle level 10 cm were greater than 100 mV. These values at two highest levels (20 cm & 30 cm) were approximately 75 mV.

There is a risk of corrosion initiating as the result of the 24-hr depolarization period chosen. This risk would likely be more pronounced at longer exposure times as the chloride concentration at the rebar trace will be higher. (Additionally, in a couple of instances the technician did not re-connect properly after the depolarization test and this could be why rebar N2 right might have become active).

Table 8-8 and Table 8-9 summarize the net depolarization values of rebar in all specimens at the different levels at those obtained after the last depolarization.

Table 8-9: Net depolarized potentials of rebar in specimens K1, K2, K3 and L1 (unit: mV)

Level	K1		K2		K3		L1	
(cm)	L	R	L	R	L	R	L	R
30	218	142	12	68	20	28	-14	66
20	162	87	17	73	63	78	-9	71
10	174	91	48	105	147	156	150	111
0	191	116	58	111	196	206	37	111
-5	188	114	60	113	194	206	44	117

Note 1: L-Left, R – Right; K4 was terminated at day 100 without performing 24-hour-depolarization testing
2: End days: Specimens M1, M2 = 1451 days; K1,K2,K3=1442 days; L1=850 days

Table 8-10: Net depolarized potentials of rebar in specimens M1, M2, N1 and N2 (unit: mV)

Level	M1		M2		N1		N2	
(cm)	L	R	L	R	L	R	L	R
30	36	115	127	72	28	66	71	63
20	63	147	147	92	29	78	112	63
10	135	220	153	98	36	143	132	14
0	197	276	206	149	33	130	180	56
-5	200	278	203	147	29	163	178	53

Note 1: L-Left, R – Right
2: End day: Specimens M1, M2 = 1451 days; N1L =1446 days; N1R=643 days; N2L=272 days; N2R=1066 days

8.4.4 Visual Inspection and Chloride Analysis

8.4.4.1 Visual inspection

Table 8-4 shows the time in which the last depolarization took place, shortly after the specimens were terminated. The specimens were cut open to inspect rebar surface condition and assess for corrosion sites. For some specimens the steel surface under the shrinkage wrap was inspected after it was removed. Unfortunately, this shrinkage warp was not removed on any of the rebars terminated after day 1400 due to a miscommunication.

Figure 8.18 shows corrosion sites on M1 right rebar at 13 cm, 14.8 cm and 16.2 cm from the bottom of specimen which is at 7.0 cm, 9.8 cm and 11.2 cm from the water line, respectively. It is unknown whether crevice corrosion also initiated underneath shrinkage wrap, as it was not removed. For M1 left rebar, M2 left and right rebars, the details can be seen in Figure F.14, Figure F.15 and Figure F.16 in the Appendix for this chapter.

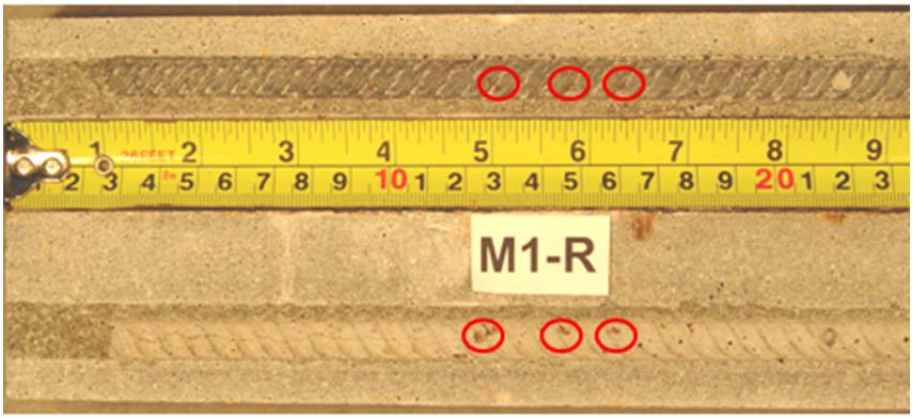

Figure 8.18: M1 right rebar - corrosion spots on right rebar at 13.00 cm, 14.80 cm and 16.20 cm from the bottom of specimen (7.00 cm, 9.80 cm and 11.20 cm from the water line)

For specimen K1, corrosion spots were observed on the left bar at elevation 8.0 cm from the bottom of specimen (3.0 cm from the water line) and on K1 right bar (see Figure 8.19) at elevation 17.5 cm from the bottom of specimen (12.5 cm from the water line). For K1 specimen, corrosion sites were seen on K2 right bar (see Fig. 8.20), but no corrosion spots were observed on K2 left bar (see Figure F.17 in the appendix). For specimen K3, corrosion was observed on the left rebar (Figure 8.21) at 16.5 cm and 28.3 cm from the bottom of specimen (11.5 cm and 23.3 cm from the water line) and on the right bar (Figure 8.22) from 14 cm to 18.25 cm from the bottom of specimen (9.0 cm ~ 13.25 cm from the water line). Specimen K4 was terminated earlier (day 100) and no corrosion was observed on either rebar. Corrosion was also observed on the rebars in specimen N1, N2 and L.

Details can be seen in Figures F.18, F.19 and F.20, respectively in the Appendix for this chapter. Table 8-11 summarizes the locations at which corrosion spots were observed on the rebars.

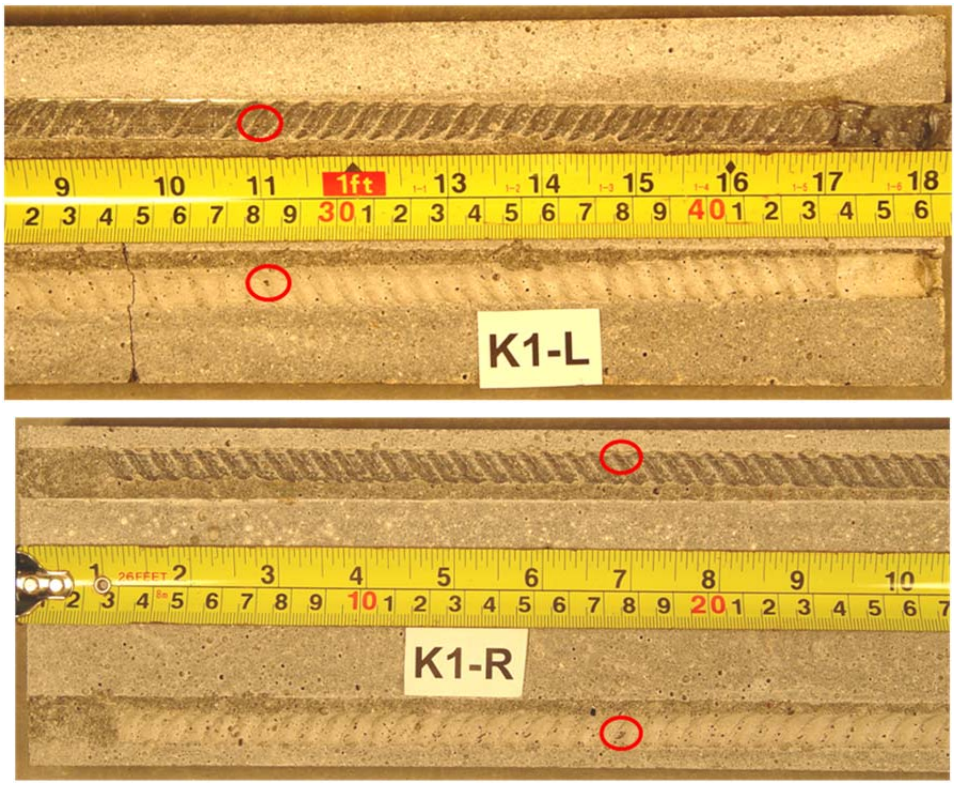

Figure 8.19: K1 right rebar low portion–corrosion spots at level 17.5 cm from the bottom of specimen (12.5 cm from the water line)

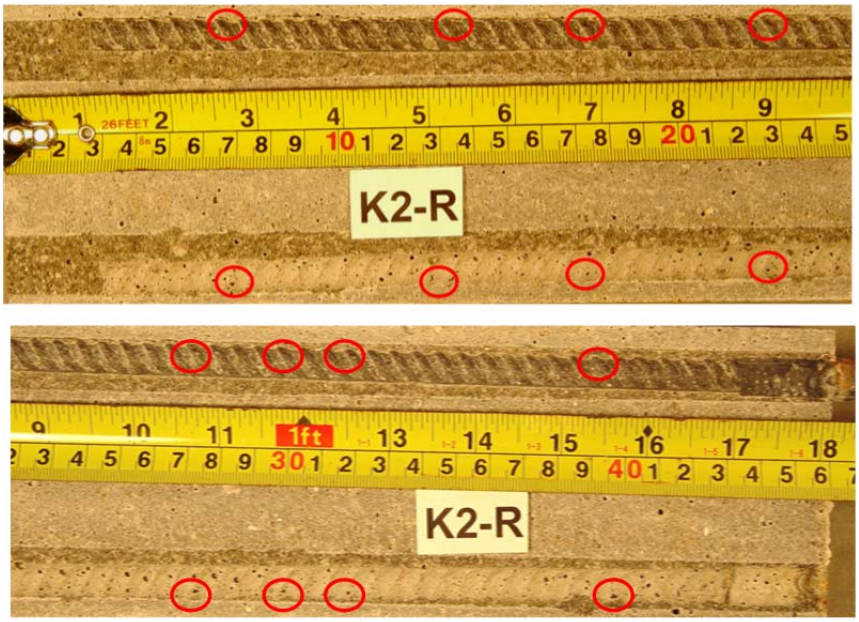

Figure 8.20 K2 right rebar–corrosion spots on rebar

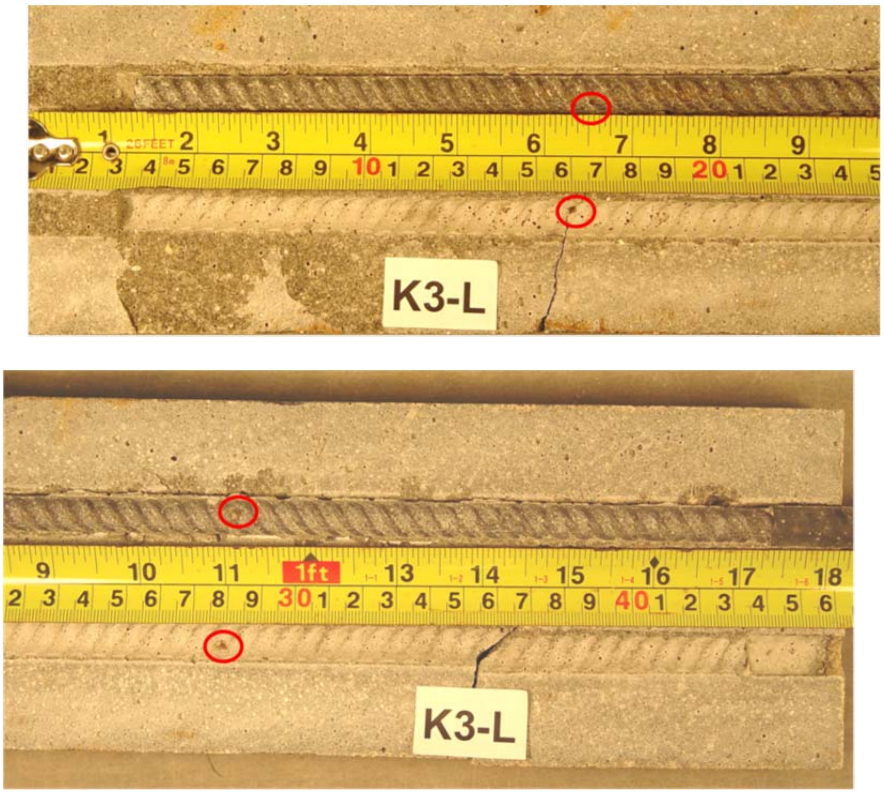

Figure 8.21: K3 left rebar–corrosion spots at 16.5 cm and 28.3 cm from the bottom of specimen (11.5 cm and 23.3 cm from the water line)

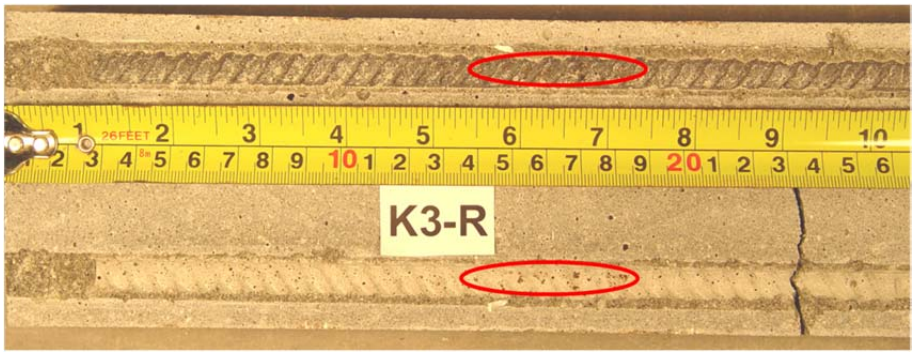

Figure 8.22: K3 right rebar–corrosion spots from 14 cm to 18.25 cm from the bottom of specimen (9.0 cm to13.25 cm from the water line)

Table 8-11: Locations of corrosion spots on rebars

Specimens	Rebar	Levels from waterline (cm)	Crevice corrosion underneath shrinkage tap
M1	L	5.0	unknown
	R	7.0, 9.8,11.2	unknown
M2	L	5.0, 11.5, 16.5, 24.0	unknown
	R	unknown	unknown
K1	L	3.0	unknown
	R	8.5, 12.5	unknown
K2	L	no corrosion	unknown
	R	2.0,8.5, 12.5,18.0 22.0, 25.0,27.0,35.0	unknown
K3	L	11.5, 23.5	unknown
	R	9.0~13.25	unknown
N1	L	no corrosion	unknown
	R	5.0	yes
N2	L	no corrosion	yes
	R	6.35, 22.86	yes
L1	L	11.6~17.8	unknown
	R	25.0	unknown

8.4.5 Chloride Concentration

Concrete milling took place at locations either below and/or above the corrosion sites along the rebar trace. Table 8-12 and Table 8-13 list the chloride concentrations at the various elevations tested from the water line. It should be pointed out that the chloride concentrations at elevations 8.0 cm ~ 12 cm (splash middle region) on all specimens were generally higher, ranging from 0.71 to 3.75% by weight of cement (2.75 to 14.58 kg/m^3 by weight of concrete), than those at other elevations.

In addition, milling was carried out at several depths between the left rebar and right rebar at four different levels on selected specimens. These mortar powders were also taken for chloride analysis and profiles prepared. Figure 8.23, Figure 8.24 and Figure 8.25 show chloride profiles for specimens K1, K3 and M1, respectively. Again, it is observed that chloride contents at level 10 cm are much greater than those at other levels.

It should be noticed that there is a difference in the chloride concentration at same elevations between different samples. This difference may be attributed to the difference in the magnitude of the electric field in different samples and as function of elevation. It may also be due in part to not-uniform splash and different splash duration on some specimens or different amount sprayed as the sprinkler tip aged.

Table 8-12: Chloride concentration of K1, K2, K3 and L1 at rebar trace

Specimen	Rebar	Elevation Range Lower (from waterline) (cm)	Elevation Range Upper (from waterline) (cm)	Chloride Concentration (kg/m3)	Chloride Concentration (% by wt of cement)
K1	L	-2.46	2.62	1.32	0.34
		8.02	12.46	3.02	0.78
		18.50	22.94	1.40	0.36
		29.29	35.01	0.60	0.15
	R	-2.46	3.26	1.64	0.42
		7.70	13.42	2.75	0.71
		18.50	23.26	1.28	0.33
		29.61	34.37	1.83	0.47
K2	L	-1.83	1.99	0.73	0.19
		8.34	12.15	2.82	0.73
		18.50	22.31	1.59	0.41
		28.66	32.47	1.38	0.36
	R	-1.83	1.99	0.99	0.26
		8.34	12.15	2.78	0.71
		18.50	22.31	1.92	0.49
		28.66	32.47	1.34	0.34
K3	L	-1.83	1.35	6.11	1.57
		2.30	5.48	8.00	2.06
		19.45	21.99	10.12	2.60
		28.66	32.47	4.34	1.12
	R	-1.83	1.99	4.95	1.27
		3.26	7.07	9.94	2.55
		13.73	17.86	12.37	3.18
		18.50	22.31	3.95	1.02
		28.66	32.47	1.31	0.34
L1	L	5.16	8.93	6.00	1.54
		14.05	17.82	4.10	1.05
		22.94	26.71	7.00	1.80
	R	5.16	8.93	7.50	1.93
		20.40	24.17	6.80	1.75

Table 8-13: Chloride concentration of M1, M2, N1 and N2 at rebar trace

Specimen	Rebar	Elevation Range Lower (from waterline) (cm)	Elevation Range Upper (from waterline) (cm)	Chloride Concentration (kg/m3)	Chloride Concentration (% by wt of cement)
M1	L	1.35	3.89	0.97	0.25
		8.34	10.88	4.35	1.12
		19.13	21.67	2.61	0.67
		29.29	31.83	2.50	0.64
	R	-1.19	1.35	1.84	0.47
		2.62	5.16	8.07	2.08
		19.13	21.67	4.32	1.11
		29.29	31.83	3.51	0.90
M2	L	-1.19	1.35	6.69	1.72
		1.99	4.53	6.78	1.74
		19.13	21.67	9.44	2.43
		29.29	31.83	6.88	1.77
	R	-1.19	1.35	5.13	1.32
		6.43	8.97	14.58	3.75
		13.42	15.96	14.26	3.67
		20.40	22.94	10.52	2.71
		29.29	31.83	7.36	1.89
N1	L	3.89	6.43	1.78	0.46
		8.97	11.51	4.59	1.18
		19.13	21.67	4.79	1.23
		29.29	31.83	1.85	0.47
N2	L	20.40	22.94	4.00	1.03
	R	2.62	6.39	12.00	3.08
		7.70	11.47	14.00	3.60
		17.86	21.63	11.00	2.83
		26.75	30.52	4.60	1.18

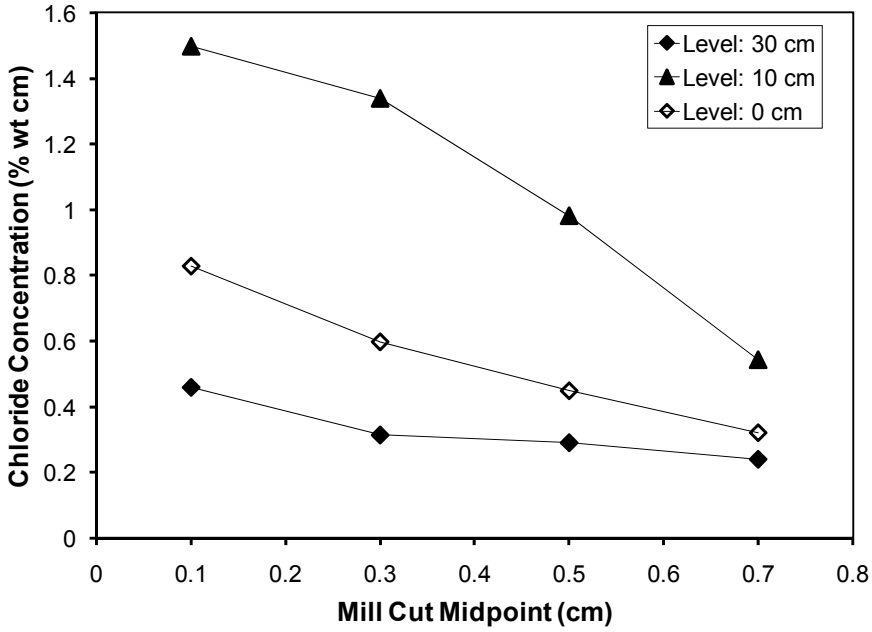

Figure 8.23: Chloride profile of specimen K1

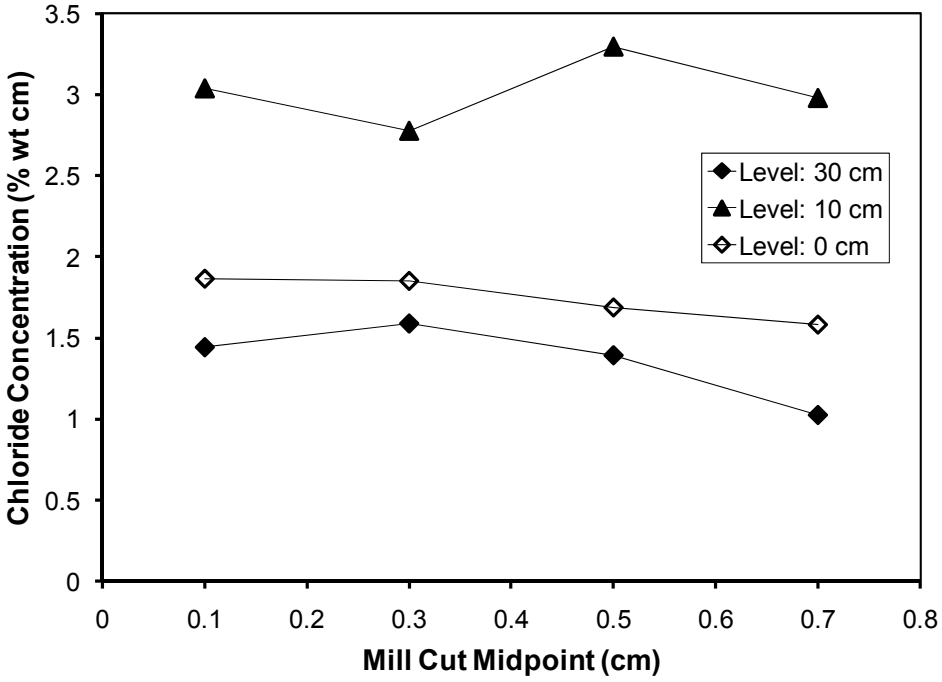

Figure 8.24: Chloride profile of specimen K3

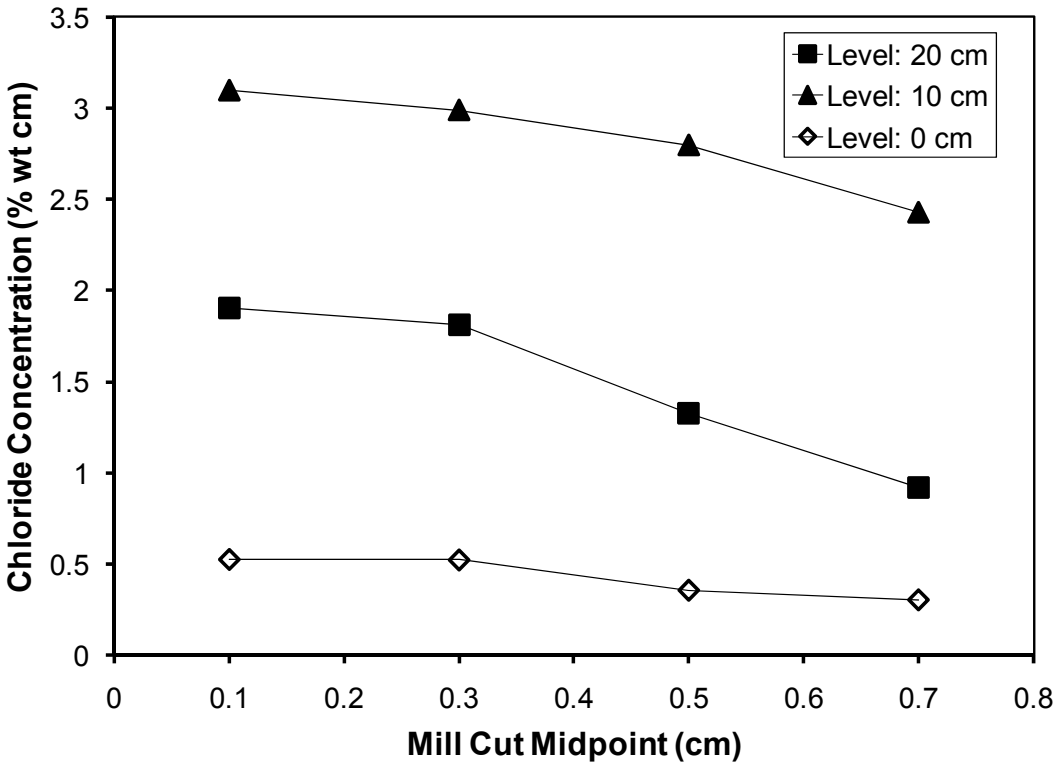

Figure 8.25: Chloride profile of specimen M1

8.5 DISCUSSION

8.5.1 Development of Testing Method

Values of chloride threshold concentrations for corrosion of reinforcing steel in concrete have been widely reported [49, 51]. However, these values may not be reliable because of the unrealistic testing setup such as the application of an electric field to accelerate chloride ingress or potentiostatic control of the rebar discussed by Angst, Elsener, Larsen and Vennesland [50]. In addition, it has been reported that chloride threshold (C_T) in splash zone can increase with increasing cathodic polarization [54-57].

The present experimental set-up physically simulated a partially immersed substructure exposed to marine environments by connecting an external source (submerged rebar), leading to a modest cathodic polarization at the splash zone. The experiment also simulated the chloride deposition from simulated splash and capillary transport. The potential profiles obtained from the present experiment have been compared with those from a bridge piling in field. The results showed that they had the similar trend. As such, present experimental set-up might realistically simulate the field condition and hence it may be a more reliable method for investigating the

chloride threshold concentrations for corrosion of reinforcing steel in bridge substructures exposed in marine environment.

8.5.2 Potentials and Corrosion Initiation

Visual inspection has showed that corrosion spots were observed on most of the rebars at different levels, but corrosion didn't initiate on some rebars. Table 8.6 to Table 8-10 have shown the 24-hours-off potentials values, net depolarization values and the rebar corrosion conditions obtained. For M1 left rebar, corrosion spot was found at elevation 5.0cm. The 24-hr-off potentials at elevations 0 ~10cm ranged from -357 to -317 mVsce, suggesting a high corrosion risk [63] and matching the inspection results [see Table 8-10]. But the net polarization values at the same elevations were between 135 mV and 197 mV (see Table 8-9), indicating rebar was polarized sufficiently [64] from a cathodic protection criteria, which would imply that the chloride concentration has exceeded the chloride threshold for corrosion to initiate. For M1 right bar, 24-hr-off potentials at elevation 0.0 cm ~ 20 cm were between -252 and -152 mVsce (see Table 8-7), representing an intermediate corrosion risk [63]. This reflects the corrosion condition of M1 right rebar where the corrosion sites were observed at levels 7.0 cm, 9.8 cm and 11.2 cm during inspection (see Table 8-10). However, the final net depolarization values at all levels were greater than 100 mV (see Table 8-9), indicating rebar was polarized sufficiently [64]. However, during the depolarization carried out around day 1300 the net polarization did not meet the 100 mV criteria. Since the corrosion sites were small, 100 mV net polarization were met at the elevations at which corrosion had initiated once the solution was refreshed.

8.5.3 Chloride Concentration of Active Sites and Potentials

It is evident that chloride threshold increases when passive steel is polarized to certain potential values[57]. Figure 8.26 shows the relationship between chloride threshold and reinforcing steel on-potentials (vs. SCE). It was originally produced by Presuel, Sagüés and Kranc [54] on the basis of previous results of studies [56, 57, 67-76] and then updated by Sanchez and Sagüés [77] (Figure 8.26(a)). Present work provides further data as shown in Figure 8.26(b) but does not included the recently added data reported by Sanchez and Sagüés [77]. Both sets of results confirm that C_T is increases once the potential is below -200 mVsce. The results from this investigation are to some extent influenced by periodic de-polarization, as well as by the low w/cm used.

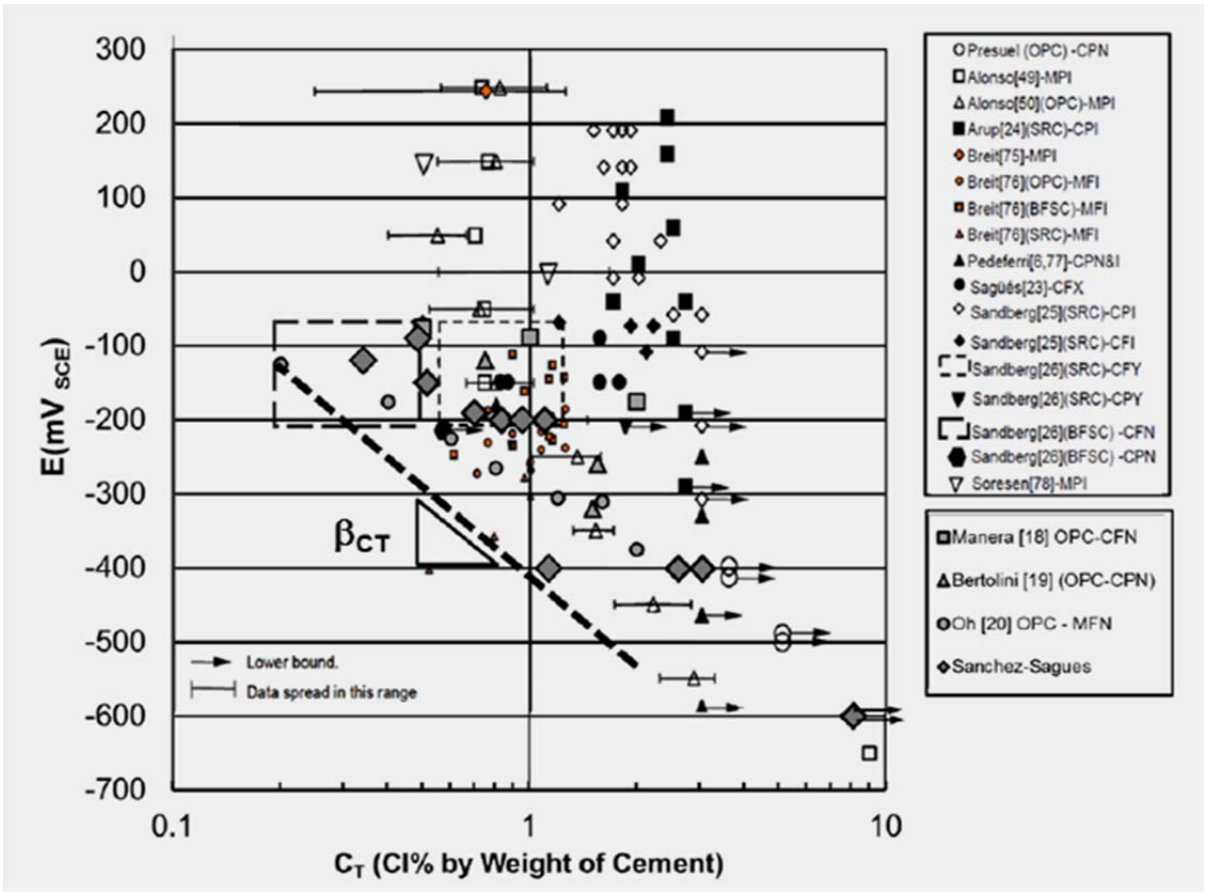

(a) Updated by Sanchez and Sagüés [77]

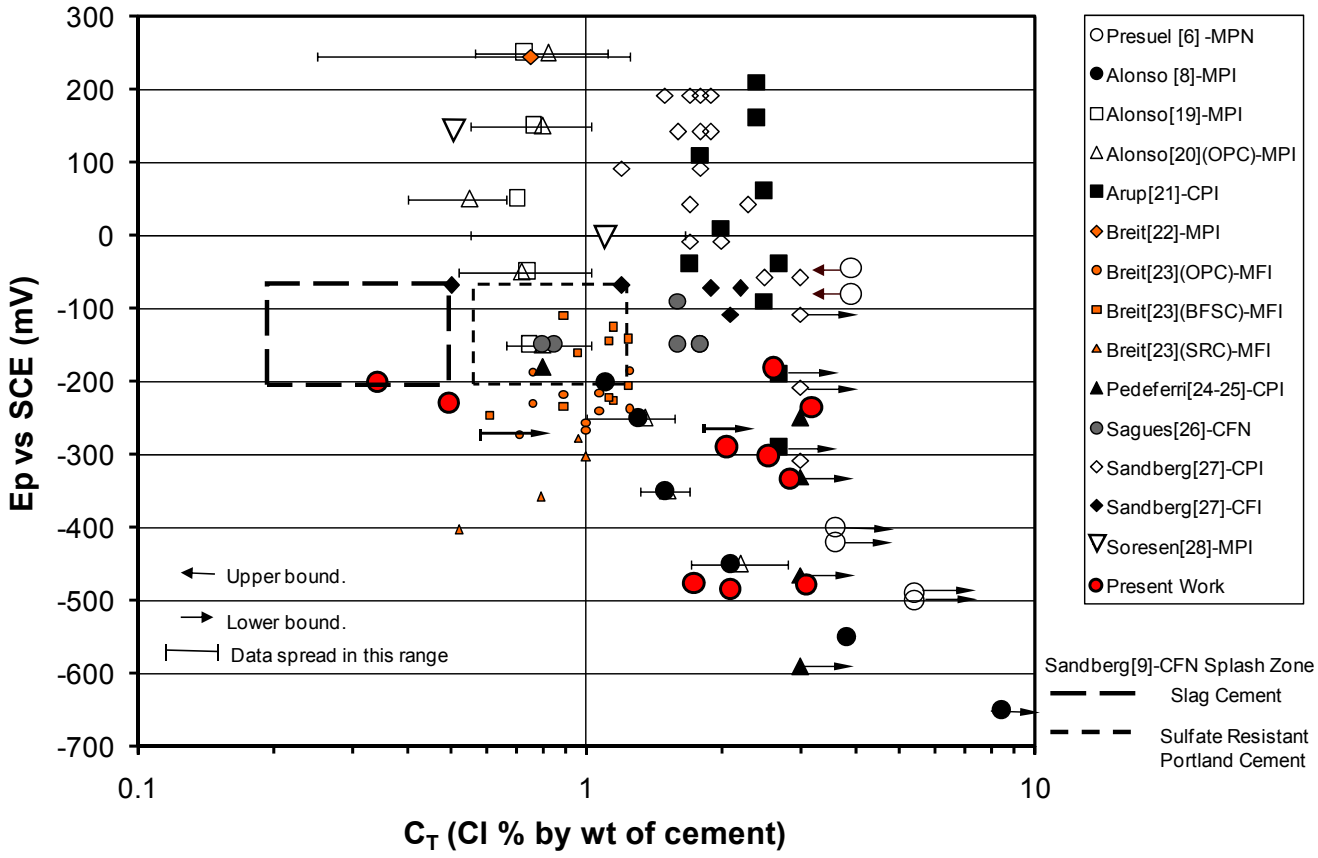

(b) Updated by present authors

Figure 8.26: Values of E_p vs C_T obtained from present work and reported by other investigators

8.6 CONCLUSIONS

This study has lead to the following conclusions:

- The specimen geometry and coupling to a submerged rebar provides a good alternative to investigate chloride threshold.
- Net depolarization profiles as a function of time and elevation appear to be a useful tool to identify when corrosion initiations has taken place.
- Off potential after 24 hr depolarization test not necessarily indicate that corrosion has initiated even if the potential is more negative than -276 mVsce.
- Observing 100 mV or more net depolarization at lower elevation is not always indicative of corrosion initiation.

9 CONCLUSIONS

Chapter 2

- The DCL of concrete mixture prepared with FA decreased close to one order of magnitude (at least 5X) from 1200 days to 5700 days, with the largest reduction observed on those with higher FA. A more modest reduction in DCL was observed on samples with SF. The observed DCL is likely influenced by not fully saturated concrete and that exposed surface did not contain solution all the time.
- The [Cl-]tmin (measured on rebars corroding) suggest that the chloride threshold for samples of concrete mixtures with 50% FA appear to be lower than those observed on the other FA admixture amounts. Corrosion initiated on more rebars from specimens with 50% FA, than with OPC only due to the lower chloride threshold.
- A good correlation was observed between ρwet (wet resistivity) and DCL.
- Further evidence was found that the rebar presence increases the chloride concentration compared to the concentration measured at the same depth

Chapter 3

- Chlorides profiles were obtained from sliced cores. These profiles were used to calculate Dapp values after approximately 5 years of exposure. The diffusivity values measured after the first visit (approx. 2.5 years of exposure) were similar to those obtained during the second visit (approx. 5 years of exposure) for each corresponding mix.
- The chloride diffusivity smaller at the higher elevation for each mix, but the diffusivities were of the same order of magnitude. However, the chloride penetration from the chloride profile was significantly smaller at this higher elevation and a corresponding smaller Cs was observed. Cs values were not the same for all mixes at the same elevations.

Chapter 4

- Specimens with 304 and 316 rebars appear to be viable rebar candidates when a long service life is desired.
- Specimens with 304 and/or 316 that experienced wire brushing before embedding them into the concrete experienced corrosion after more than five years of exposure, but the corrosion appears to be propagating at a slow rate.
- When considering placing high performance corrosion resistant alloys on the outer layer and carbon steel in the inner portion, concrete quality should be such that the permeability is low. Otherwise, situations as shown above might occur.

- Intermediate CRA as 3CR12 produced cracks at the rebar surface due to corrosion products build up. The cover was small on these specimens due to simulated crack and also crevice condition was present. Specimens with similar geometry that contained 316 show no signs of corrosion.
- Specimens with 2304 rebar appear to initiated corrosion at 5 wt% cement, but propagate at a slow rate.

Chapter 5

- Developed a methodology that allows for corrosion to initiate and propagate on concrete specimens embedded with CRAs and initially chloride free.
- Stray current might have caused an accelerated corrosion rate (due to additional electric field application once corrosion had initiated) on reinforcing bar(s) where corrosion had initiated.
- The results from this investigation suggest that UNS S32304 rebars corrode at a slower rate than UNS S32101 rebars (once corrosion has initiated).
- The average CT for UNS S32101 rebars was found to range between 0.95 and 2.95 WC%, whereas for UNS32304 the range was between 1.05 and 2.6 WC% (i.e. % by cementitious).
- The results of chloride concentration at the rebar trace from this investigation, of UNS S32101 rebars and UNS S32304, are found to be lower compared to reported C_T values on specimens under non-accelerated chloride transport. As indicated in the discussion this likely was due to stray corrents.
- On several rebars corrosion propagation caused the concrete to crack. The corrosion propagated at a fast rate due to stray currents (on rebars where corrosion initiated first) present while trying to initiate corrosion on the other rebars.
- Mass loss as little as 0.65 gr caused a surface crack on specimens with UNS32304. The smallest mass loss observed on UNS32101 was ~1.4 gr, but it is likely that a crack appeared with smaller corrosion mass loss.

Chapter 6.1

- Mill scale presence is detrimental to the chloride threshold of CRA. Removal of mill scale via sandblasting still produces a material with lower chloride threshold than properly pickled rebar.
- Rebars segments immersed in SPS for a few weeks followed by NaCl additions over time appears to provide a methodology to follow-up corrosion propagation

Chapter 6.2

- Mill scale presence is detrimental to the chloride threshold of CRA. Removal of mill scale via sandblasting still produces a material with lower chloride threshold than properly pickled rebar. Corrosion propagation during the monitored time did not cause cracks on the mortars by alloys UNS S30400 and S32304, whereas some of the S32101 did experienced cracks.

- The implement method appears to provide a methodology to follow-up corrosion propagation. Even with a reduced mortar cover, corrosion initiation takes several months/years on higher performance CRA rebars. Improvements to the set-up as to minimize differential aeration are recommended.
- The chloride threshold for as received specimens appear to be greater than 1.4 percent of the mortar unit weight (for the mortar investigated unit weight assumed was 2200 kg/m3), which corresponds to approx. ~6 percent of the cement weight used in the mix based on the observed results on specimens with w/c=0.41. The threshold appears to be somewhat lower on specimens with w/c=0.5, but might have been influenced by differential aeration cell.

Chapter 7

- Concrete prisms prepared with Spratt and Sudbury aggregates showed the larger elongations. The presence of Li inhibitor and FA even with high EqA reduced significantly the amount of elongation, but did not prevent ASR. FL coarse aggregates appear to be less prone to ASR in the presence of FA and Li particularly FL1 and FL3.
- The resistivity values measured at room temperature was found to be affected by the presence of FA, Li inhibitor and the type of aggregate. LiNO3 significantly increase the resistivity on concretes with H1, H2, GG and NG aggregates. The lowest resistivity was measured on FL3 specimens, this is believed to be due to the higher porosity of this aggregate.
- It appears that most specimens selected for petrographic and thin section experienced some degree of ASR, except FL1 and FL2. This was not always obvious from low magnification (stereo microscope pics), but some degree of ASR as observed upon examining the thin sections.

Chapter 8

- The specimen geometry and coupling to a submerged rebar provides a good alternative to investigate chloride threshold.
- Net depolarization profiles as a function of time and elevation appear to be a useful tool to identify when corrosion initiations has taken place.
- Off potential after 24 hr depolarization test not necessarily indicate that corrosion has initiated even if the potential is more negative than -276 mVsce.
- Observing 100 mV or more net depolarization at lower elevation is not always indicative of corrosion initiation.

REFERENCES

[1] Hartt W.H., Charvin S.C., Lee S.K. (1999), "Influence of Permeability Reducing and Corrosion Inhibiting Admixtures in Concrete upon Initiation of Salt Induced Embedded Metal Corrosion" Final Report WPI 0510716 Tallahassee, FL: Florida Department of Transportation Research Center.

[2] FM5-516 (2005). "Florida Method of Test For Determining Low-Levels of Chloride in Concrete and Raw Materials," Florida Department of Transportation (FDOT).

[3] FM5-578 (2004). "Florida Method of Test for Concrete Resistivity as an Electrical Indicator of its Permeability," Florida Department of Transportation (FDOT).

[4] Angst U.M.; Elsener B.; Larsen C.K.; Vennesland O., (2011), "Chloride induced reinforcement corrosion: Electrochemical monitoring of initiation stage and chloride threshold values", Corrosion Science, Vol 53, pp 1451-1464.

[5] Kranc, S.C., Sagüés, A.A., and Presuel-Moreno, F.J., (2002) "Decreased Corrosion Initiation Time of Steel in Concrete Due to Reinforcing Bar Obstruction of Diffusional Flow", ACI Materials Journal, Vol.99, pp 51-53.

[6] Yu H. and Hartt W.H., Corrosion, (2007) Vol. 63, p. 843.

[7] Justnes H., Weerdt K.D., Geiker M. (2013), "Chloride Binding in concrete exposed to seawater and salt solutions", in Concrete under Severe Conditions, Eds. Li Z.J.; Sun W, et. al., RILEM Proceeding PRO84, p. 647-659.

[8] Presuel-Moreno F., Powers R. G., Hartt W. H. (2008). "Corrosion Resistant Alloys for Reinforced Concrete" Final Report BD228, Tallahassee, FL: Florida Department of Transportation Research Center.

[9] Hurley, M.F. and Scully, J.R. (2006). "Threshold Chloride Concentrations of Selected Corrosion-Resistant Rebar Materials Compared to Carbon Steel" Corrosion 62, 892-904.

[10] Gutierrez, F. (2013). "Corrosion Initiation and Propagation on Corrosion Resistant Alloys Embedded In Concrete by Accelerated Chloride Transport". Ms Thesis, Boca Raton: Florida Atlantic University.

[11] Sederholm B., Almqvist J., Randstrom S. (2009). "Corrosion Properties of Stainless Steel as Reinforcement in Concrete in Swedish Outdoor Environment" NACE International; Corrosion 2009, Houston, TX.

[12] Scully J.R., Hurley M.F. (2007). "Investigation of the Corrosion Propagation Characteristics of New Metallic Reinforcing Bars" Final Report VTRC 07-CR9, Charlottesville: VA Transportation Research Council.

[13] Schönning M., Randström S., Adair M. (2011). "Adaption of EN 480-14:2006 as a Test Method for Determining a Critical Chloride Threshold Level for Stainless Steel Rebar" *Eurocorr 2011*. Stockholm, Sweden.

[14] Hanson C., (2013) The Case for Cyclic Corrosion Testing", ACI Fall/2013.

[15] Presuel-Moreno F., Liu Y., Suarez A., (2010) "Characterization of New and Old Concrete Structures Using Surface Resistivity Measurements" Final Report BD546-08, Tallahassee, FL: Florida Department of Transportation Research Center.

[16] Nordtest. NT BUILD 492 (1999). "Chloride migration coefficient from non-steady-state migration experiment" Spoo, Finland.

[17] Nordtest NT BUILD 443 (1995) "Concrete, hardened: Accelerated chloride penetration" Spoo, Finland.

[18] Castellote C., Andrade M.C. (2011). Assessment of the behavior of concrete in the initiation period of chloride induced corrosion of rebars. In Concrete Repair, Rehabilitation and Retrofitting II.

[19] Bertolini L. and Gastaldi G. (2011). Corrosion Resistance of Low Nickel Duplex Stainless Steel Rebars. Materials and Corrosion, 62(2), 120 -129.

[20] Presuel-Moreno, F. (2012). FHWA/Florida DOT Research on Alternative CRRB's Corrosion Resistant Alloys for Steel Reinforcement in Concrete. *Corrosion Resistant Reinforcing Bar (CRRB) Seminar, organized by the FHWA and Florida DOT.* Tampa, FL.

[21] Trejo D., Pillai R.G.. (2004). Accelerated Chloride Threshold testing: Part II – Corrosion-Resistant reinforcement. *ACI Materials Journal, 101*(1), 57 - 64.

[22] Busba E. and Sagues A.A. (2013). Critical localize corrosion penetration of steel reinforcement for concrete cover cracking. *NACE Corrosion 2013* . Orlando, FL.

[23] Torres-Acosta A. and Sagues, A.A. (2004) "Concrete cracking by localized steel corrosion - geometry effects," ACI Materials Journal, Vol. 101, no. 6, pp. 501-507, 2004.

[24] Hansson C.M. and Mammoliti, L., "Is it Necessary to Remove the Mill Scale from Stainless Steel Reinforcing Bar? Part 1: Test in Symmetric Pore Solution" Report HIIFP-015; Ontario, Canada: Ministry of Transportation Provincial Highways Division.

[25] Hartt W., FHWARD- 04-093, "Critical Literature Review of High-Performance Corrosion Reinforcements in Concrete Bridge Applications" McLean, VA: Federal Highway Administration - Turner-Fairbank Highway Research Center.

[26] Presuel-Moreno F., Scully J.R., Sharp S., (2010) "Literature Review of Commercially Available Alloys that Have Potential as Low-Cost Corrosion Resistant Concrete Reinforcement" Corrosion V 66, 8 pp. 086001.

[27] Nürnberger, N. (2005) "Stainless Steel Reinforcement: A Survey", Otto Graf Journal 16, p. 111-138.

[28] Clemeña, G.G. and Virmani, Y.P. (2004) "Comparing the Chloride Resistance of Reinforcing Bars", Concrete International 26, 11, p. 39-49.

[29] Clemeña, G.G., (2004) "Investigation of the Resistance of Several New Metallic Reinforcing Bars to Chloride-Induced Corrosion in Concrete" Report VTRC 04-R7. Charlottesville, VA: Virginia Transportation Research Council.

[30] Clemeña, G. G. and Virmani, Yash Paul. (2002) "Testing of Selected Metallic Reinforcing Bars for Extending the Service Life of Concrete Bridges: Testing Outdoor Concrete Blocks" Report VTRC 03- R6. Charlottesville, VA: Virginia Transportation Research Council.

[31] S. Randström, M. Almen, R. Pettersson, M. Adair, (2010) "Stainless Steel Rebars – Influence of the Surface State on the Critical Chloride Threshold Level", Stainless Steel World 2010, Houston, TX; paper no PSA10_051.

[32] Li, L., and Sagüés, A.A. (2001) Chloride Corrosion Threshold of Reinforcing Steel in Alkaline Solutions: Open-Circuit Immersion Tests. *Corrosion*, Vol. 57, No. 1 pp. 19-28.

[33] ASTM Standard G1-03 (2003)"Standard Practice for Preparing, Cleaning, and Evaluating Corrosion Test Specimens" Vol 03.02 (ASTM International: West Conshohocken PA.

[34] Hartt W., Nam J., (2004) "Critical Parameters for Corrosion Induced Deterioration of Marine Bridge Substructures in Florida" Final Report BD-166, Tallahassee, FL: Florida Department of Transportation Research Center.

[35] Nam J., Hartt W.H., and Kim K., (2005)"Time-to-Corrosion of Reinforcing Steel in Concrete Specimens as Affected by Cement Alkalinity and Rebar Surface Condition," paper no. 05256 presented at CORROSION/05, Houston, TX.

[36] Dehwah, H.; Maslehuddin, M., and Austin, S. (2002) "Effect of cement alkalinity on pore solution chemistry and chloride-induced reinforcement corrosion", ACI Materials Journal, V 99 N2 pp 227-233.

[37] Hartt W., Suarez J., (2007) "Utility of High Alkalinity Cement for Control of Reinforcing Steel Corrosion in Concrete" Tallahassee, FL: Final Report BD-546 for Florida Department of Transportation Research Center..

[38] ASTM C1293, “Standard Test Method for Determination of Length Change of Concrete Due to Alkali-Silica Reaction” Vol. 04.02, Annual Book of ASTM Standards, American Society for Testing and Materials, Philadelphia.

[39] CSA A23.2-27A “Standard Practice to Identify Potential for Alkali-Reactivity of Aggregates and Measures to Avoid Deleterious Expansion in Concrete” Canadian Standards Association.

[40] Castellote, M.; Andrade, C.; Alonso, M. C., (2002) “Standardization, to a Reference of 25°C, of Electrical Resistivity for Mortars and Concretes in Saturated or Isolated Conditions,” ACI Materials Journal, V.99, No. 2.

[41] Presuel-Moreno, F. and Liu, Y, (2012) “Temperature Effect on Electrical Resistivity Measurements on Mature Saturated Concrete” Corroison/2012, paper No. C2012-01732, Salt Lake City, UT, March 11-15 (Proceedings published on CD).

[42] Bertolini, L.; Polder, R. B., (1997) “Concrete Resistivity and Reinforcement Corrosion Rate as a Function of Temperature and Humidity of the Environment,” TNO Report 97-BT-R0574.

[43] Liu, Y. (2012) “Accelerated Curing of Concrete with High Volume Pozzolans-Resistivity, Diffusivity and Compressive Strength”. PhD Dissertation, Boca Raton, FL: Florida Atlantic University.

[44]. McCarter, W.J.; Starrs, G.; Chrisp, T.M., (2000) “Electrical Conductivity, Diffusion, and Permeability of Portland Cement-based Mortars,” Cement and Concrete Research 30, pp.1395-1400.

[45] Villagrán Zaccardi, Y.A.; Fullea García, J.; Huélamo, P.; Di Maio, Á. A., (2009)“Influence of Temperature and Humidity on Portland Cement Mortar Resistivity Monitored with Inner Sensors,” Materials and Corrosion 60, No. 4.

[46] Chrisp, T.M.; Starrs, G.; McCarter, W. J.; Rouchotas, E.; Belewett, J., (2001) “Temperature-conductivity Relationships for Concrete: An Activation Energy Approach,” Journal of Materials Science Letters 20, pp.1085-1087.

[47] Fournier, B. and Malhotra, M., (1999) “Evaluation of laboratory tests methods for alkali-silica reactivity”, Cement, concrete and aggregates, CCAGDP V21 N.2., pp 173-184.

[46] Feng, X.; Thomas, M.D.A.; Bremner, T.W.; Folliard, K.J.; and Fournier, B. (2010) “Summary of research on the effect of LiNO3 on alkali–silica reaction in new concrete” Cement and Concrete Research 40 pp. 636-642.

[47] Thomas, M.; Baxter, S.; and Stokes, D.; (2001) "The Combined Use of Fly Ash and Lithium Nitrate for Controlling Expansion Due to Alkali-Silica Reaction." ICAR 2001.

[48] Thomas, M. (2011) “The effect of supplementary cementing materials on alkali-silica reaction: A review” Cement and Concrete Research 41 pp. 1224–1231.

[49] Glass, G.K. and Buenfeld, N.R., (1997) “The Presentation of The Chloride Threshold Levels for Corrosion of Steel in Concrete,” Corrosion Science, Vol. 39 No. 5, , p.1001-1013.

[50] Angst, C., Elsener, B., Larsen, C. K. and Vennesland Ø., (2009) “Critical chloride content in reinforced concrete – A review”, Cement and Concrete Research, Vol. 39, p.1122-1138.

[51] Yu, H., Himiob, R.J., and Hartt, W.H., (2007) "Effect of Reinforcement and Coarse Aggregates on Chloride Ingress into Concrete and Time-to-Corrosion: Part II-Spatial Distribution of Aggregates," Corrosion Vol. 63, p. 924.

[52] ACI Committee 201, (2001) Guide to Durable Concrete, Chapter IV – Corrosion of Steel and Other Materials embedded in Concrete, Manual of Concrete Practice, Part I, American Concrete Institute, Detroit.

[53] Bamforth, P.B. and Chapman-Andrews, J.F., (1994) “Long-Term Performance of RC Elements under UK Coastal Exposure Conditions,” Proc. Intl. Conf. on Corrosion and Corrosion Protection of Steel in Concrete, Vol. 1, University of Sheffield, p. 139.

[54] Presuel-Moreno, F.J., Sagüés, A.A., and Kranc, S.C., (2005) "Steel Activation in Concrete Following Interruption of Long-Term Cathodic Polarization," Corrosion, Vol. 61, 2005, p. 428-436.

[55] Presuel-Moreno, F.J., Kranc, S.C., and Sagüés, A.A., (2005) "Cathodic Prevention distribution in Partially Submerged Reinforced Concrete," Corrosion, Vol. 61, 2005, p. 548-558.

[56] Alonso C., Castellote M., Andrade C., (2002) "Chloride threshold dependence of pitting potential of reinforcements ," Electrochimica Acta, 47, 2002, p. 3469-3481.

[57] Sandberg P., (1998) "Chloride Initiated Reinforcement Corrosion in Marine Concrete", Lund University, Division of Building Materials, Dissertation, TVBM-1015.

[58] Standard Specification for Road and Bridge Construction, Section 346: (2007) Portland Cement Concrete, Florida Department of Transportation, Tallahassee, FL.

[59] ASTM G109-07, "Standard Test Method for Determining Effects of Chemical Admixtures on Corrosion of Embedded Reinforcing Steel in Concrete Exposed to Chloride Environments," Annual Book of Standards, American Society for Testing and Materials, West Conshohocken, PA.

[60] ASTM C231-04, "Standard Test Method for Air Content of Freshly Mixed Concrete by the Pressure Method," Annual Book of Standards, American Society for Testing and Materials, West Conshohocken, PA.

[61] ASTM C192-07, "Standard Practice for making and Curing Concrete Specimens in the Laboratory," Annual Book of Standards, American Society for Testing and Materials, West Conshohocken, PA.

[62] Presuel-Moreno, F.J. and Hartt W. (2009) "Characterization of Chloride Thresholds in Florida- Coastal Concrete Bridge Substructures" Tallahassee, FL: Final Report BD546-05 Florida Department of Transportation Research Center.

[63] ASTM C876-09, (2009) "Standard Test Method for Corrosion Potentials of Uncoated Reinforcing Steel in Concrete," Annual Book of ASTM Standards – Section Four Construction, American Society for Testing and Materials, West Conshohocken, PA.

[64] NACE SP0290-2007**,** (2003) **"**Impressed Current Cathodic Protection of Reinforcing Steel in Atmospherically Exposed Concrete Structures," NACE International, Houston, TX, March, 2003.

[65] Monteiro, P., P. Helene, I. Aoki, P. Barbosa, and E. Monteiro.(2005) "Influence of Water-Cement Ratio and Cover Thickness on Chloride Extraction of Reinforced Concrete." ACI Materials Journal Vol 102.1: p9-14.

[66] Unpublished data provided by Mr. Ivan Lasa, Florida Department of Transportation – State Materials Office, Gainesville, FL.

[67] Alonso, C., Andrade, C., Castellote, M., (1997) "The influence of the Electrical Potential in the Chloride Threshold for Rebar Depassivation", In Proceedings of 10th International Congress on the Chemistry of Cement, Vol. 4, paper No. 4iv082, edited by H. Justness, GÖtheborg, Sweden.

[68] Alonso, C., Andrade, C., Castellote, M., (2000) "Dependence of Chloride Threshold with the Electrical Potential of Reinforcements,", in 2nd International RILEM Workshop on Testing and Modeling the Chloride Ingress into Concrete, Cachan, France, RILEM Publication, p. 415.

[69] Arup, H., (1996) "A New Method for Determining Chloride Thresholds as a Function of Potential in Field Exposure Tests," in Durability of Concrete in Saline Environment, Lund, Sweden,p.107.

[70] Breit, W., Schiesl, P., (1997) "Investigation on the Threshold Value of the Critical Chloride Content," In Concrete Durability, American Concrete Institute SP 170, Detroit, MI, p. 363-378.

[71] Breit, W. (1997) "Investigation on the Critical Chloride Content for Steel in Concrete," Ph.D. Dissertation, Aachen, in German.

[72] Pedeferri P., (1997) “Principles of Cathodic Protection and Cathodic Prevention in Atmospherically Exposed Concrete Structures”, In Corrosion of reinforcement in concrete: monitoring, prevention and rehabilitation,papers from EUROCORR '97, Trondheim, Norway, J. Mietz, B. Elsener and R. Polder Eds, pp163-171.

[73] Bertolini L., Bolzoni F., Lazzari L., Pedeferri P., (2000) Internationale Zeitschrift fur Bauinstandsetzen und Baudenkmalpflege, Vol 6, : pp. 655-668.

[74] Sagüés A.A. et. al., (2001) “Corrosion Resistance and Service Life of Drainage Culverts” Final Report to Florida Department of Transportation, Tallahassee, FL: Final Report WPI 0510756 Florida Department of Transportation Research Center.

[75] Sandberg P., (1998) “The effect of defects at the steel – concrete interface, exposure regime and cement type on pitting corrosion in concrete”, Report TVBM-3081, Lund, Sweden.

[76] Sorensen B., Jensen P.B., Maahn E., (1990) “The corrosion properties of Stainless Steel Reinforcement”, In Corrosion of Reinforcement in Concrete, Ed. Page C.L., Treadaway K.W.J., Bamforth P.B. : p. 601-610.

[77] Sanchez, A., Sagüés A.A., (2012) “Chloride Threshold Dependence on Potential in Reinforced Mortar”, NACE CORROSION 2012, Paper No. C2012-0001728, 11pp, Houston, TX.

APPENDIX A: Pictures of Terminated Specimens (Chapter 2)

AO1

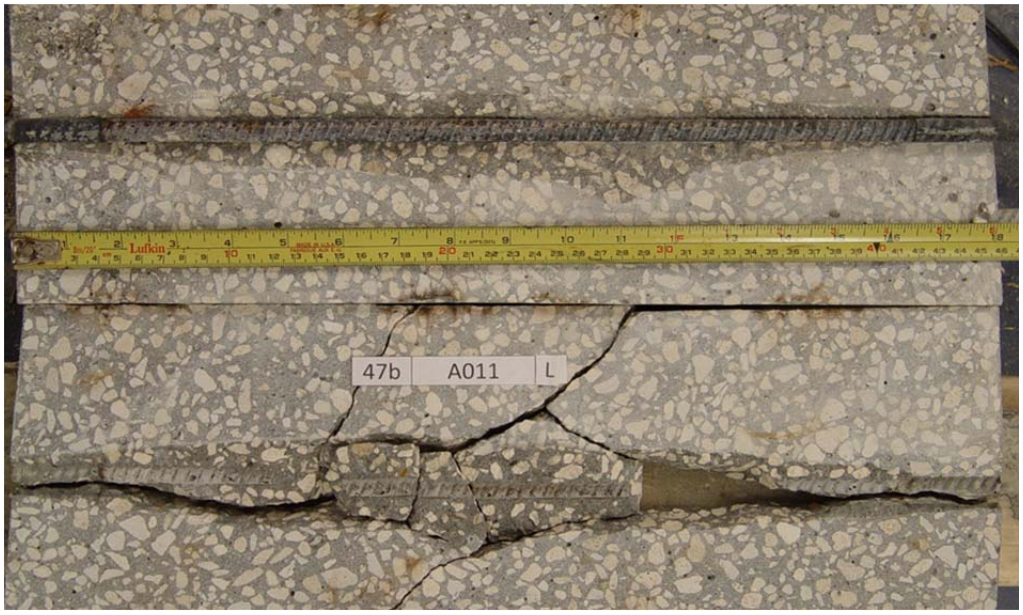

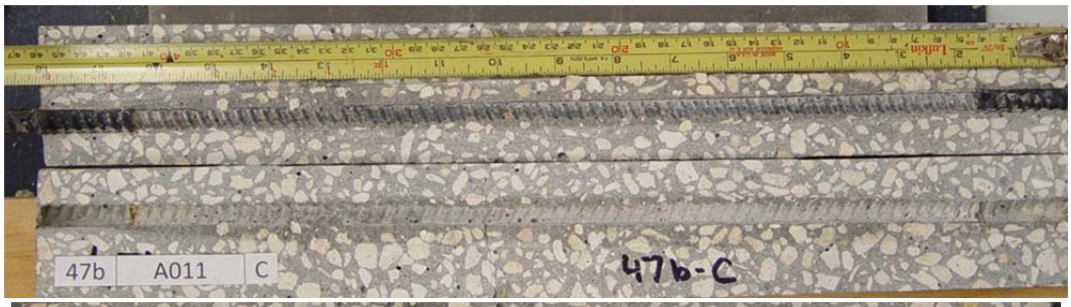

AO2

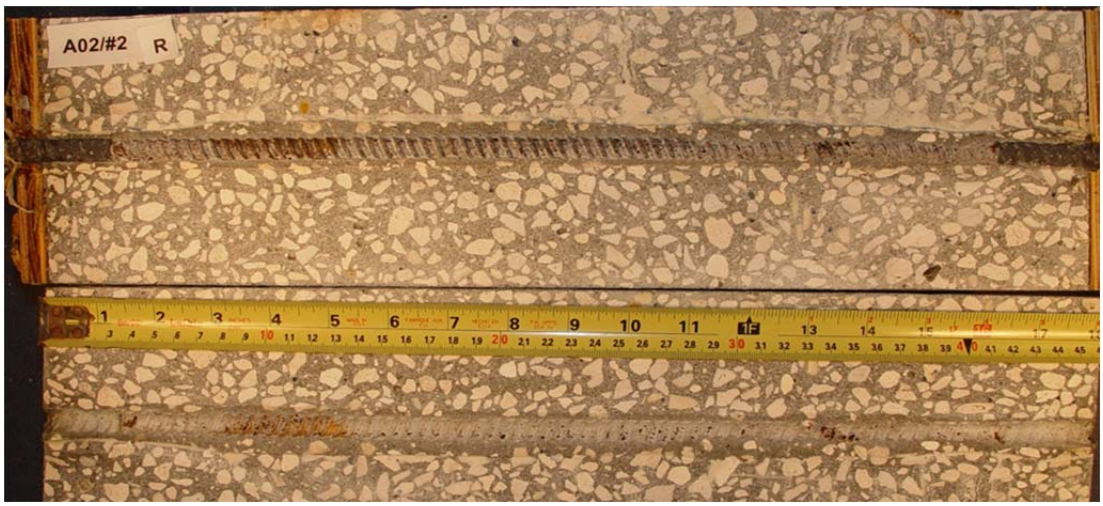

AO3

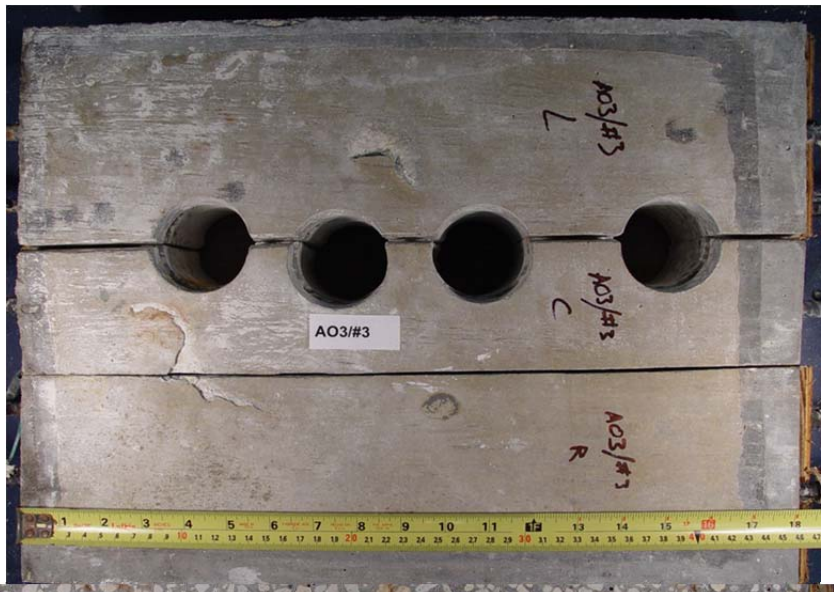

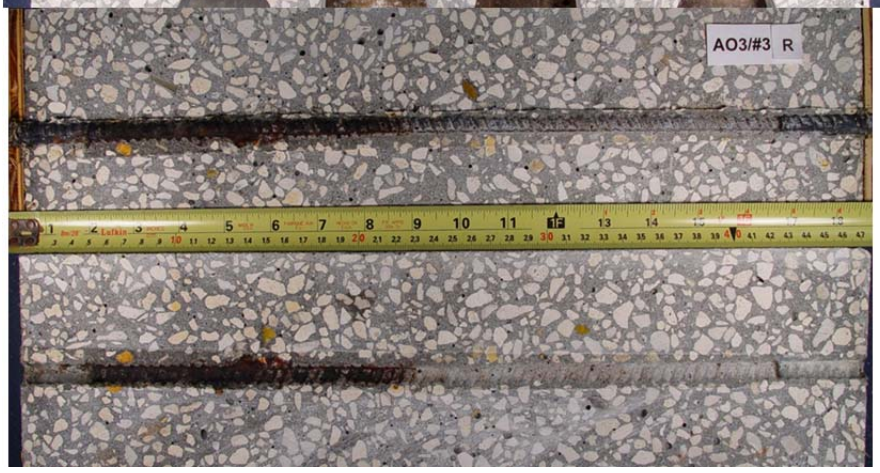

AO8

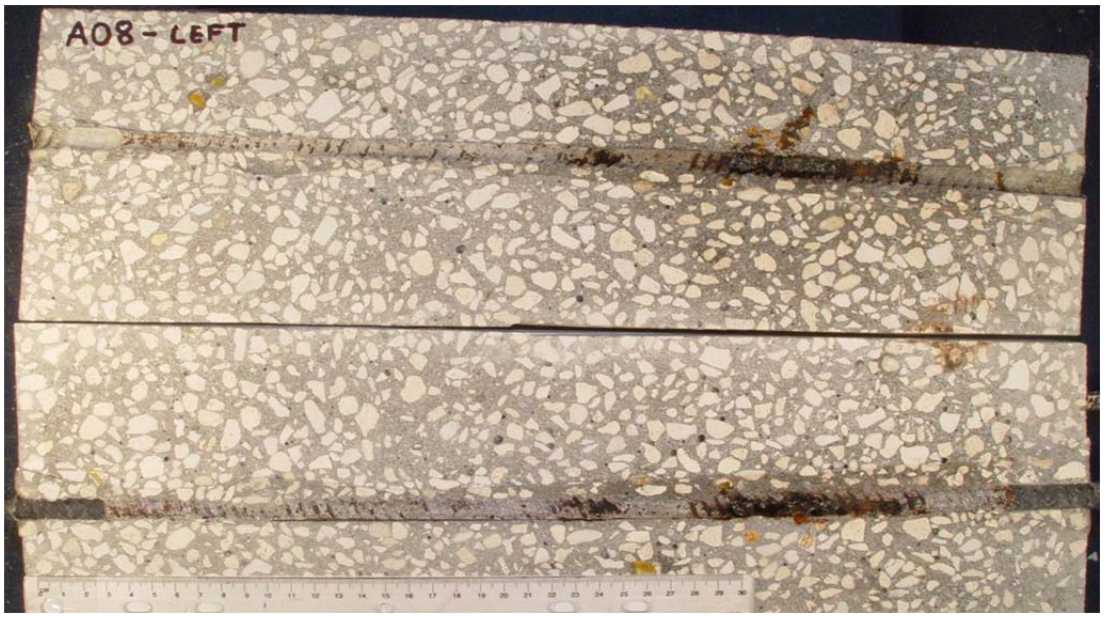

CO1

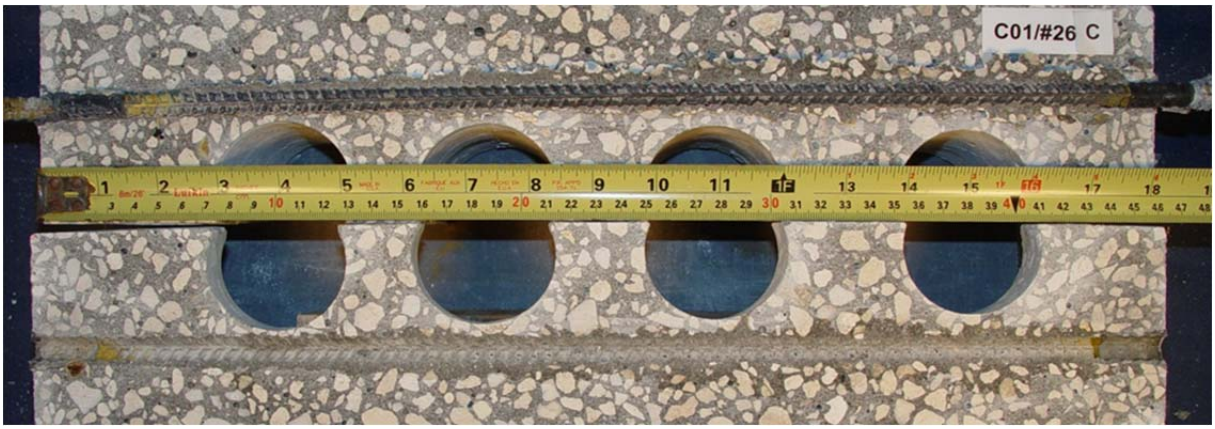

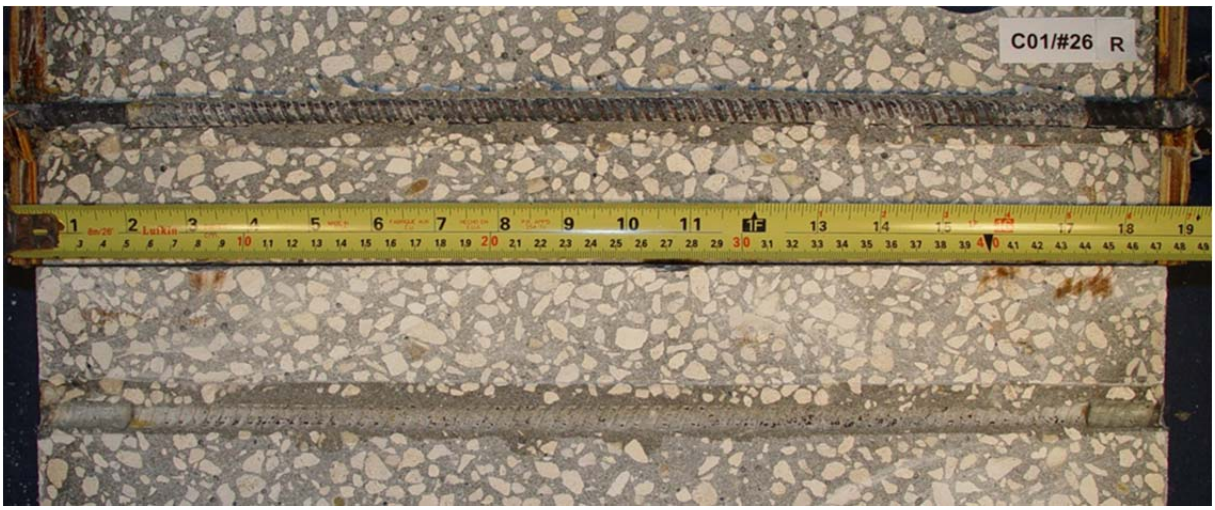

CO3

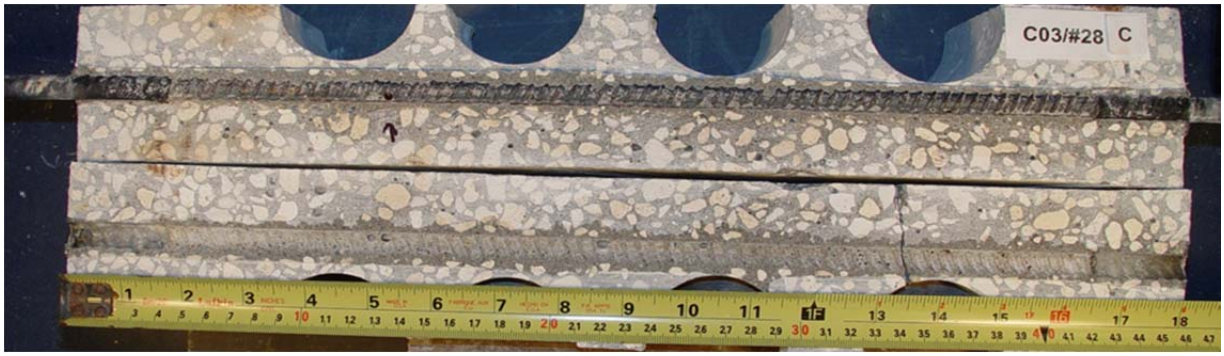

FA1-1

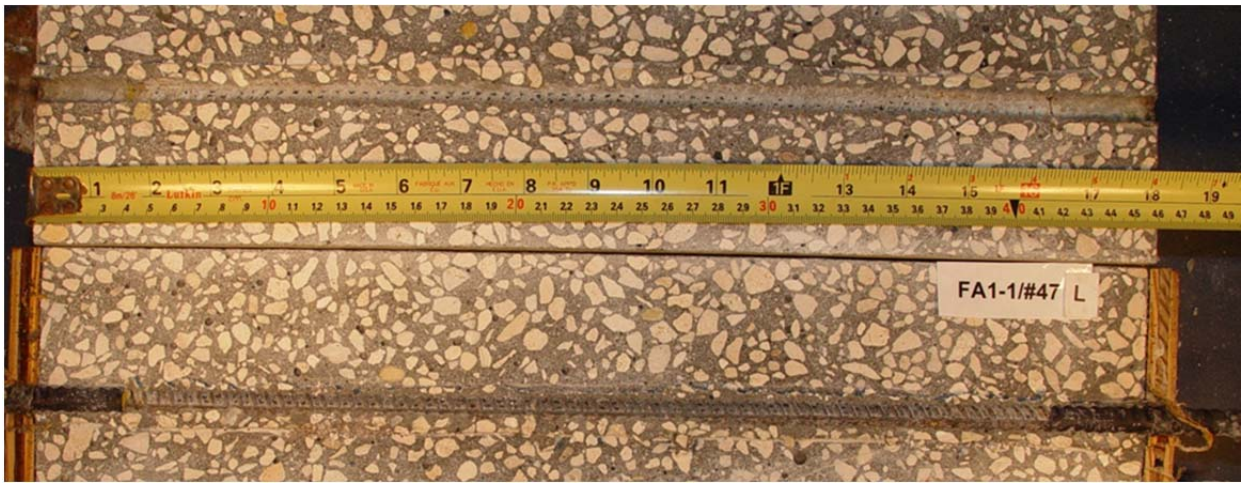

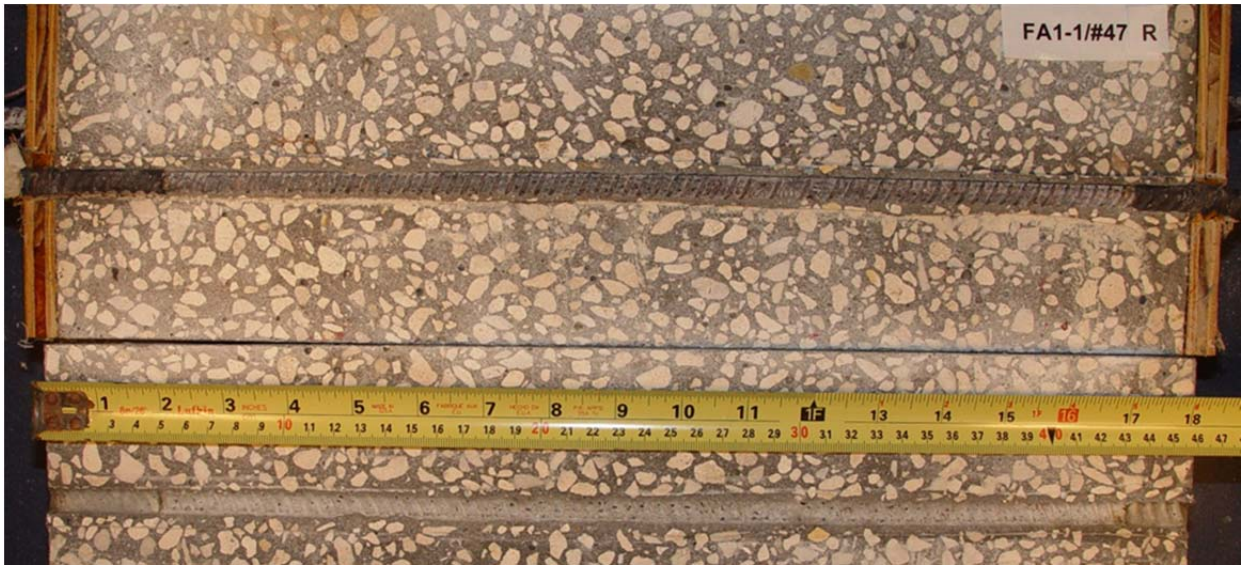

FA1-3

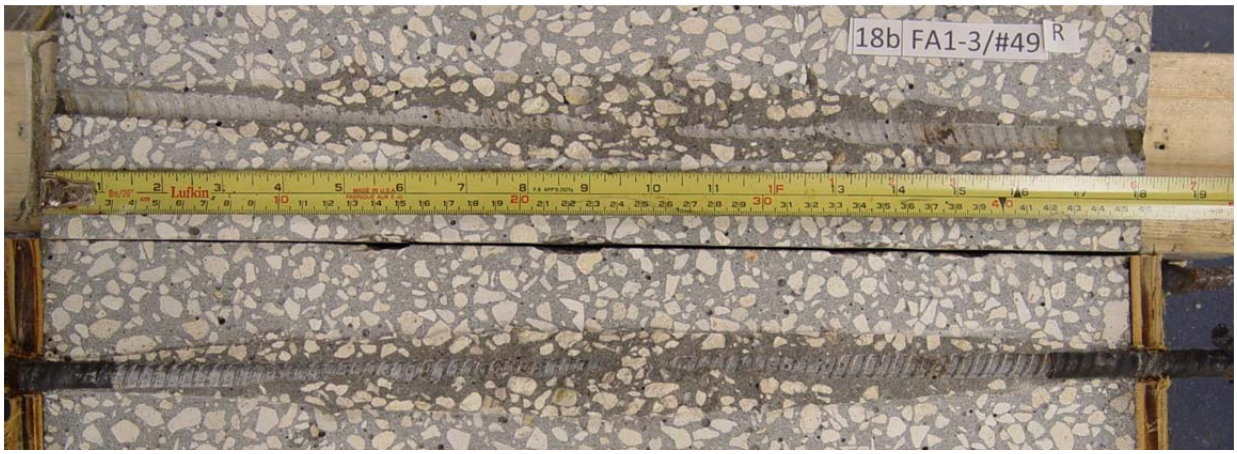

FA2-1

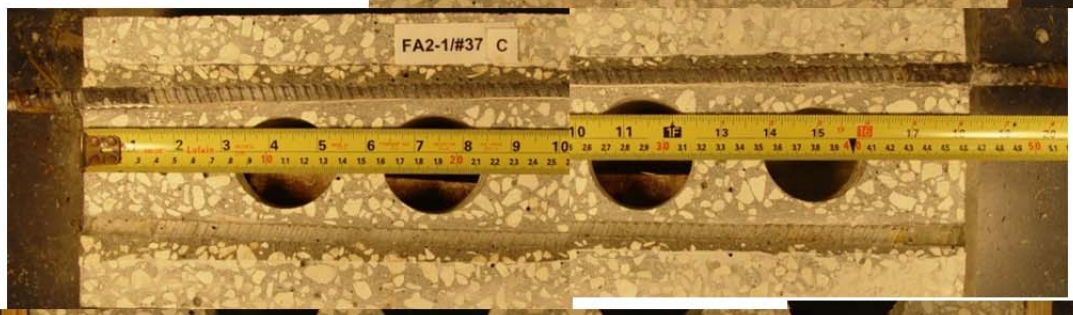

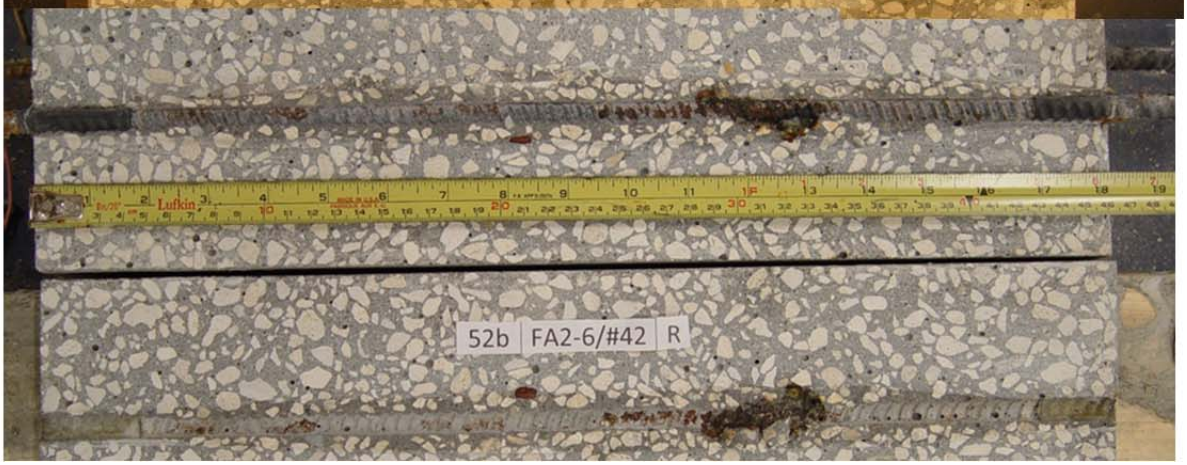

FA3-1

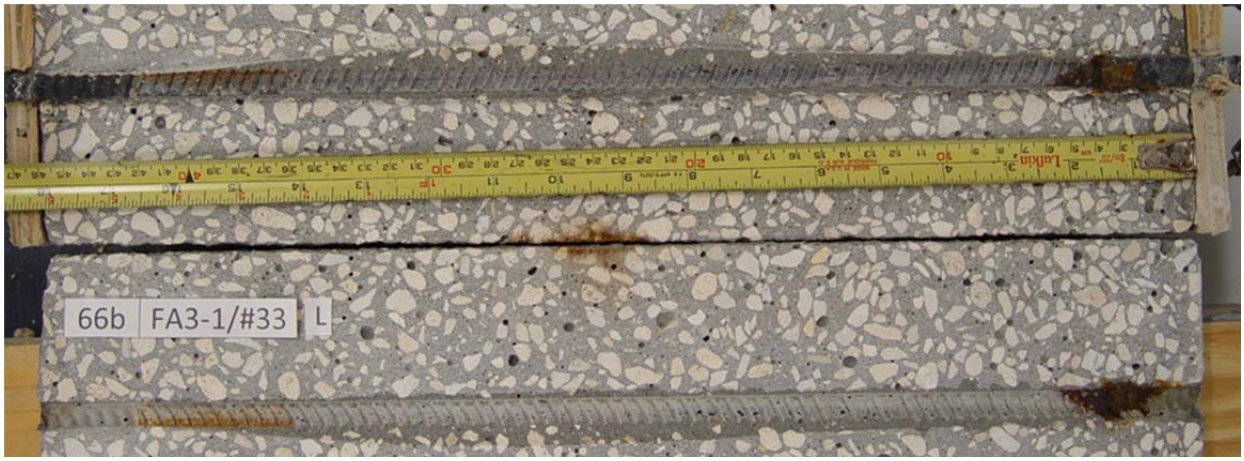

FA3-2

FA3-4

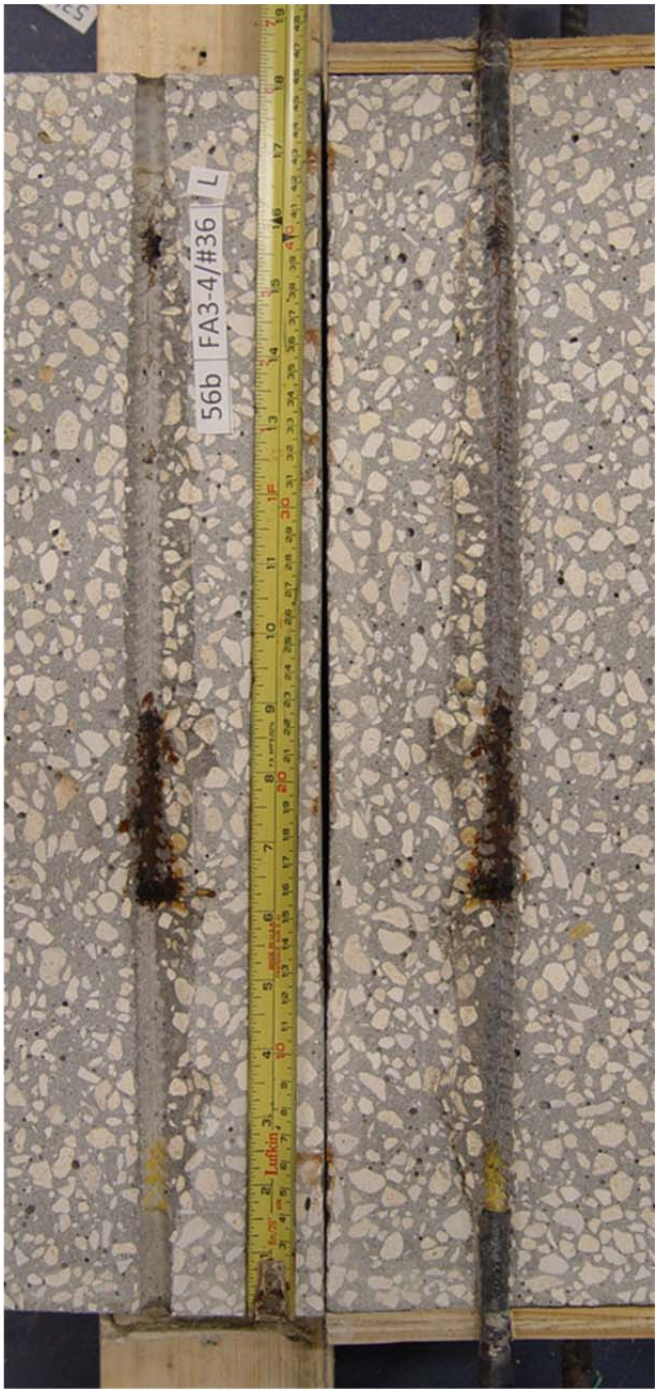

FA3-5

FA3-7

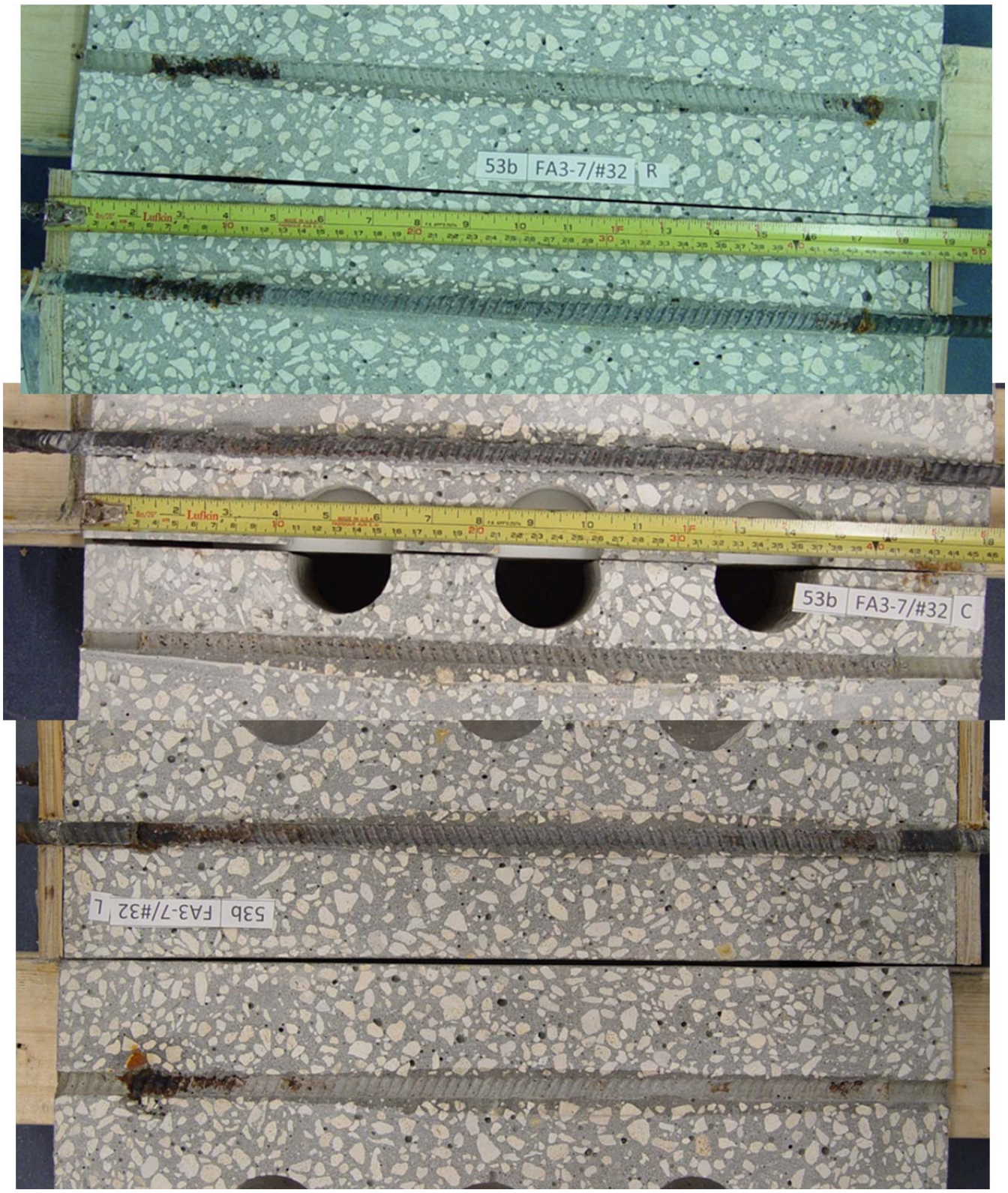

FA4-1

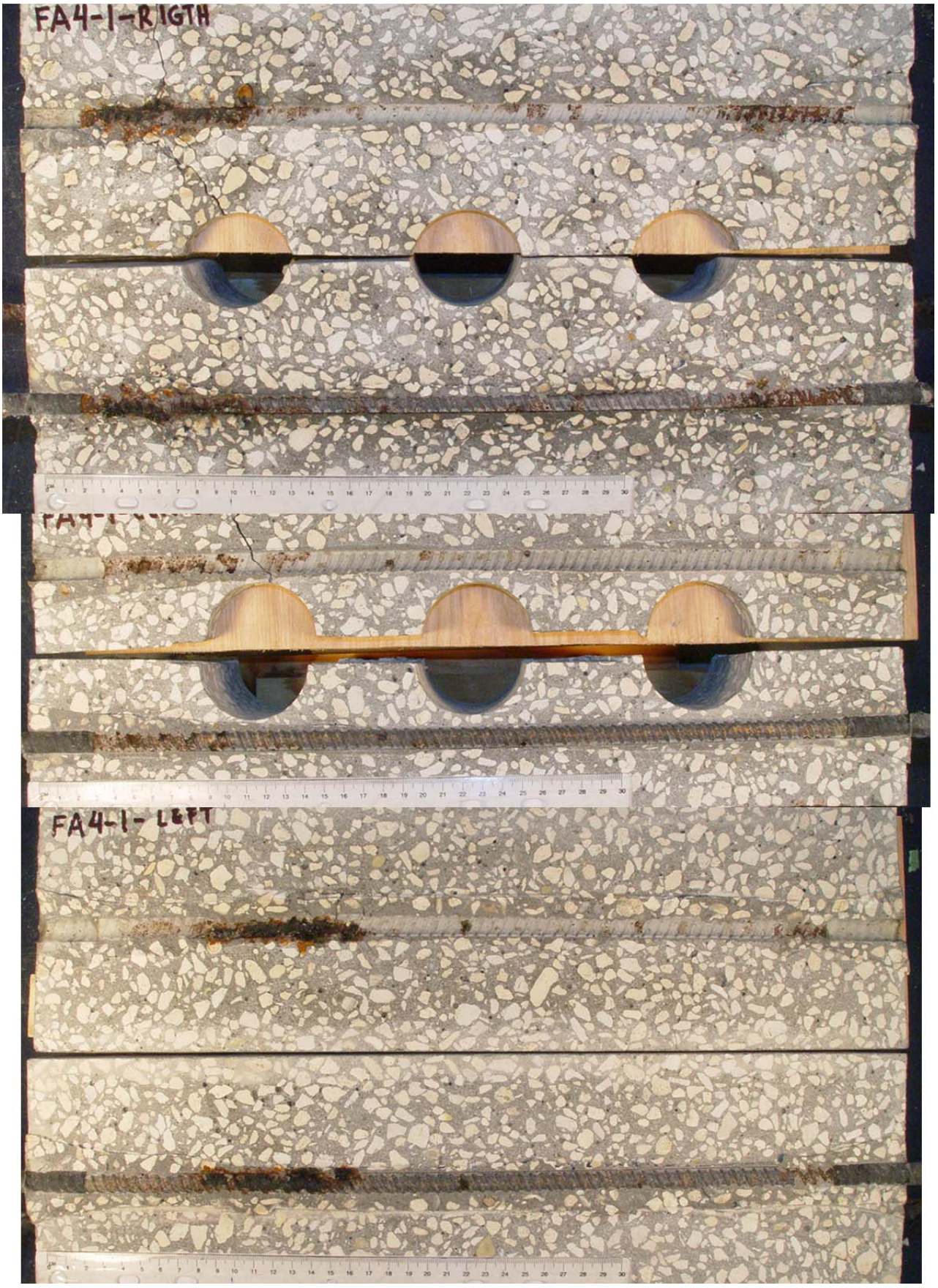

FA4-2

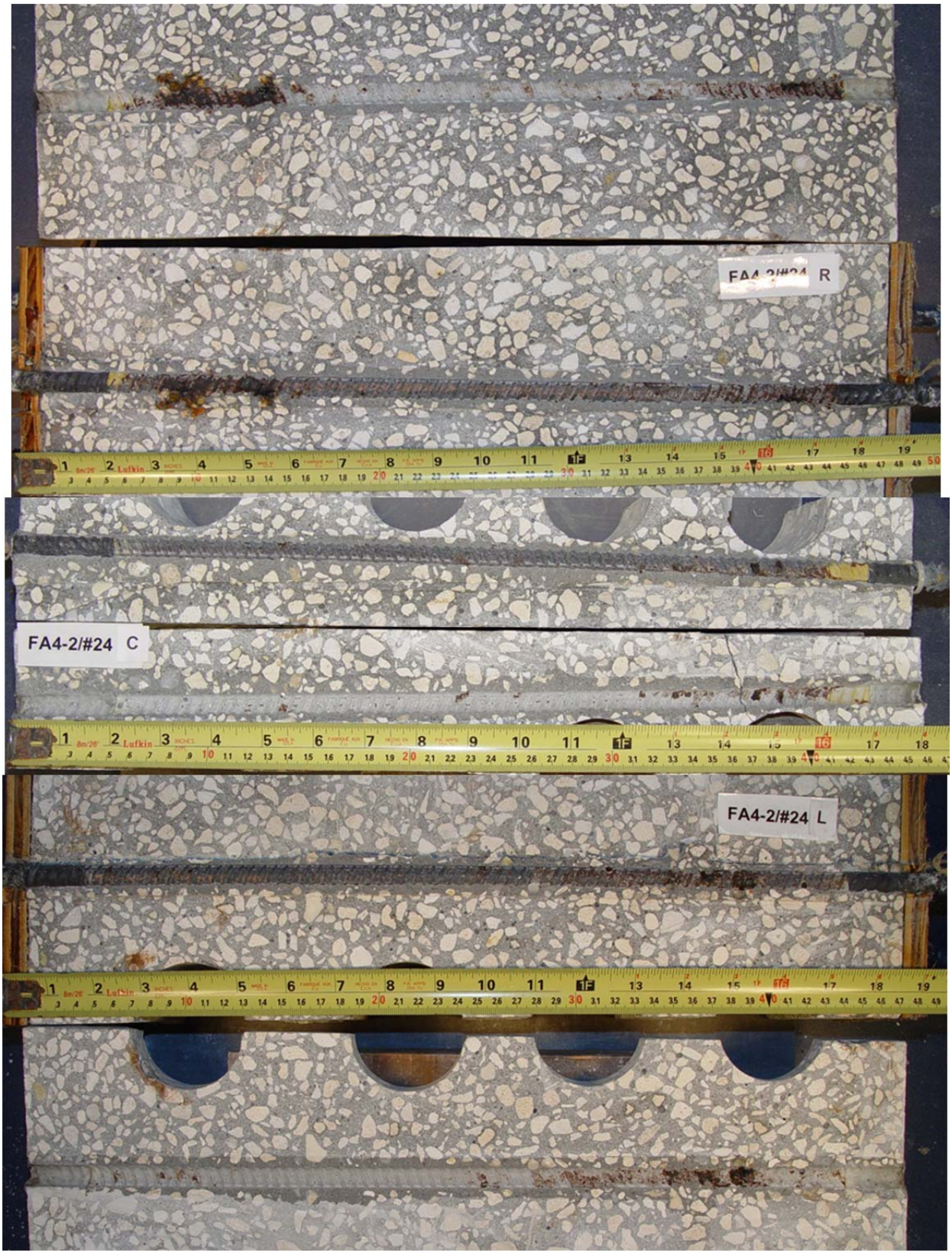

FA4-3

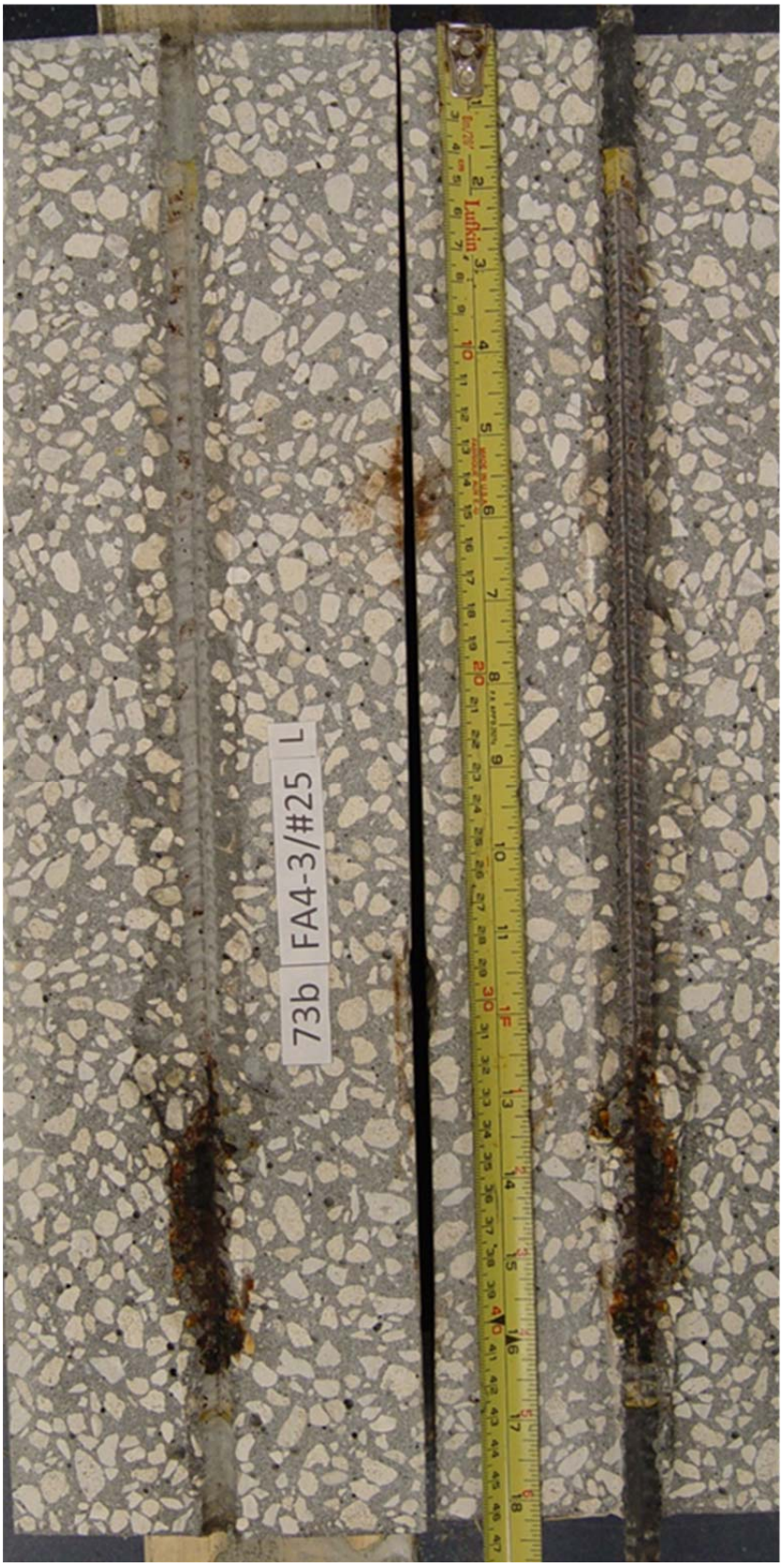

SF1-1

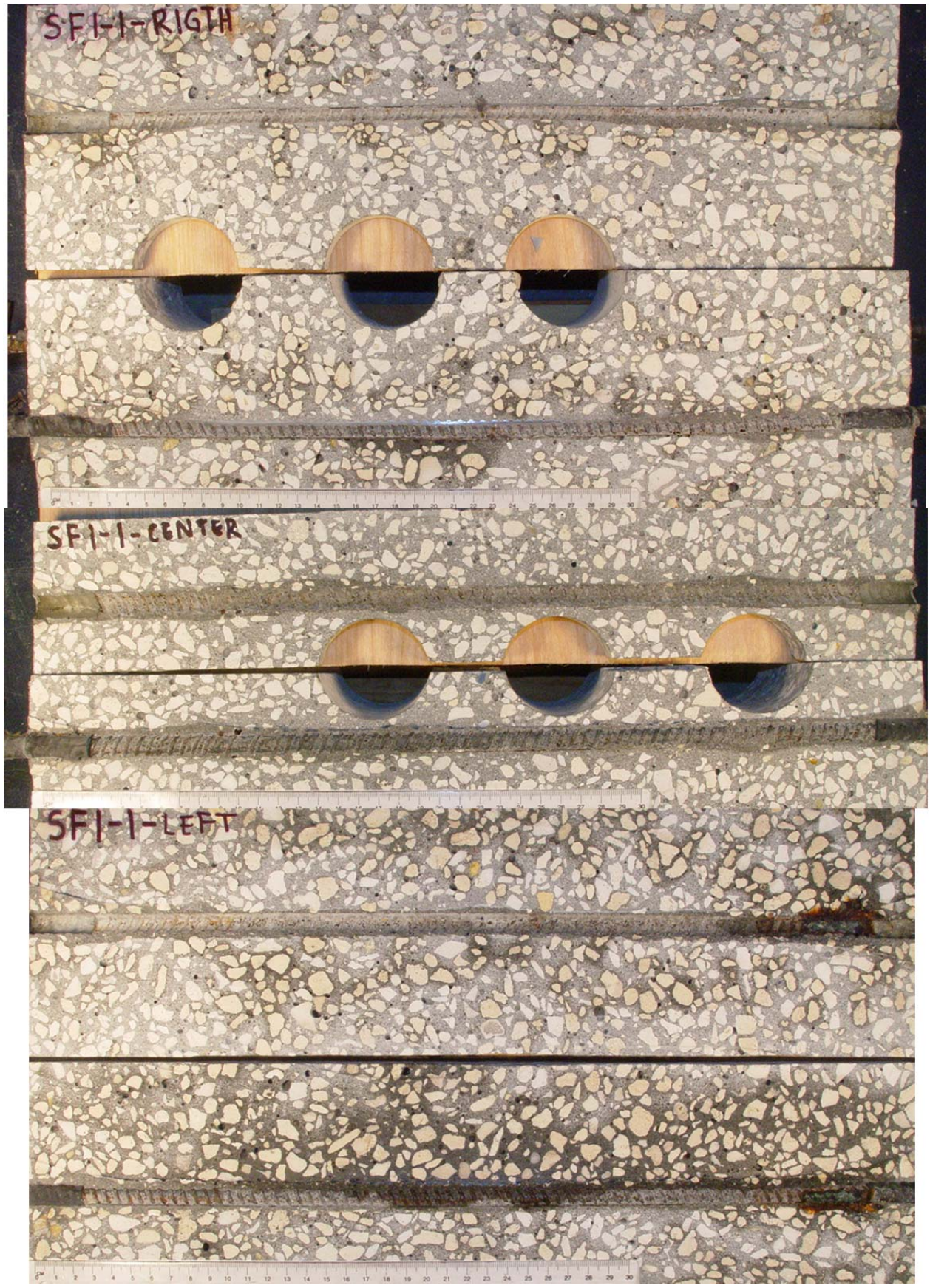

SF1-3

SF2-1

SF2-2

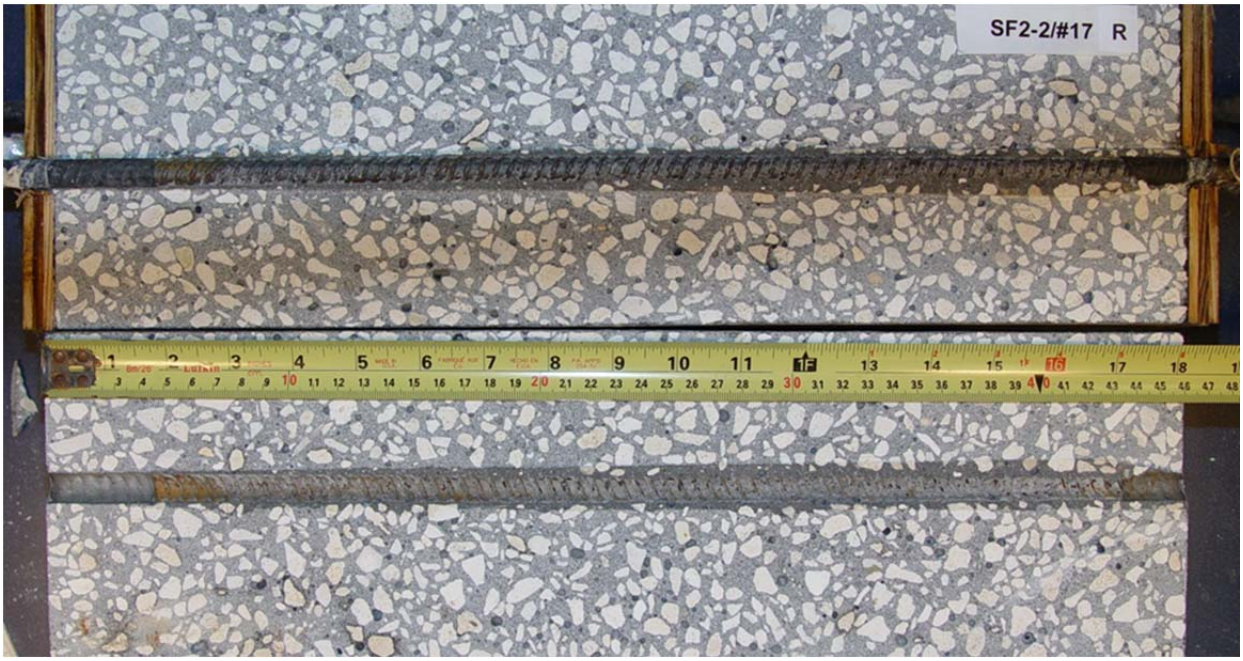

SF3-2

SF4-3

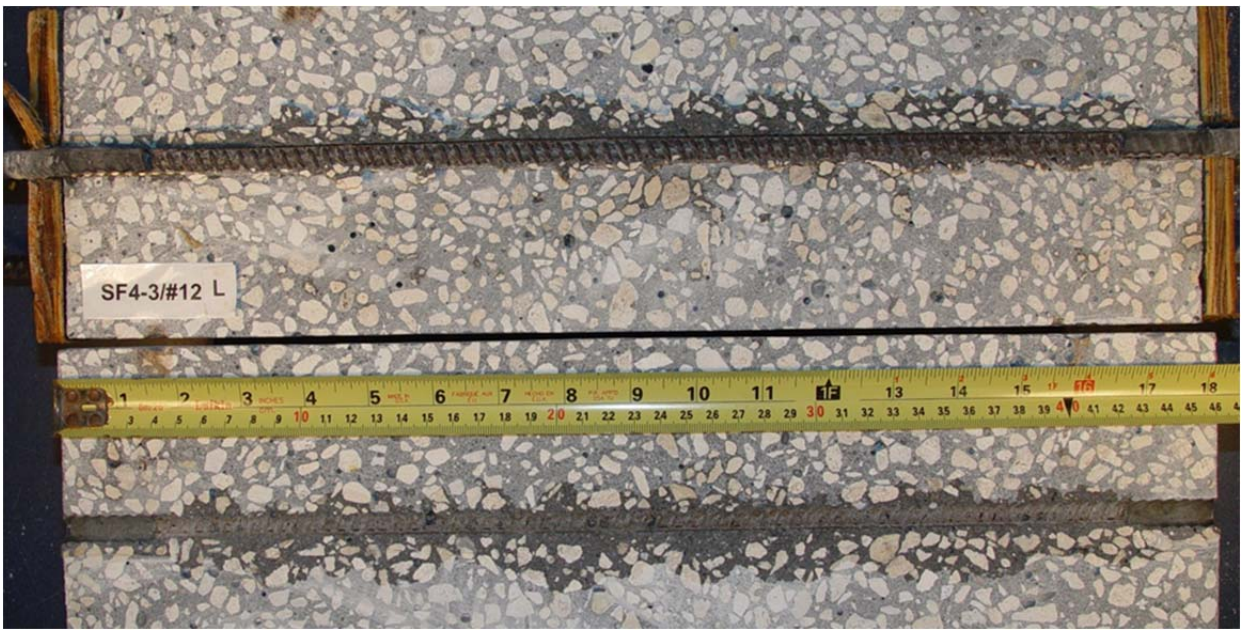

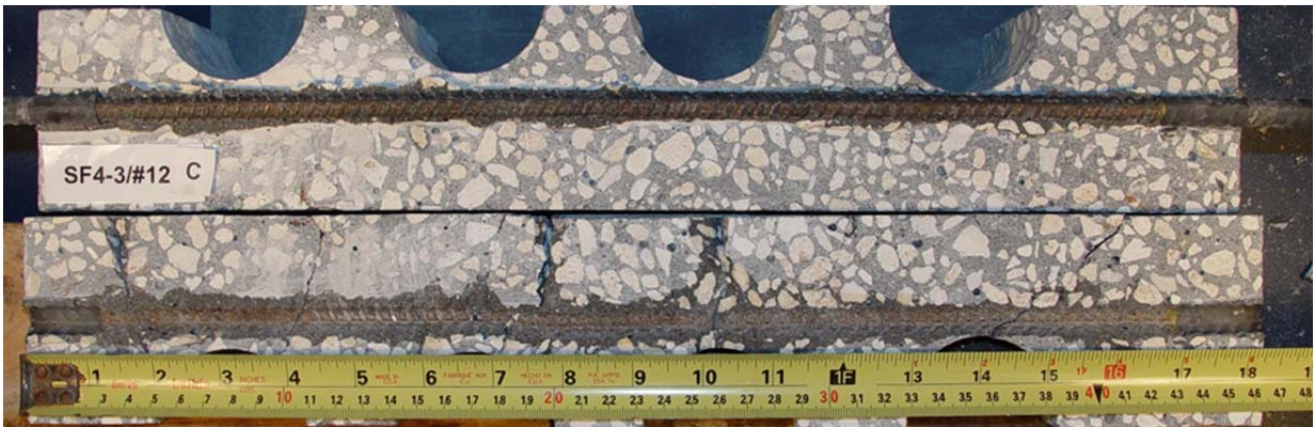

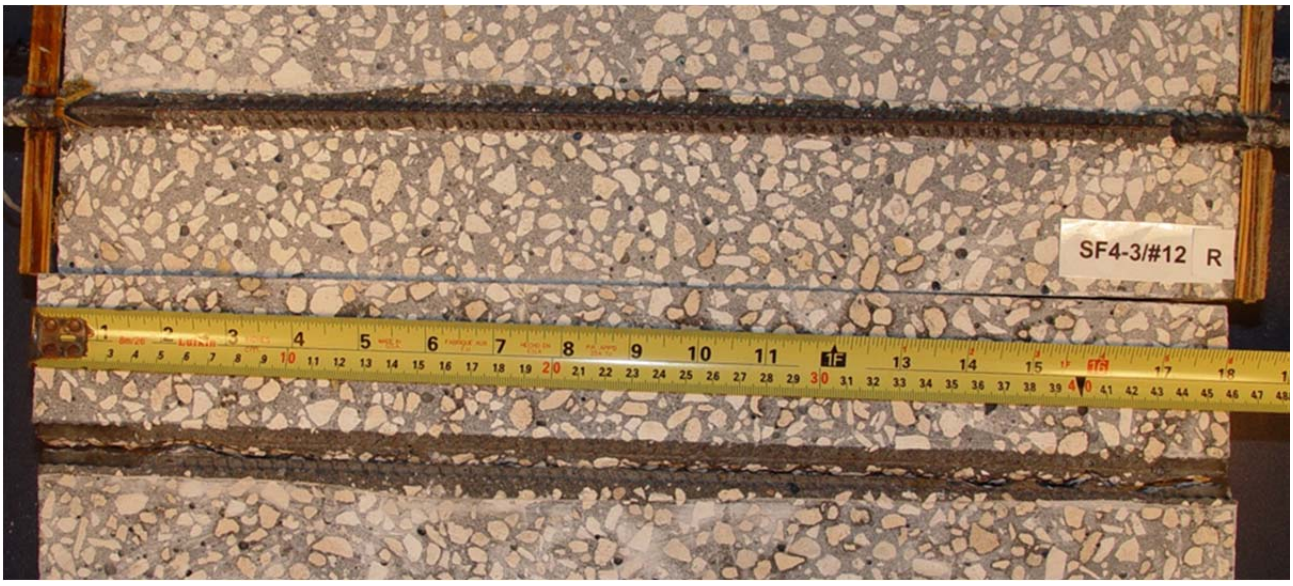

APPENDIX B: Rebar Potential vs. Time (Chapter 2)

AO

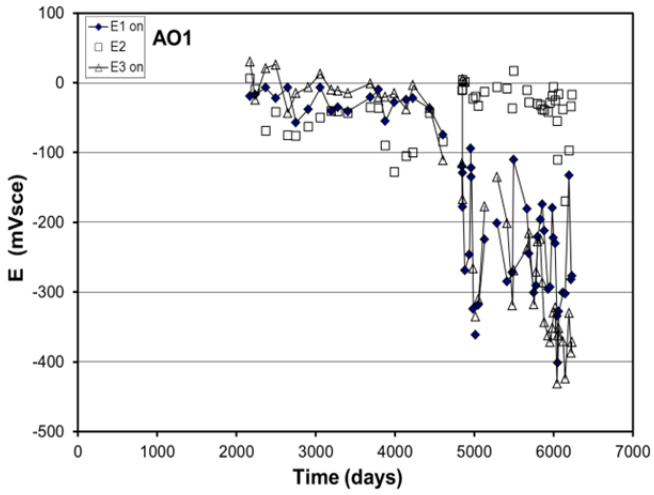

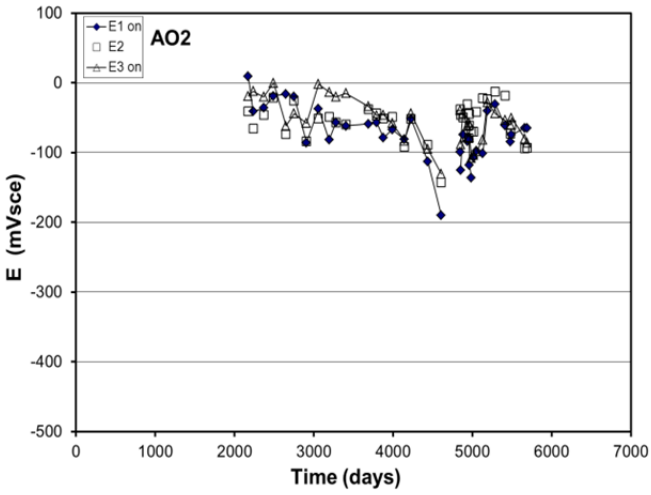

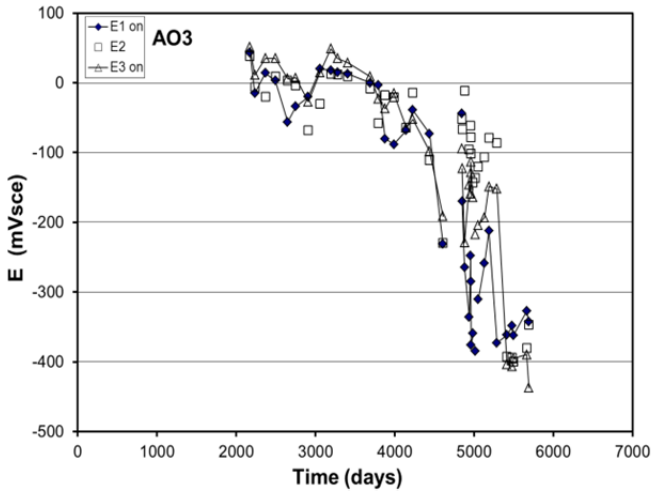

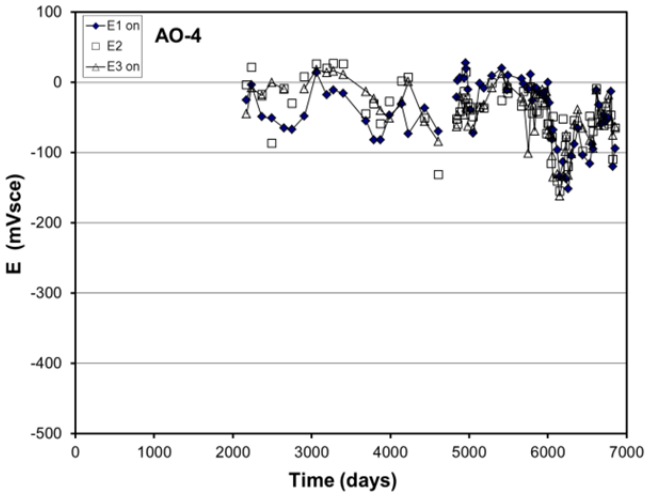

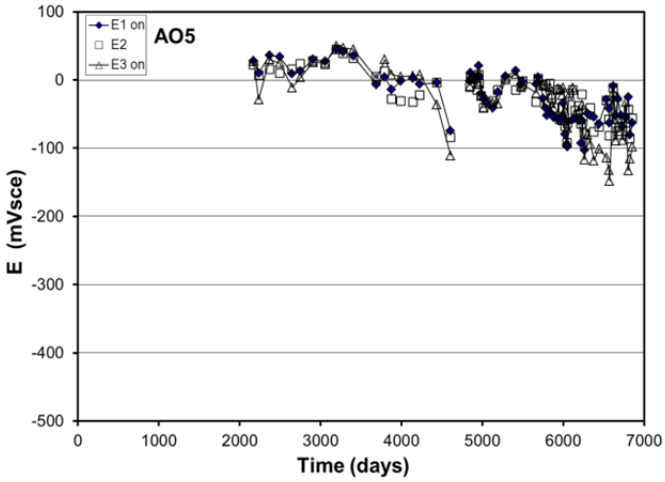
AO5
E1 on
E2
E3 on
E (mVsce)
Time (days)

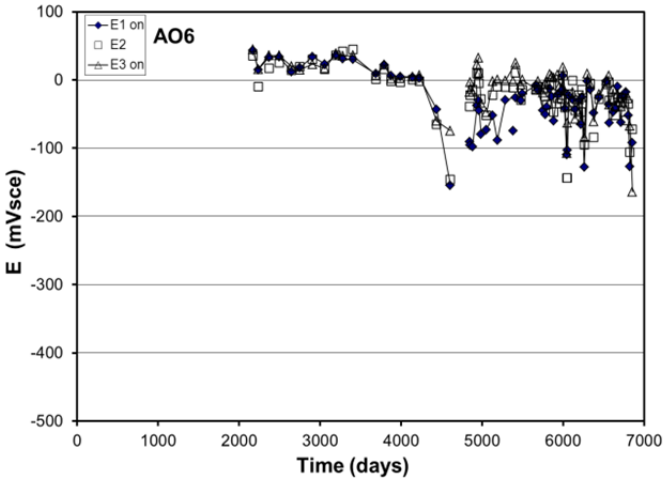
AO6
E1 on
E2
E3 on
E (mVsce)
Time (days)

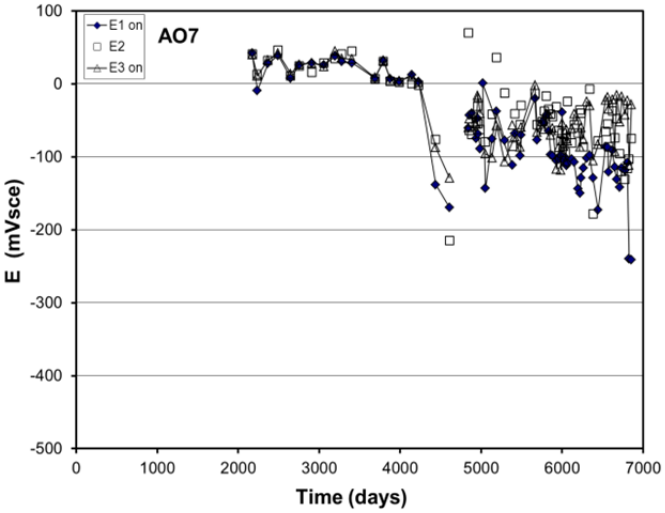
AO7
E1 on
E2
E3 on
E (mVsce)
Time (days)

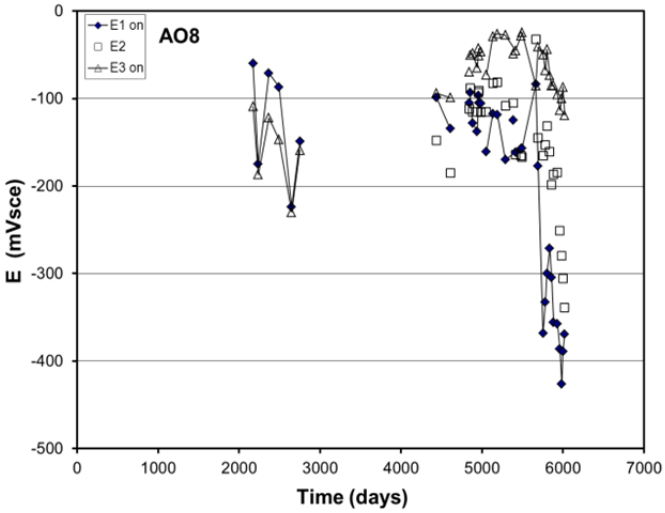
AO8
E1 on
E2
E3 on
E (mVsce)
Time (days)

CO

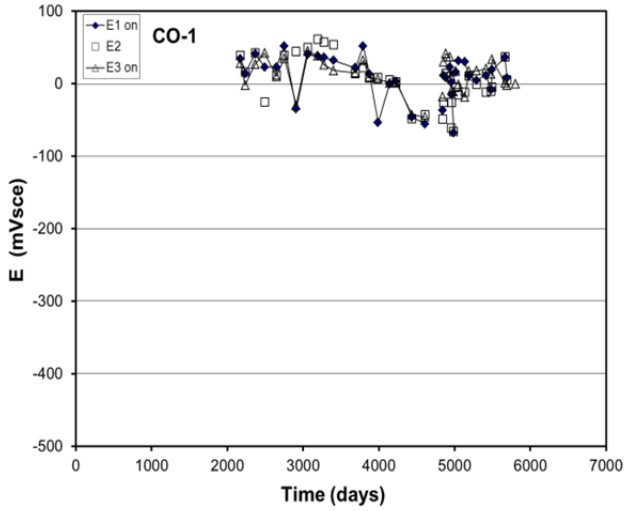
CO-1
E1 on
E2
E3 on
E (mVsce)
Time (days)

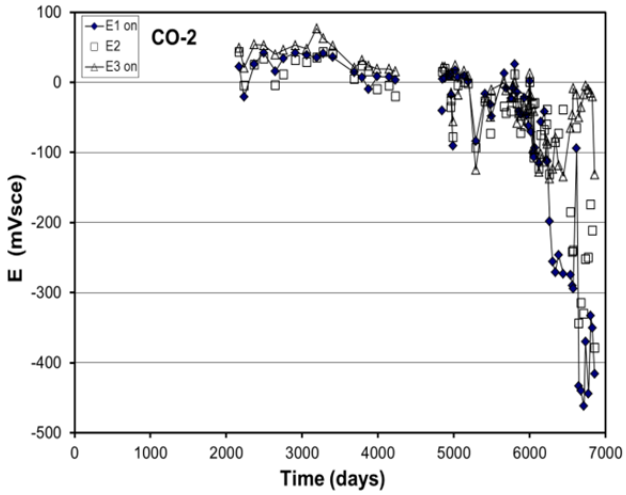
CO-2
E1 on
E2
E3 on
E (mVsce)
Time (days)

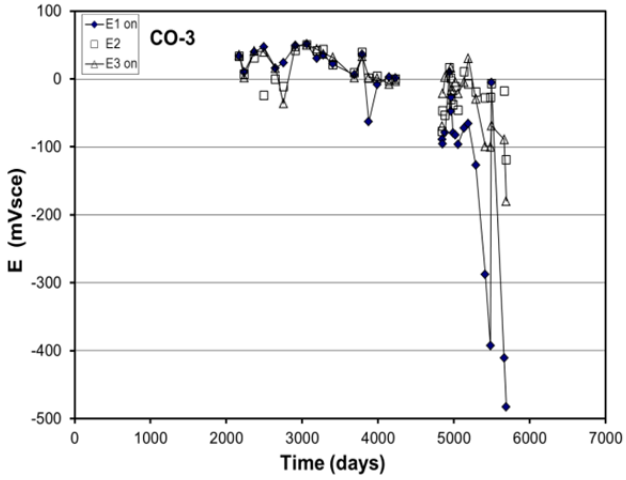
CO-3
E1 on
E2
E3 on
E (mVsce)
Time (days)

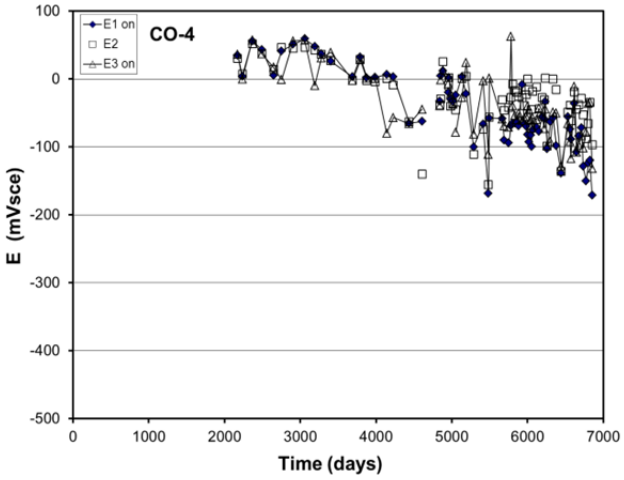
CO-4
E1 on
E2
E3 on
E (mVsce)
Time (days)

FA1

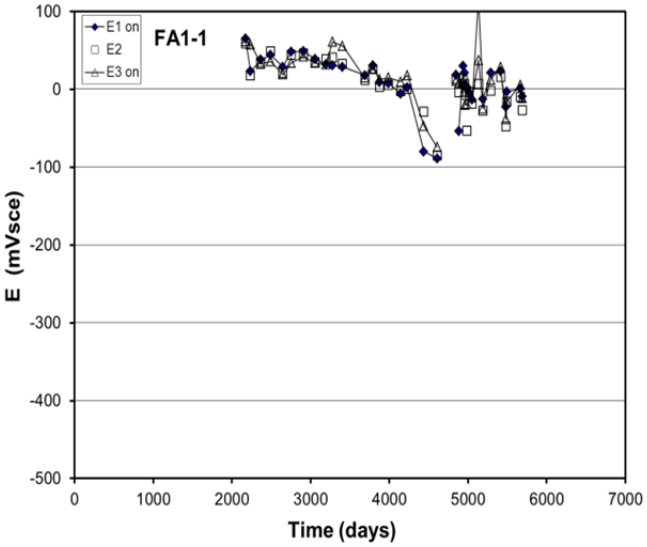
FA1-1
E1 on
E2
E3 on
E (mVsce)
Time (days)

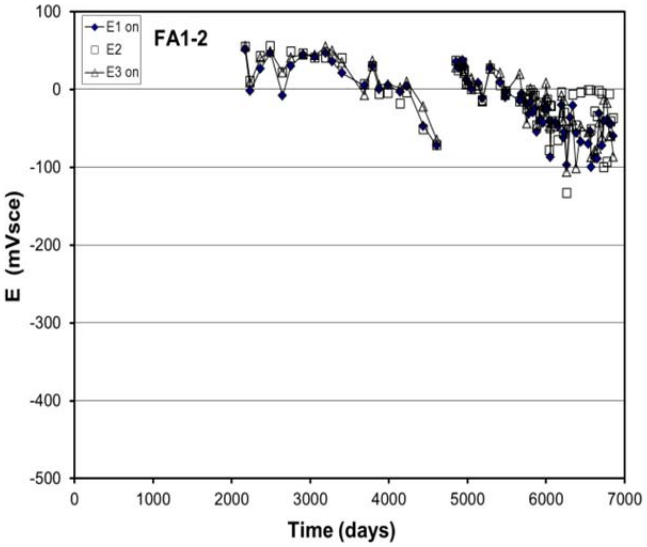
FA1-2
E1 on
E2
E3 on
E (mVsce)
Time (days)

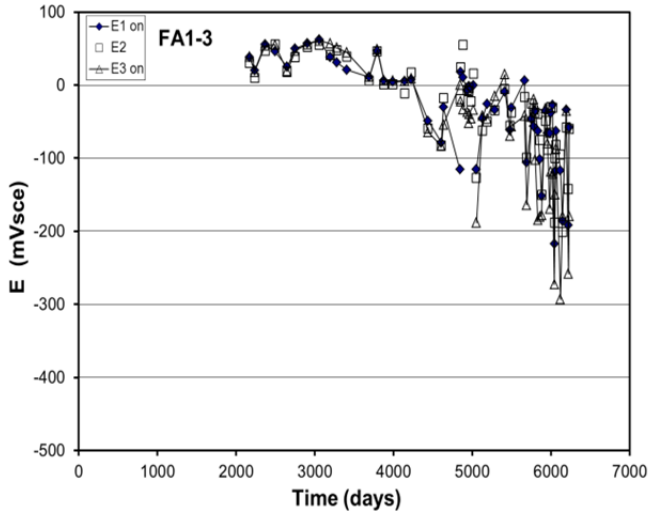
FA1-3
E1 on
E2
E3 on
E (mVsce)
Time (days)

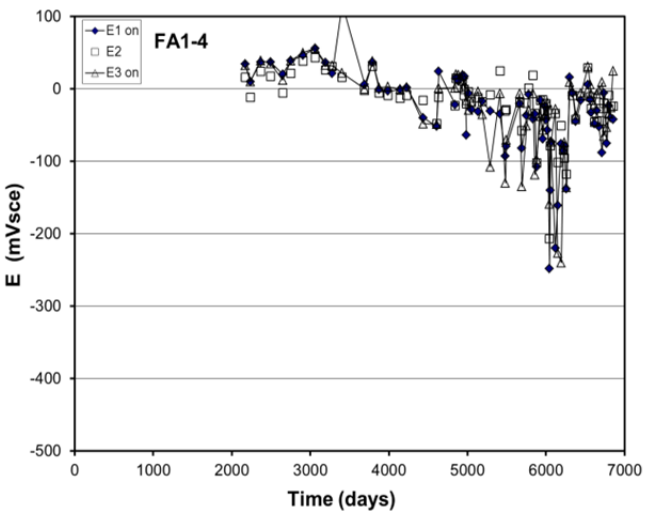
FA1-4
E1 on
E2
E3 on
E (mVsce)
Time (days)

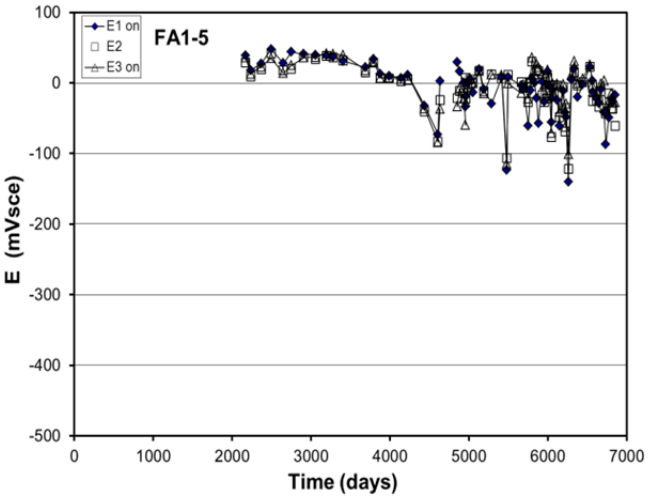
FA1-5
E1 on
E2
E3 on
E (mVsce)
Time (days)
100
0
-100
-200
-300
-400
-500
0
1000
2000
3000
4000
5000
6000
7000

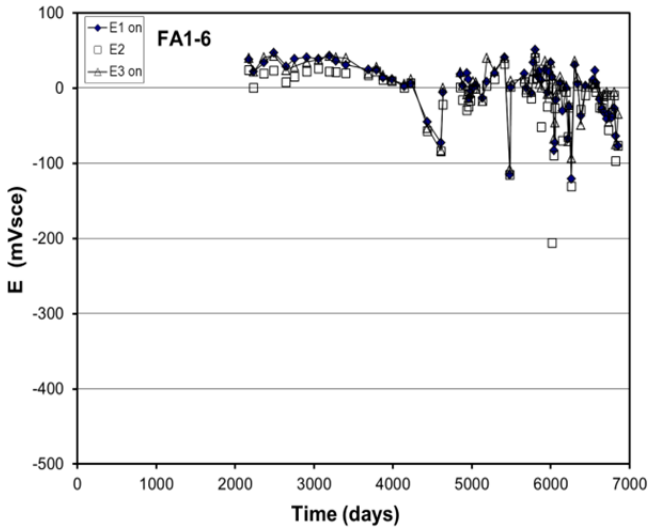
FA1-6
E1 on
E2
E3 on
E (mVsce)
Time (days)
100
0
-100
-200
-300
-400
-500
0
1000
2000
3000
4000
5000
6000
7000

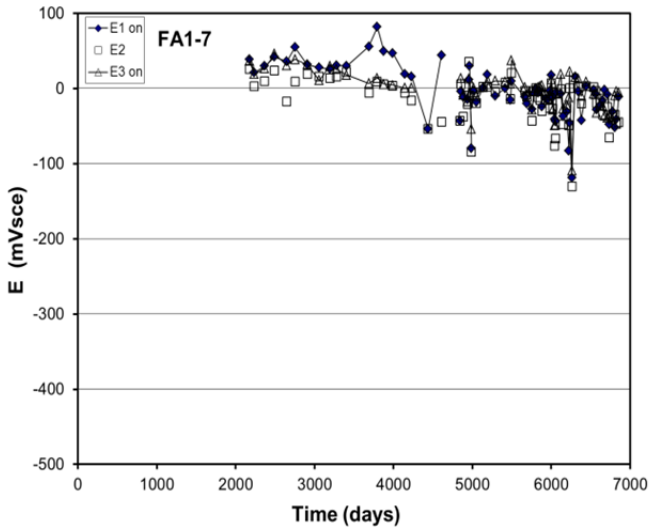
FA1-7
E1 on
E2
E3 on
E (mVsce)
Time (days)
100
0
-100
-200
-300
-400
-500
0
1000
2000
3000
4000
5000
6000
7000

FA2

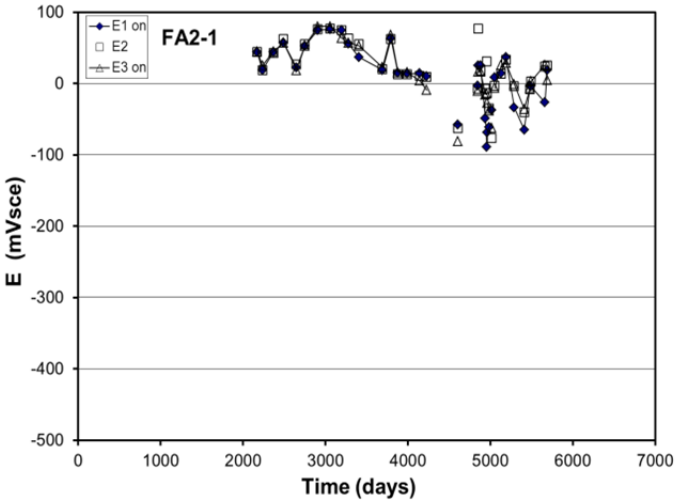
FA2-1
E1 on
E2
E3 on
E (mVsce)
Time (days)
100
0
-100
-200
-300
-400
-500
0
1000
2000
3000
4000
5000
6000
7000

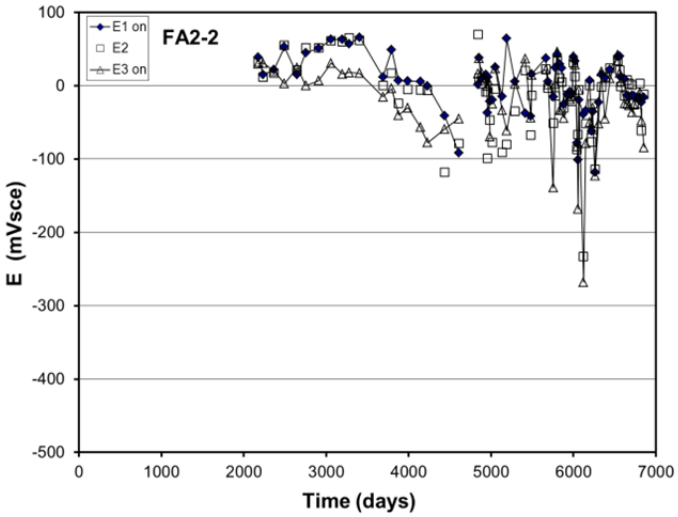
FA2-2
E1 on
E2
E3 on
E (mVsce)
Time (days)
100
0
-100
-200
-300
-400
-500
0
1000
2000
3000
4000
5000
6000
7000

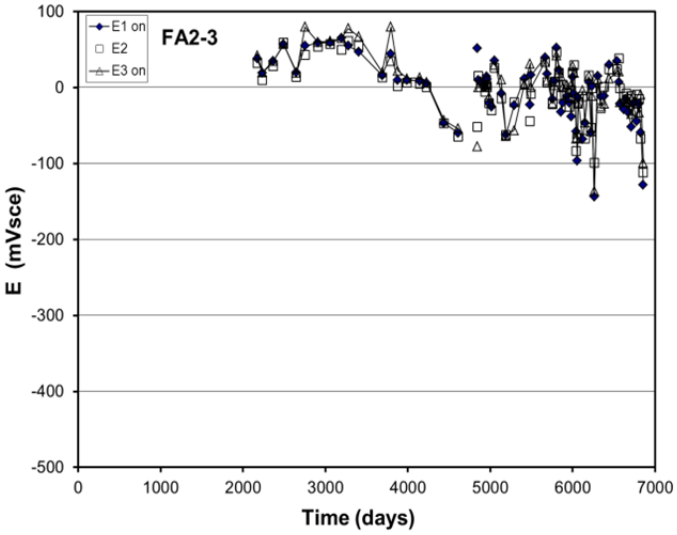
FA2-3
E1 on
E2
E3 on
E (mVsce)
Time (days)
100
0
-100
-200
-300
-400
-500
0
1000
2000
3000
4000
5000
6000
7000

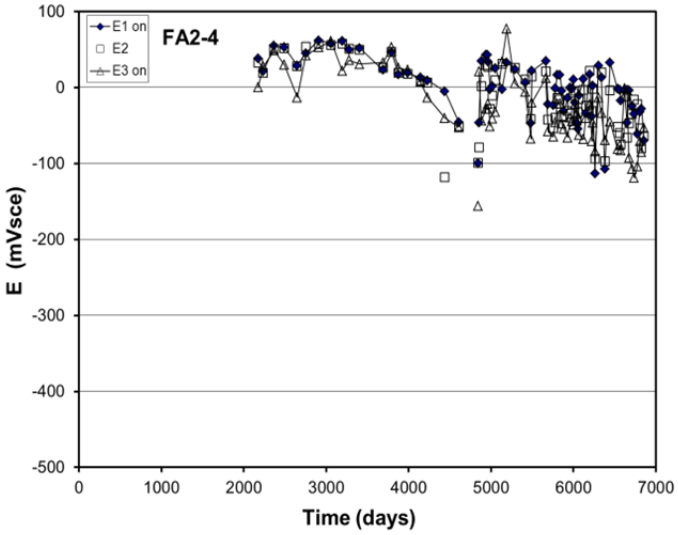
FA2-4
E1 on
E2
E3 on
E (mVsce)
Time (days)
100
0
-100
-200
-300
-400
-500
0
1000
2000
3000
4000
5000
6000
7000

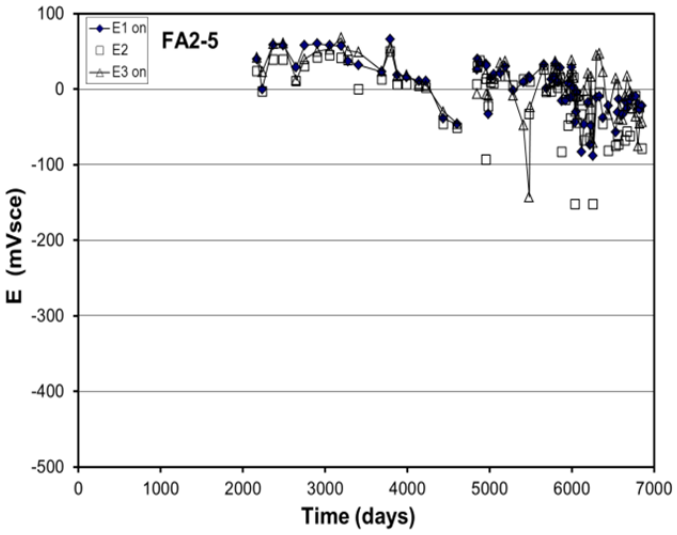
FA2-5
E1 on
E2
E3 on
E (mVsce)
Time (days)
100
0
-100
-200
-300
-400
-500
0
1000
2000
3000
4000
5000
6000
7000

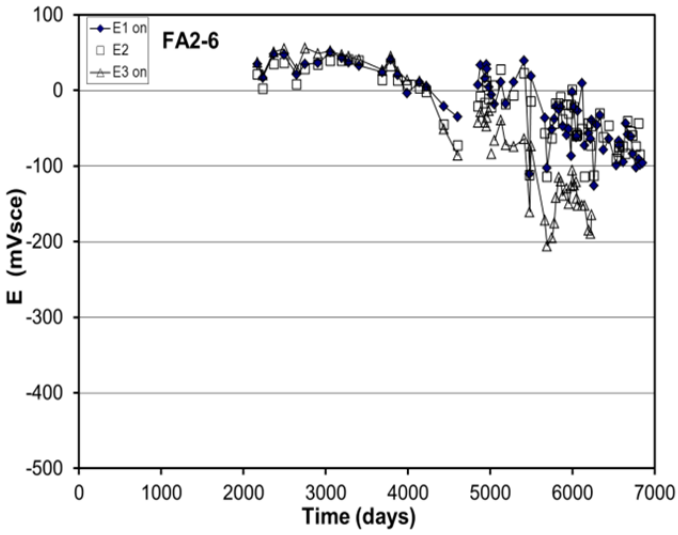
FA2-6
E1 on
E2
E3 on
E (mVsce)
Time (days)
100
0
-100
-200
-300
-400
-500
0
1000
2000
3000
4000
5000
6000
7000

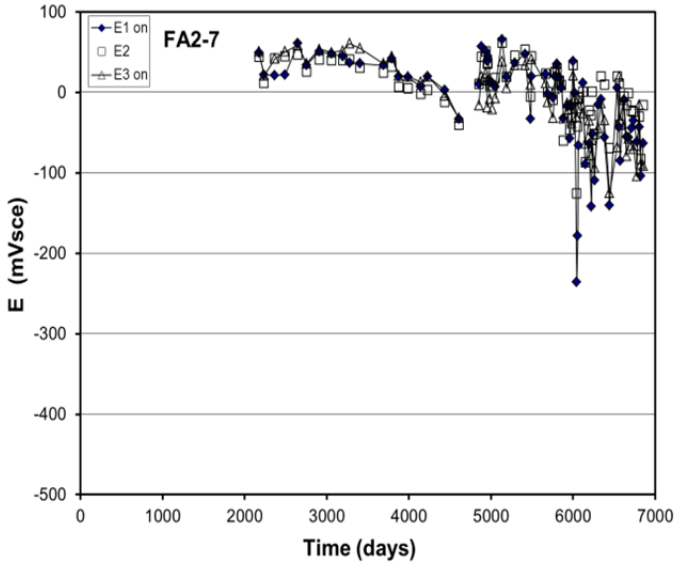
FA2-7
E1 on
E2
E3 on
E (mVsce)
Time (days)
100
0
-100
-200
-300
-400
-500
0
1000
2000
3000
4000
5000
6000
7000

FA3

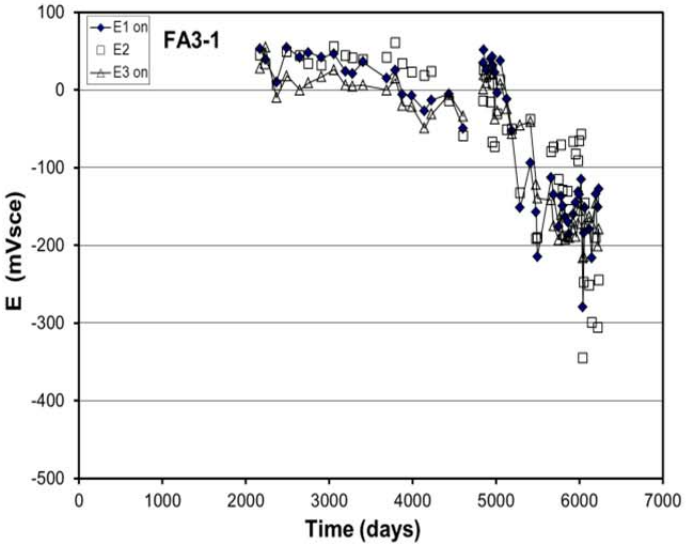
FA3-1
E1 on
E2
E3 on
E (mVsce)
Time (days)

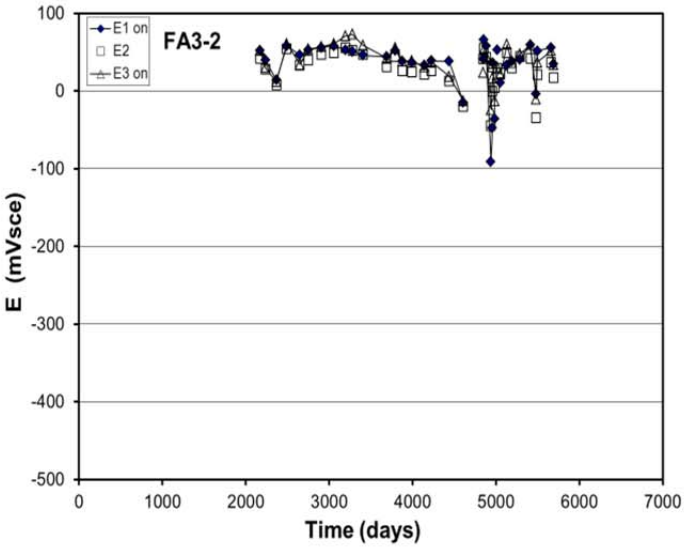
FA3-2
E1 on
E2
E3 on
E (mVsce)
Time (days)

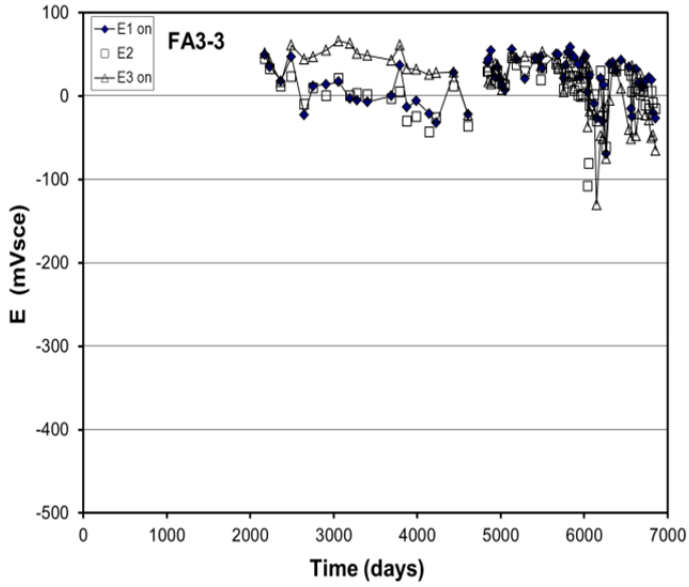
FA3-3
E1 on
E2
E3 on
E (mVsce)
Time (days)

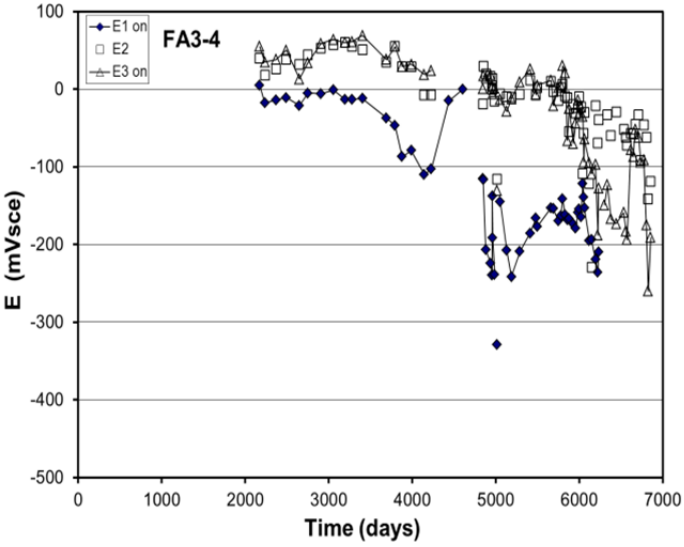
FA3-4
E1 on
E2
E3 on
E (mVsce)
Time (days)

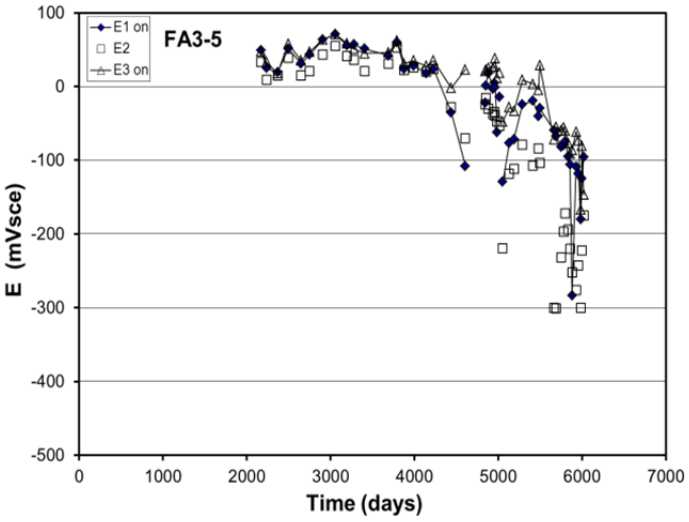
FA3-5
E1 on
E2
E3 on
E (mVsce)
Time (days)
100
0
-100
-200
-300
-400
-500
0
1000
2000
3000
4000
5000
6000
7000

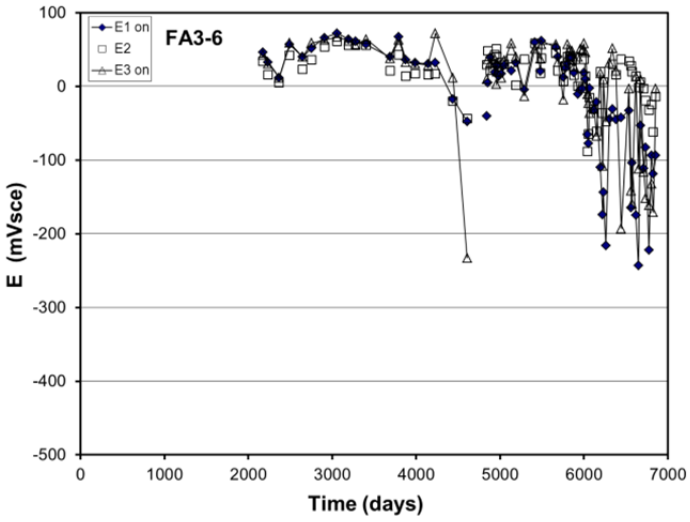
FA3-6
E1 on
E2
E3 on
E (mVsce)
Time (days)
100
0
-100
-200
-300
-400
-500
0
1000
2000
3000
4000
5000
6000
7000

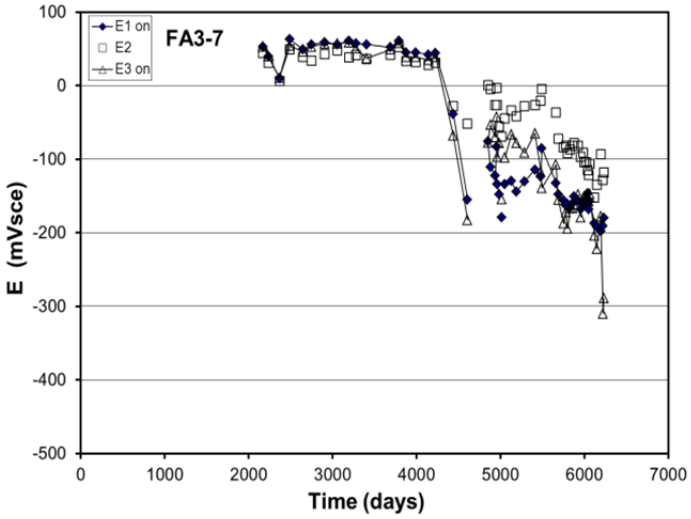
FA3-7
E1 on
E2
E3 on
E (mVsce)
Time (days)
100
0
-100
-200
-300
-400
-500
0
1000
2000
3000
4000
5000
6000
7000

FA4

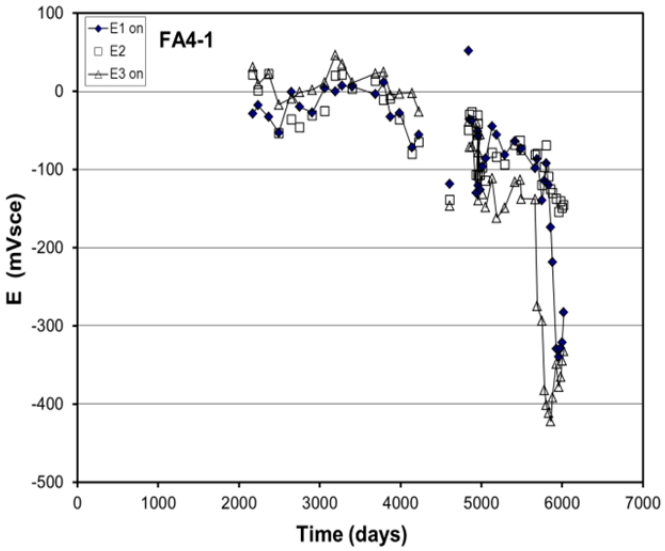
FA4-1
E1 on
E2
E3 on
E (mVsce)
Time (days)
100
0
-100
-200
-300
-400
-500
0
1000
2000
3000
4000
5000
6000
7000

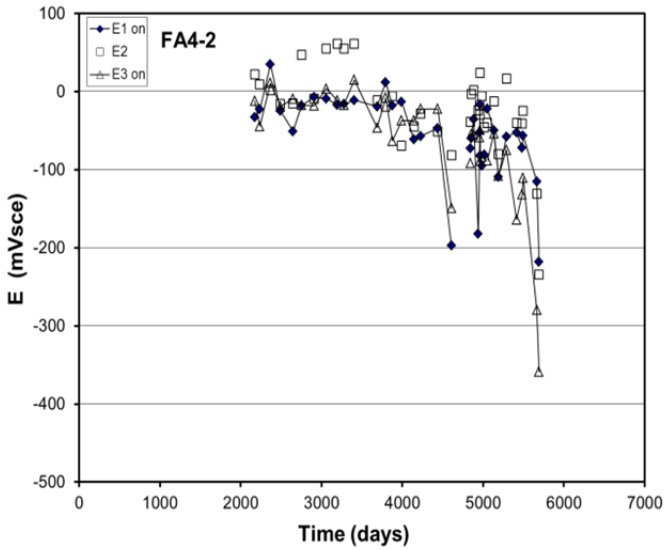
FA4-2
E1 on
E2
E3 on
E (mVsce)
Time (days)
100
0
-100
-200
-300
-400
-500
0
1000
2000
3000
4000
5000
6000
7000

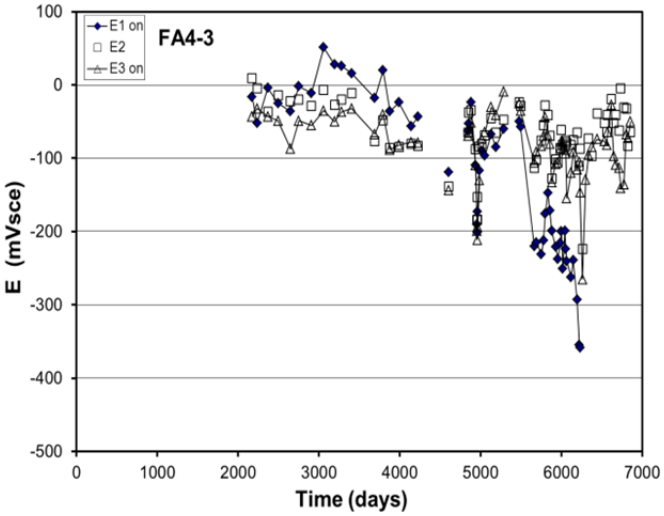
FA4-3
E1 on
E2
E3 on
E (mVsce)
Time (days)
100
0
-100
-200
-300
-400
-500
0
1000
2000
3000
4000
5000
6000
7000

SF1

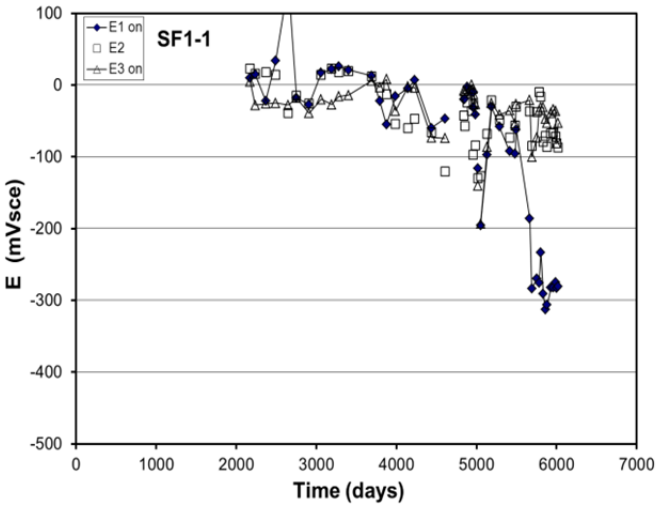
SF1-1
E1 on
E2
E3 on
E (mVsce)
Time (days)
100
0
-100
-200
-300
-400
-500
0
1000
2000
3000
4000
5000
6000
7000

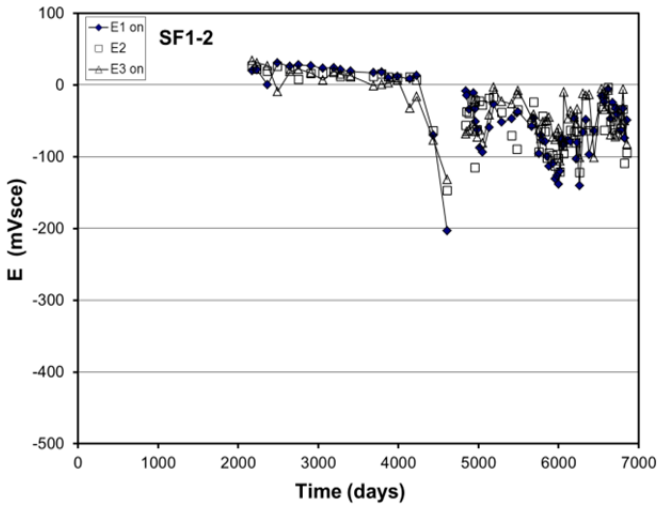
SF1-2
E1 on
E2
E3 on
E (mVsce)
Time (days)
100
0
-100
-200
-300
-400
-500
0
1000
2000
3000
4000
5000
6000
7000

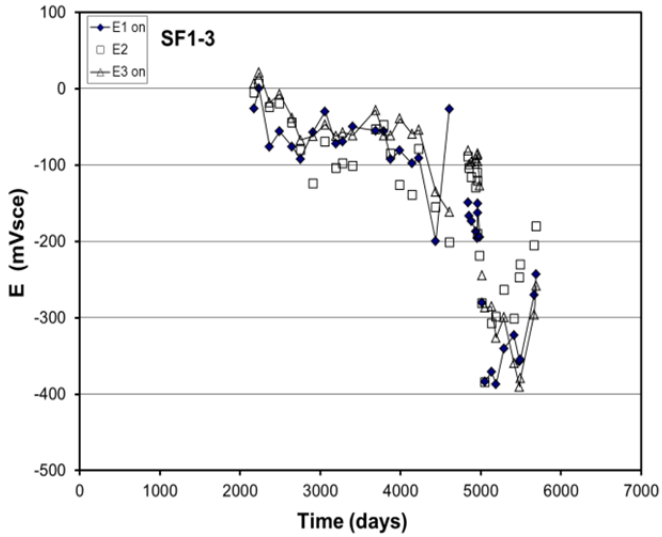
SF1-3
E1 on
E2
E3 on
E (mVsce)
Time (days)
100
0
-100
-200
-300
-400
-500
0
1000
2000
3000
4000
5000
6000
7000

SF2

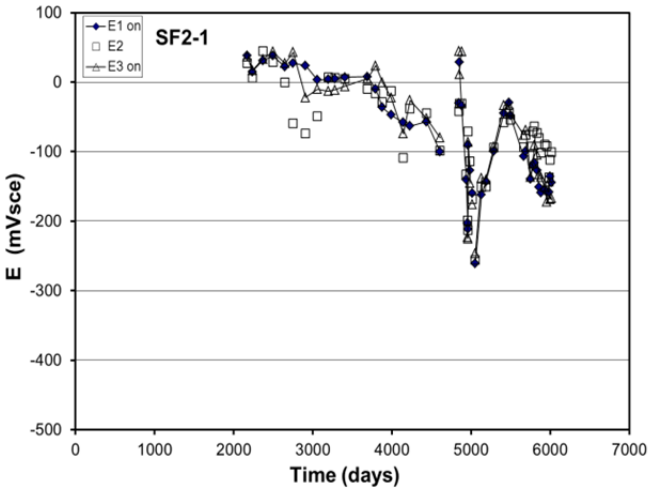
SF2-1
E1 on
E2
E3 on
E (mVsce)
Time (days)
100
0
-100
-200
-300
-400
-500
0
1000
2000
3000
4000
5000
6000
7000

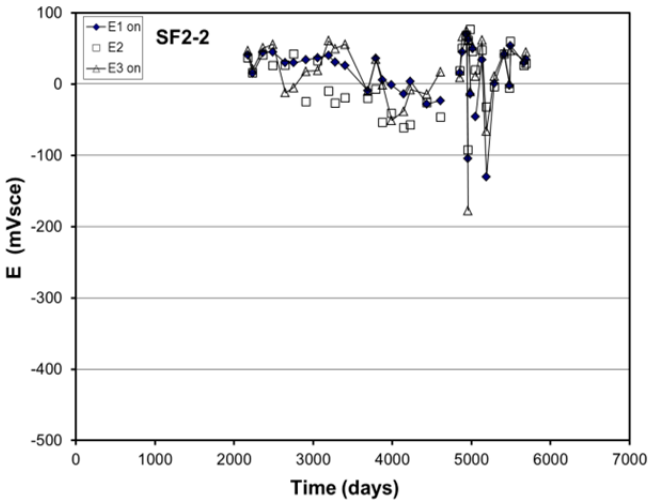
SF2-2
E1 on
E2
E3 on
E (mVsce)
Time (days)
100
0
-100
-200
-300
-400
-500
0
1000
2000
3000
4000
5000
6000
7000

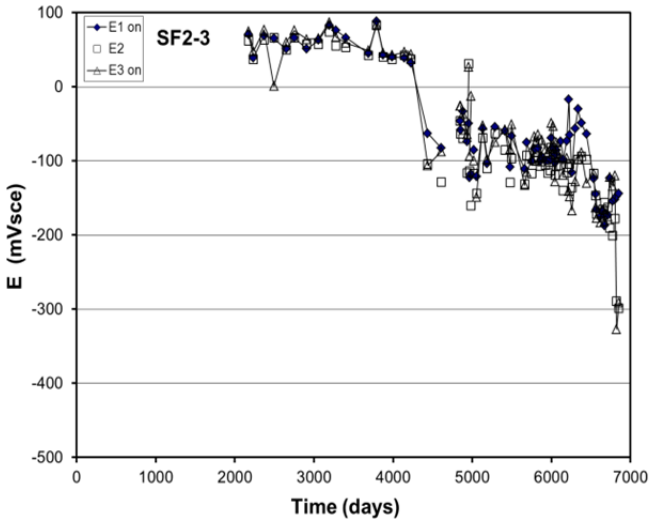
SF2-3
E1 on
E2
E3 on
E (mVsce)
Time (days)
100
0
-100
-200
-300
-400
-500
0
1000
2000
3000
4000
5000
6000
7000

SF3

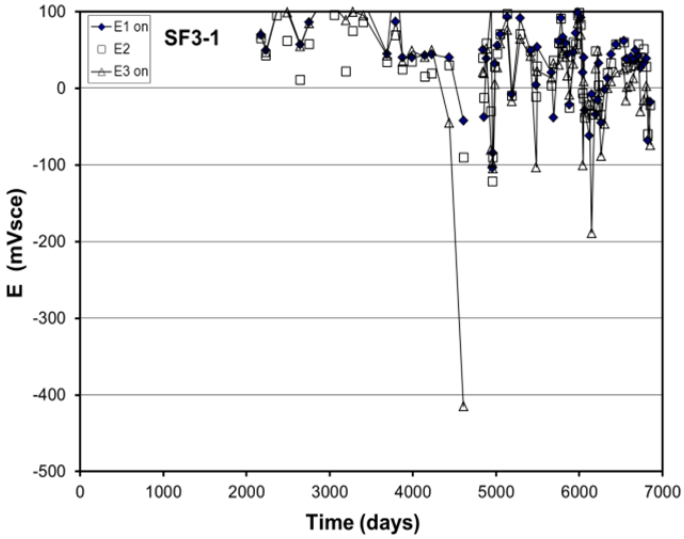
SF3-1
E1 on
E2
E3 on
E (mVsce)
Time (days)
100
0
-100
-200
-300
-400
-500
0
1000
2000
3000
4000
5000
6000
7000

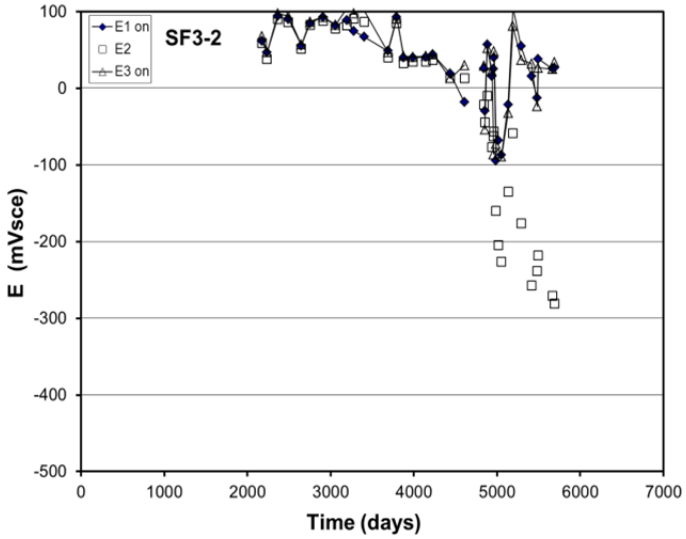
SF3-2
E1 on
E2
E3 on
E (mVsce)
Time (days)
100
0
-100
-200
-300
-400
-500
0
1000
2000
3000
4000
5000
6000
7000

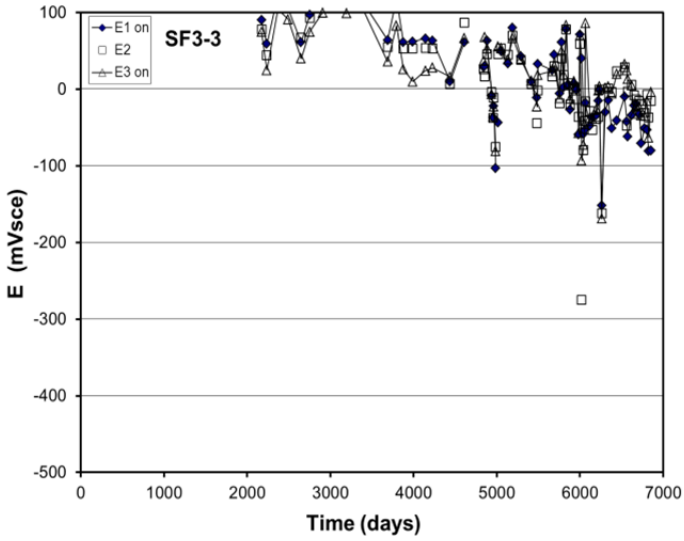
SF3-3
E1 on
E2
E3 on
E (mVsce)
Time (days)
100
0
-100
-200
-300
-400
-500
0
1000
2000
3000
4000
5000
6000
7000

SF4

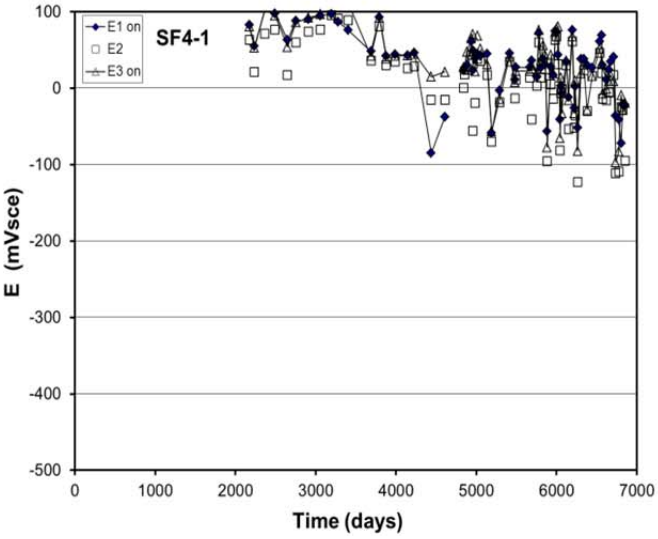
SF4-1
E1 on
E2
E3 on
E (mVsce)
Time (days)
100
0
-100
-200
-300
-400
-500
0
1000
2000
3000
4000
5000
6000
7000

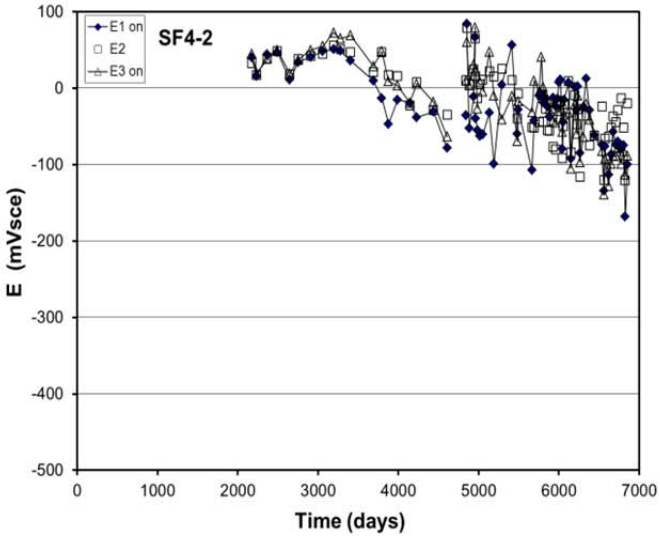
SF4-2
E1 on
E2
E3 on
E (mVsce)
Time (days)
100
0
-100
-200
-300
-400
-500
0
1000
2000
3000
4000
5000
6000
7000

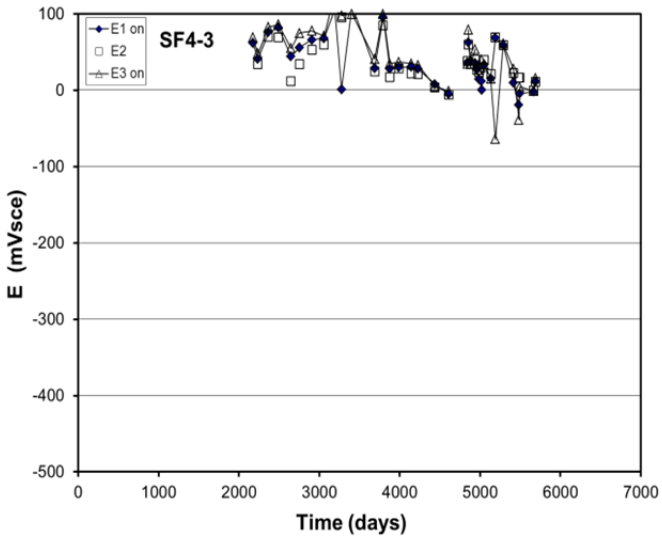
SF4-3
E1 on
E2
E3 on
E (mVsce)
Time (days)
100
0
-100
-200
-300
-400
-500
0
1000
2000
3000
4000
5000
6000
7000

APPENDIX C: Applied Electric Field on Specimens of Chapter-5

Table 1 Applied voltage schedule

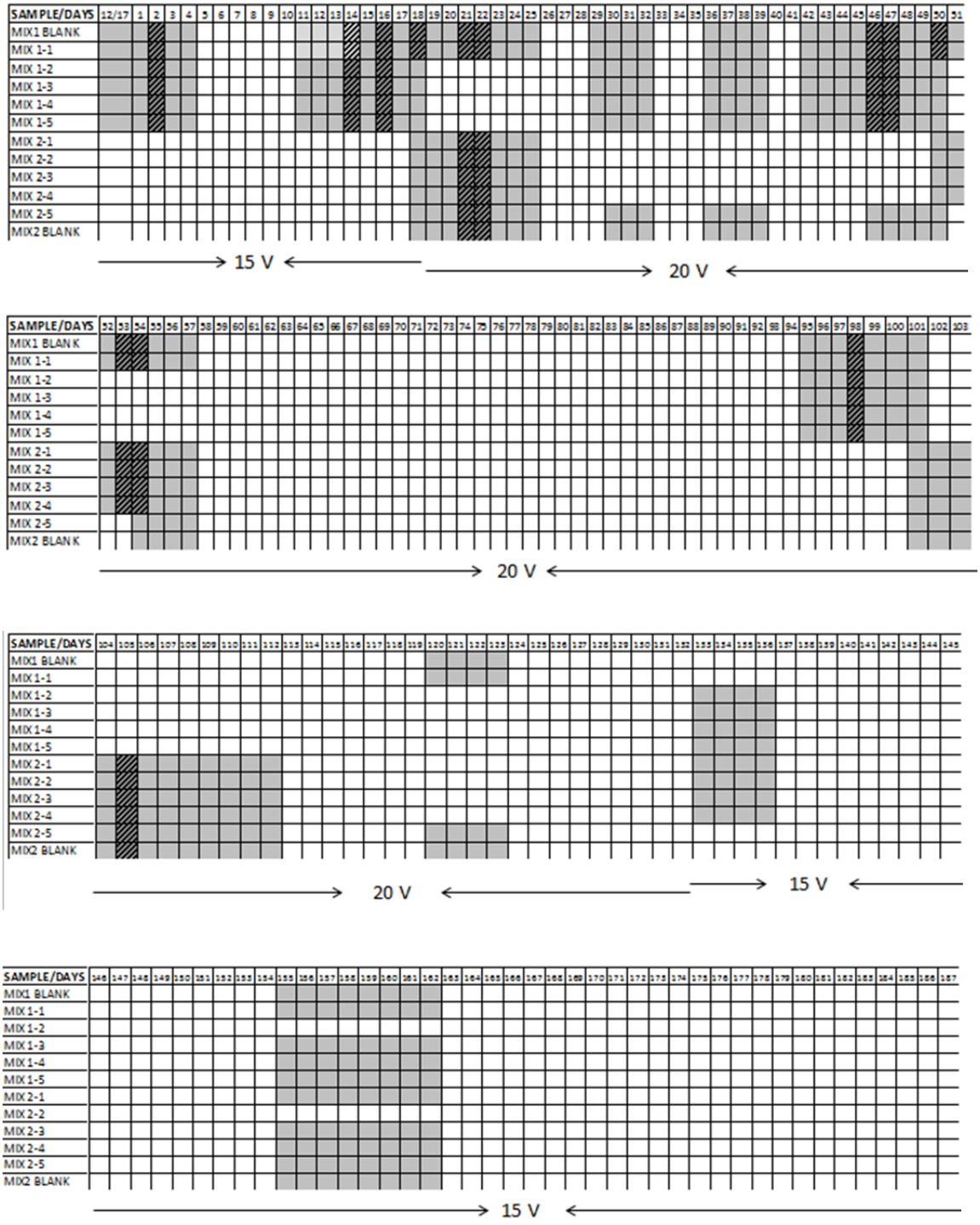

APPENDIX D: Potential vs. time and Forensic Examination for specimens in Chapter-5

Figure D.1 Open Circuit Potential (OCP) Measurements during Phase I – Batch 1 Samples

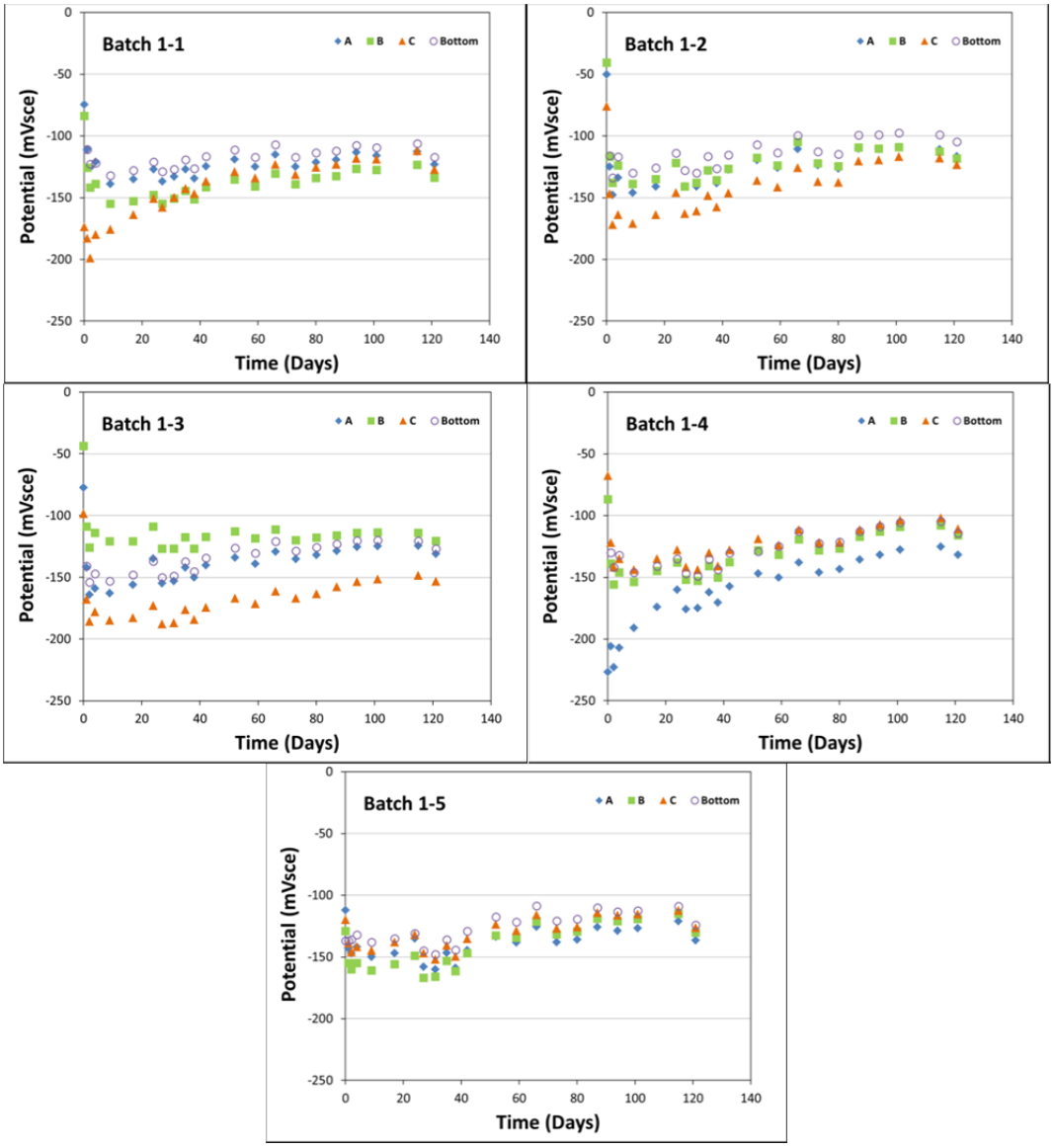

Figure D.2 Open Circuit Potential Measurements (OCP) of Phase I – Batch 2 Samples

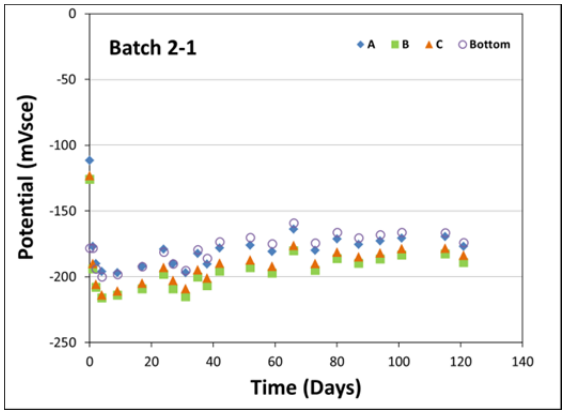

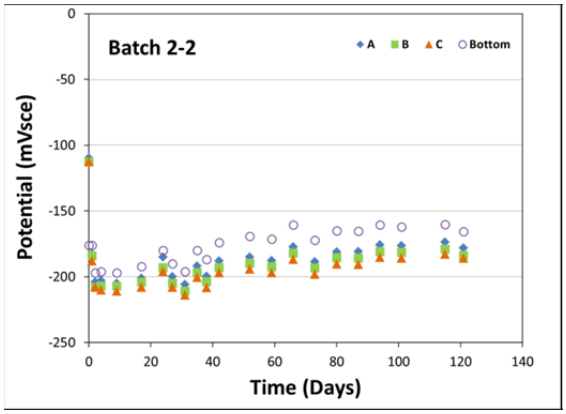

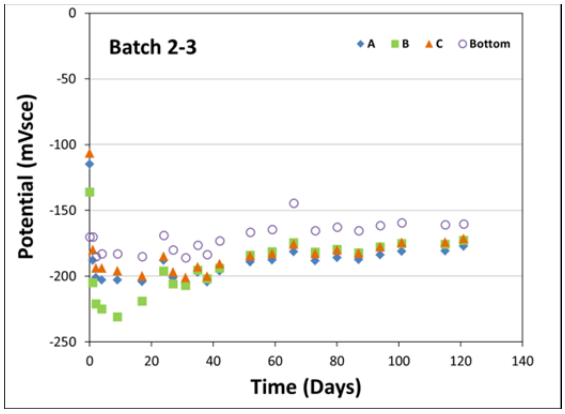

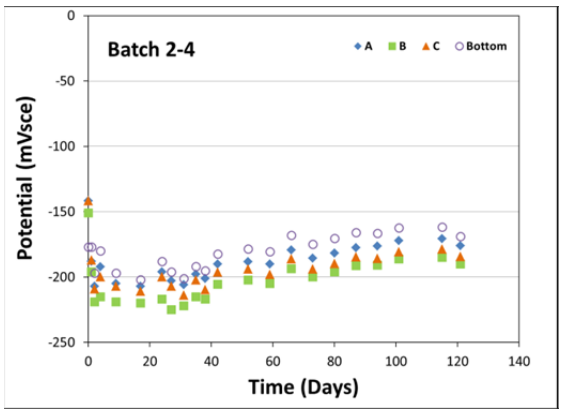

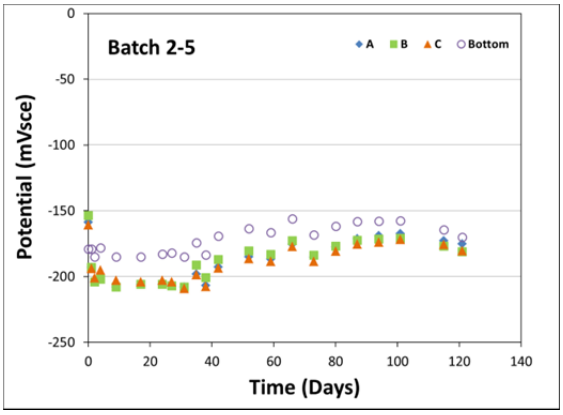

Figure D.3 Rebar potential measurements over time for batch 1 samples during Phase II

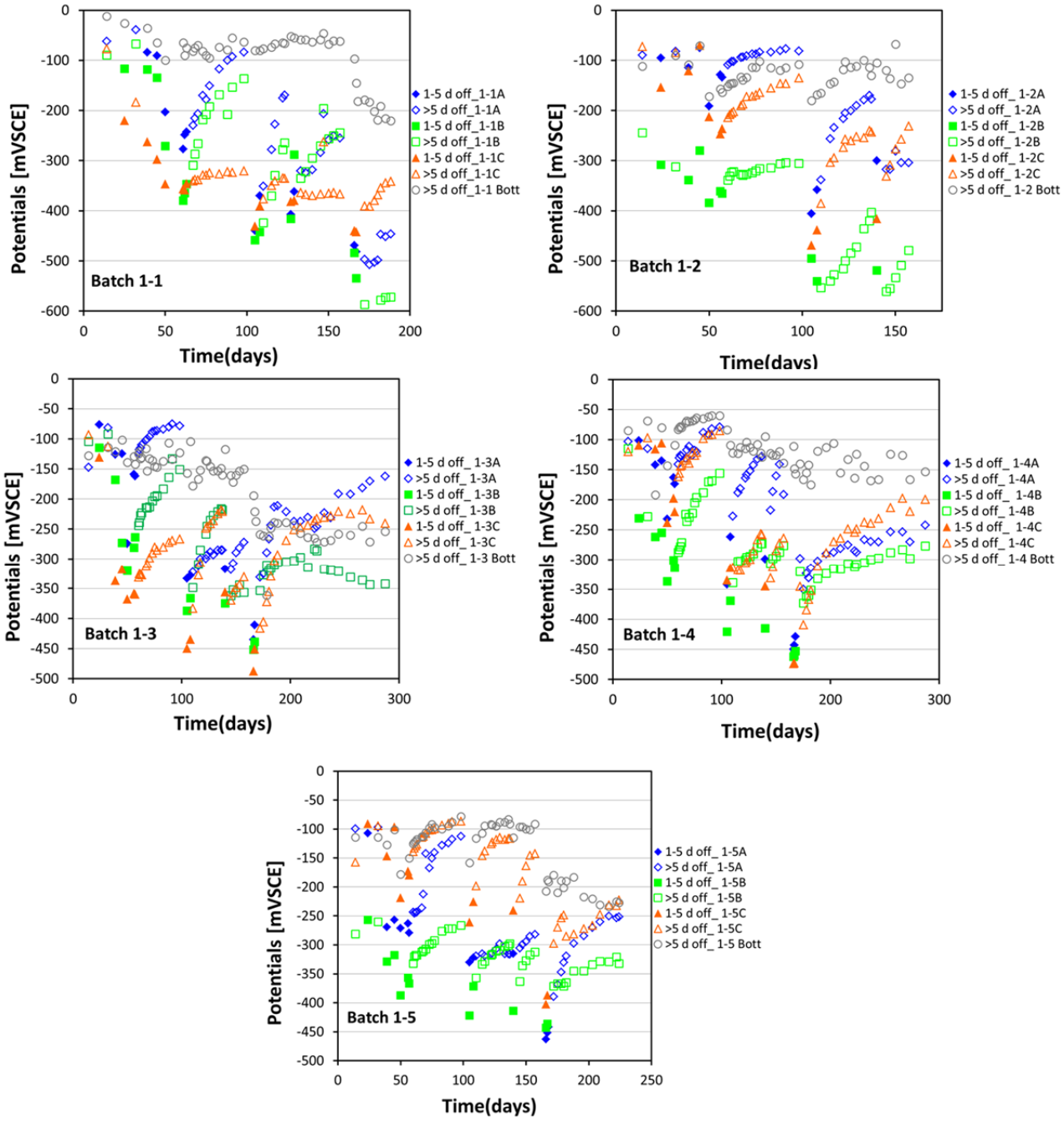

Figure D.4 Rebar potential measurements over time for batch 2 samples during Phase II

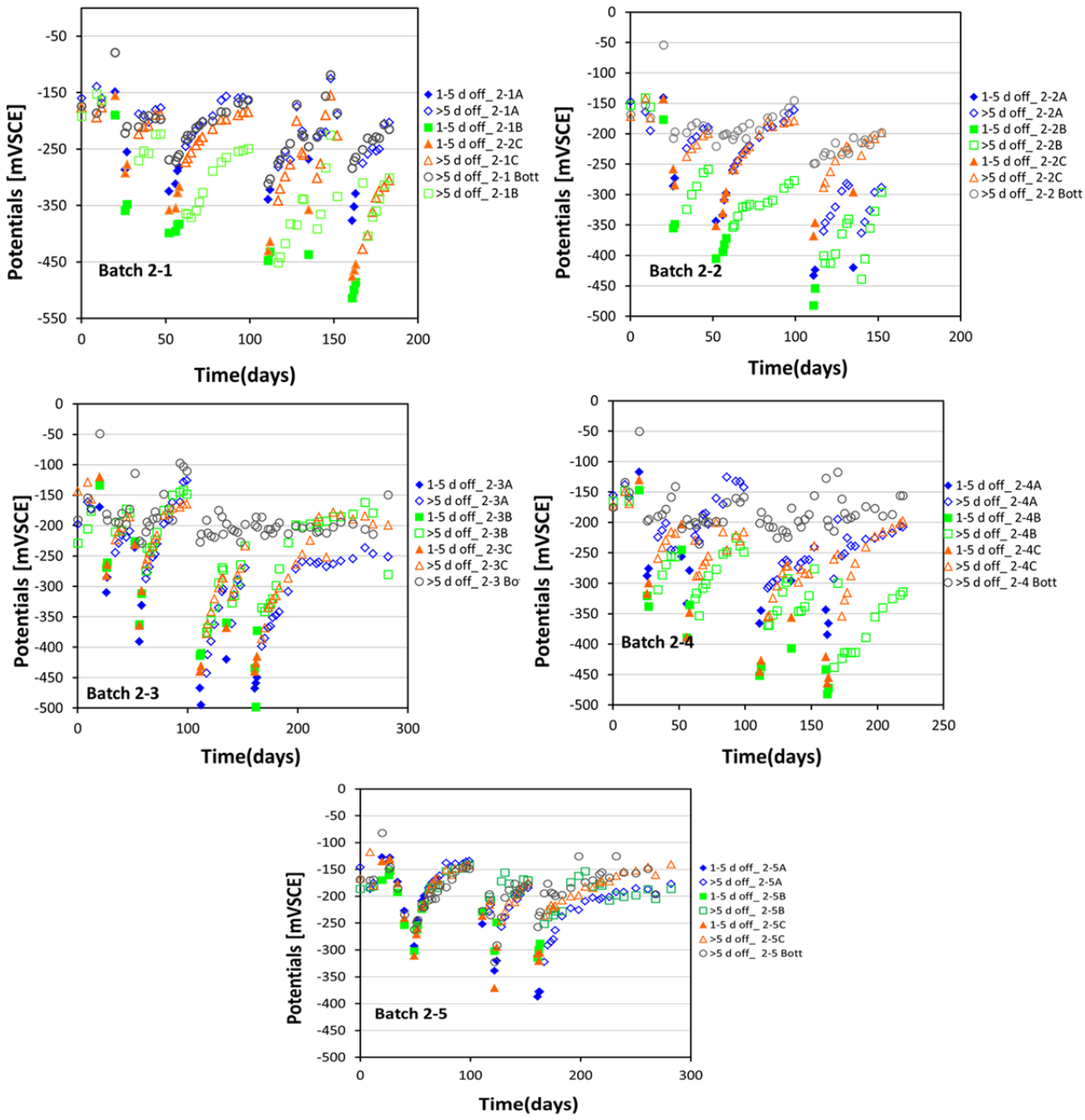

Figure D.5 Solution Resistance over time for samples batch 1 phase II

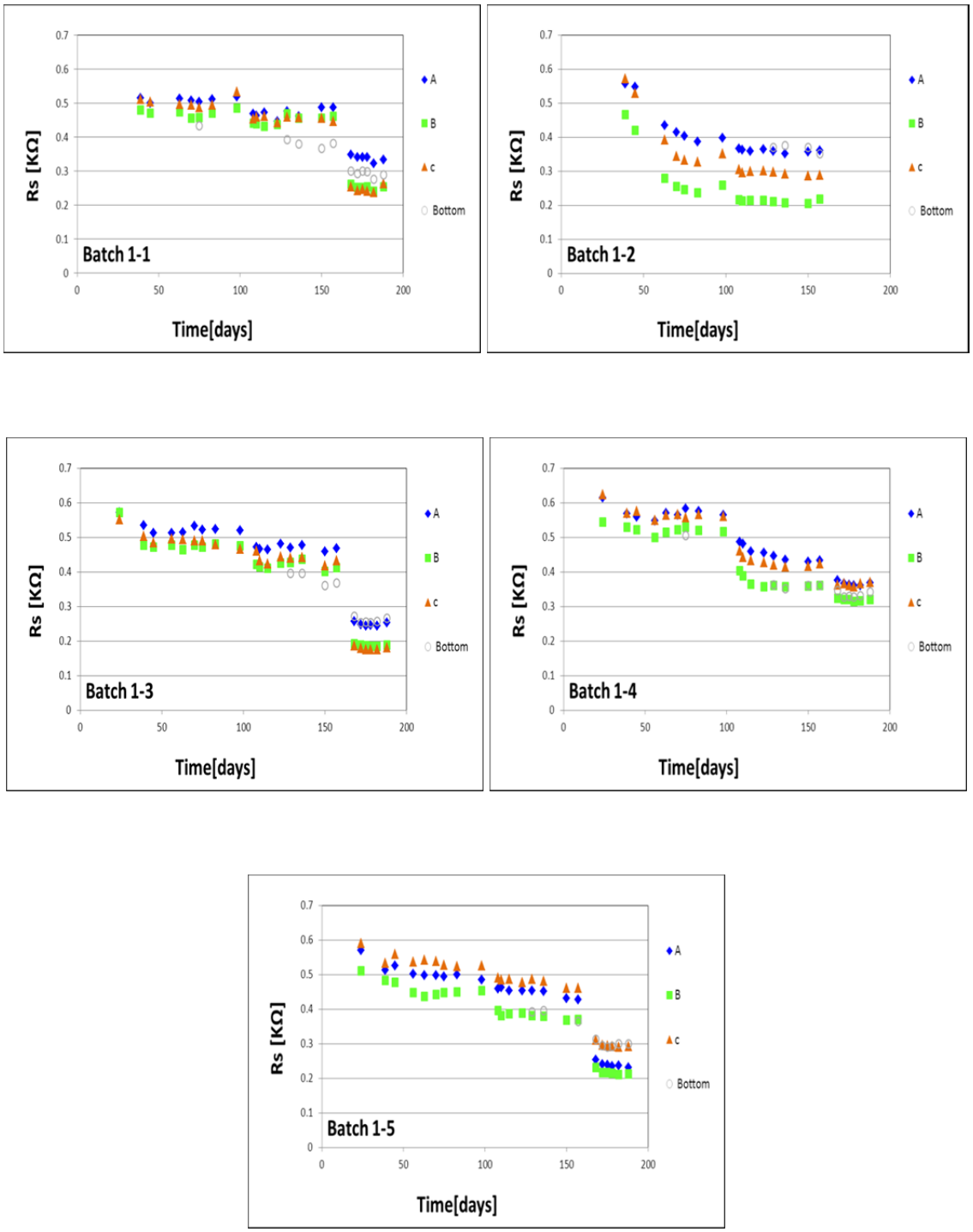

Figure D.6 Solution Resistance over time for samples batch 2 phase II

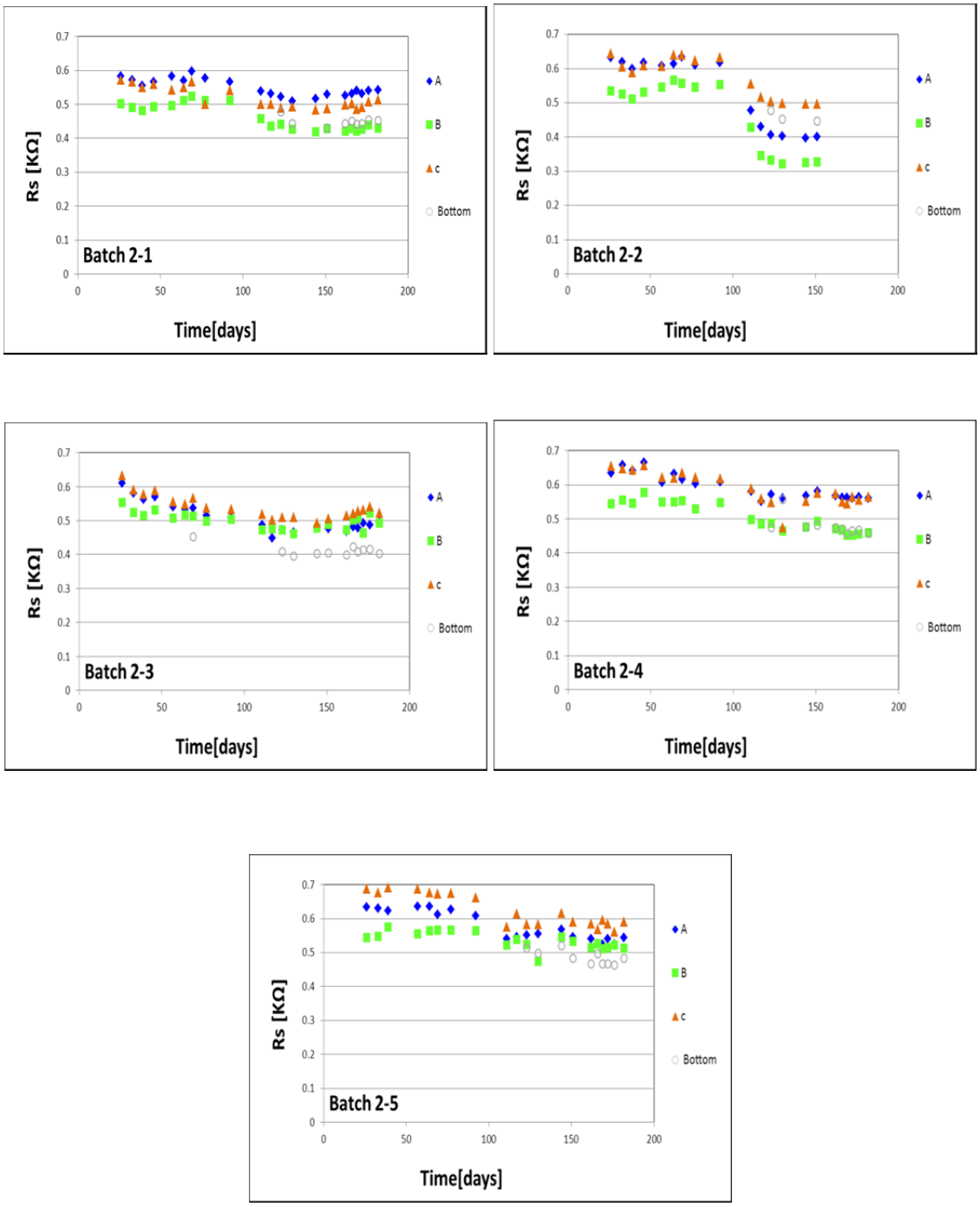

Figure D.7 Rc (Rp_meas-Rs) over time for batch 1 samples at Phase II

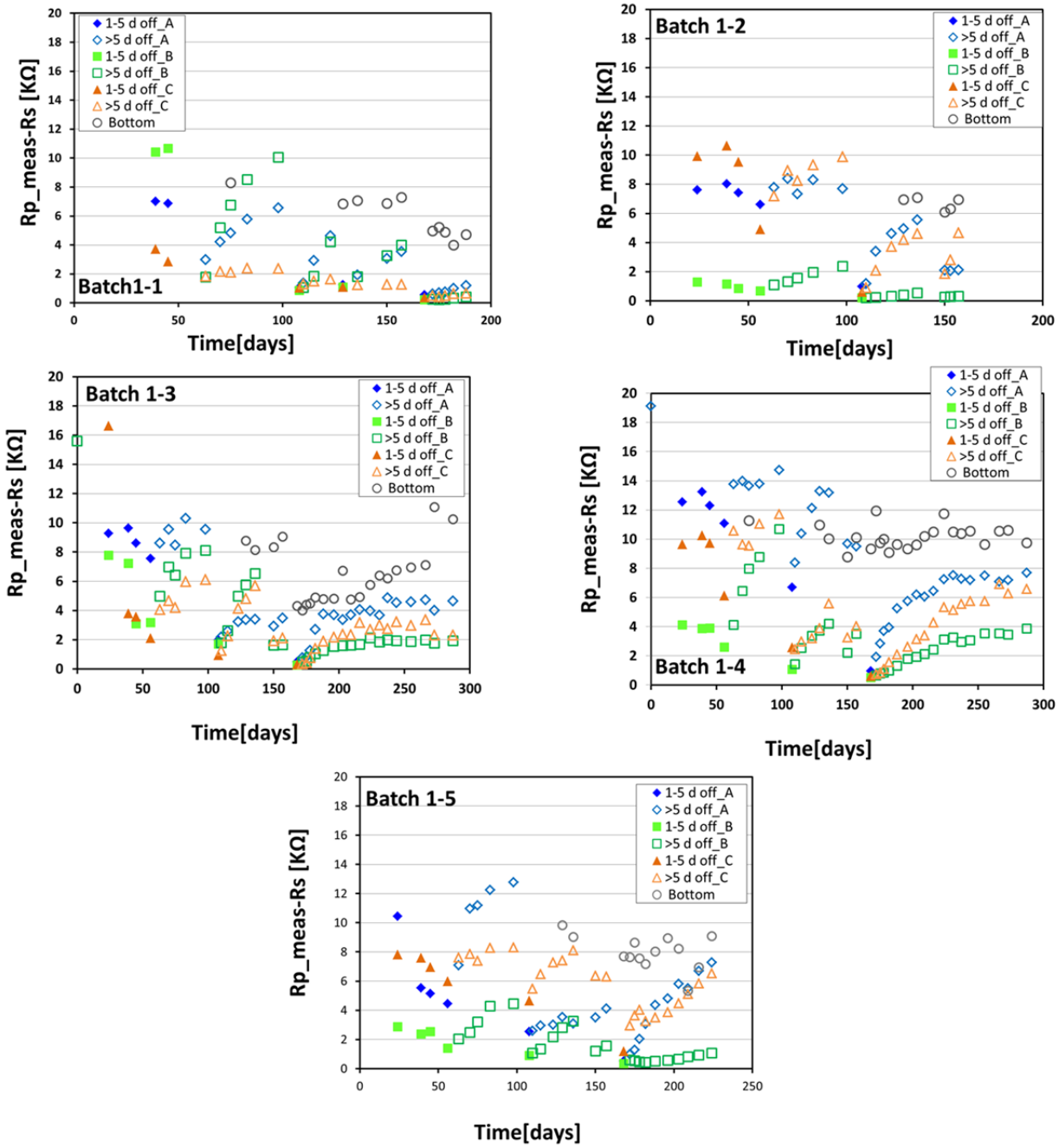

Figure D.8 Rc (Rp_meas-Rs) over time for batch 2 samples at Phase II

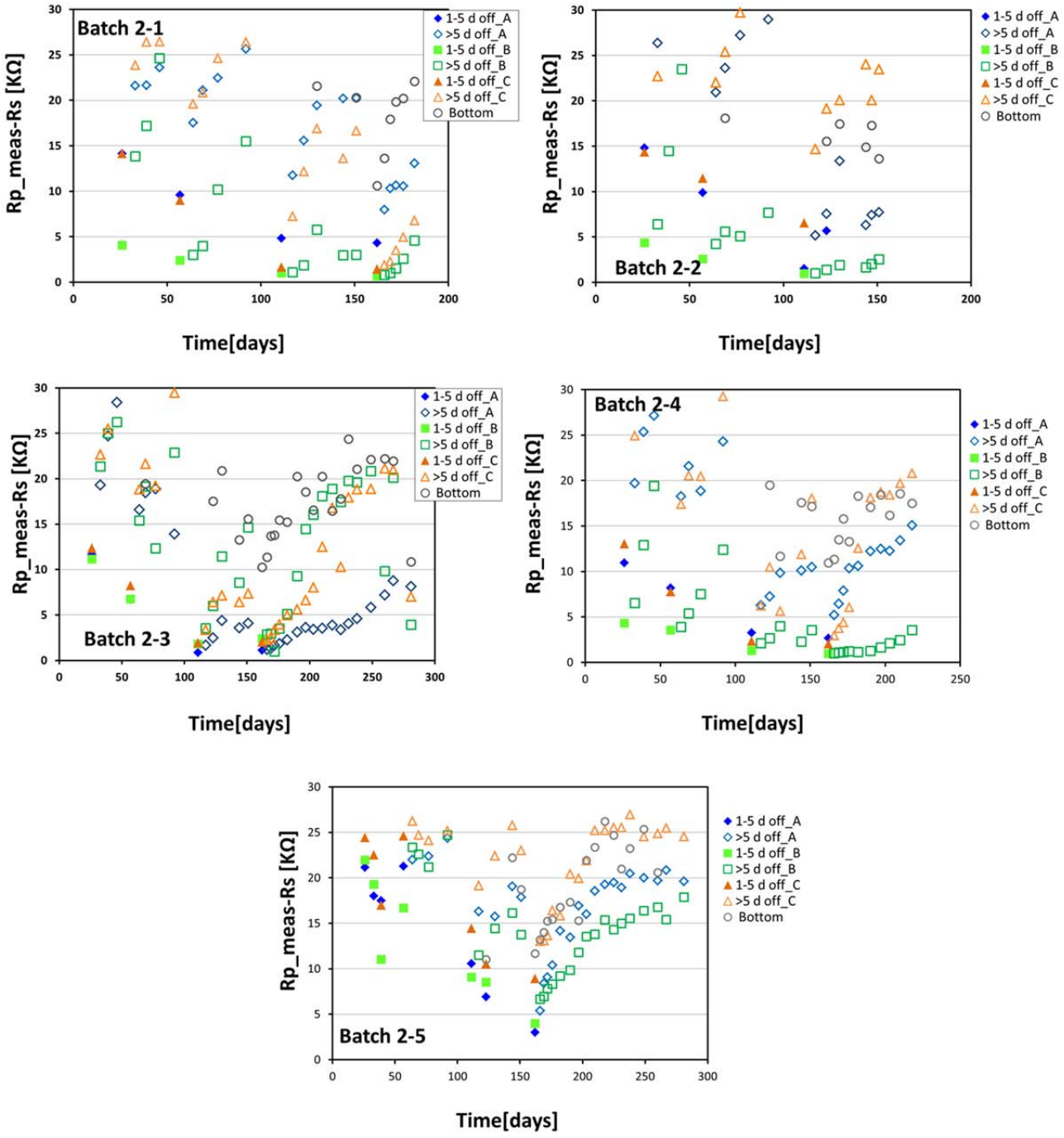

Figure D.9 Crack by inspection day for batch 1 and 2 (multiple pages)

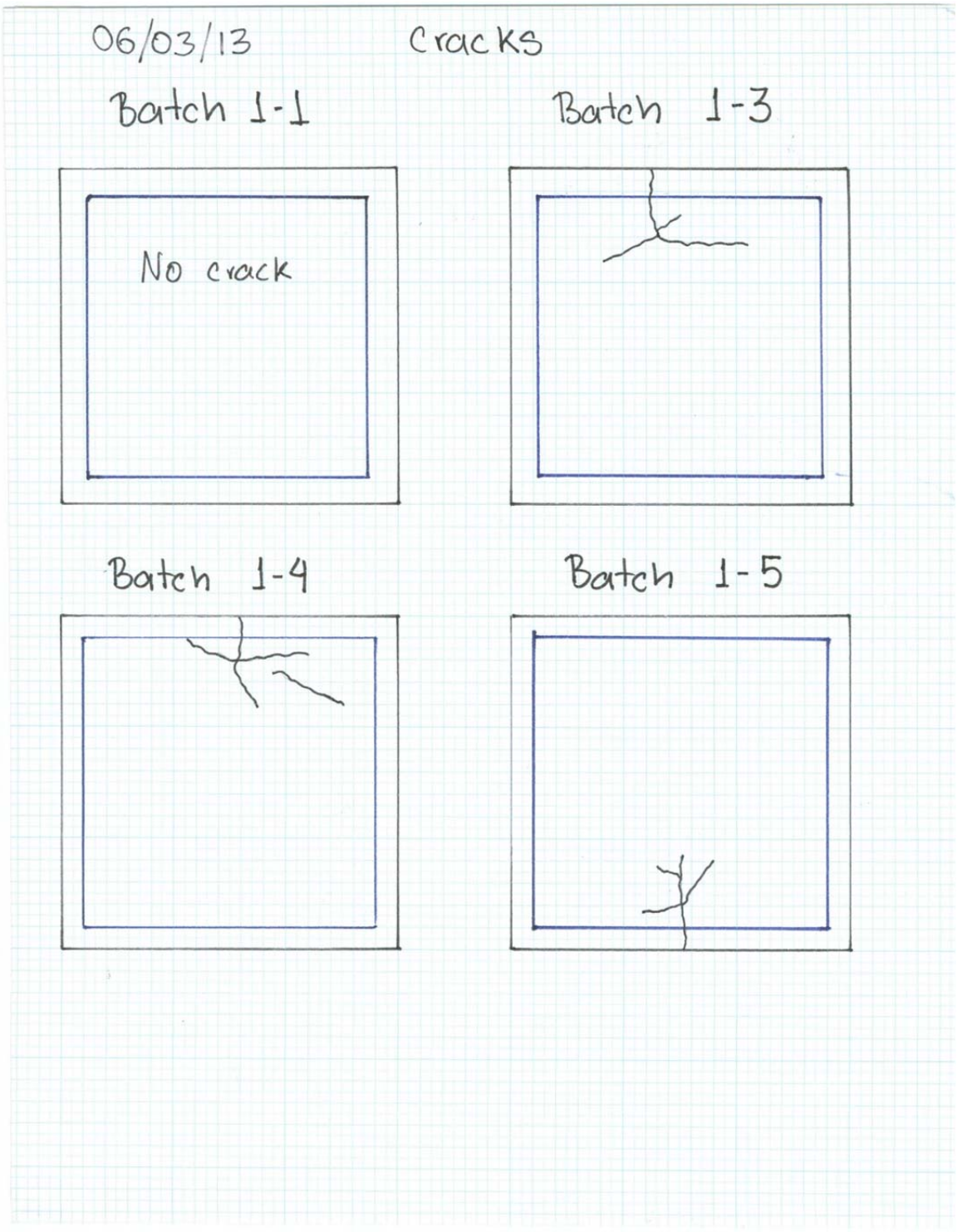

Figure D.9 Continue

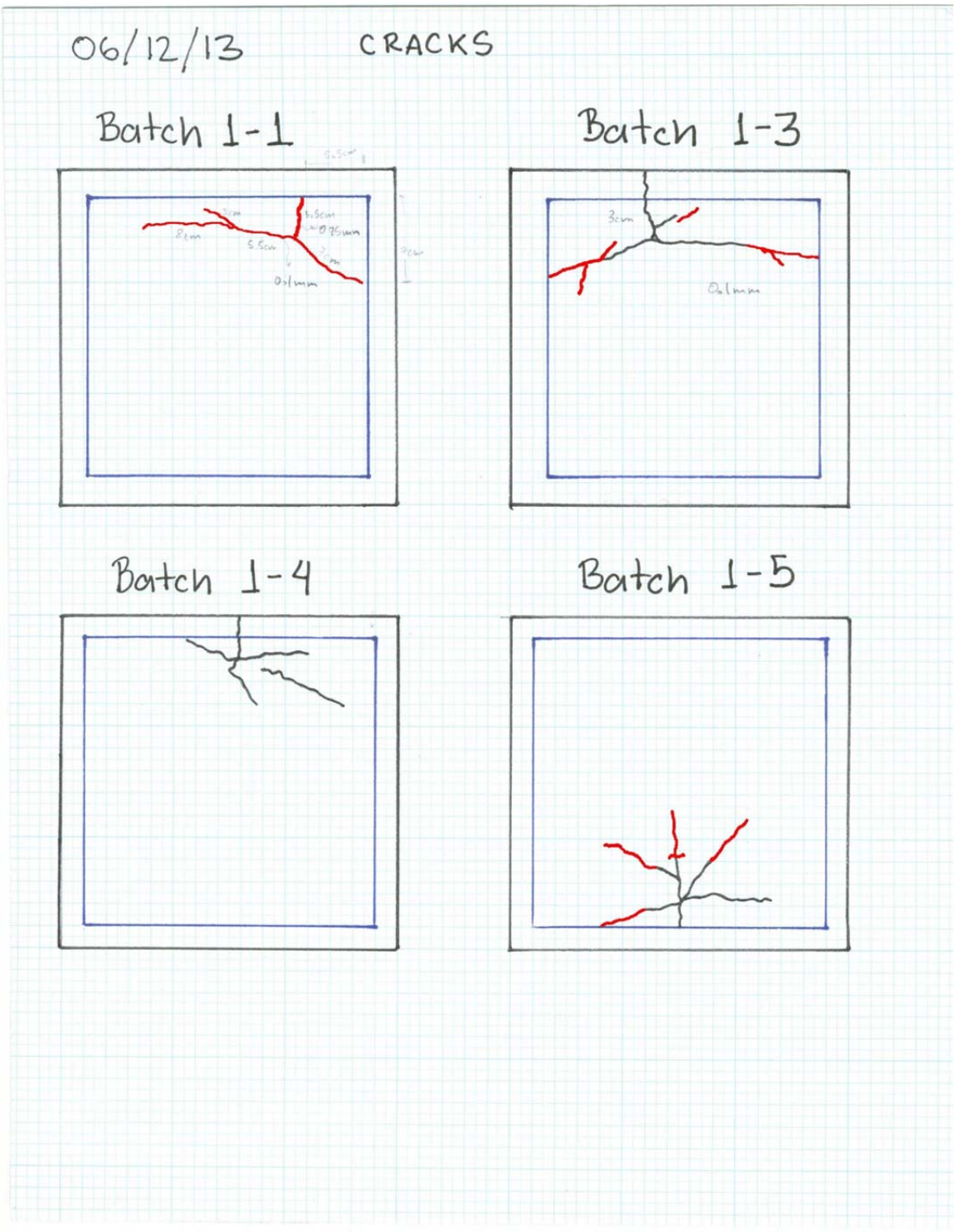

Figure D.9 Continue

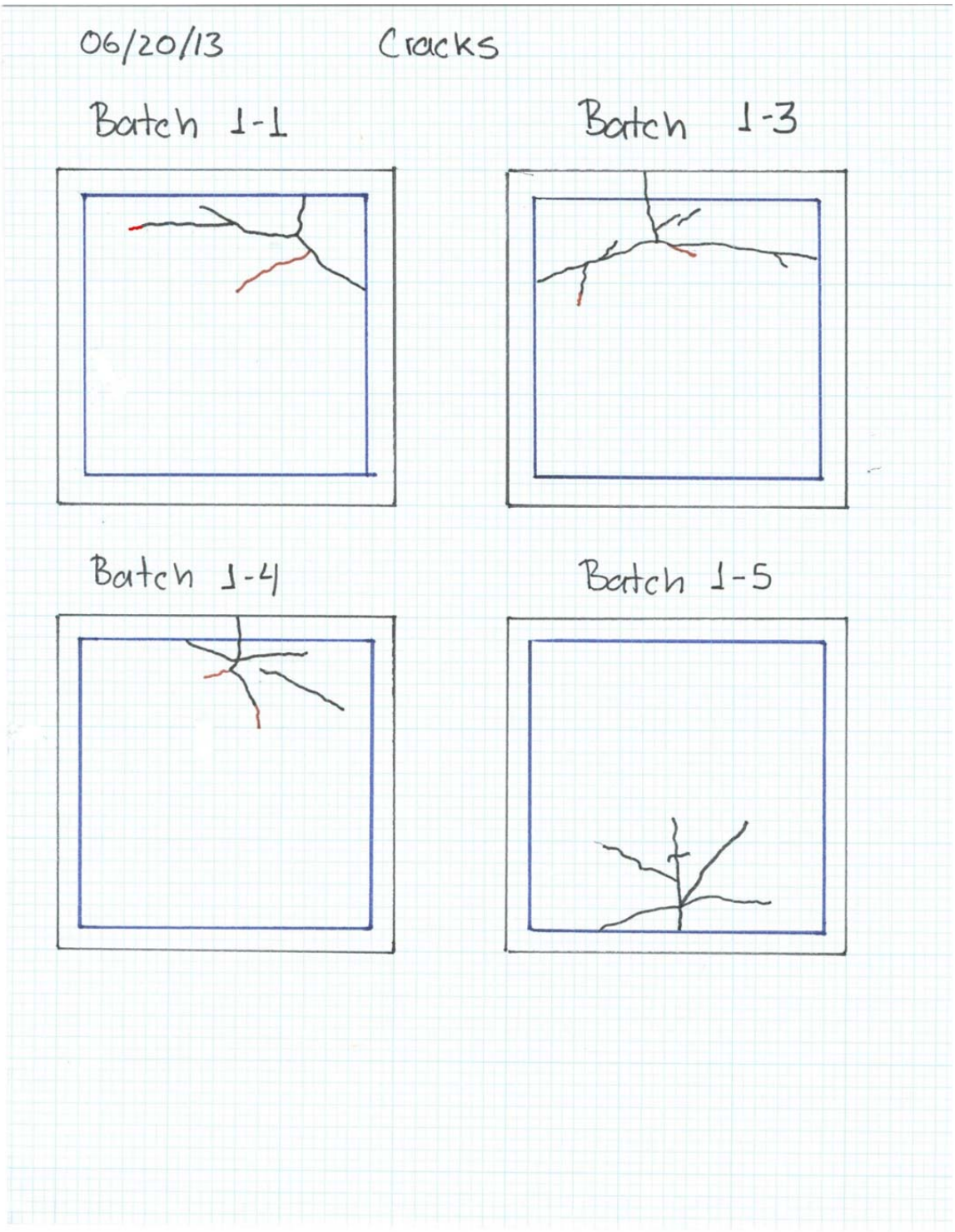

Figure D.9 Continue

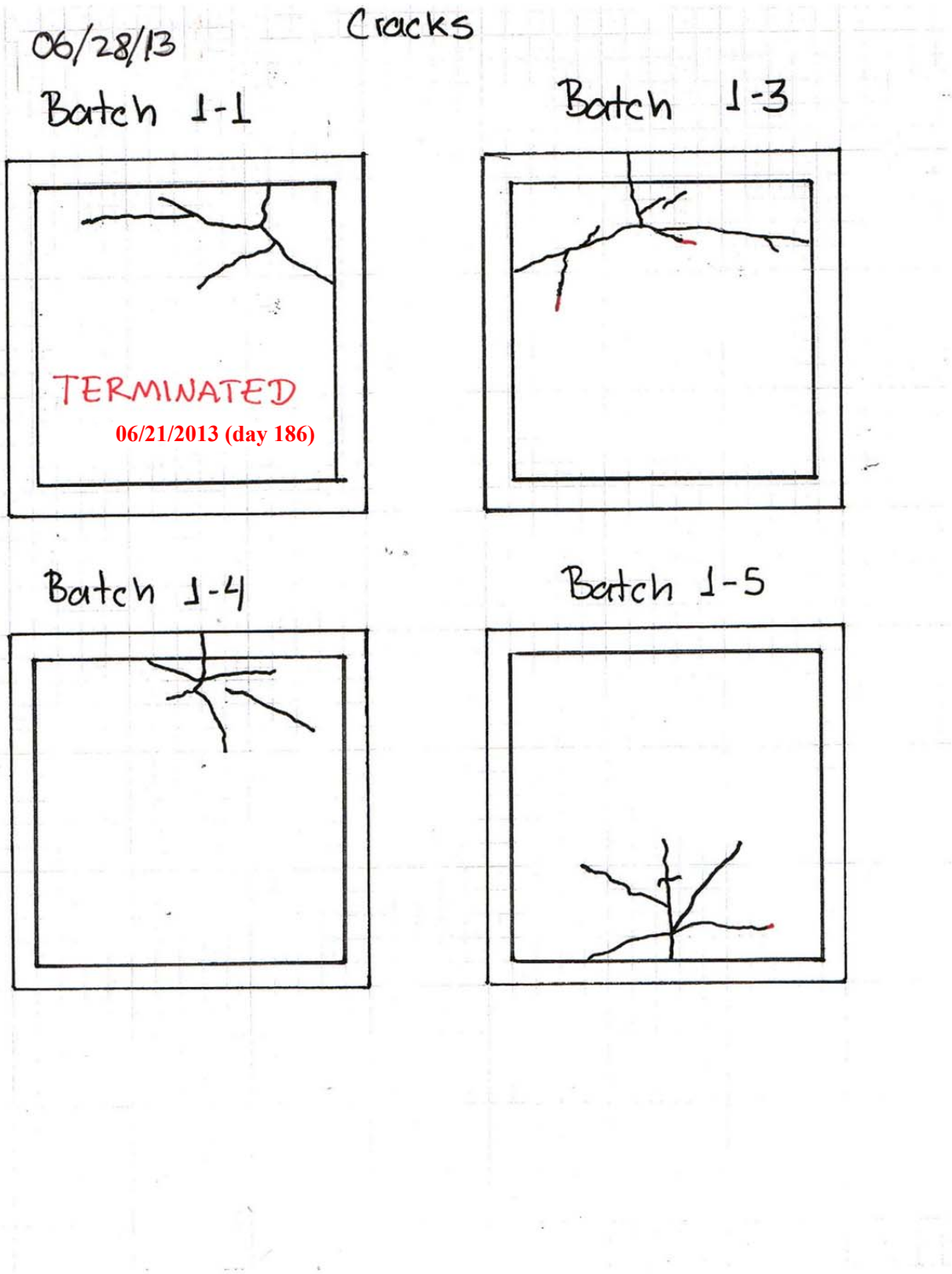

Figure D.9 Continue

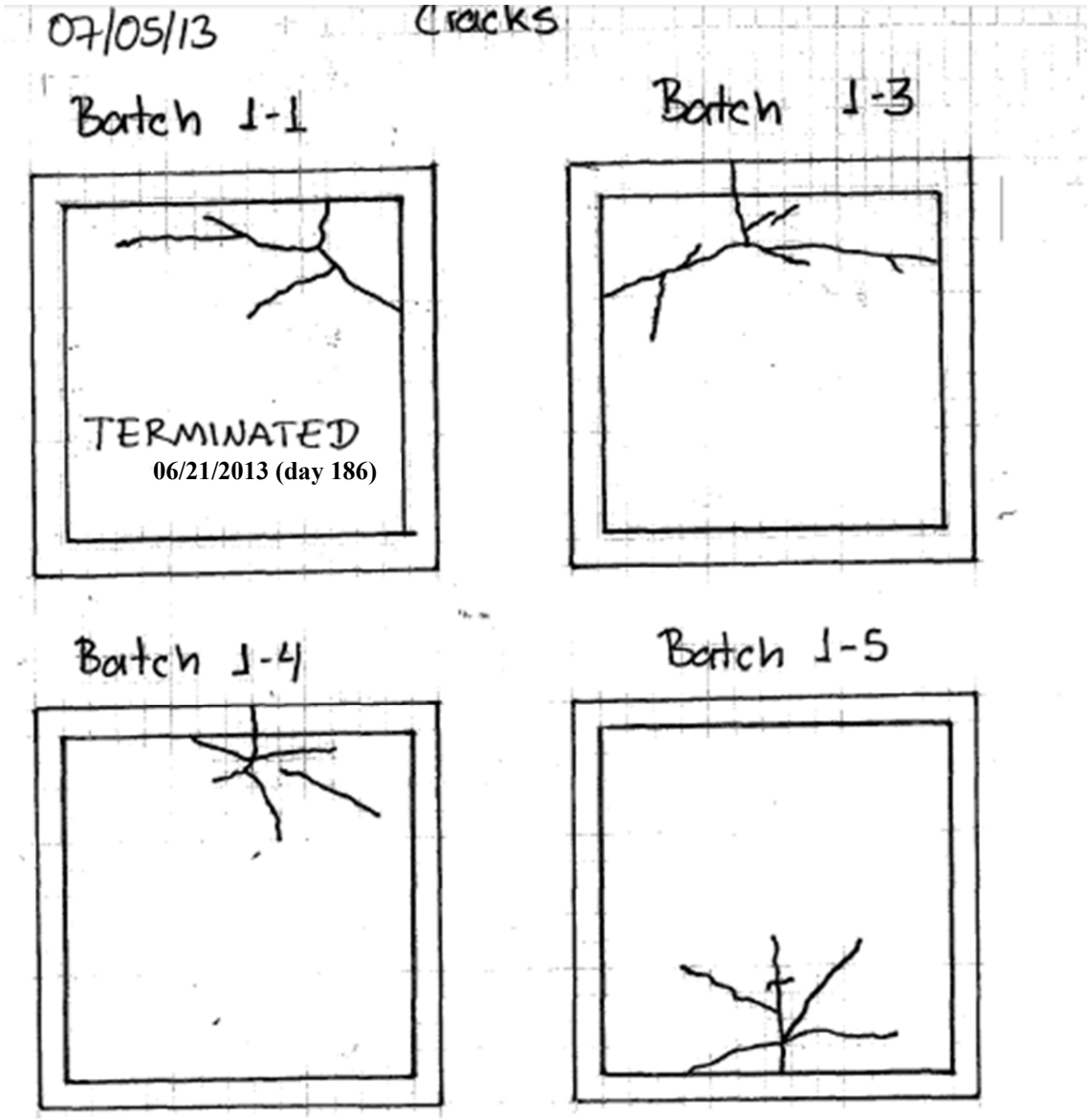

Figure D.9 Continue

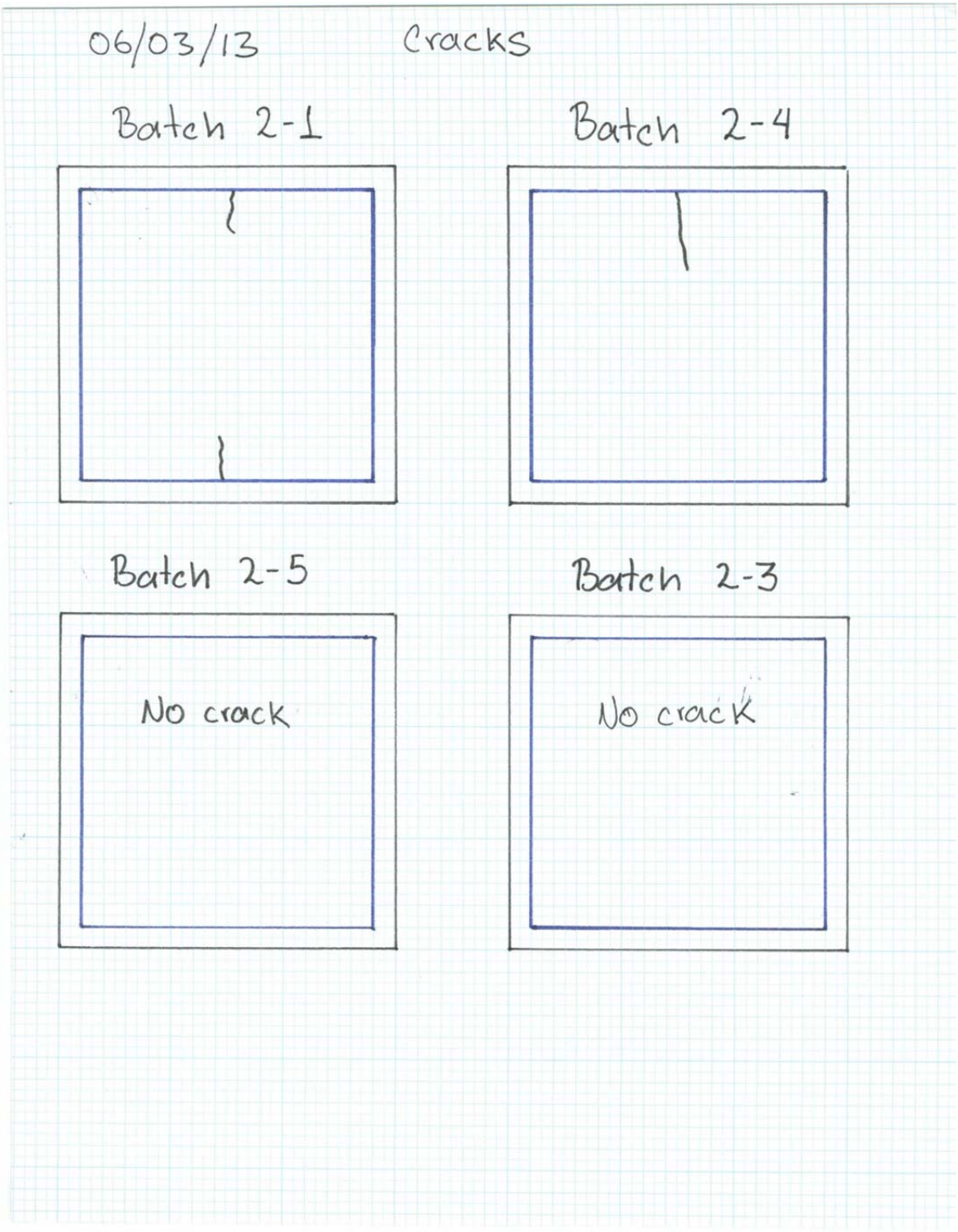

Figure D.9 Continue

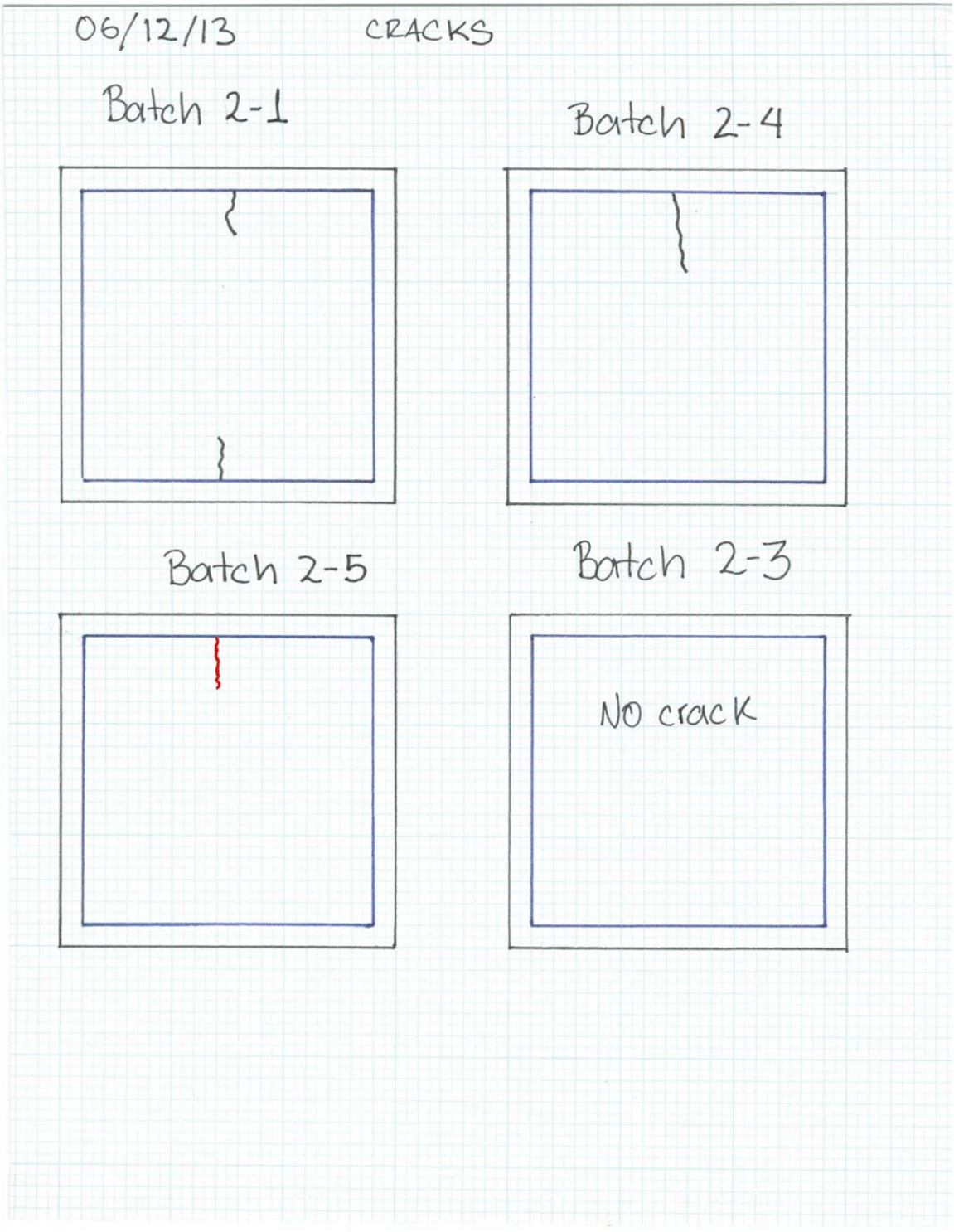

Figure D.9 Continue

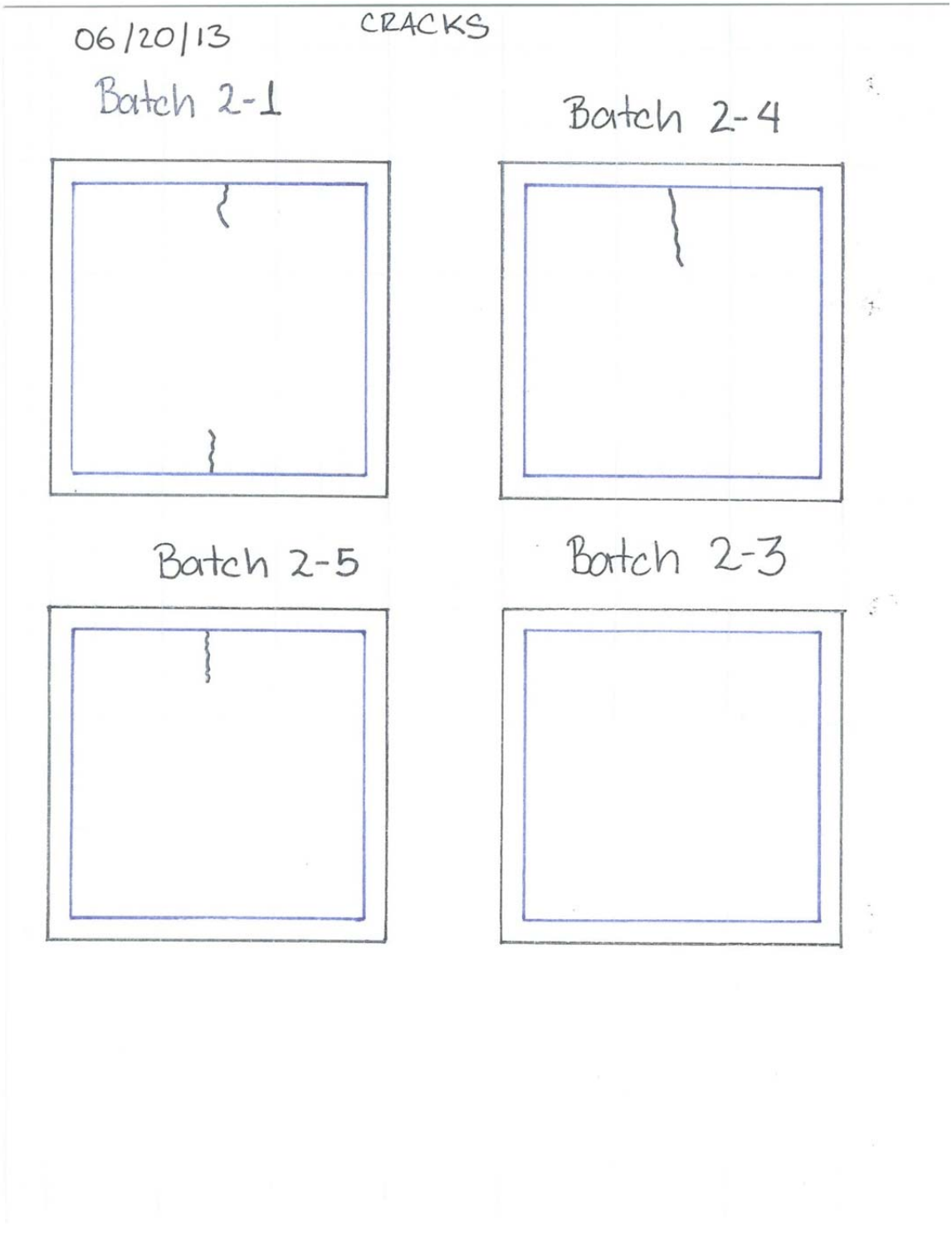

Figure D.9 Continue

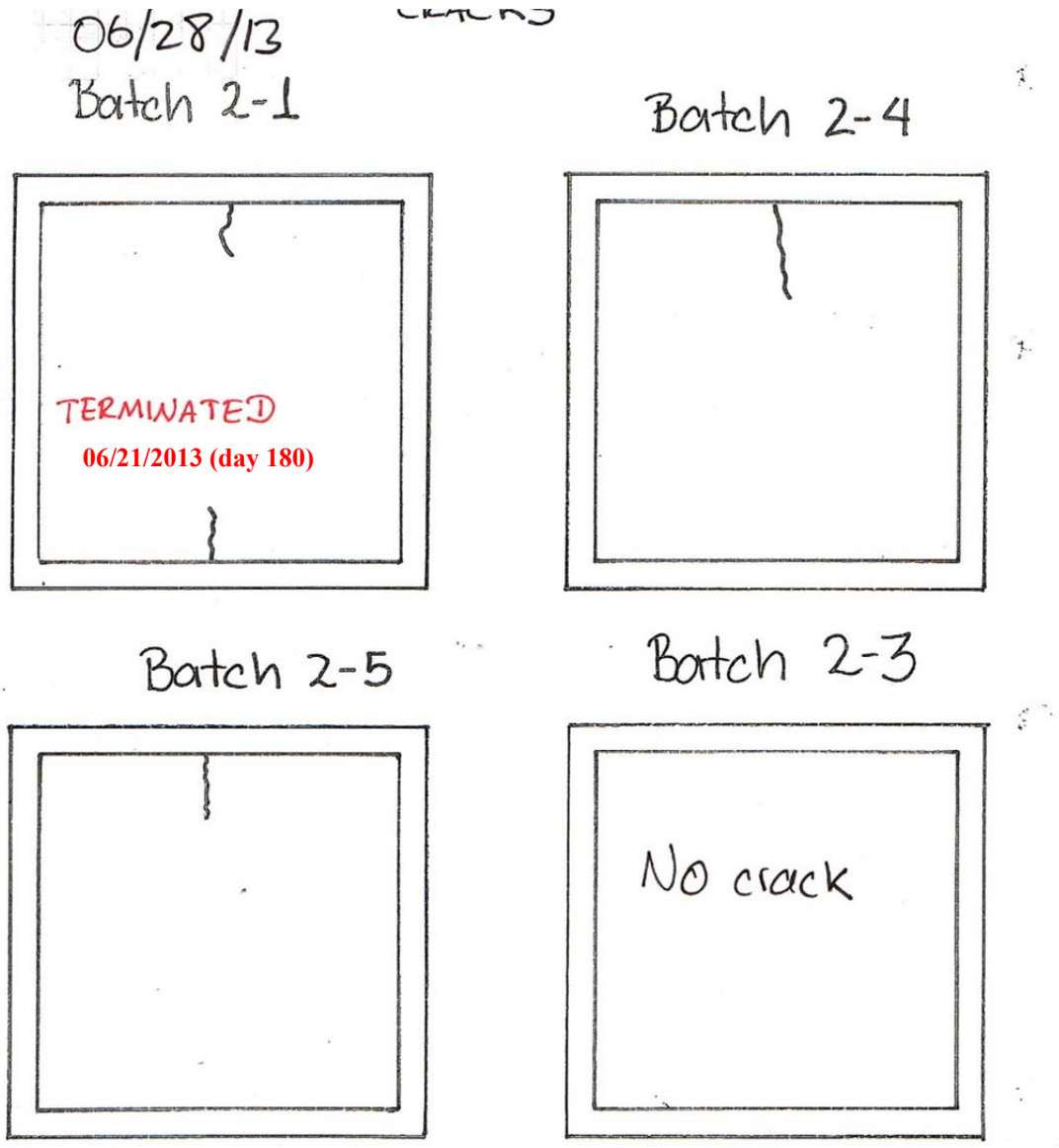

Figure D.9 Continue

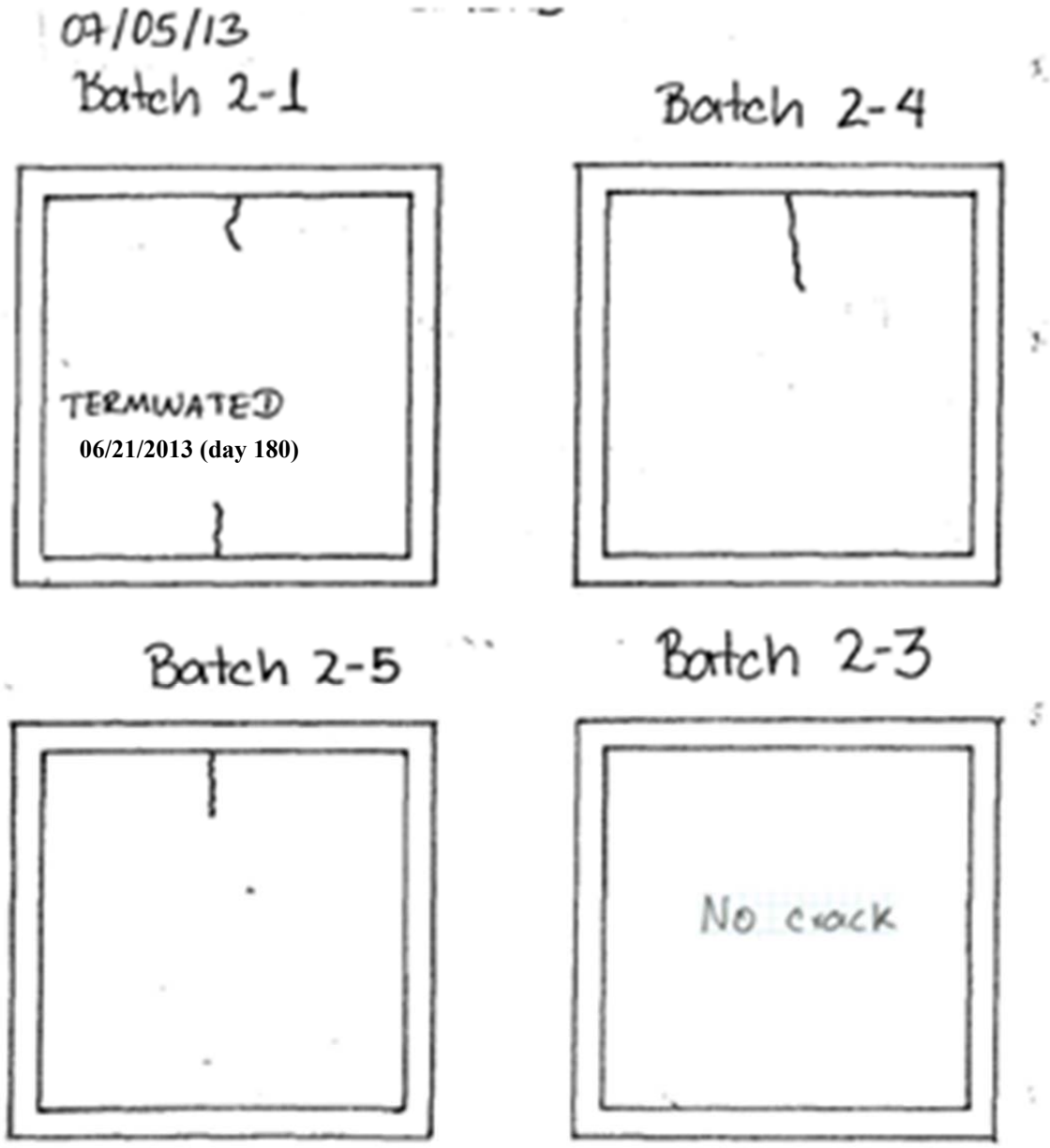

Figure D.9 Continue

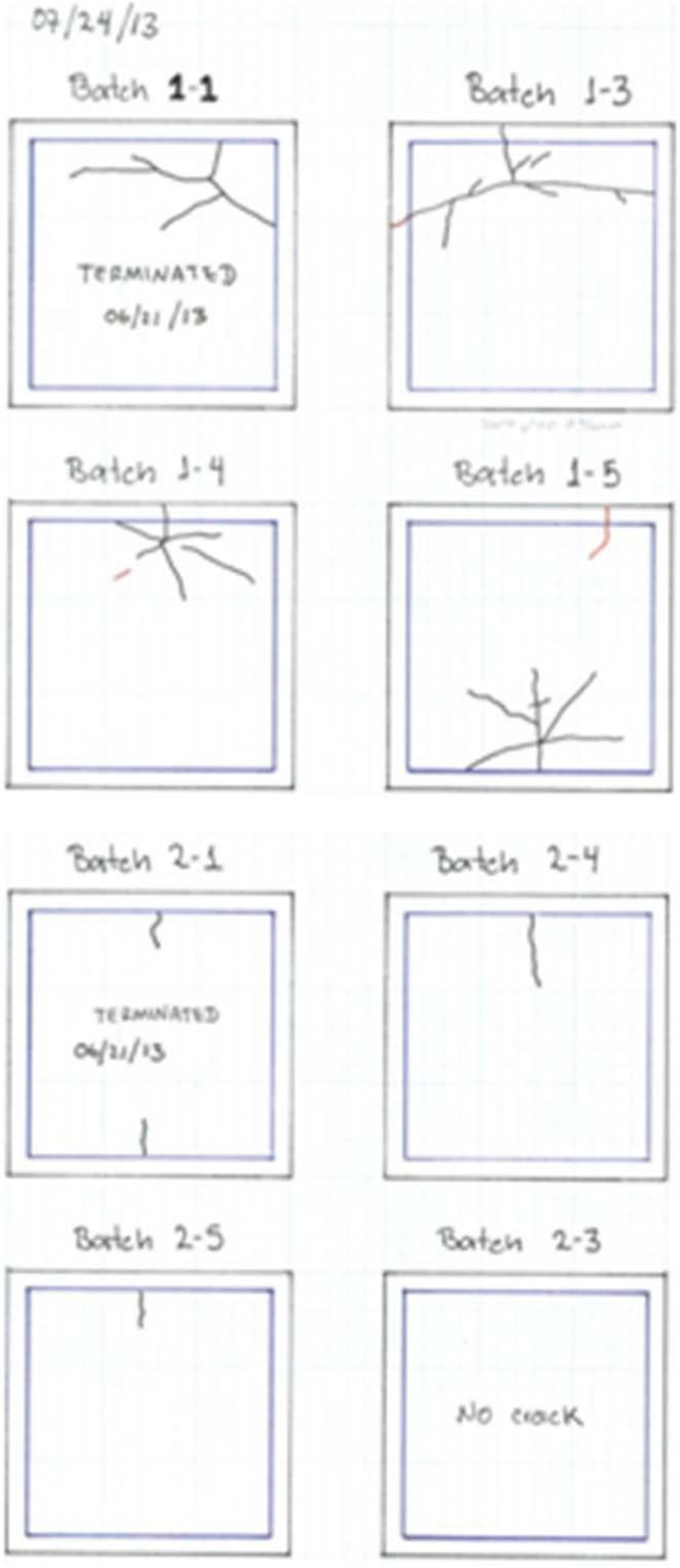

Figure D.9 Continue

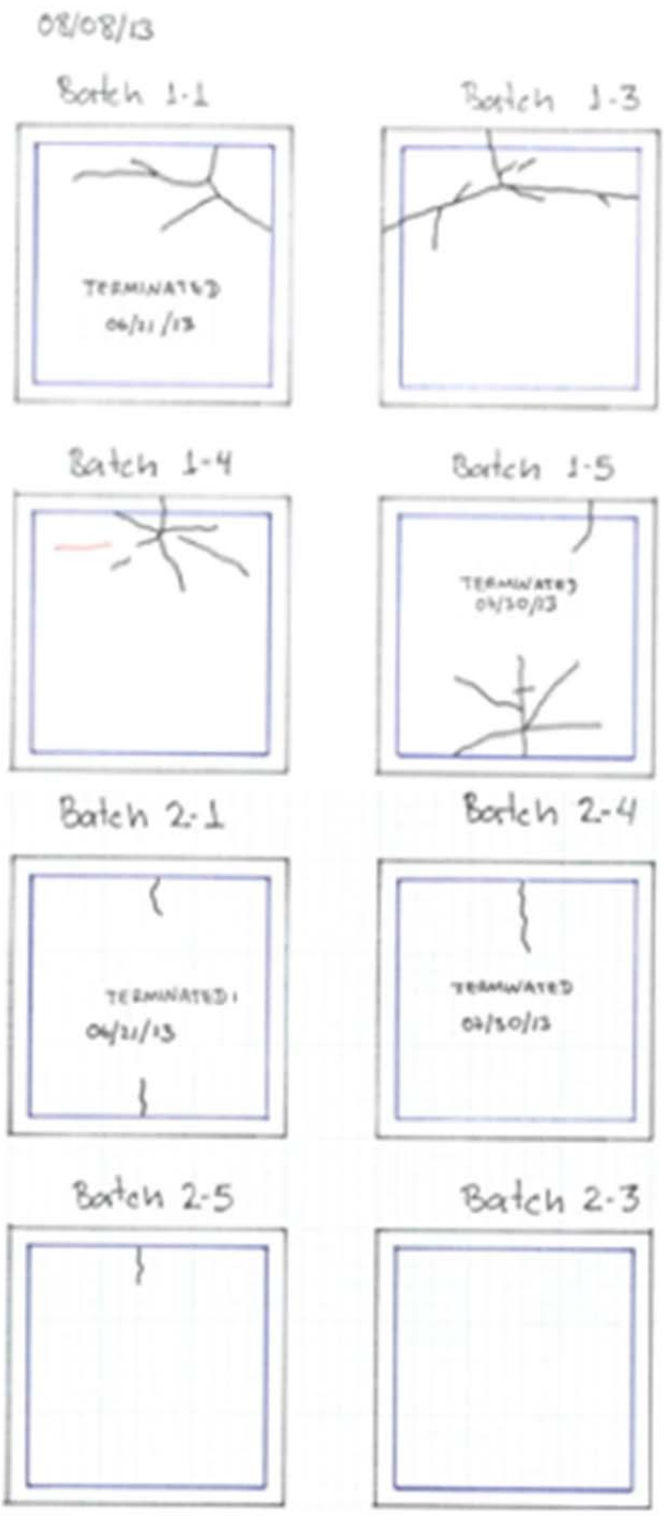

Figure D.9 Continue

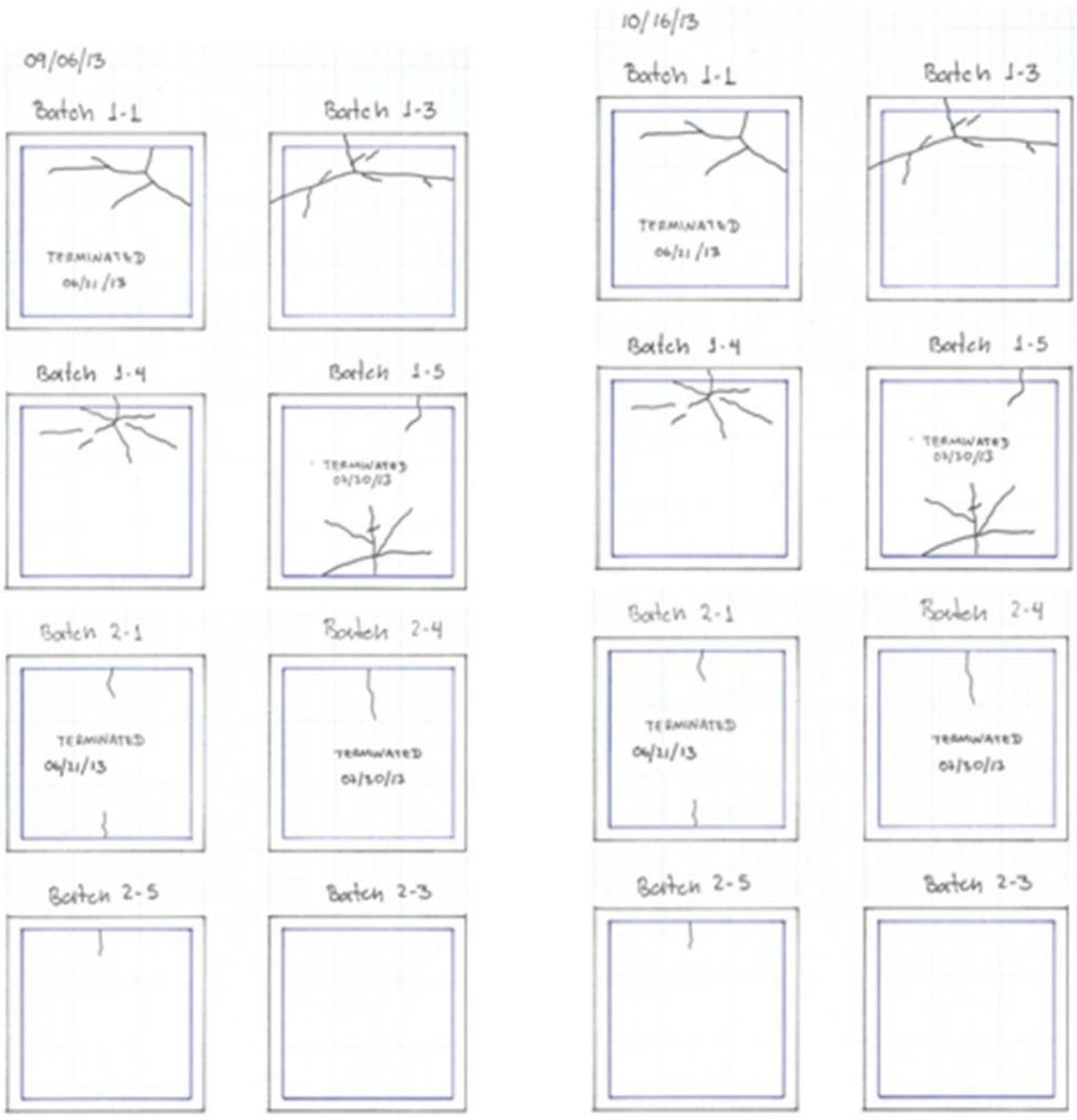

Figure D.10 Autopsy and visual examination of bottom rebars batch 1-1

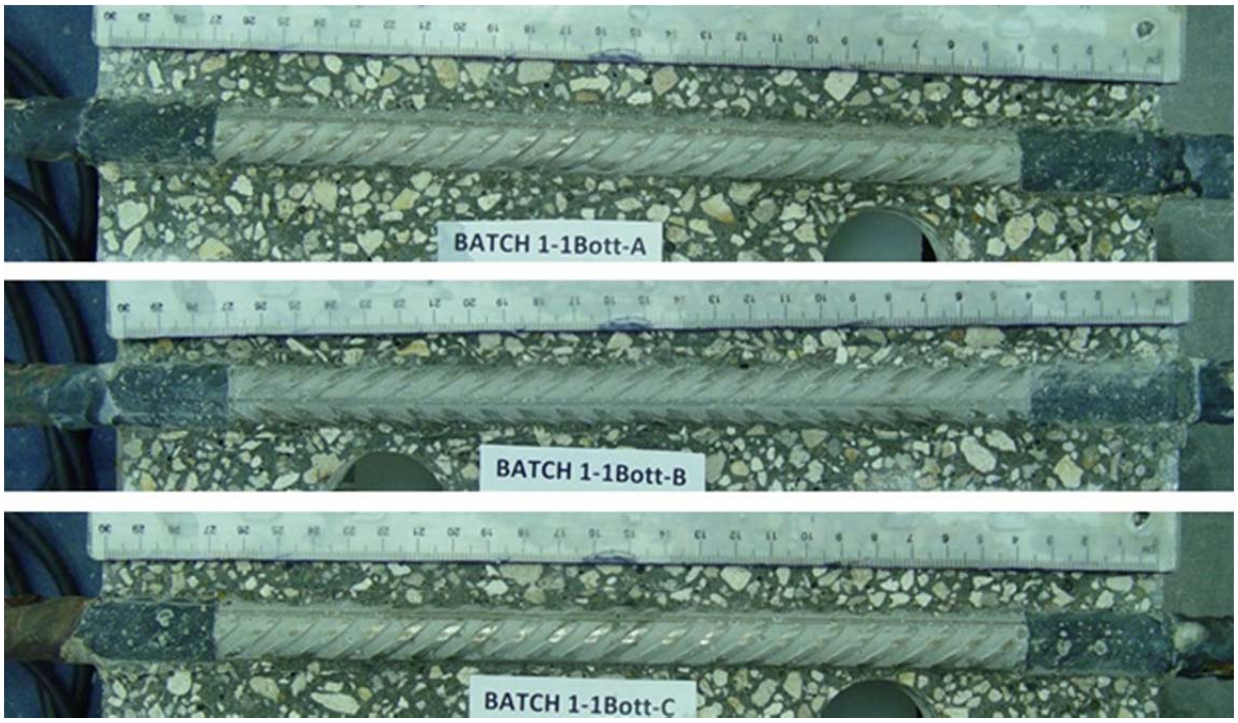

Figure D.11 Close-up picture of sample batch 1-1A rebar before and after cleaning

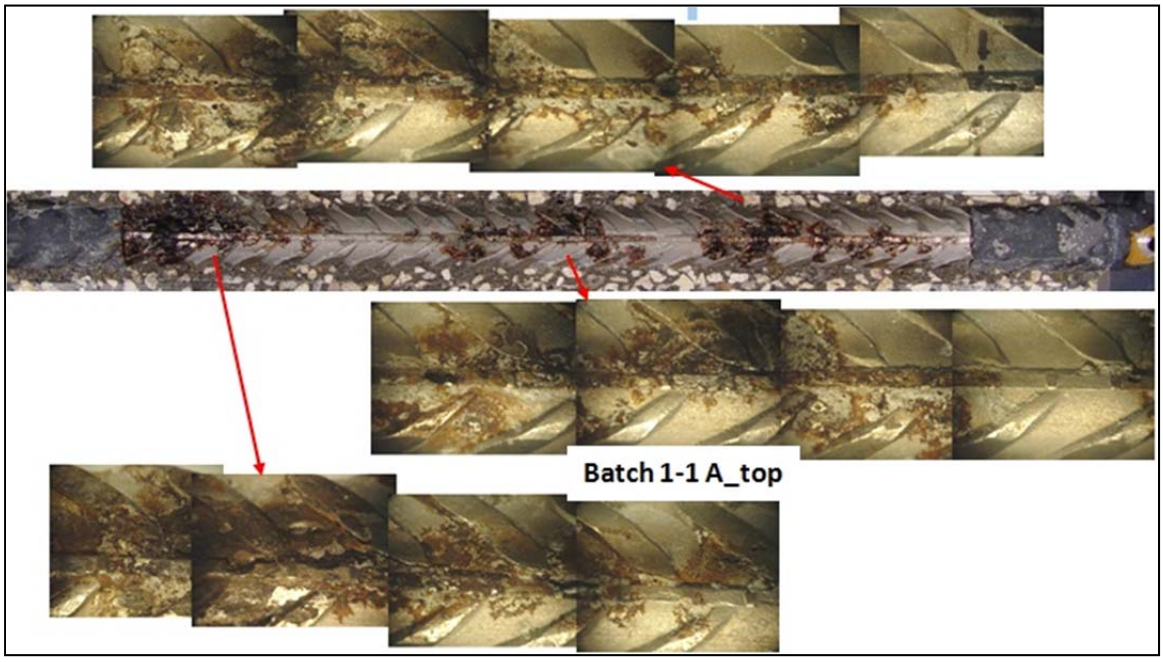

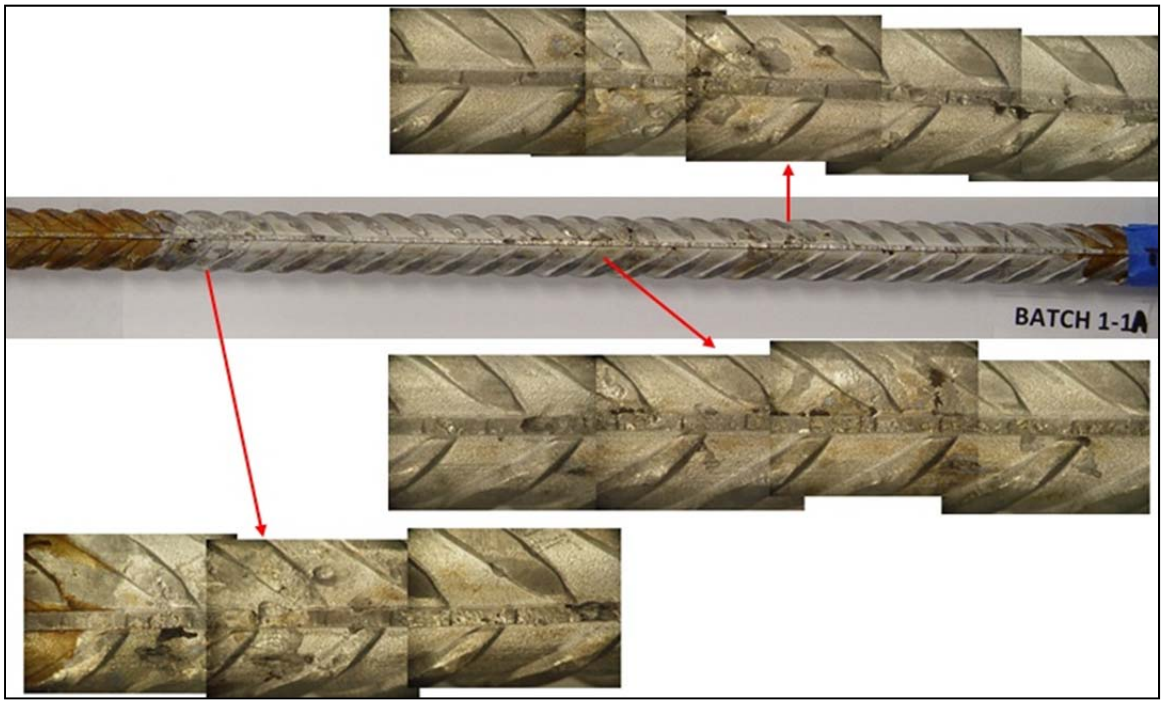

Figure D.12 Close-up picture of sample batch 1-1C rebar before and after cleaning

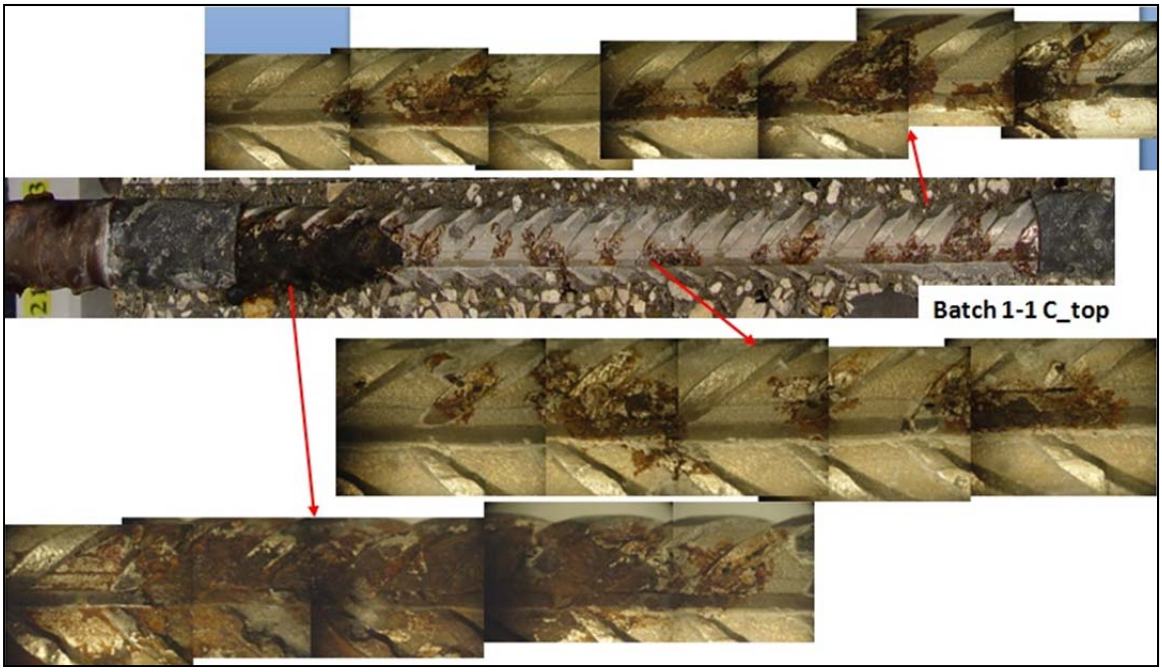

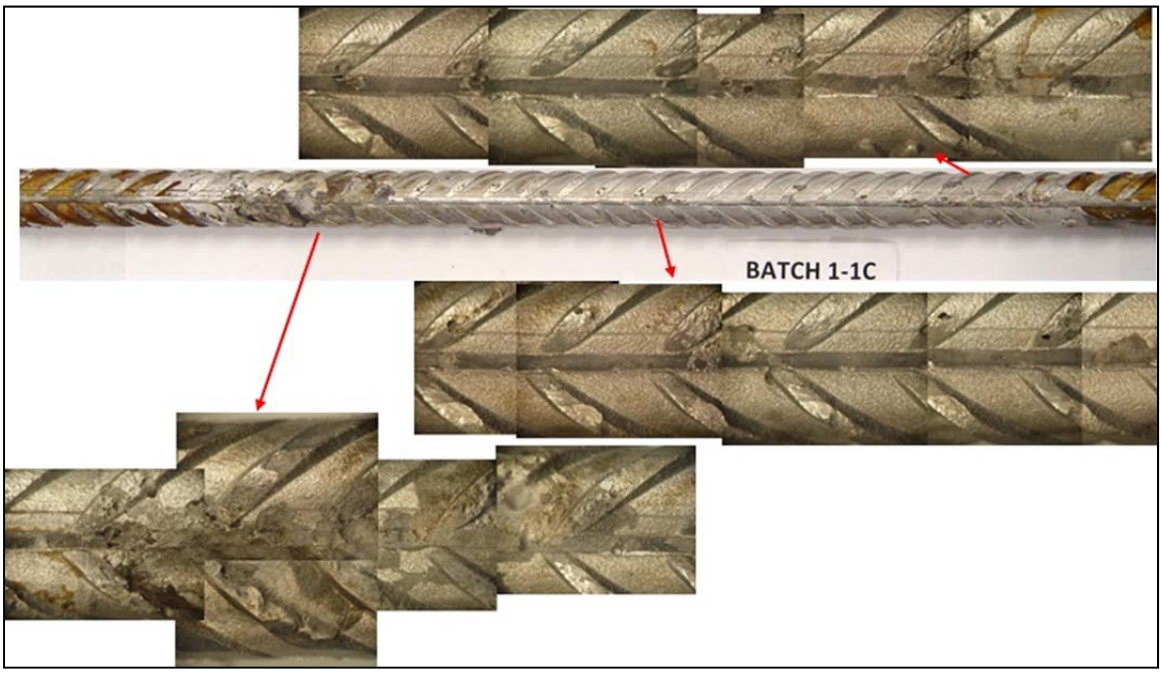

Figure D.13 Autopsy and visual examination of bottom rebars batch 1-2

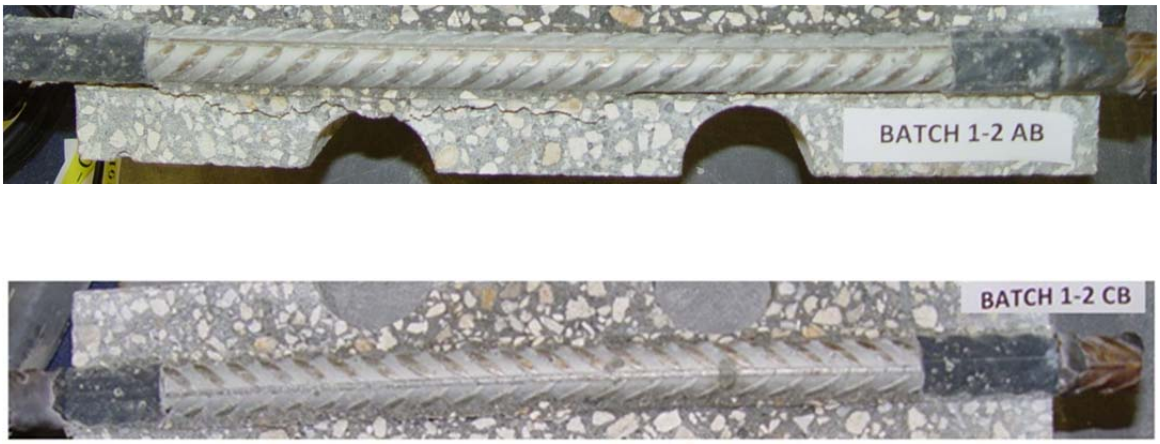

Figure D.14 Close-up pictures before and after cleaning for batch 1-2

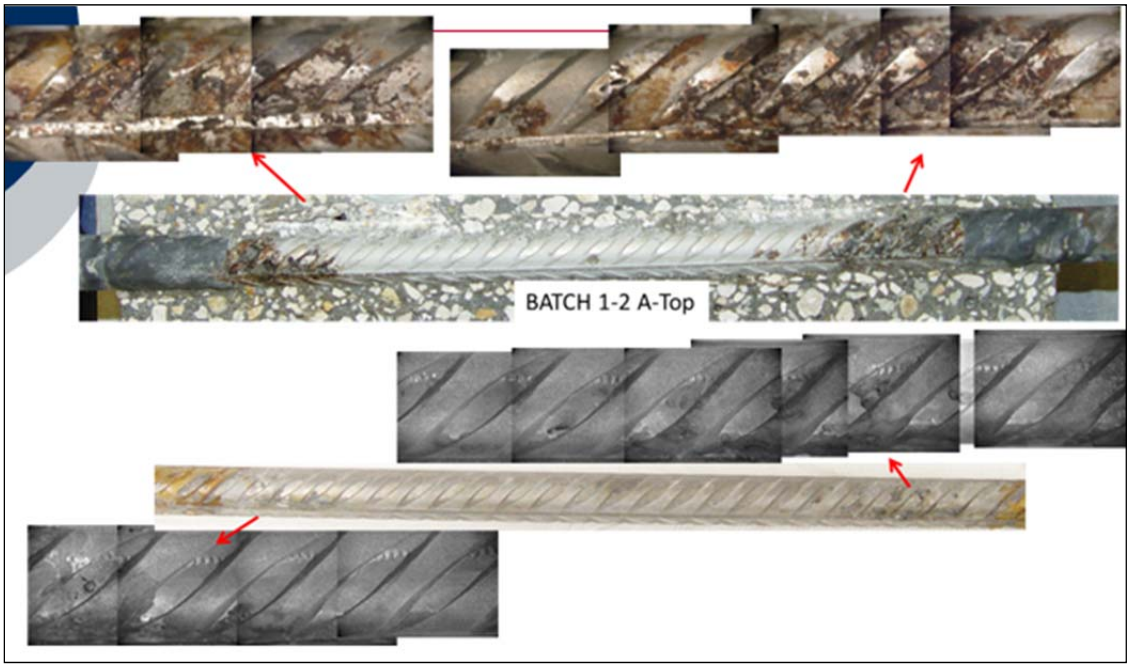

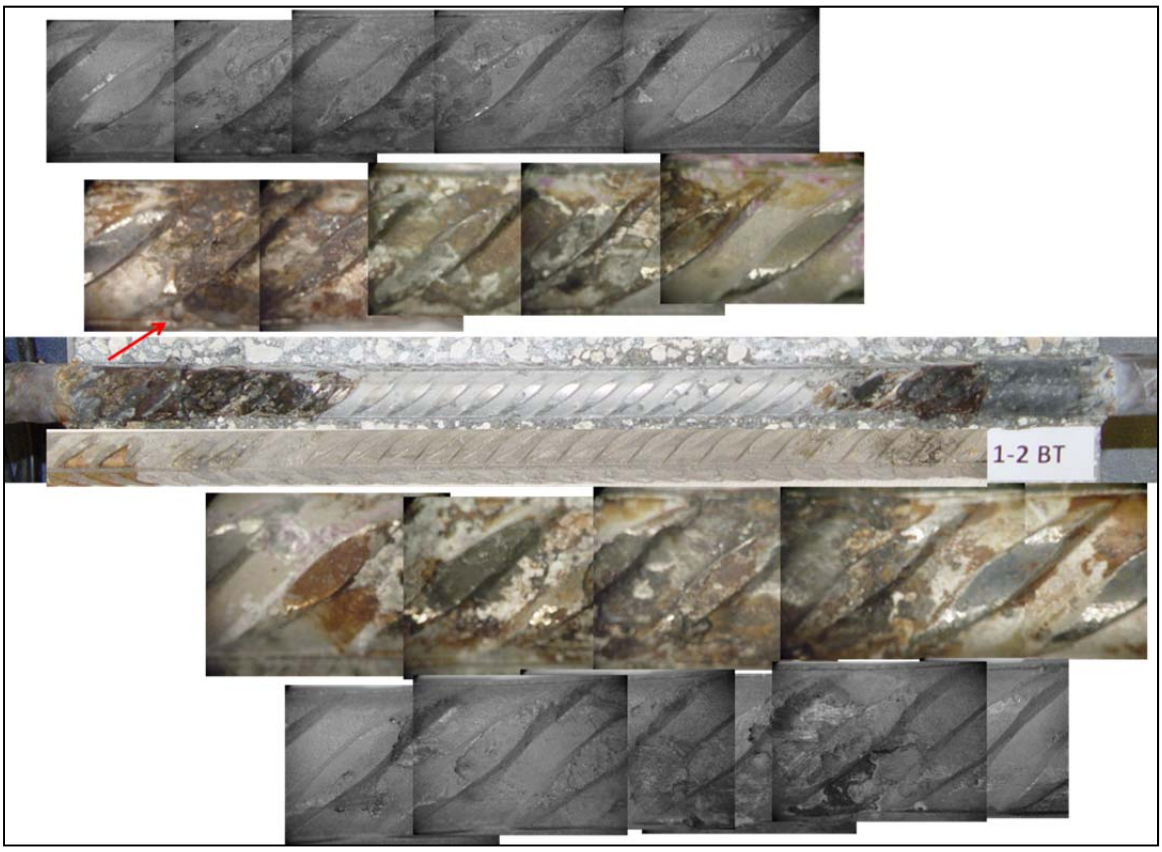

Figure D.14 Continue

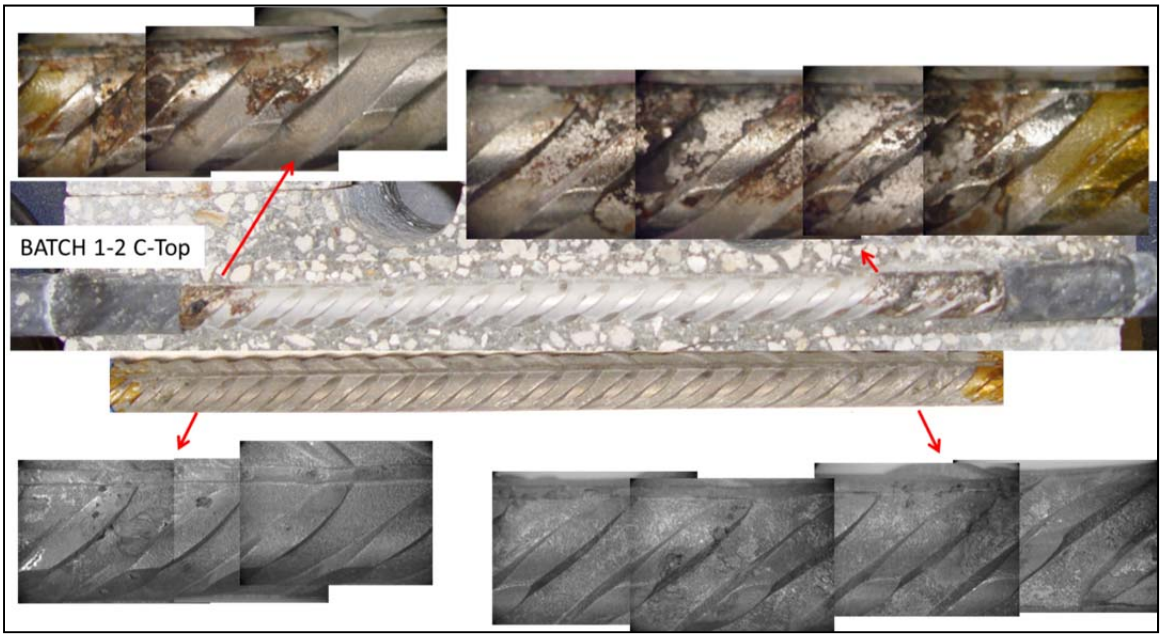

Figure D.15 Close-up pictures before and after cleaning for batch 1-5

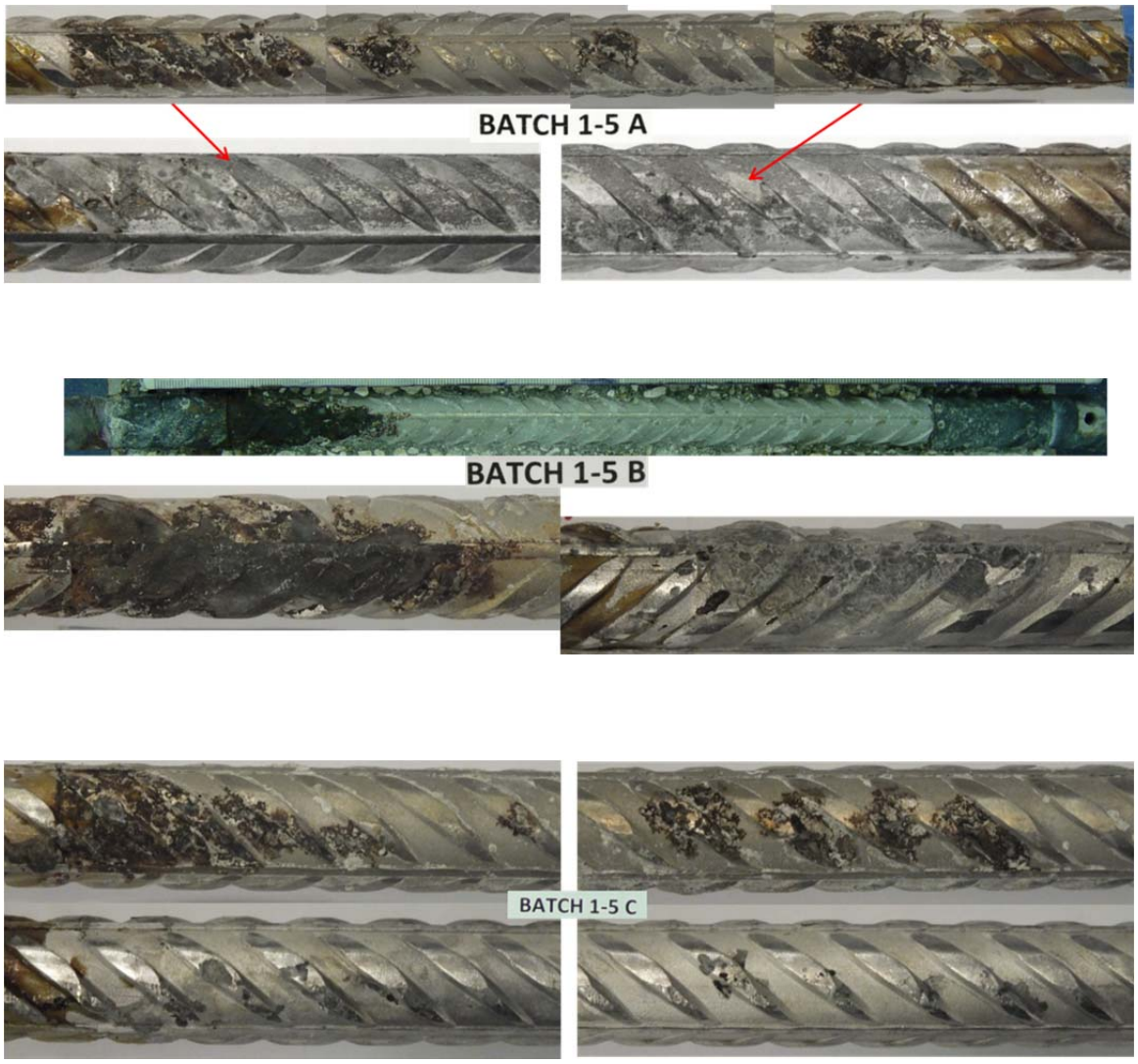

Figure D.16 Autopsy and visual examination of bottom rebars batch 2-1

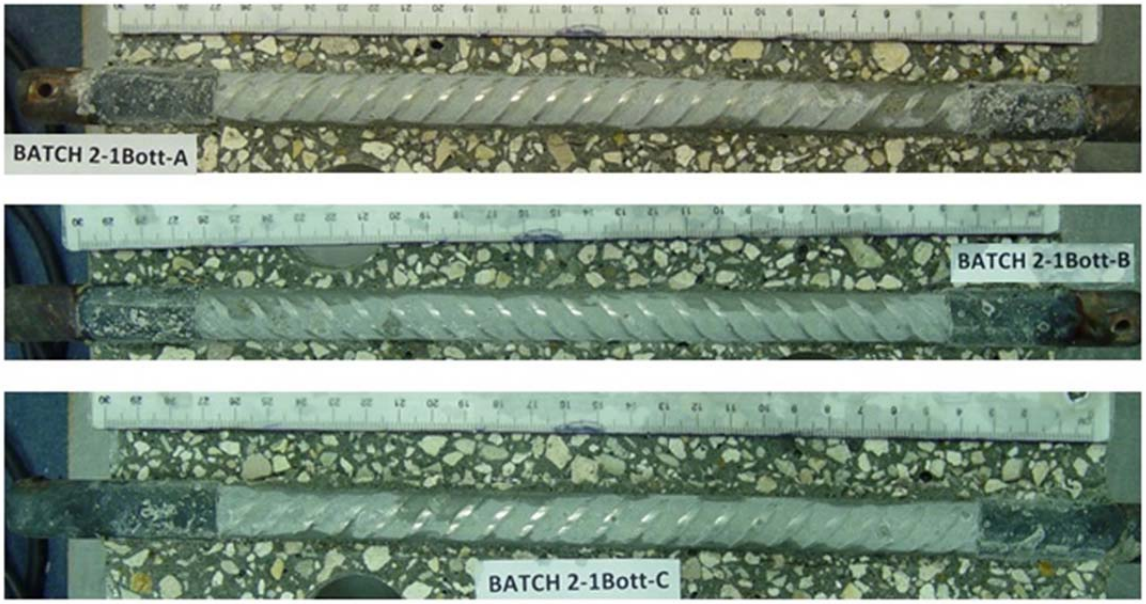

Figure D.17 Close-up pictures before and after cleaning for batch 2-1

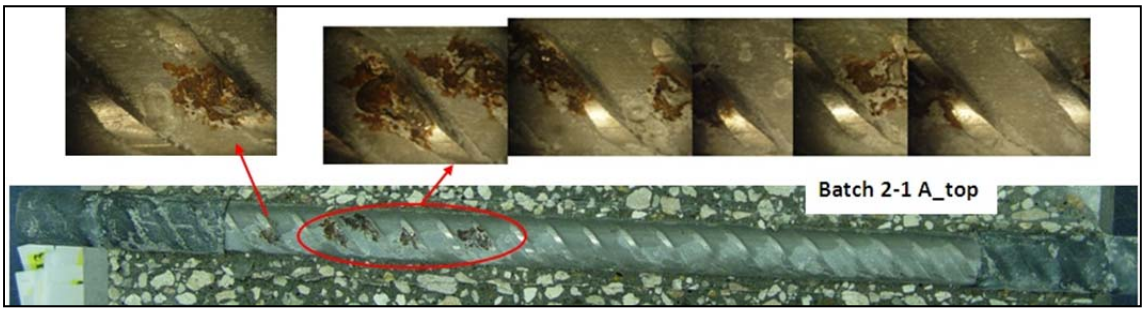

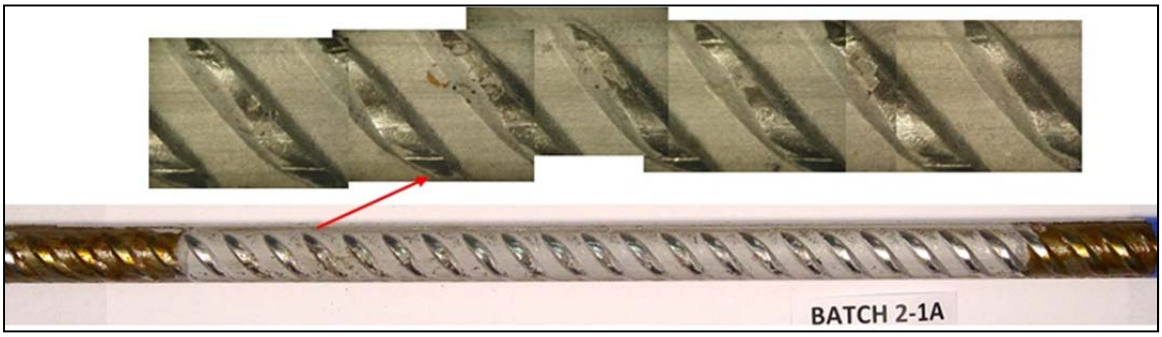

Figure D.17 Continue

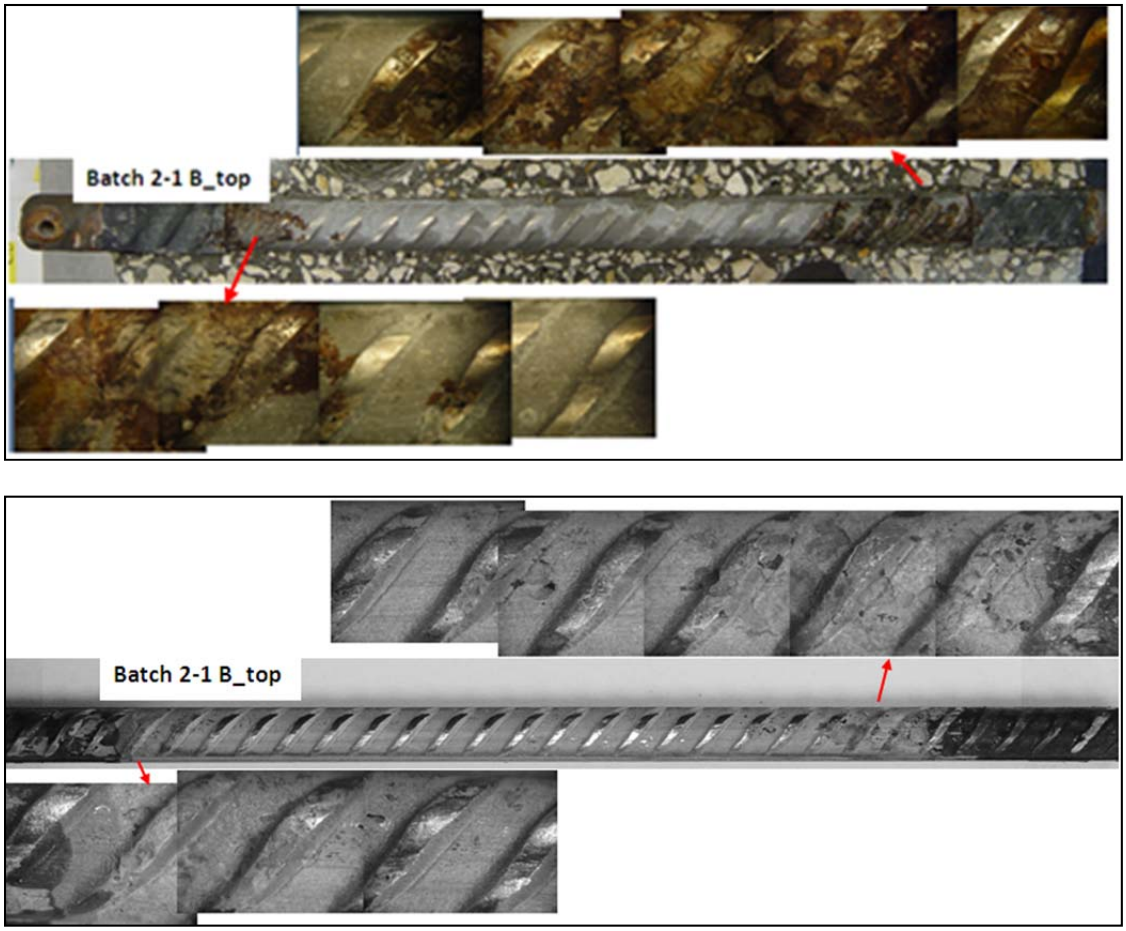

Figure D.17 Continue

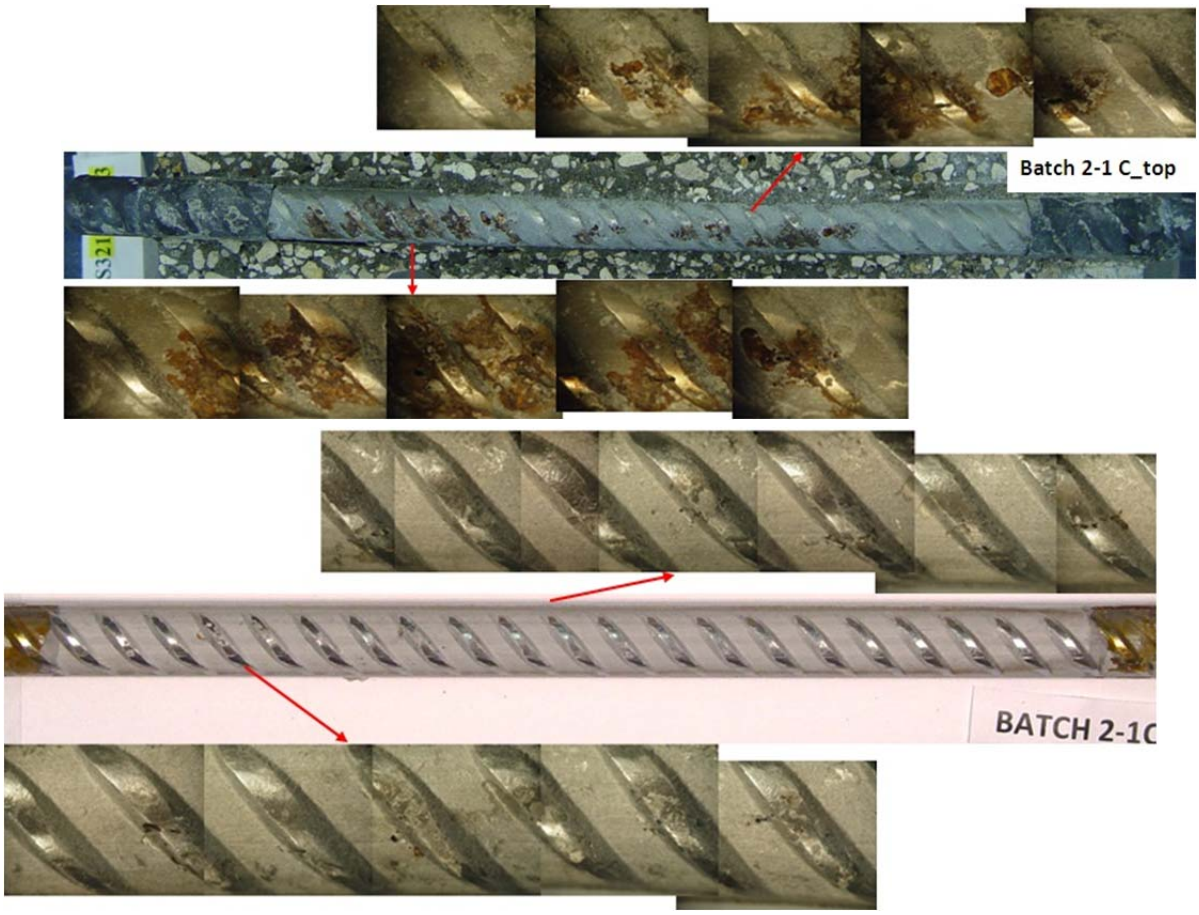

Figure D.18 Pictures Autopsy bottom rebars for batch 2-2

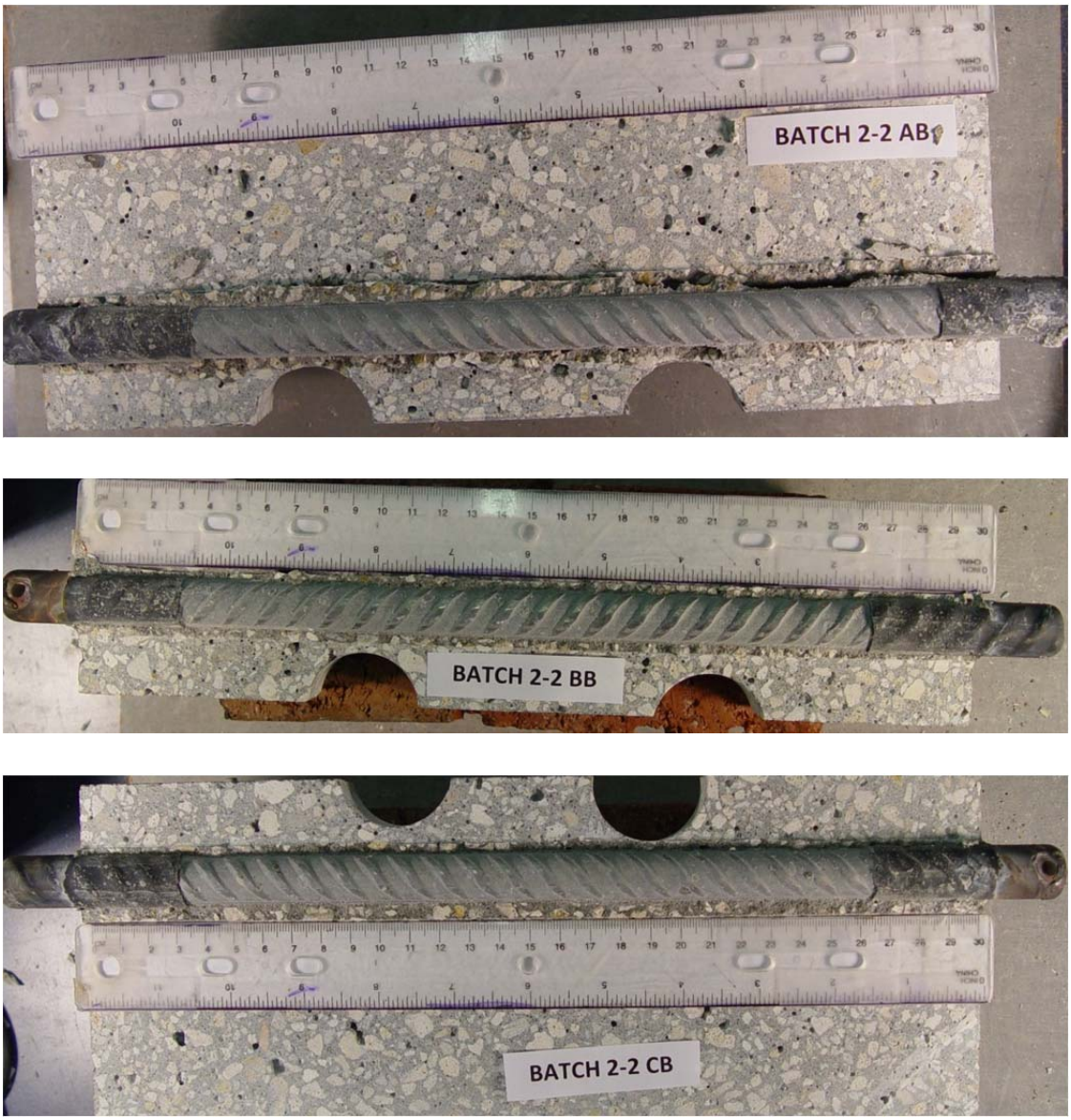

Figure D.19 Close-up pictures before and after cleaning for batch 2-2

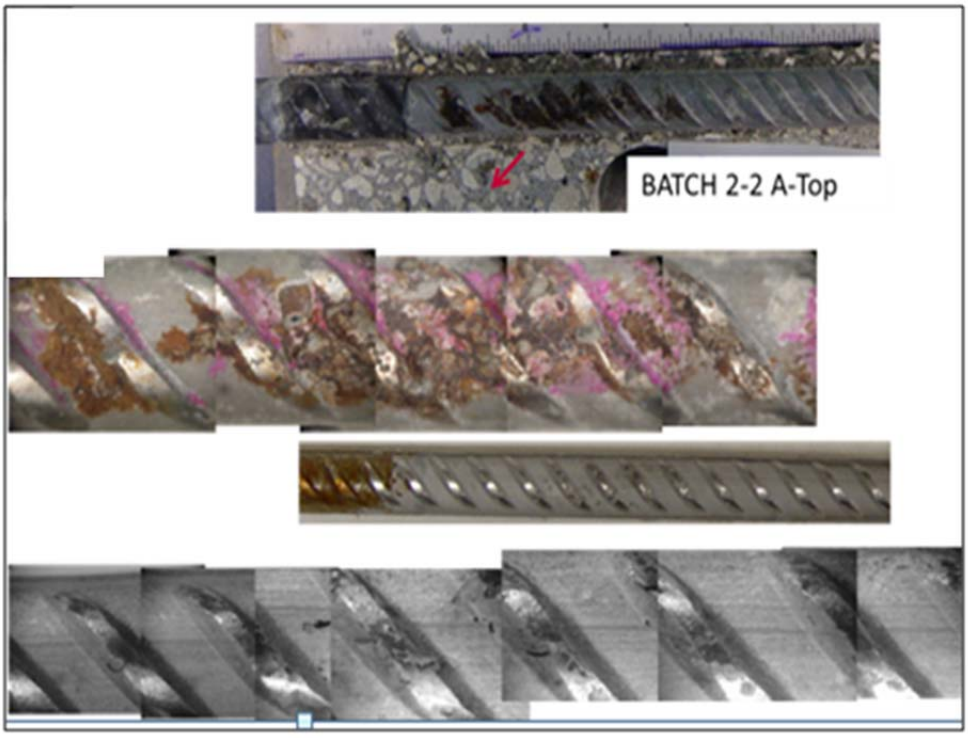

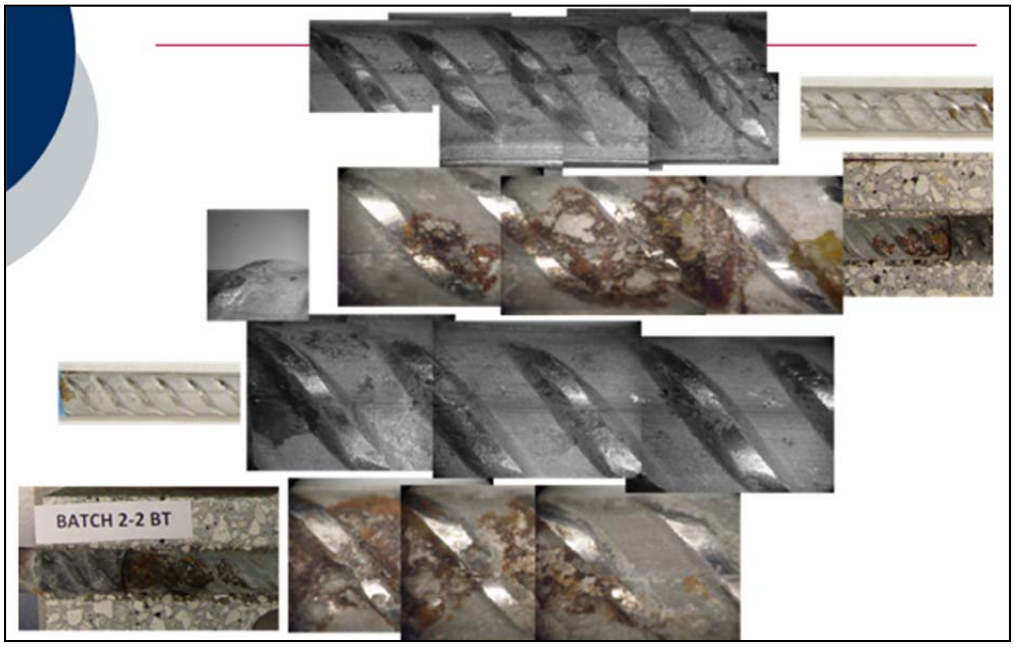

Figure D.20 Close-up pictures before and after cleaning for batch 2-4

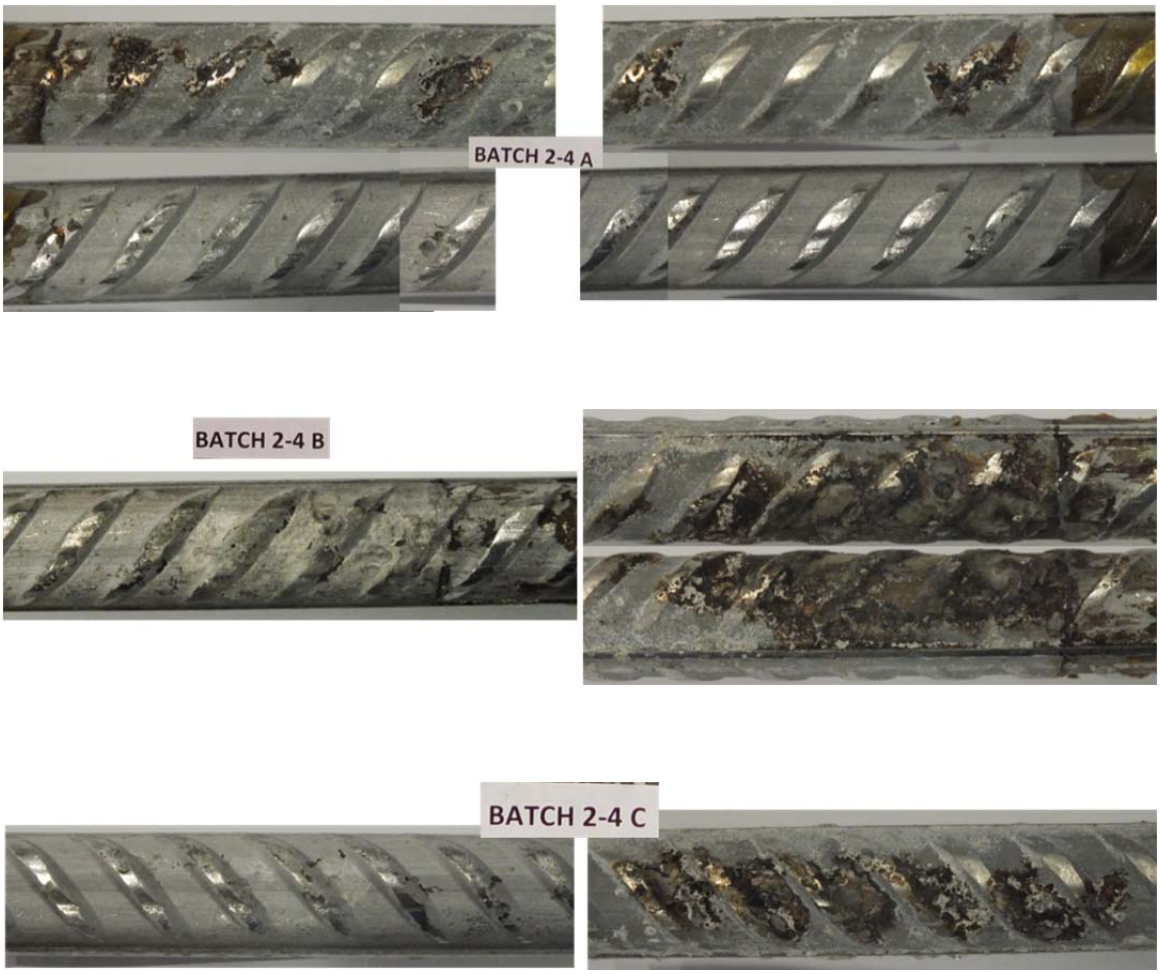

APPENDIX E: Petrographic and Polarizing Micrographs of Terminated ASR Specimens (Chapter 7)

FL1

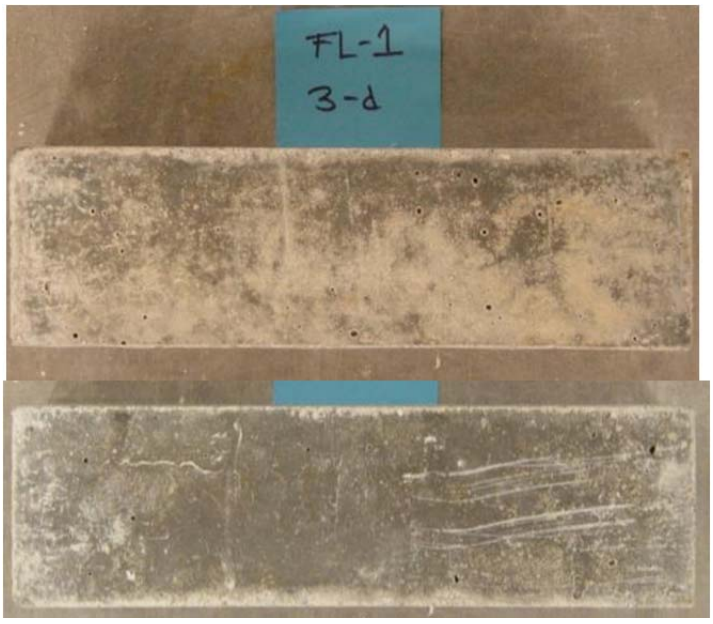

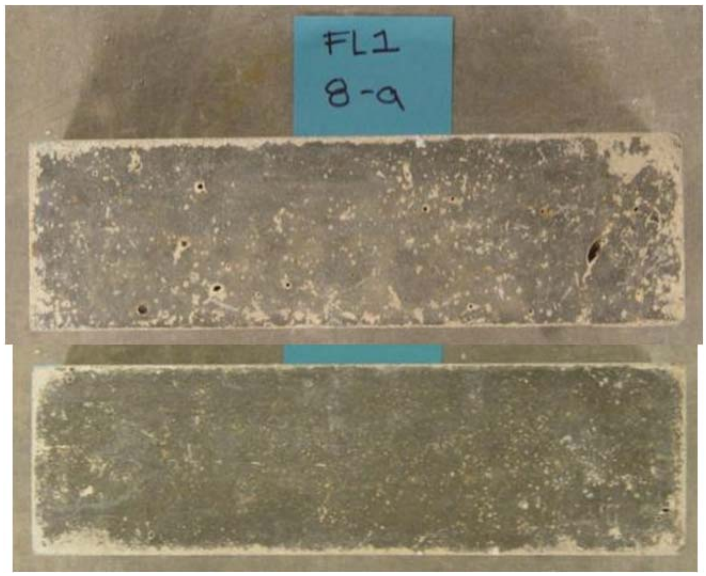

03D-1

03D-2

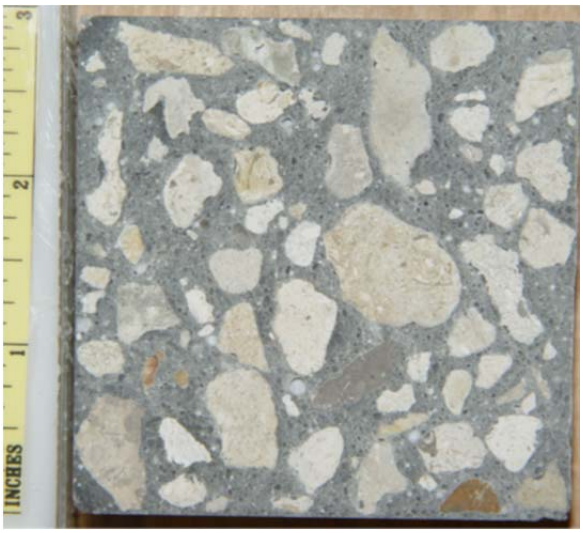

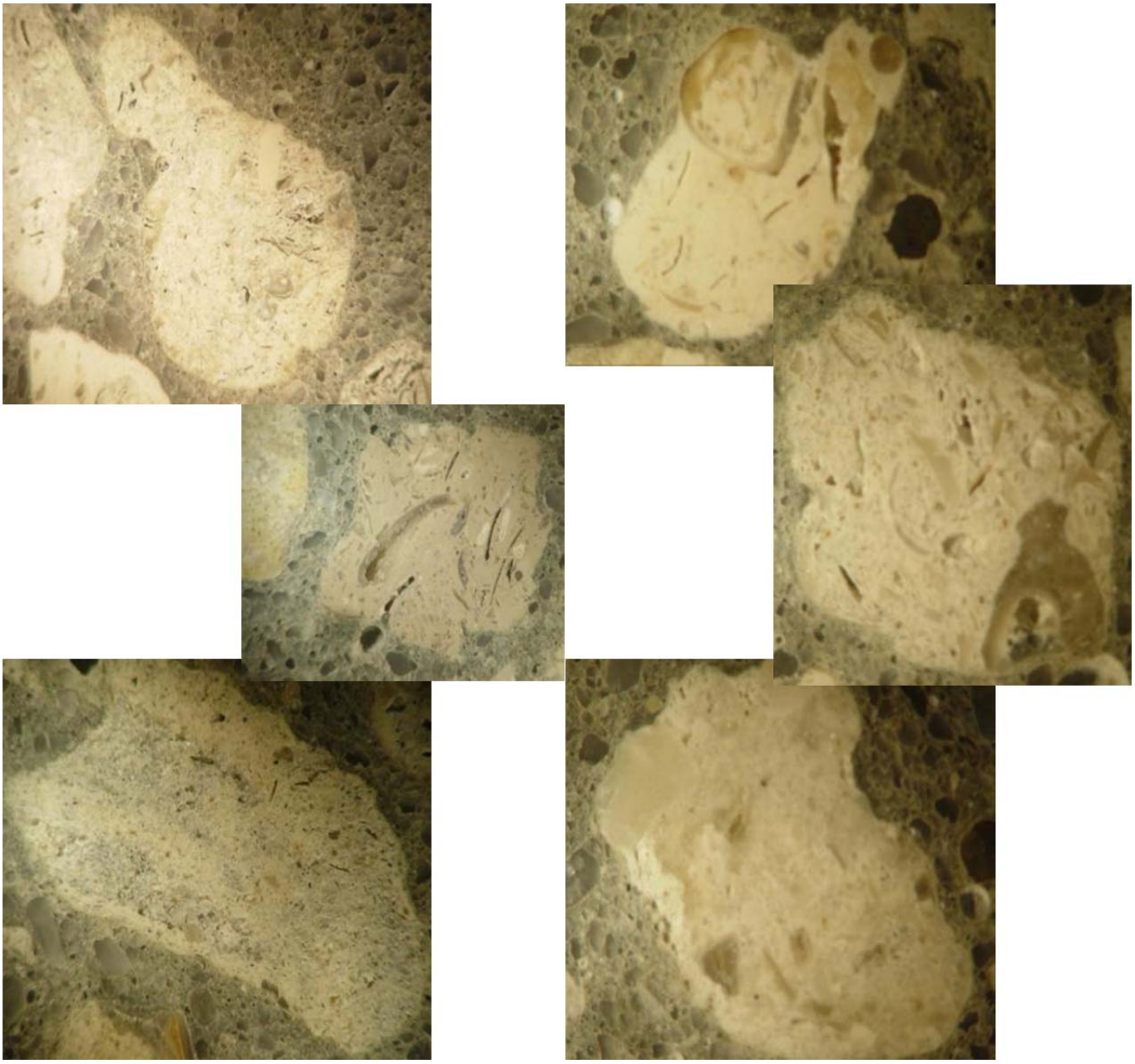

3D-1.2
45%

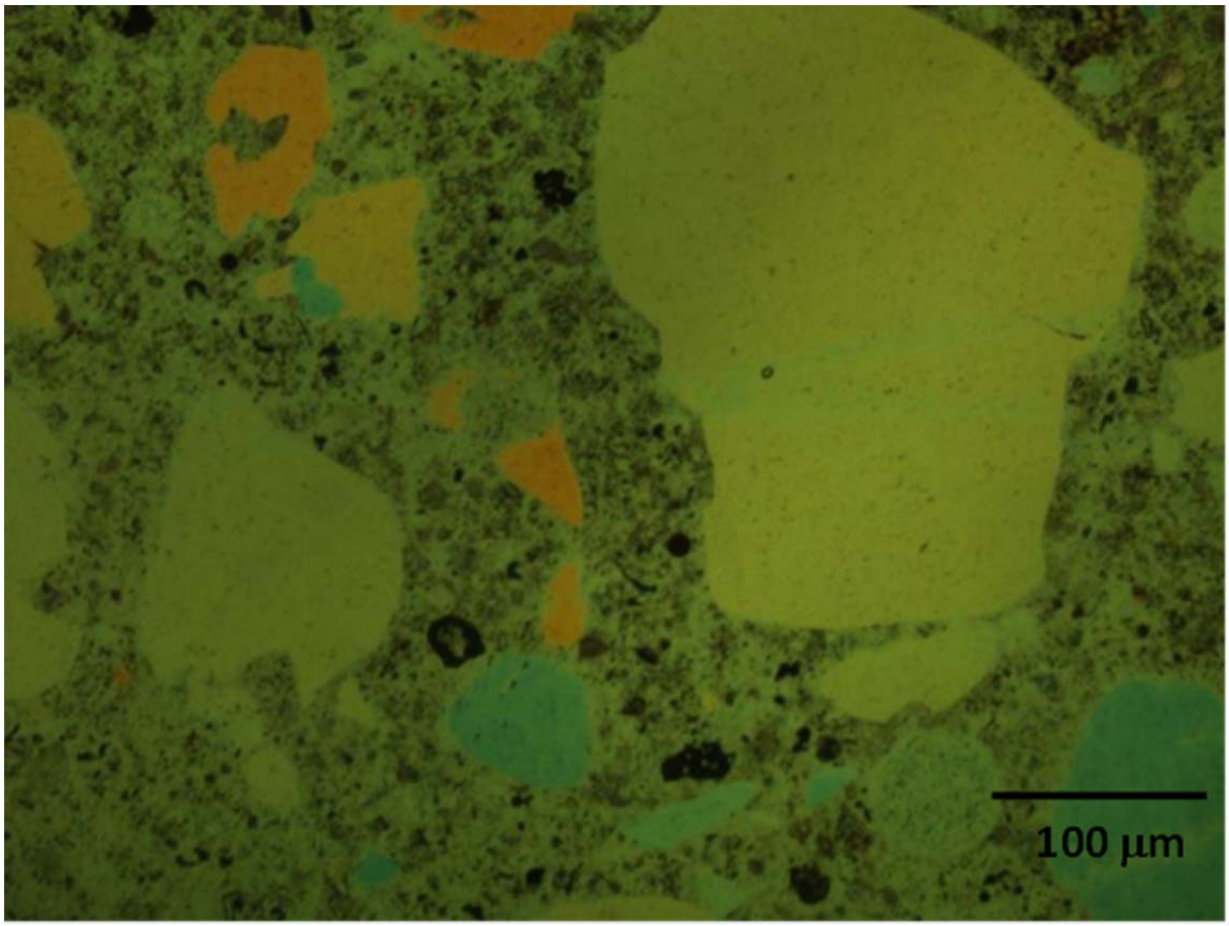

3D-3.2
45%

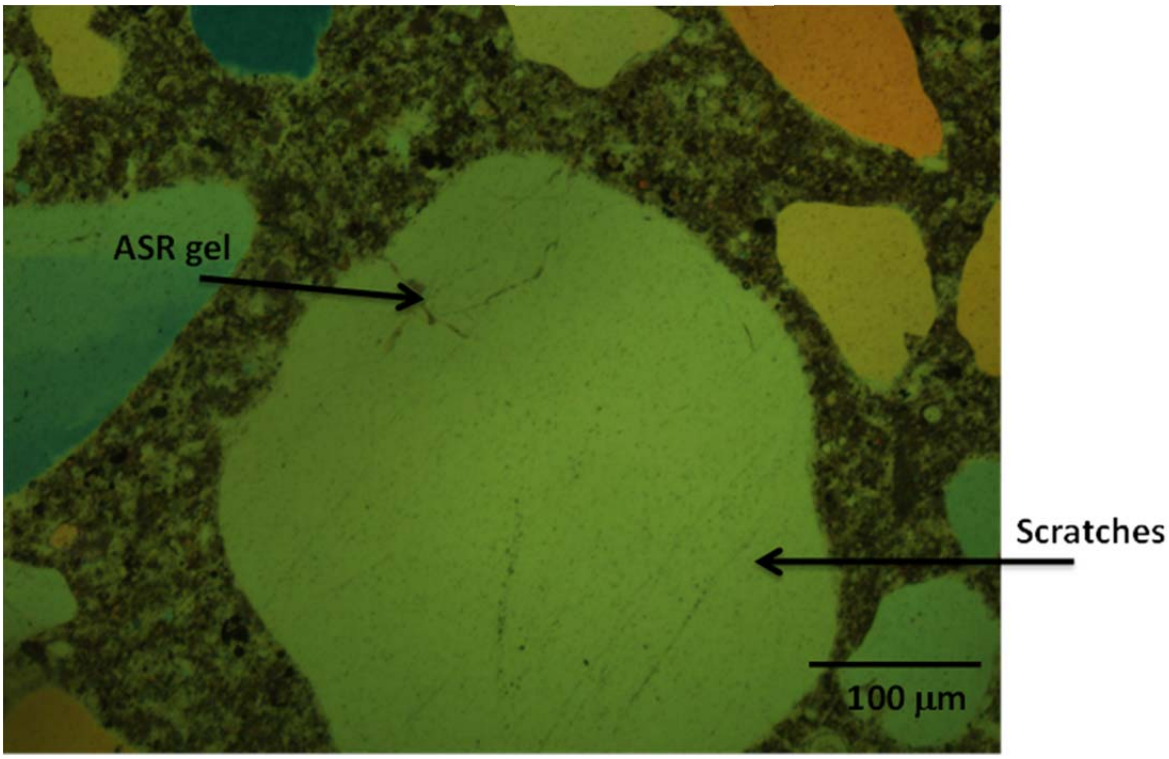

3D-4.3
45%

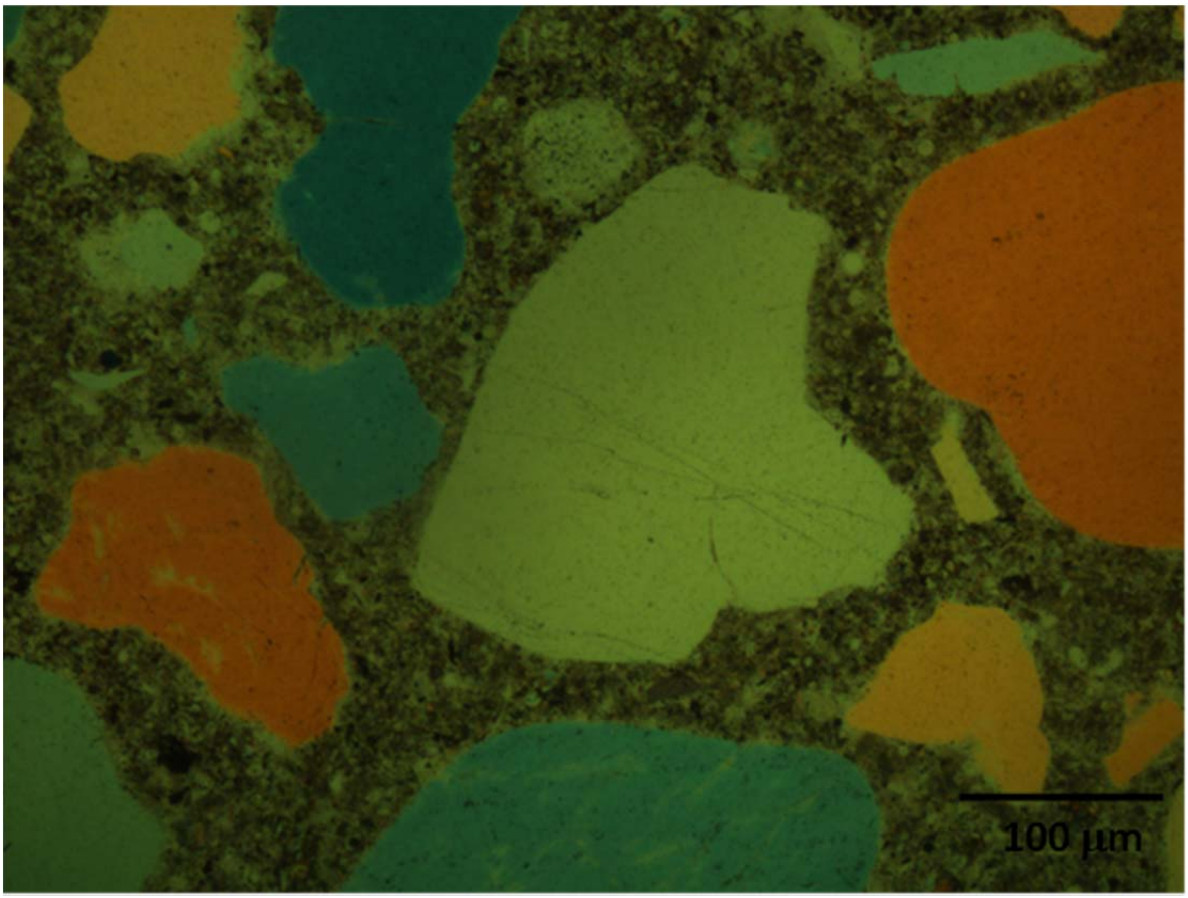

3D-5.1
45%

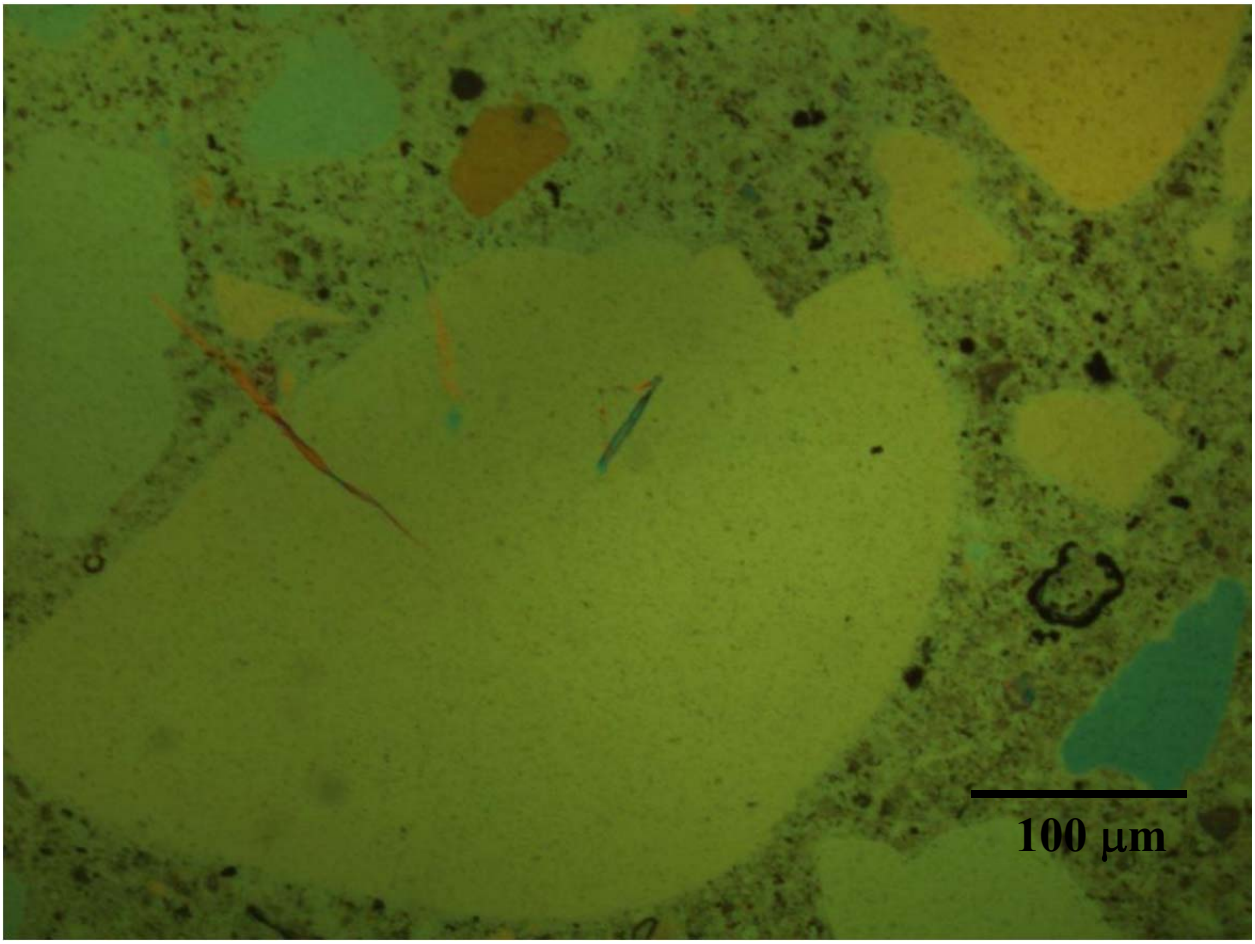

08A-1

08A-2

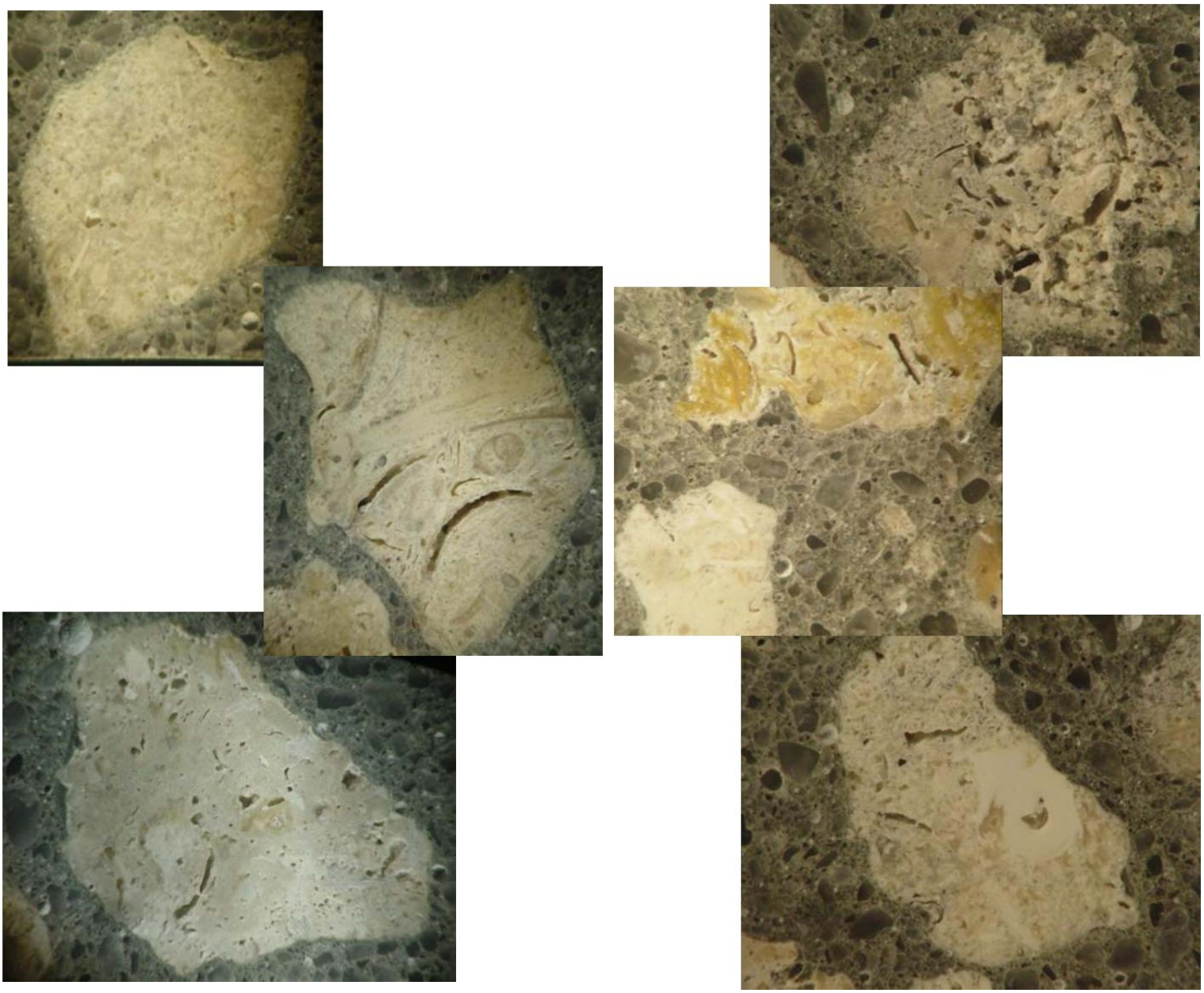

8A-1.1
45%

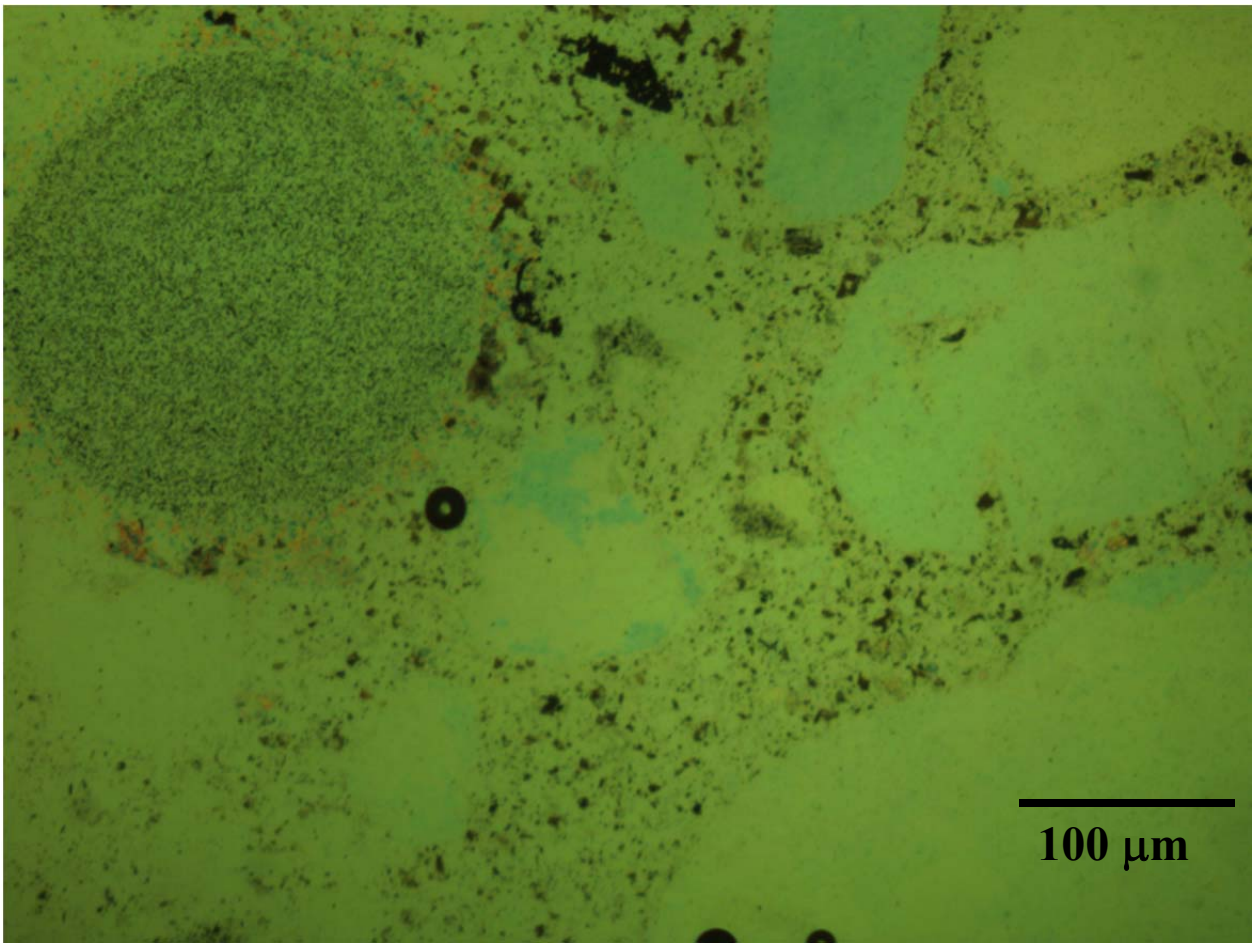

8A-2.1
45%

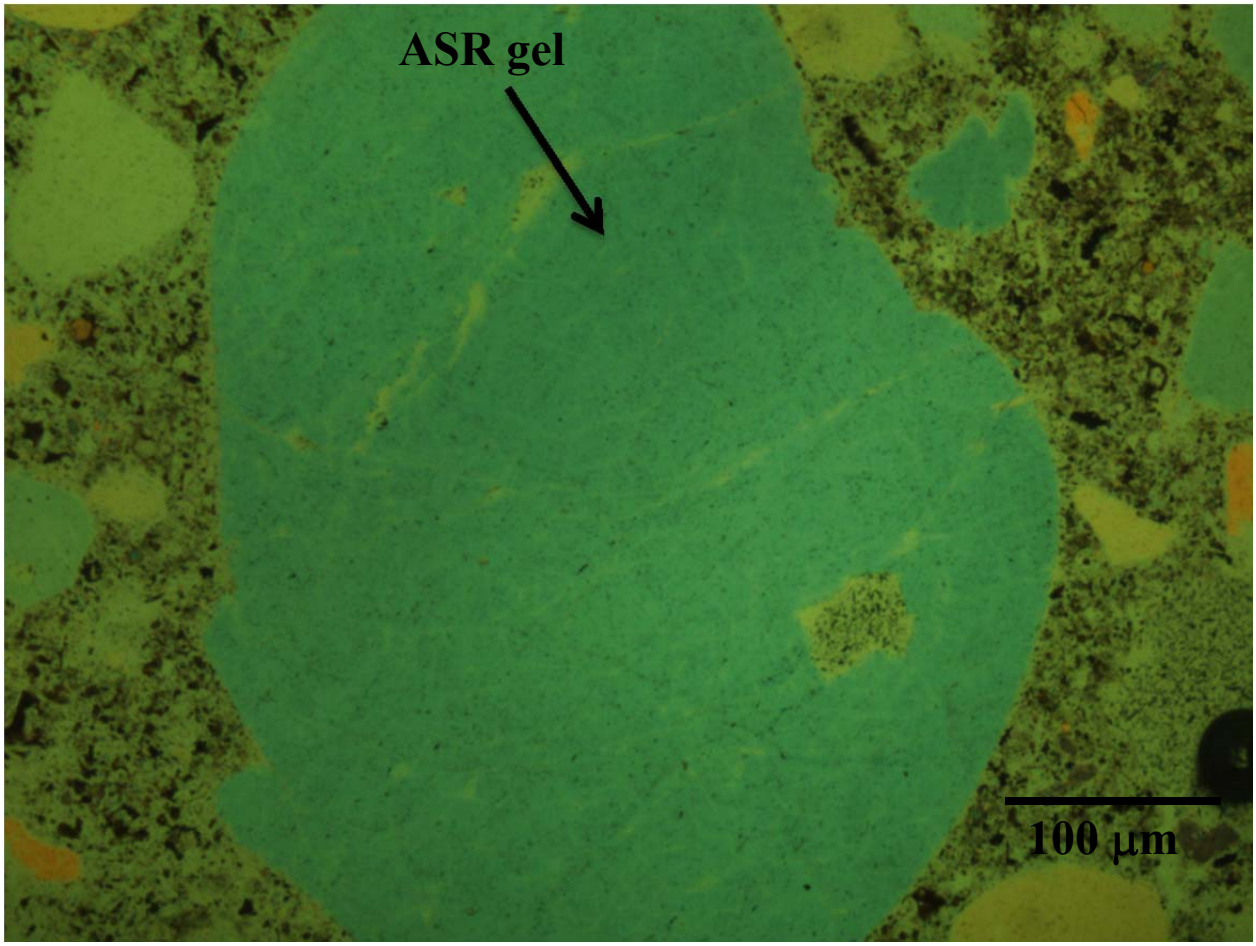

8A-5.1
45%

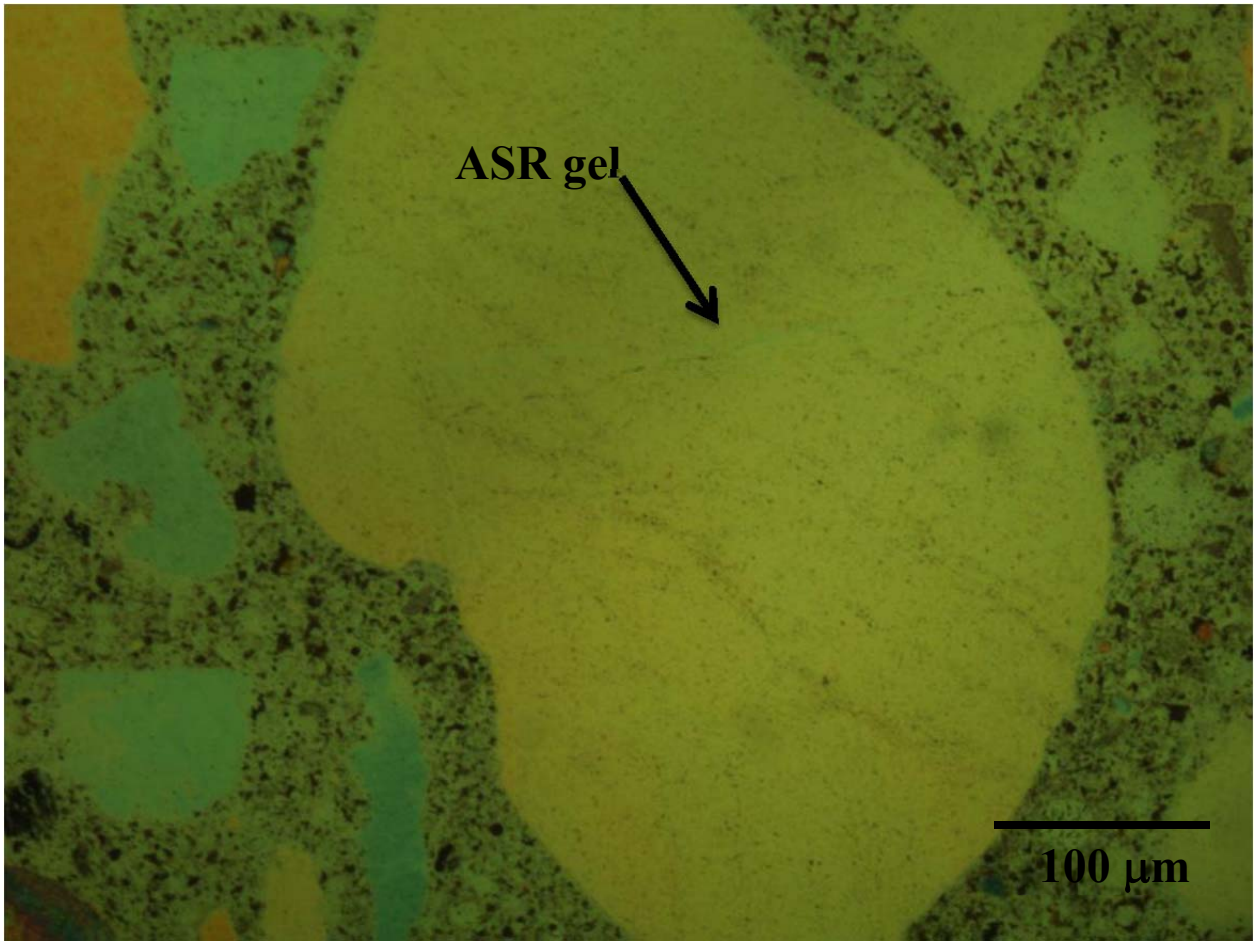

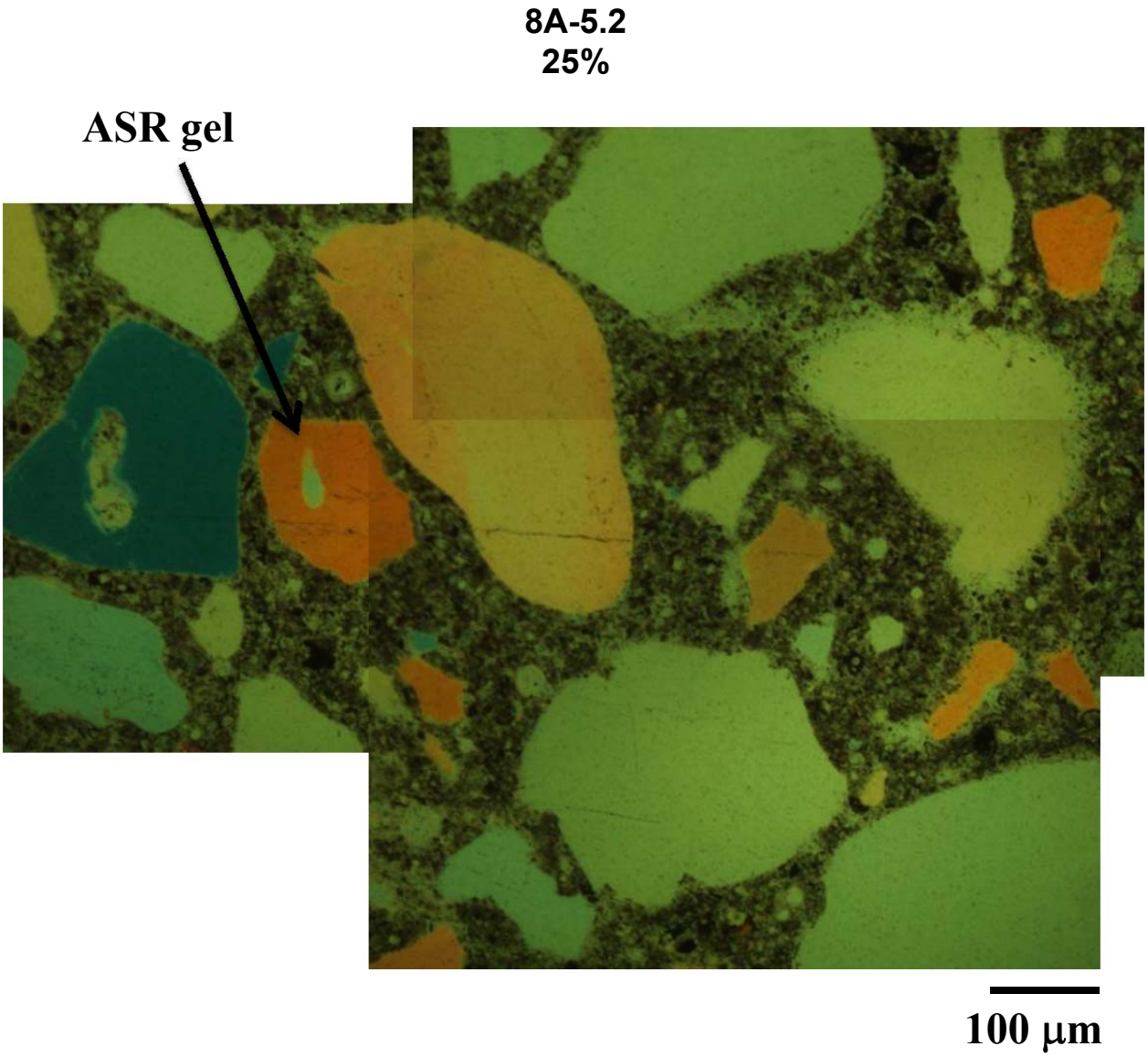
8A-5.2
25%
ASR gel
100 μm

8A-5.2
25%

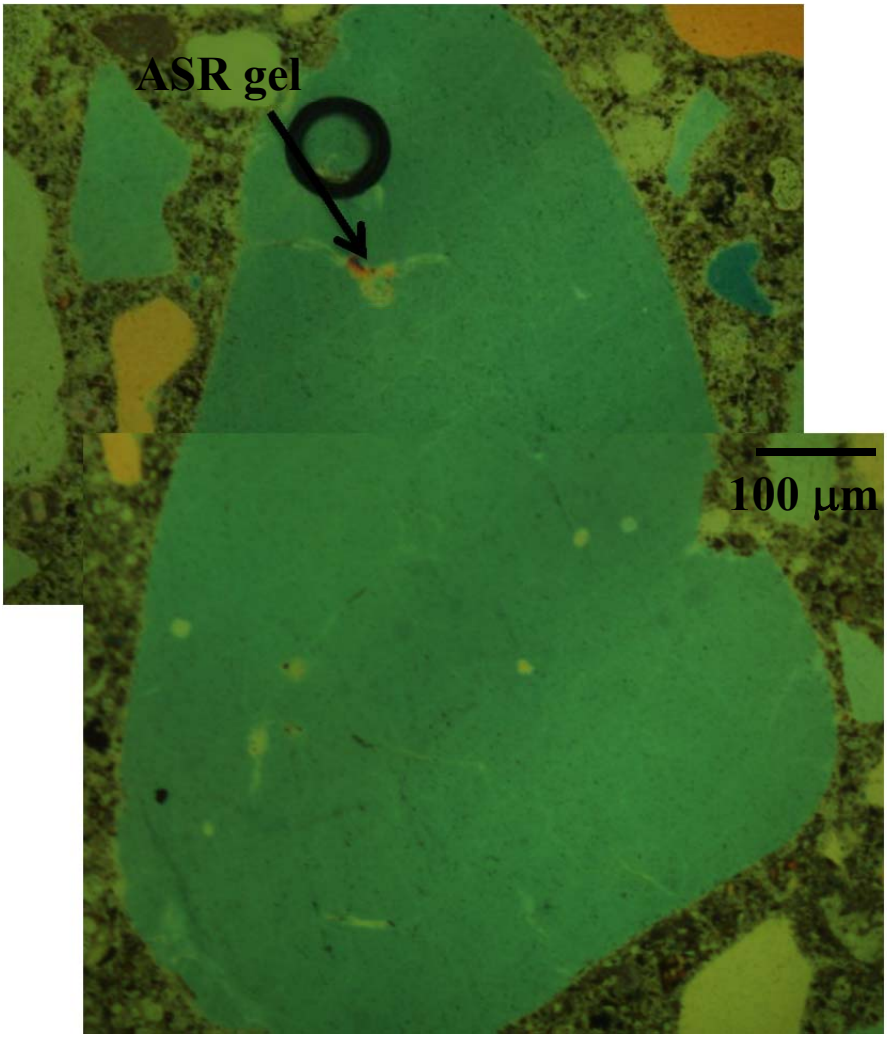

8A-5.3
45%

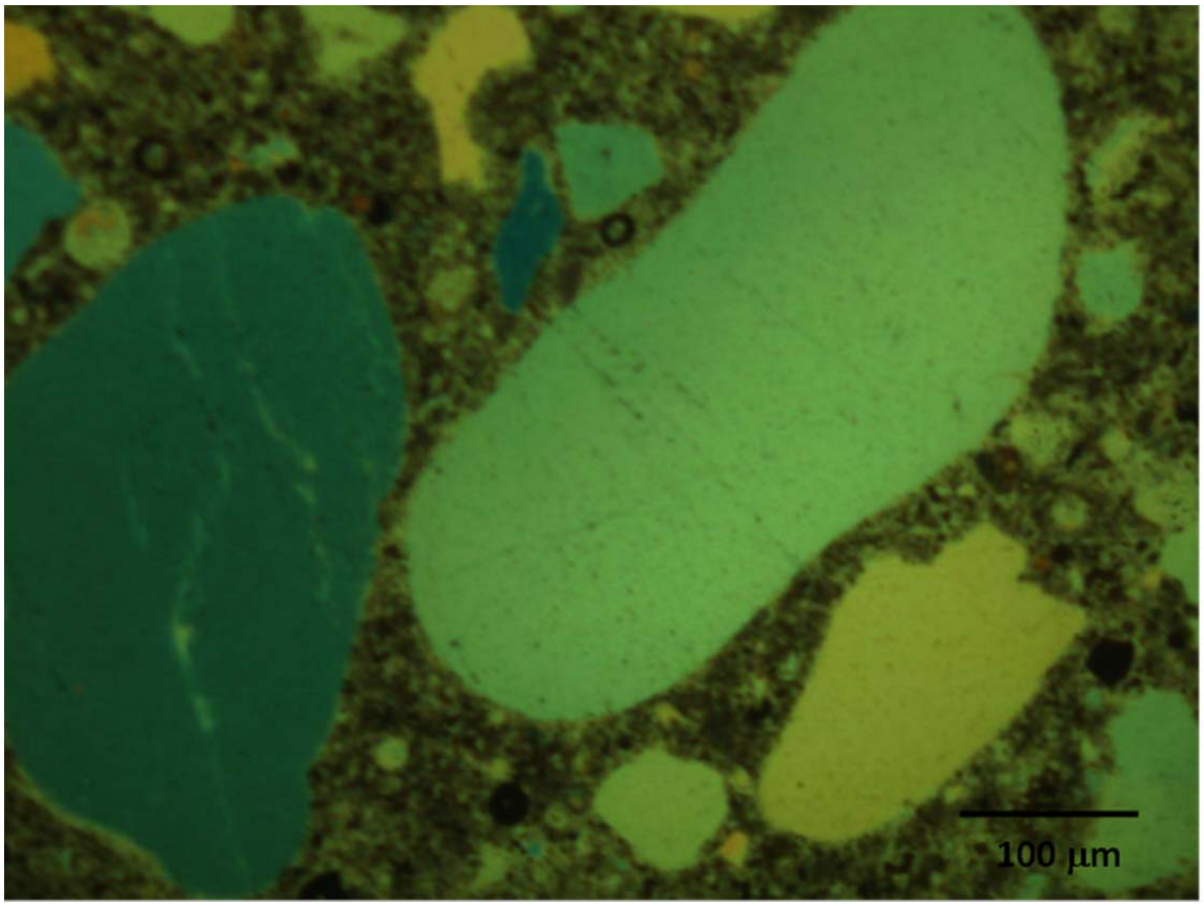

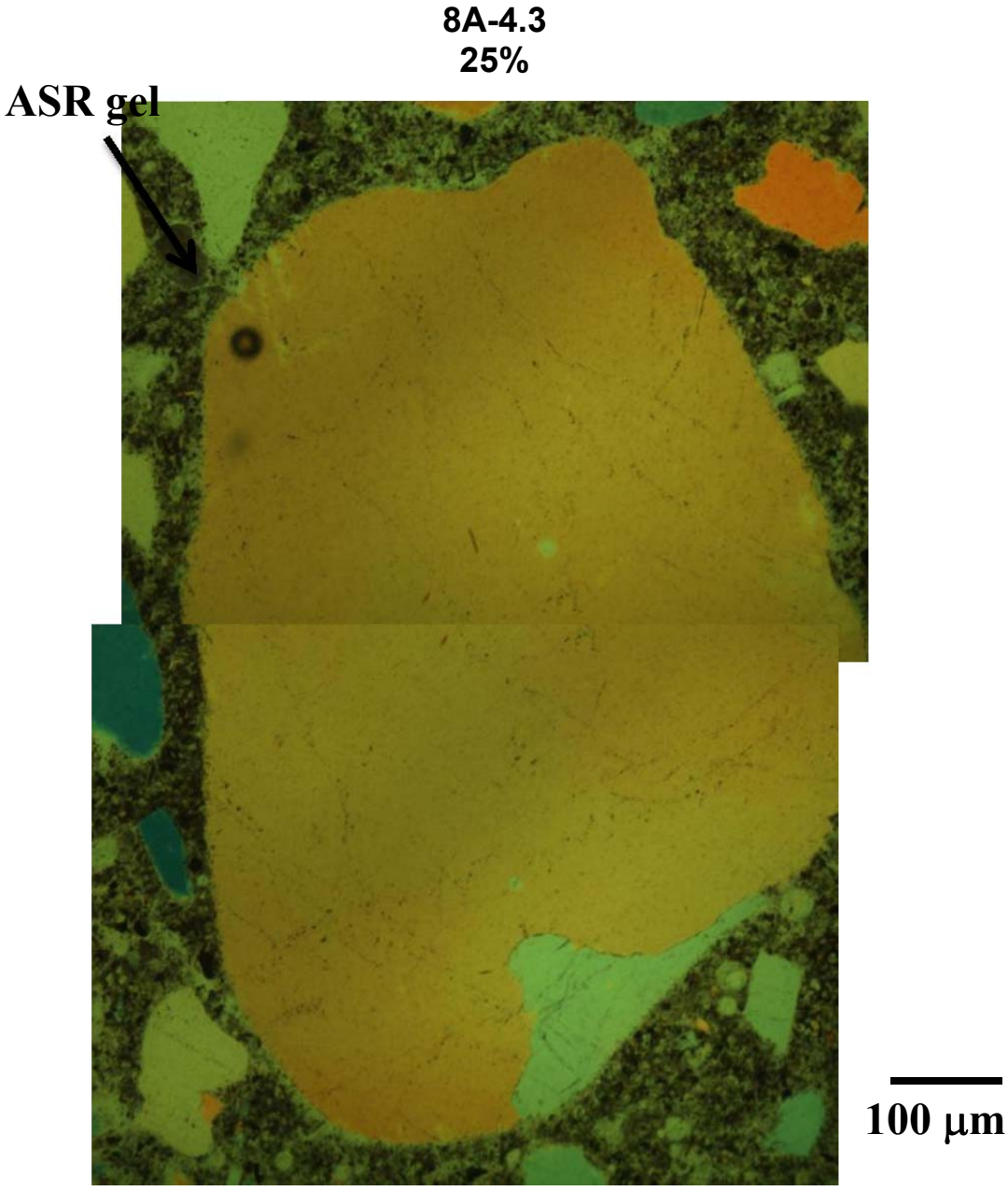
8A-4.3
25%
ASR gel
100 μm

8A-3.2
45%

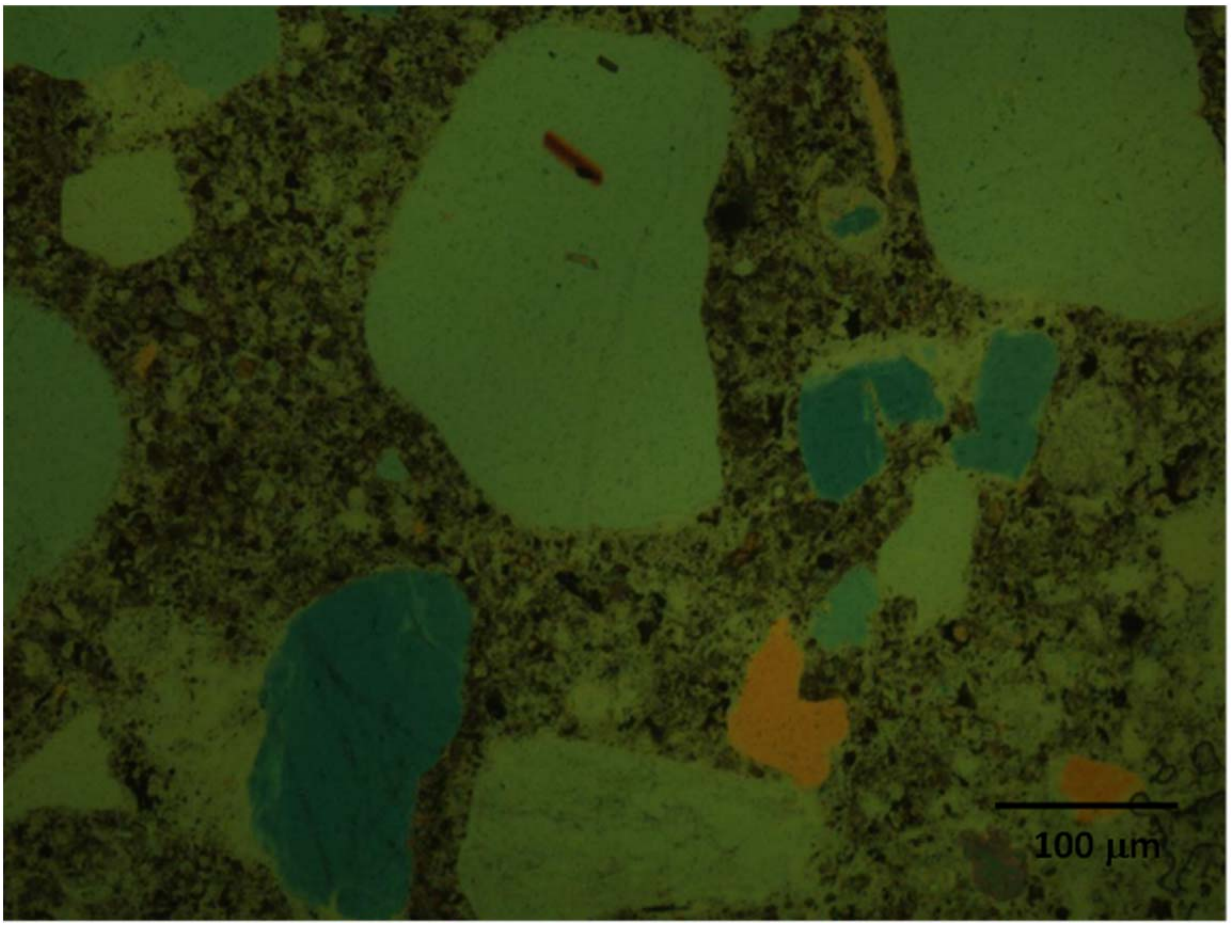

8A-3.3
45%

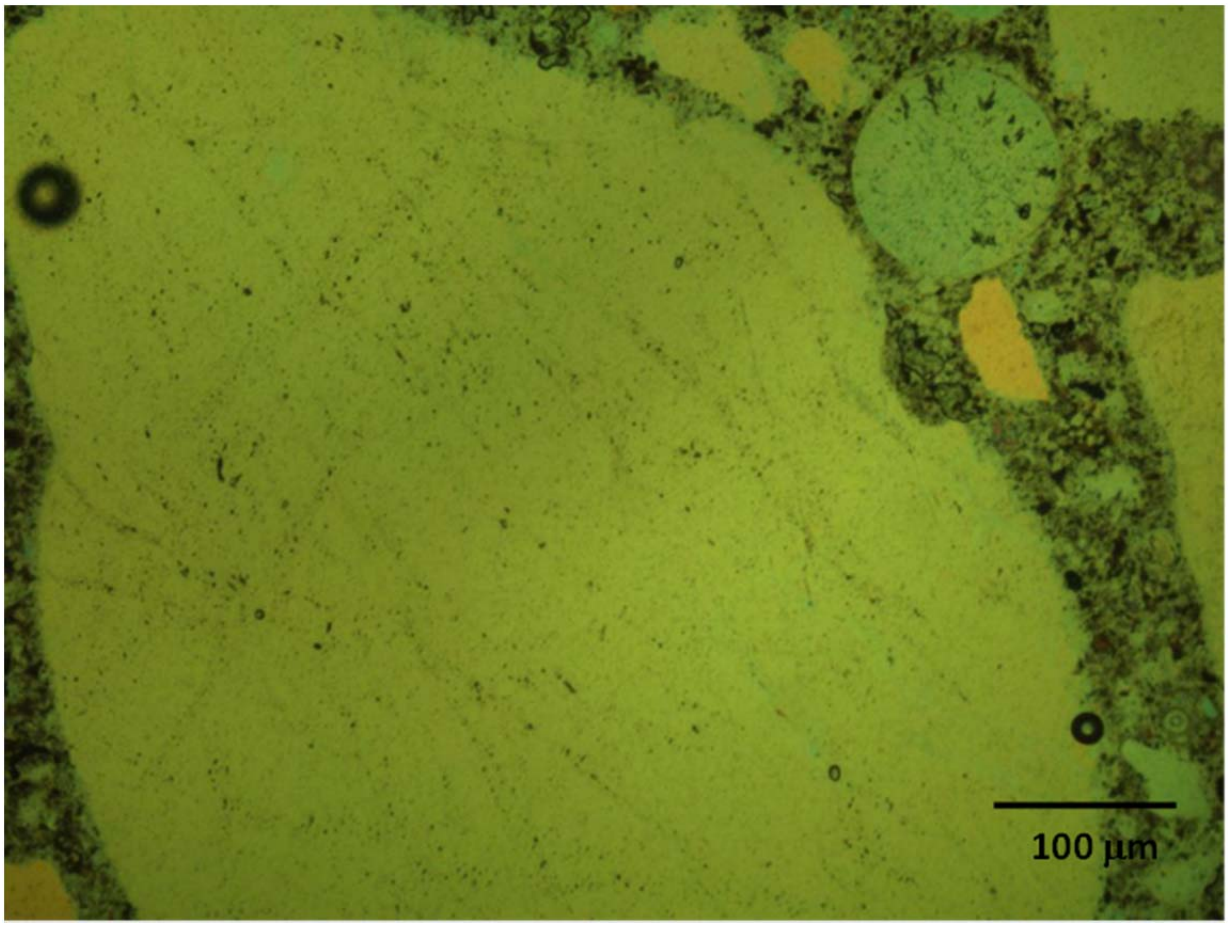

8A-3.4
45%

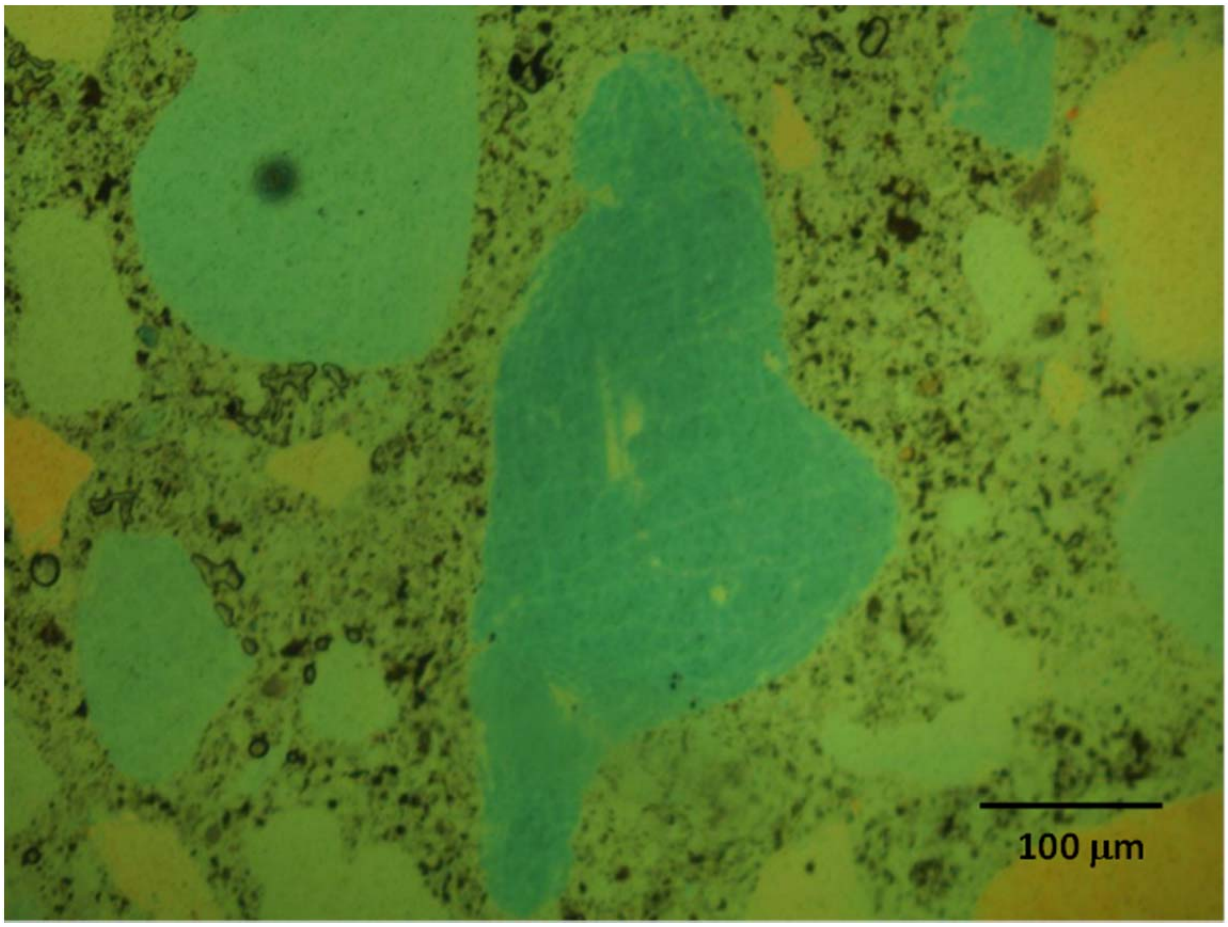

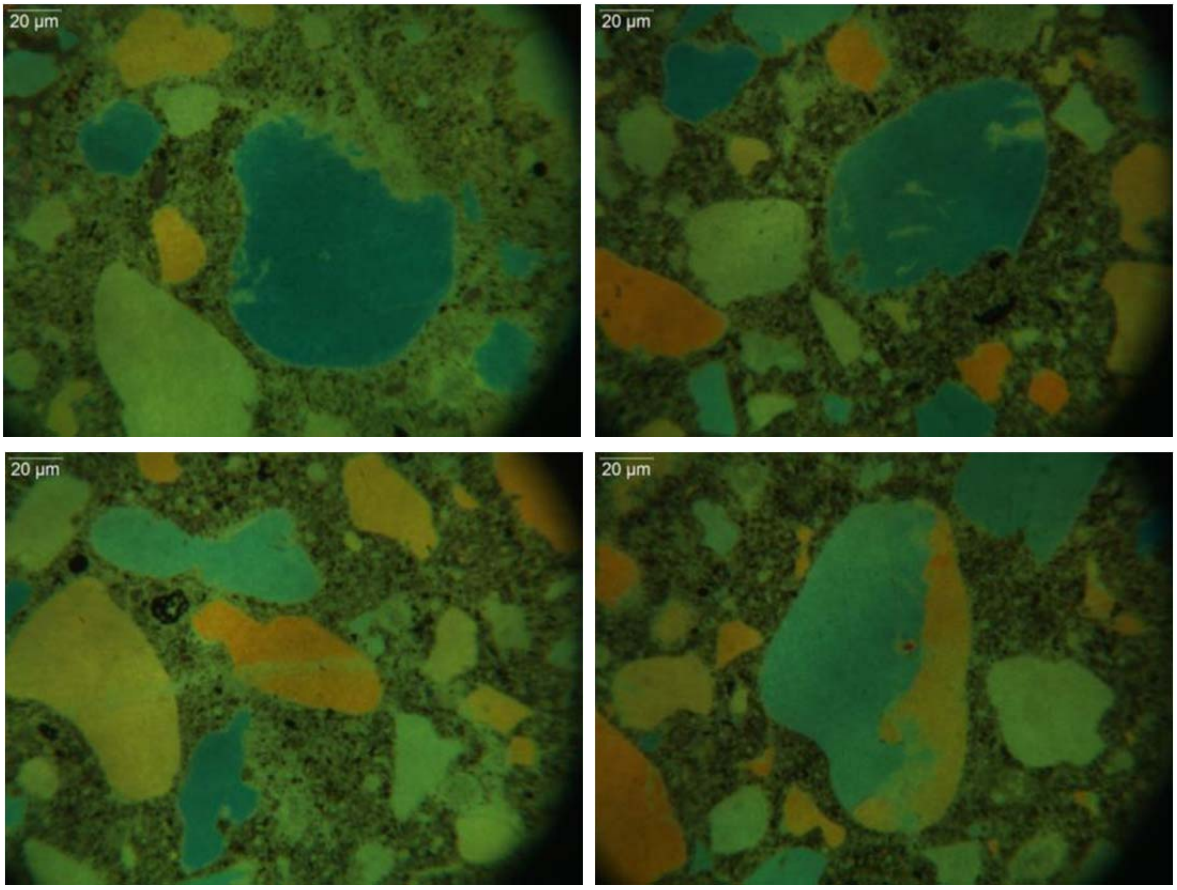
20 µm
20 µm
20 µm
20 µm

FL2

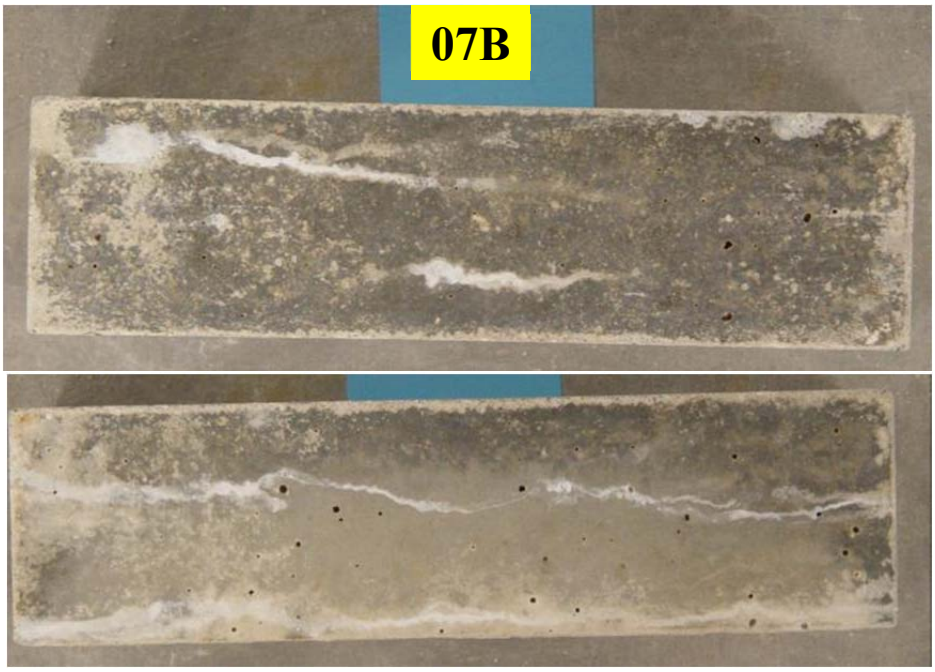

27A

29B

07B-1

07B-2

07B-1.2
45%

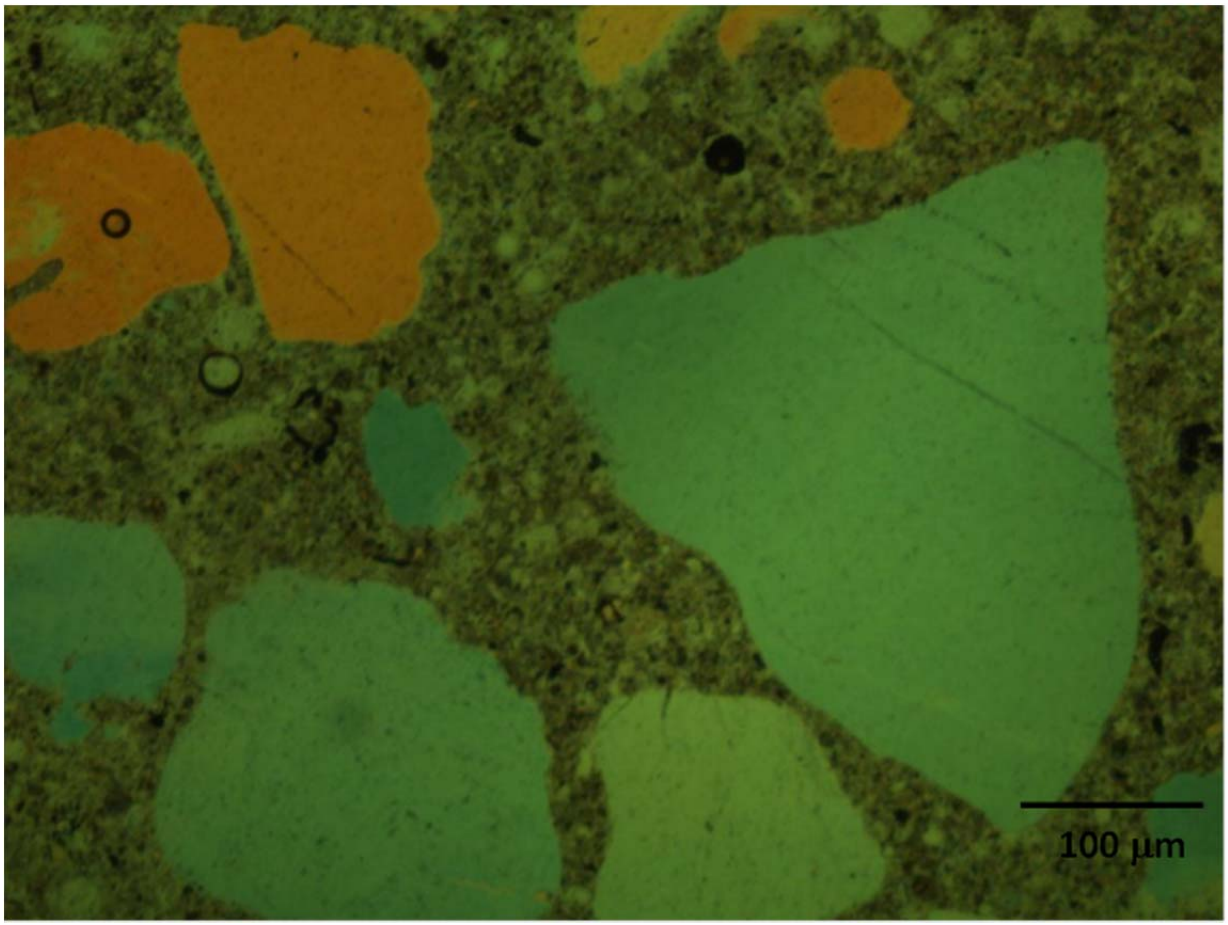

07B-2.1
45%

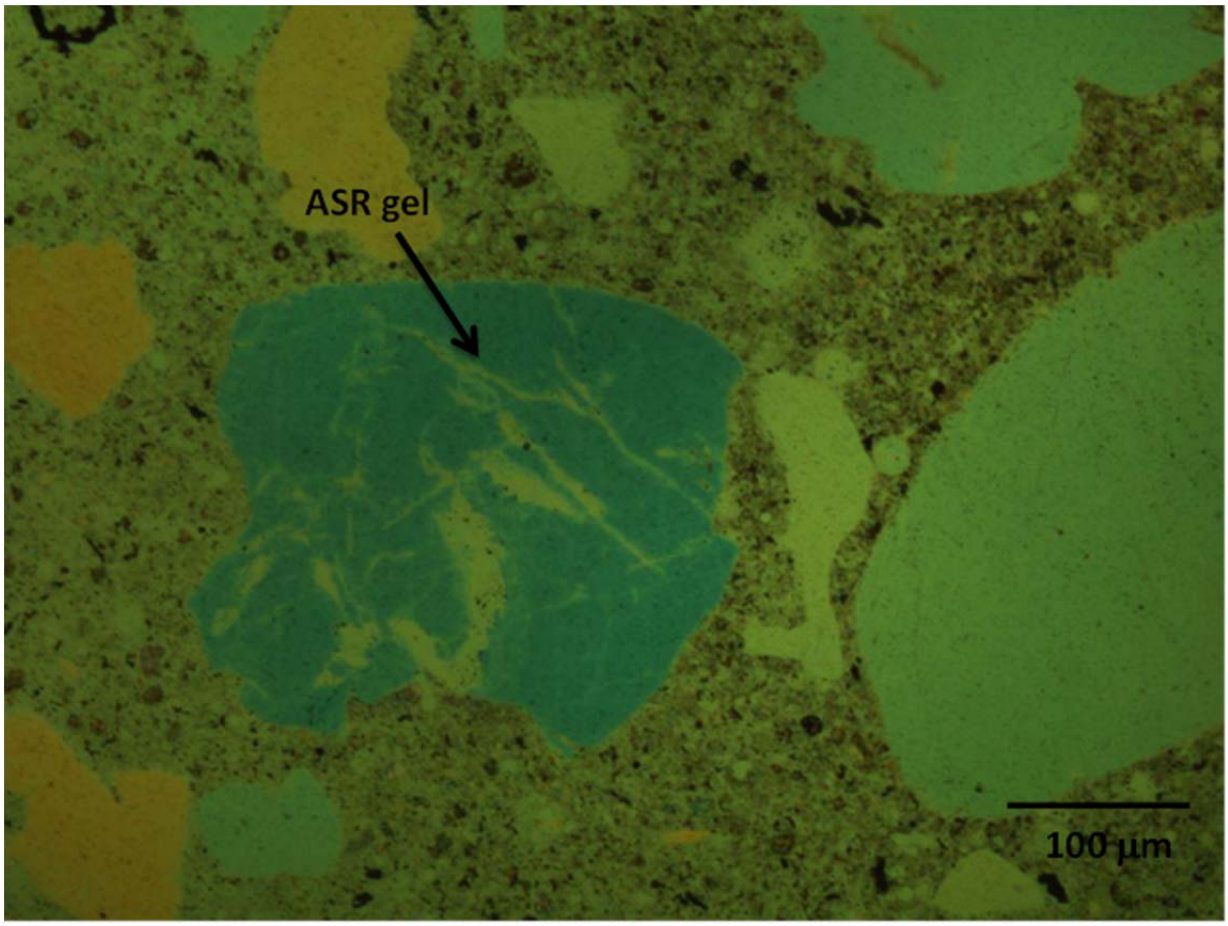

07B-2.3
45%

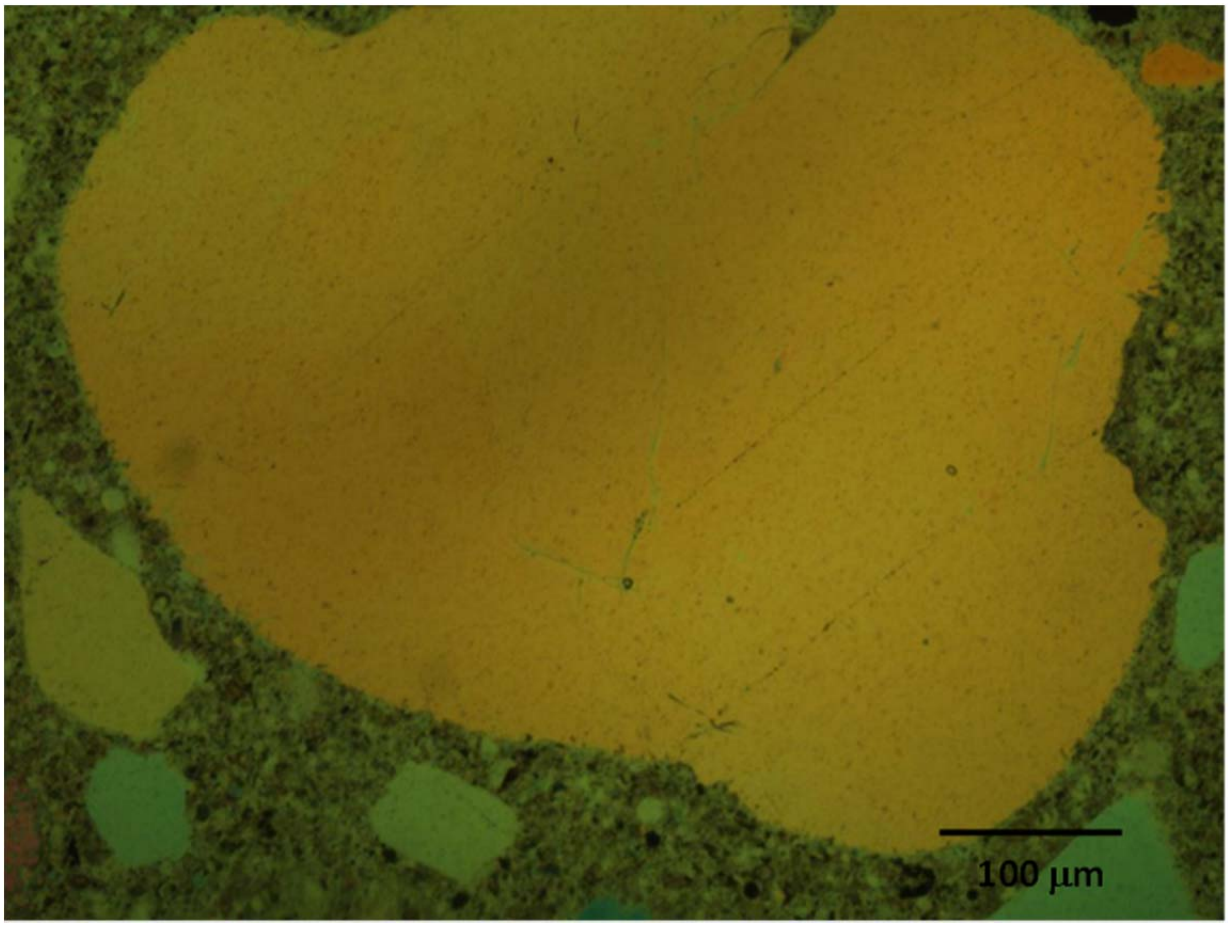

07B-3.2
45%

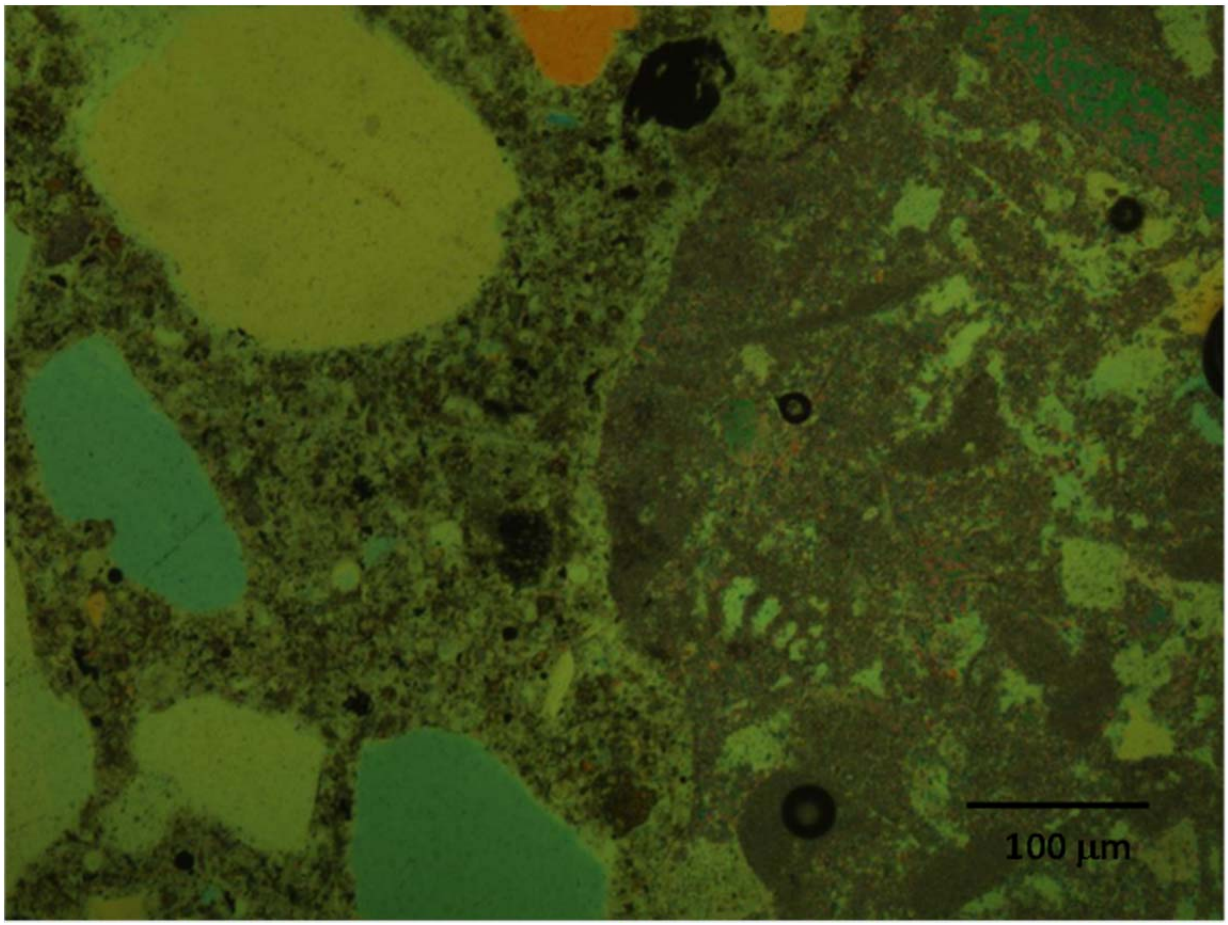

07B-4.4
45%

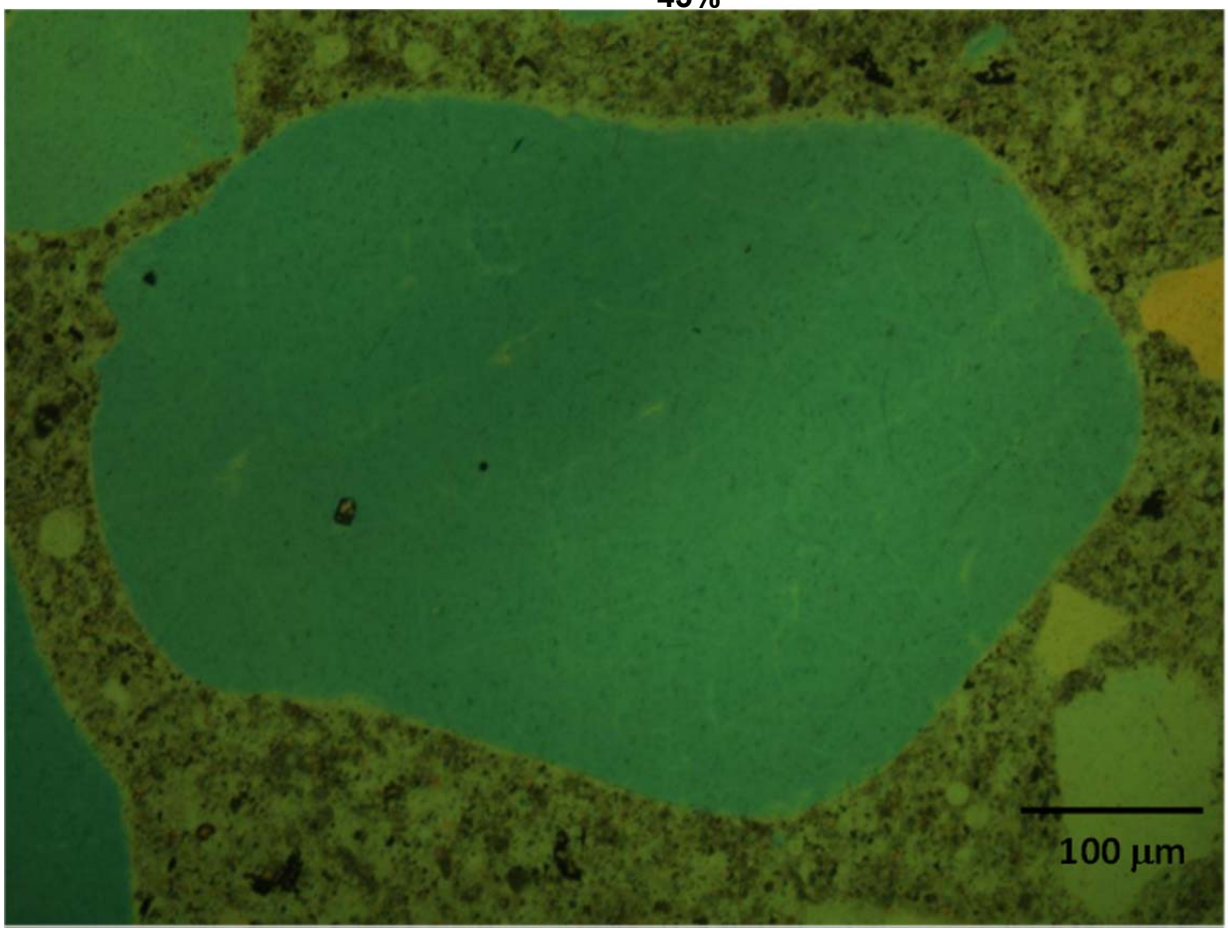

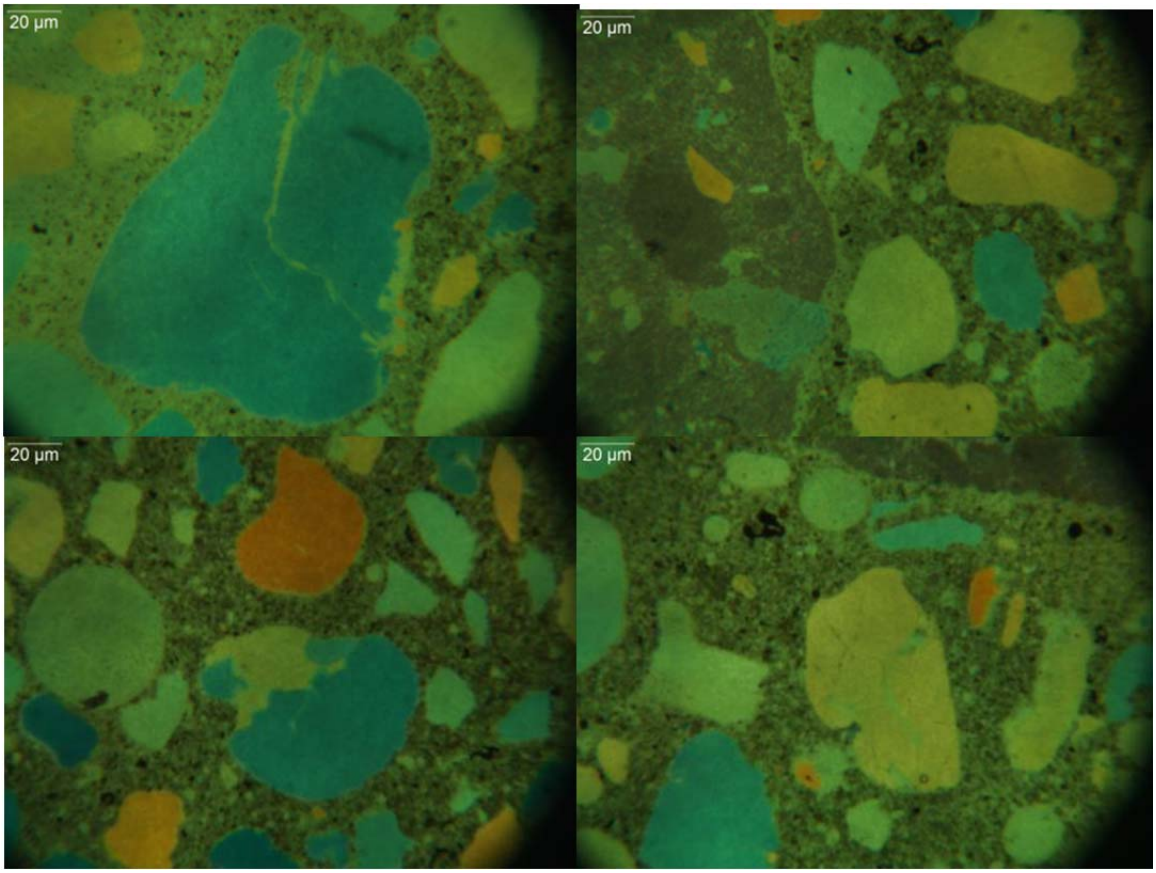
20 µm
20 µm
20 µm
20 µm

27A-1

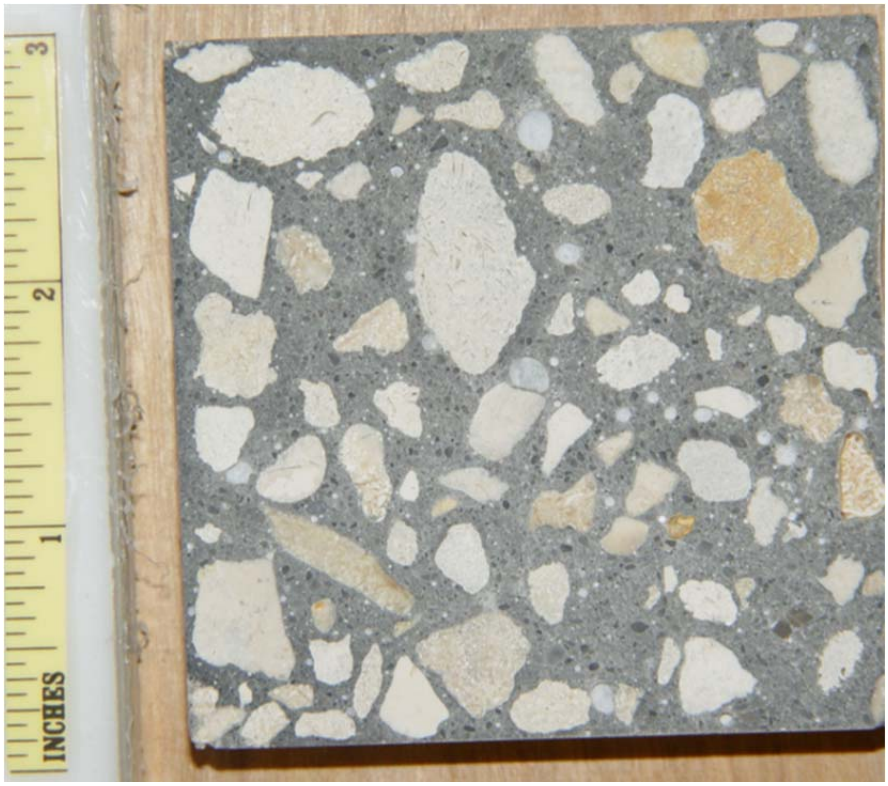

27A-2

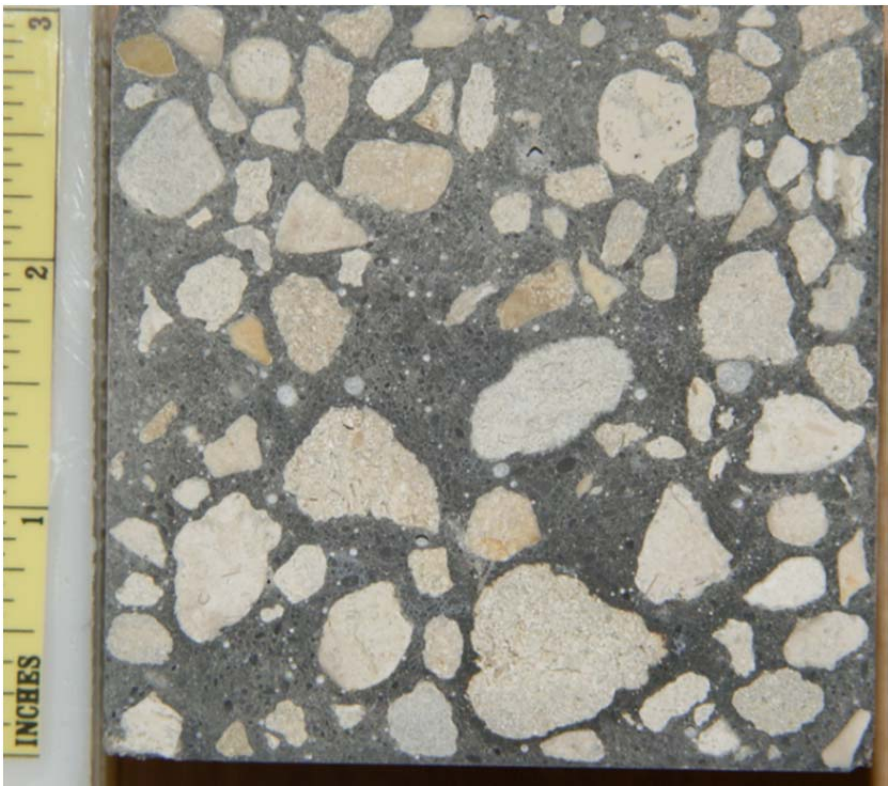

27A-1.2
25%

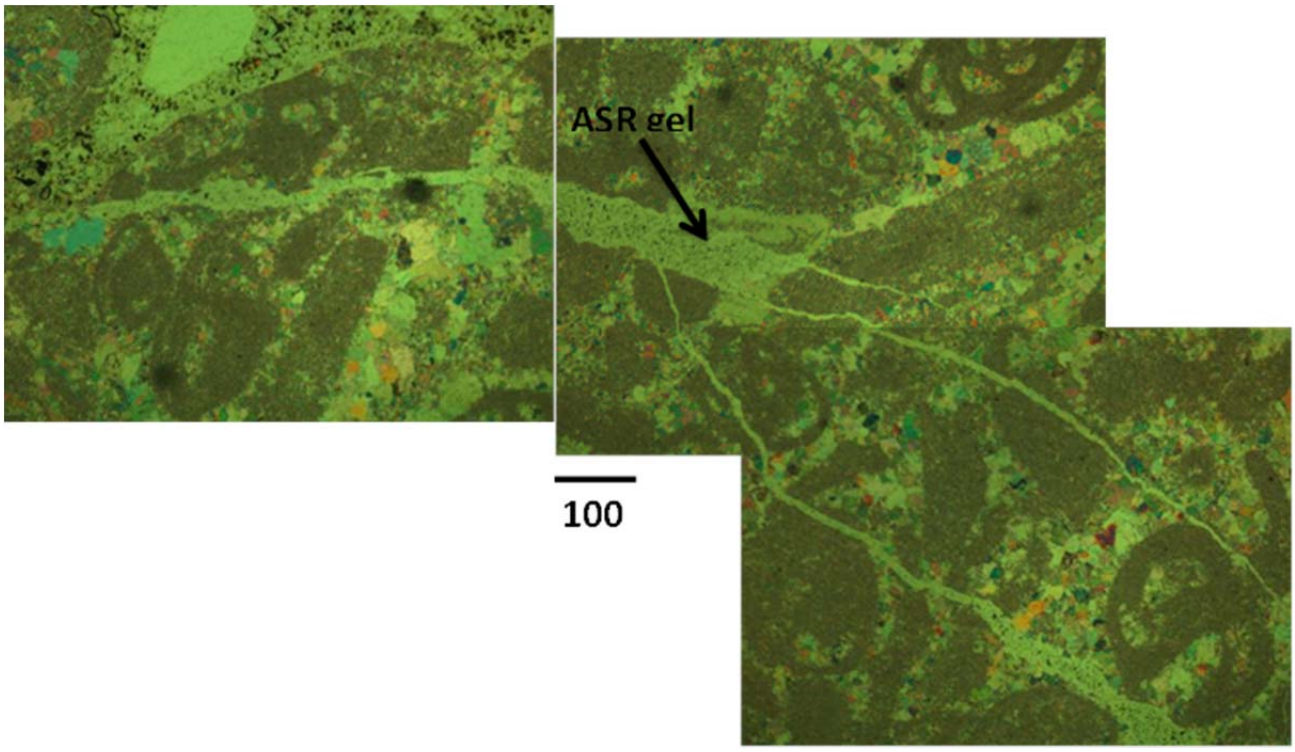

27A-2.1
45%

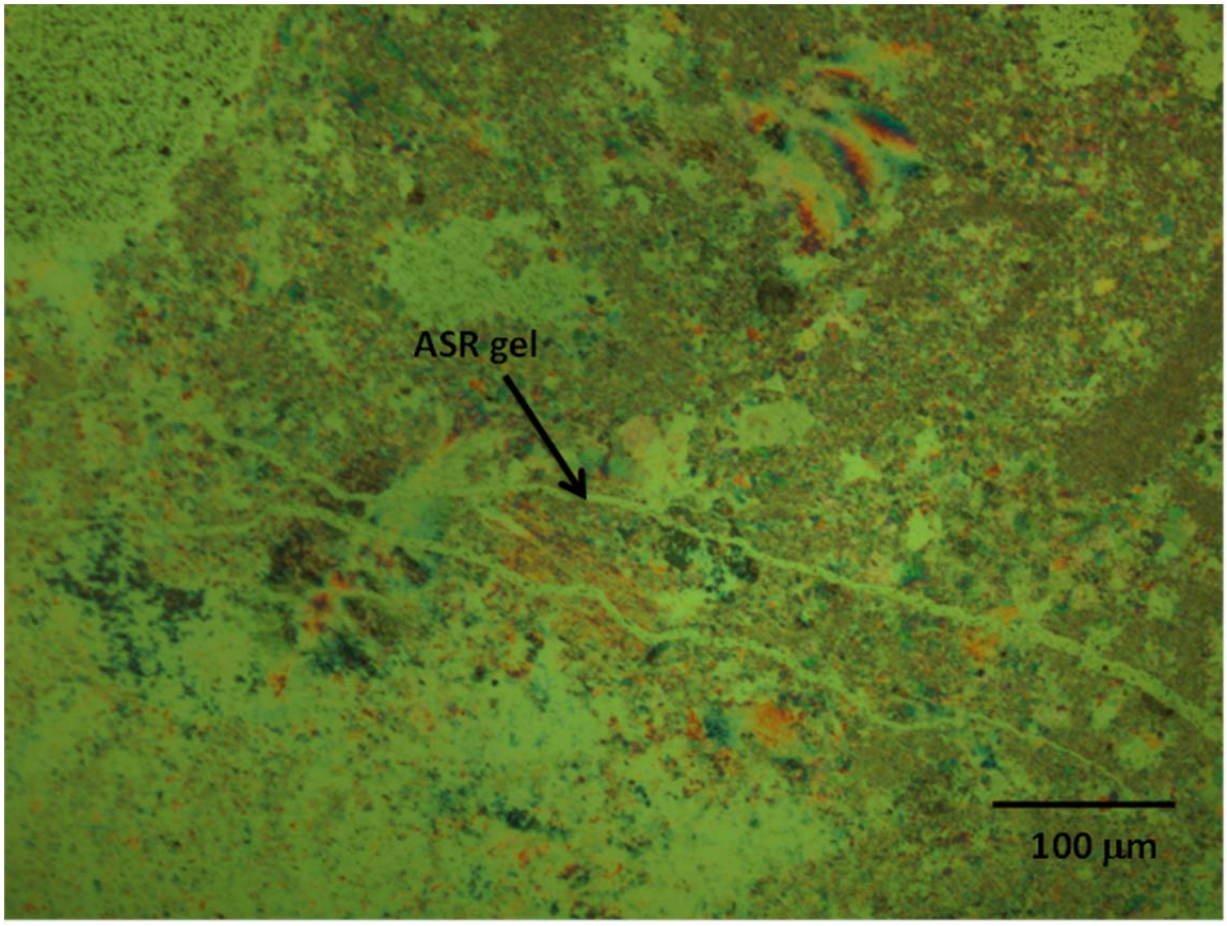

27A-3.2
45%

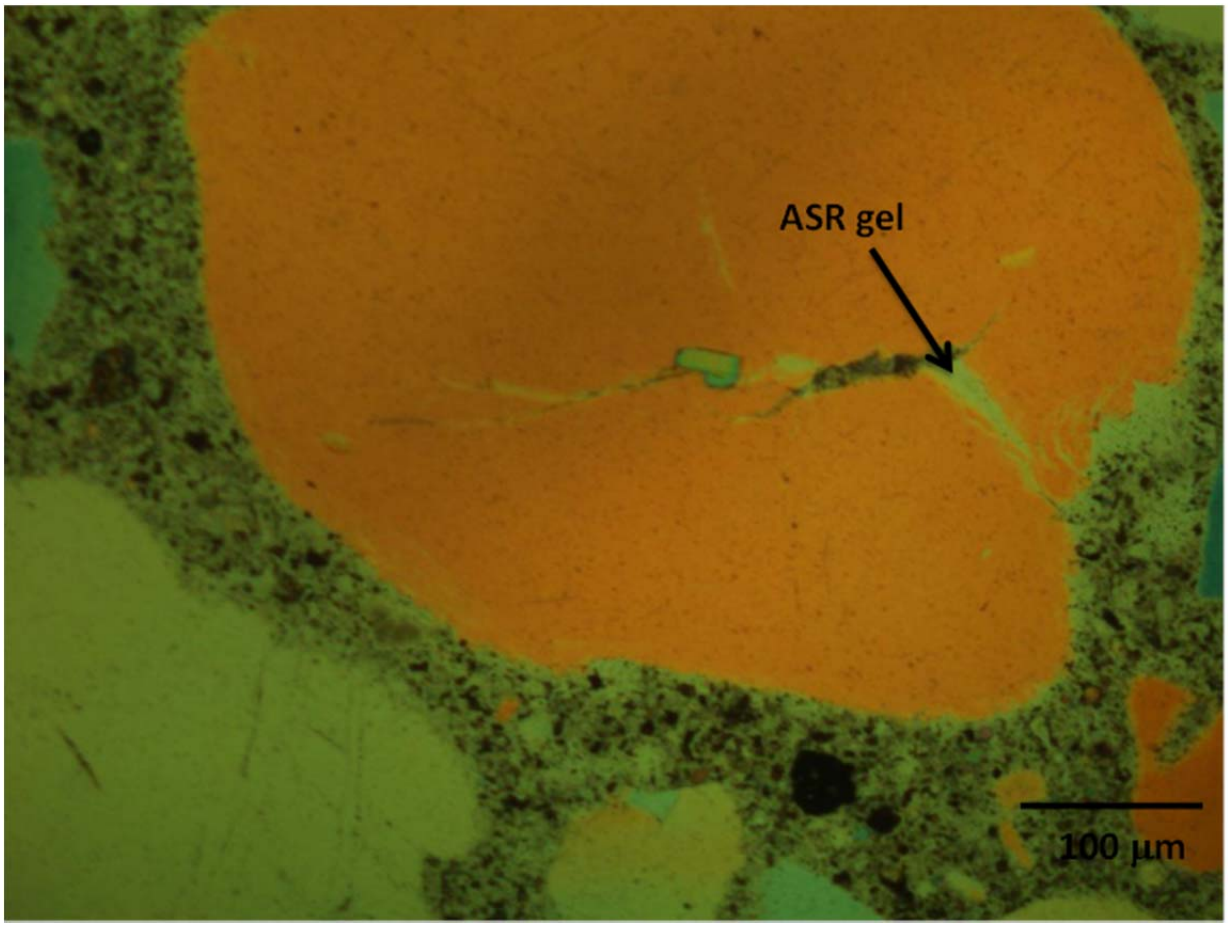

27A-4.3
45%

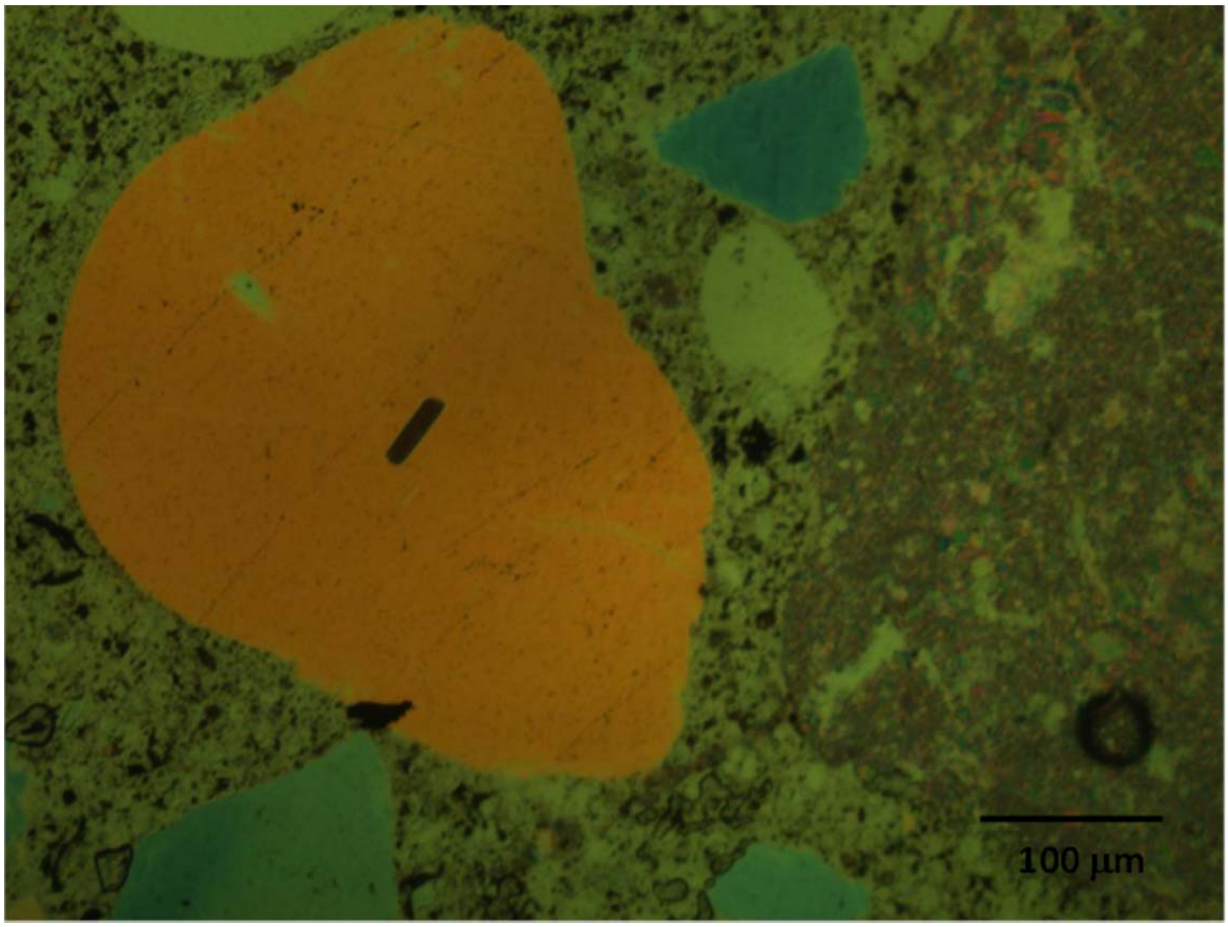

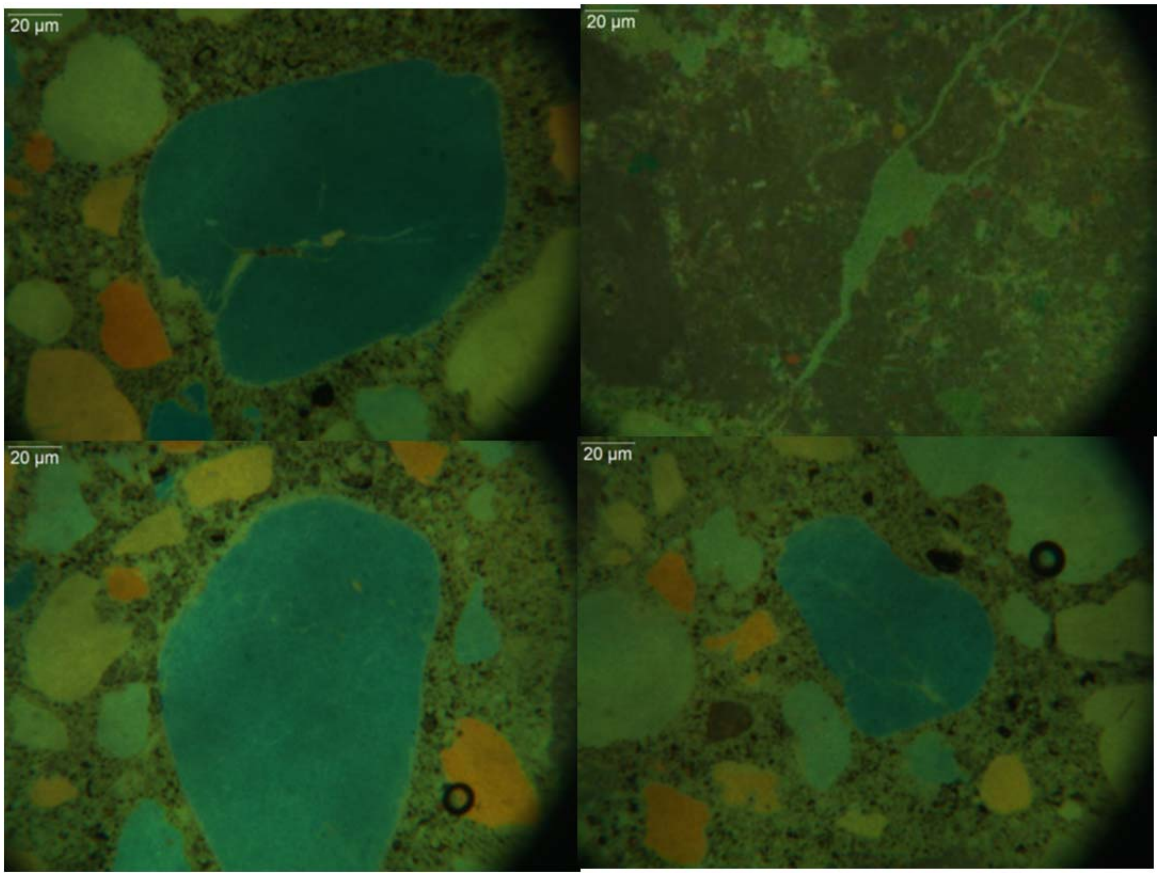
20 µm
20 µm
20 µm
20 µm

29B-1

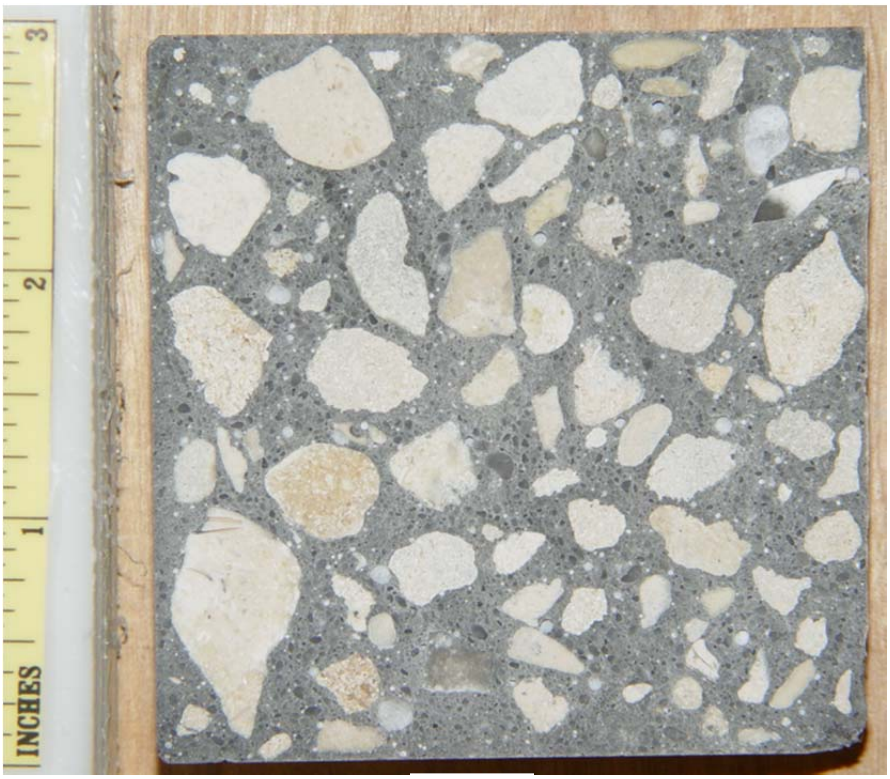

29A-2

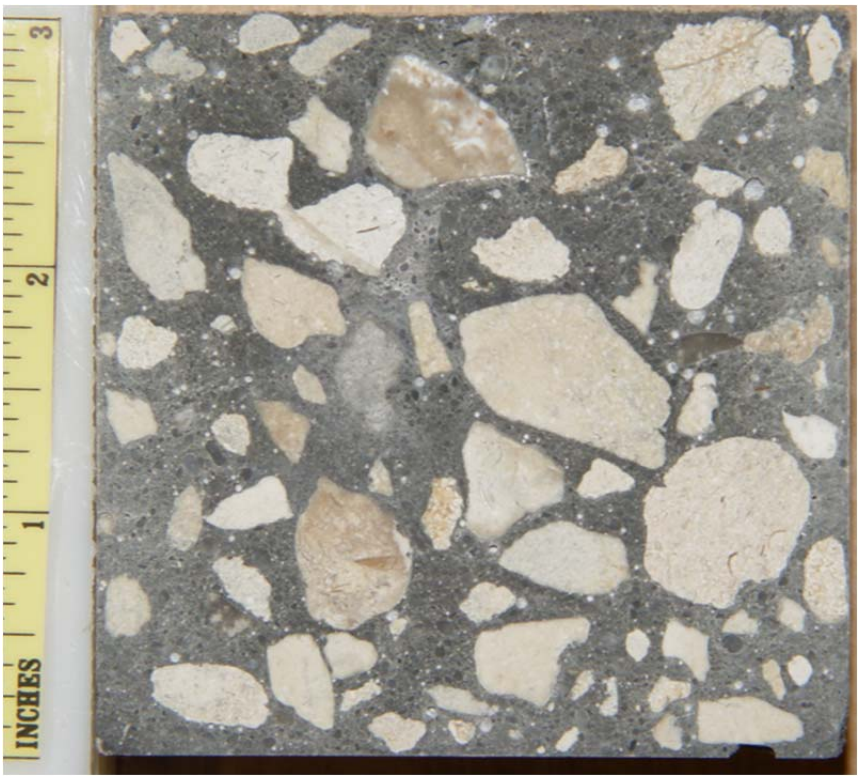

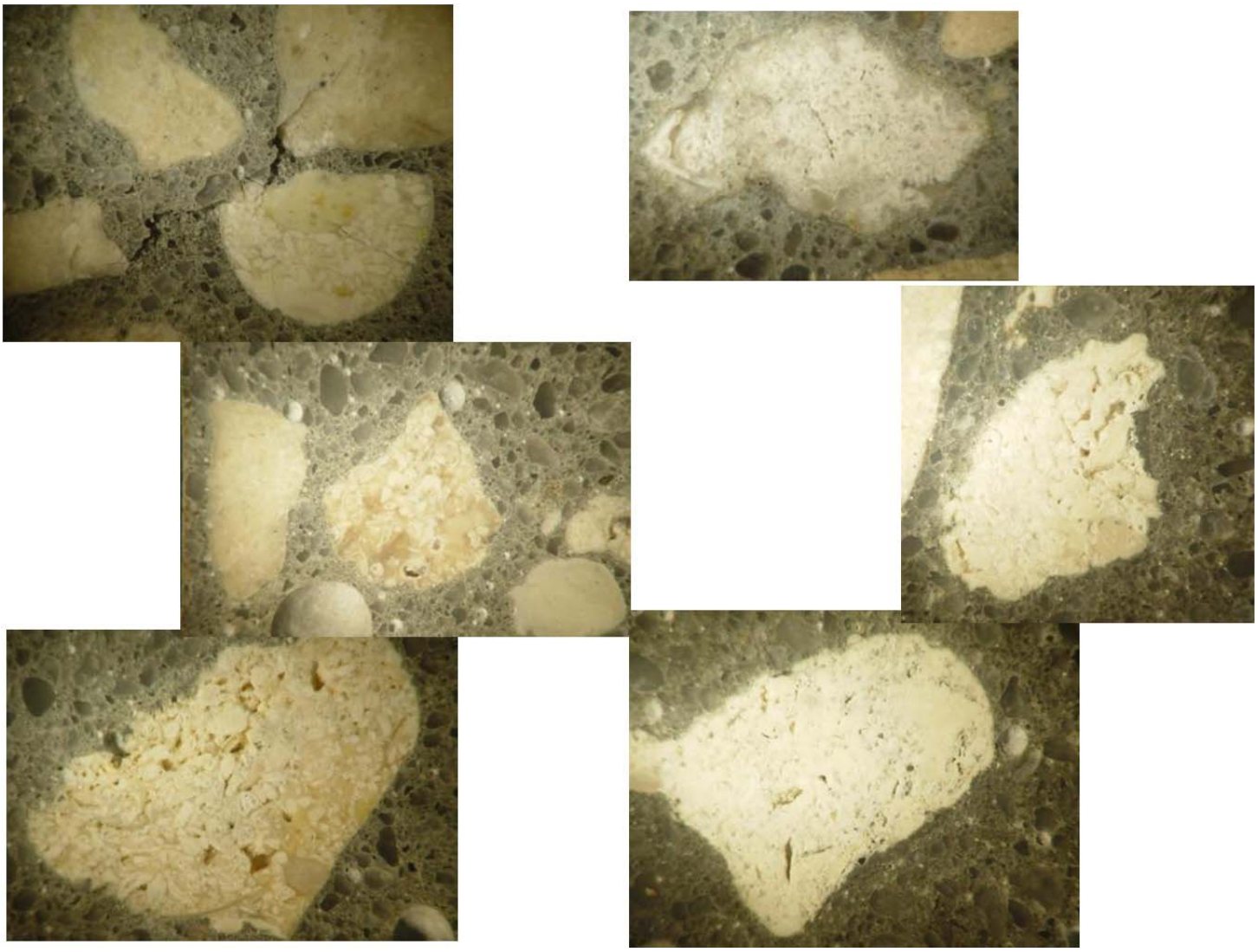

29B-1.3
30%

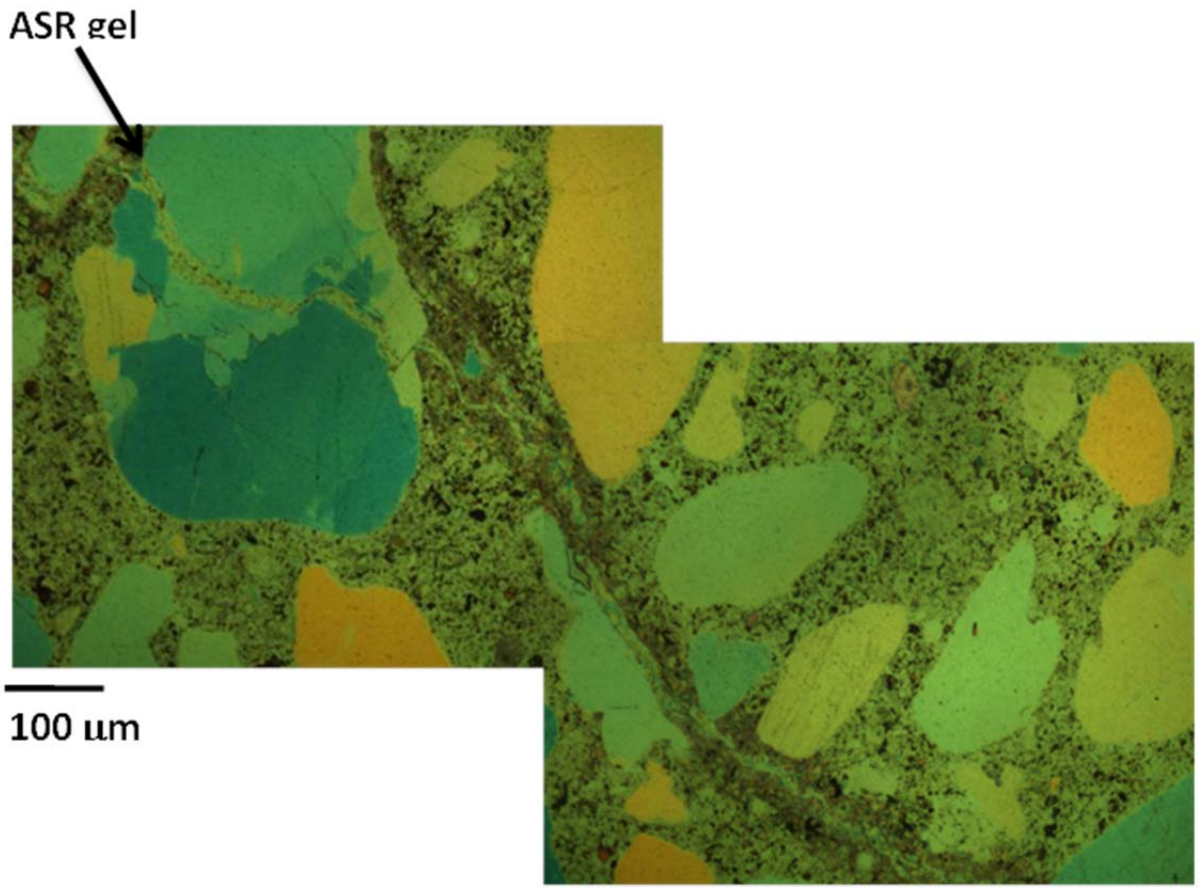

29B-1.4
45%

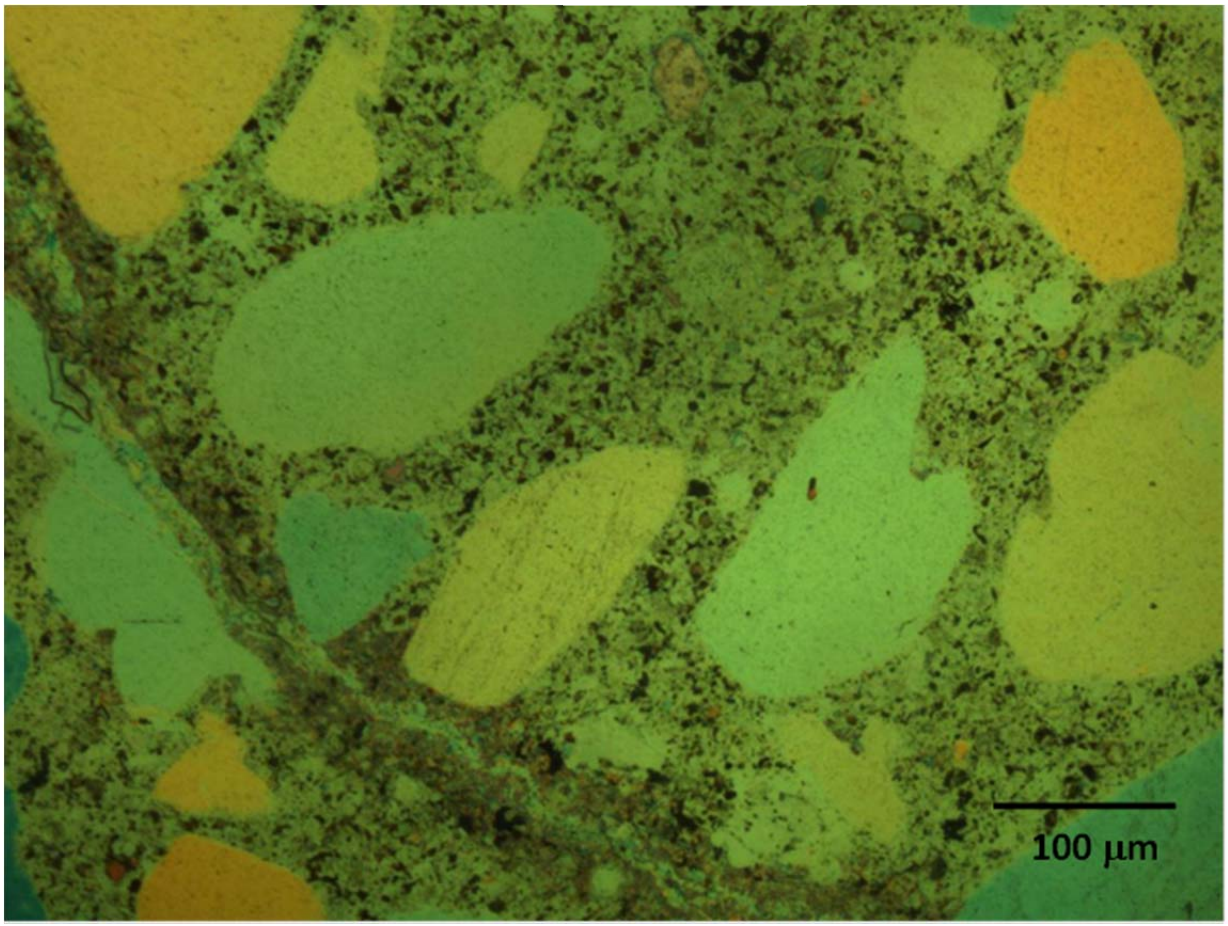

29B-2.1
15%

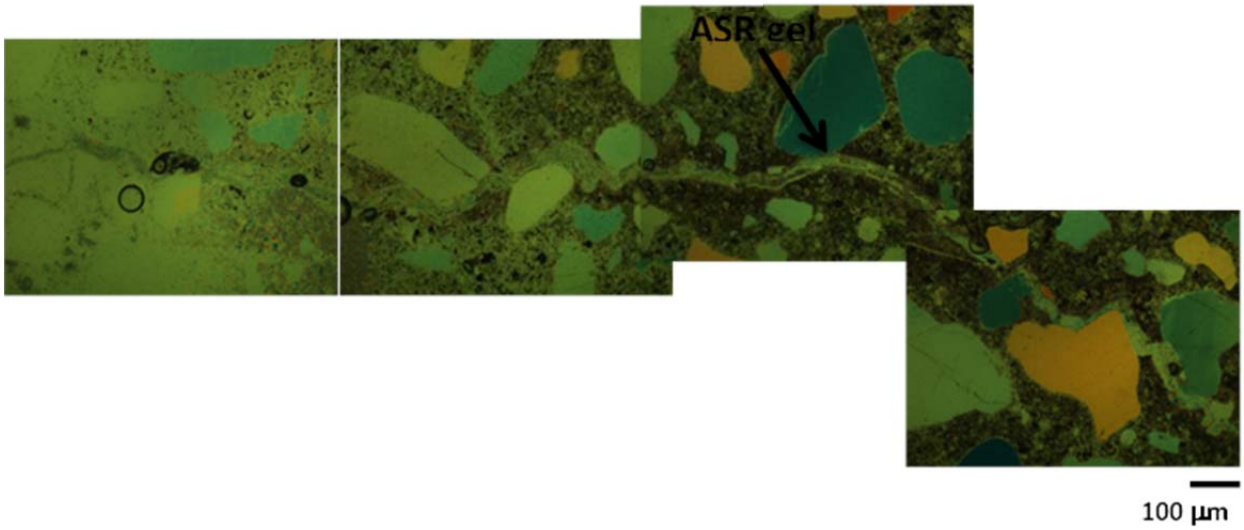

29B-2.2
25%

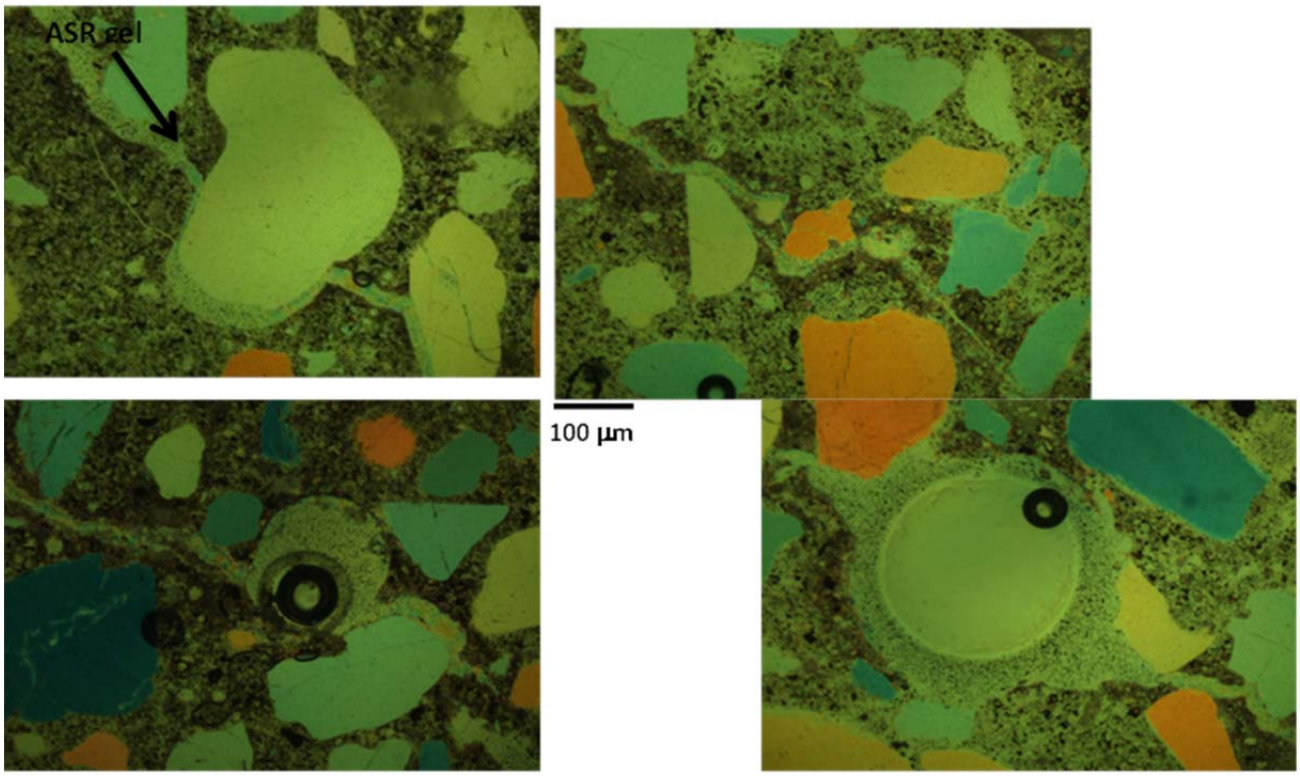

29B-2.3
45%

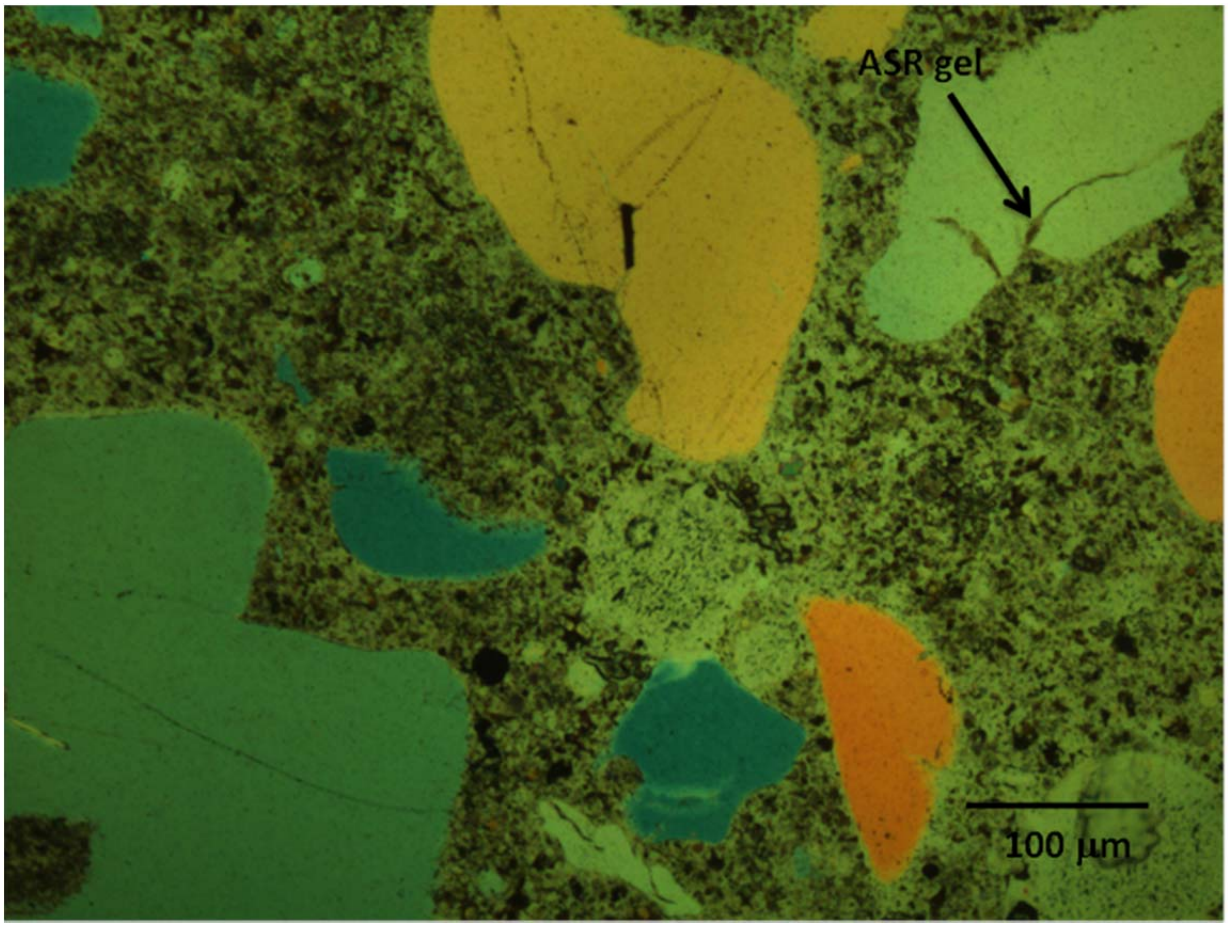

29B-3.2
30%

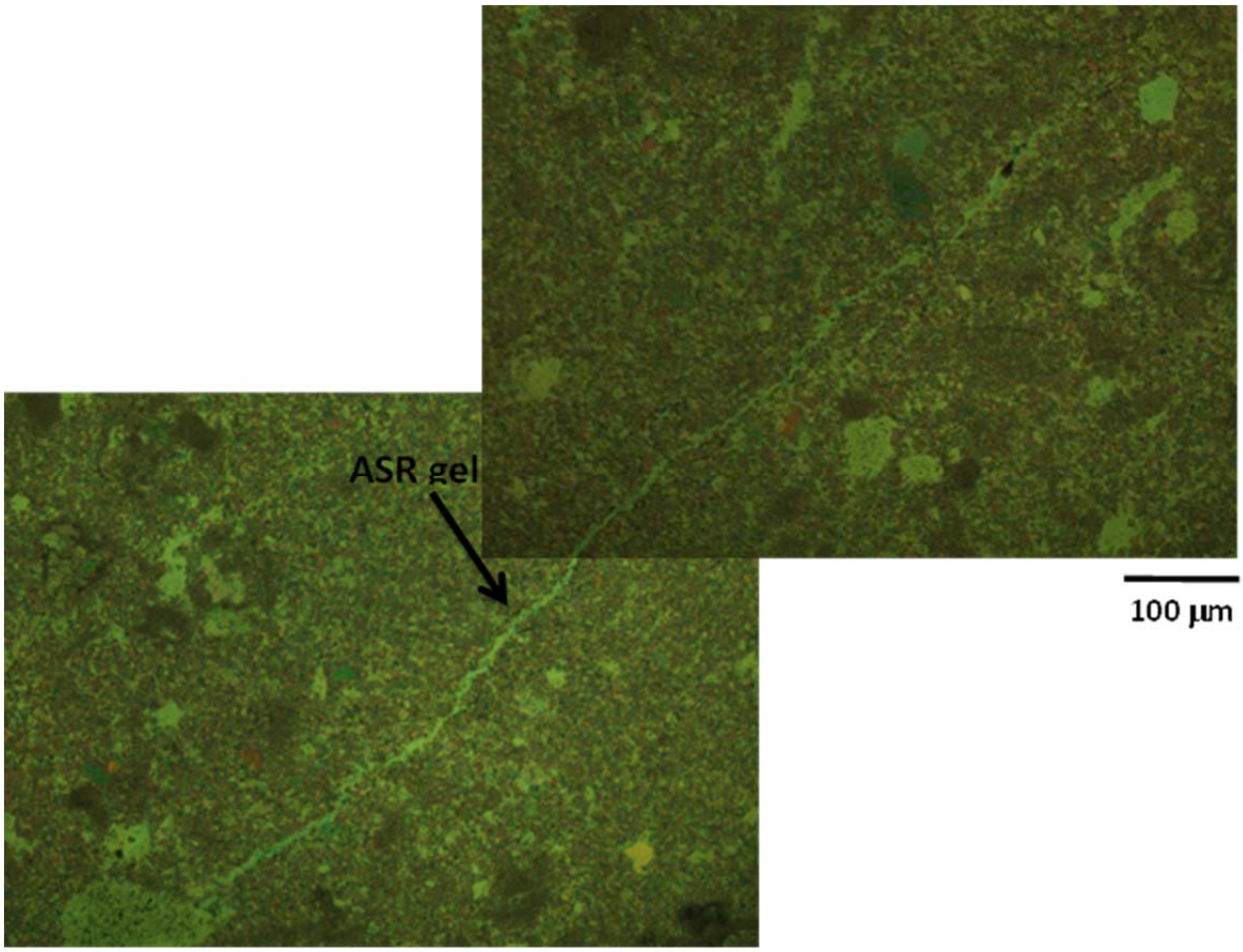

FL3

– Specimens 49A and 45A contained EqA=1, latter by NaOH the former by HA cement
- 45A-1, 45A-2
- 49A-1, 49A-2

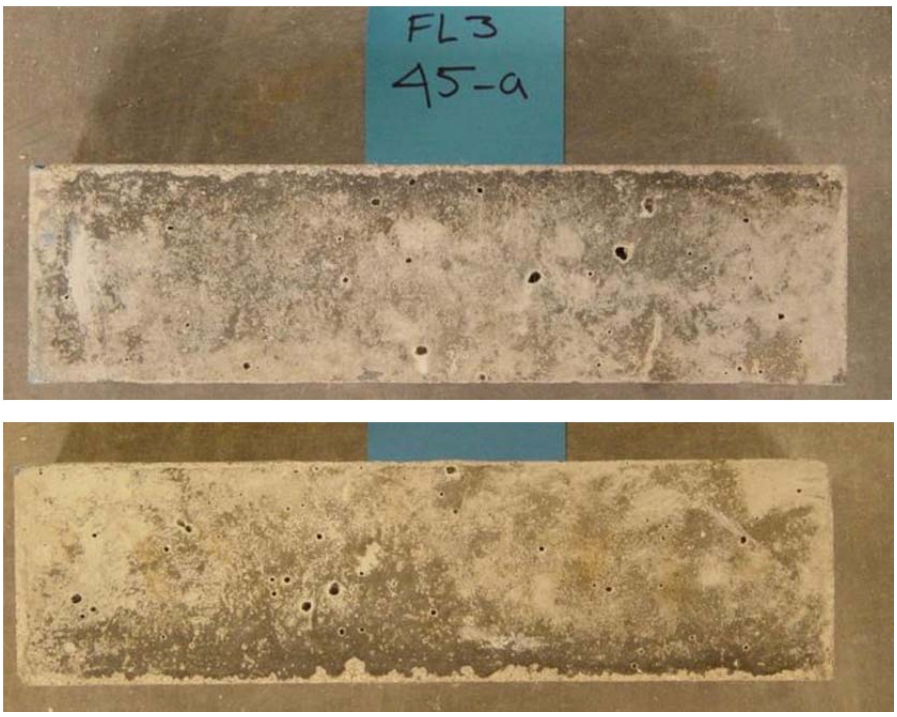

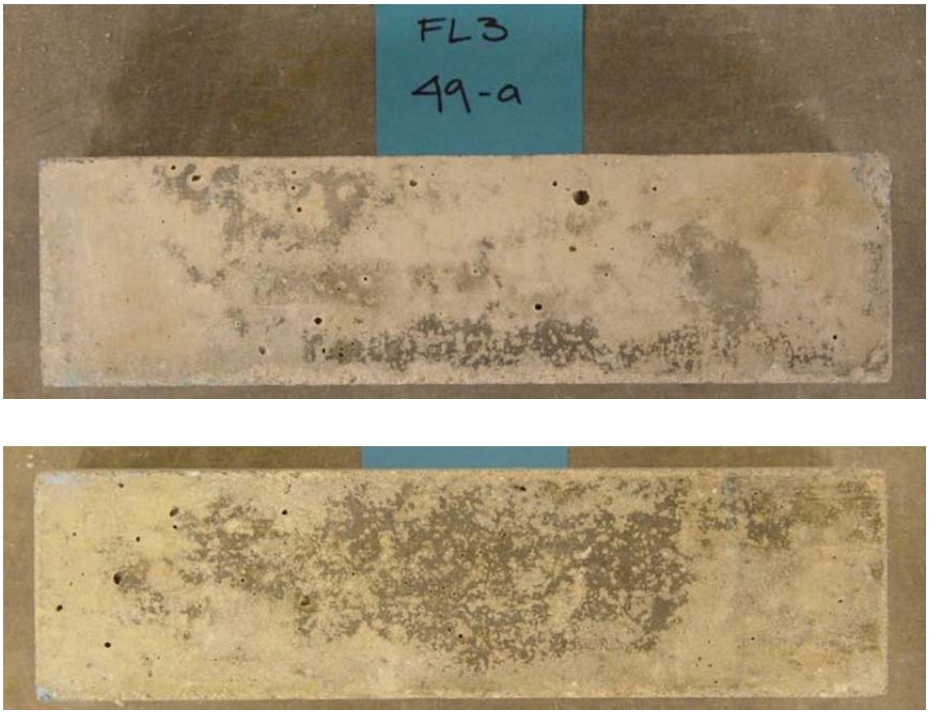
FL3
49-a

45A-

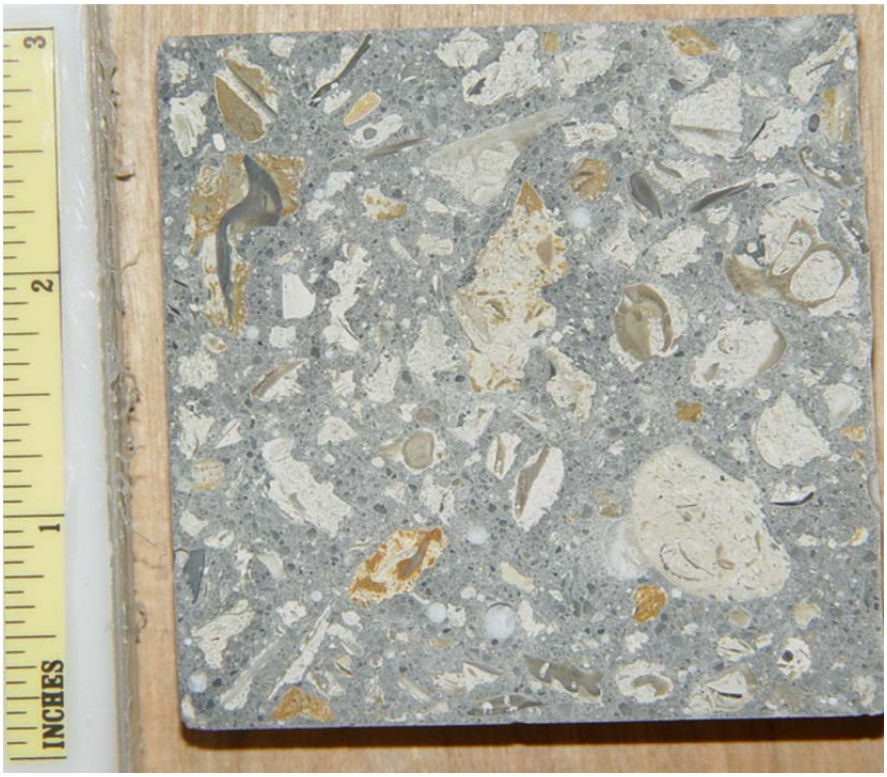

45A-2

45A-1.3
45%

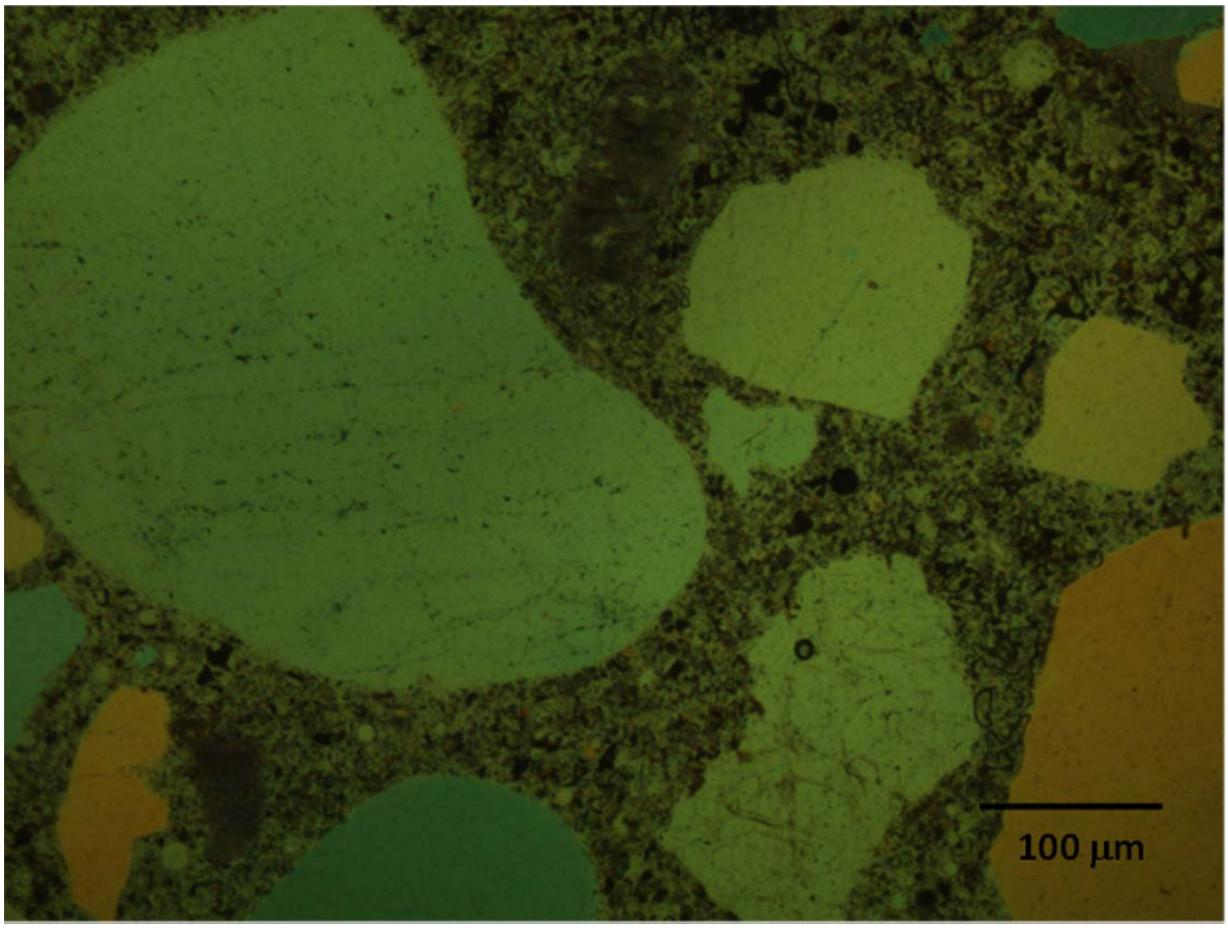

45A-2.3
45%

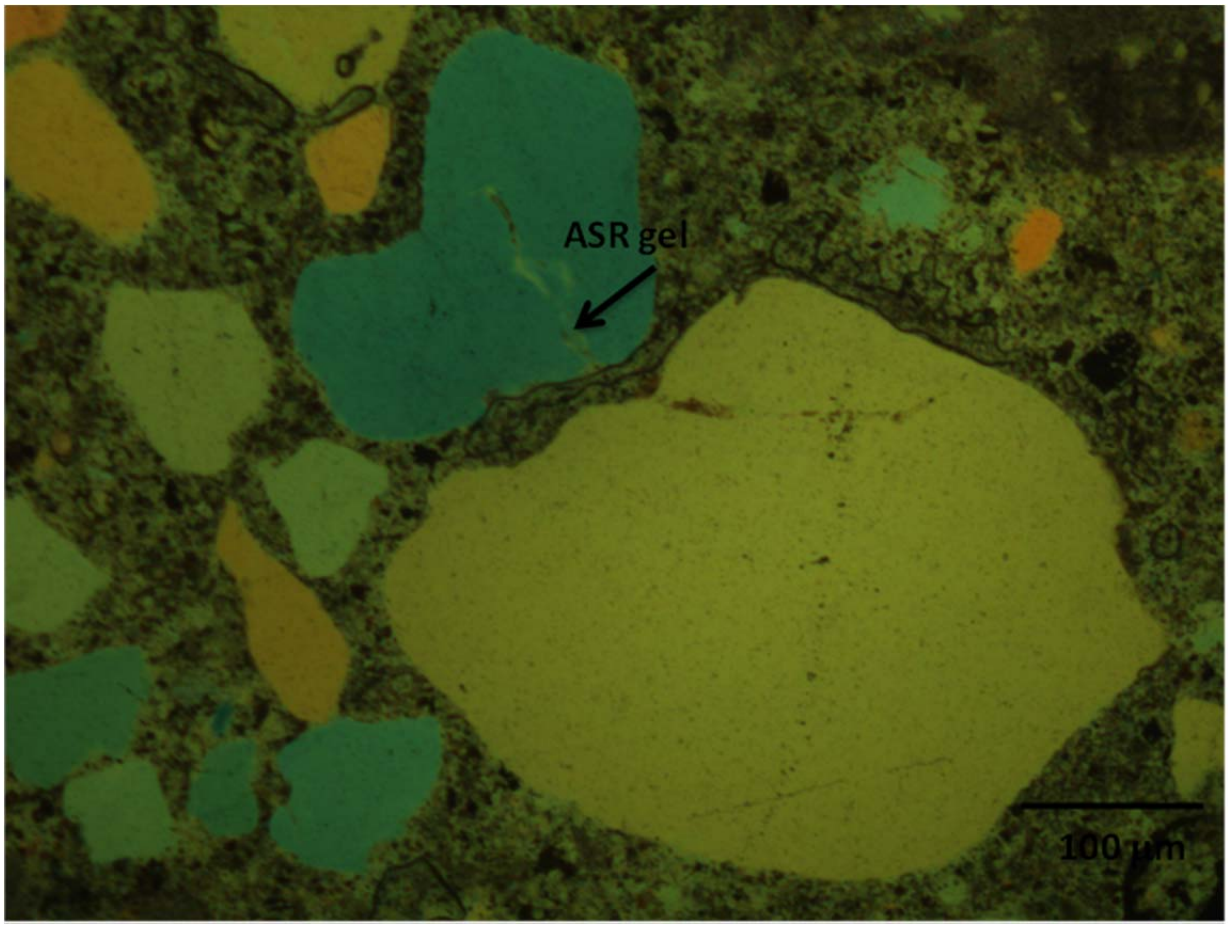

45A-3.4
45%

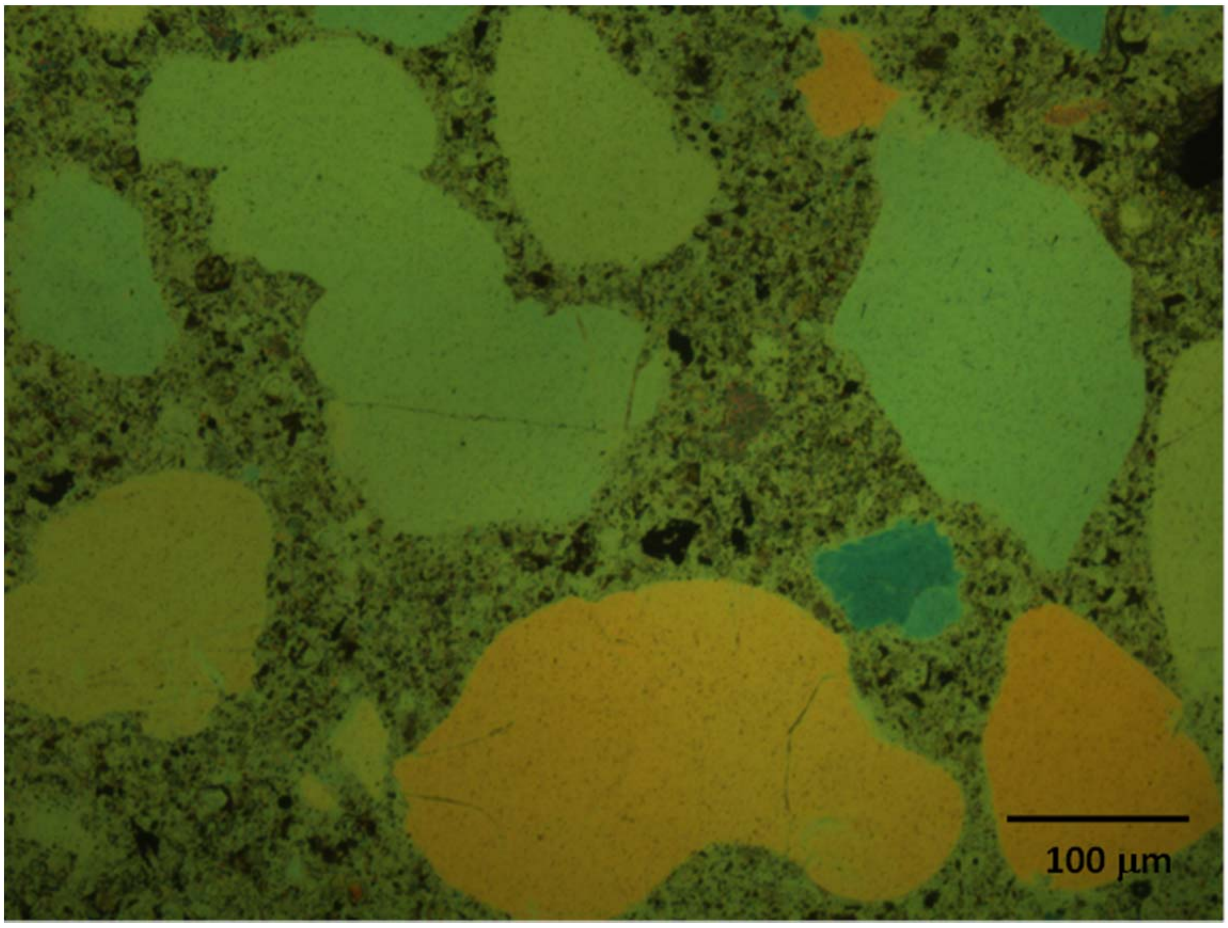

45A-4.1
45%

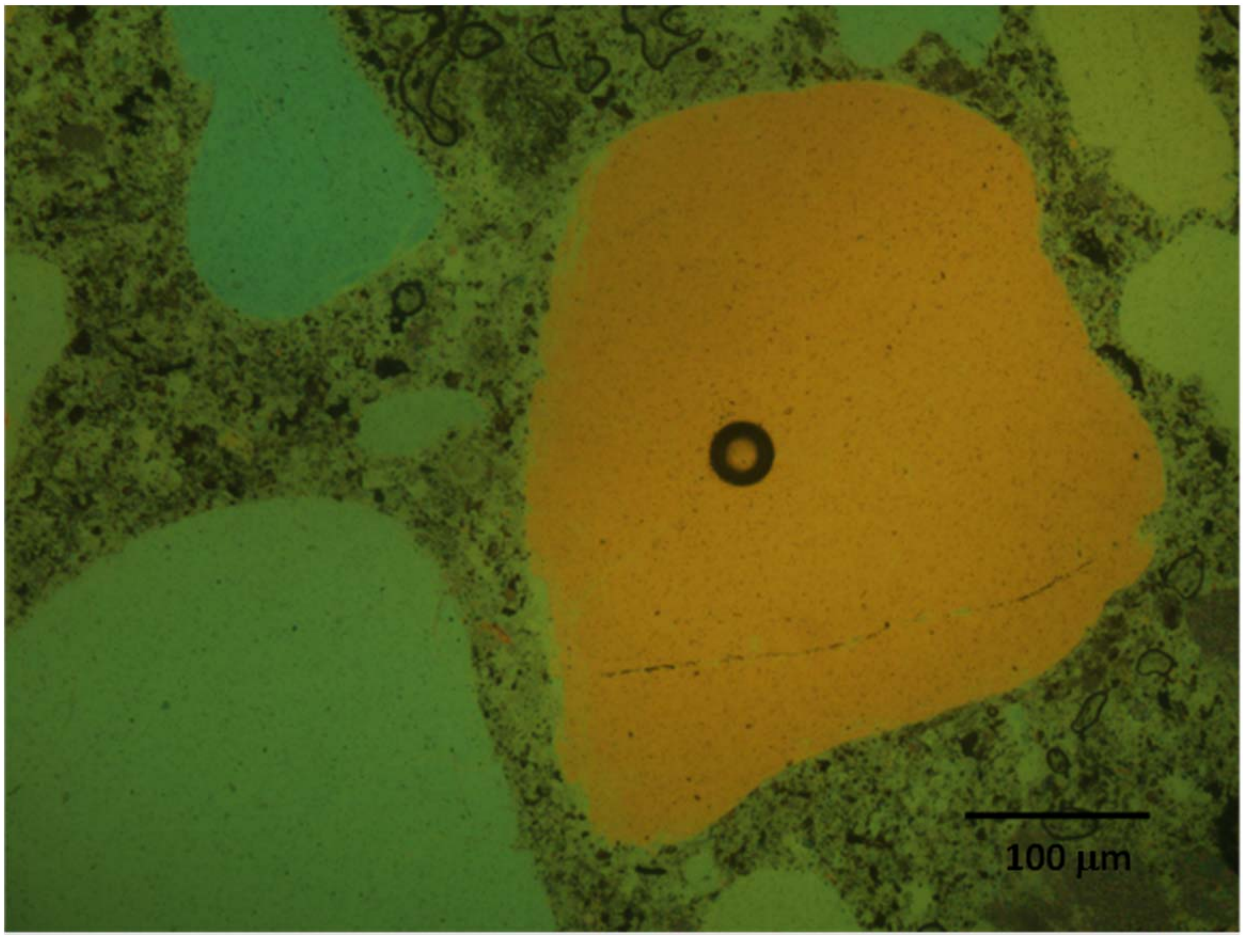

45A-5.1
45%

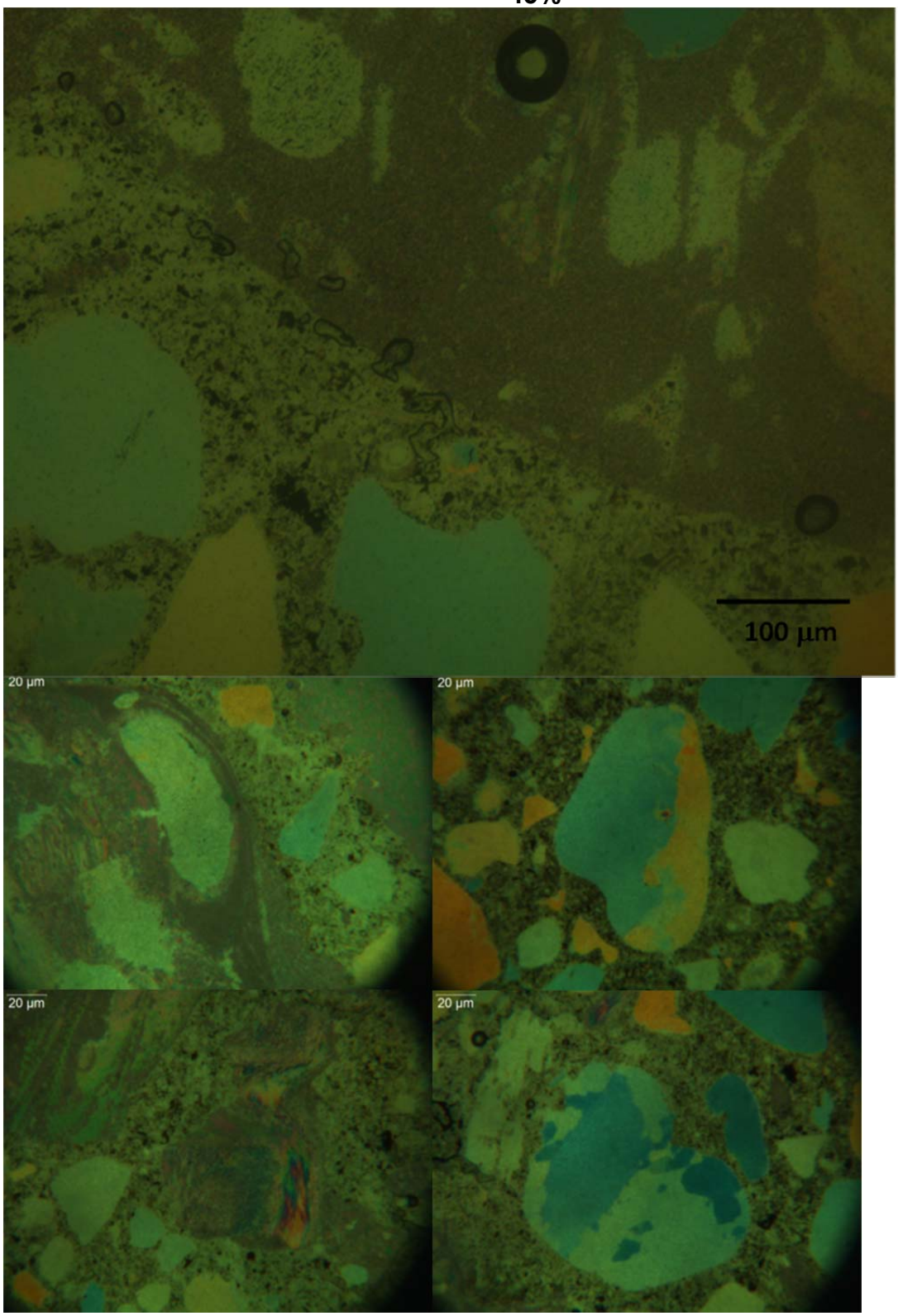

49A-1

49A-2

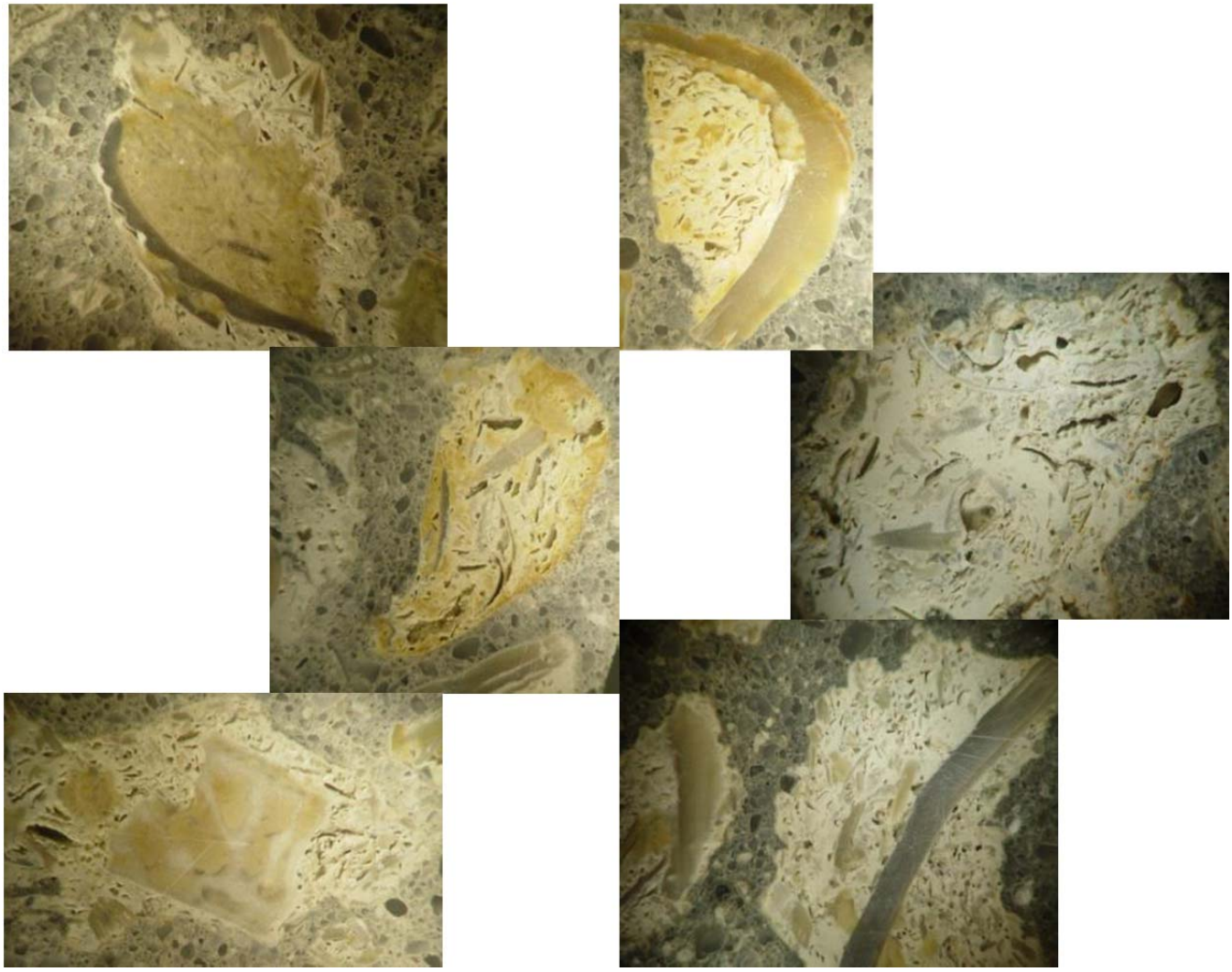

49A-1.3
45%

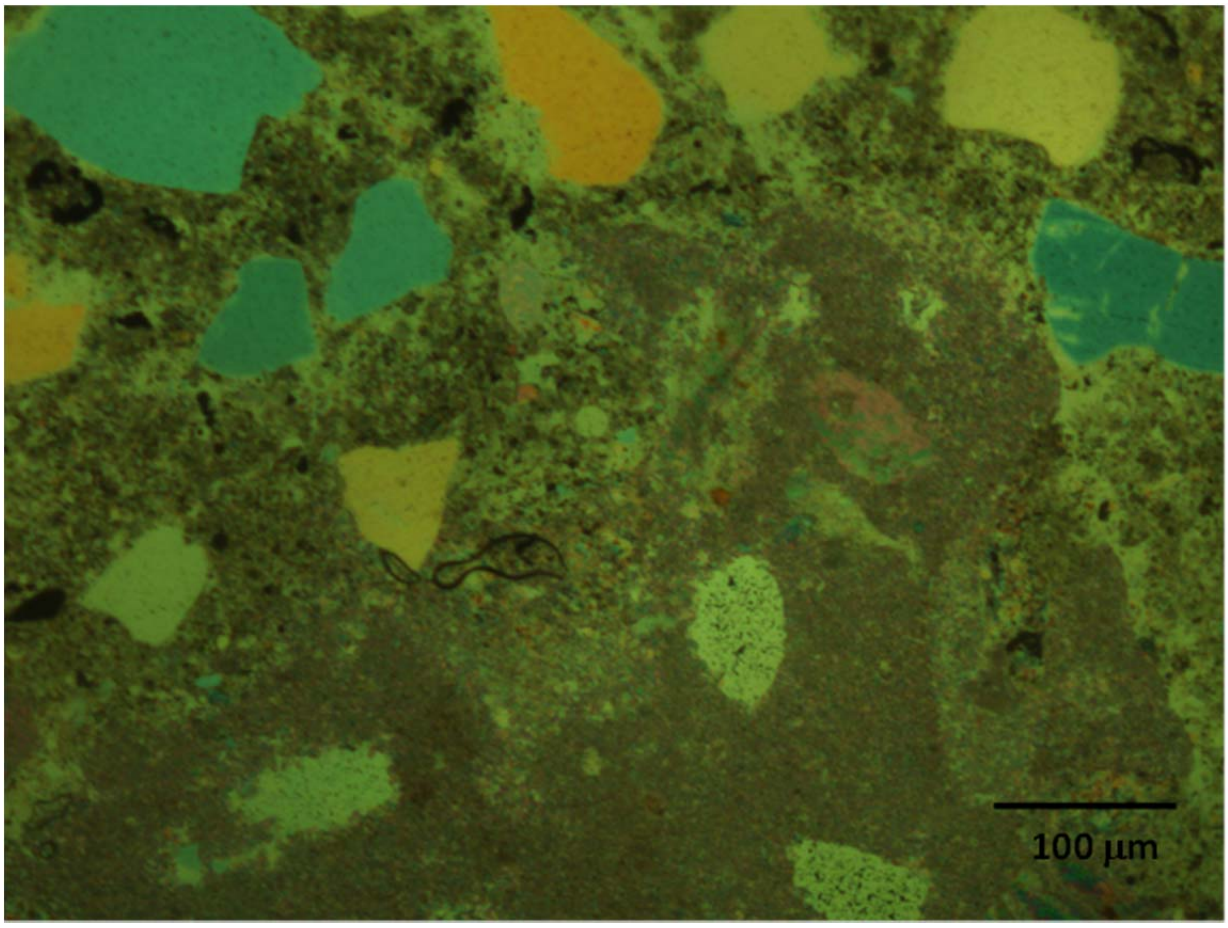

49A-2.1
45%

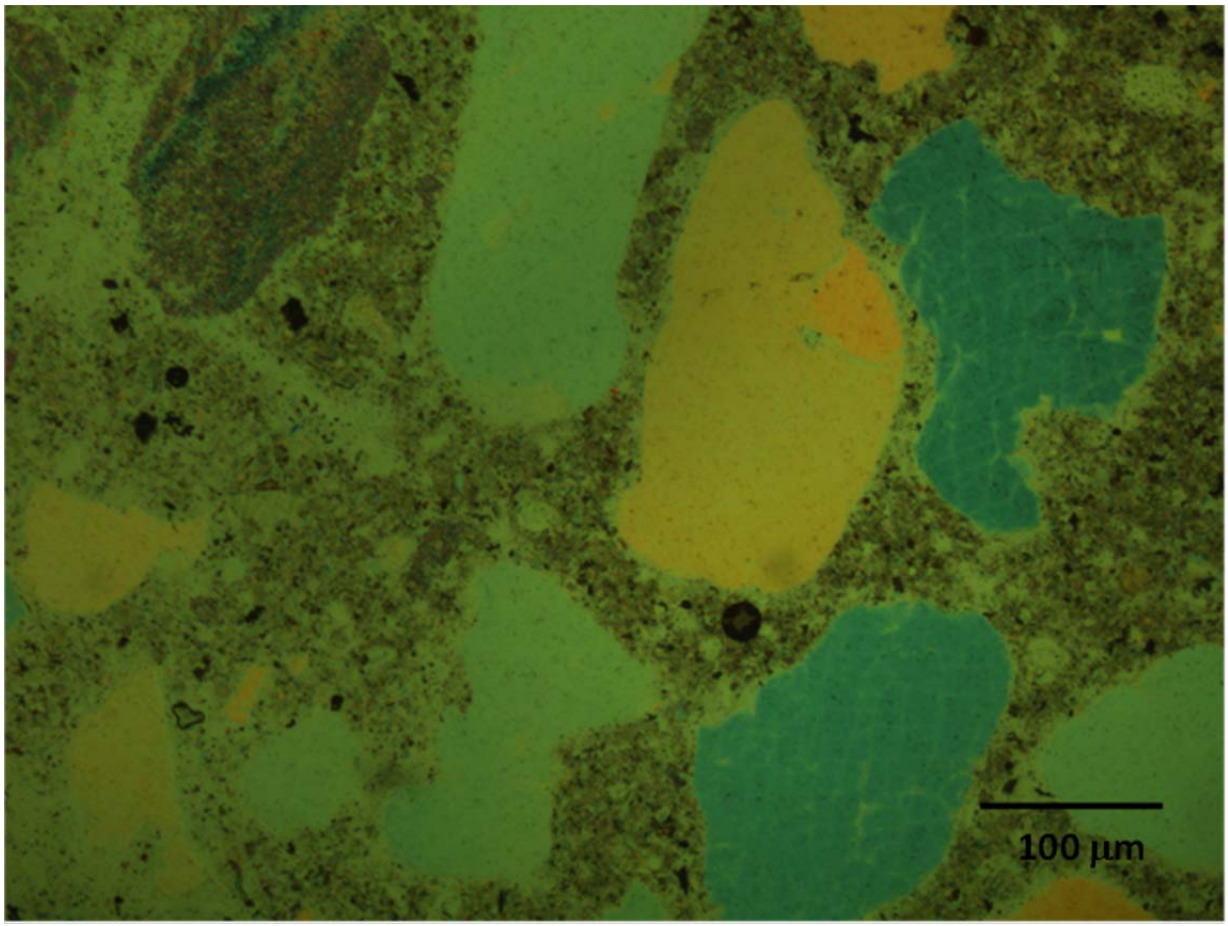

49A-3.1
45%

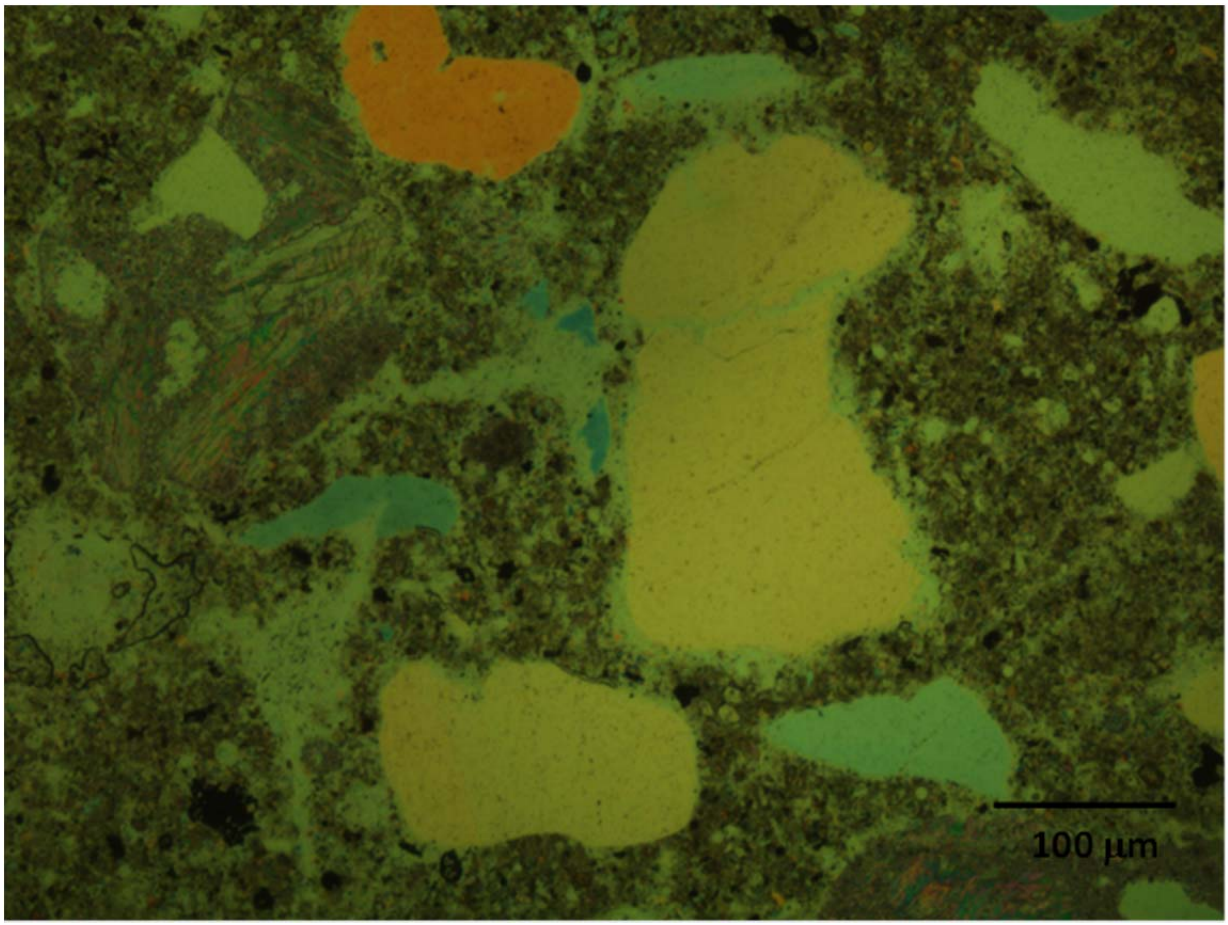

49A-4.2
45%

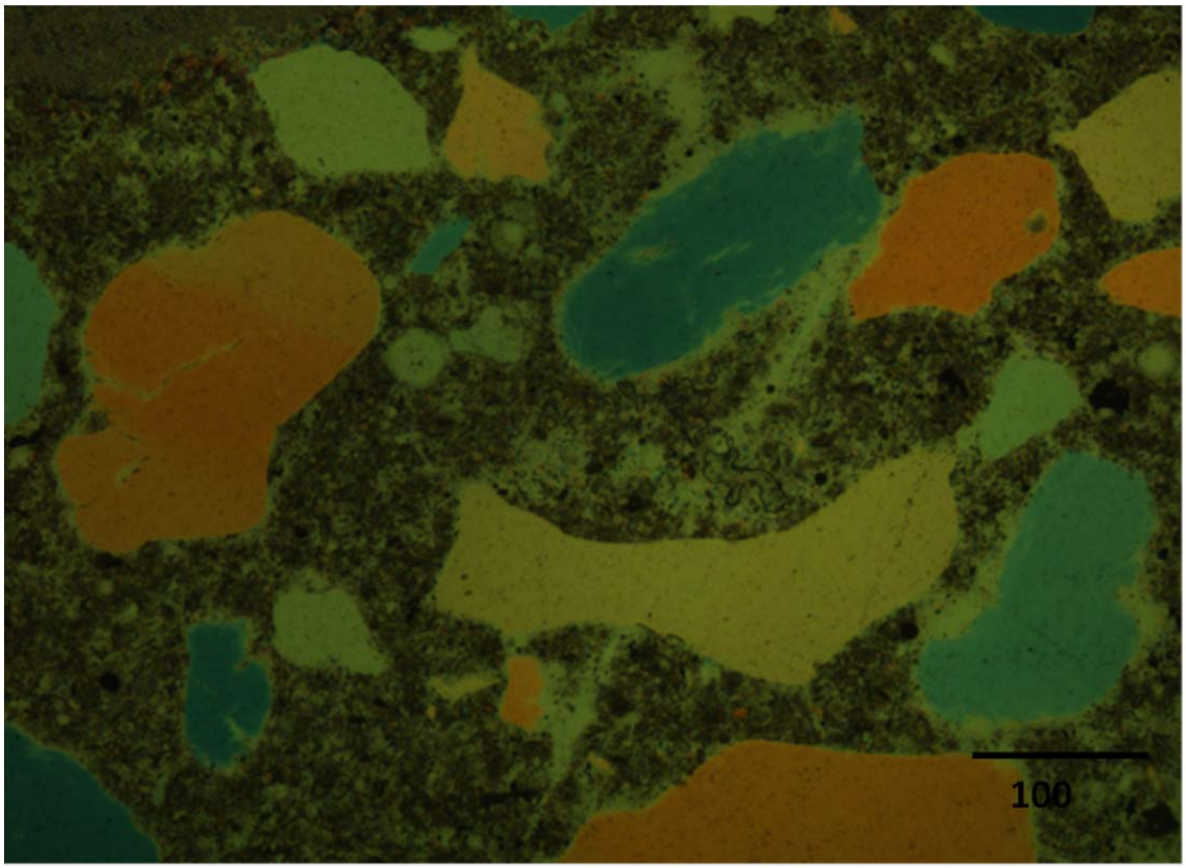

49A-4.3
45%

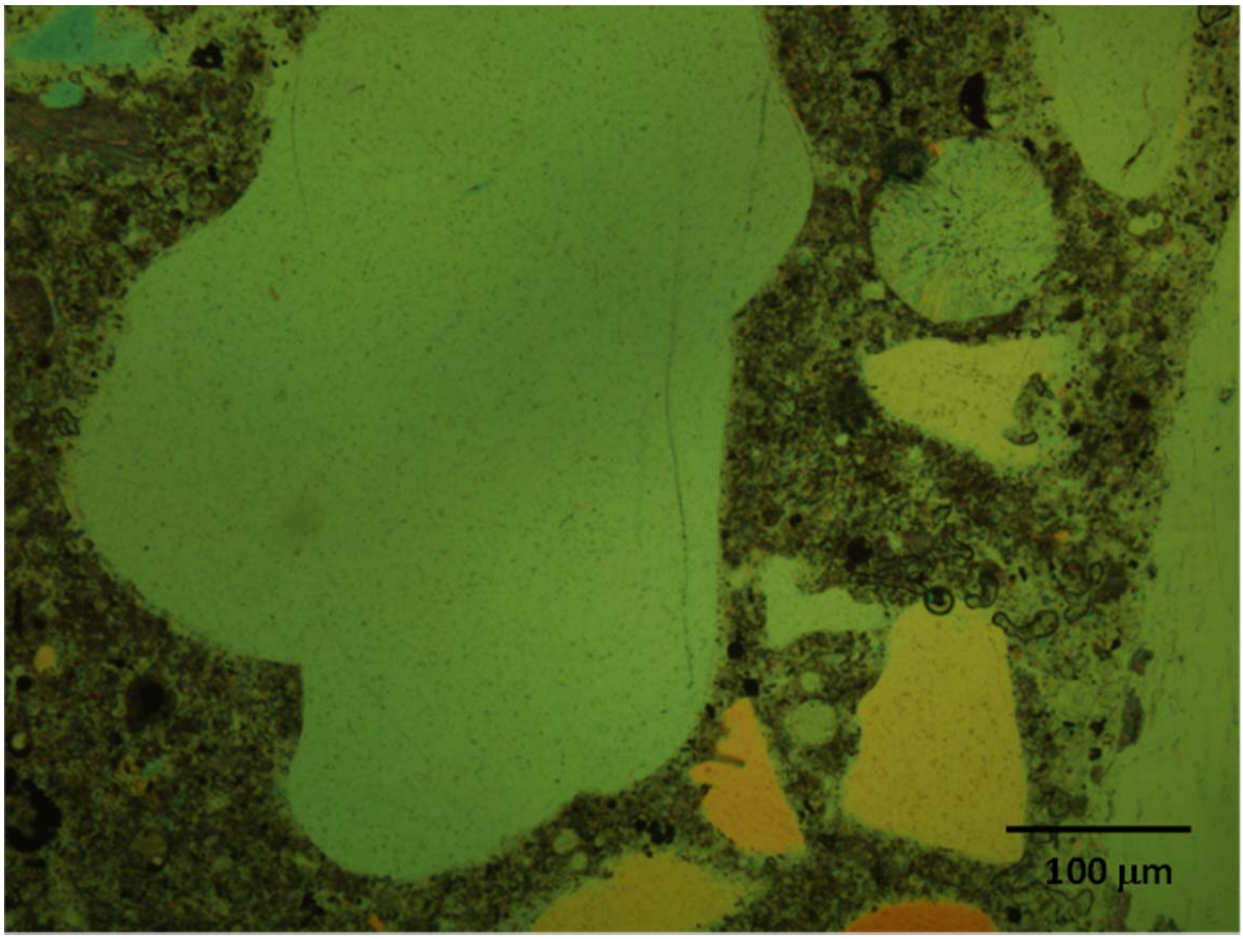

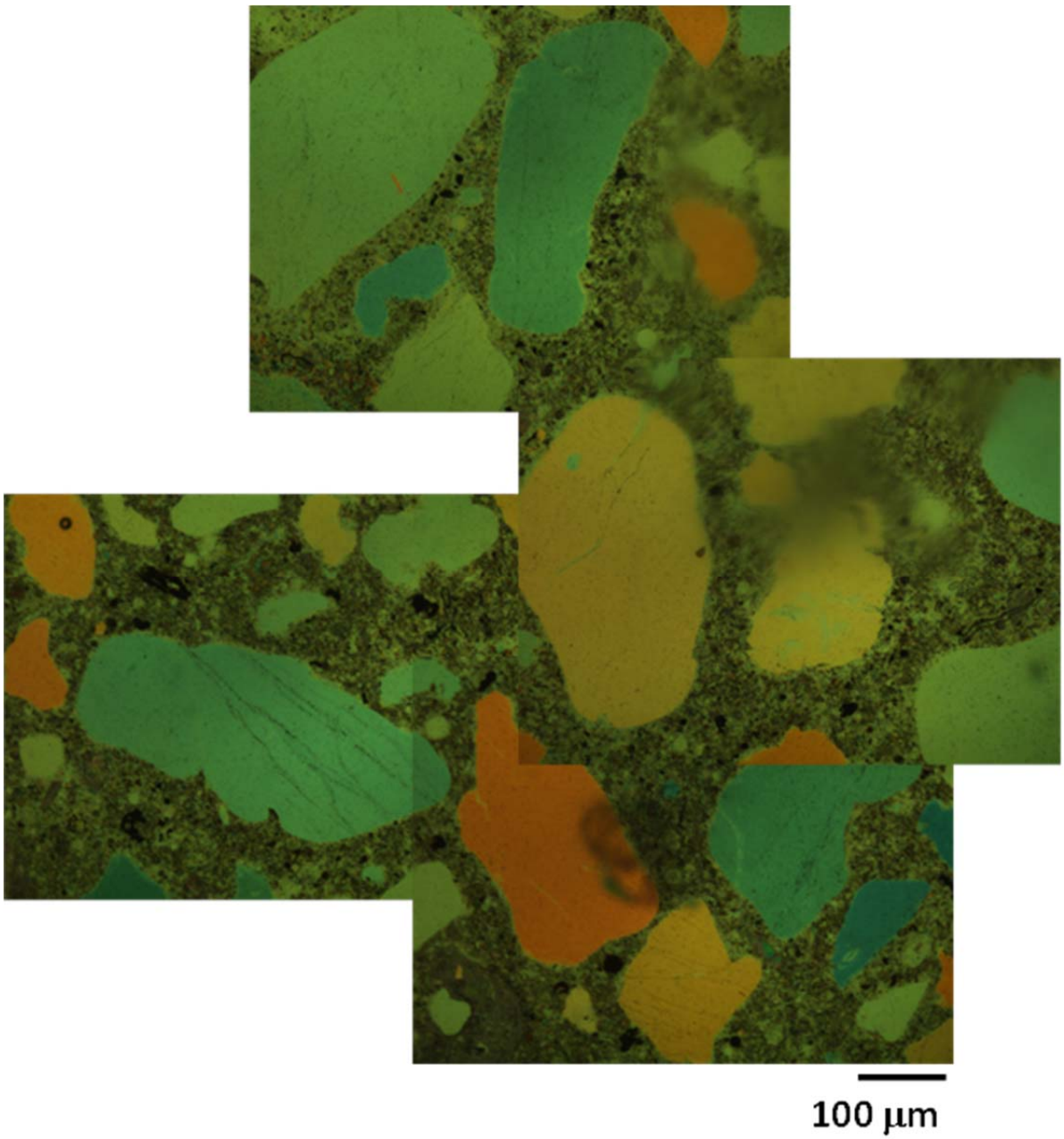
100 µm

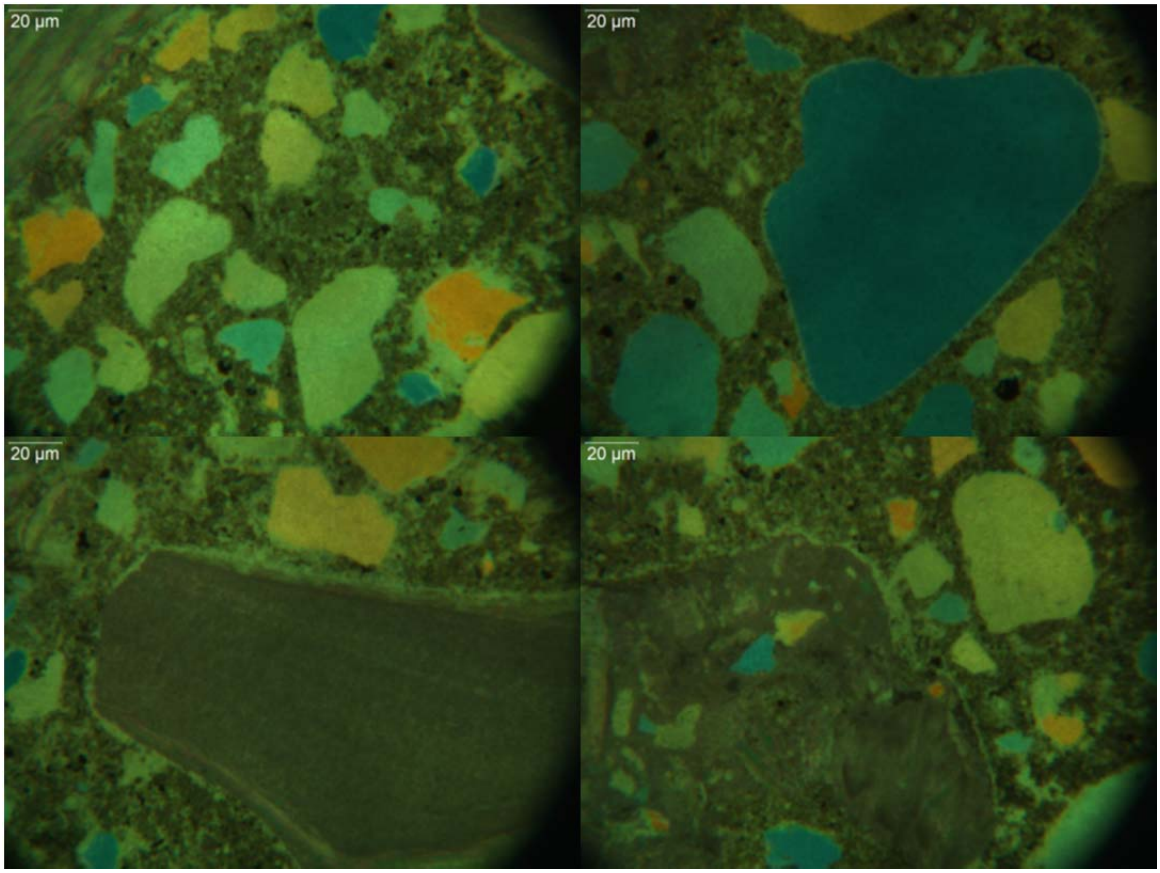
20 µm
20 µm
20 µm
20 µm

GG

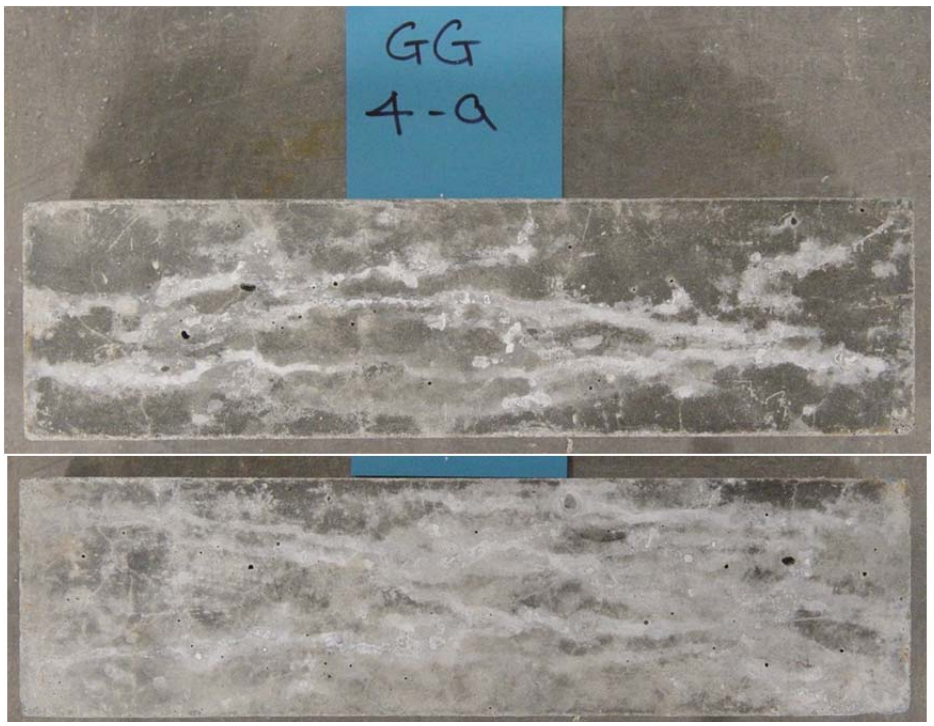

15D

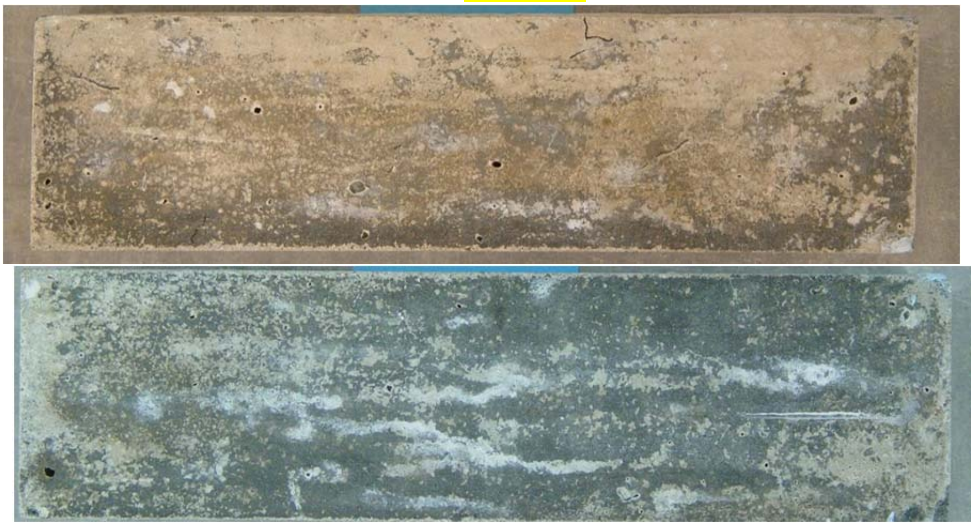

16C

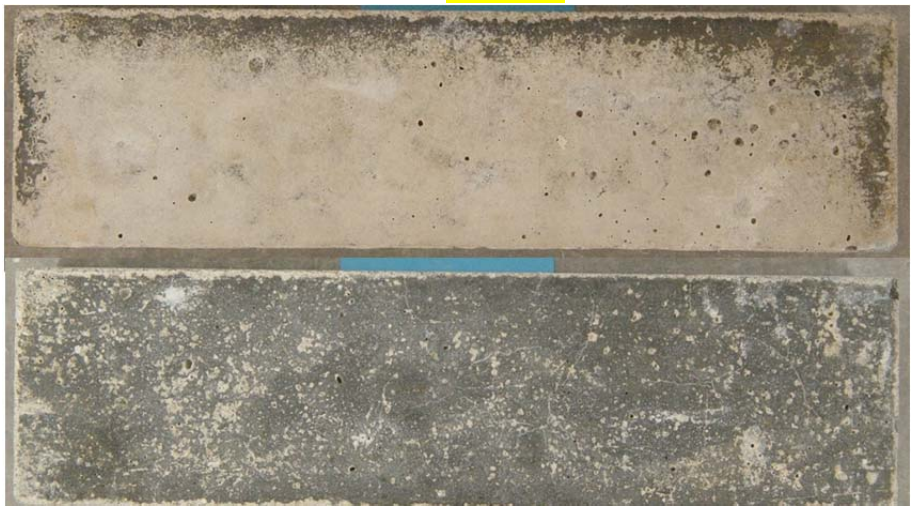

04A-1

04A-2

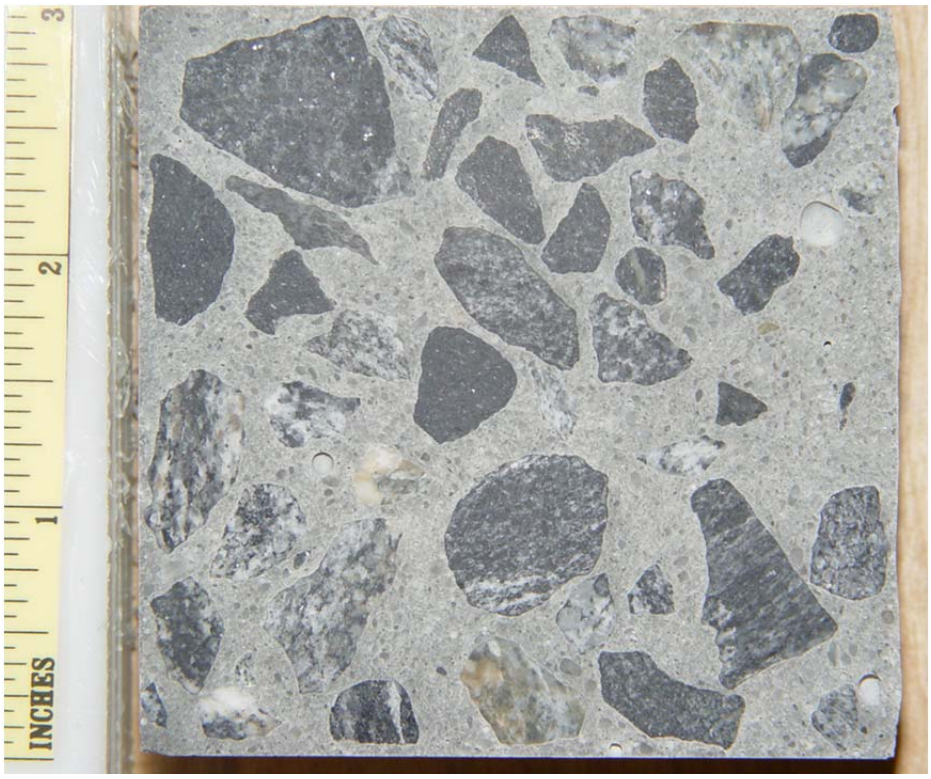

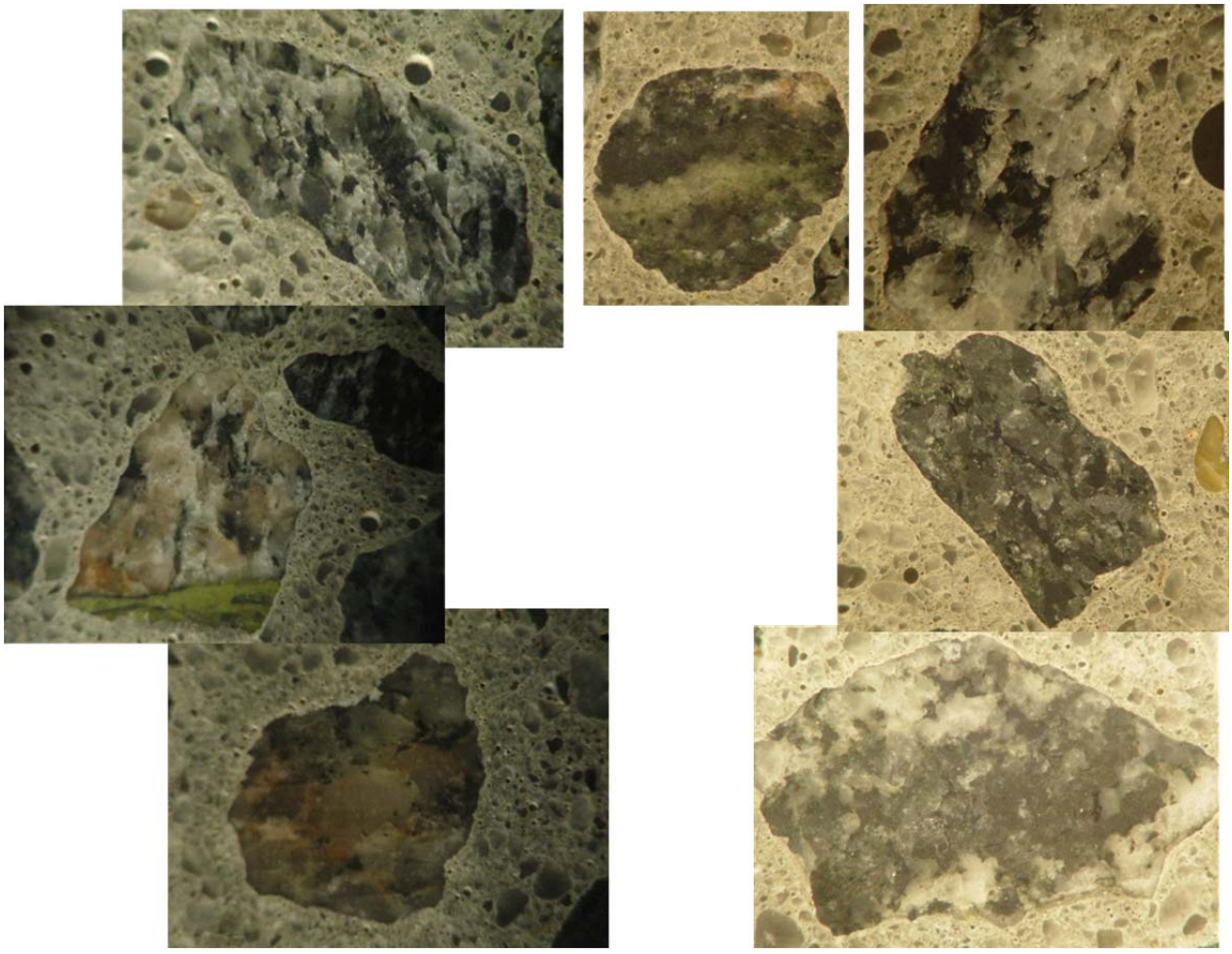

4A-3.2 45%

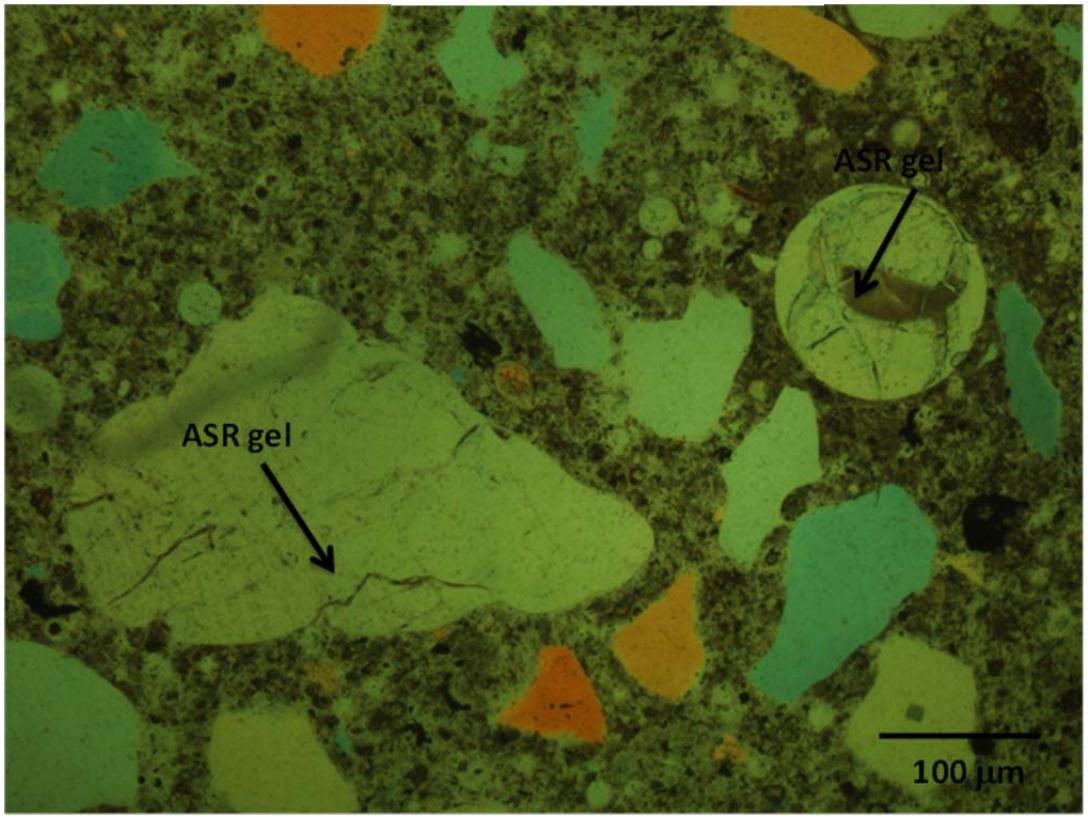

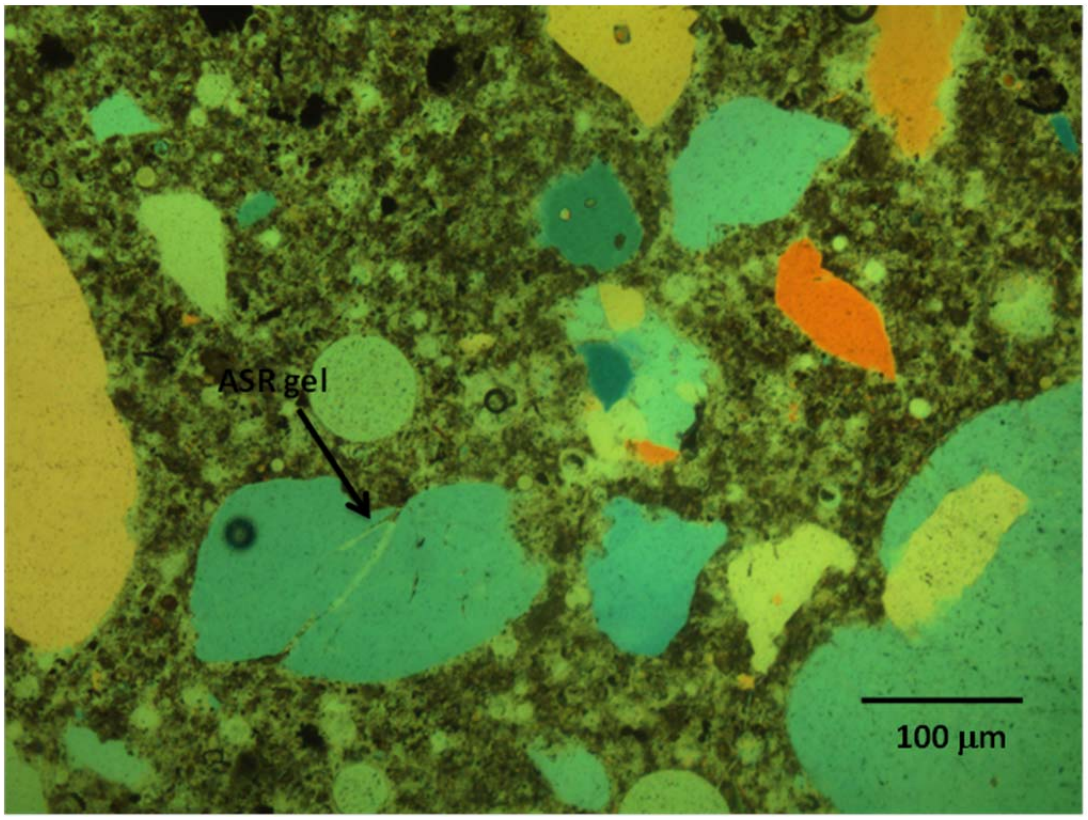

4A-3.3 45%

4A-3.3b
45%

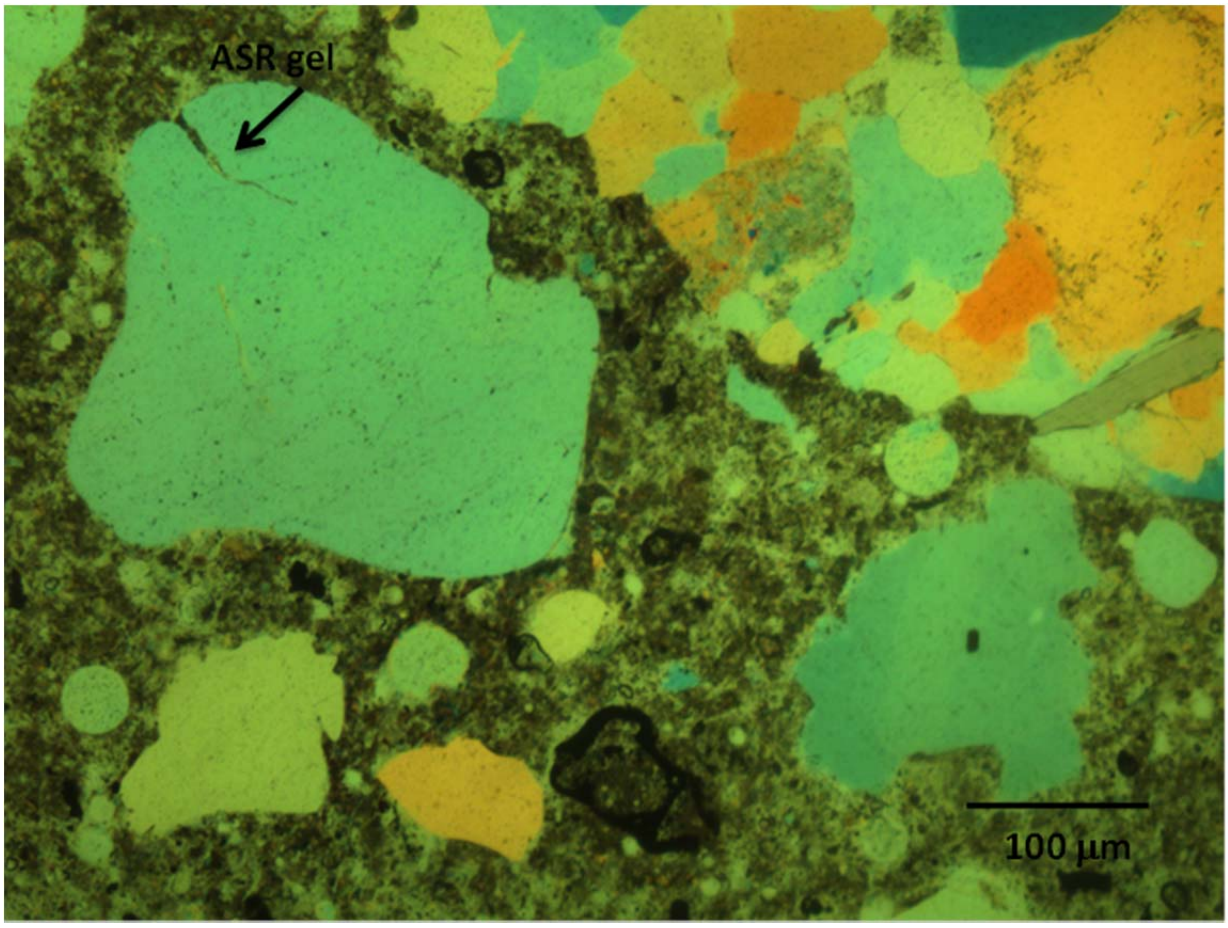

4A-2.1
45%

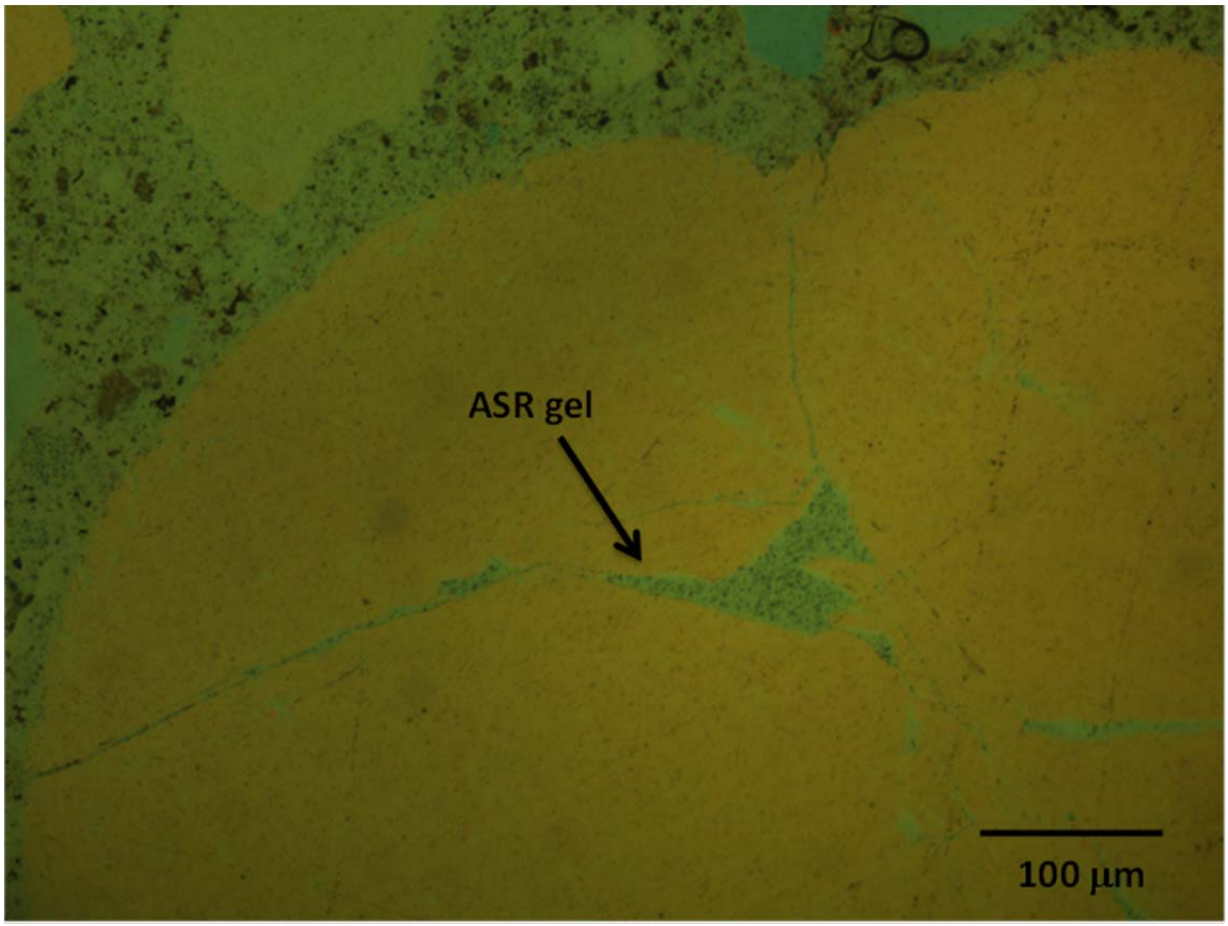

4A-2.1b 45%

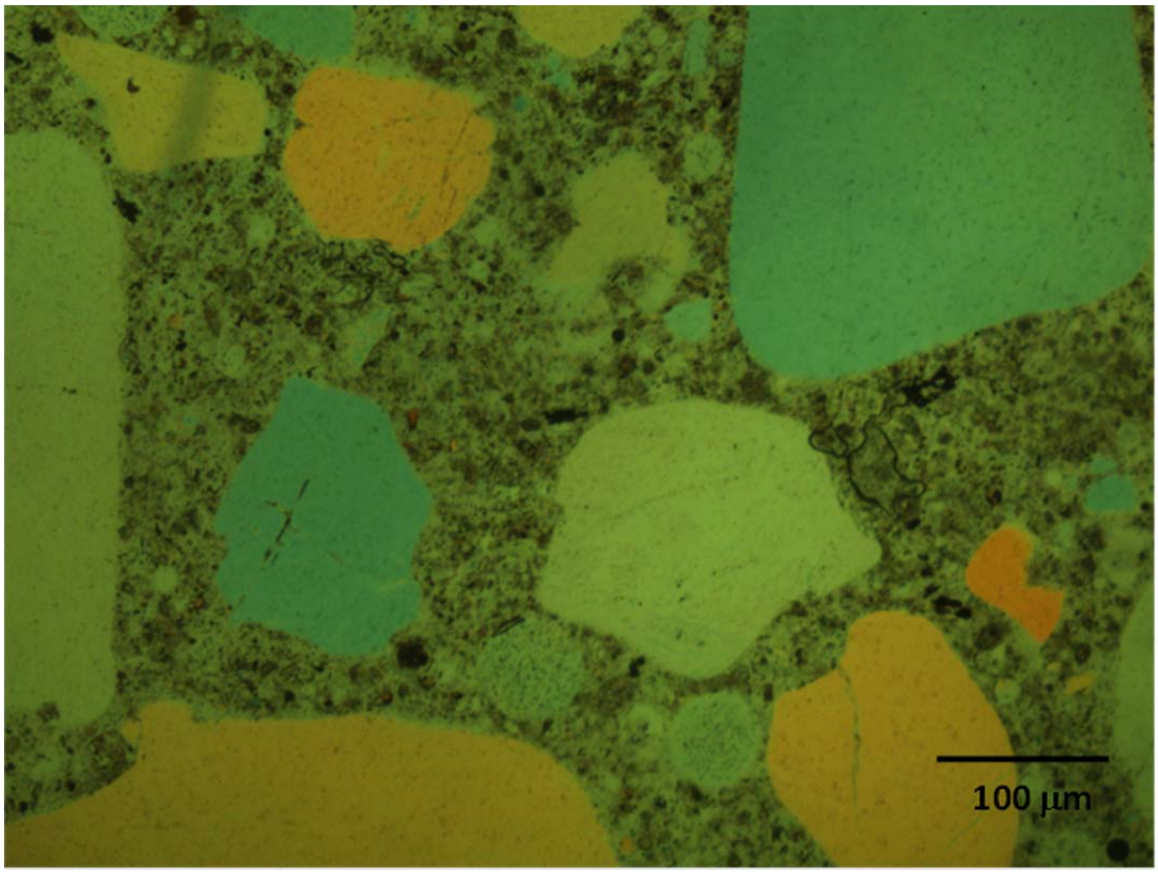

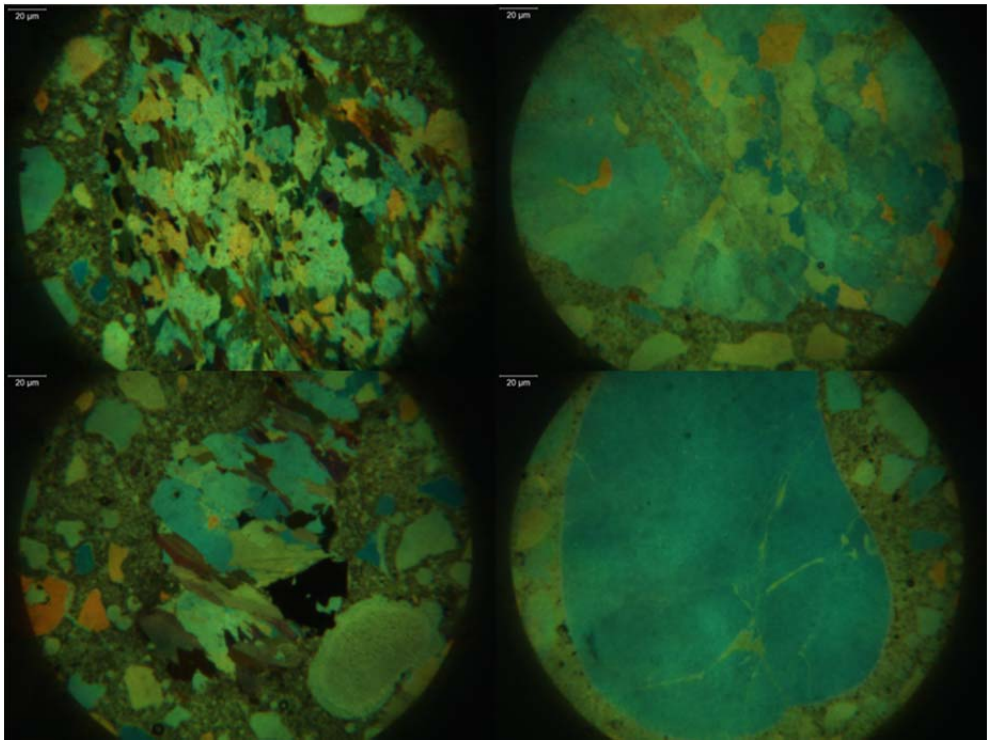

15D-1

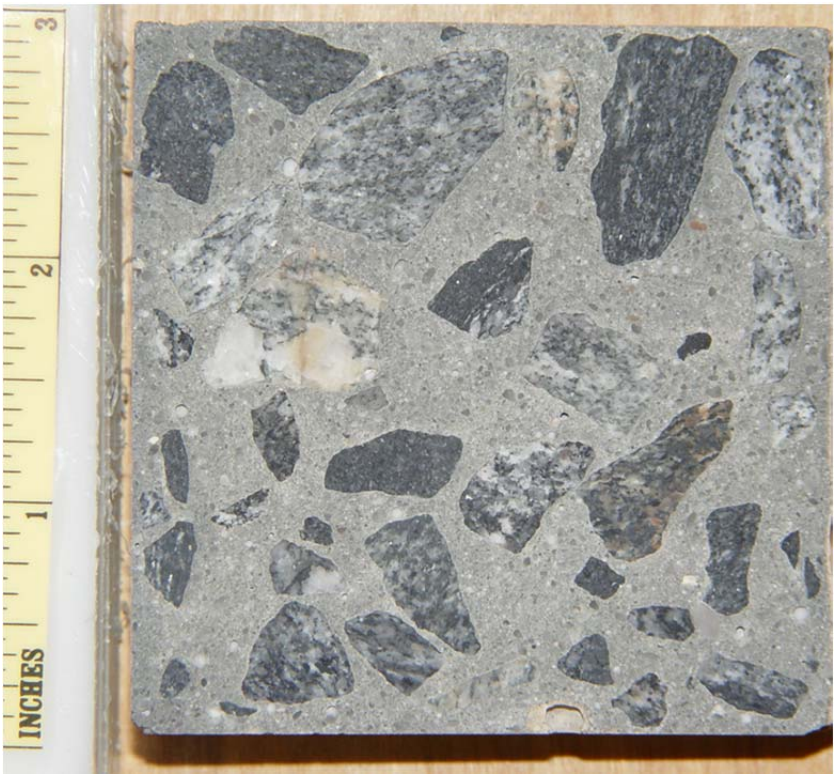

15D-2

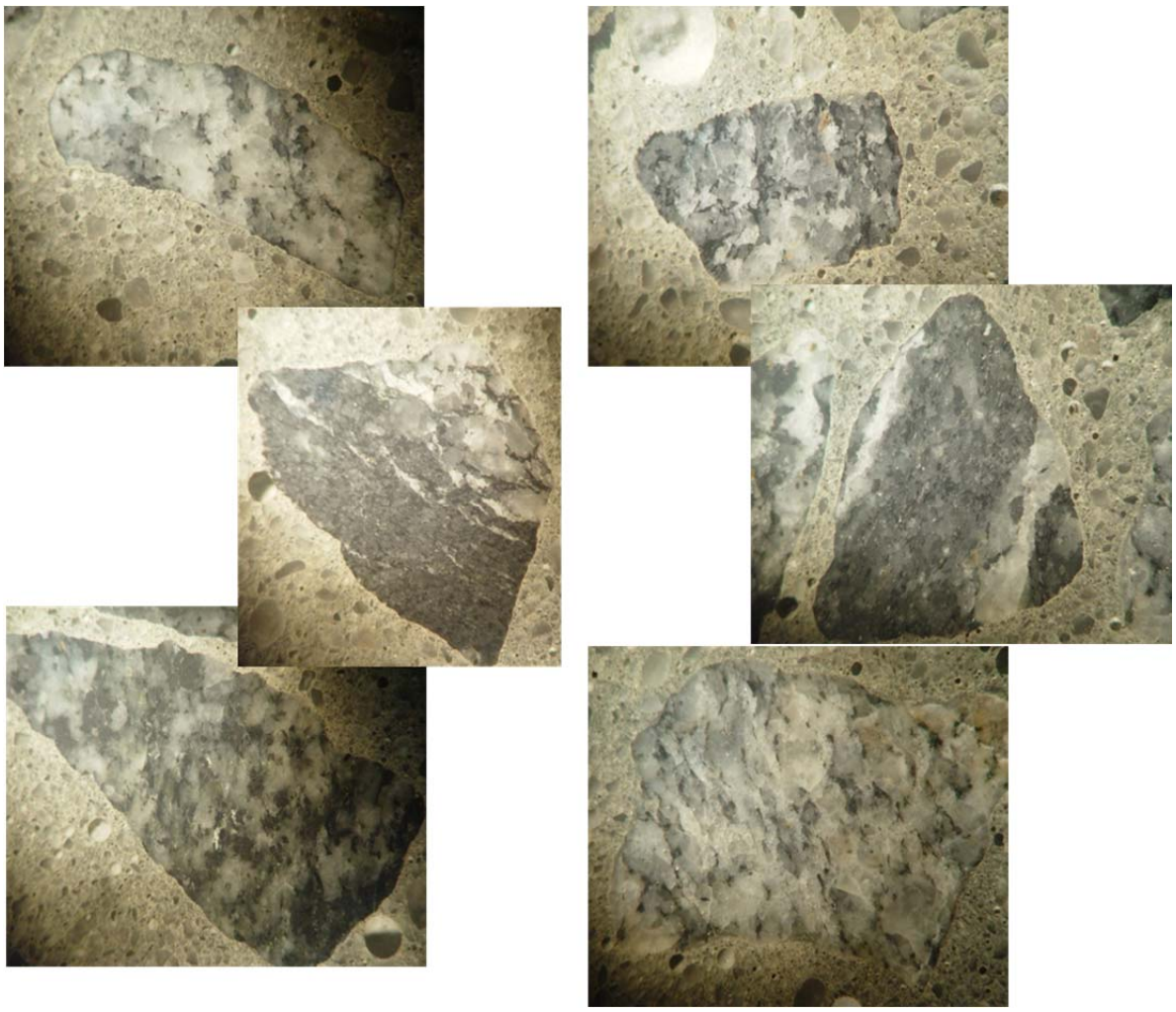

15D-1.3
45%

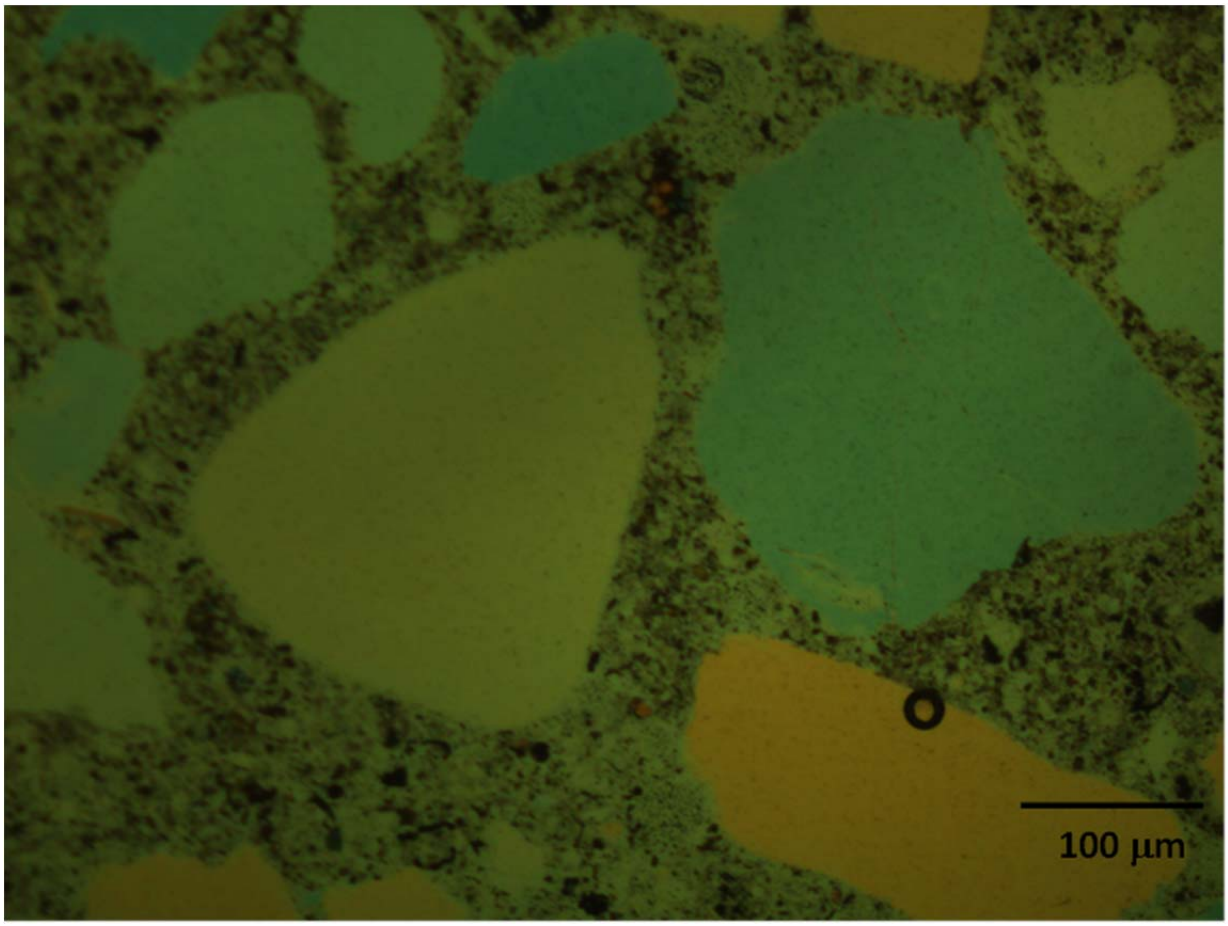

15D-3.1
45%

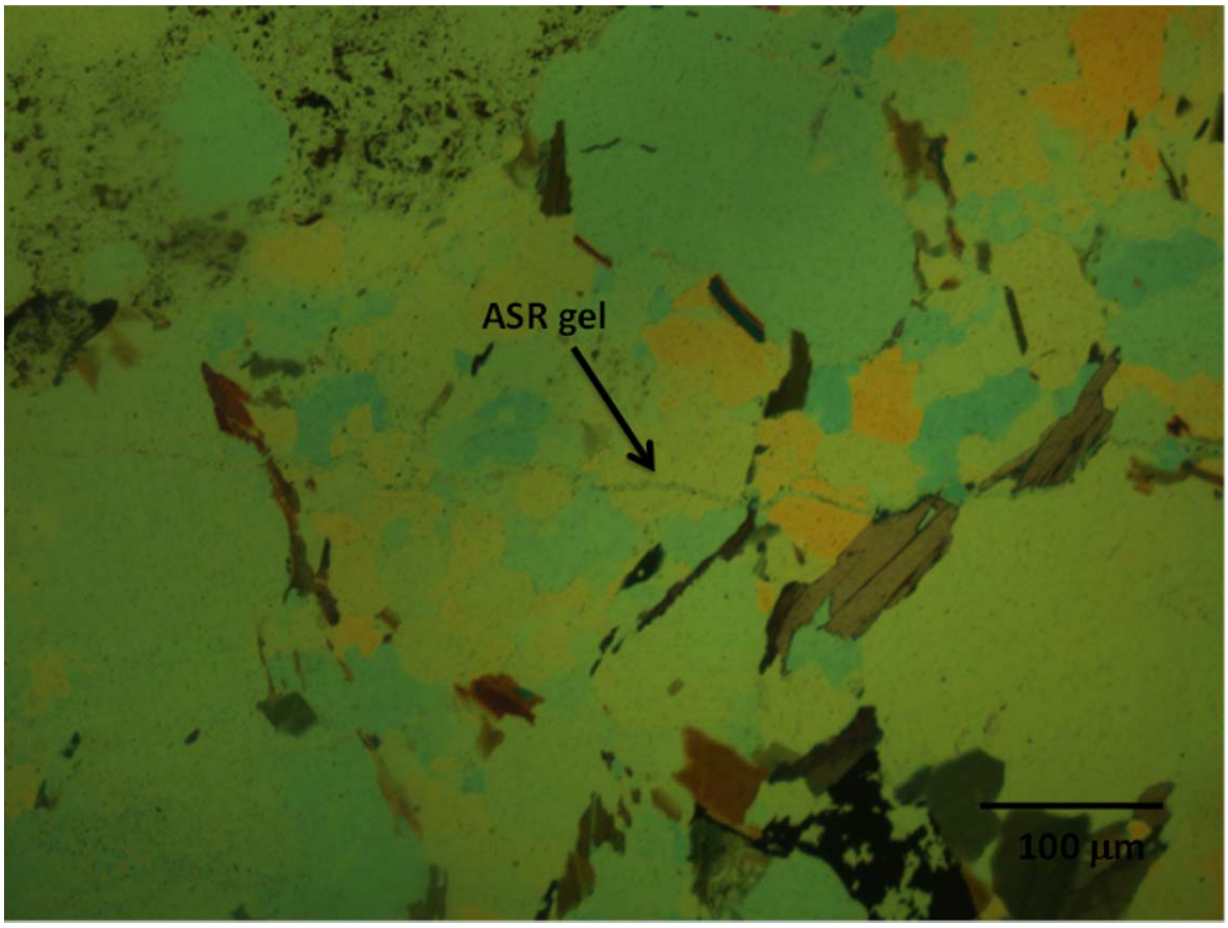

15D-3.3
45%

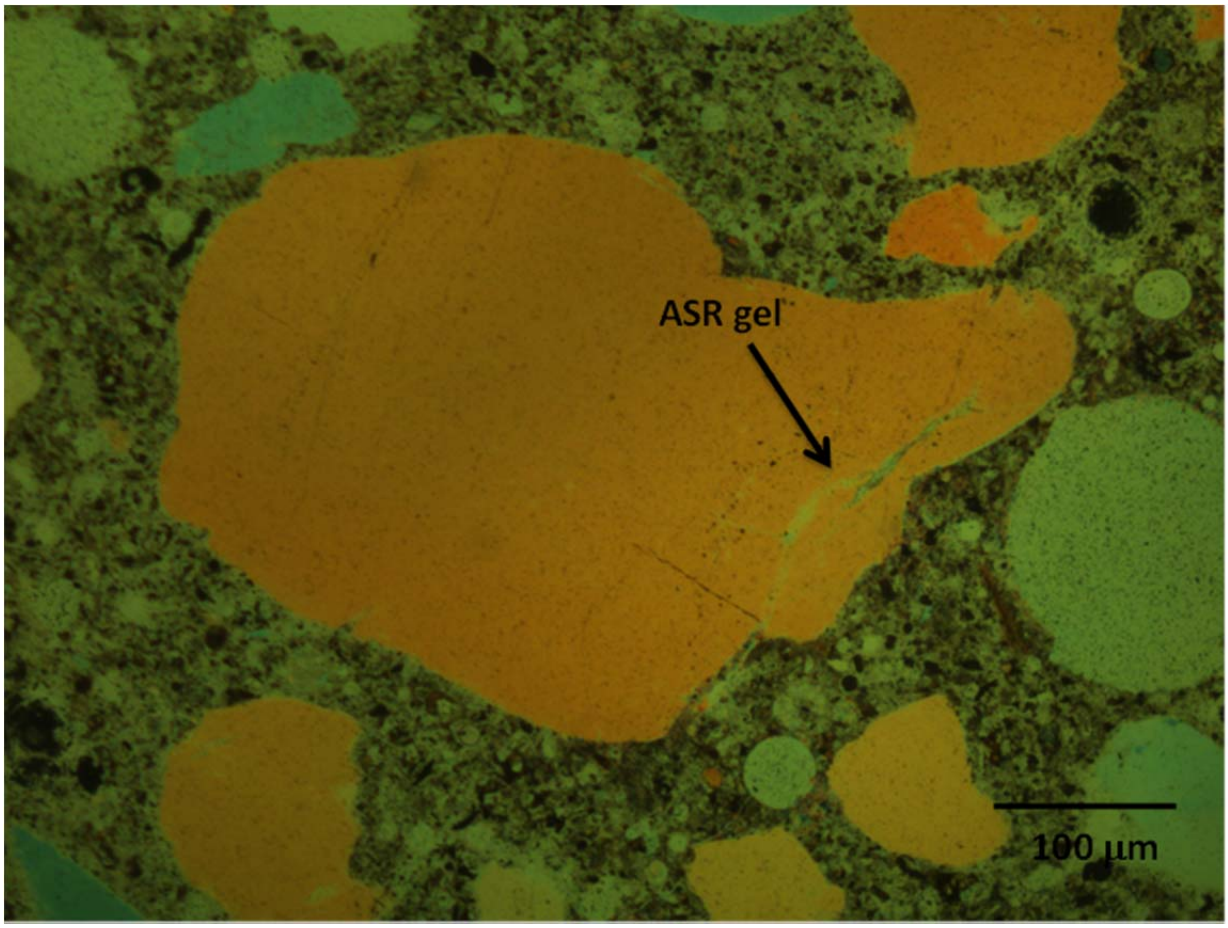

15D-4.2
30%

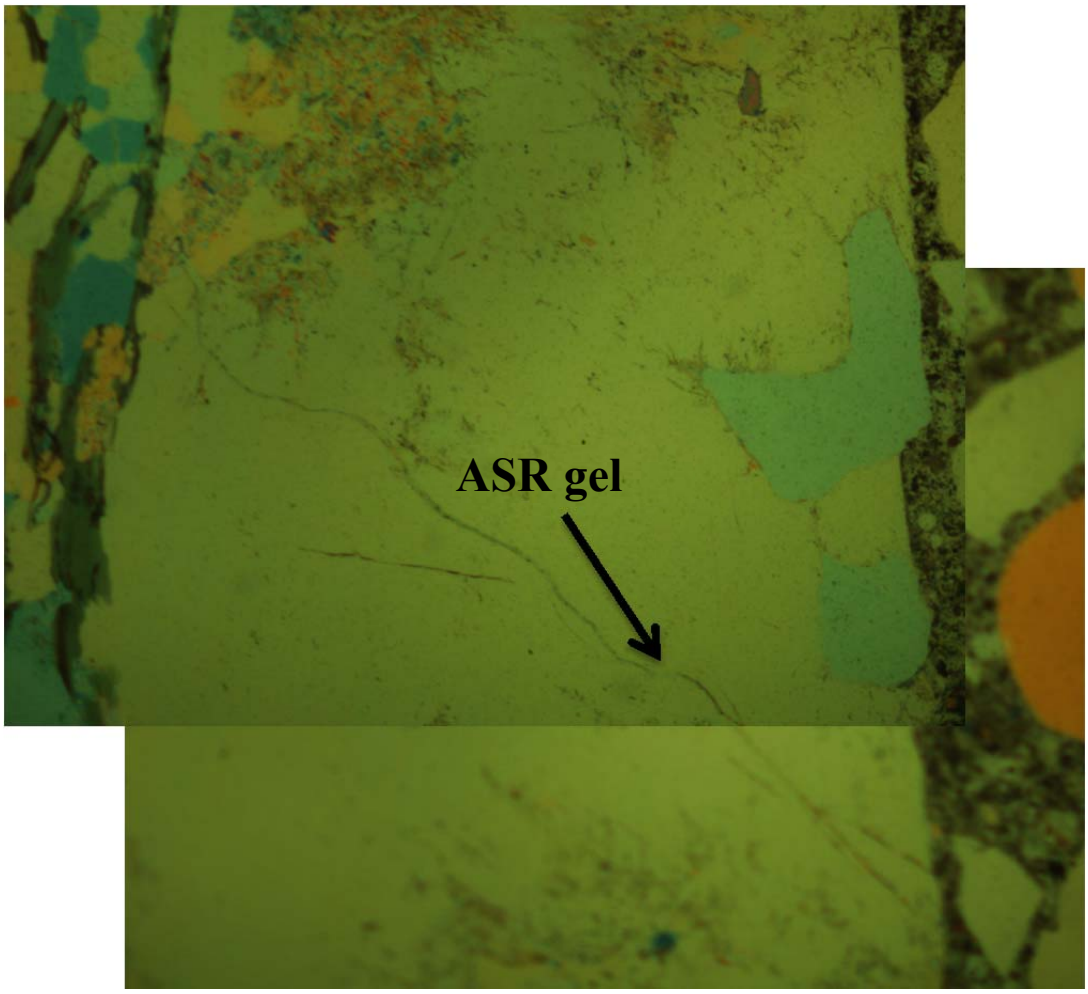

100 μm

15D-4.3
45%

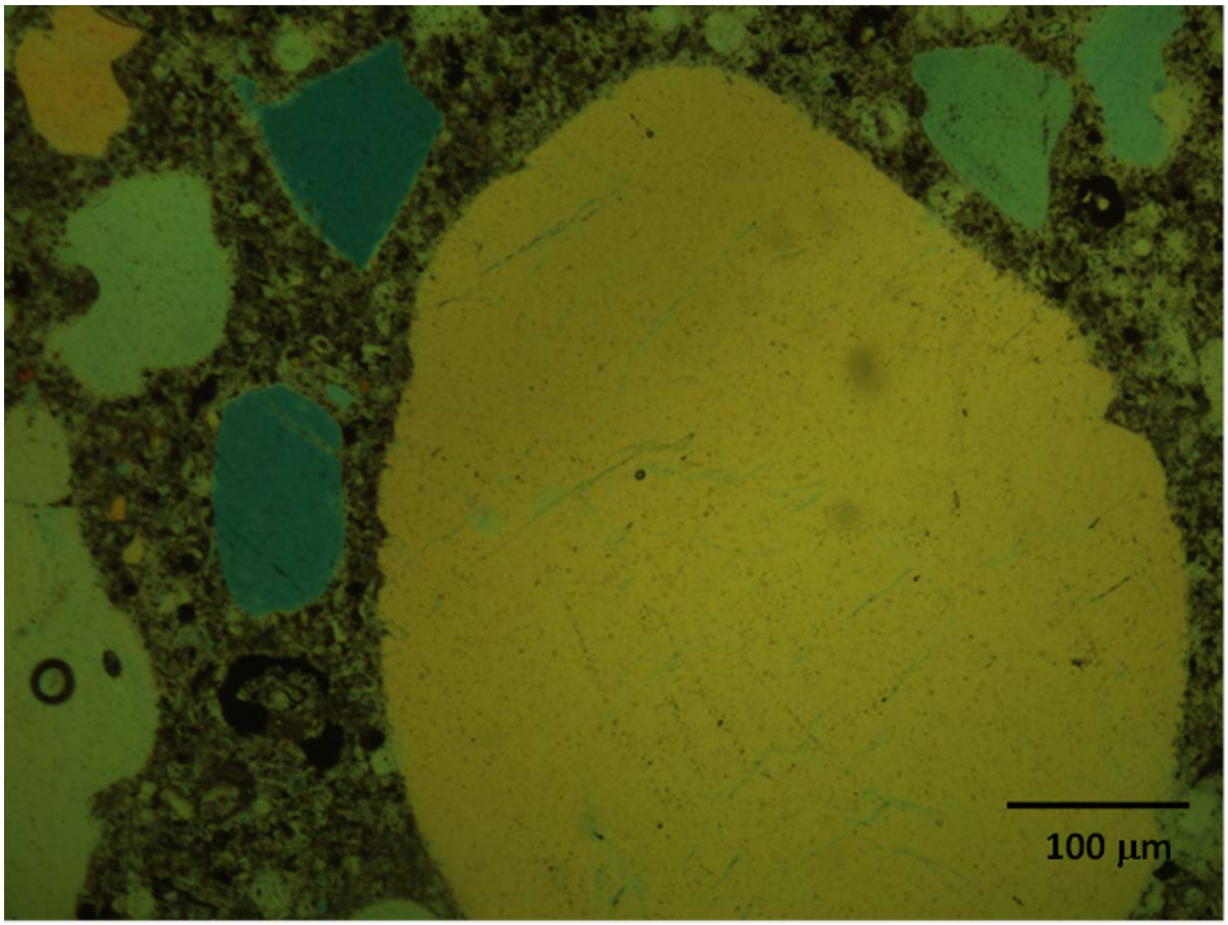

15D-4.3
45%

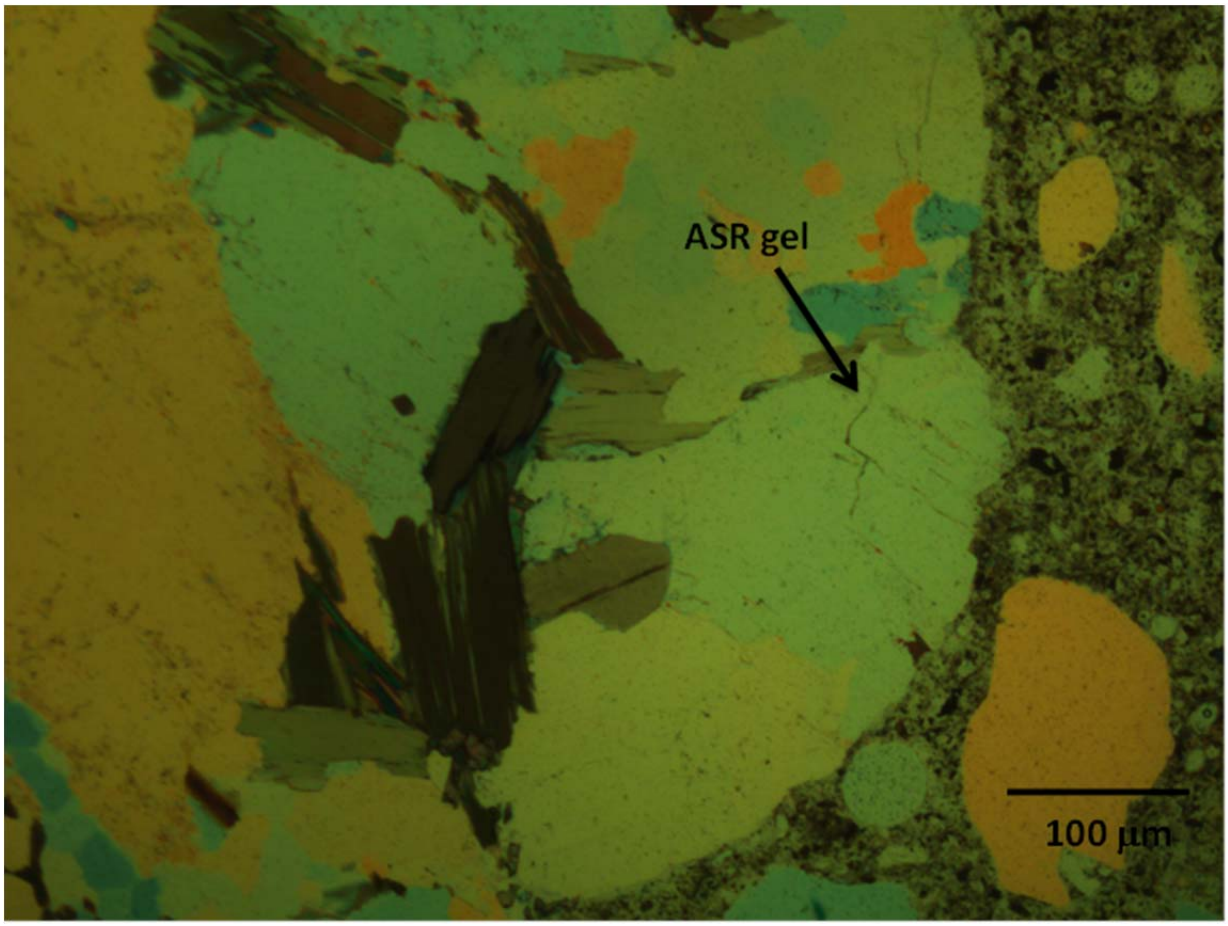

15D-5.1 45%

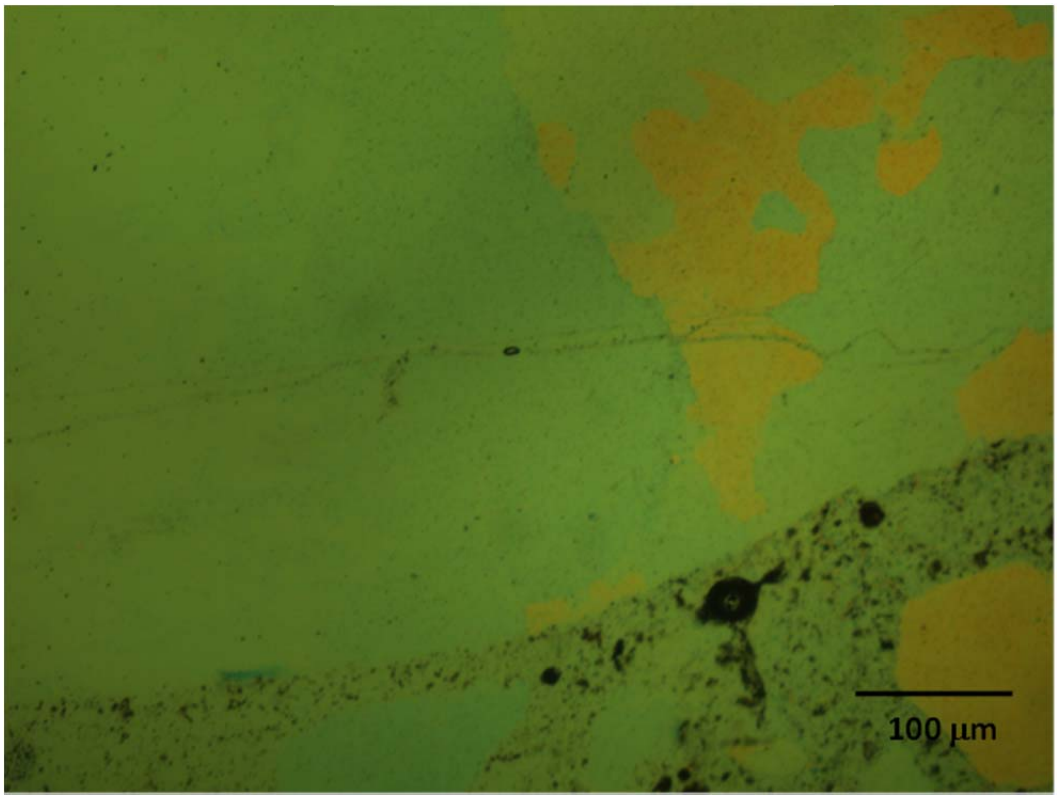

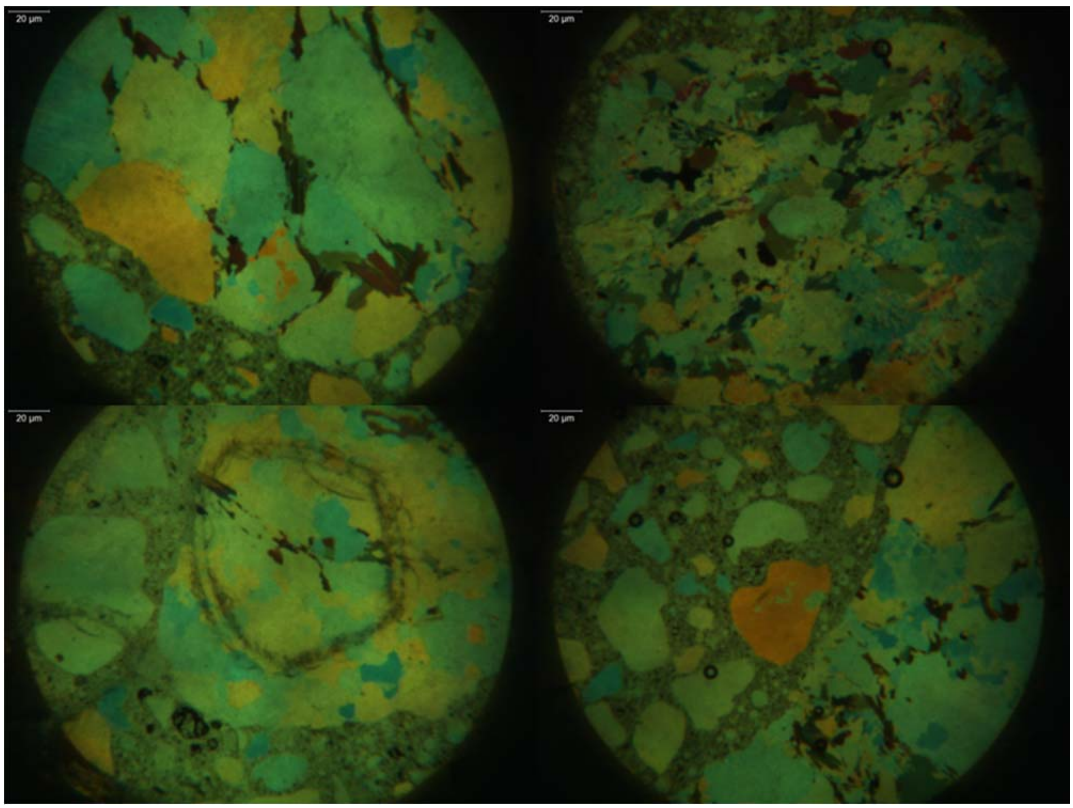

16C-1

16C-2

16C-1.1
45%

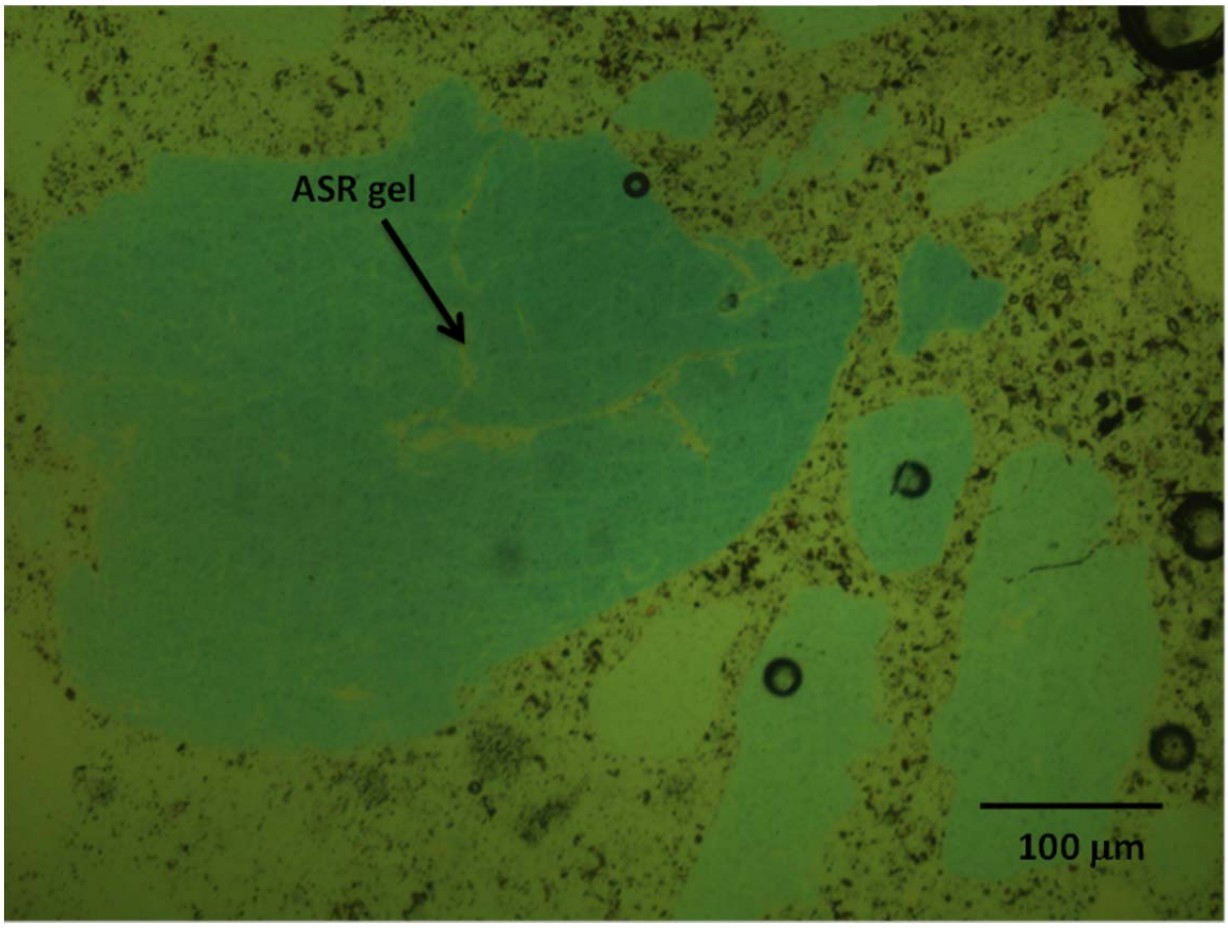

16C-2.1
30%

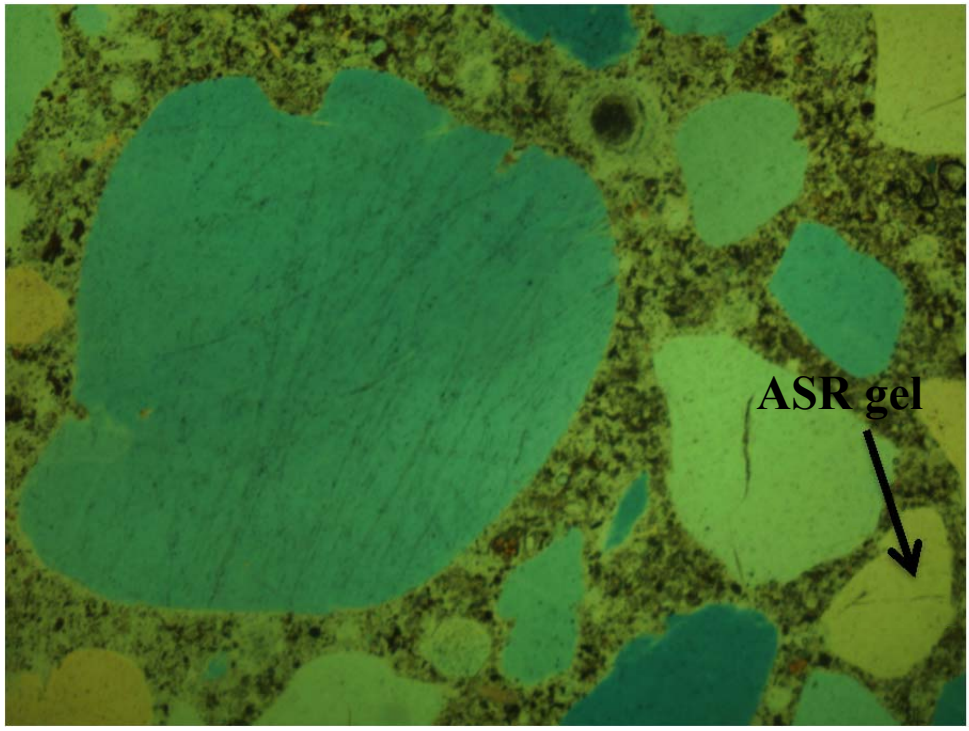

100 μm

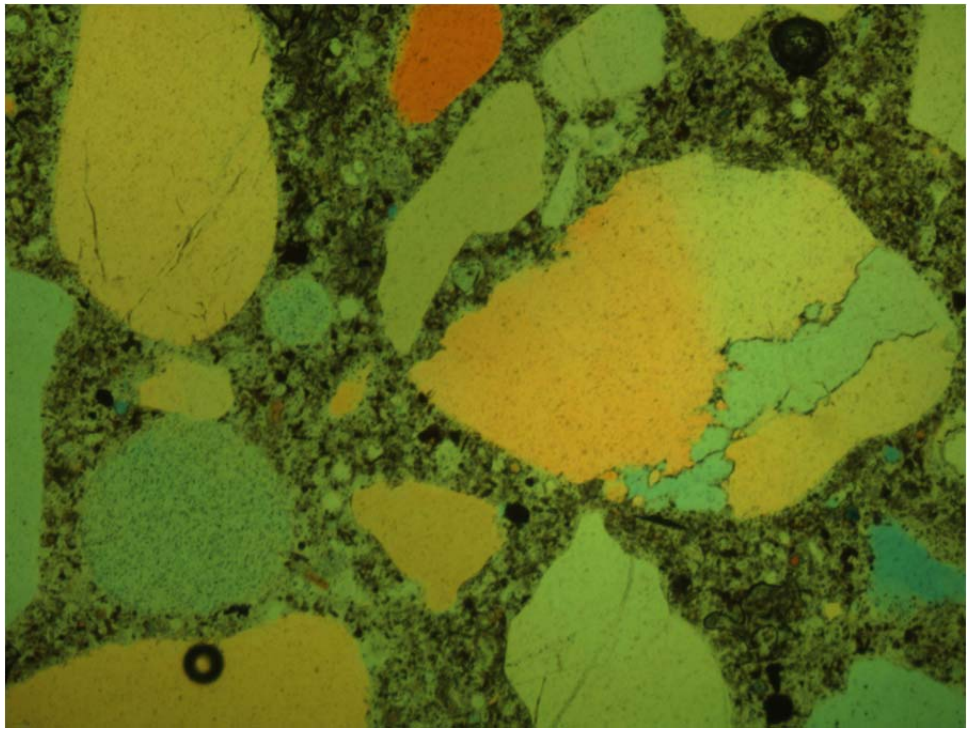

16C-2.3
20%

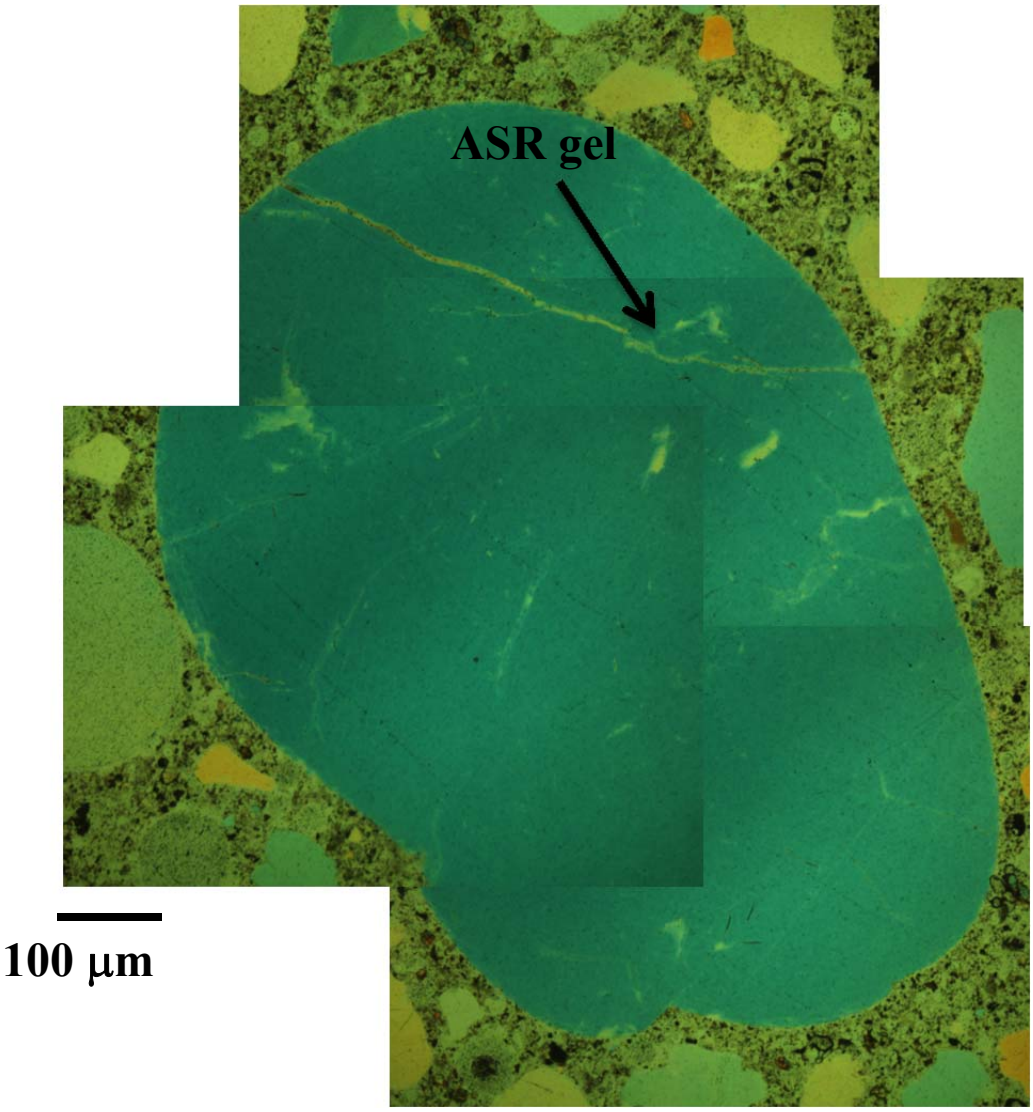

16C-3.1
45%

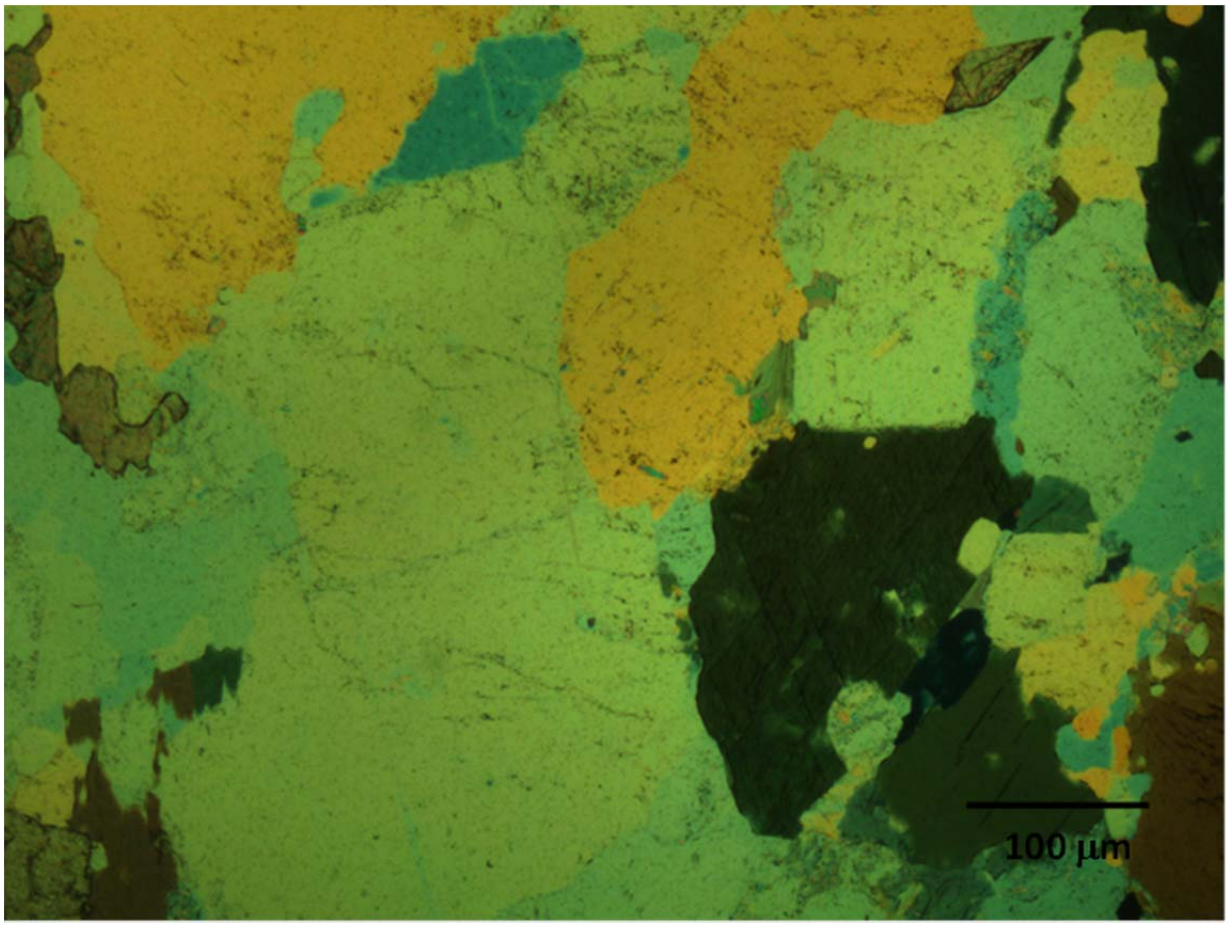

16C-3.4
45%

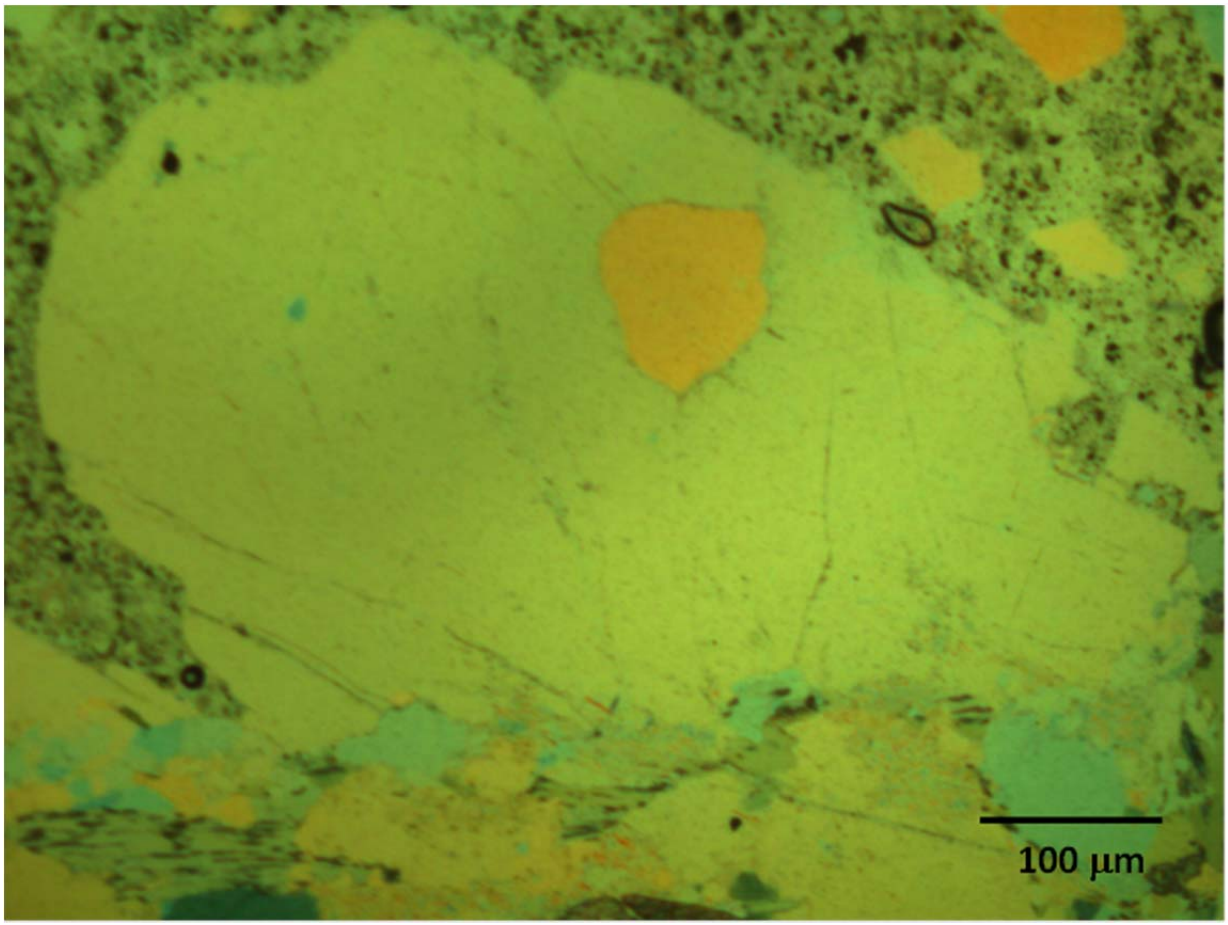

16C-4.1
30%

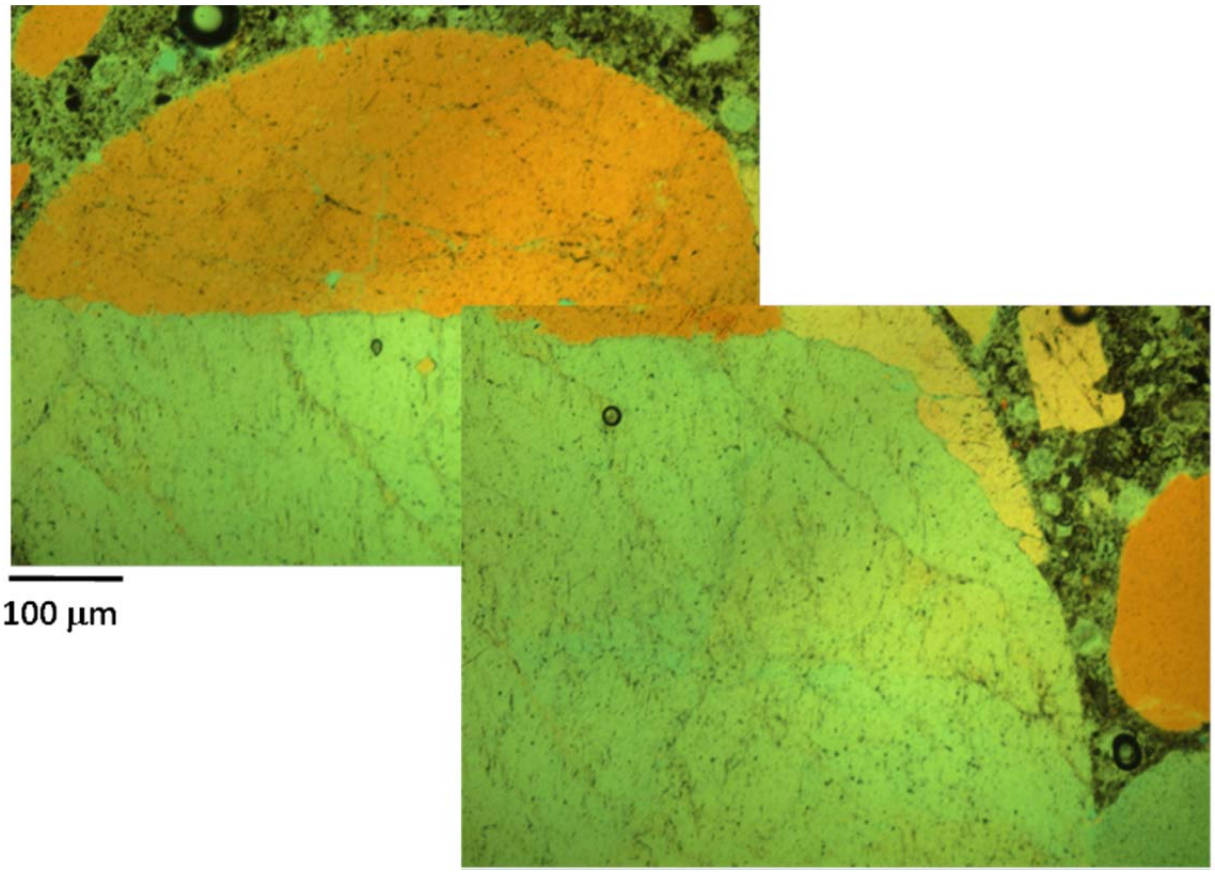

16C-4.2
45%

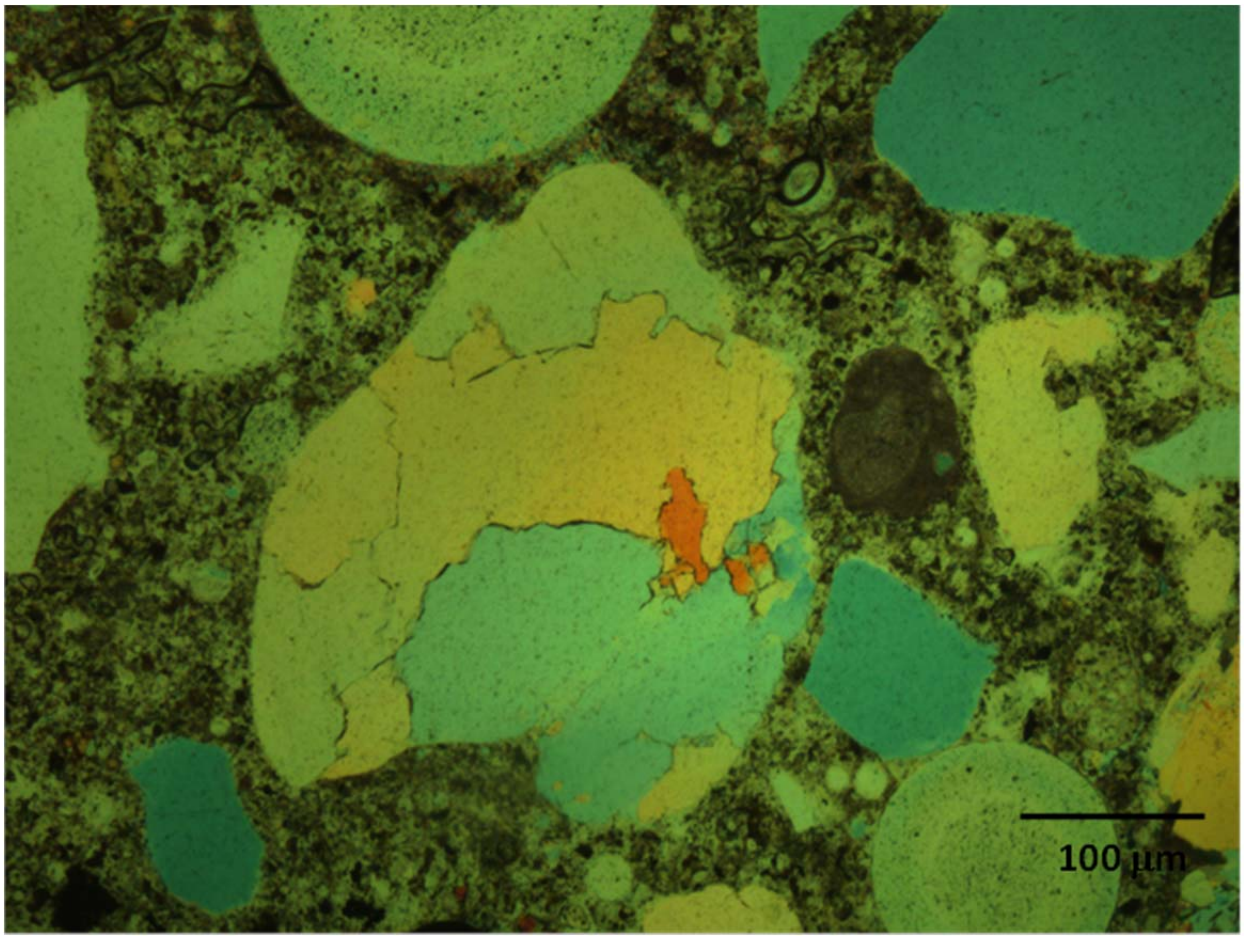

16C-5.1 45%

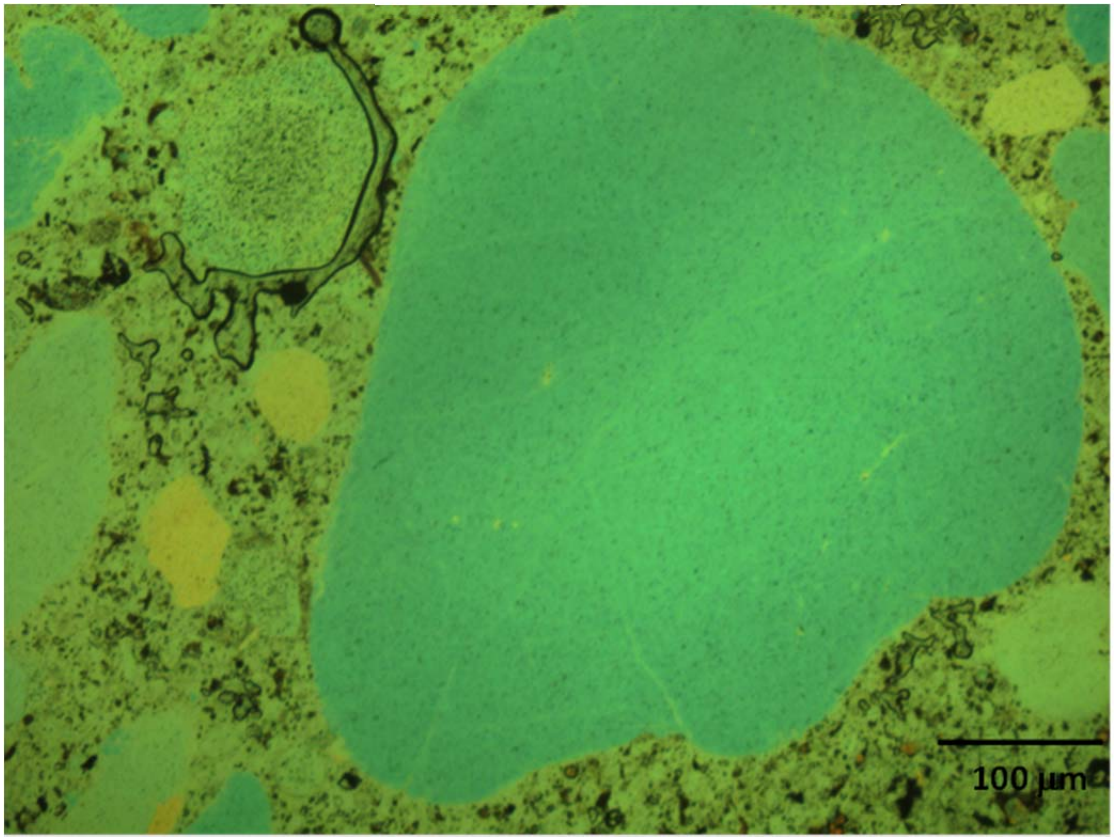

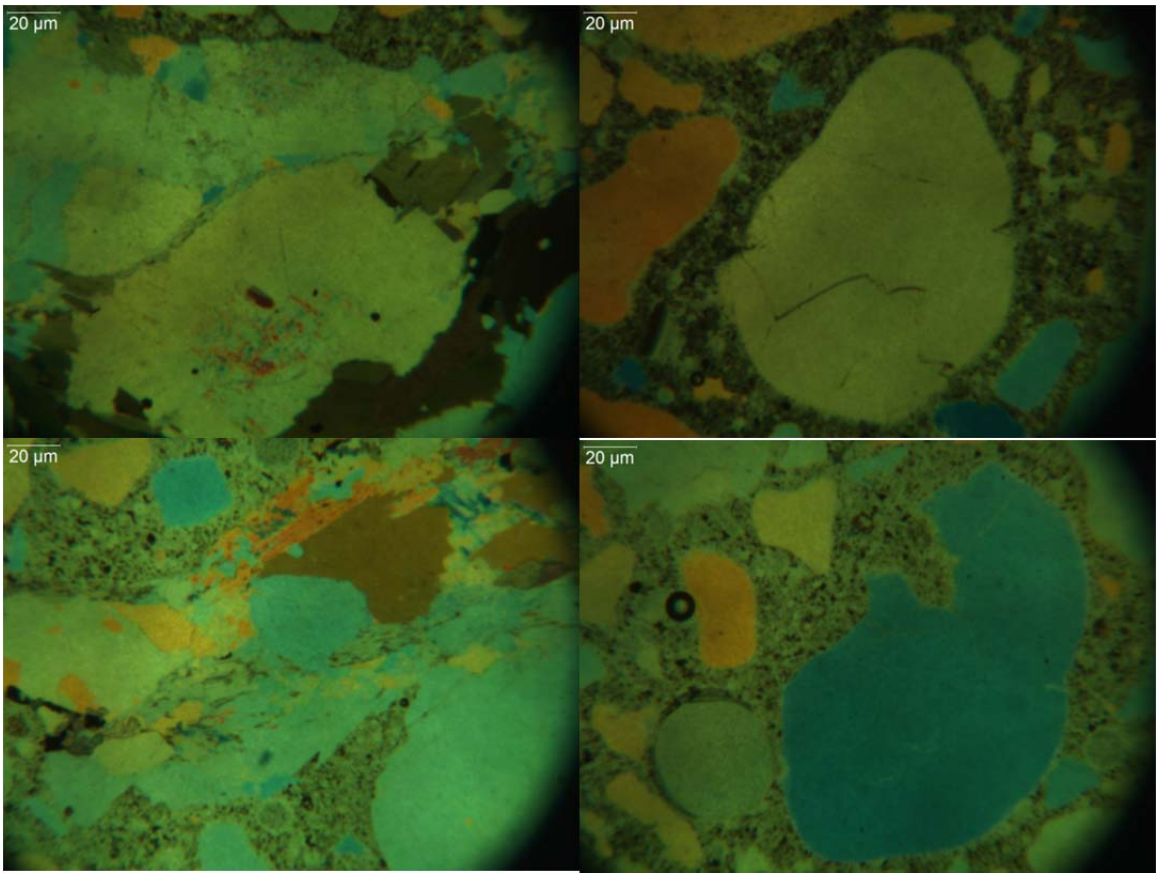

NG

02C

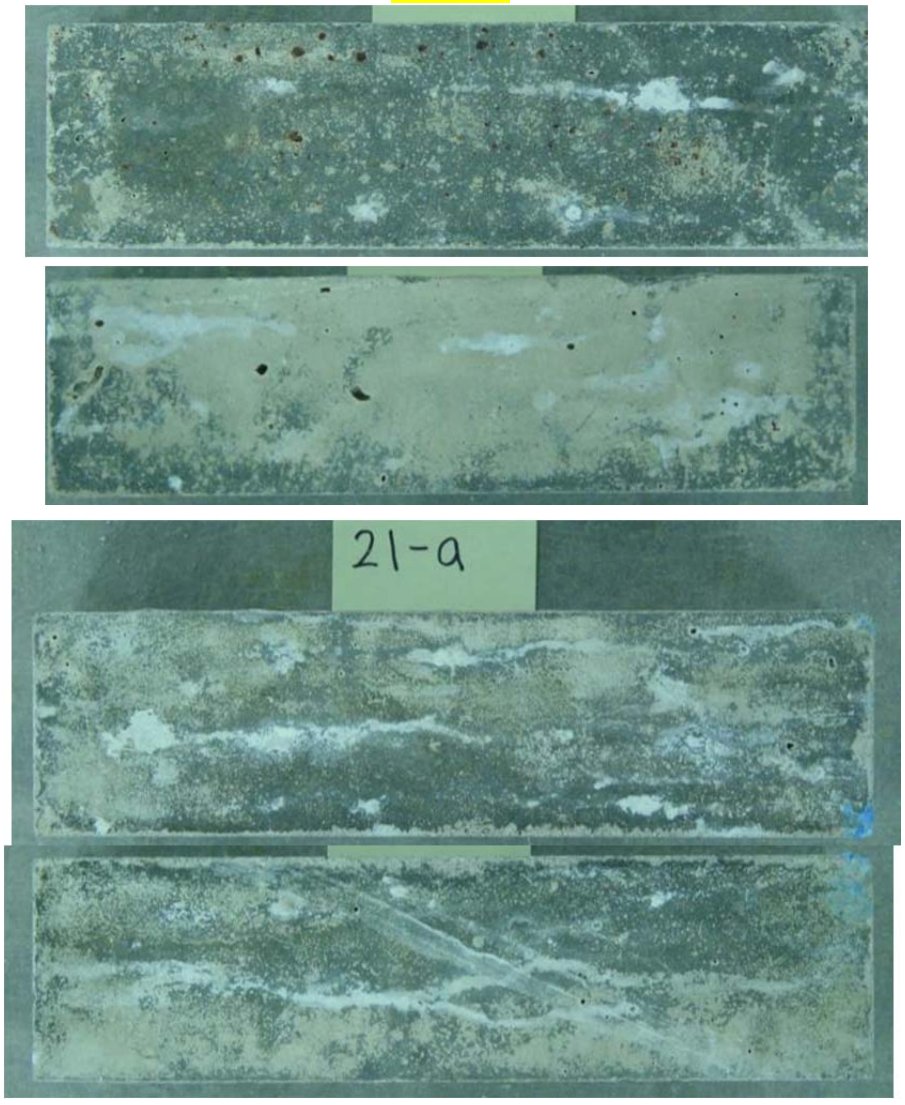

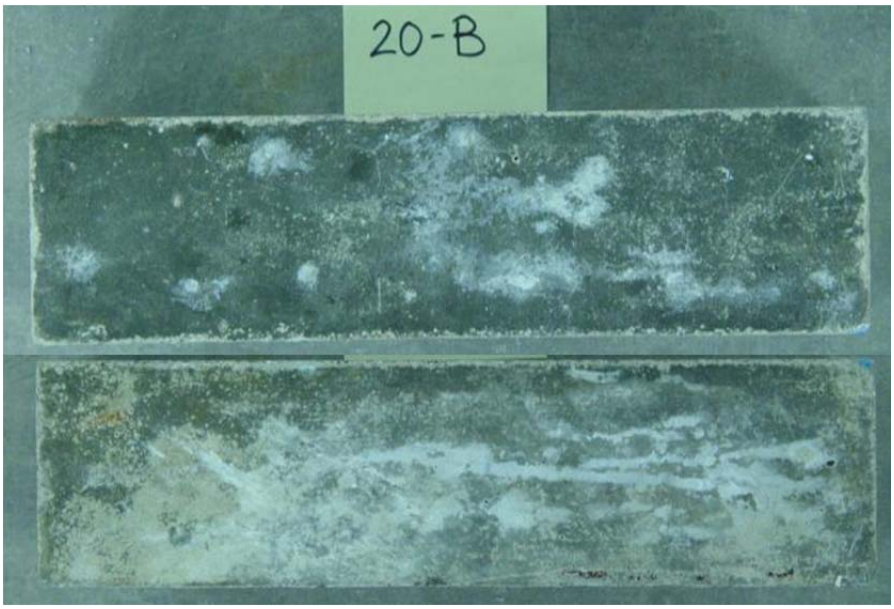
20-B

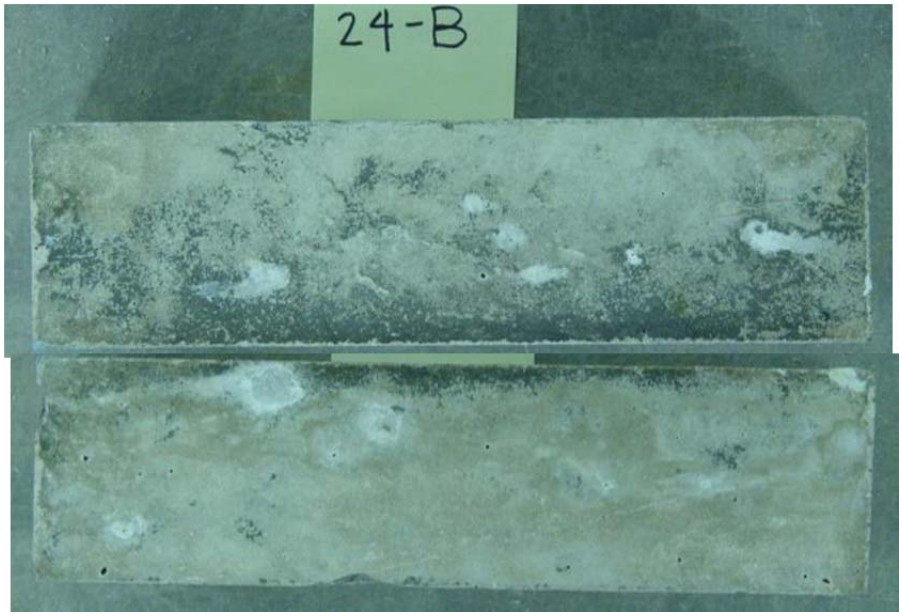
24-B

02C-1

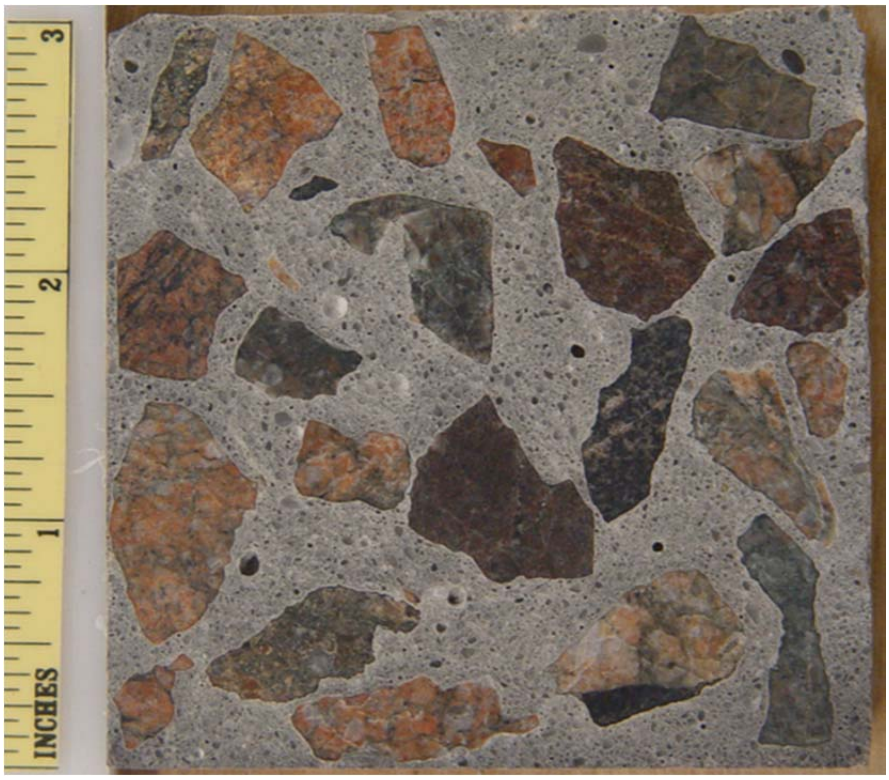

02C-2

02C-1

02C-2

02C-1.1
45%

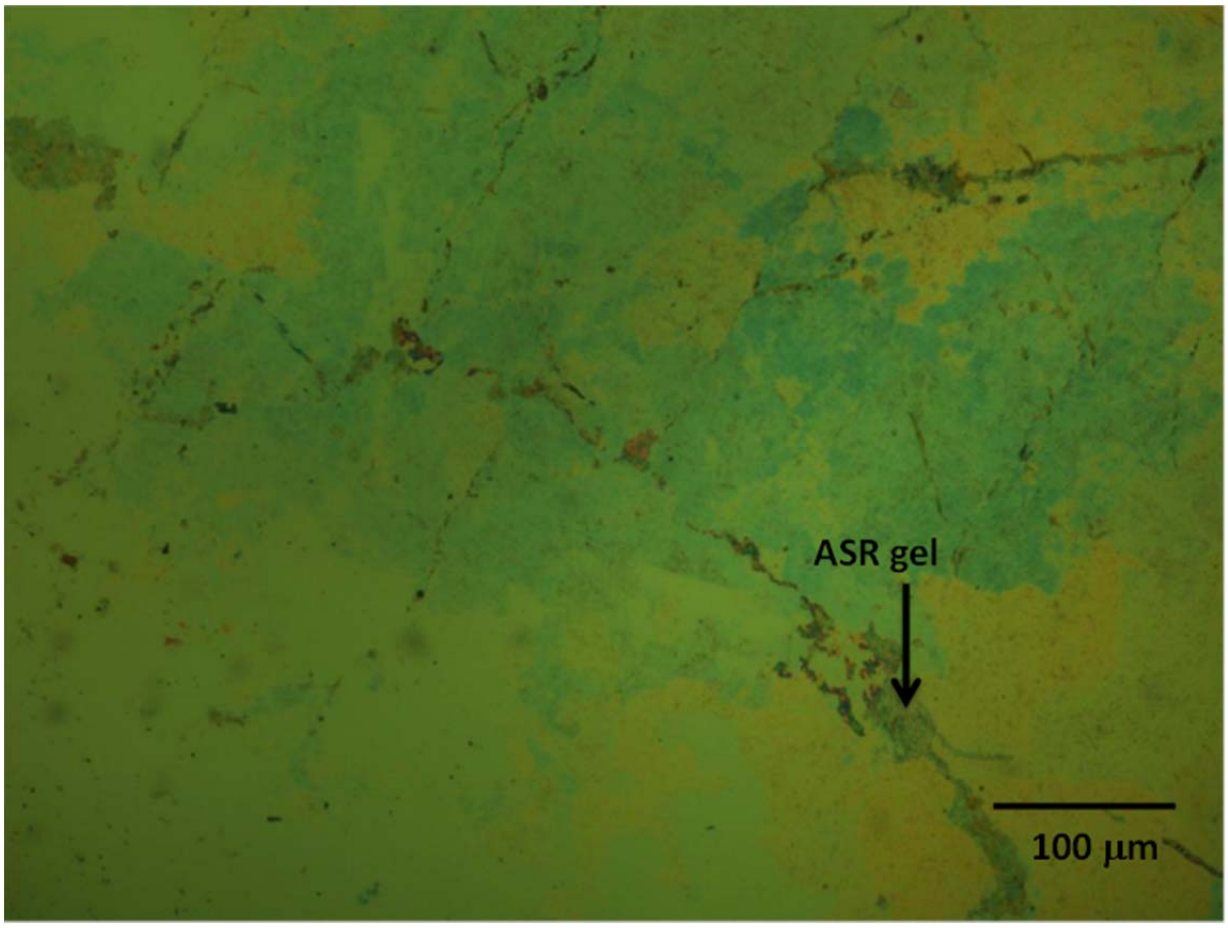

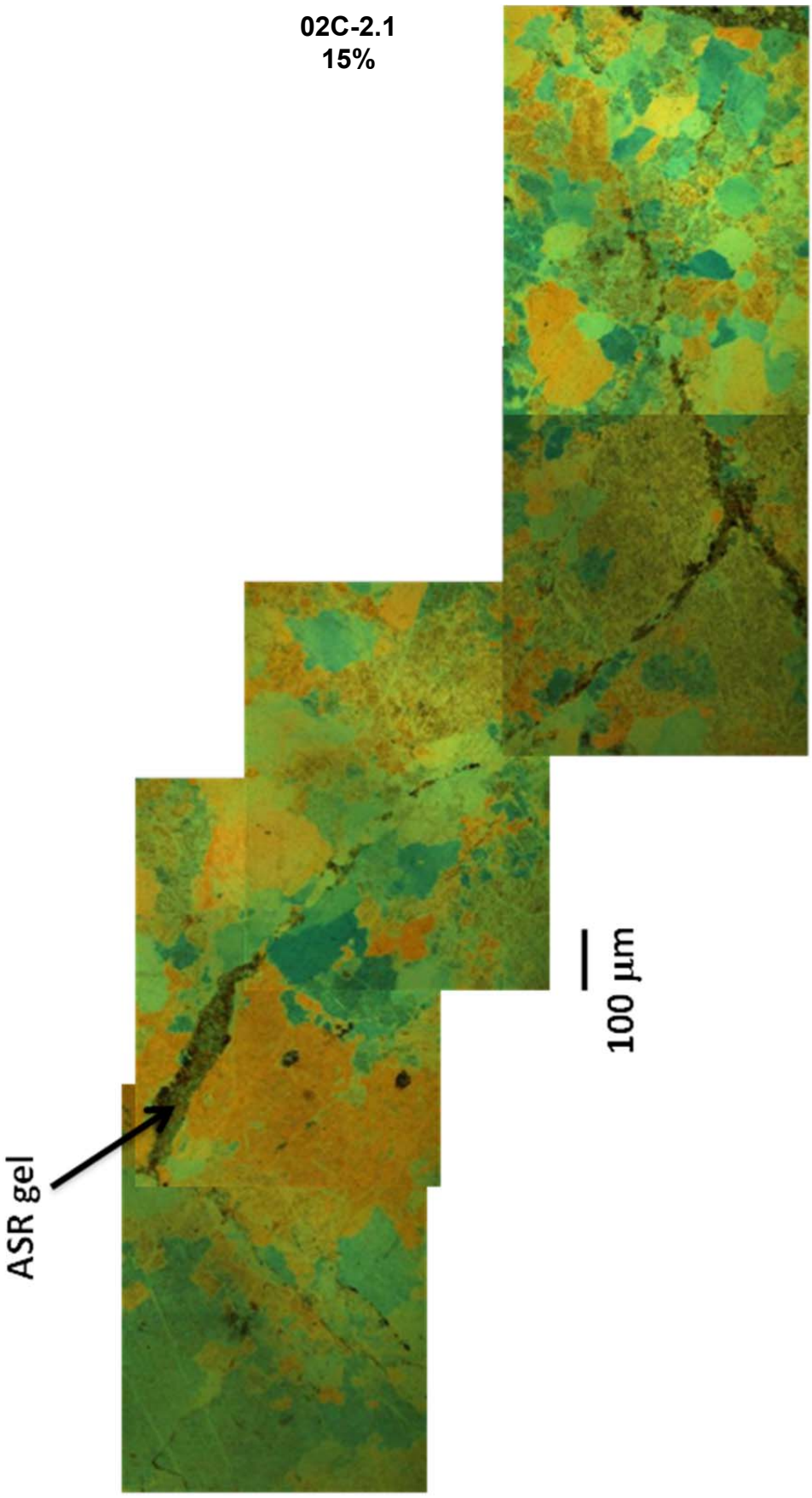
02C-2.1
15%
ASR gel
100 µm

02C-3.2
45%

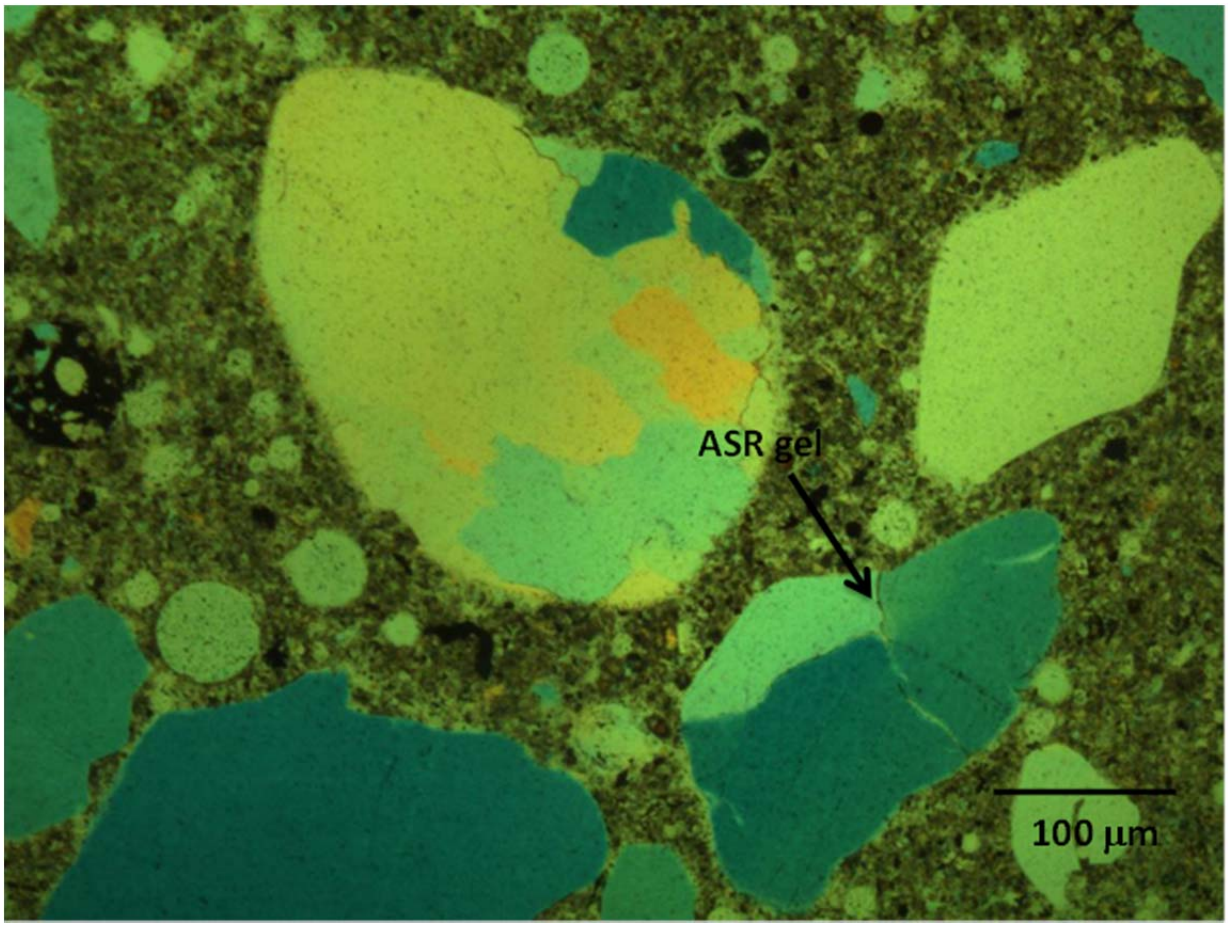

02C-4.2
45%

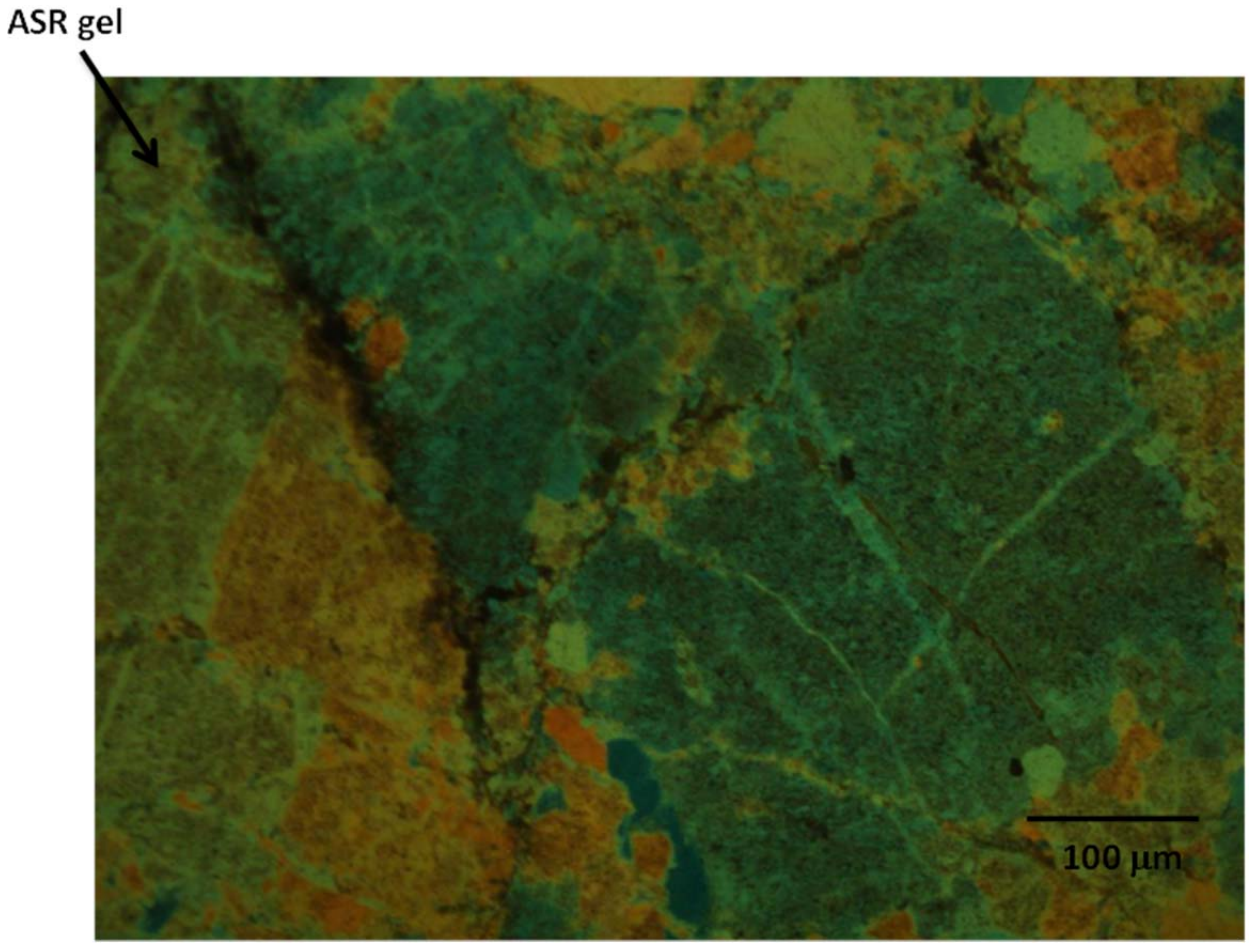

02C-4.4
45%

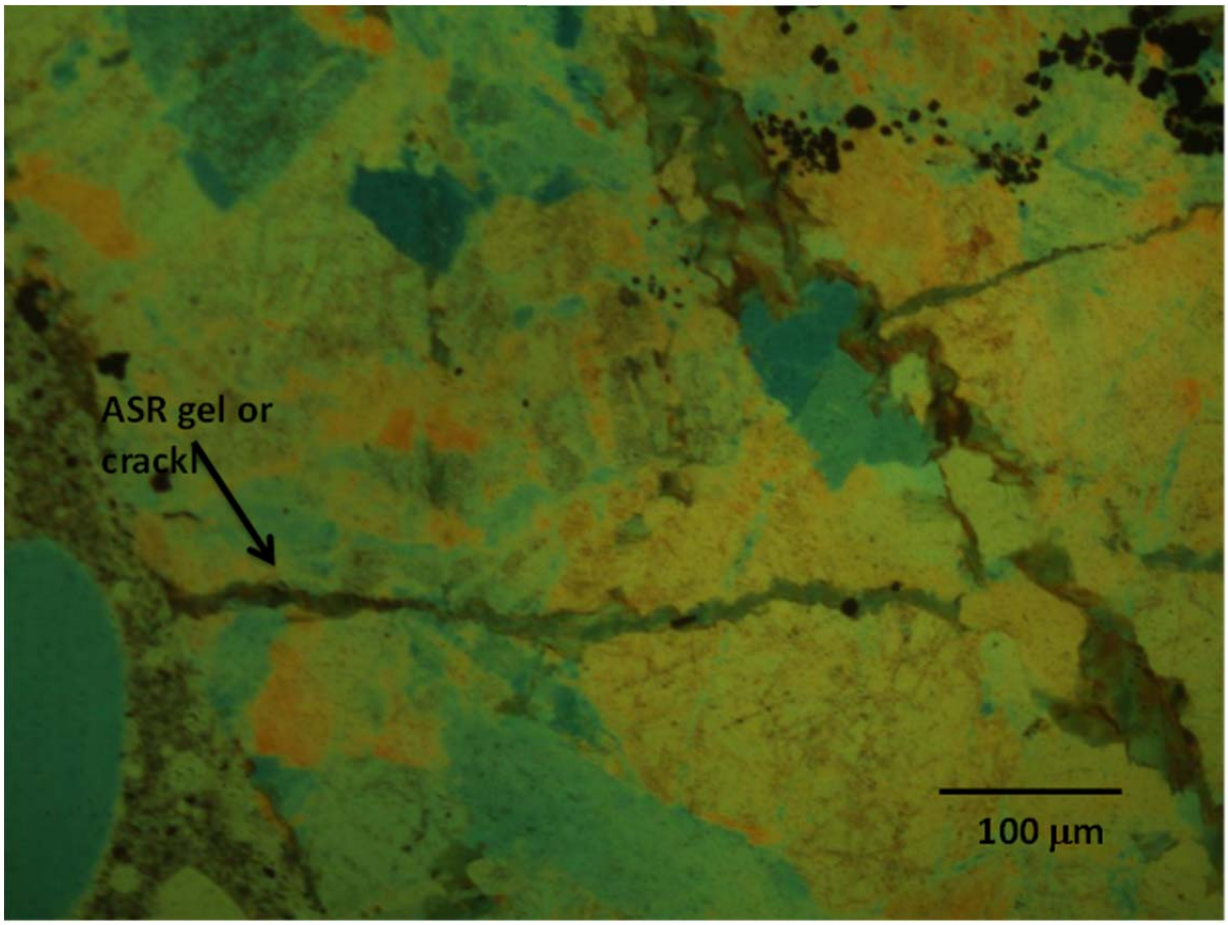

02C-5.1
45%

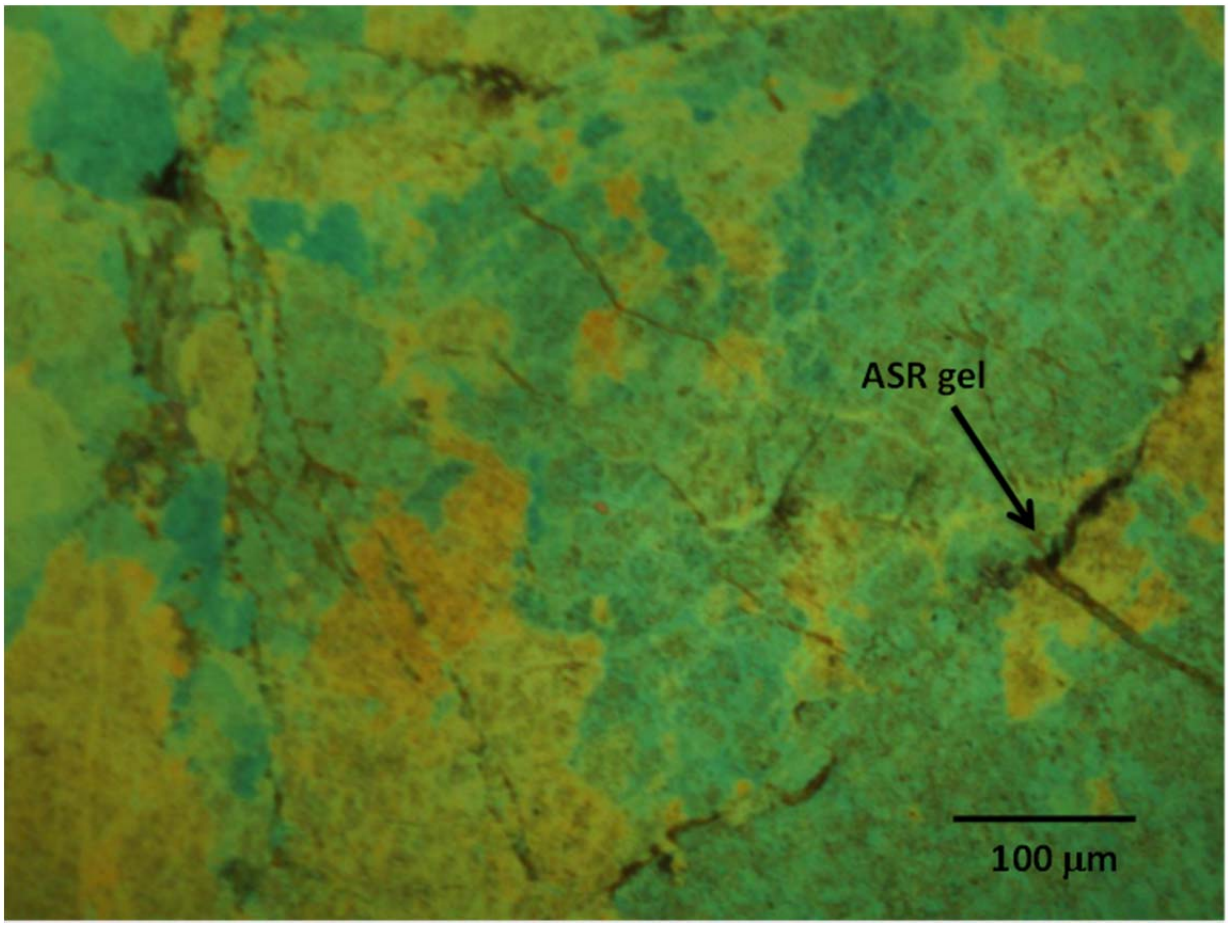

02C-5.3
45%

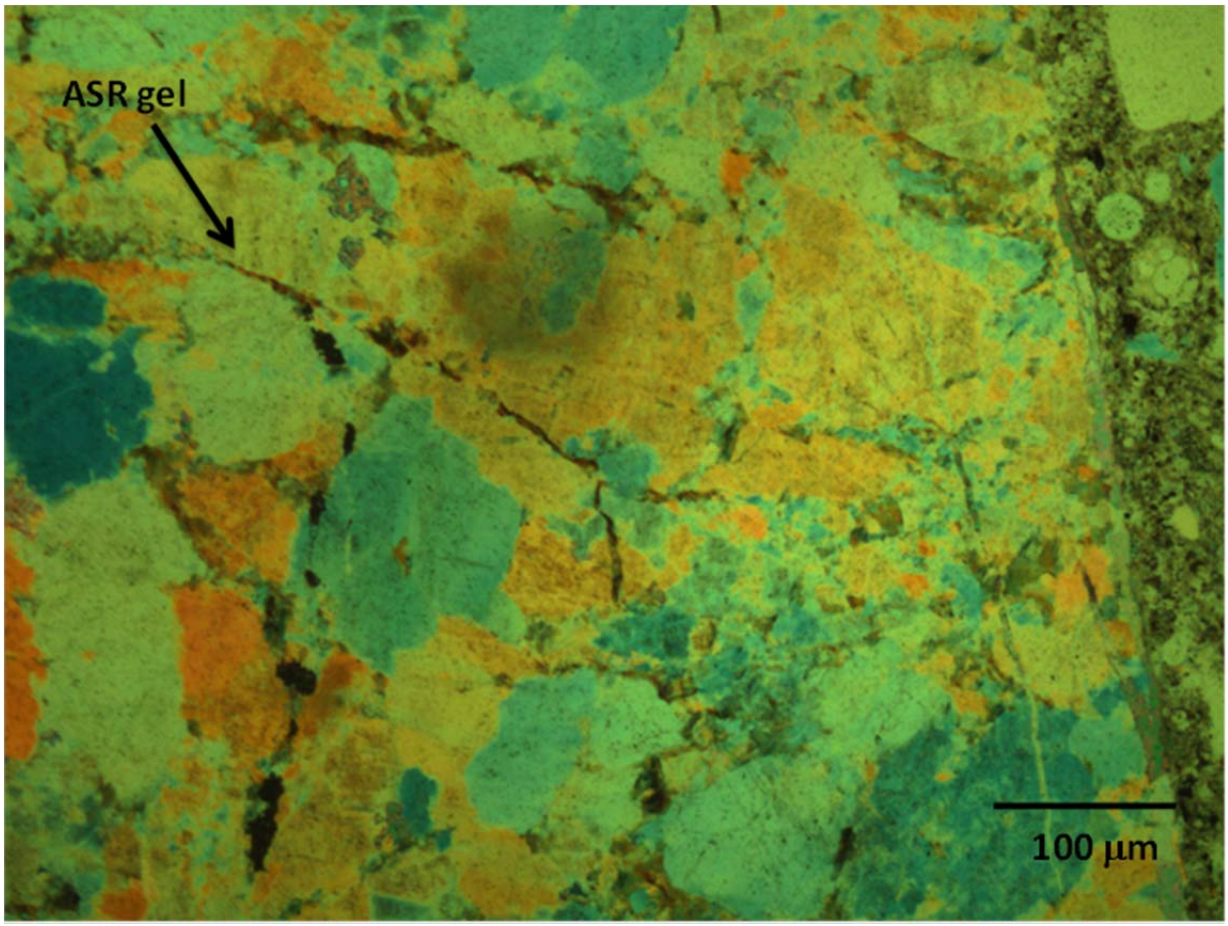

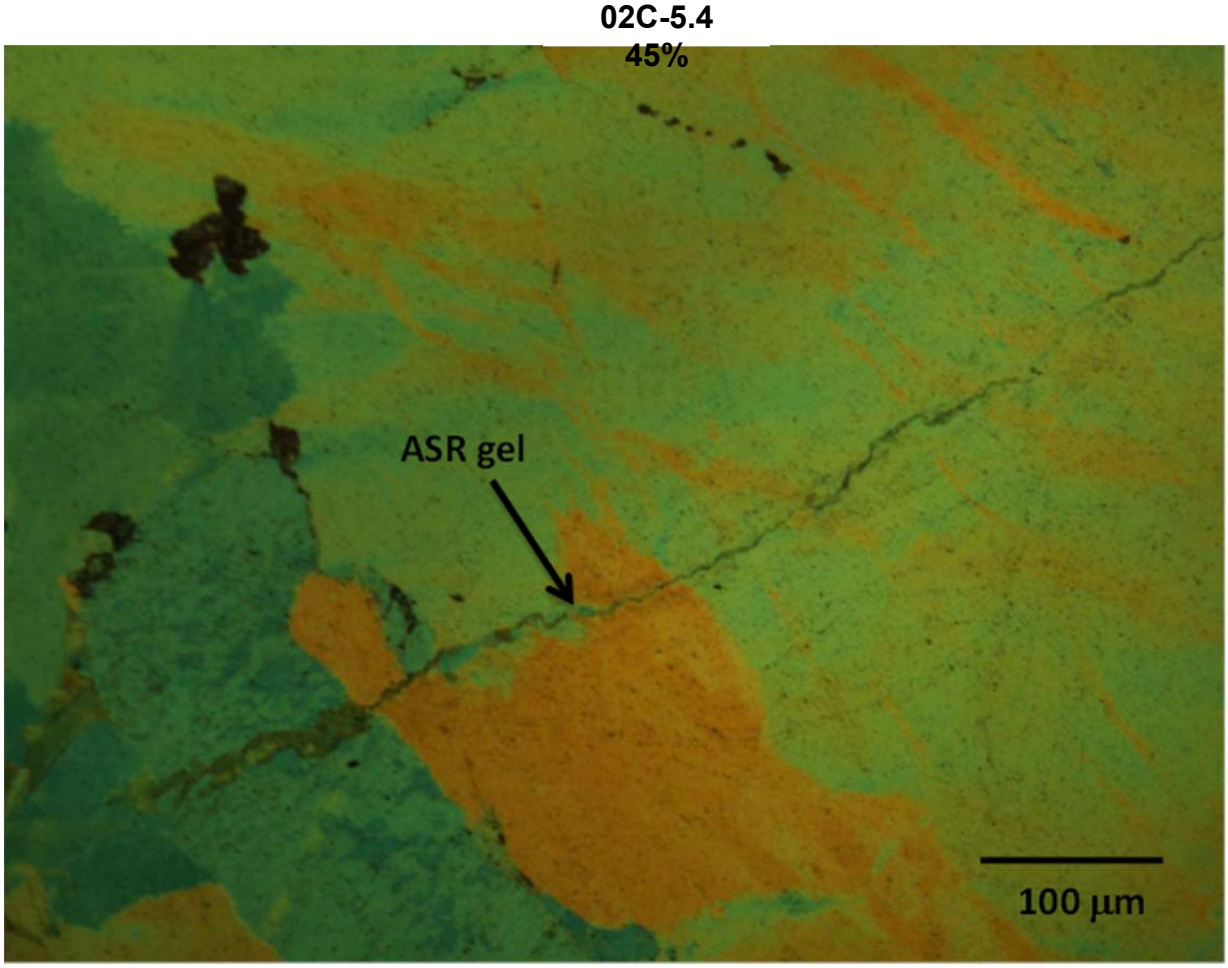
02C-5.4
45%
ASR gel
100 µm

02C

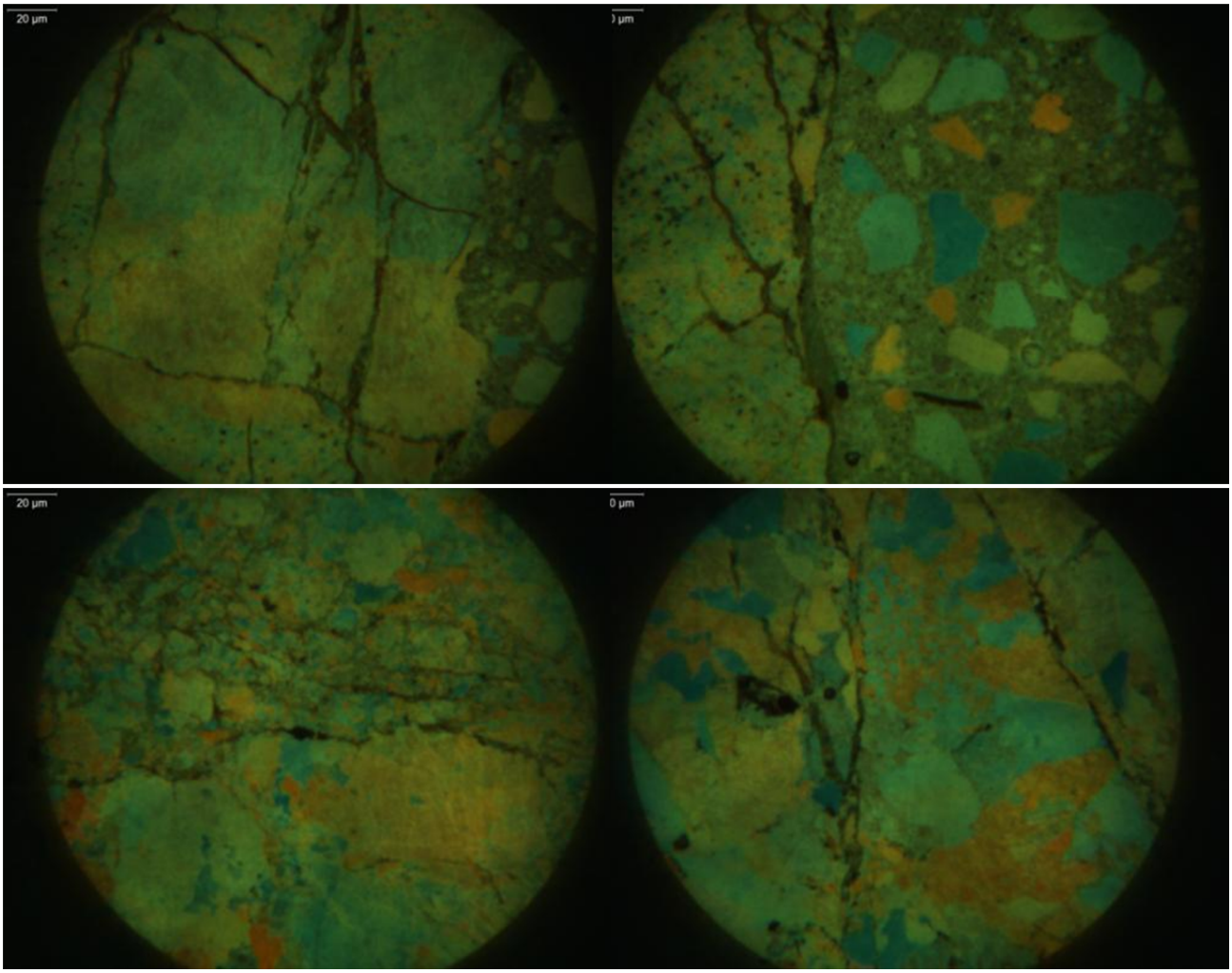

20B-1

20B-2

20B-1

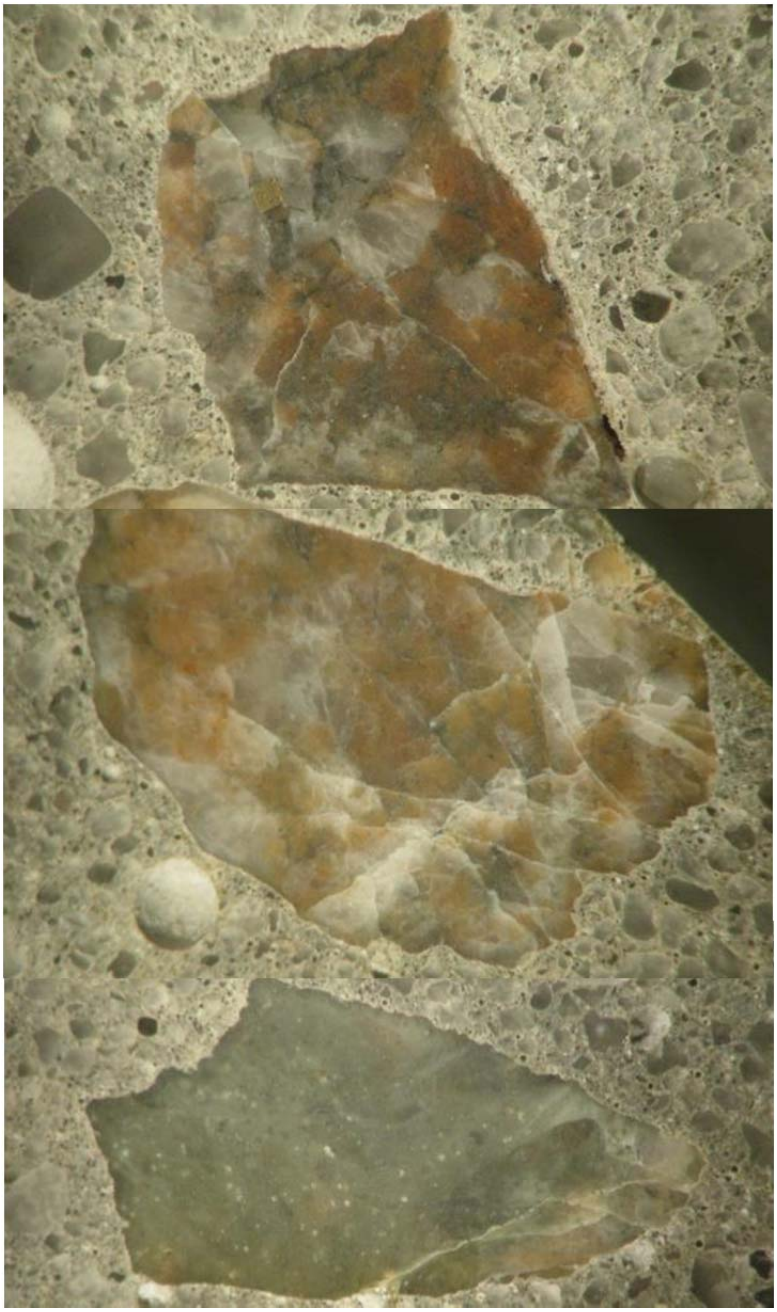

20B-2

20B-1.1
45%

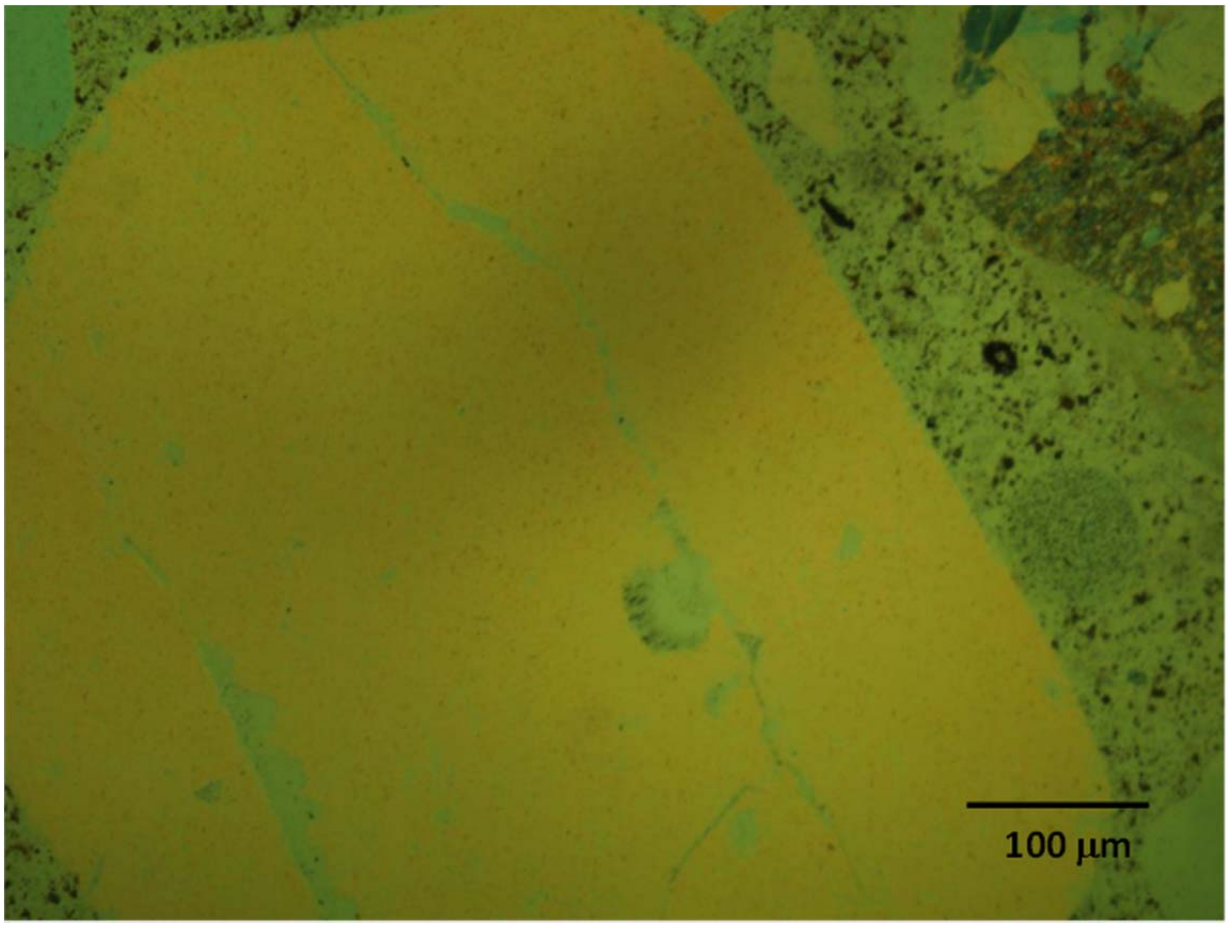

20B-1.4
20%

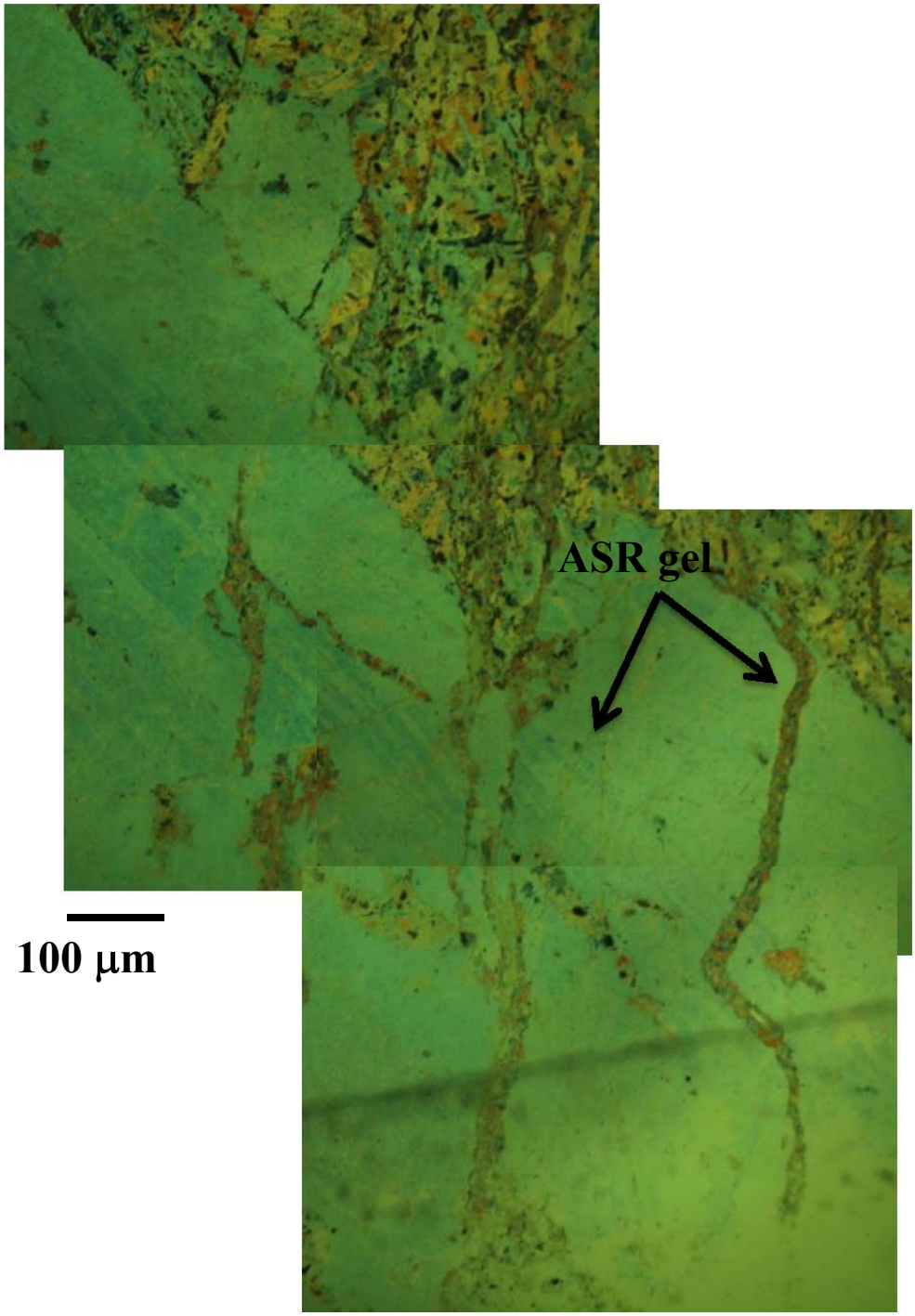

20B-2.1
45%

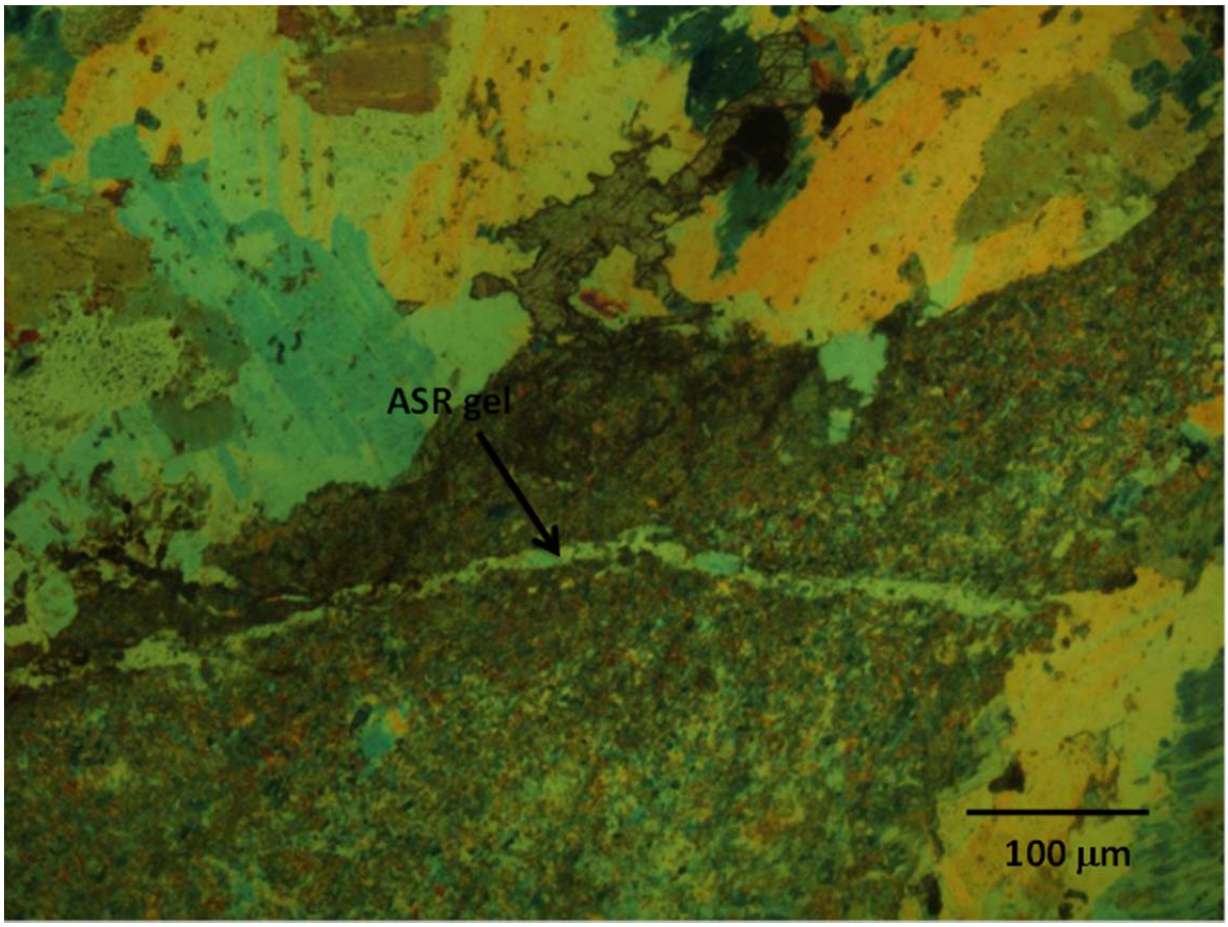

20B-2.3
45%

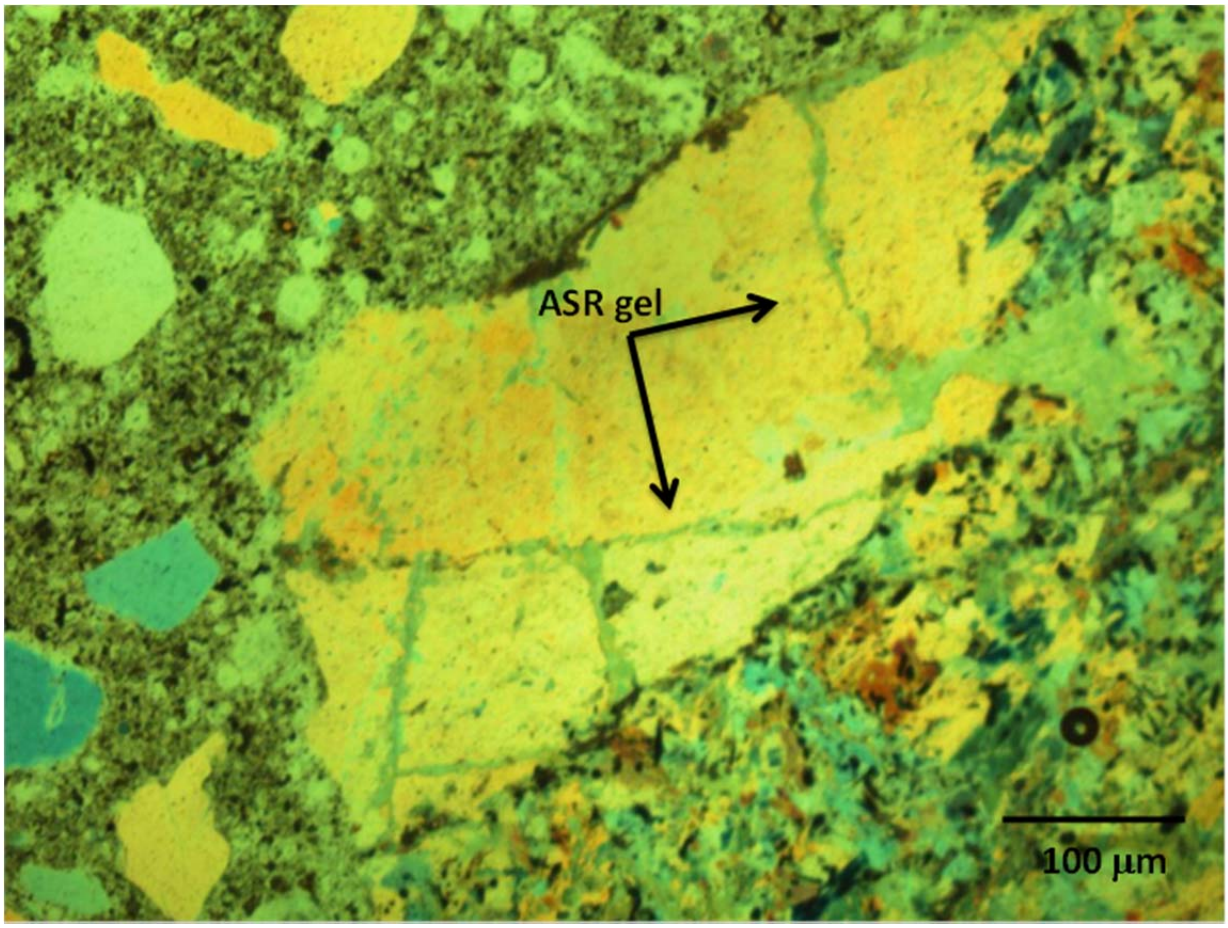

20B-4.1
20%

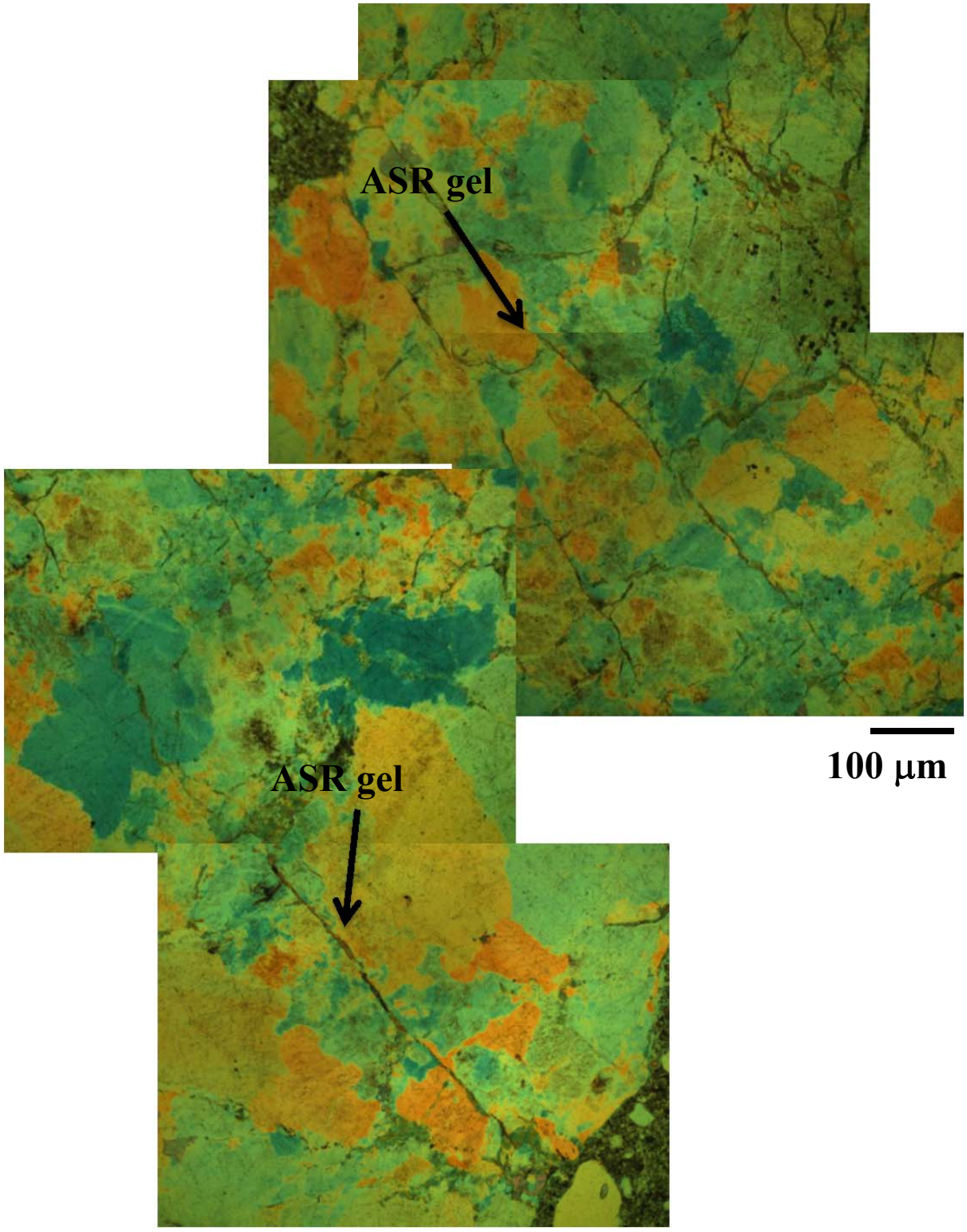

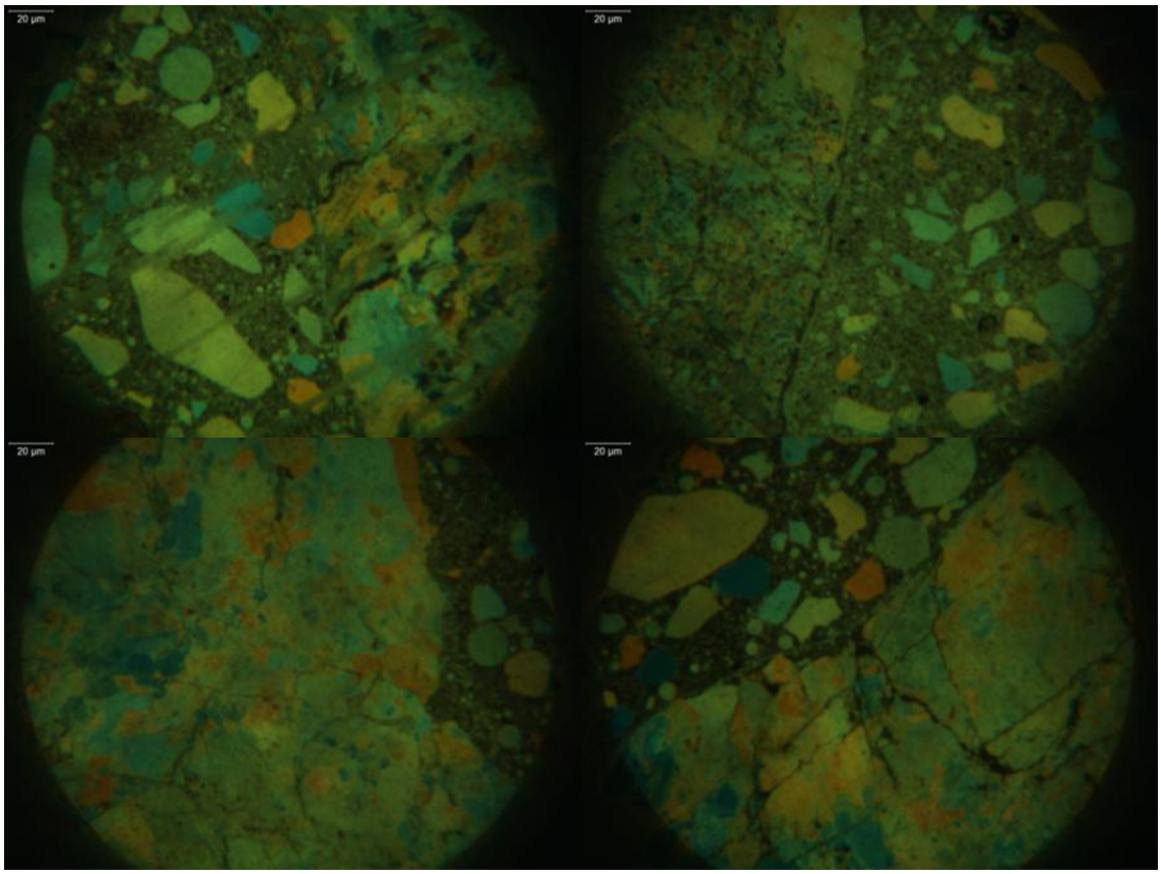
20 µm
20 µm
20 µm
20 µm

21A-1

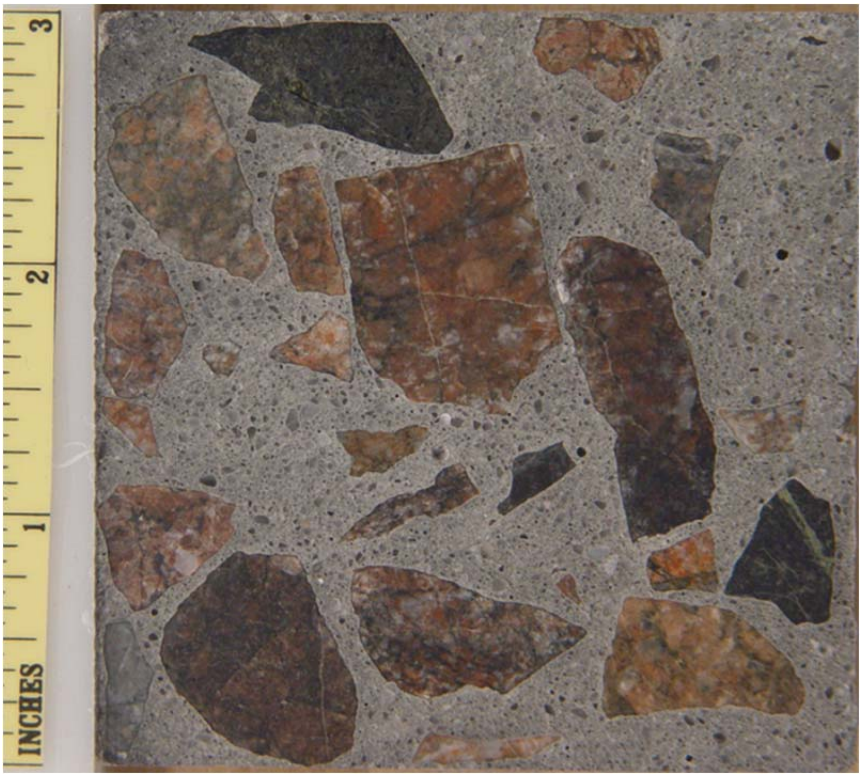

21A-2

21A-1.3
45%

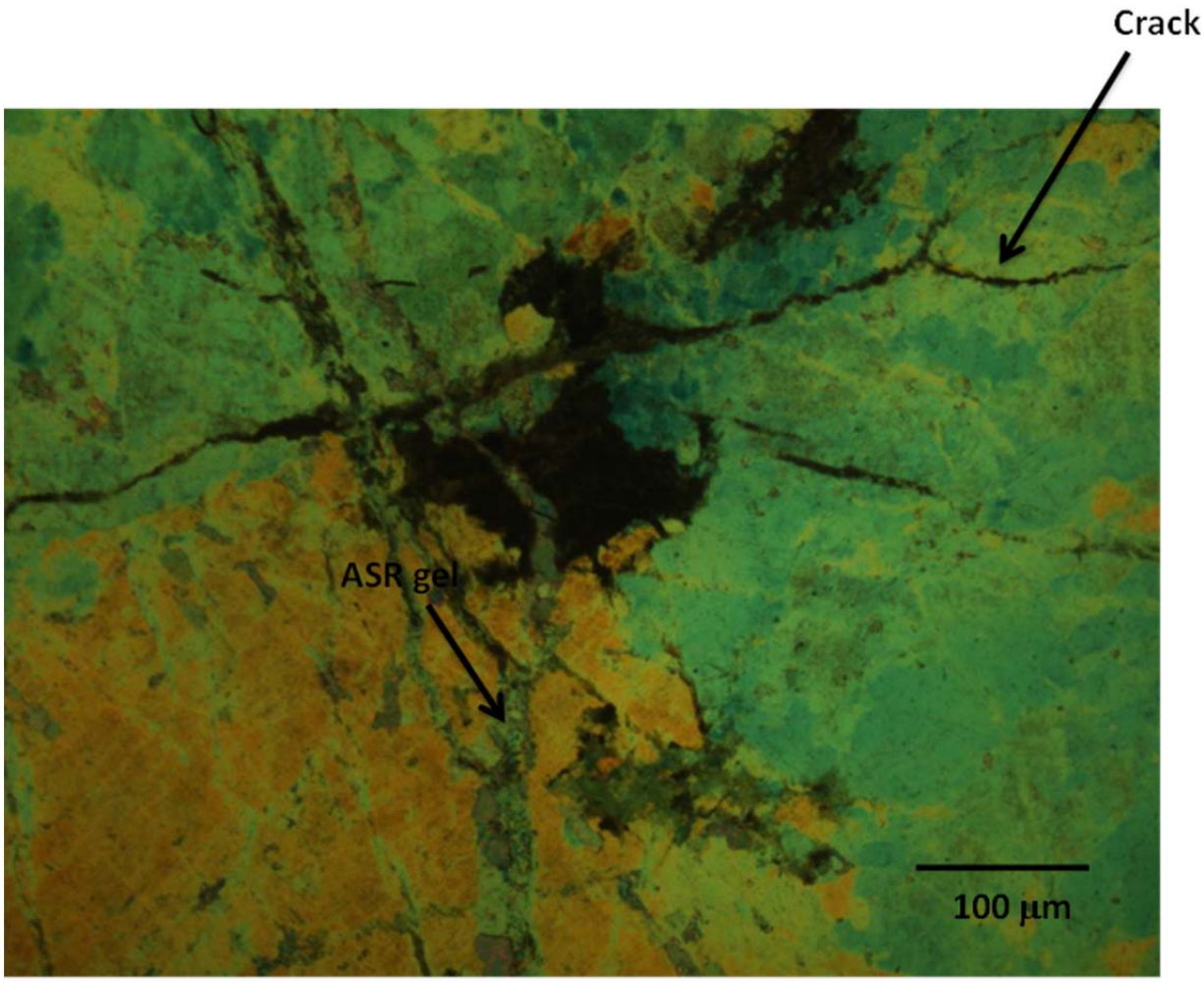

21A-2.1
45%

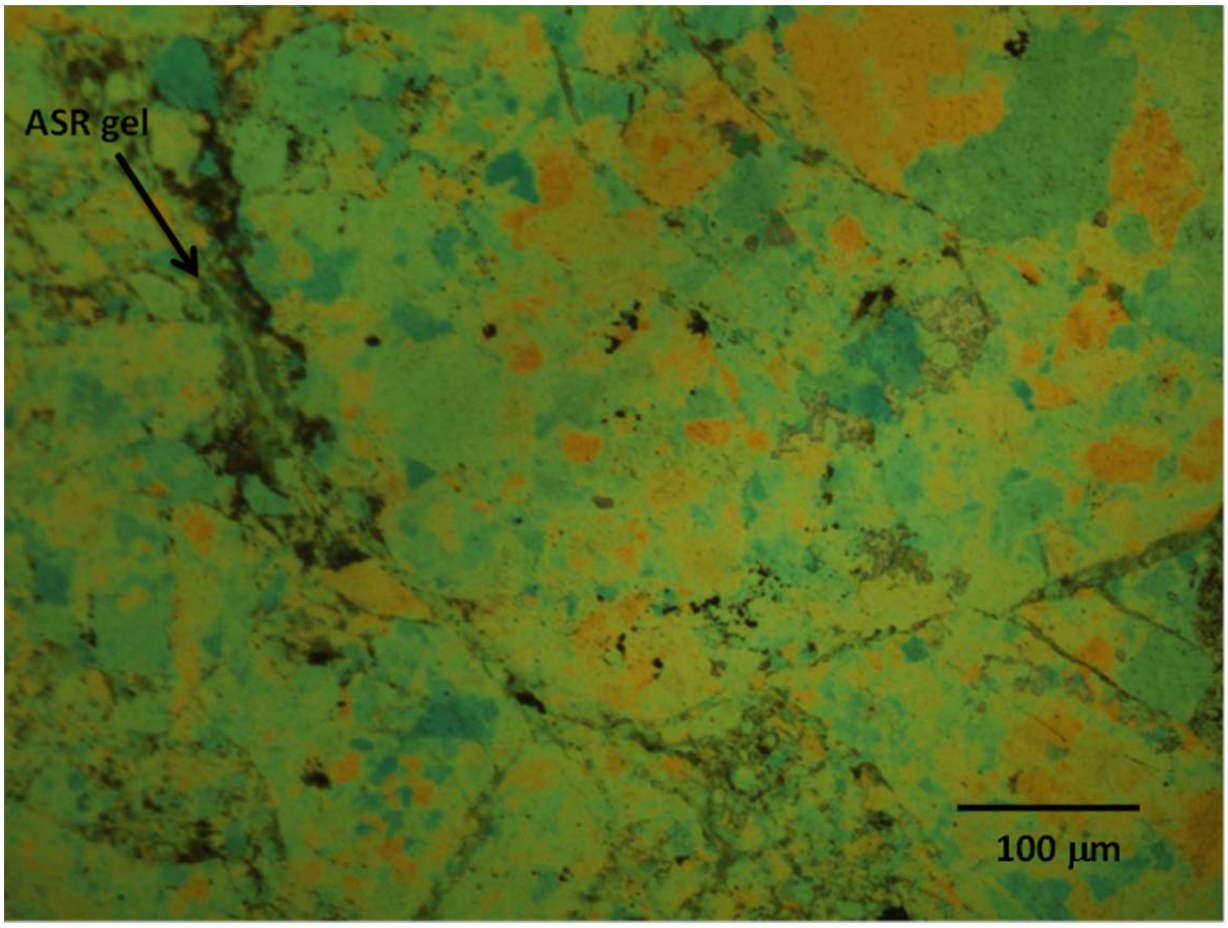

21A-2.3
25%

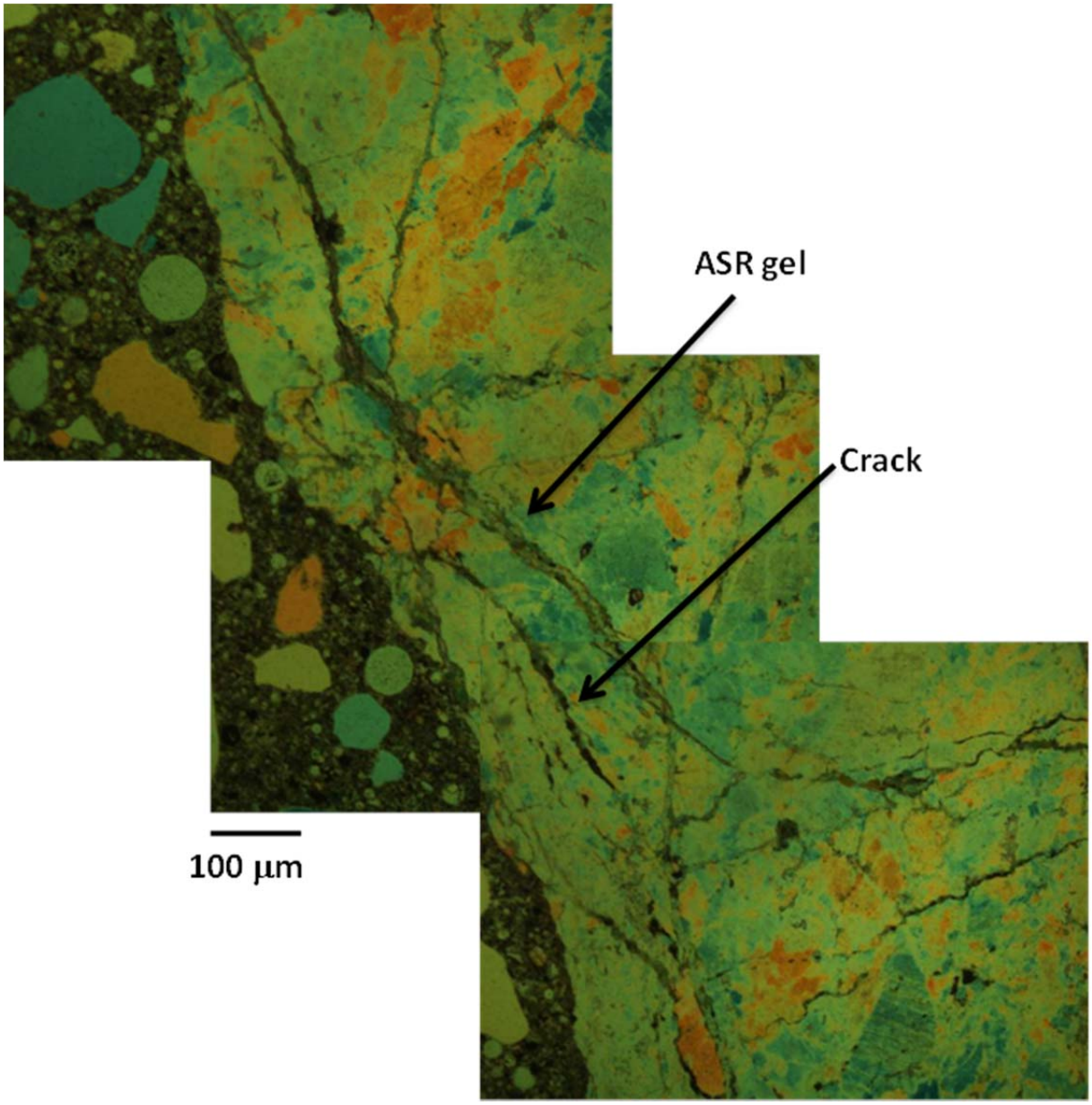

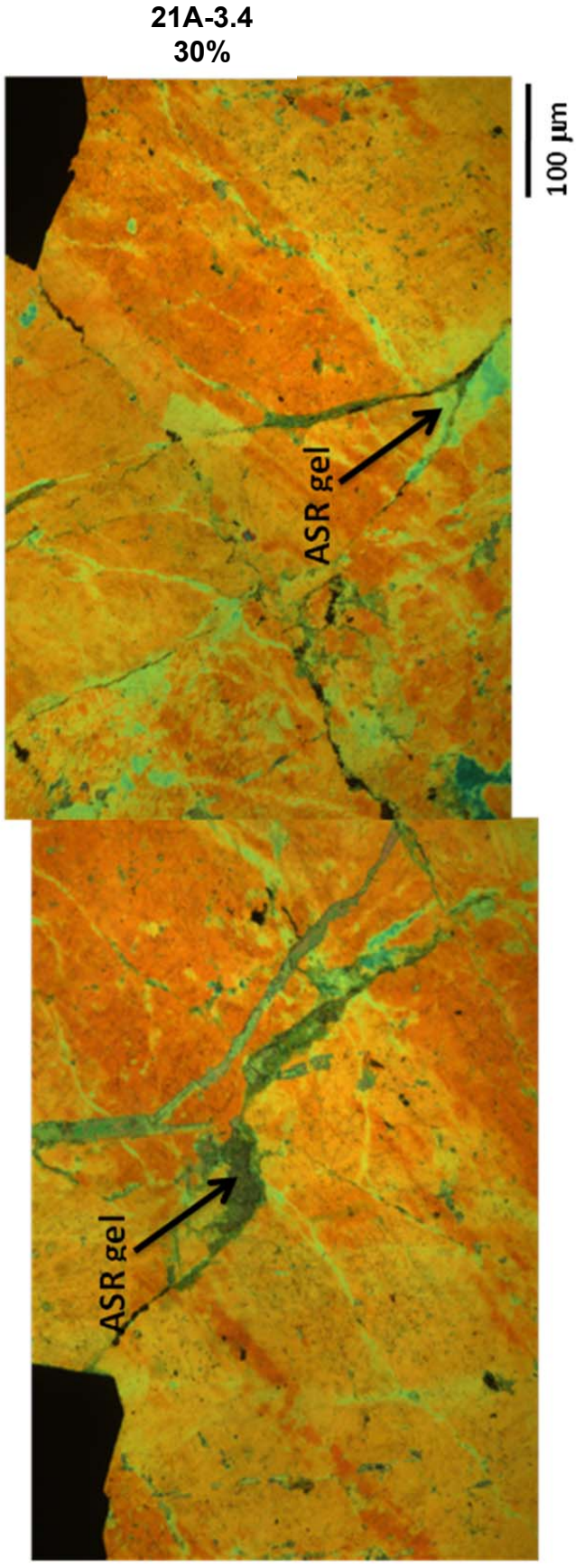
21A-3.4
30%
100 µm
ASR gel
ASR gel

21A-4.3
45%

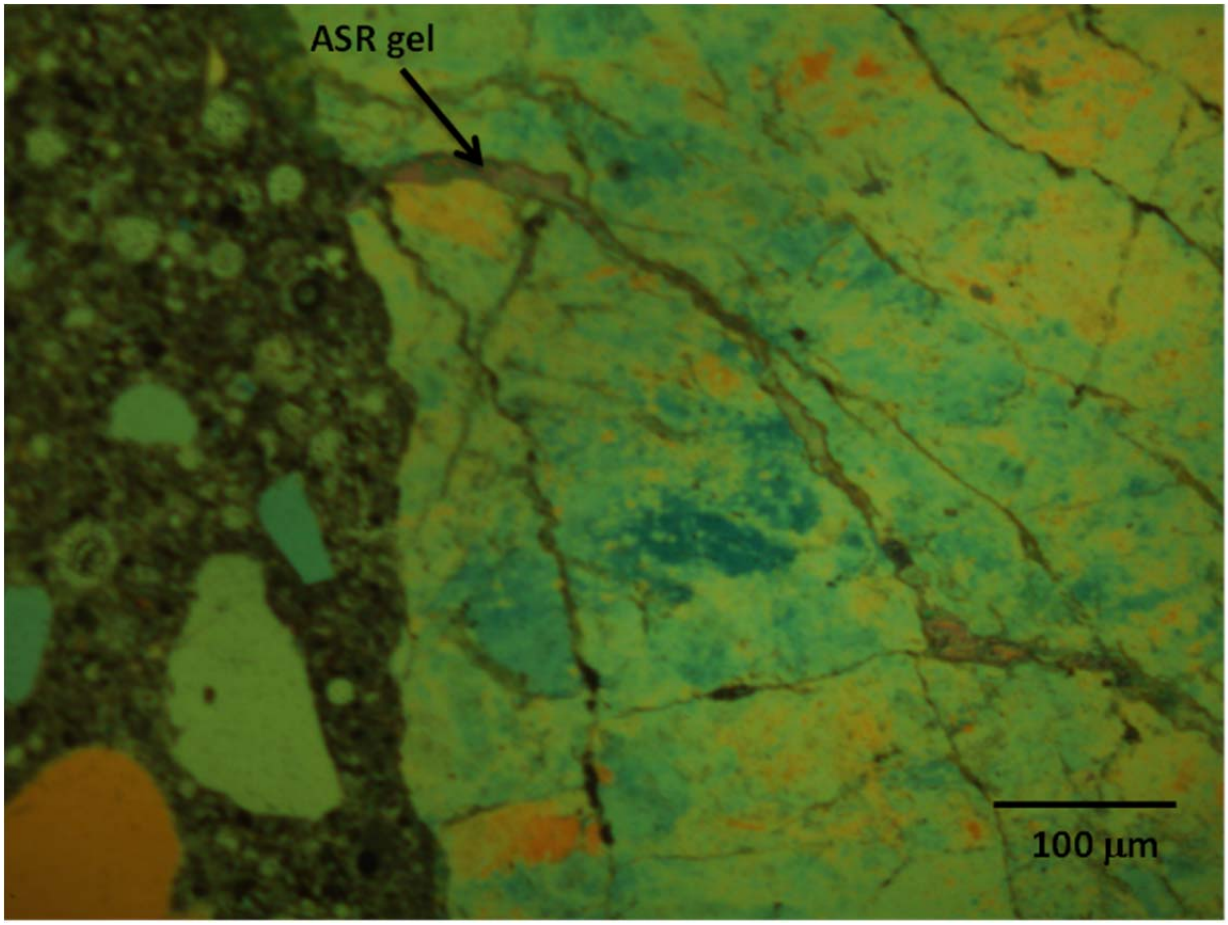

24B-1

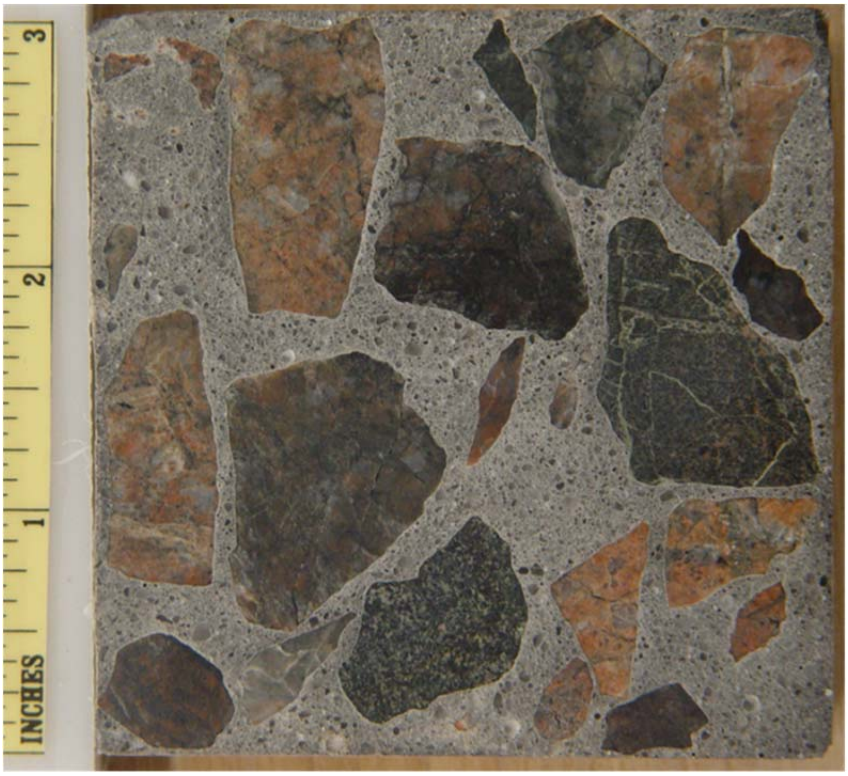

24B-2

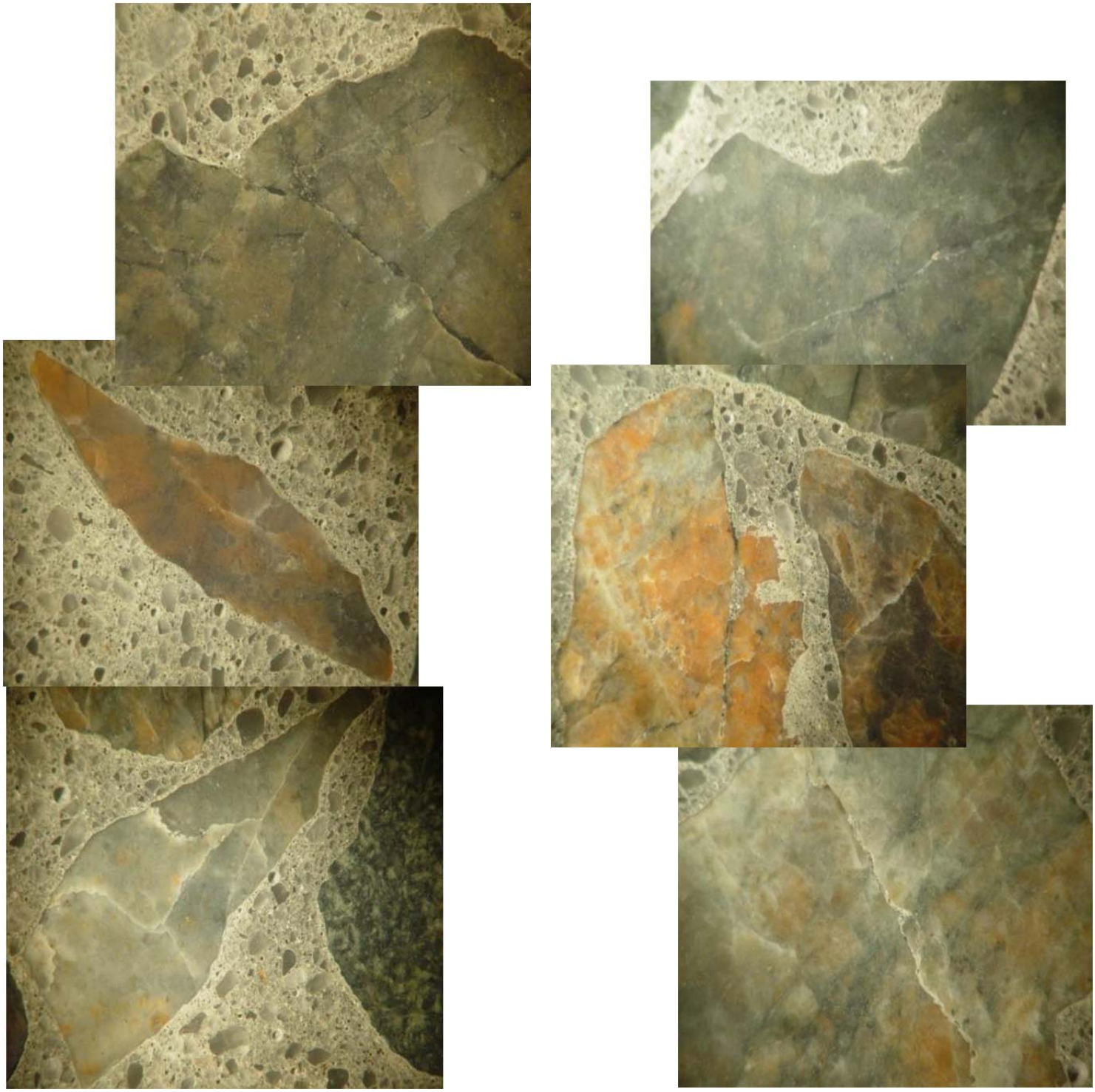

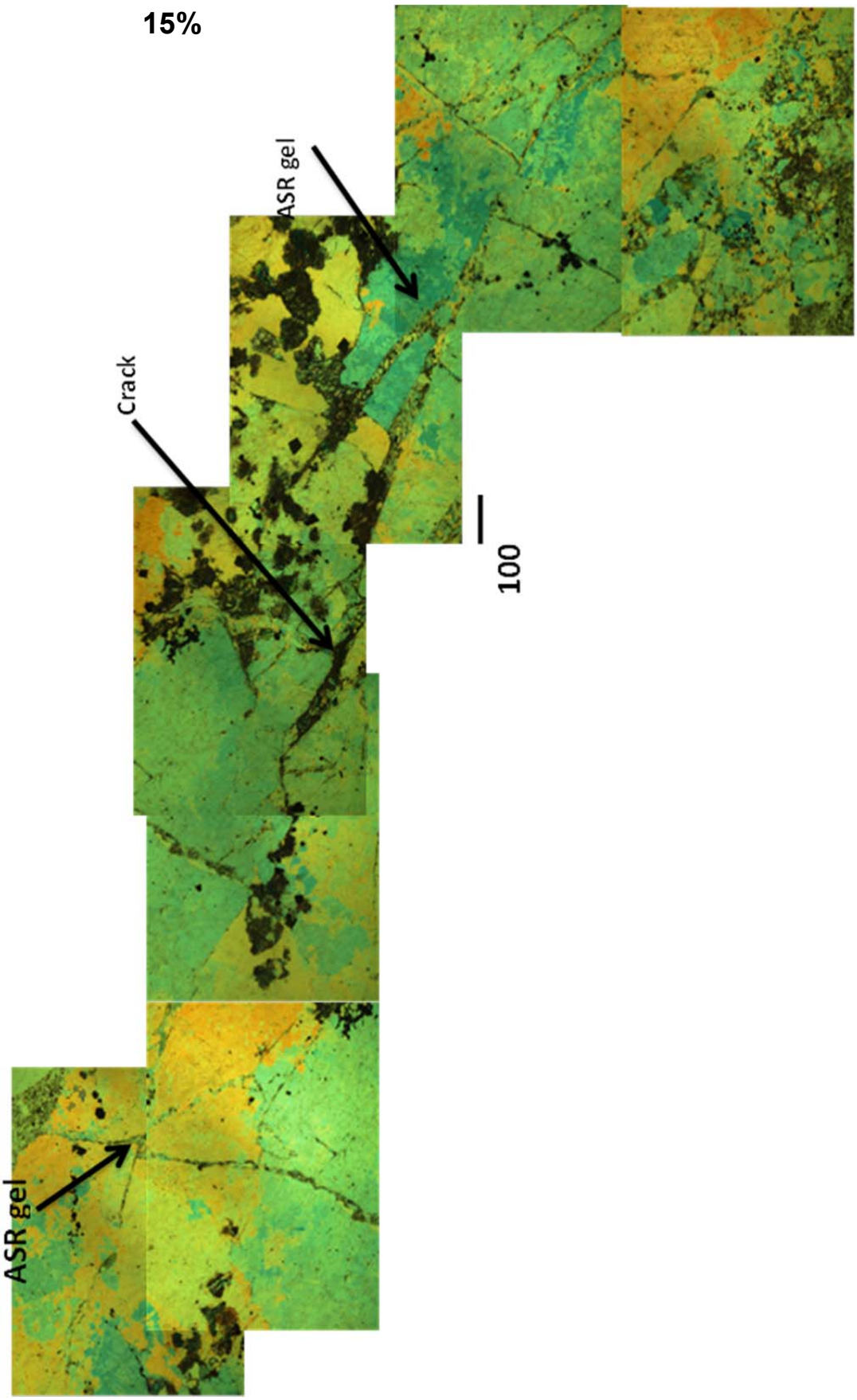
24B-1.4
15%
ASR gel
Crack
100
ASR gel

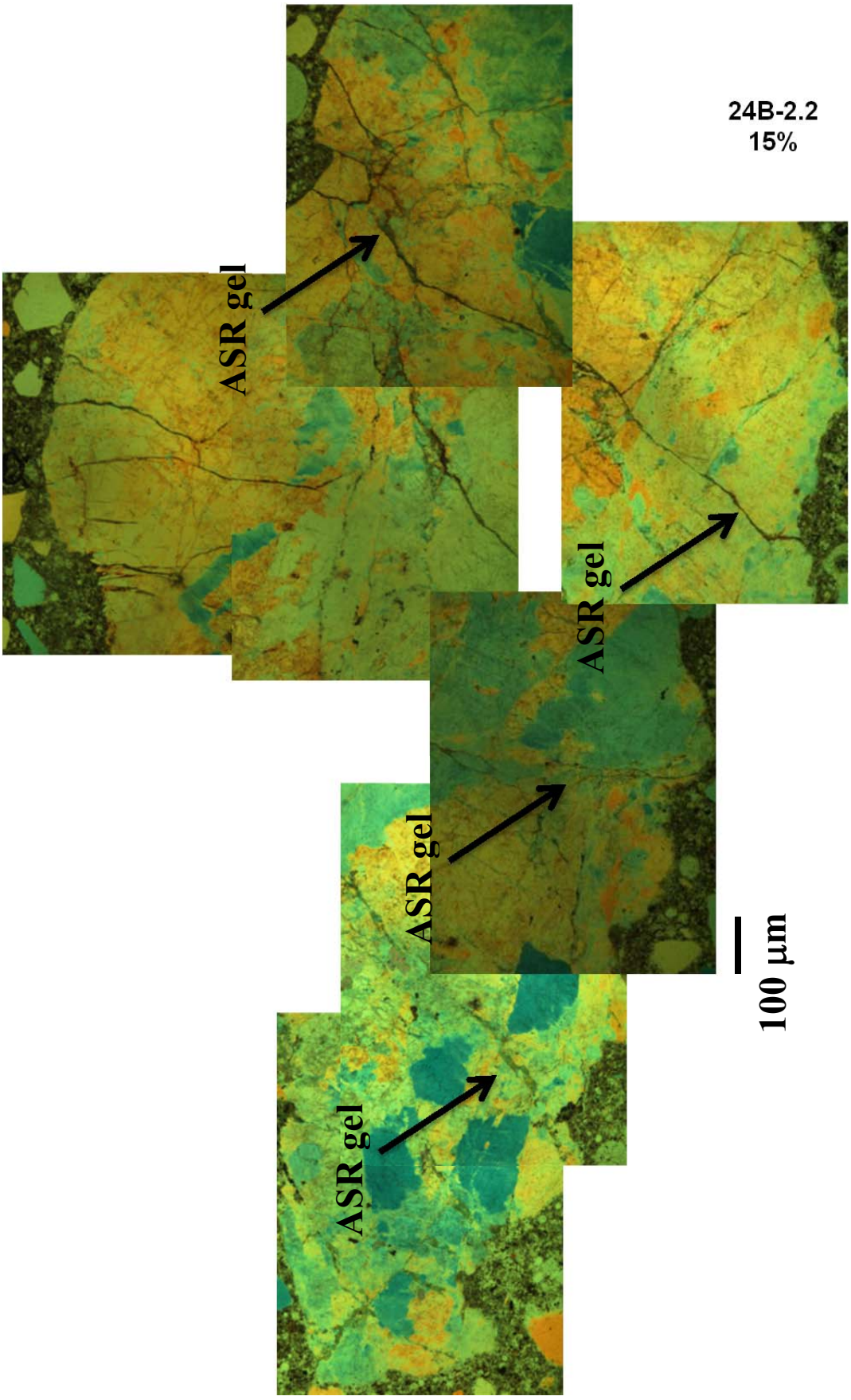
24B-2.2
15%
ASR gel
ASR gel
ASR gel
ASR gel
100 µm

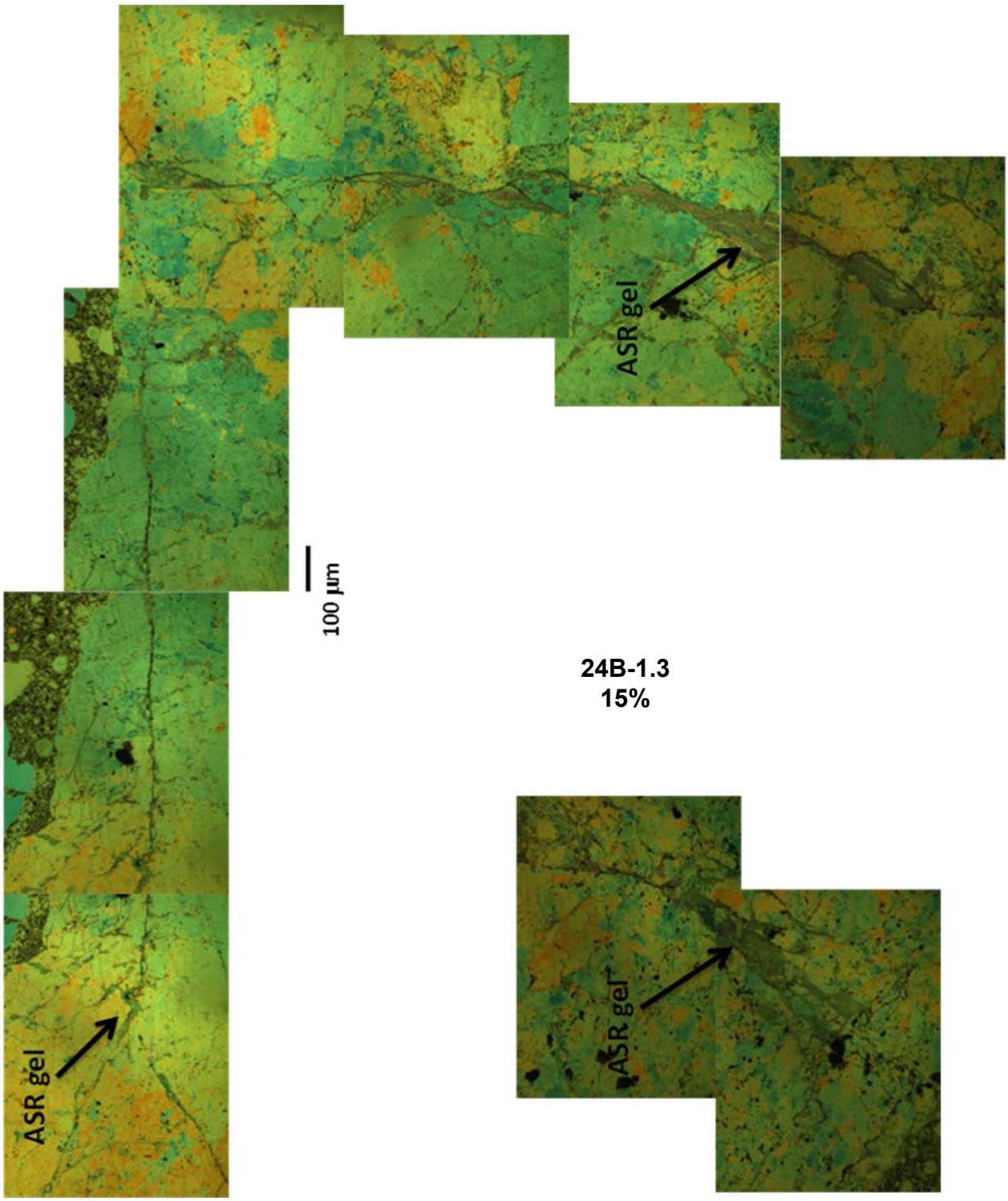
ASR gel
100 µm
24B-1.3
15%
ASR gel
ASR gel

H1

54A

31C

33A

31C-1

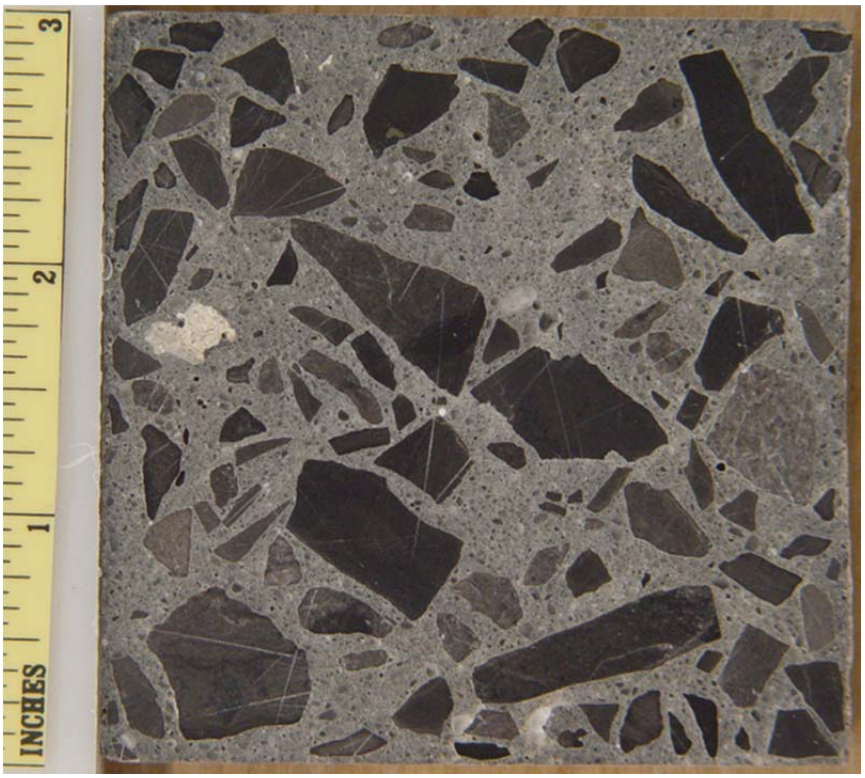

31C-2

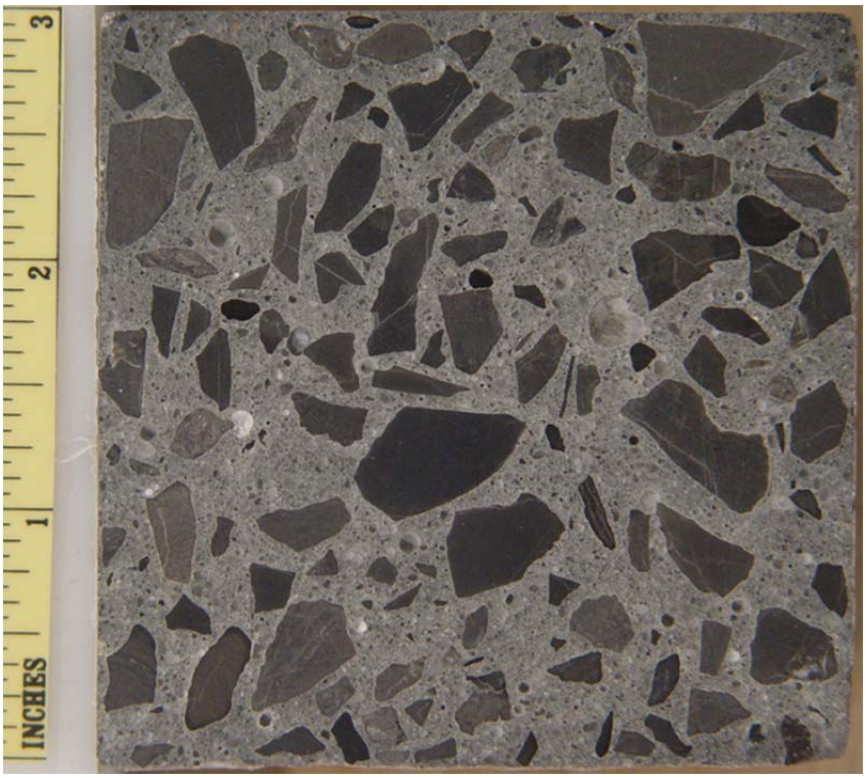

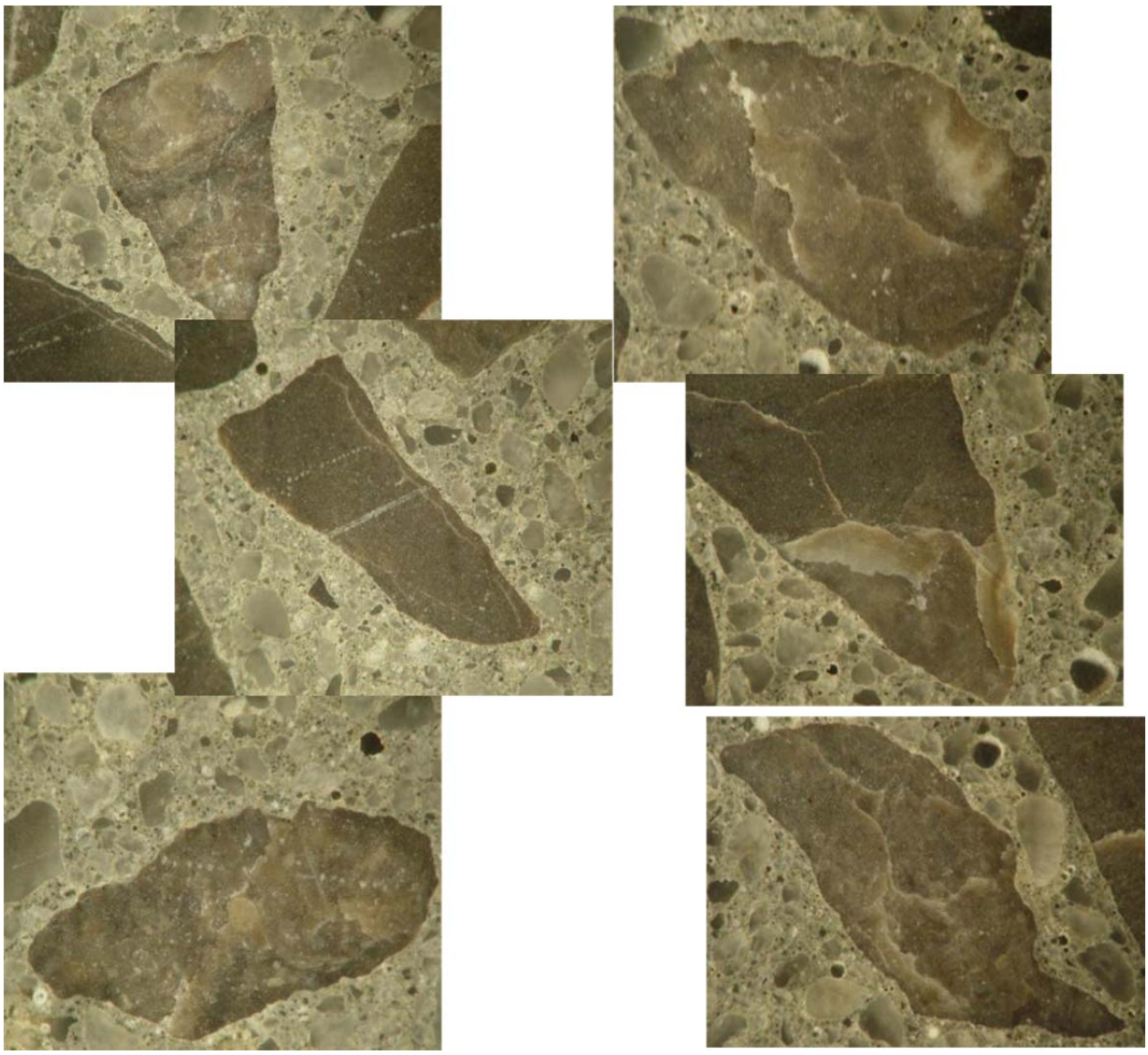

31C-2.1 45%

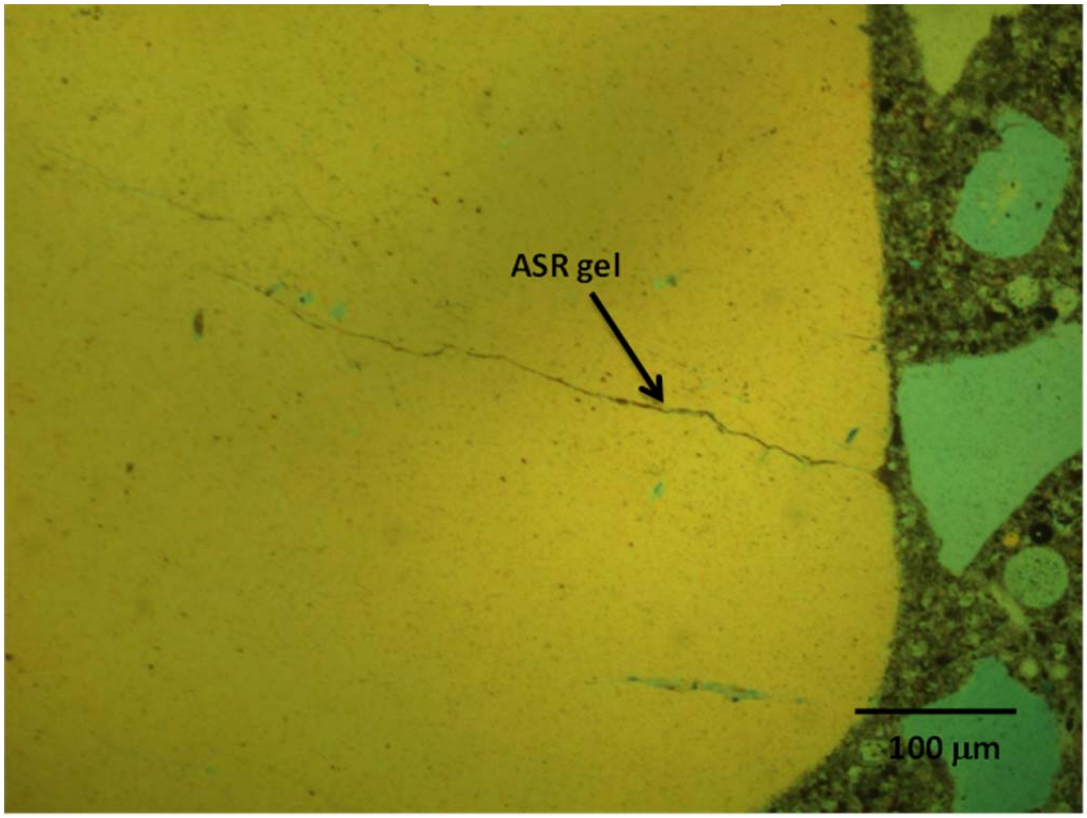

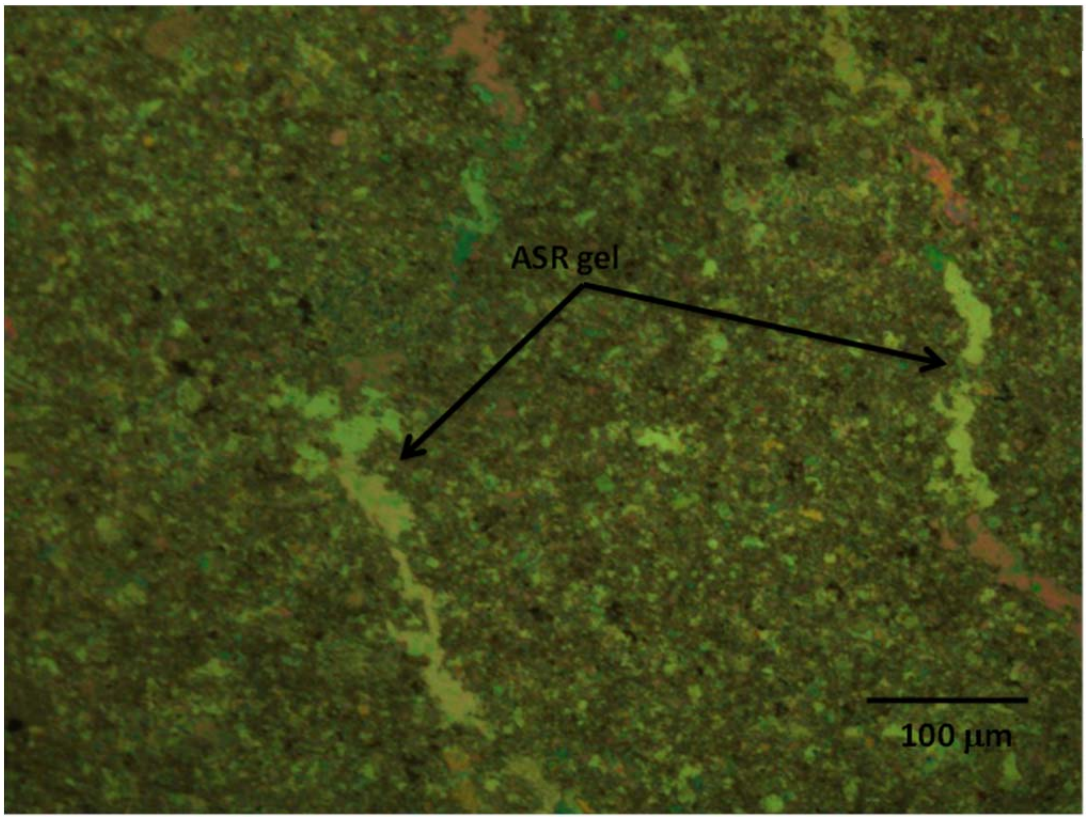

31C-2.3
45%

31C-2.4
45%

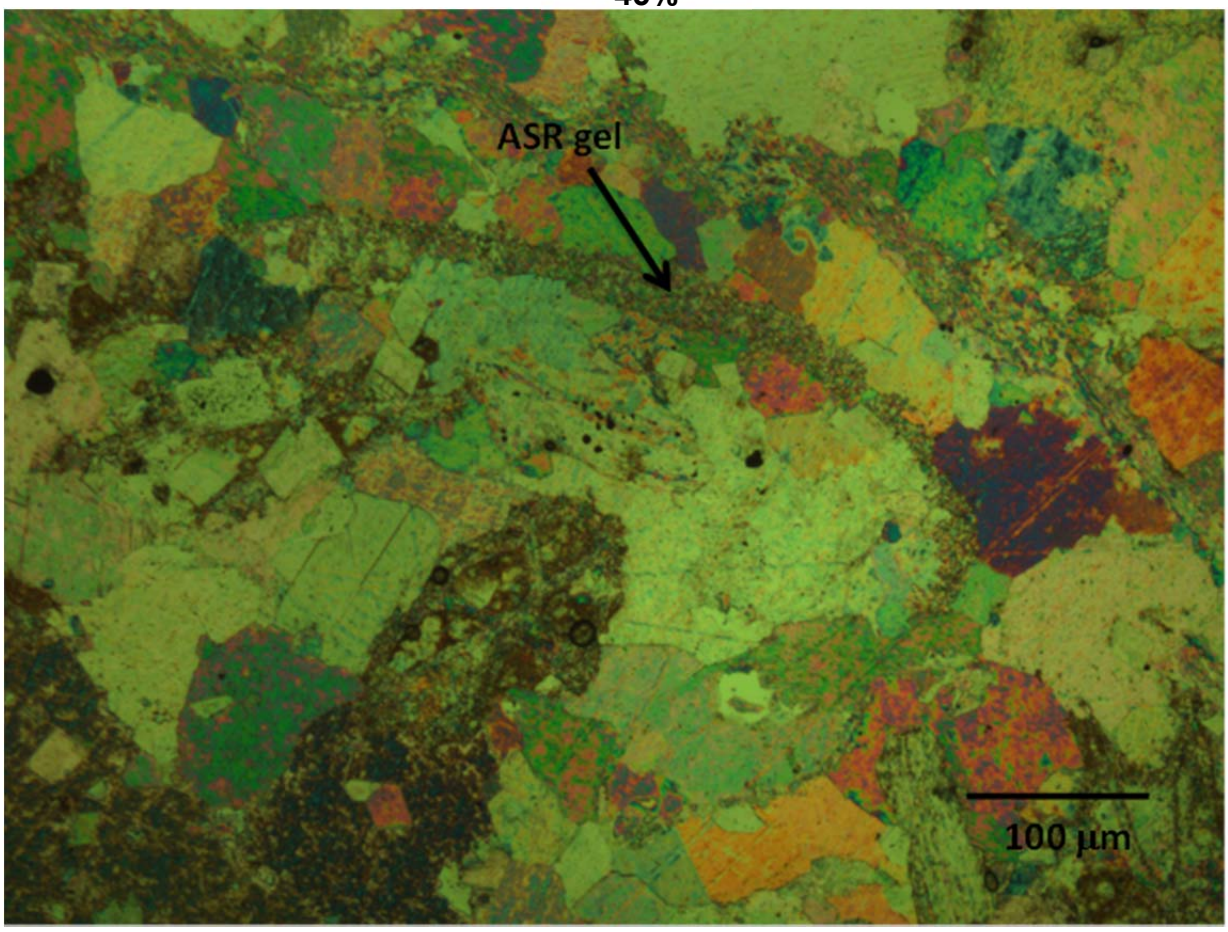

31C-3.1
45%

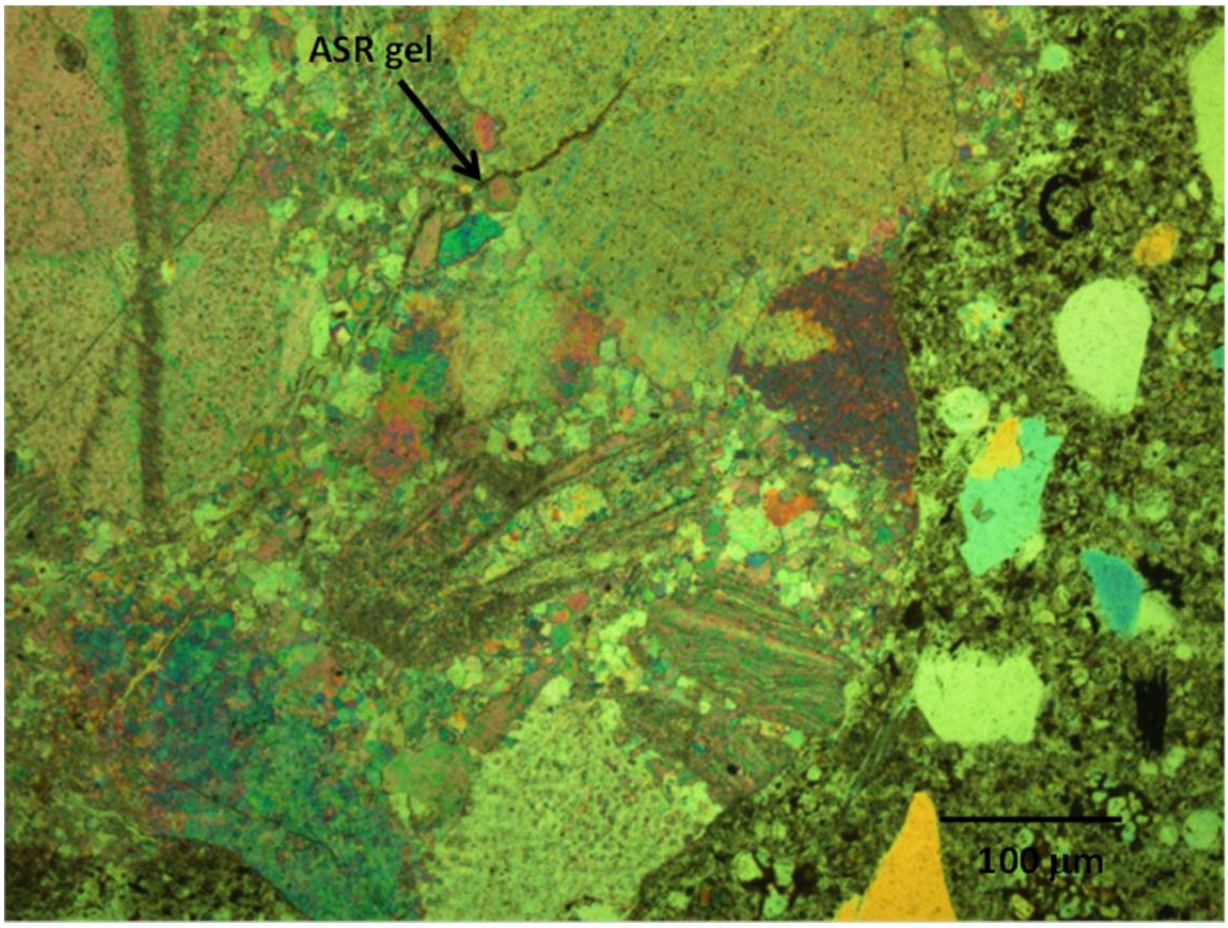

33A-1

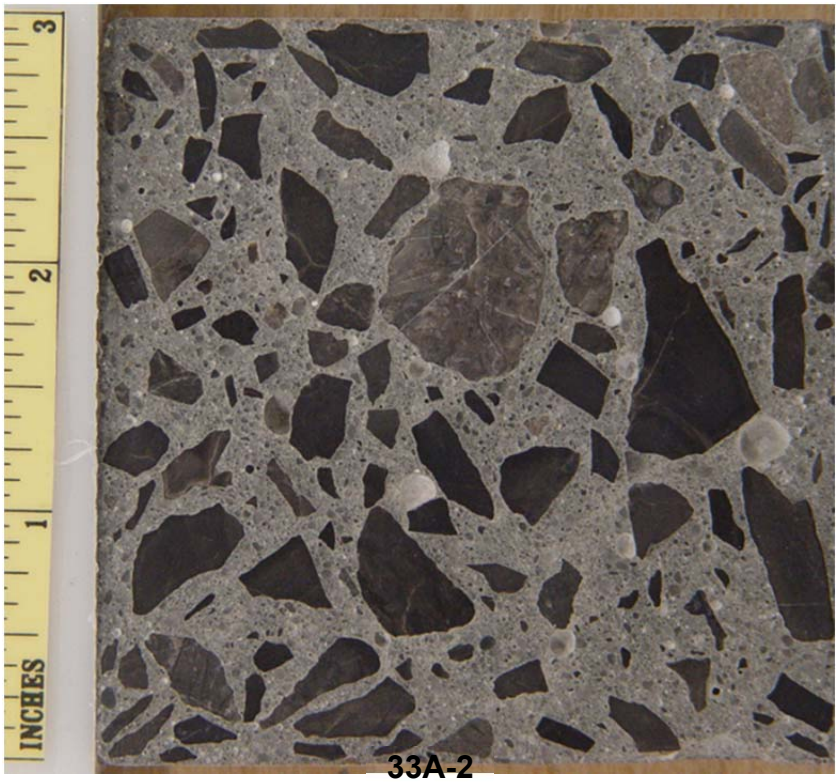

33A-2

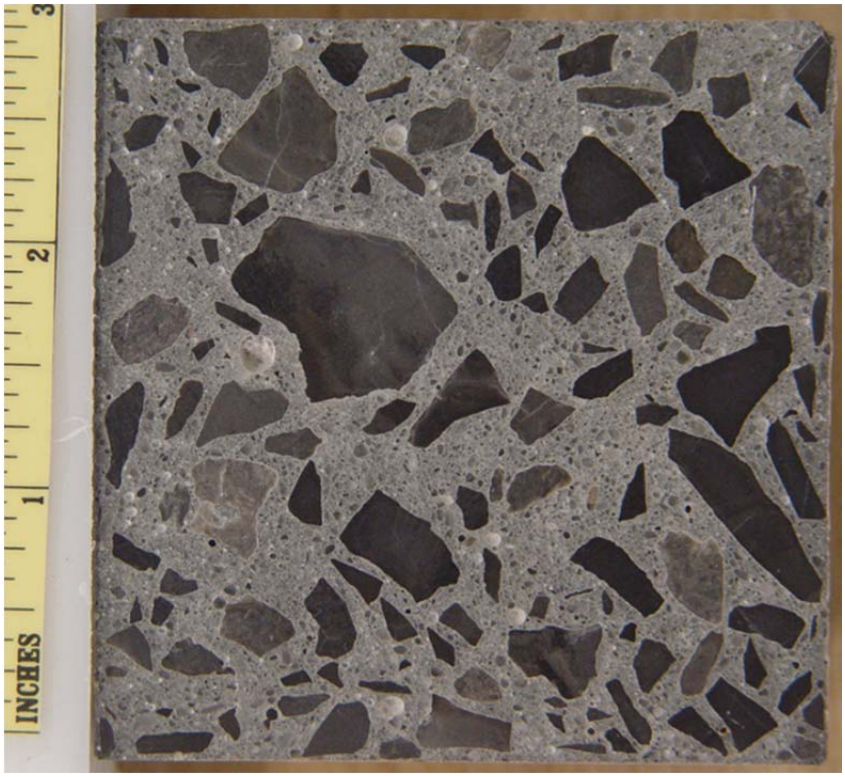

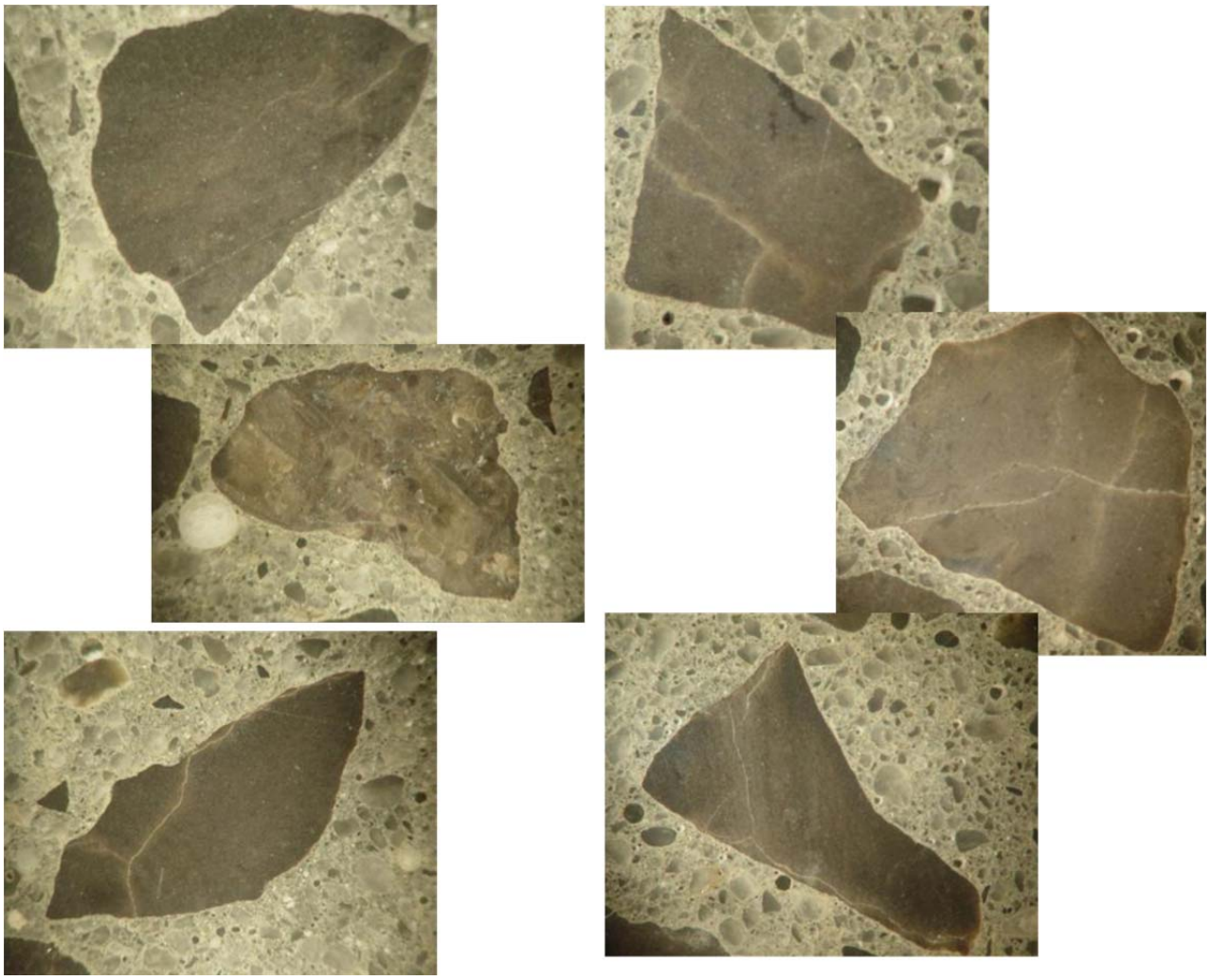

33A-3.2
45%

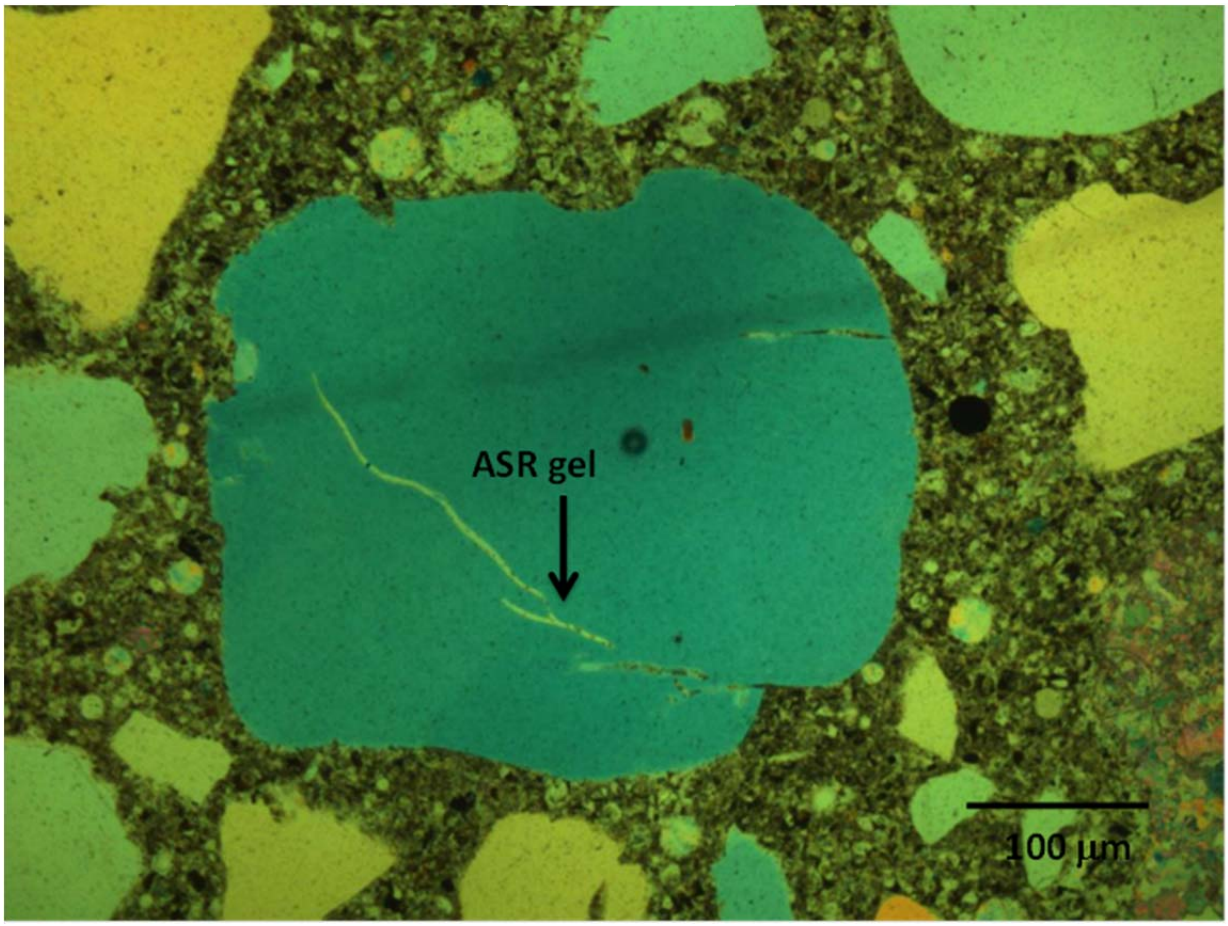

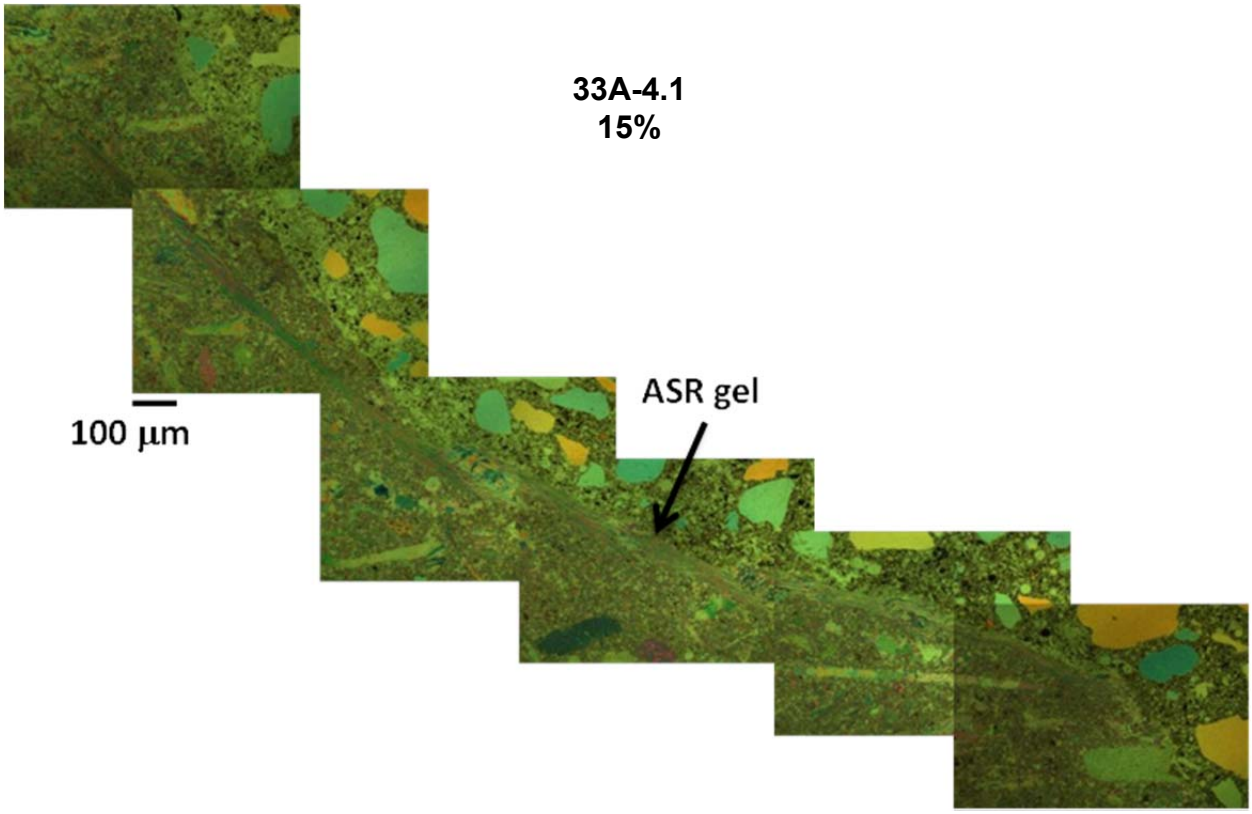
33A-4.1
15%
ASR gel
100 µm

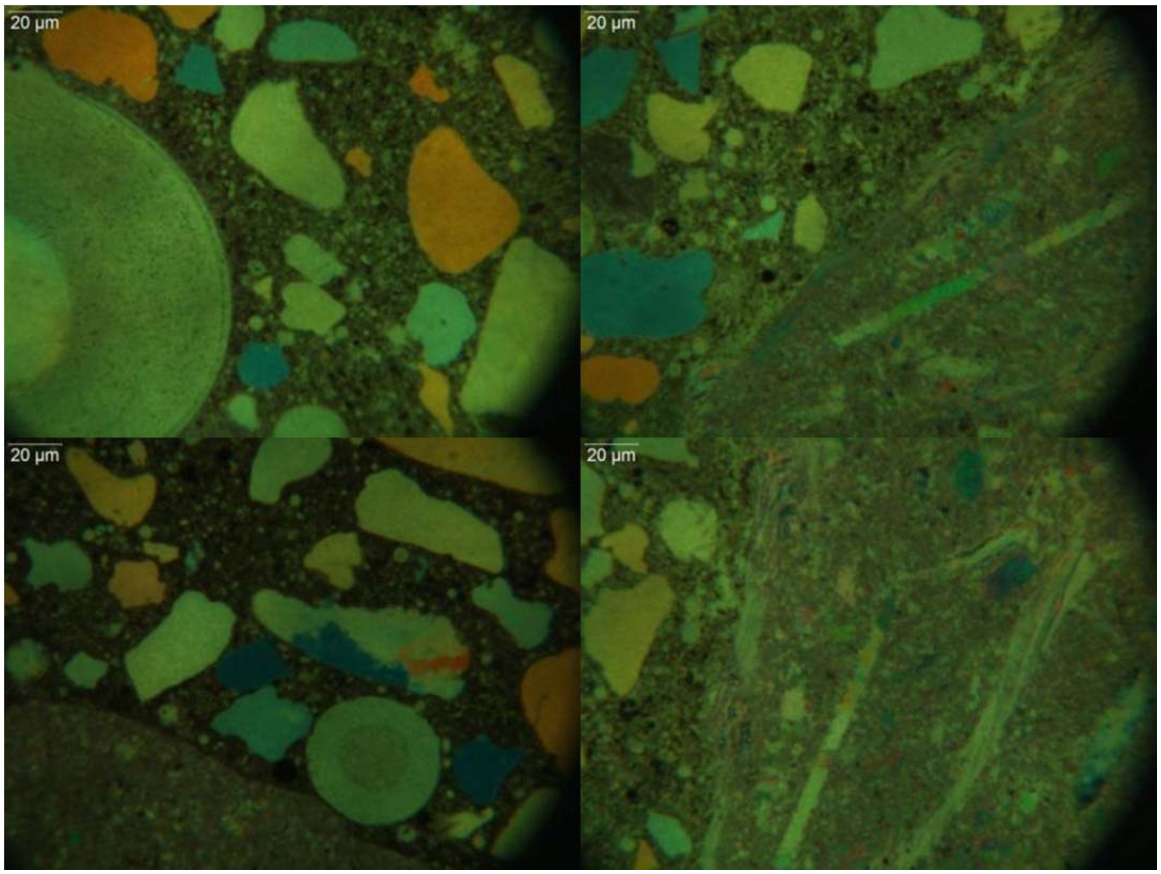
20 µm
20 µm
20 µm
20 µm

36B-1

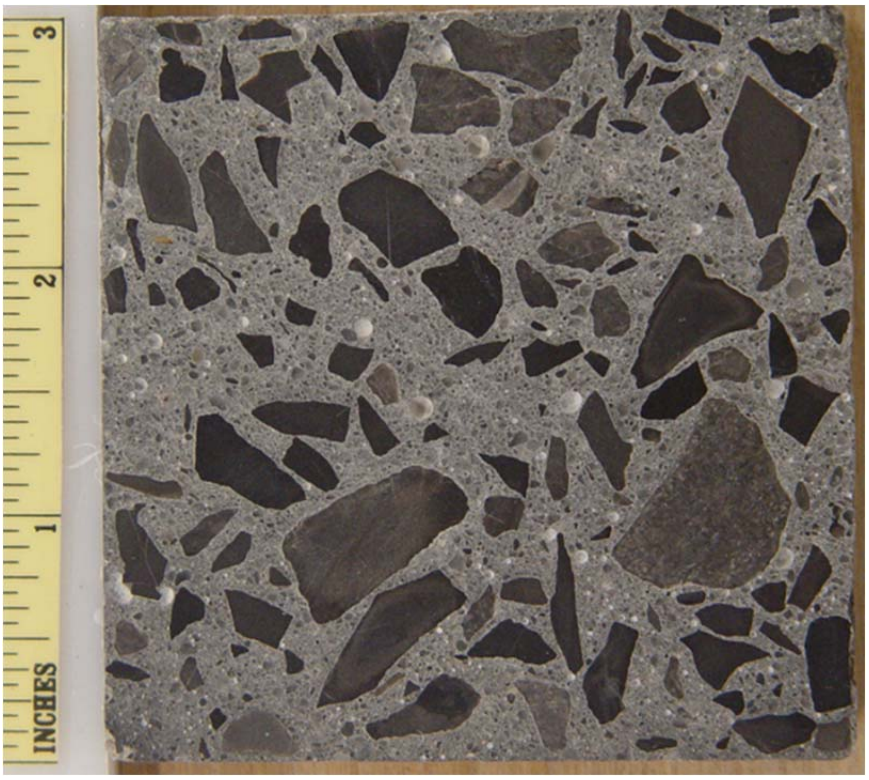

36B-2

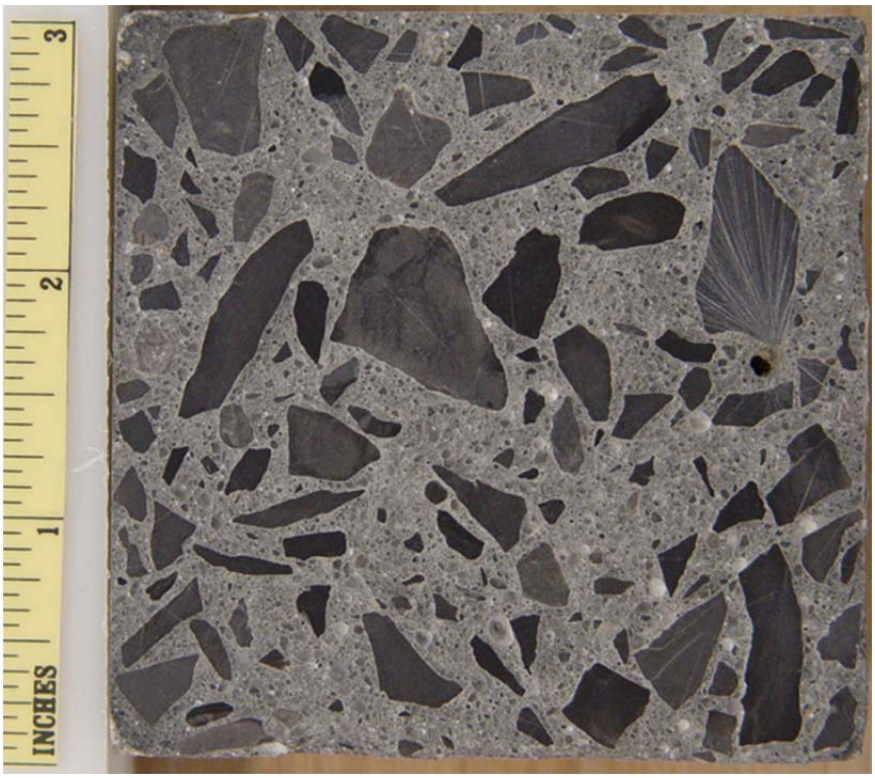

36B-1.1
45%

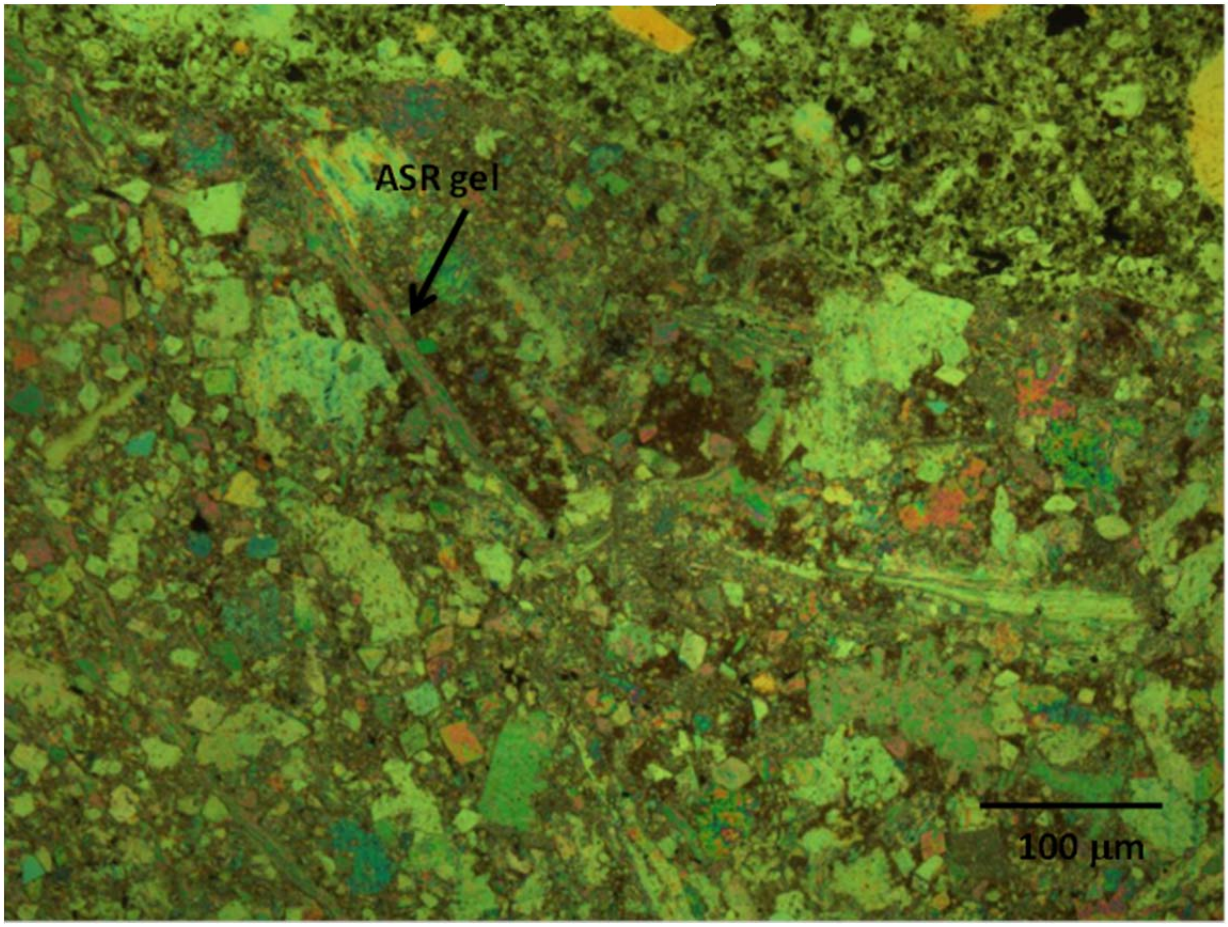

36B-3.2 25%

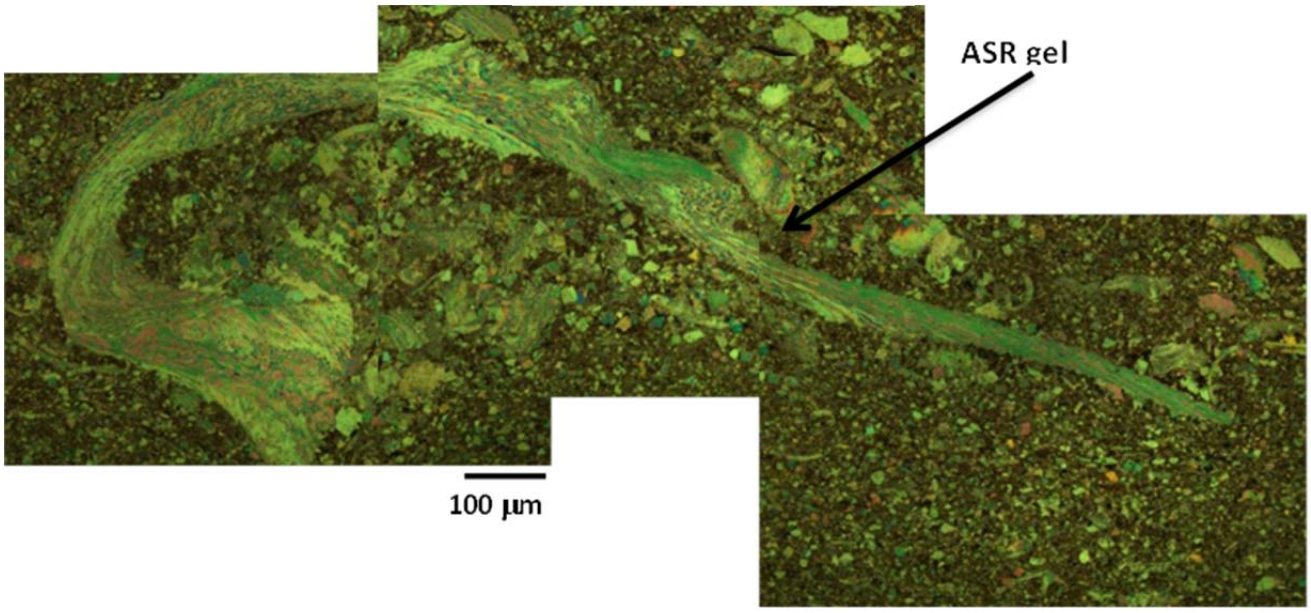

54A-

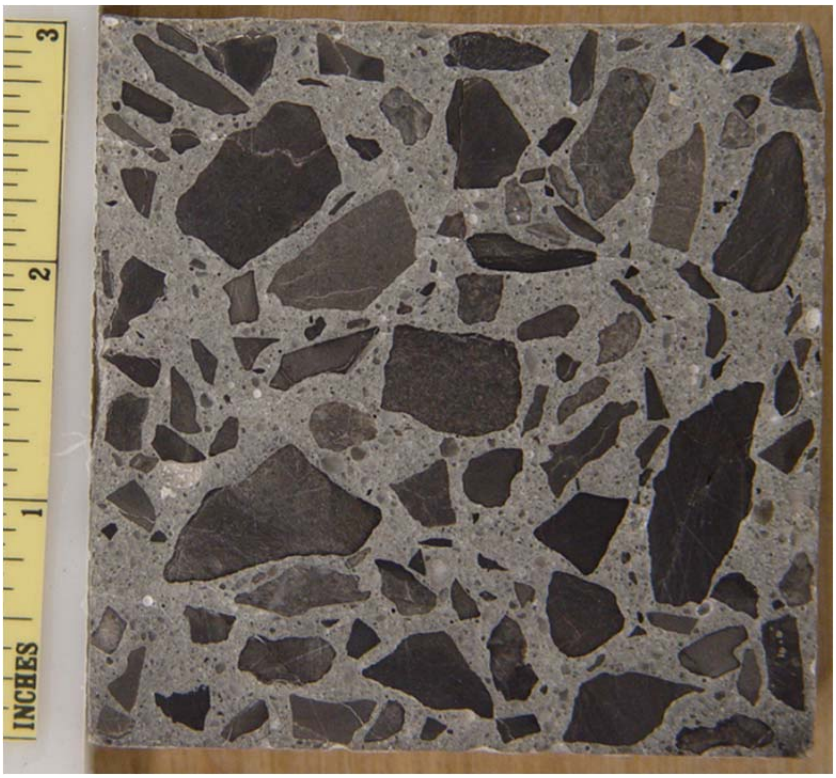

54A-2

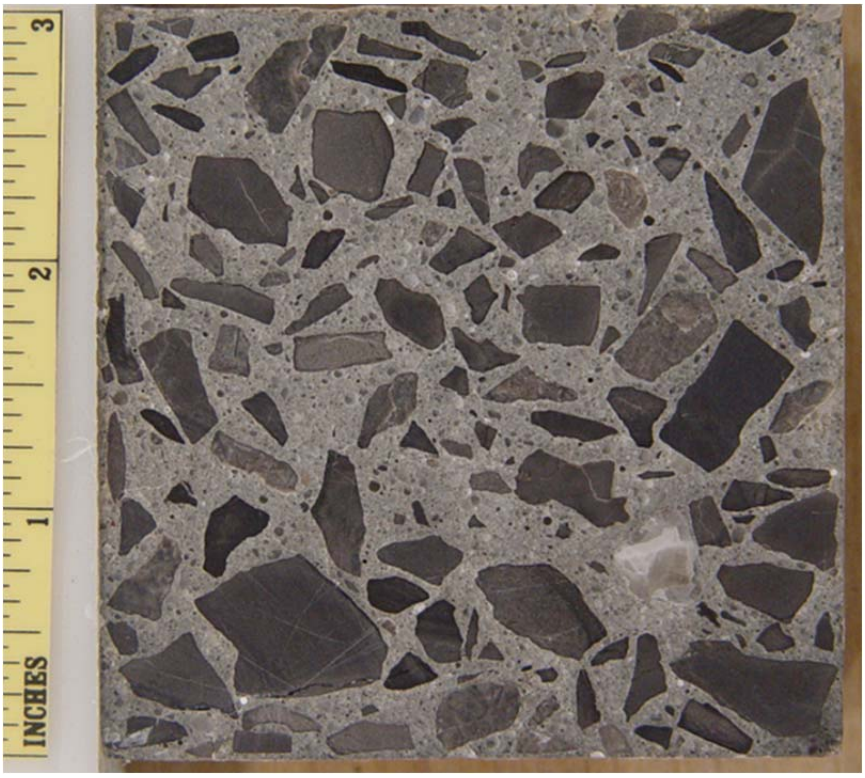

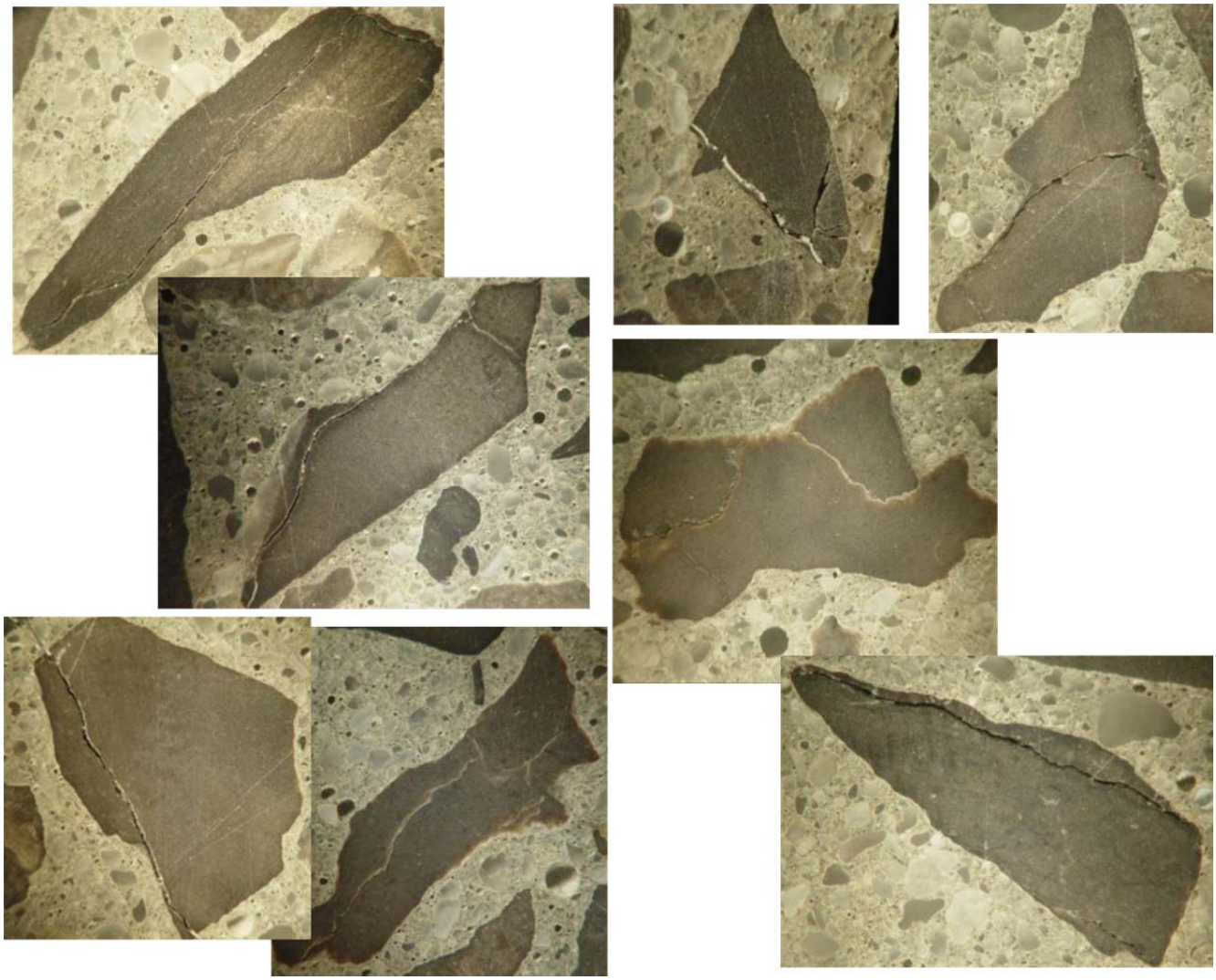

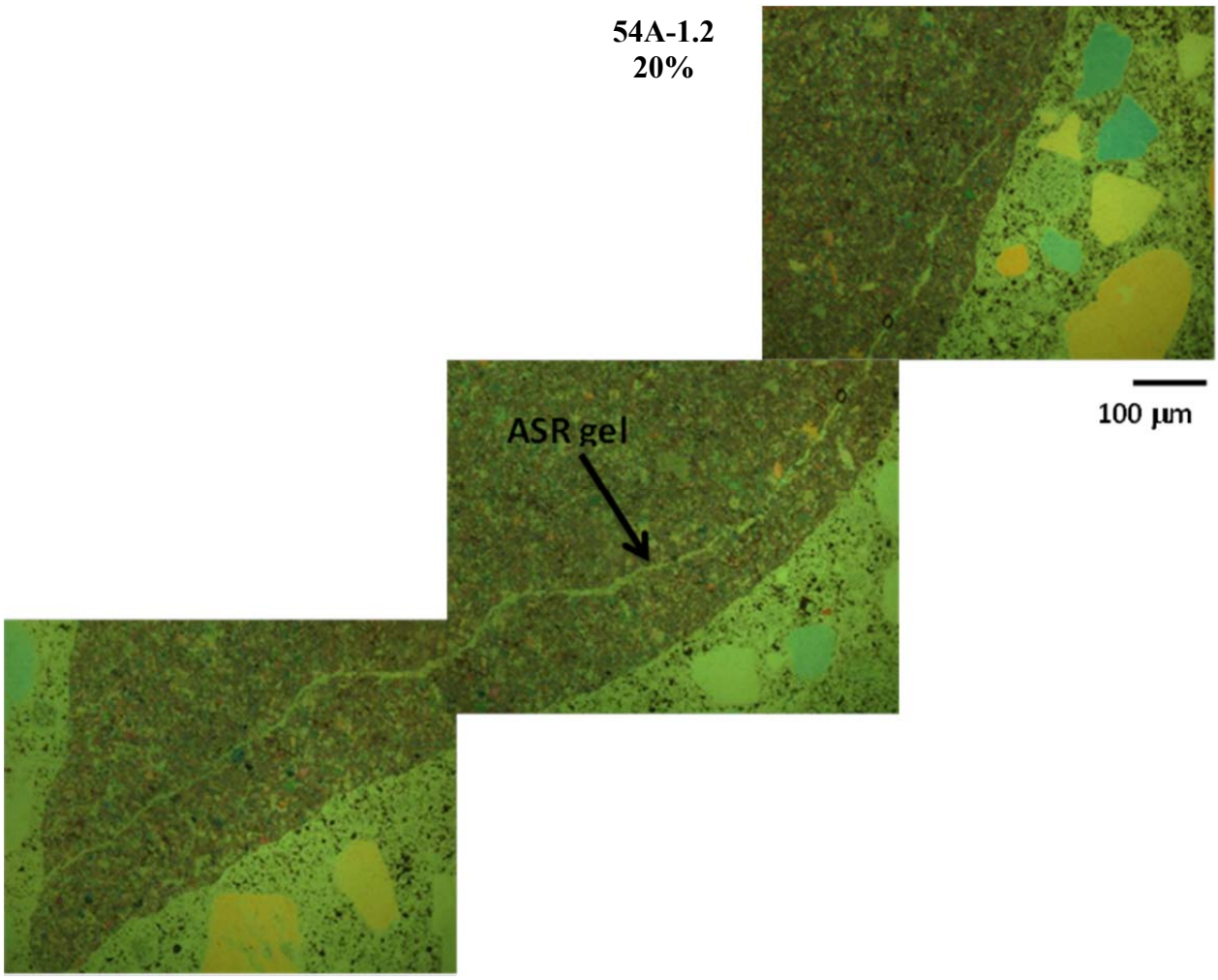
54A-1.2
20%
ASR gel
100 µm

54A-1.3
30%

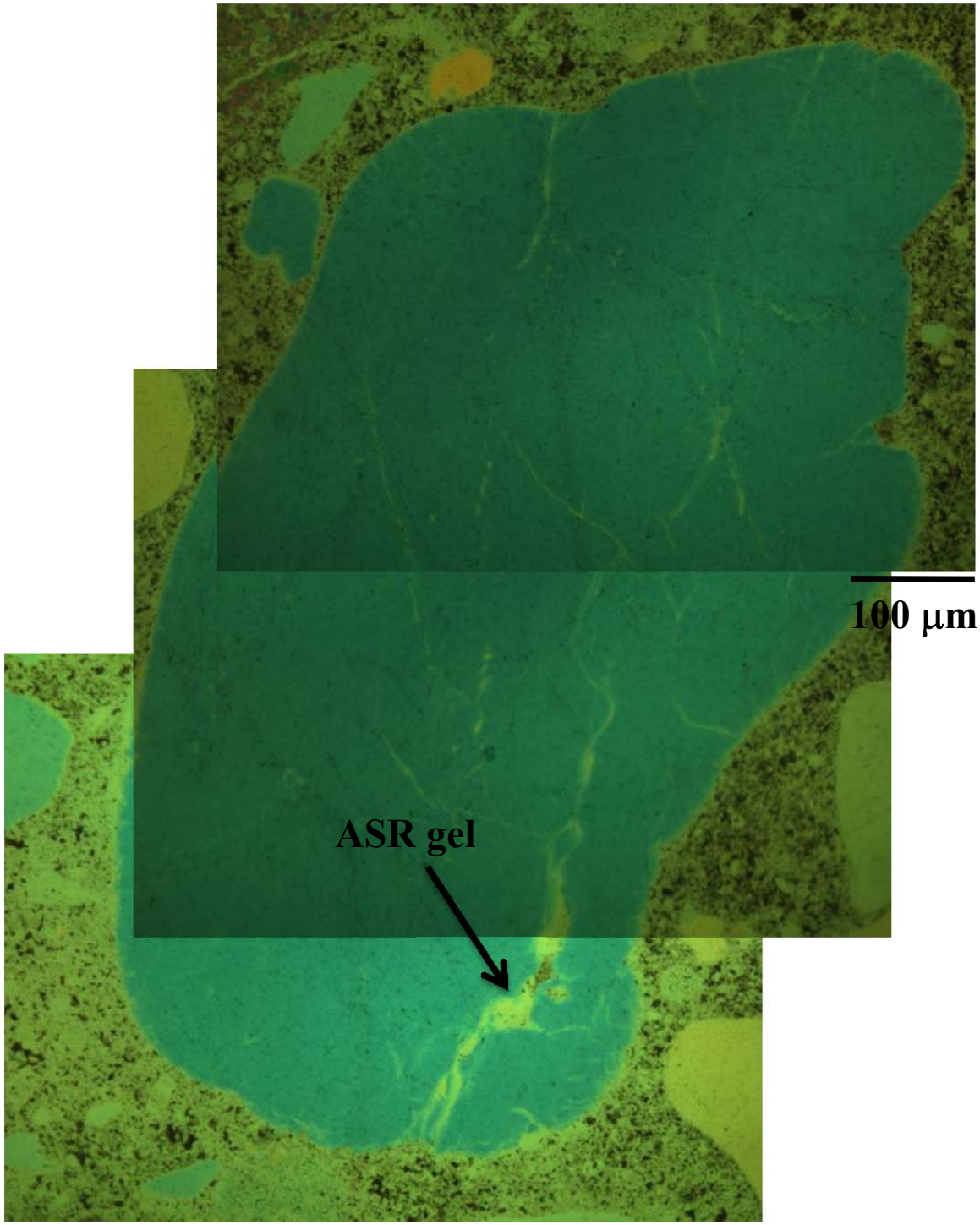

54A-1.3
25%

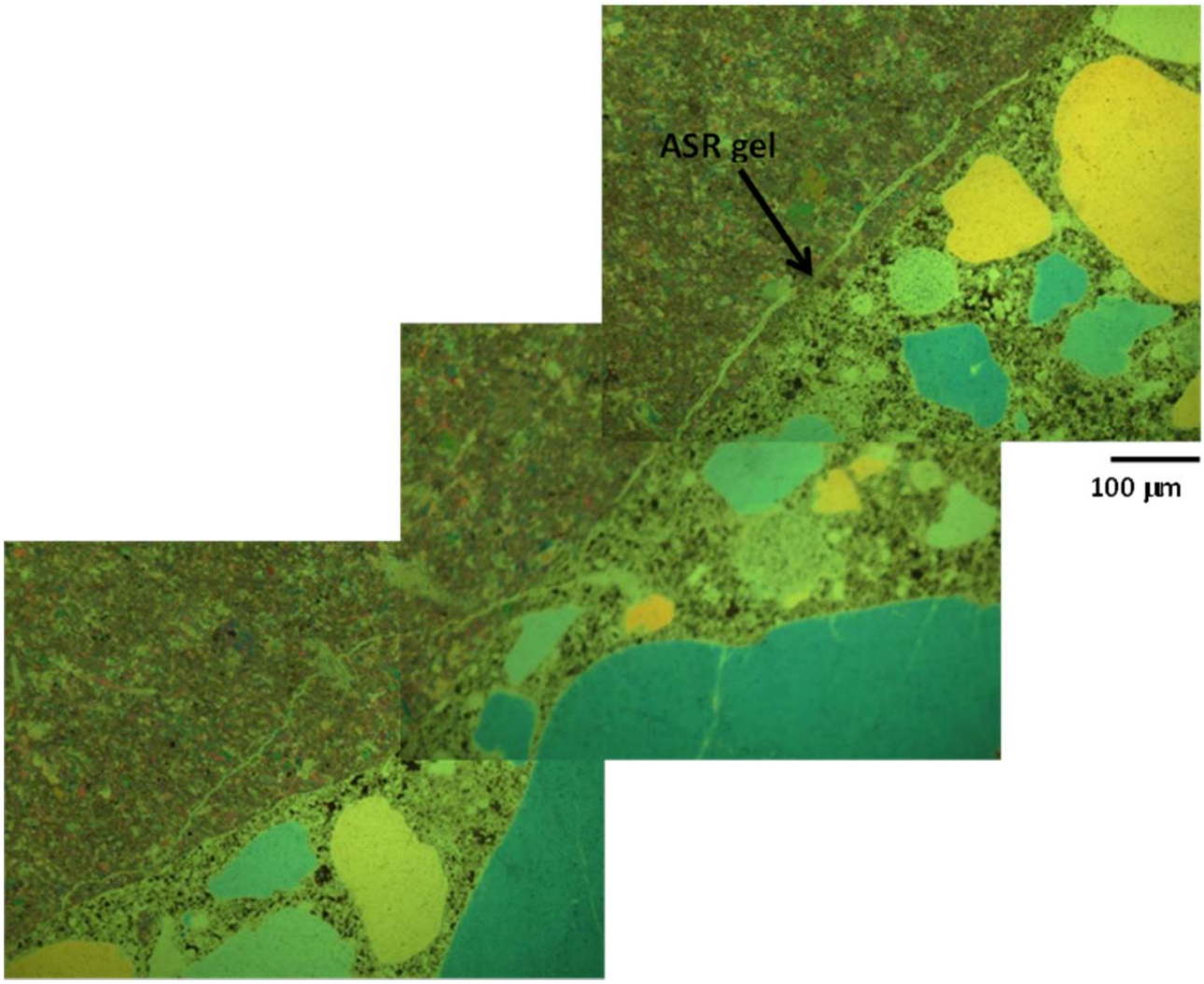

54A-1.5
45%

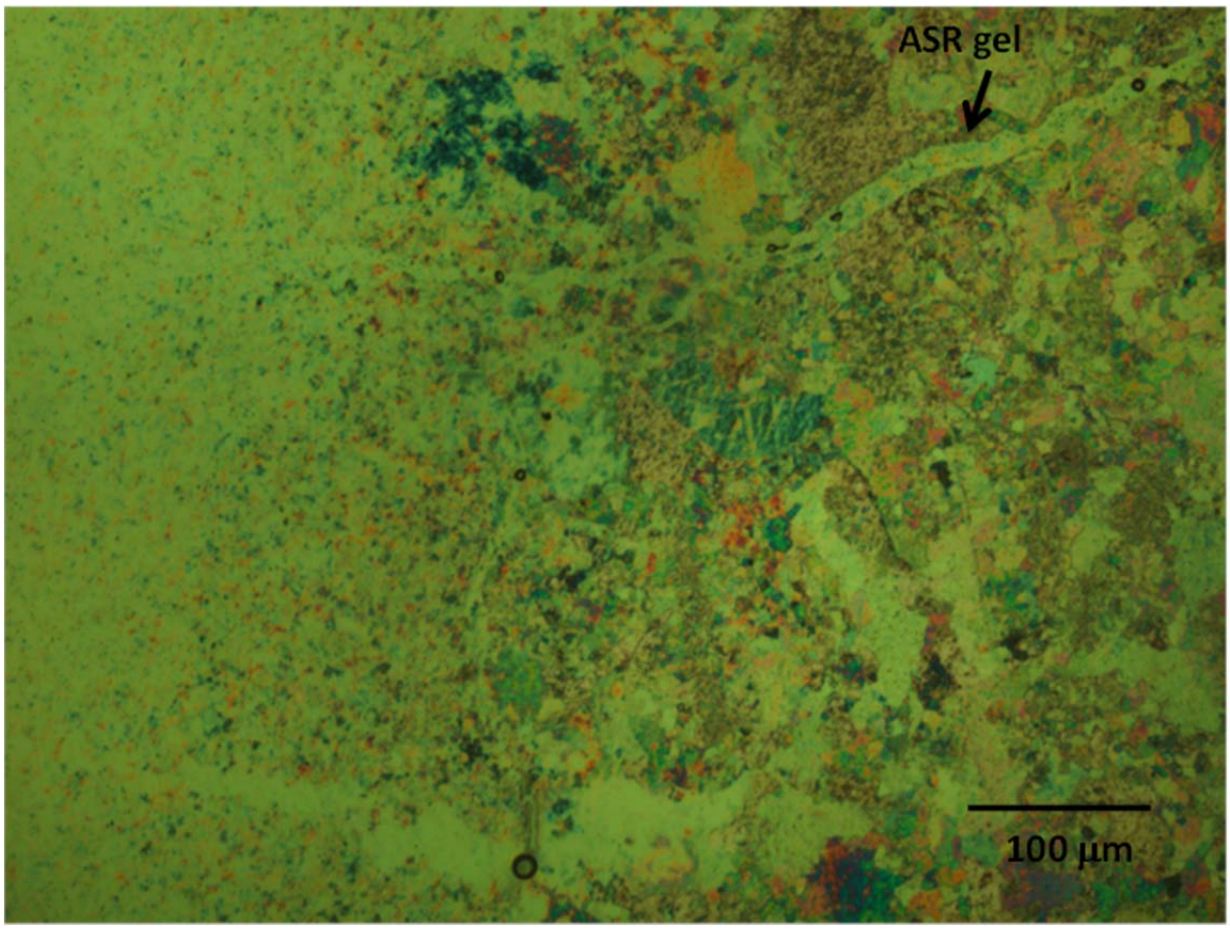

54A-2.3
30%

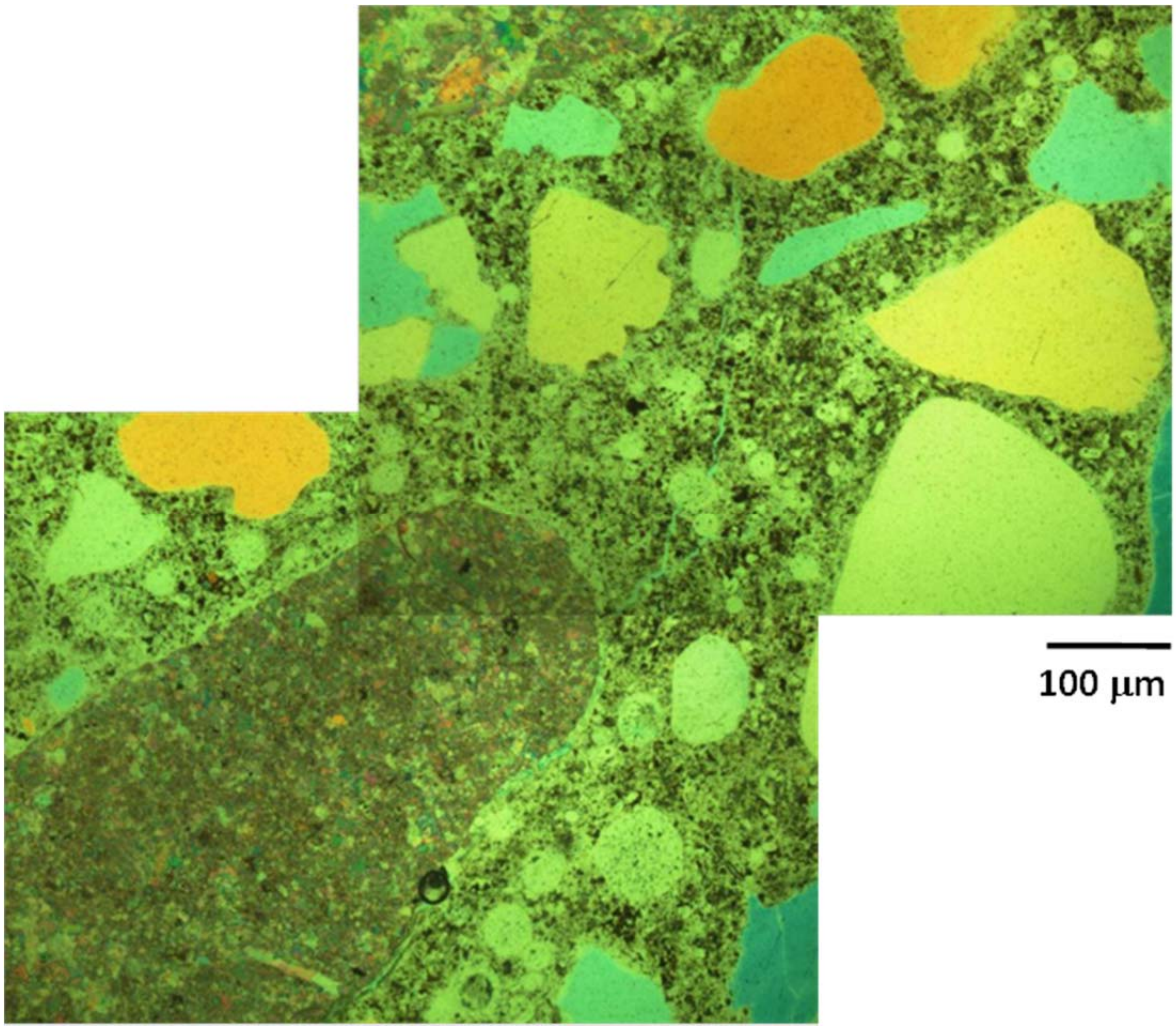

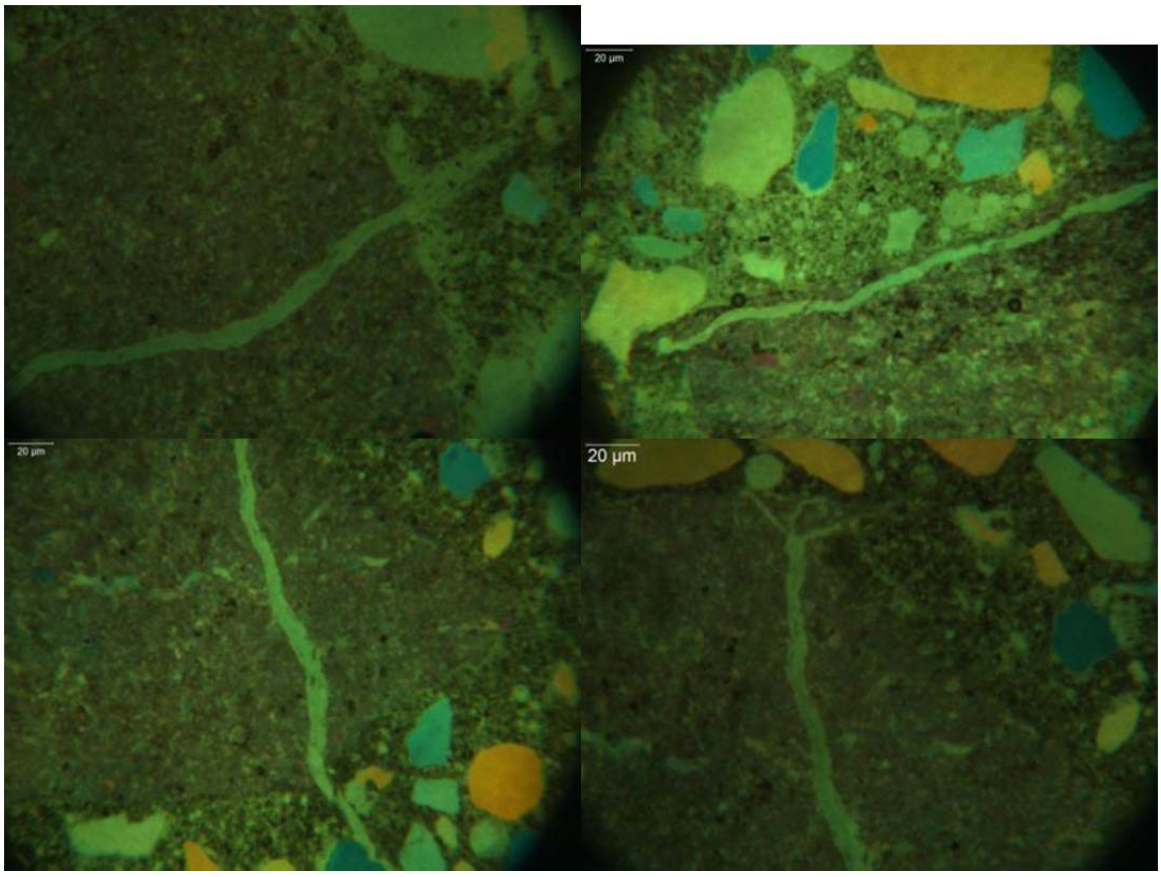
20 µm
20 µm
20 µm

H2

39B

40C

55A

42A

39B-1

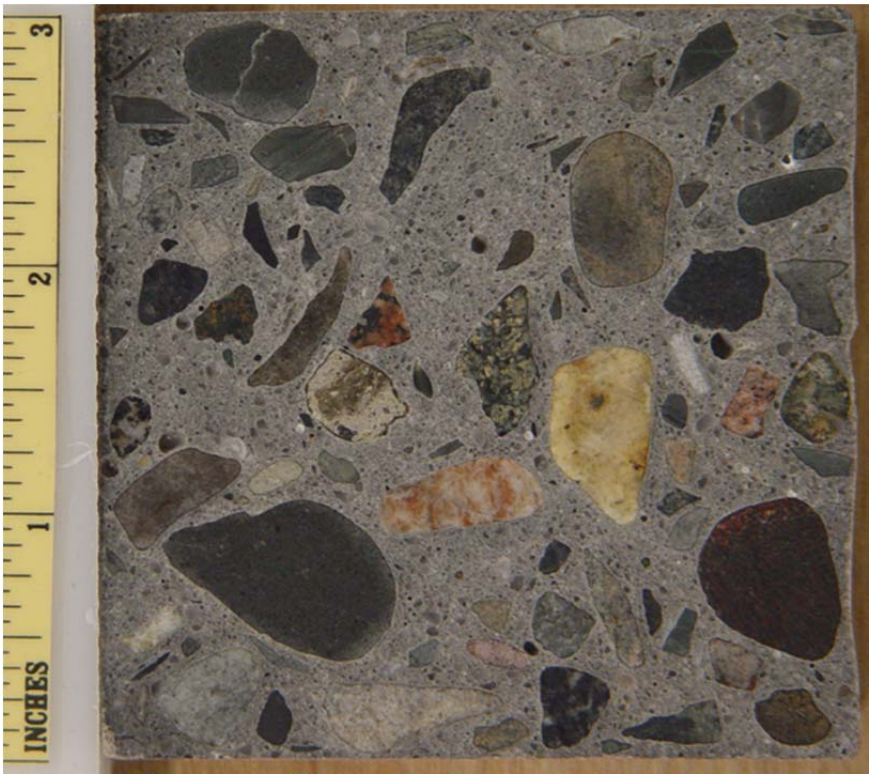

39B-2

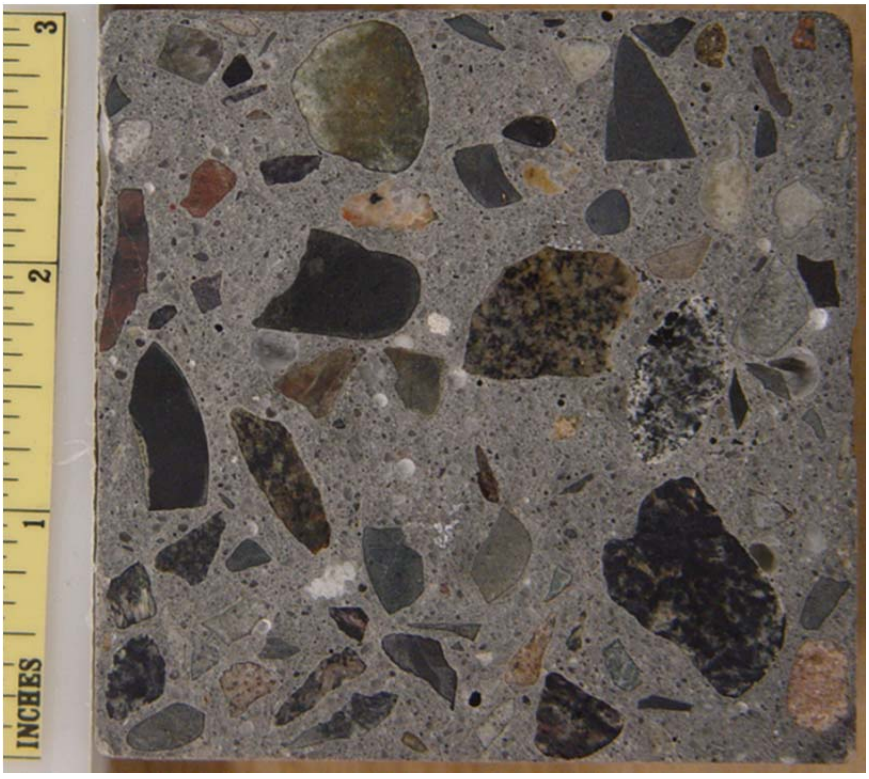

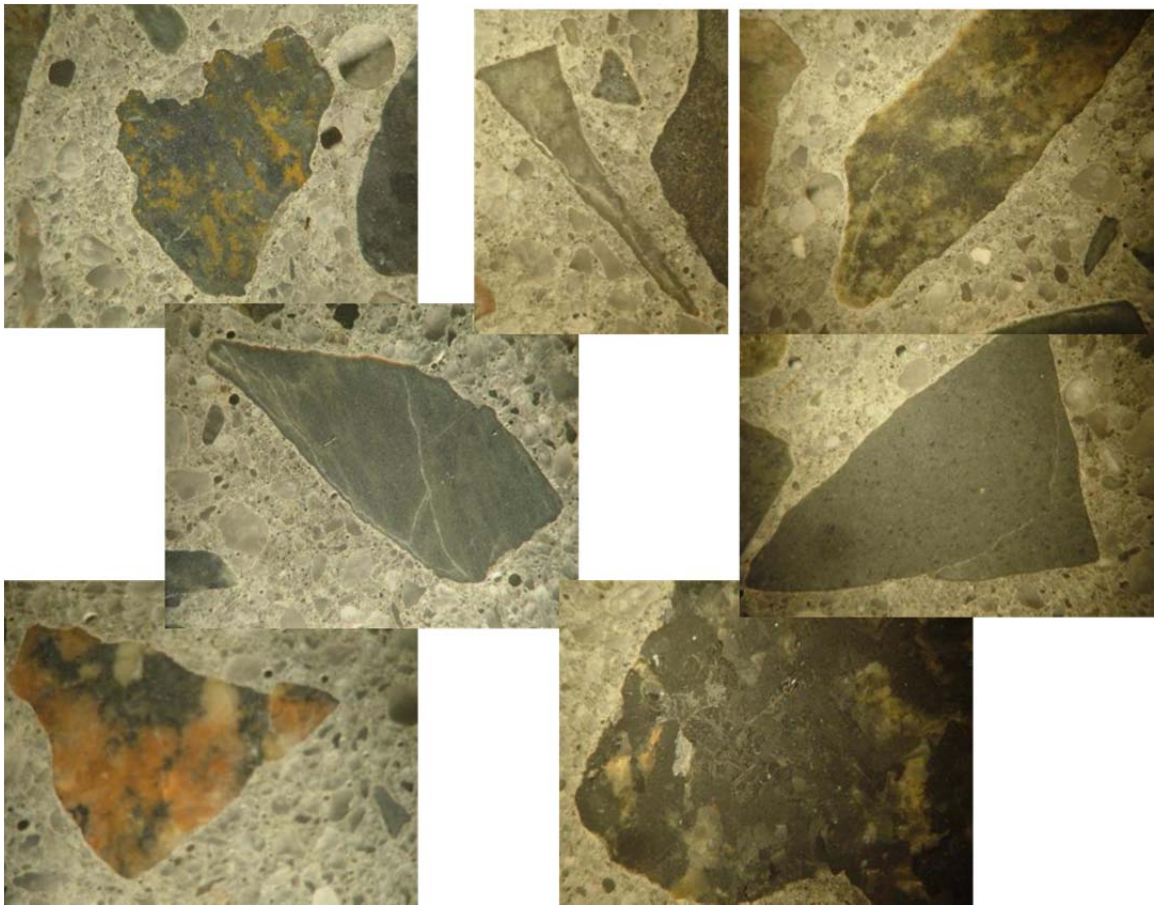

39B-2.1
15%

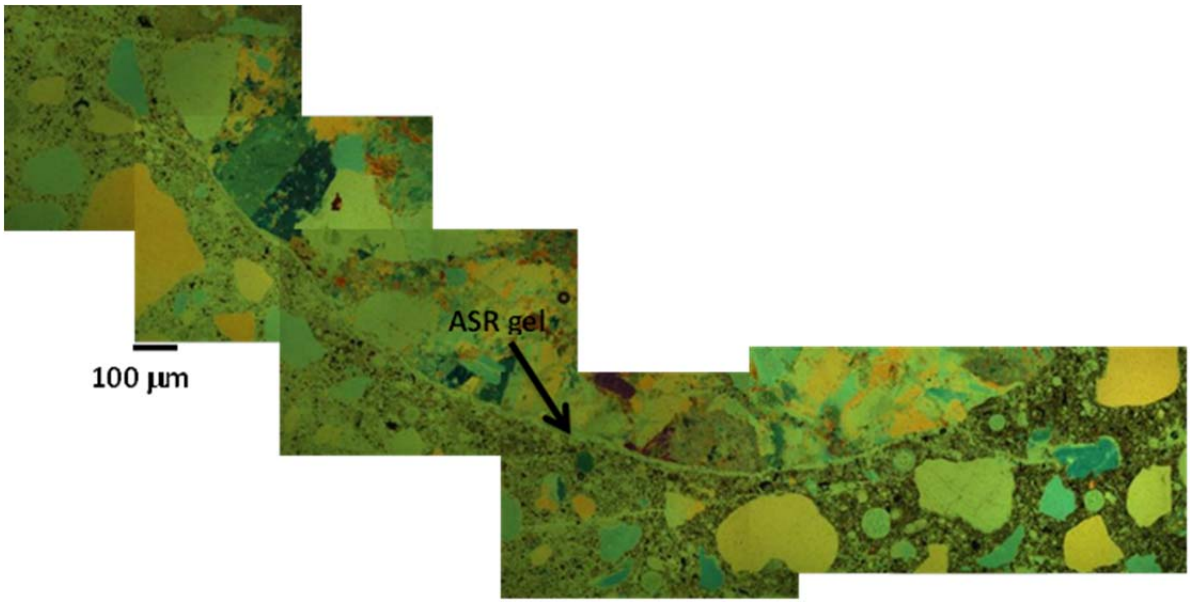

39B-2.4
45%

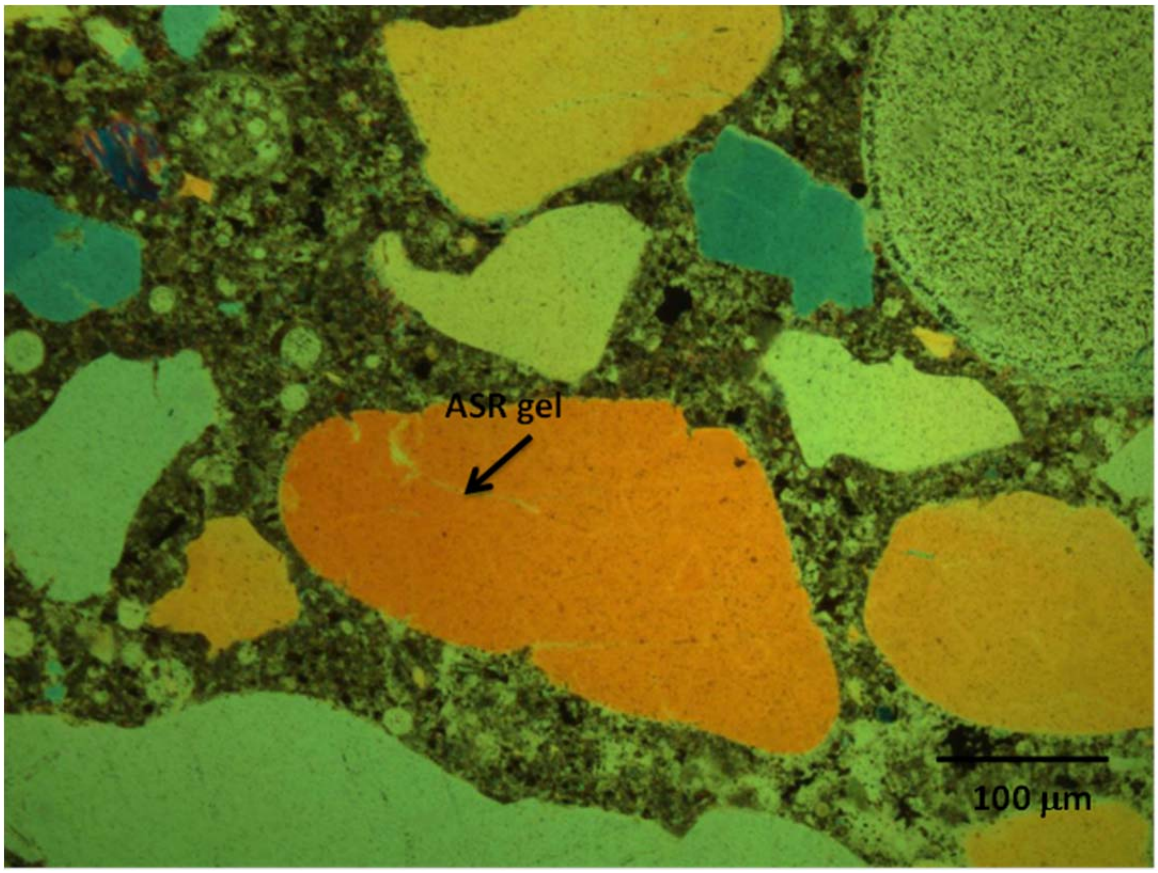

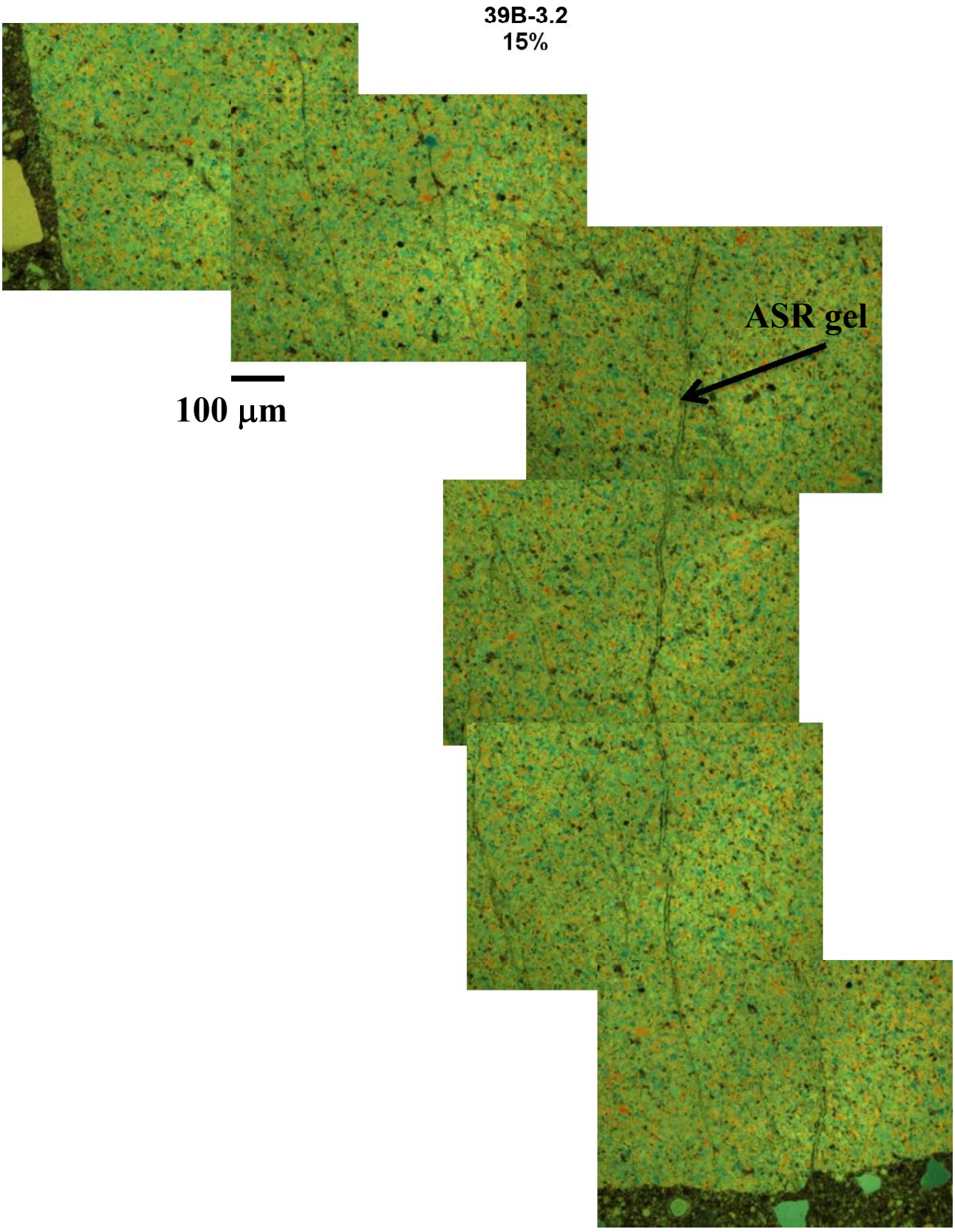
39B-3.2
15%
ASR gel
100 μm

39B-3.4 45%

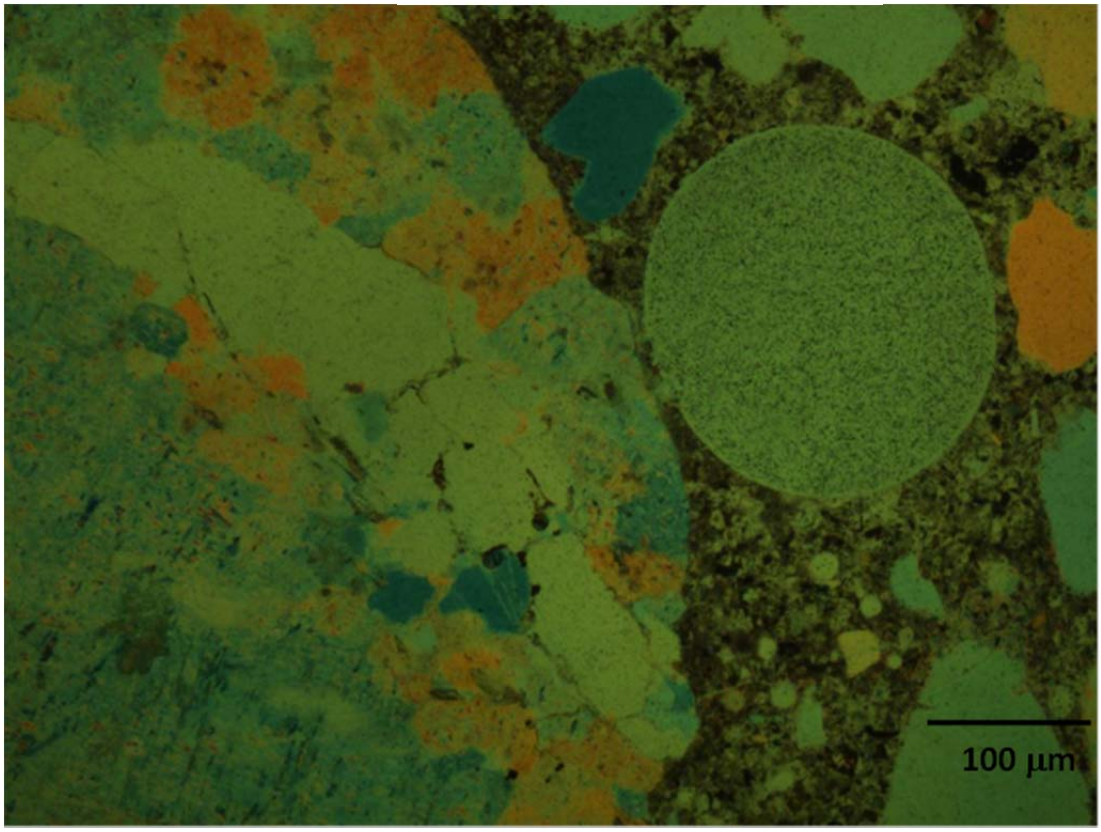

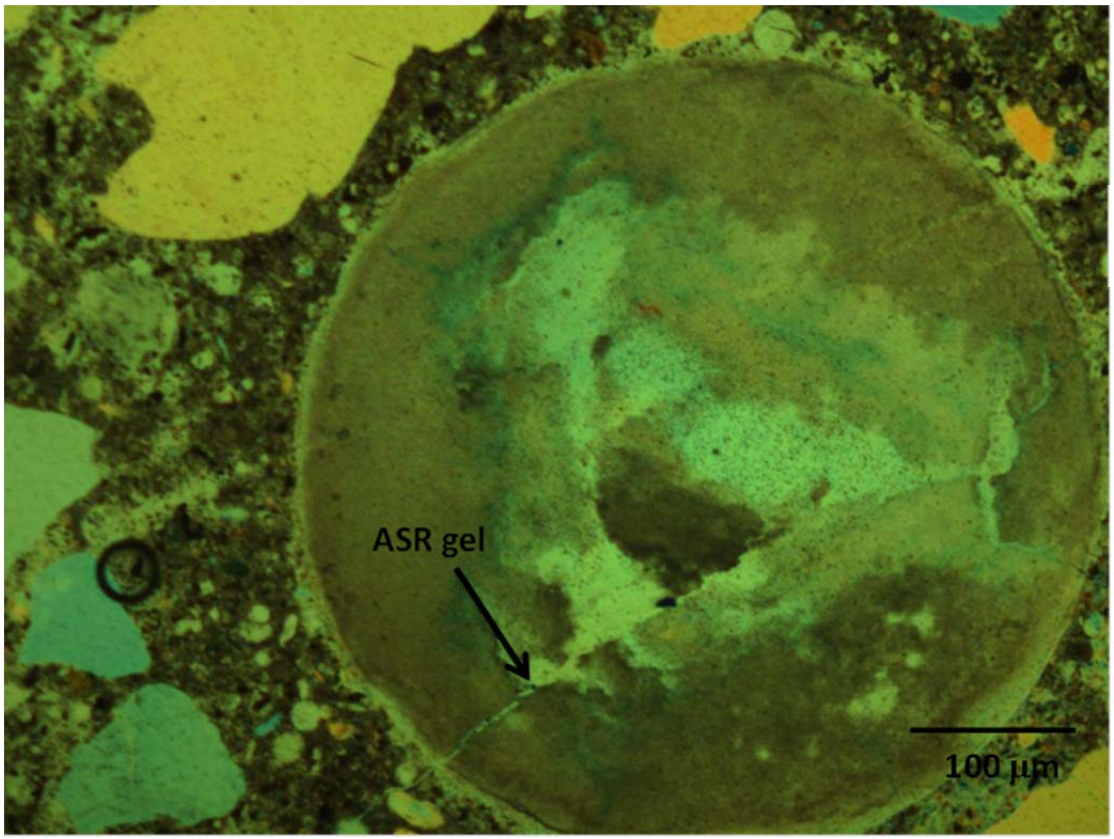

39B-4.2
45%

39B-5.3 45%

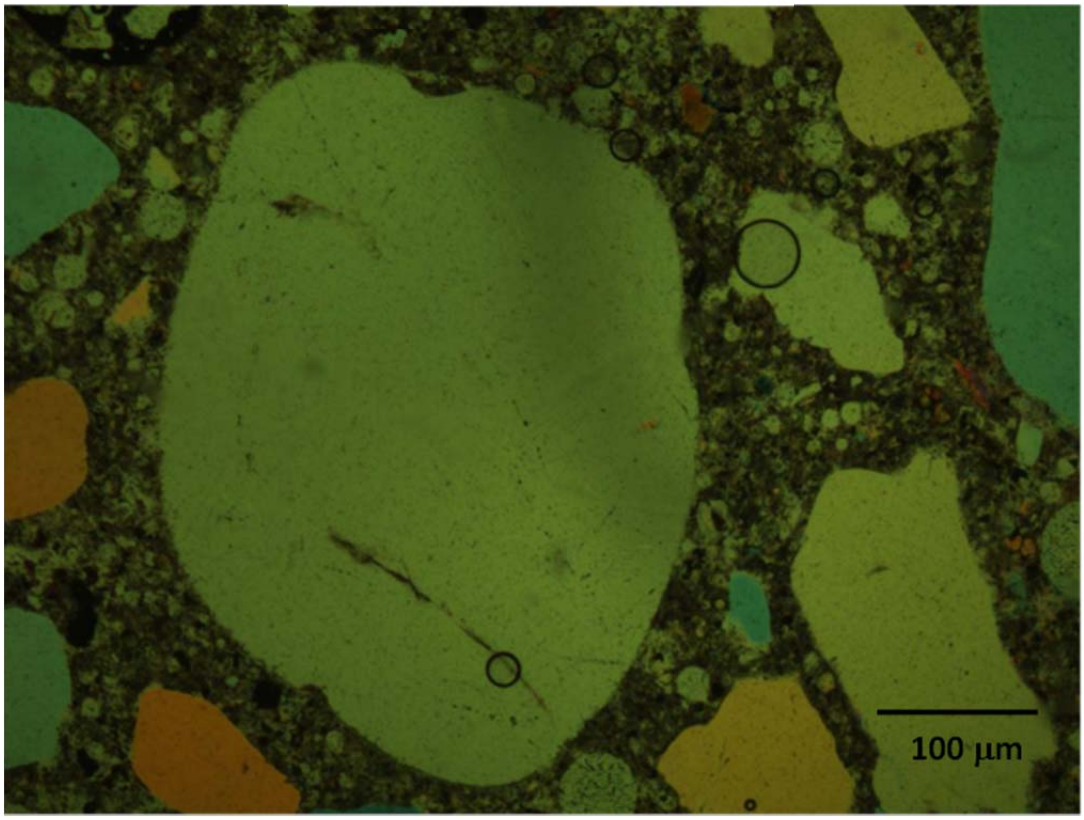

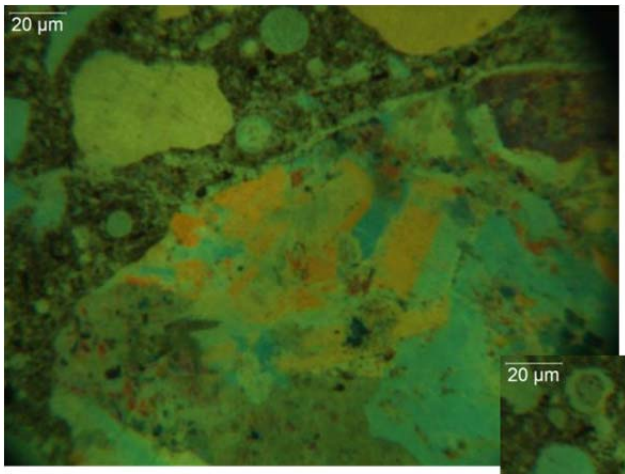

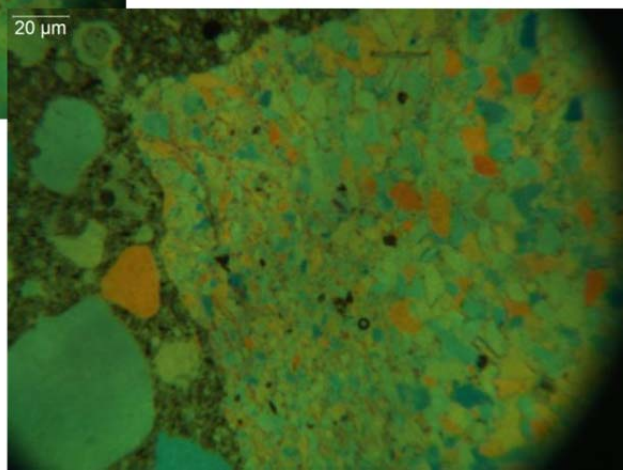

40C-1

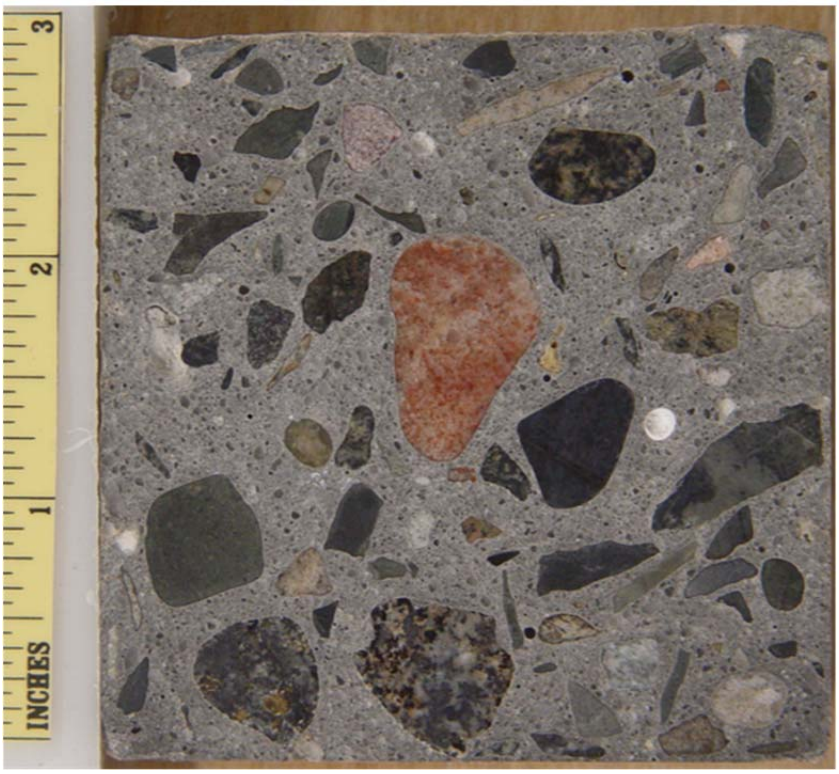

40C-2

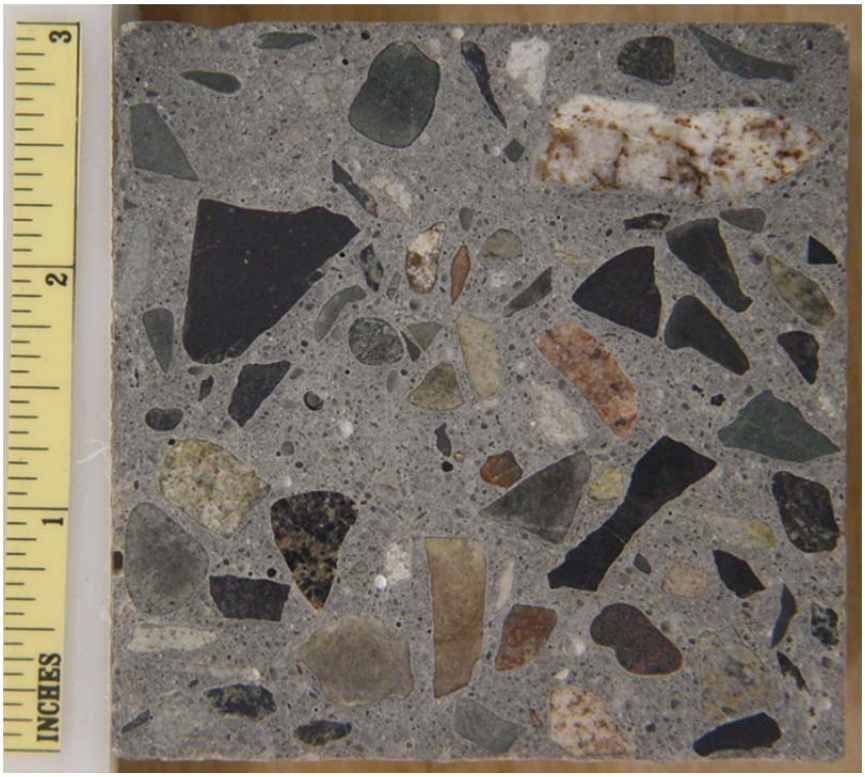

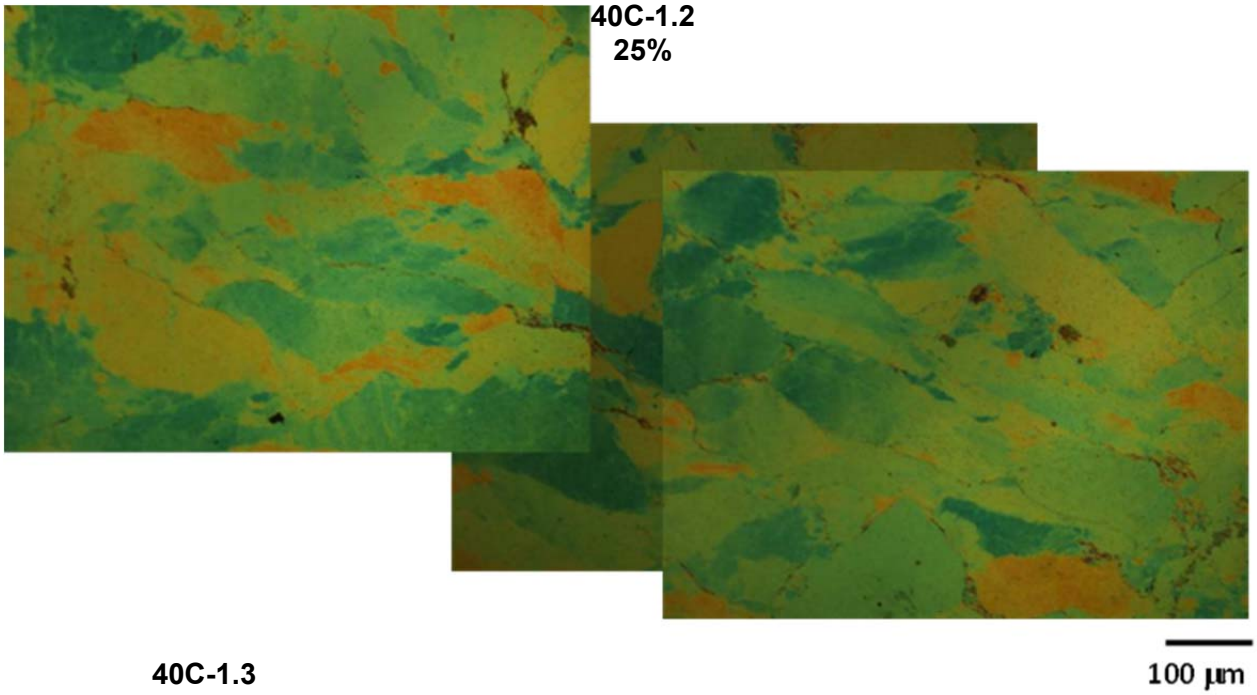
40C-1.2
25%
100 µm

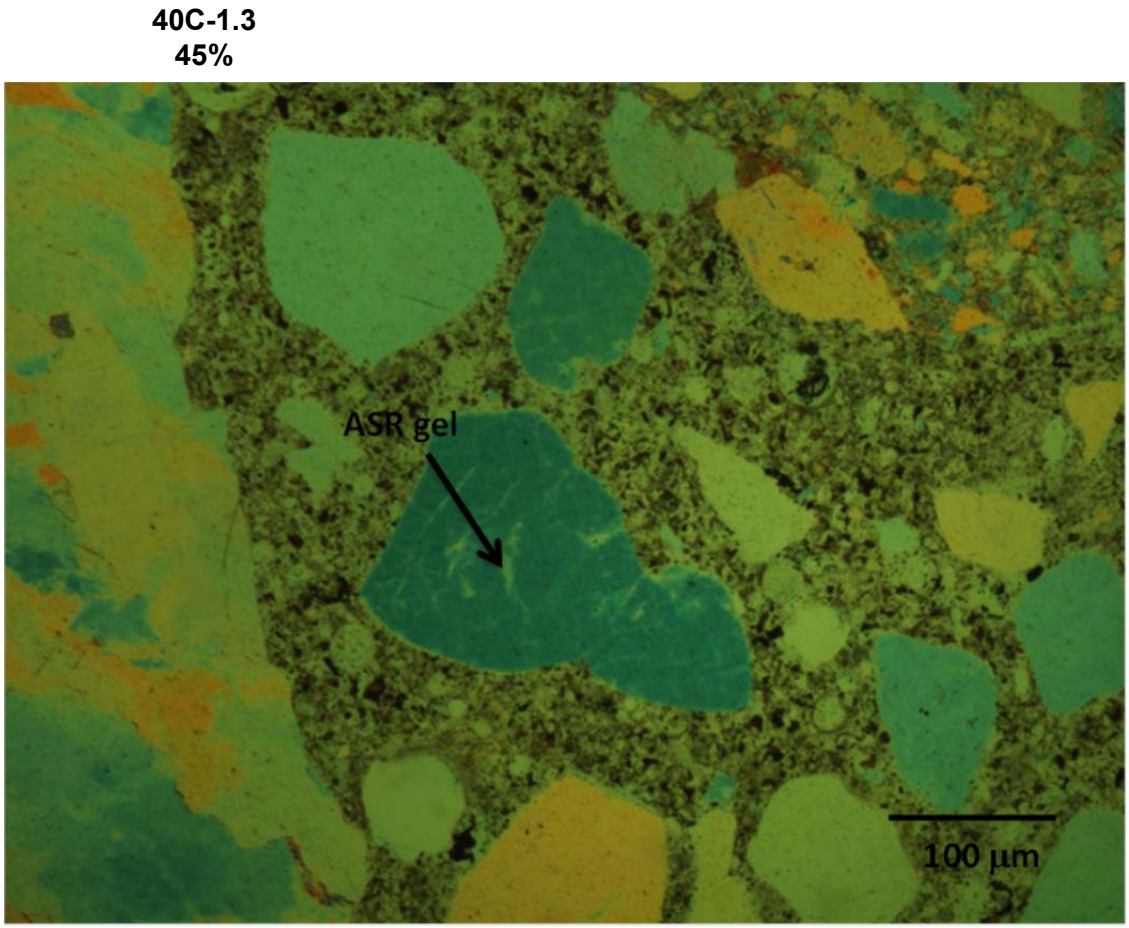
40C-1.3
45%
ASR gel
100 µm

40C-2.1
45%

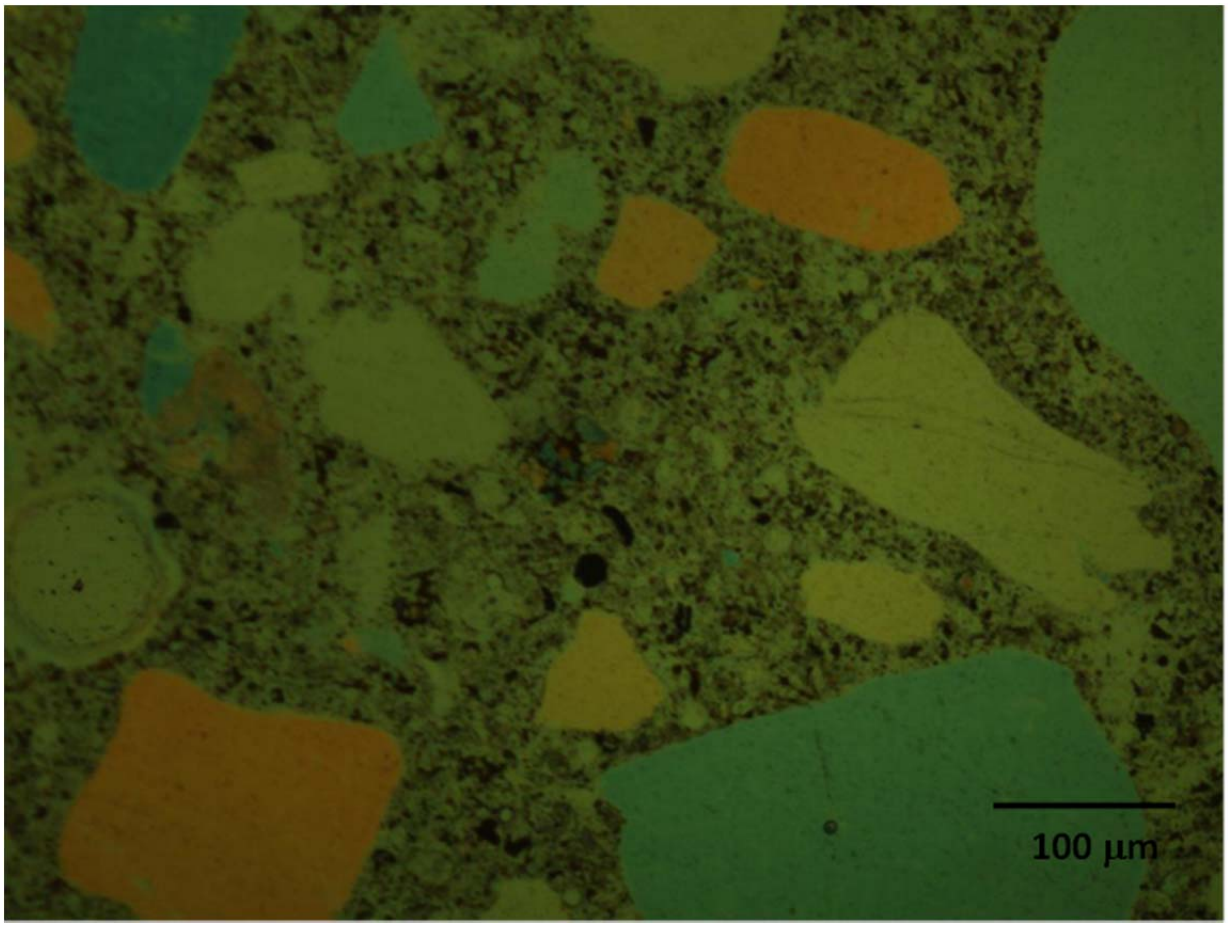

40C-2.3
30%

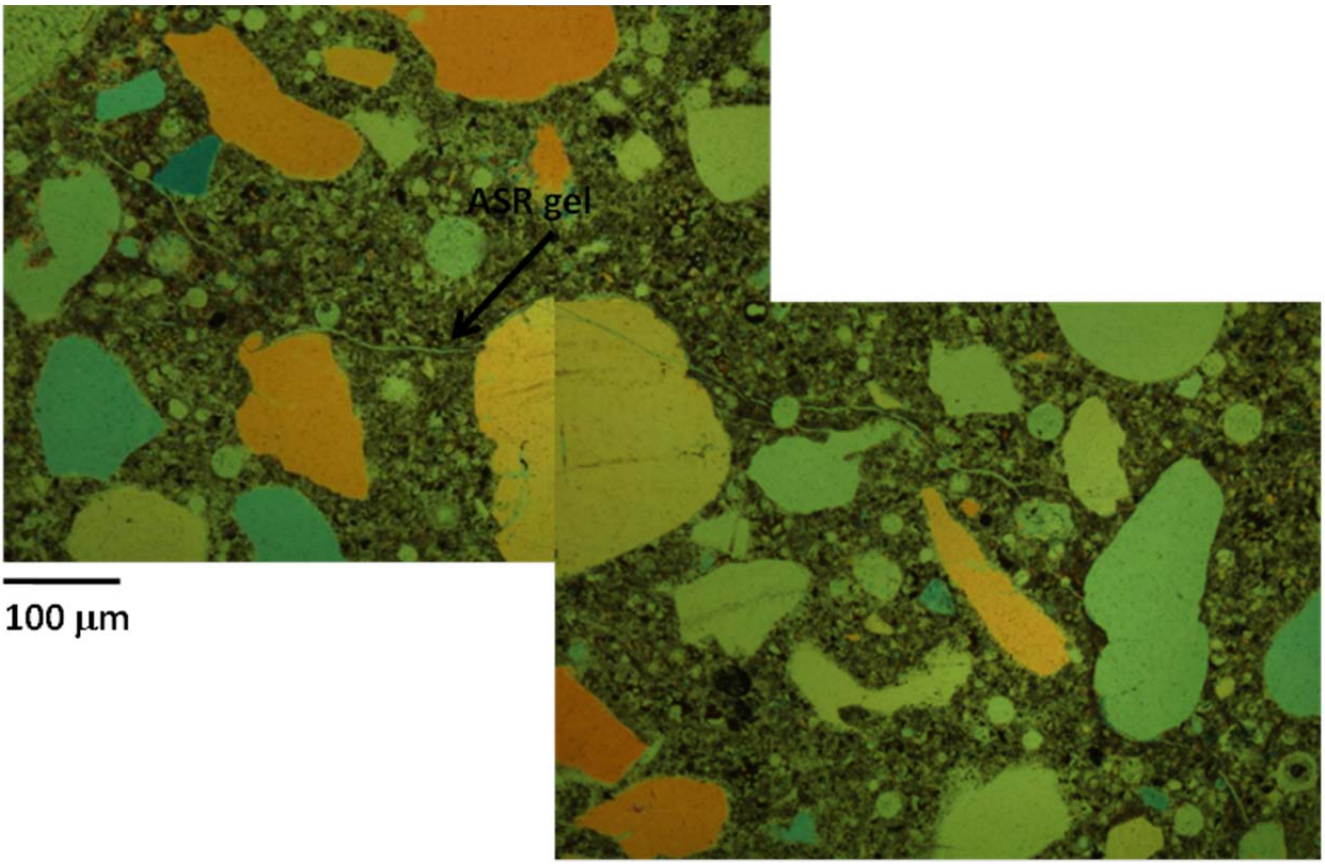

40C-4.1
30%

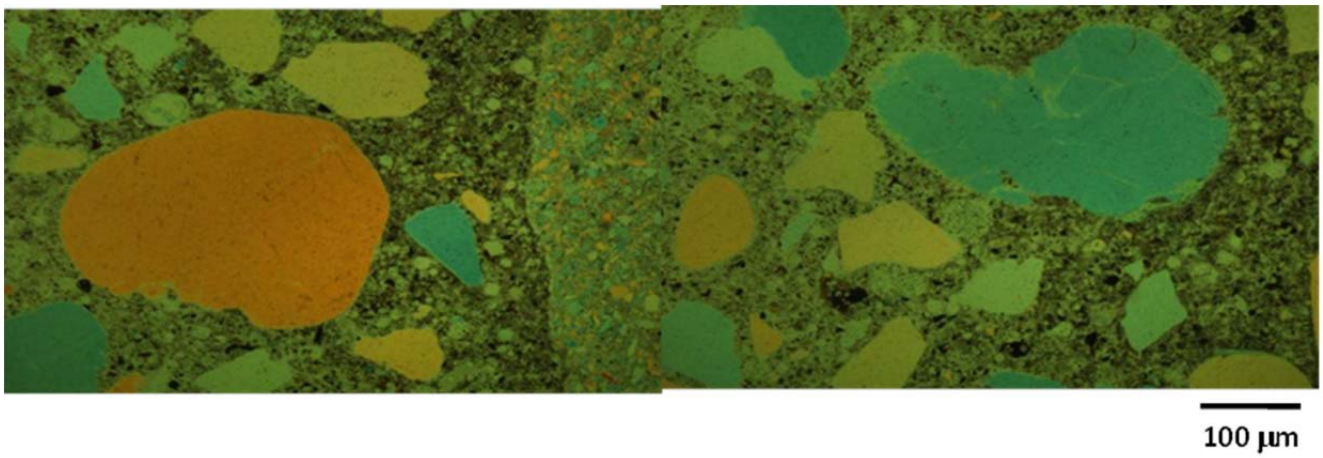

40C-4.3
45%

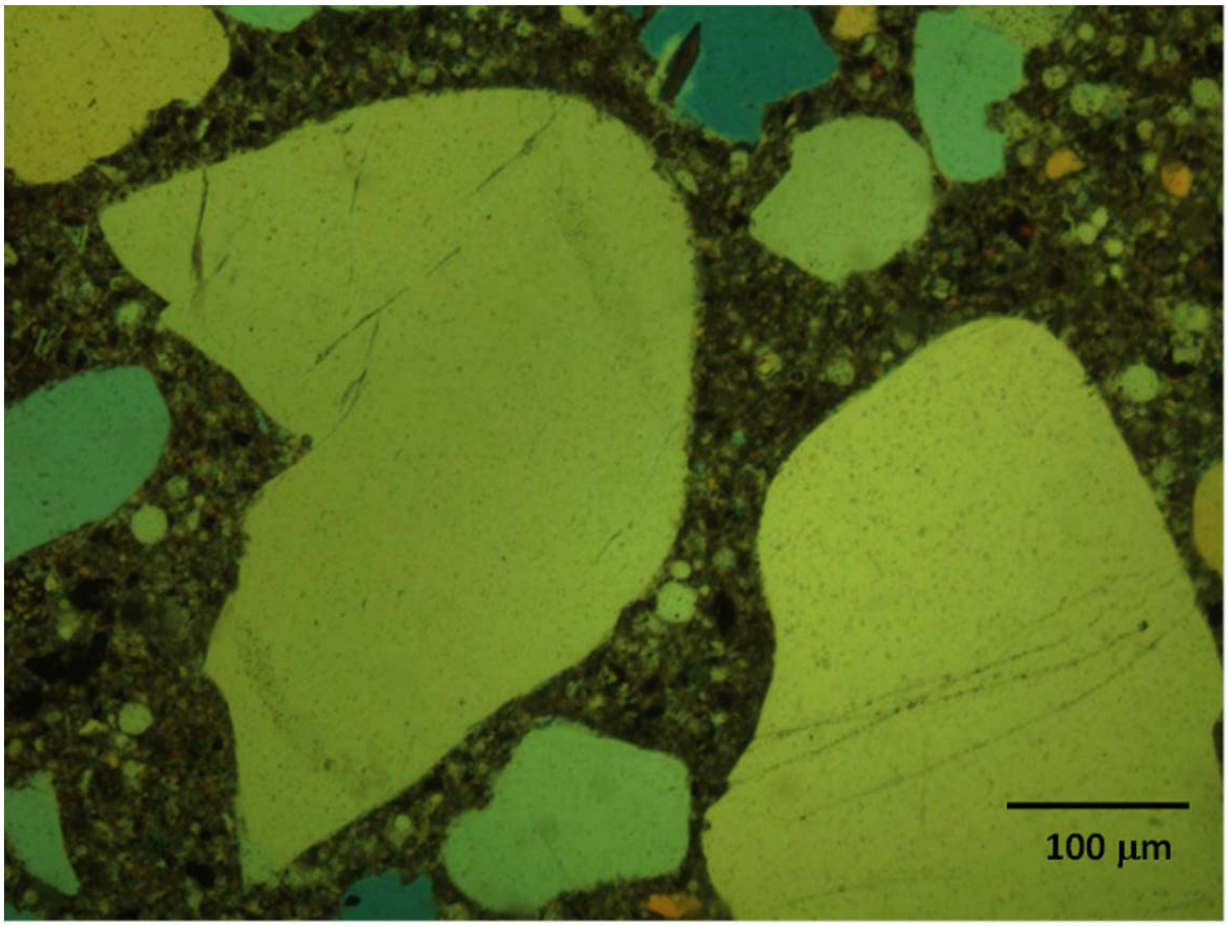

40C-4.4
45%

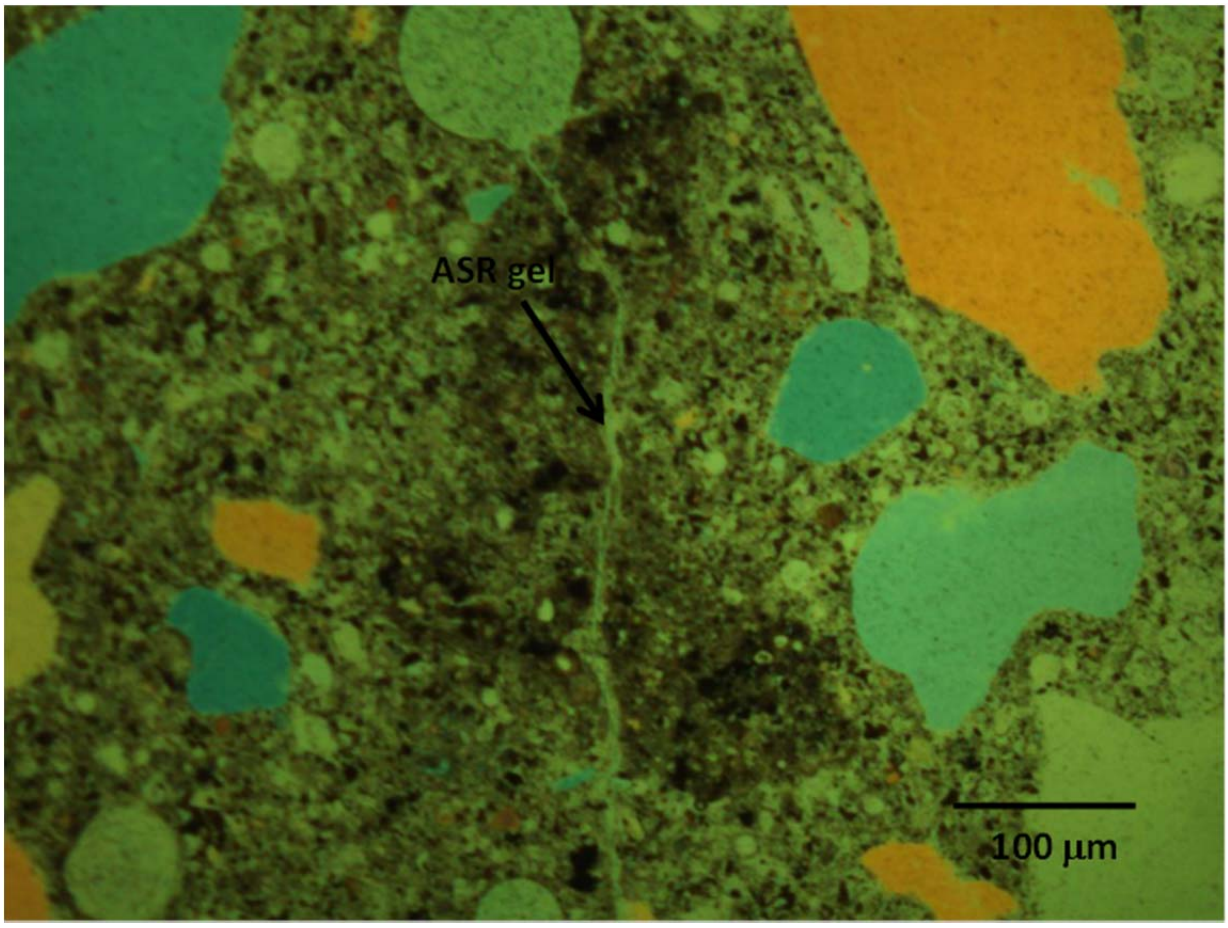

42A-1

42A-2

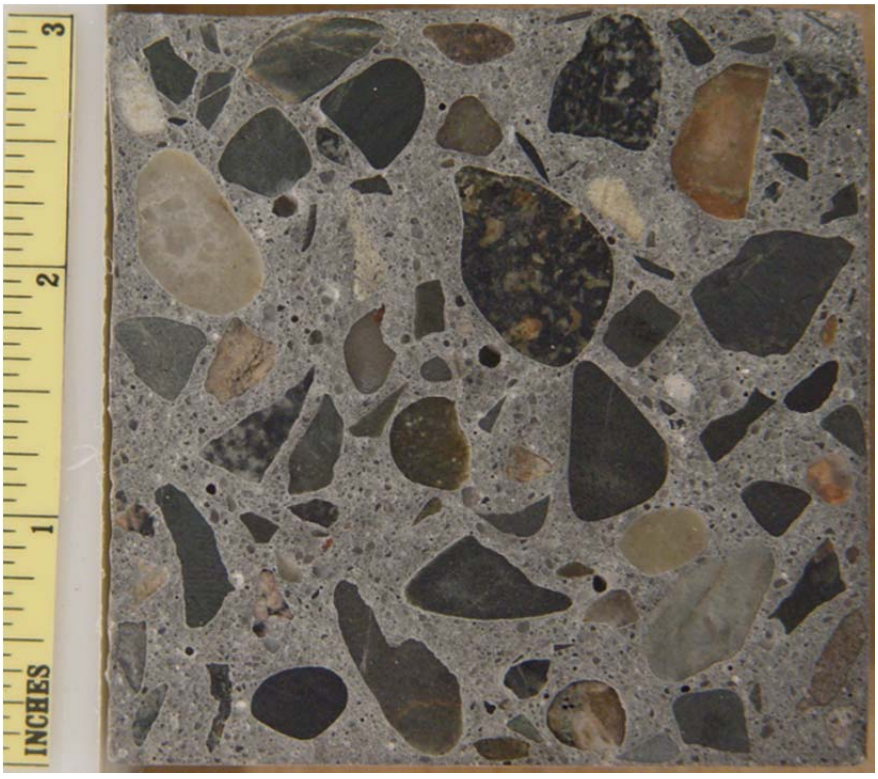

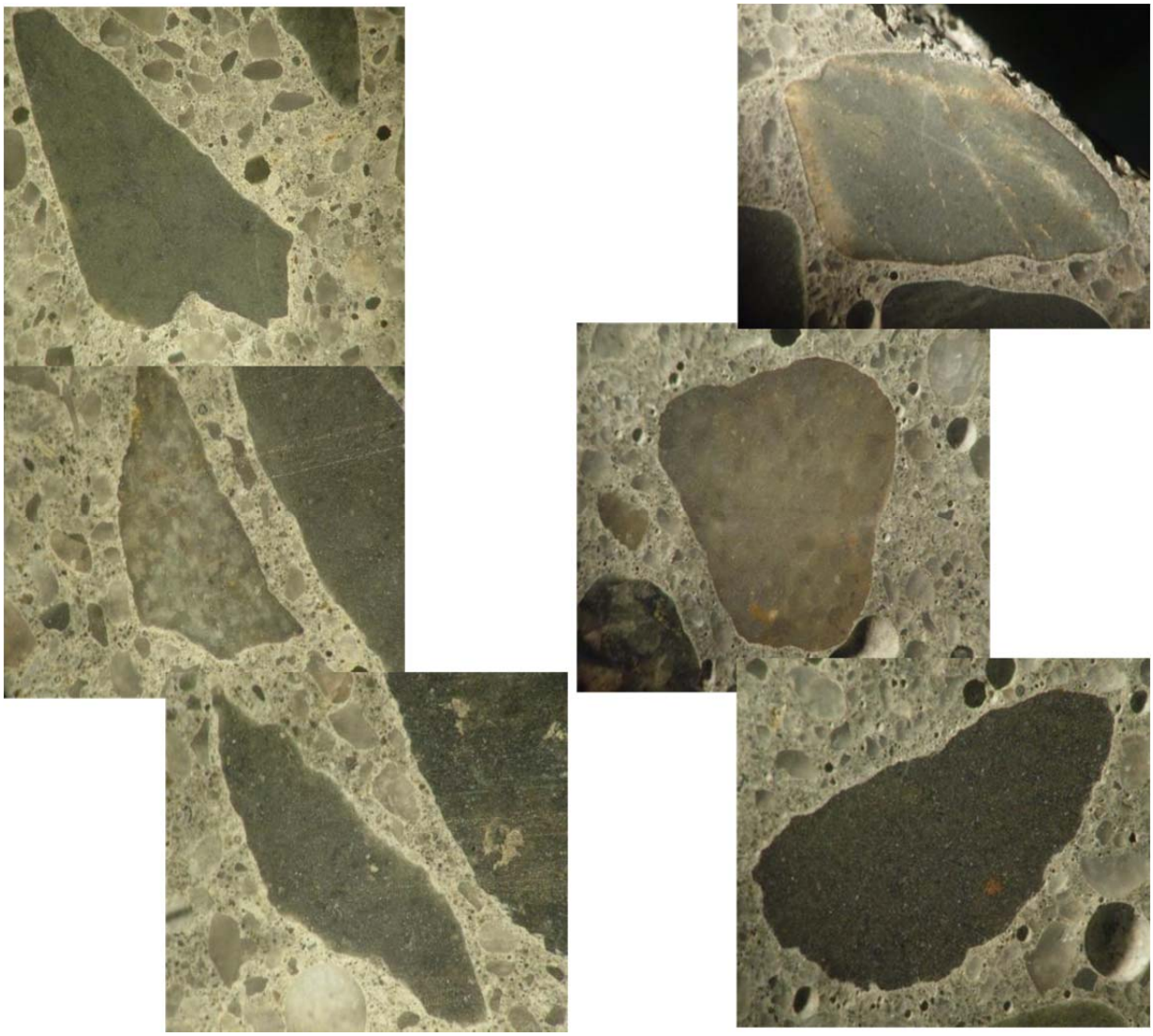

42A-3.2
25%

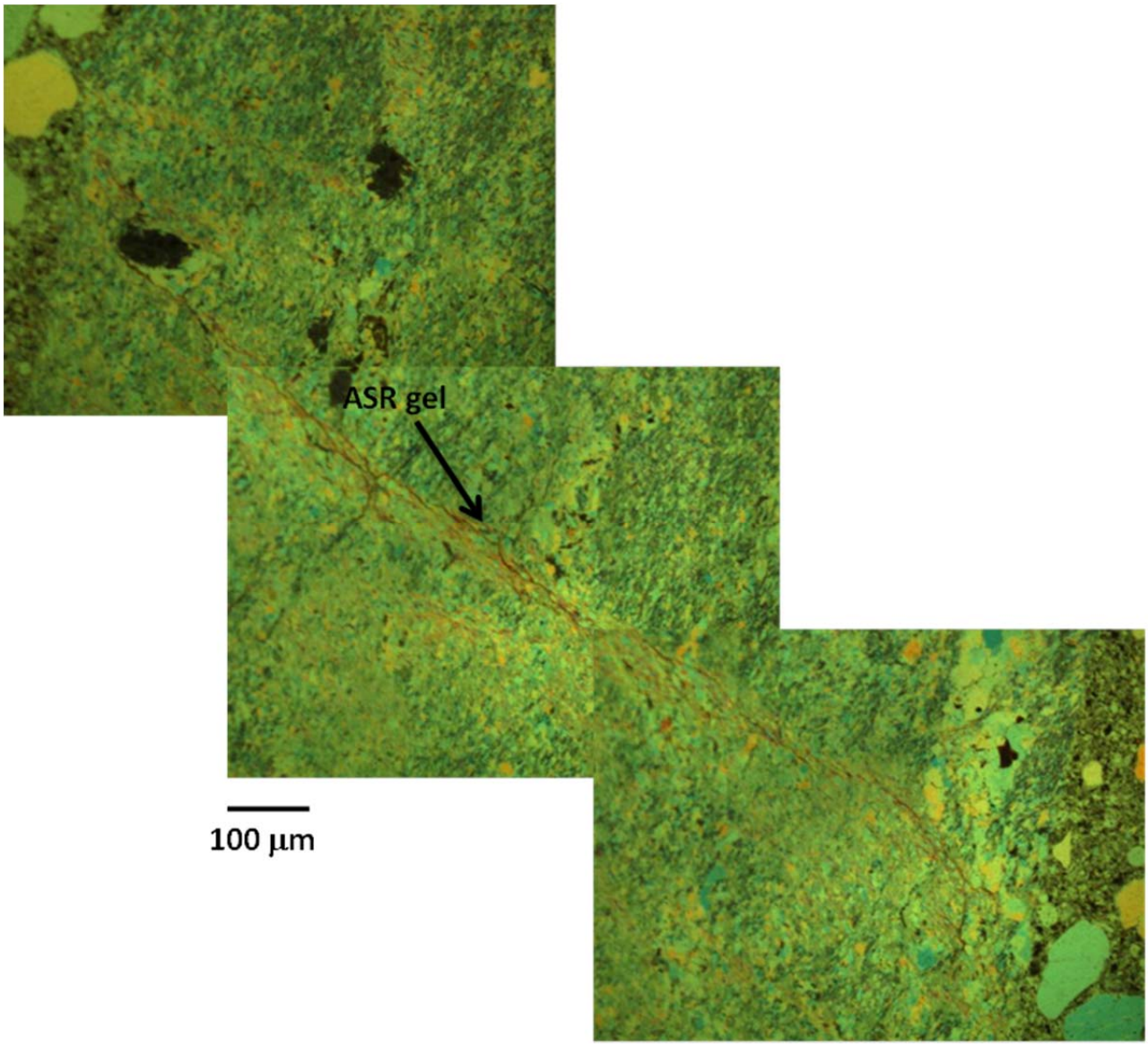

42A-4.3
45%

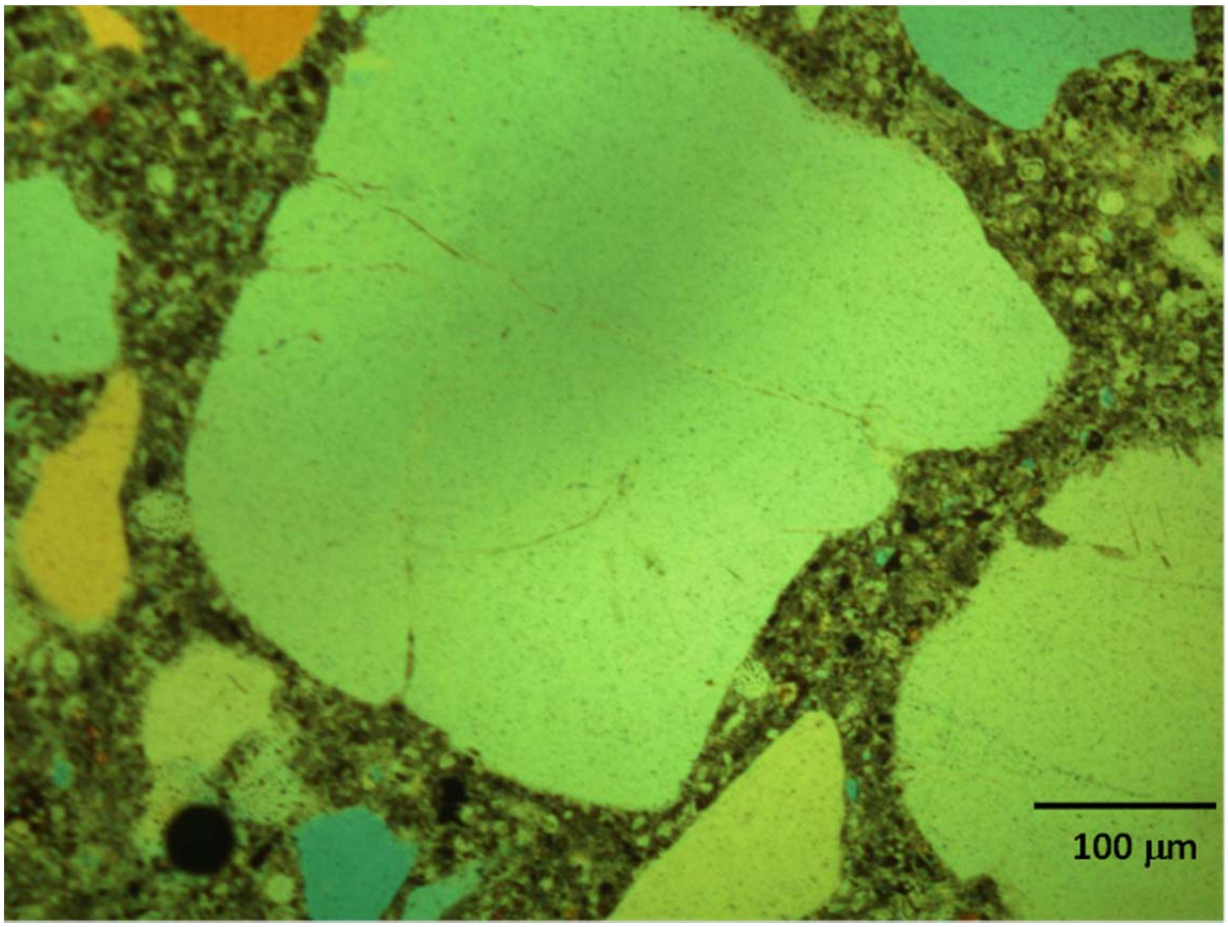

42A-5.4
45%

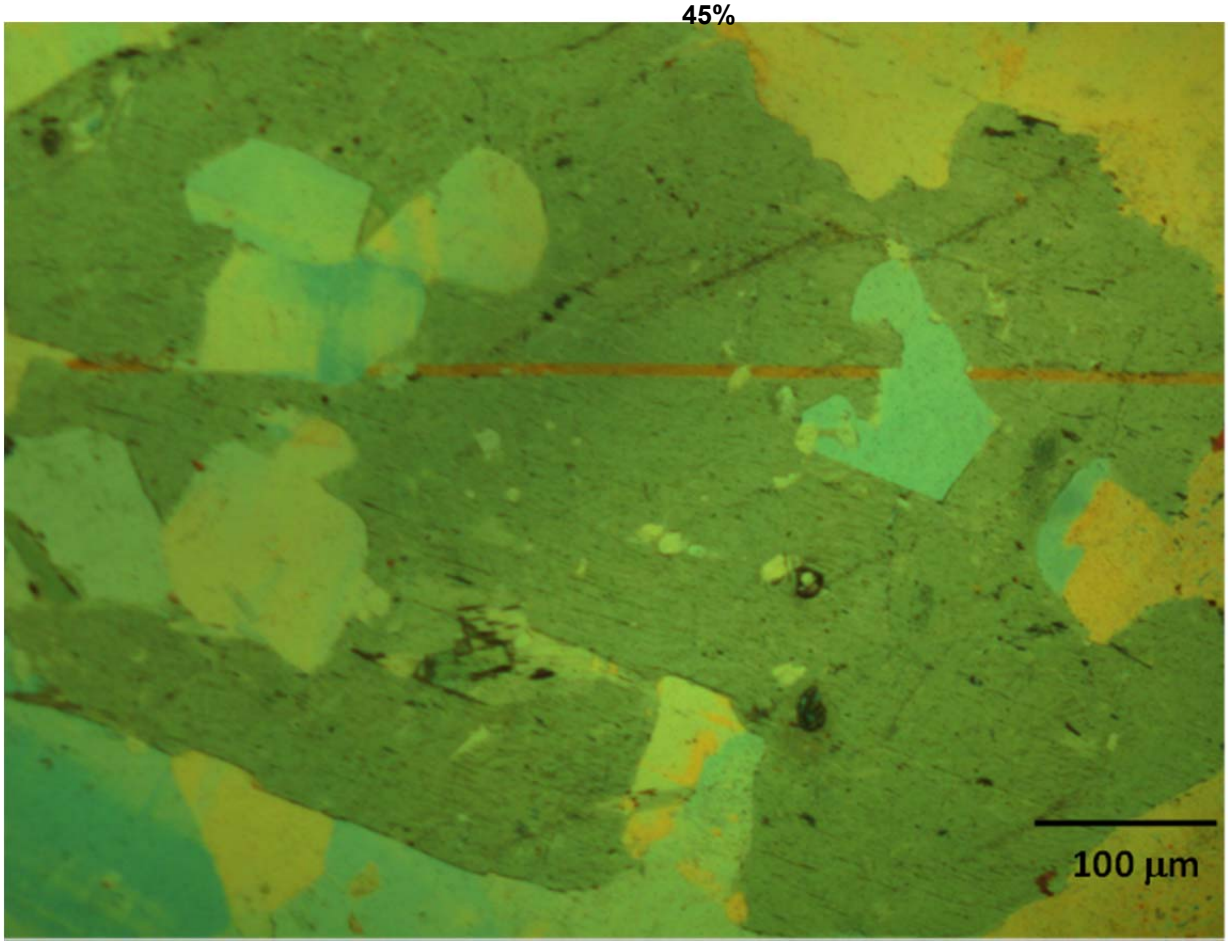

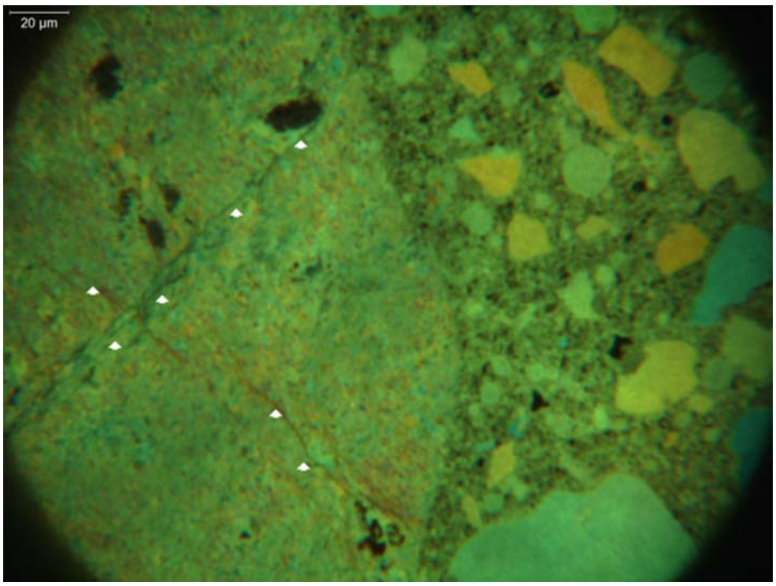
20 µm

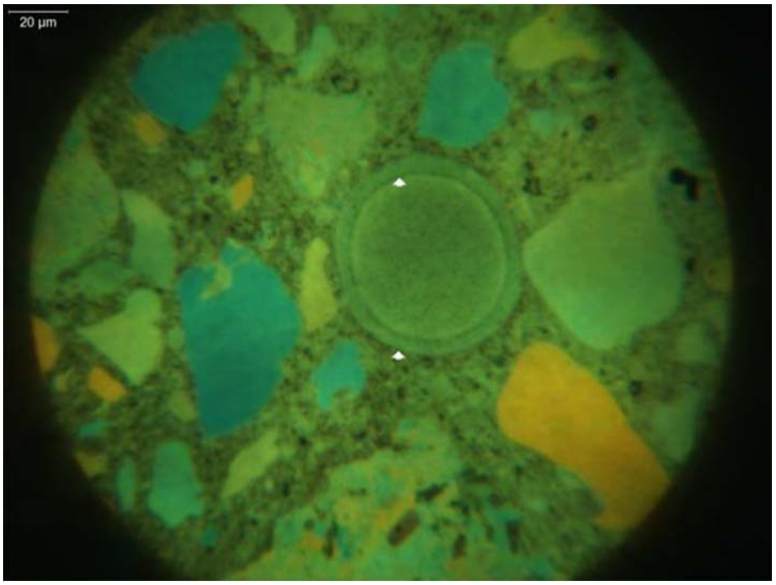
20 µm

55A-1

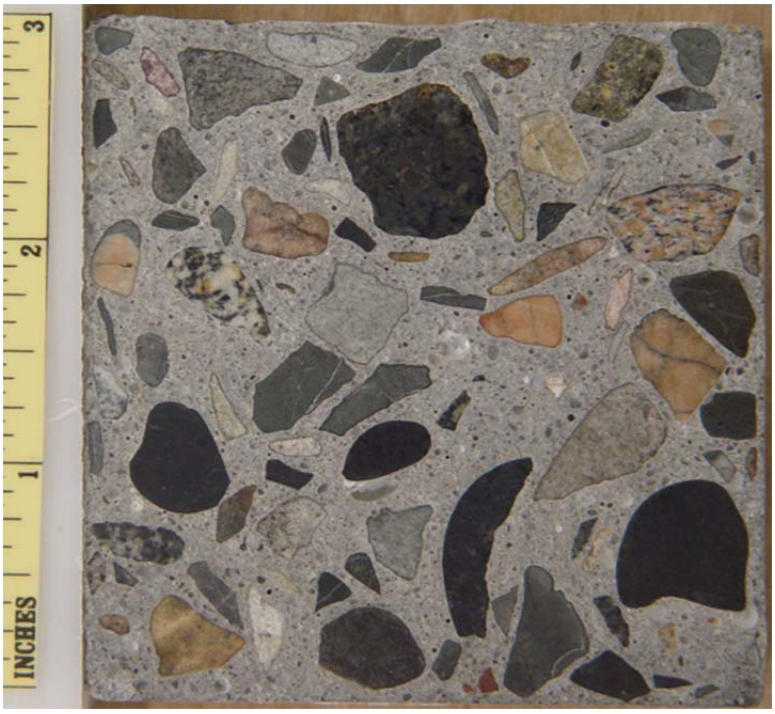

55A-2

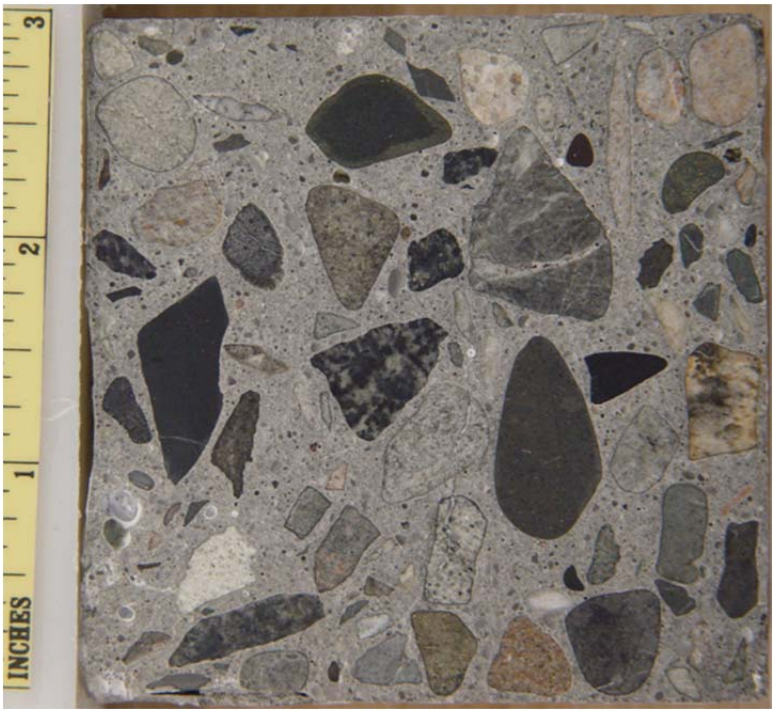

55A-2.2
20%

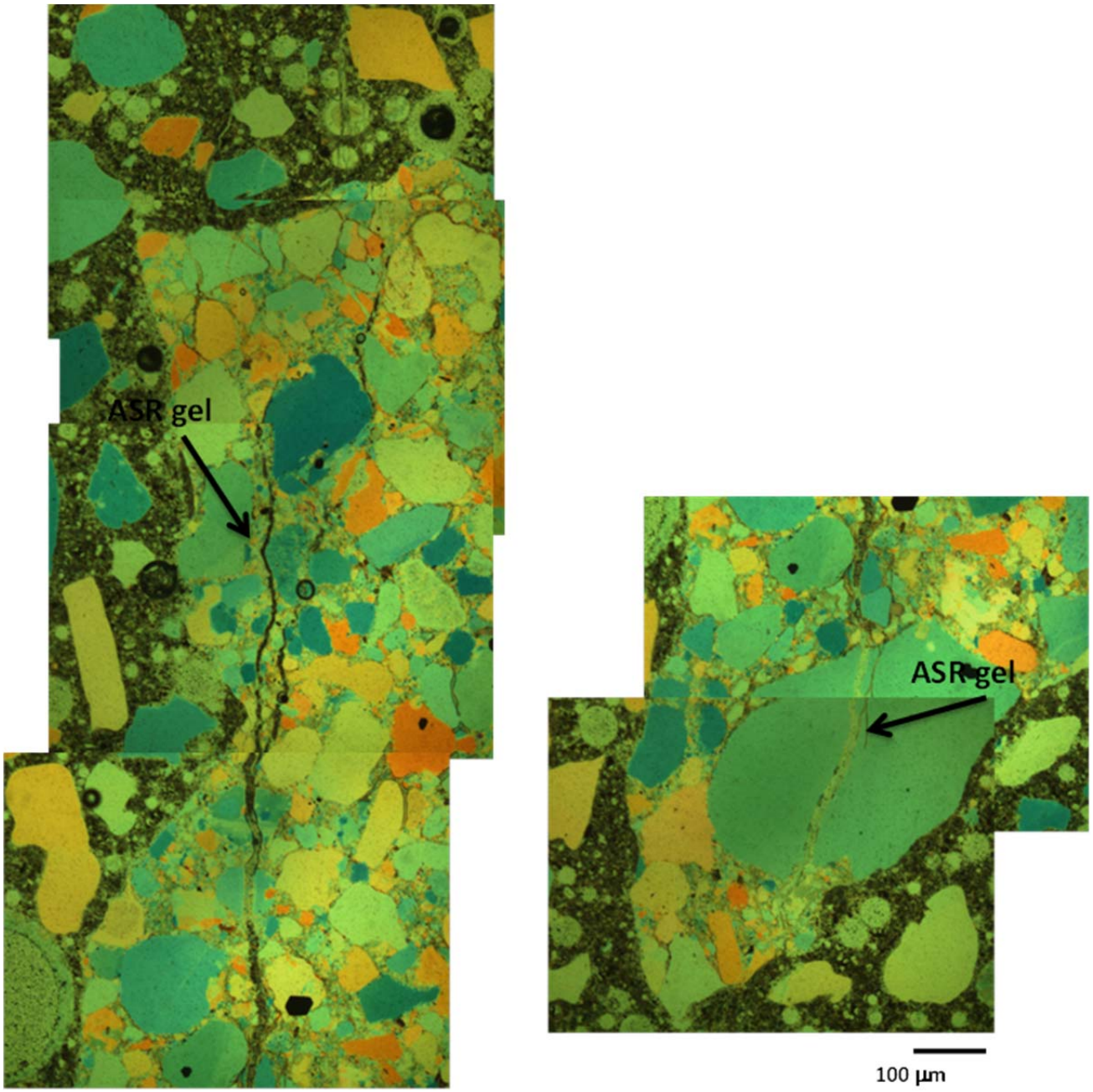

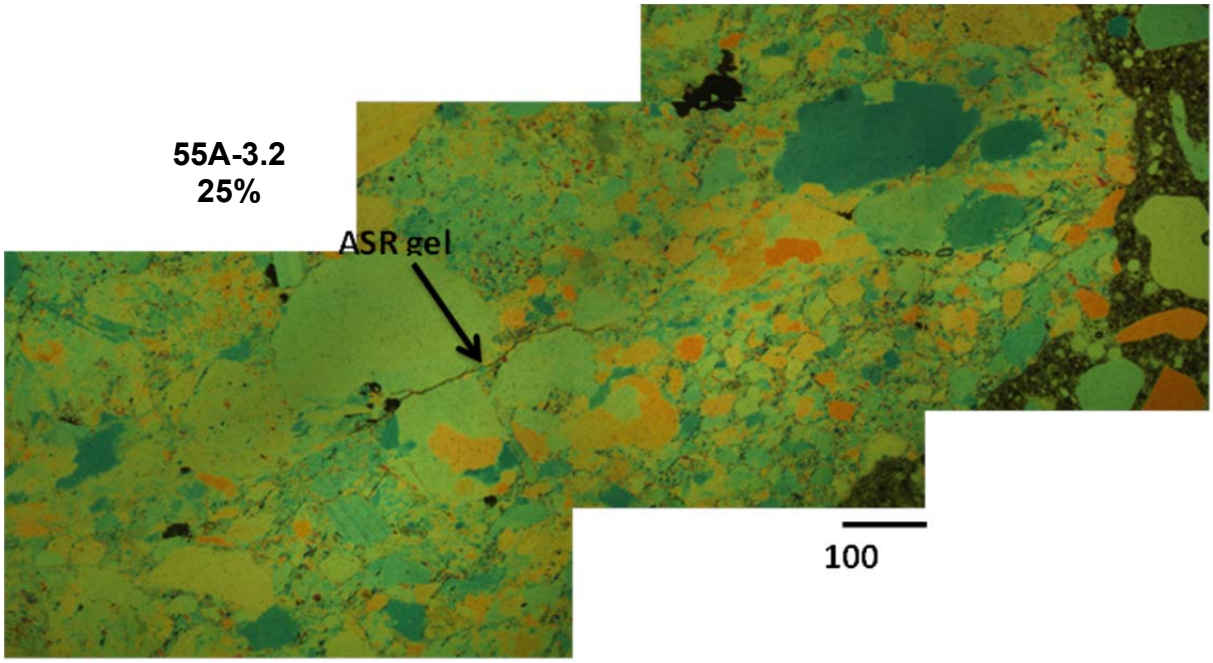
55A-3.2
25%
ASR gel
100

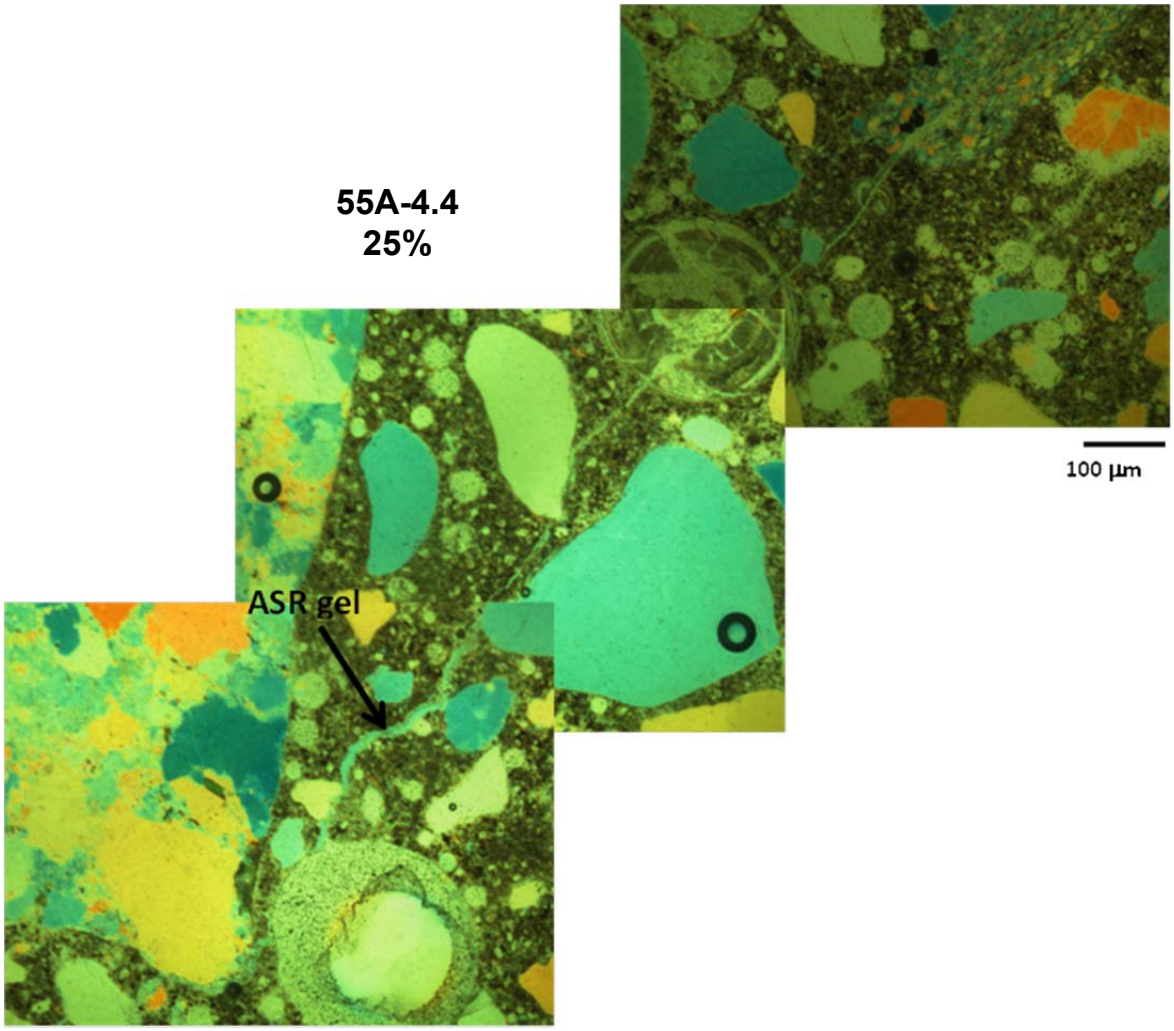
55A-4.4
25%
ASR gel
100 µm

55A-5.3
20%

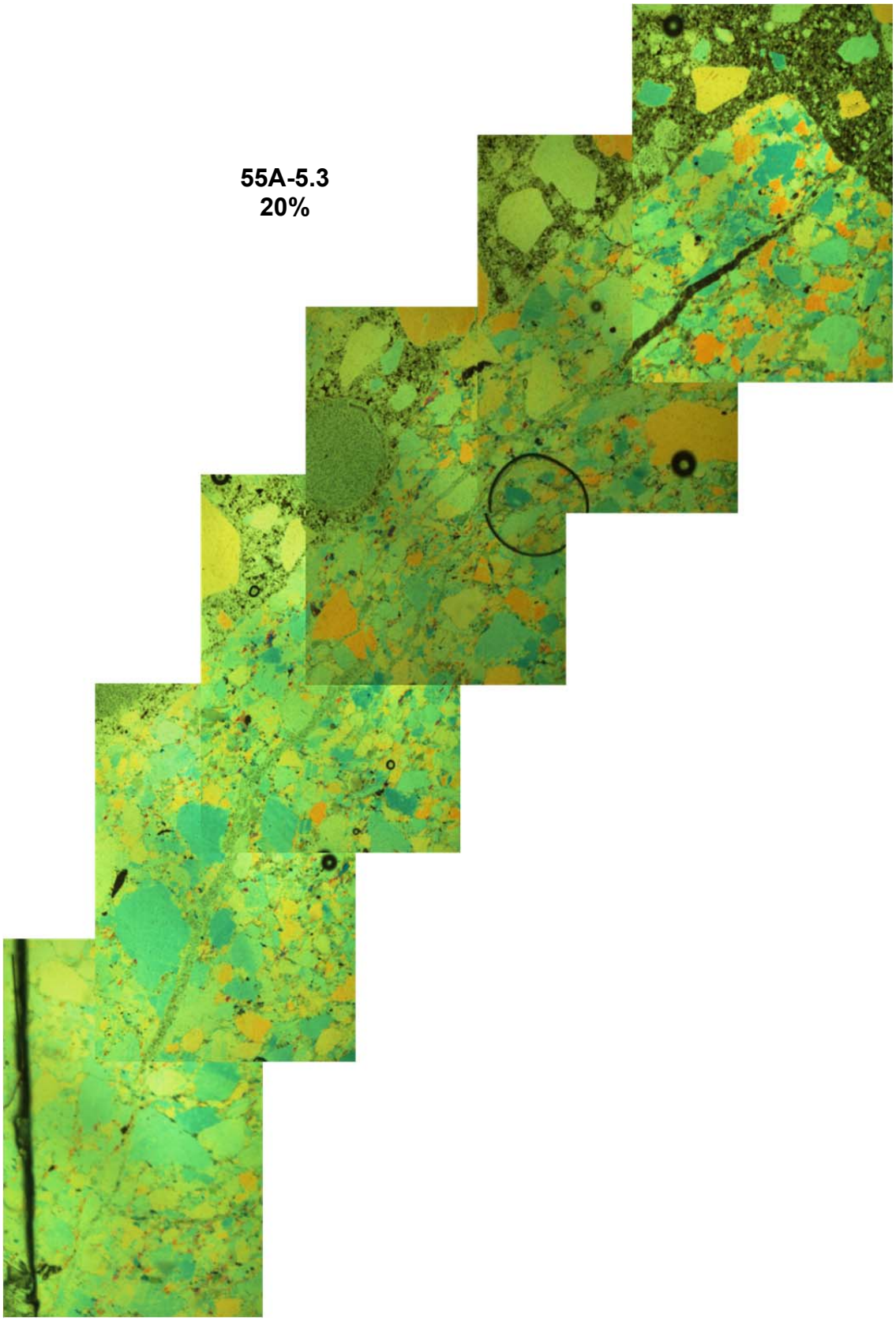

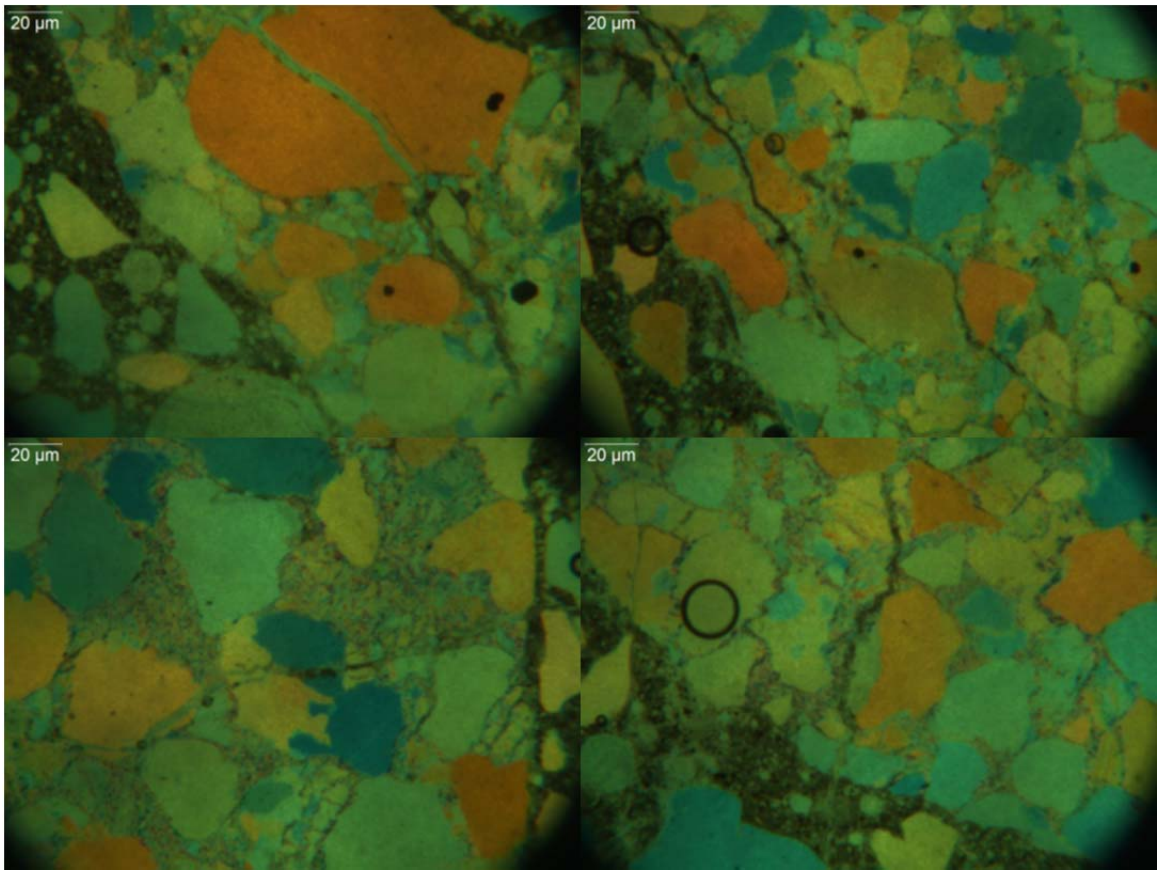
20 µm
20 µm
20 µm
20 µm

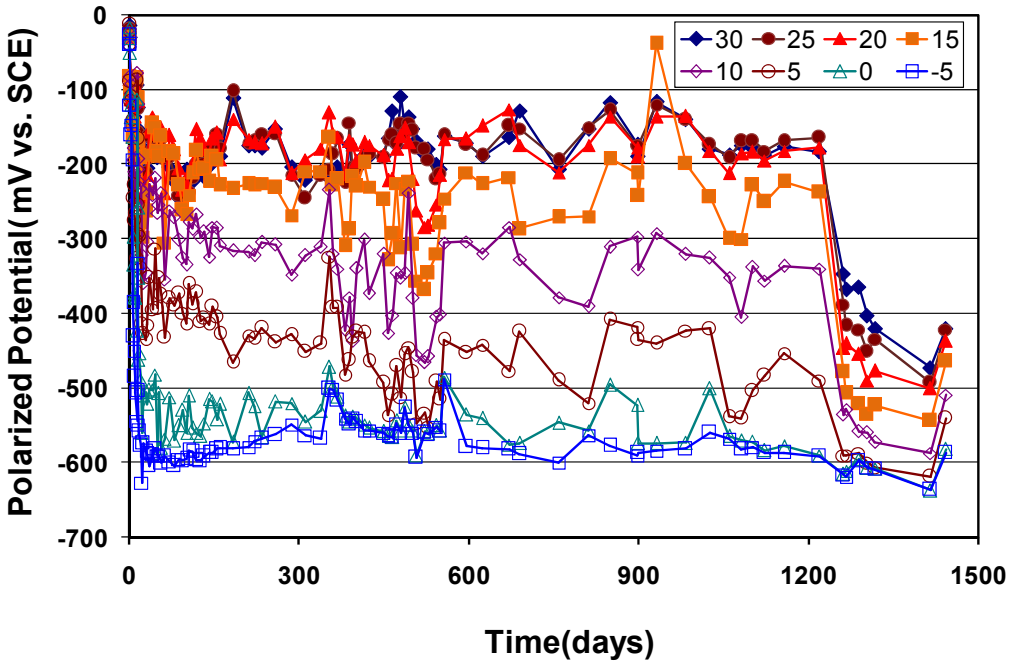

(a) Polarized potentials of left rebar in specimen M2 at eight (8) levels

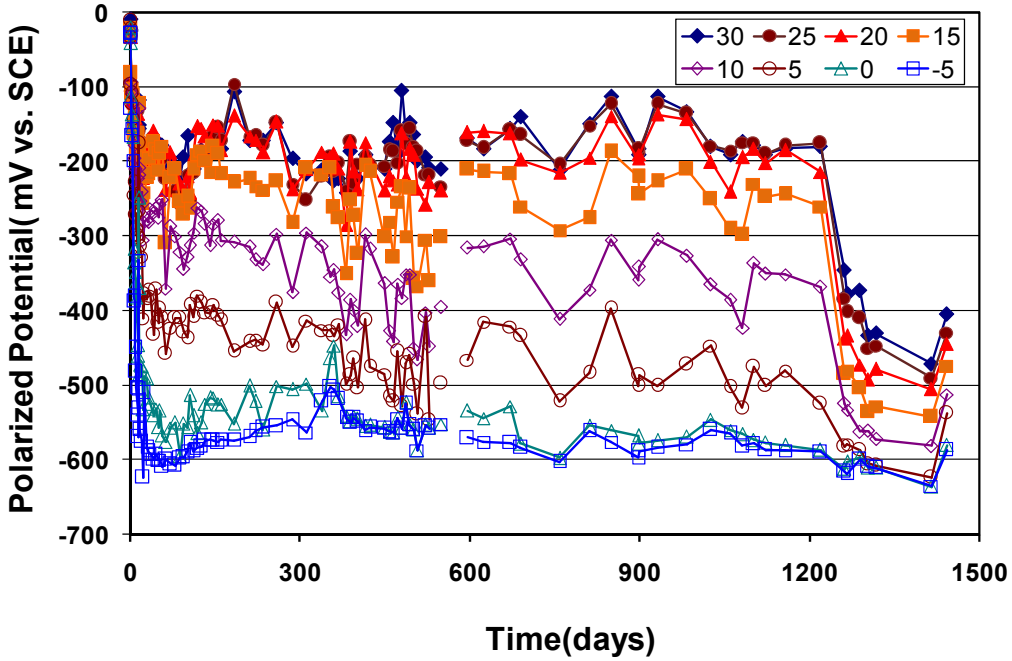

(b) Polarized potentials of right rebar in specimen M2 at eight (8) levels

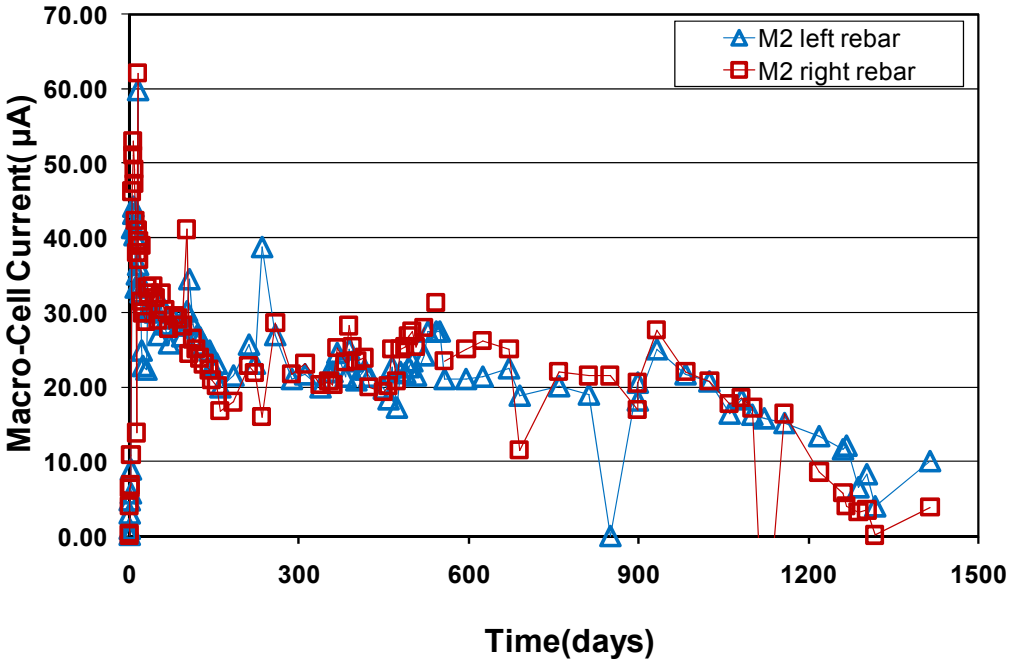

(c) Macro-cell current from left rebar and right rebar in specimen M2

Figure F.1: Potential of the left and right bars at eight elevations and macro-cell current in specimen M2 as a function of exposure time (measurement elevations in cm relative to the waterline).

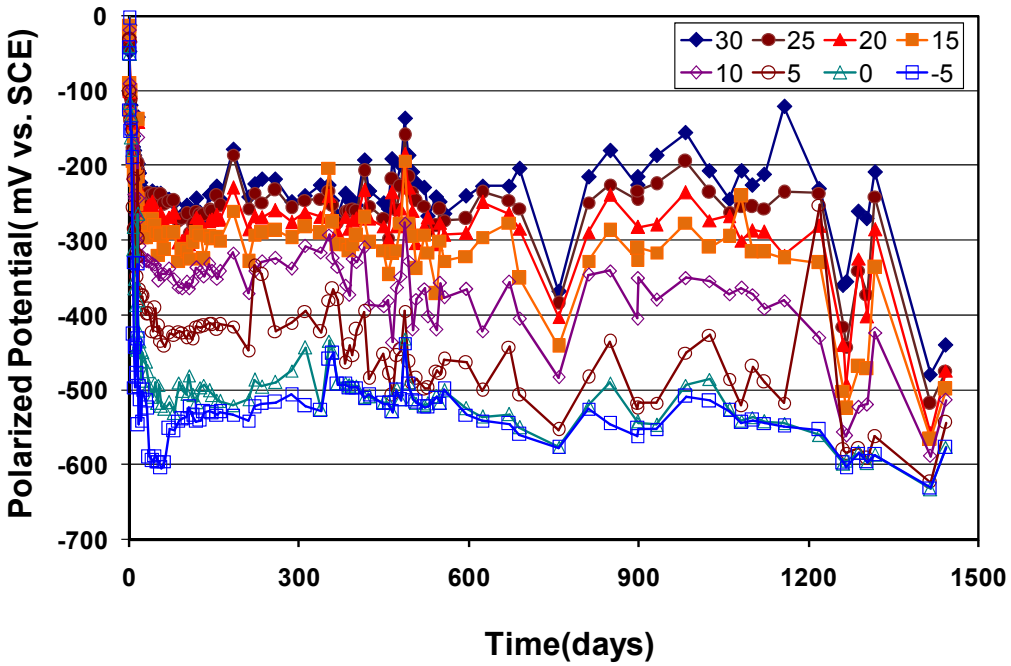

(a) Polarized potentials of left rebar in specimen K1

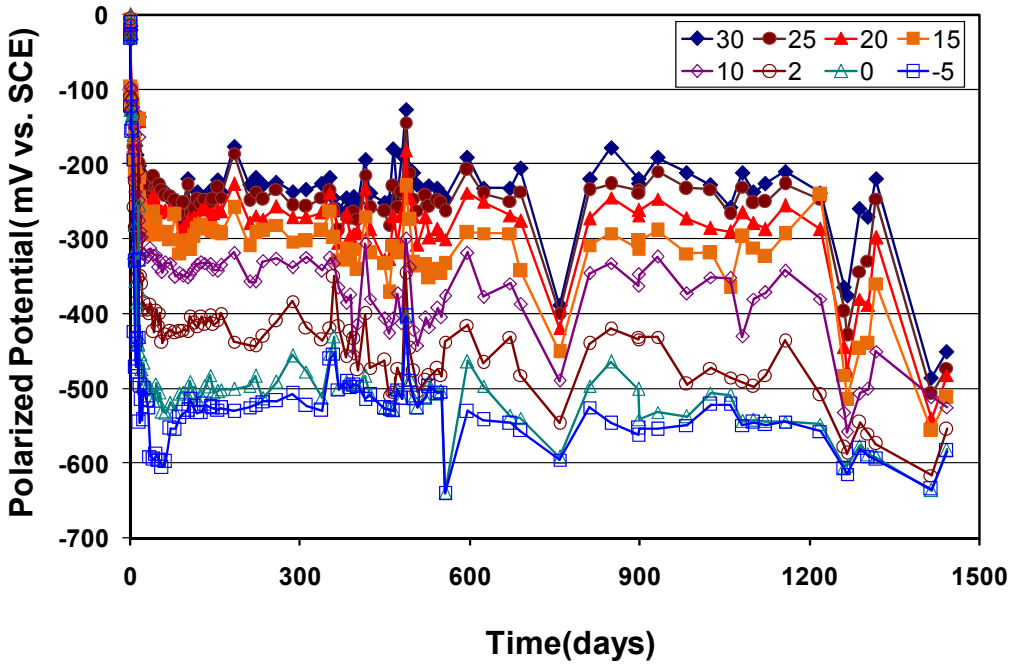

(b) Polarized potentials of right rebar in specimen K1

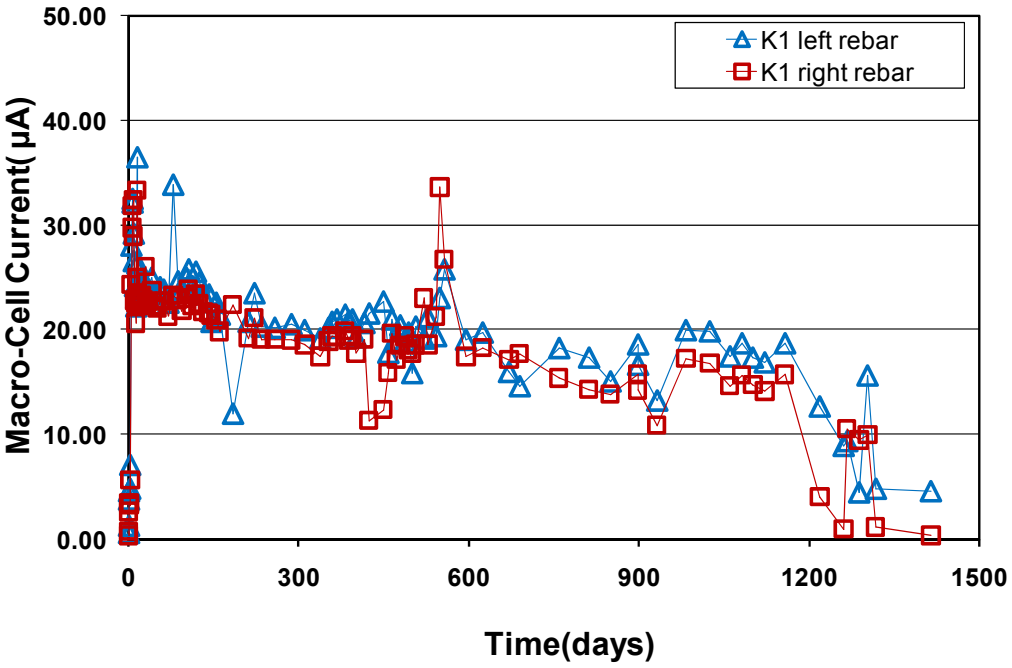

(c) Macro-cell current from left rebar and right rebar in specimen K1

Figure F.2: Potential of the left and right bars at eight elevations and macro-cell current in specimen K1 as a function of exposure time (measurement elevations in cm relative to the waterline).

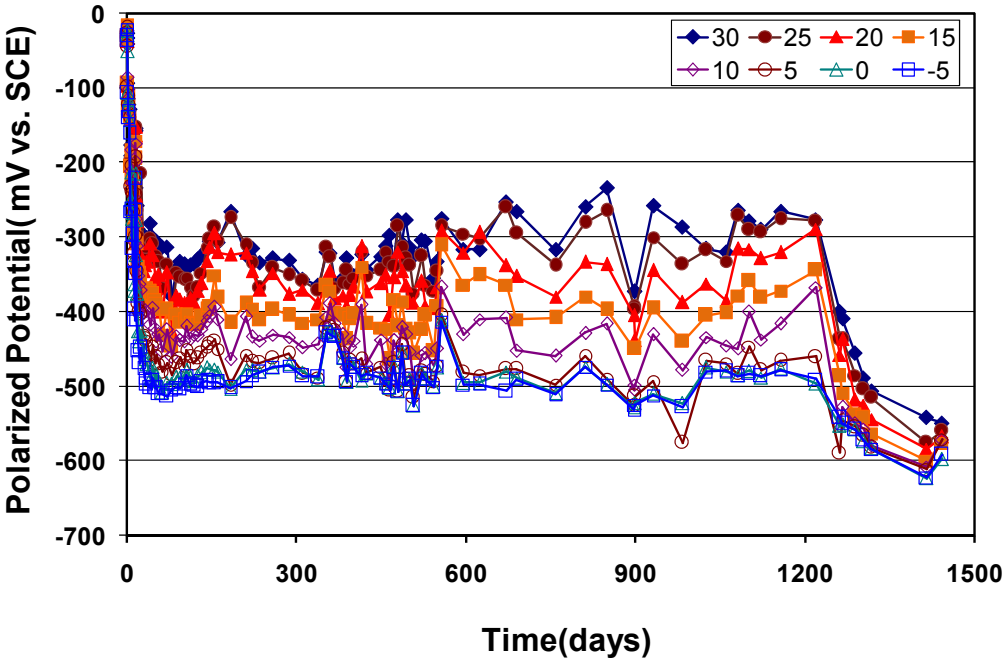

(a) Polarized potentials of left rebar in specimen N1

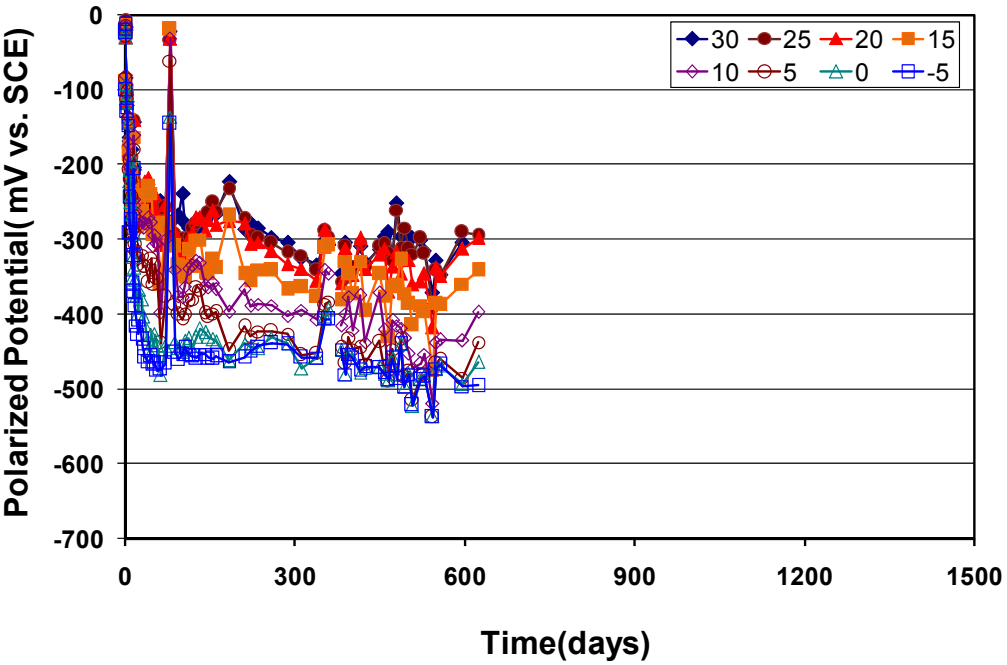

(b) Polarized potentials of right rebar in specimen N1

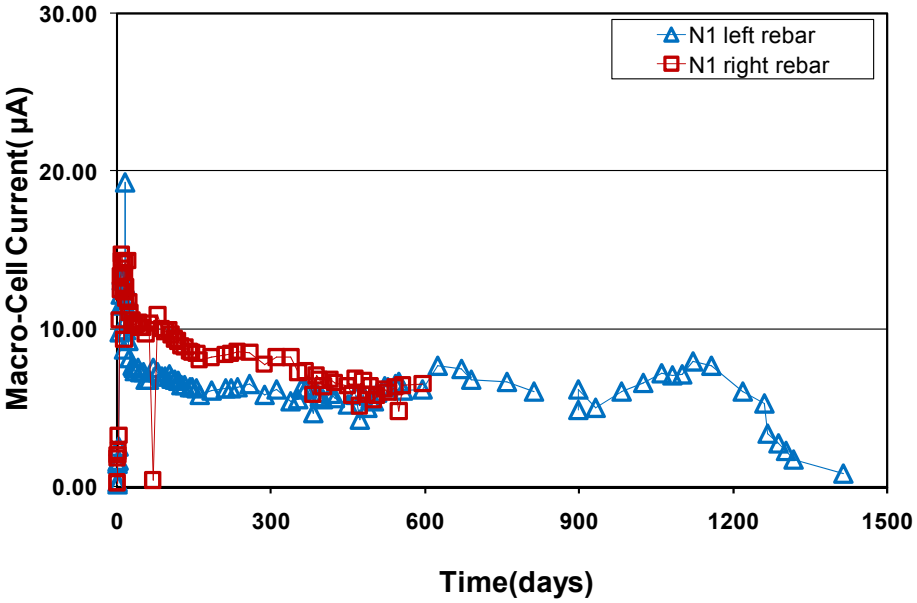

(c) Macro-cell current from left rebar and right rebar in specimen N1

Figure F.3: Potential of the left and right bars at eight elevations and macro-cell current in specimen N1 as a function of exposure time (measurement elevations in cm relative to the waterline).

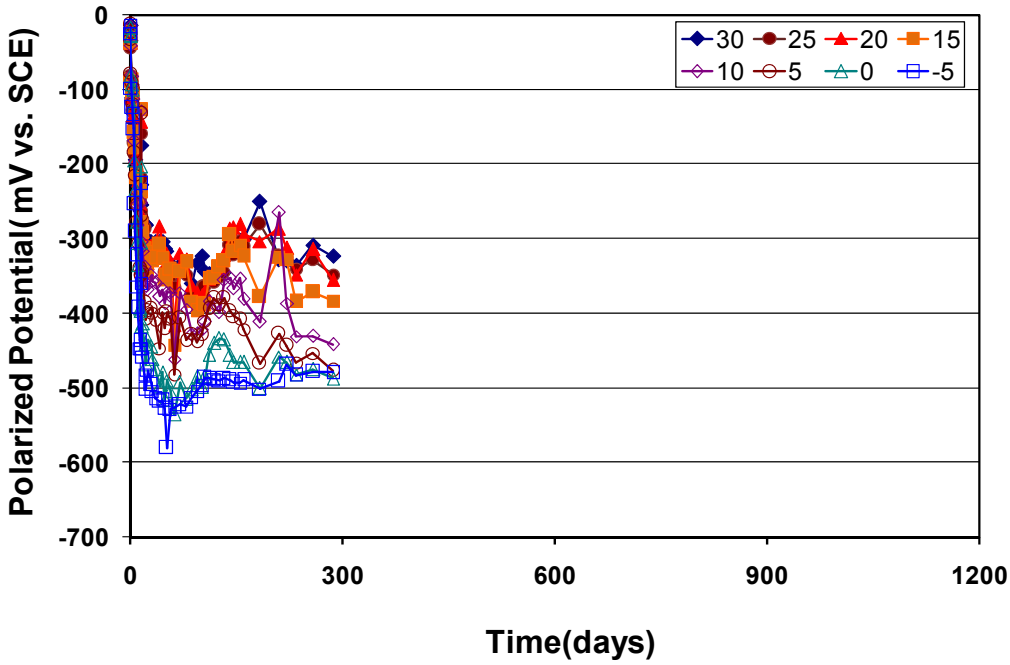

(a) Polarized potentials of left rebar in specimen N2

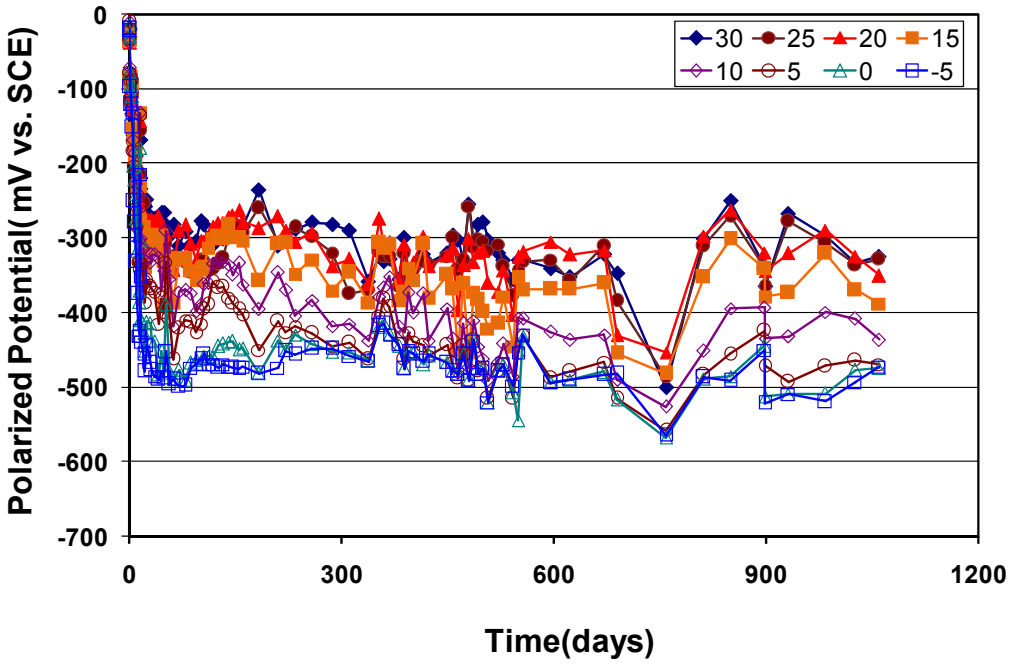

(b) Polarized potentials of left rebar in specimen N2

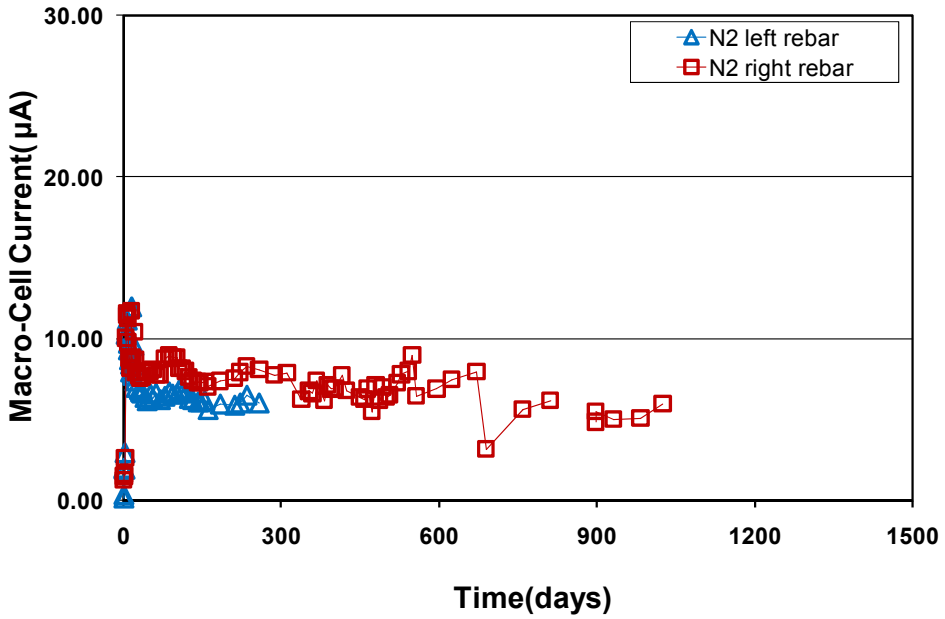

(c) Macro-cell current from left rebar and right rebar in specimen N2

Figure F.4: Potential of the left and right bars at eight elevations and macro-cell current in specimen N2 as a function of exposure time (measurement elevations in cm relative to the waterline).

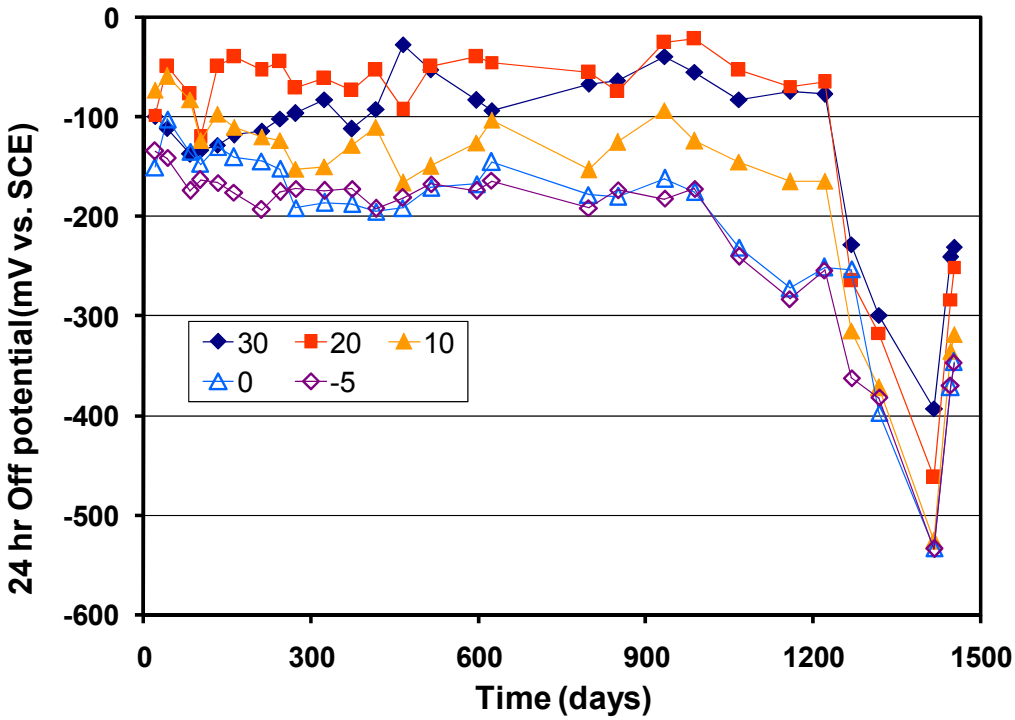

(a) 24 hr off potentials of left rebar in specimen M2

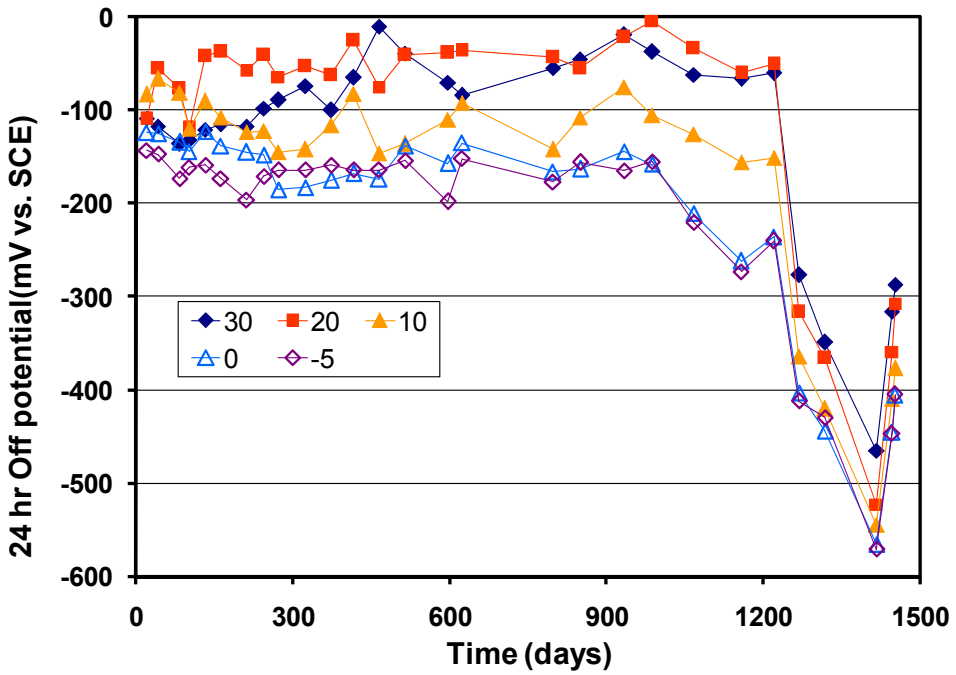

(b) 24 hr off potentials of right rebar in specimen M2

Figure F. 5: 24-hr off potential plots of the M2 left bar and right bar at different elevations as a function of exposure time (measurement elevations in cm relative to the waterline).

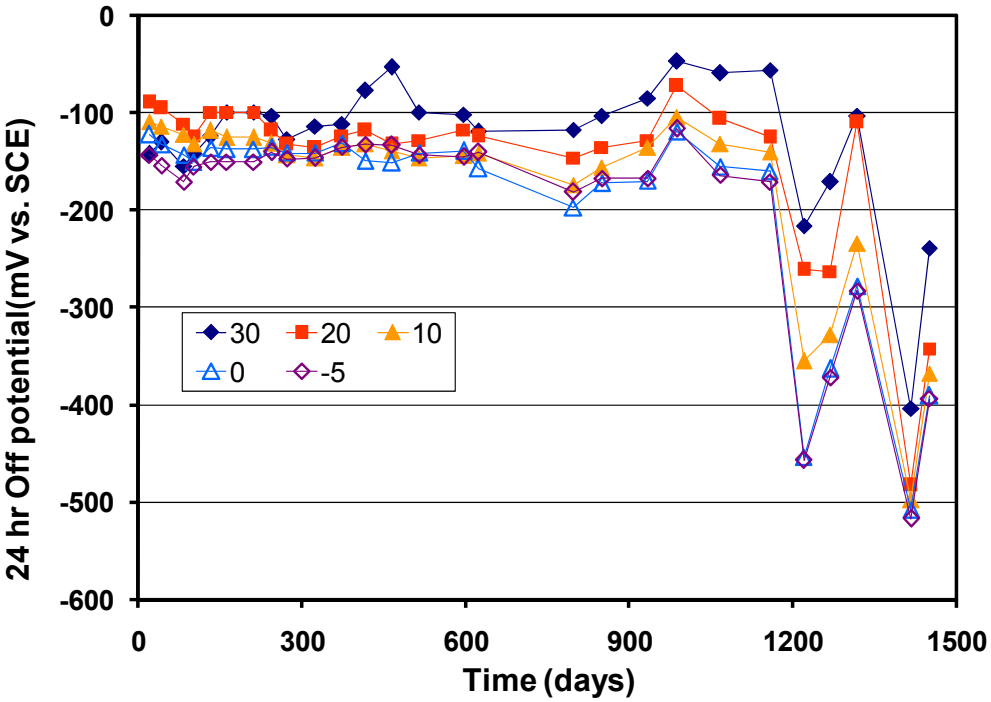

(a) 24 hr off potentials of left rebar in specimen K1

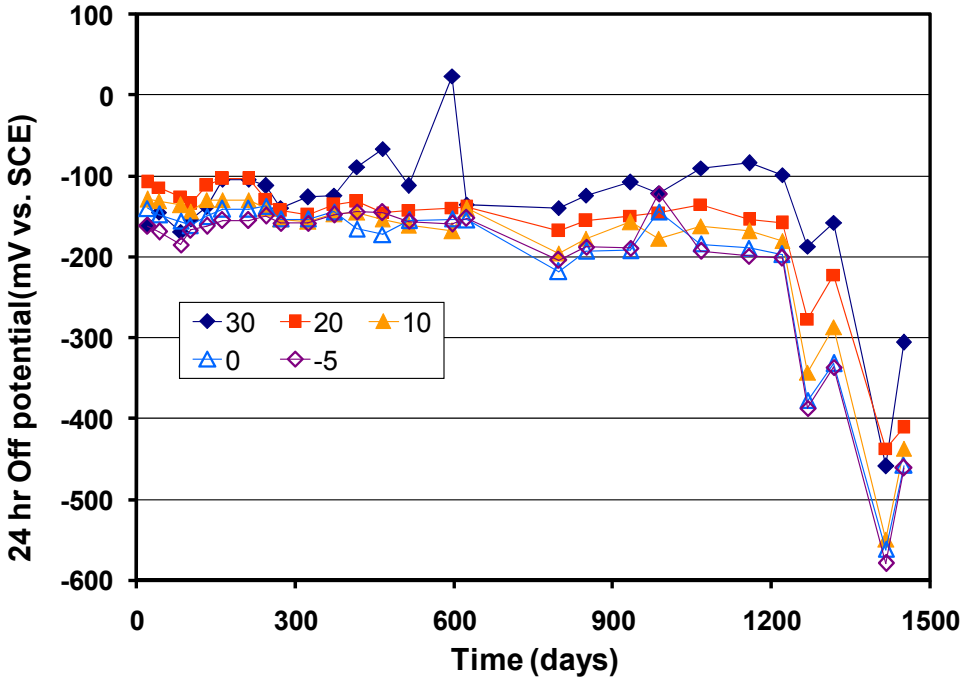

(b) 24 hr off potentials of right rebar in specimen K1

Figure F.6: 24-hr off potential plots of the K1 left bar and right bar at different elevations as a function of exposure time (measurement elevations in cm relative to the waterline).

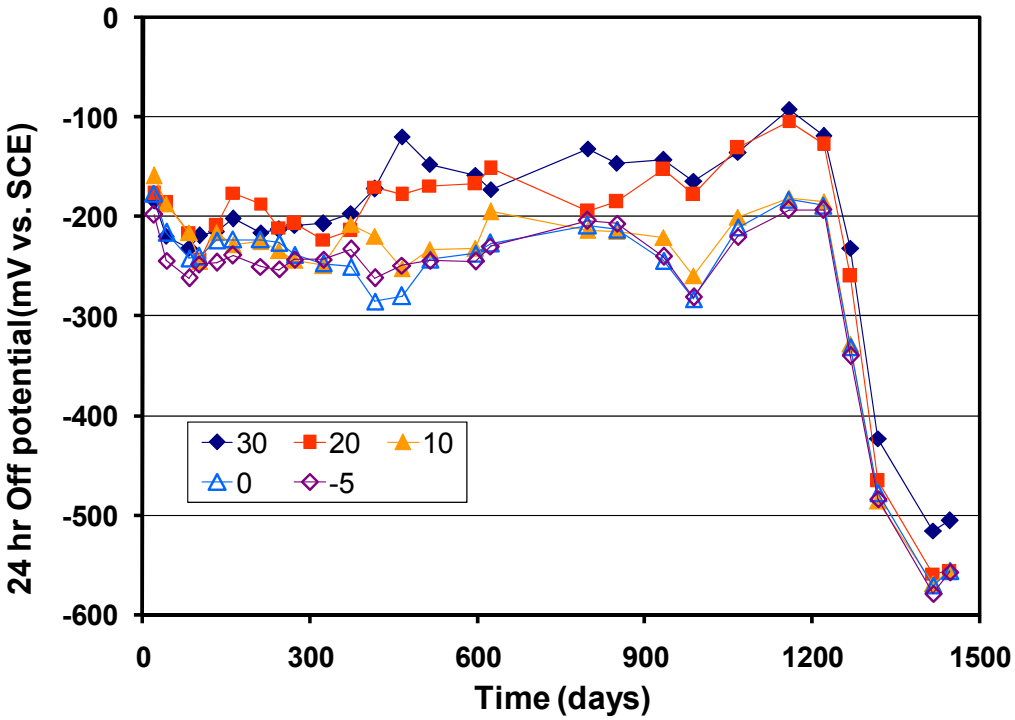

(a) 24 hr off potentials of left rebar in specimen N1

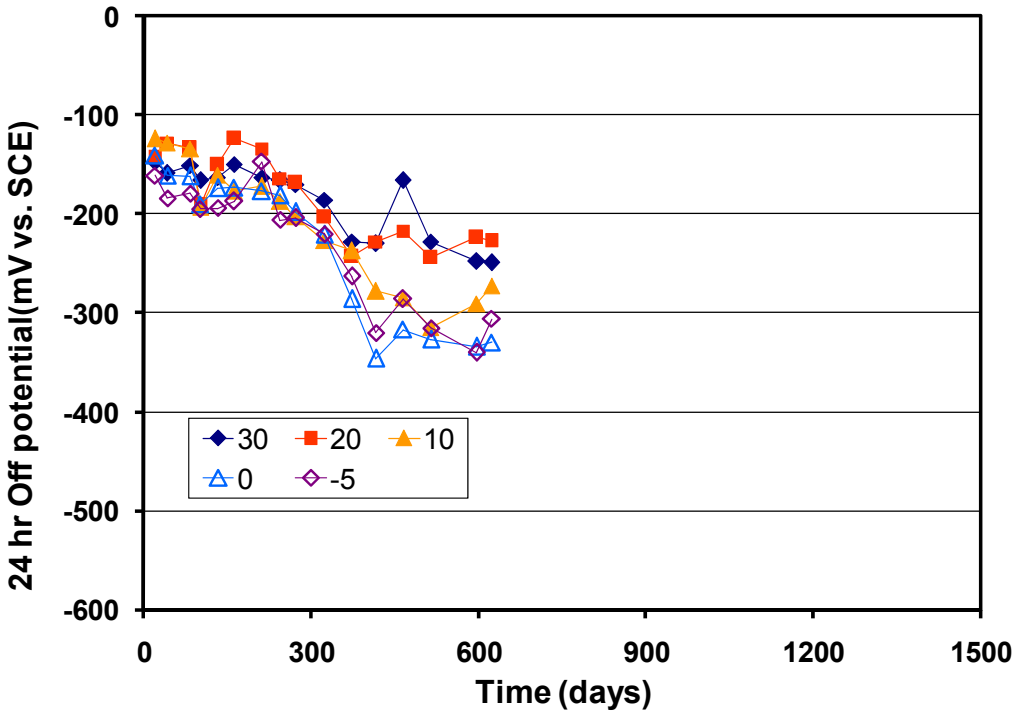

(b) 24 hr off potentials of right rebar in specimen N1

Figure F.7: 24-hr off potential plots of the N1 left bar and right bar at different elevations as a function of exposure time (measurement elevations in cm relative to the waterline).

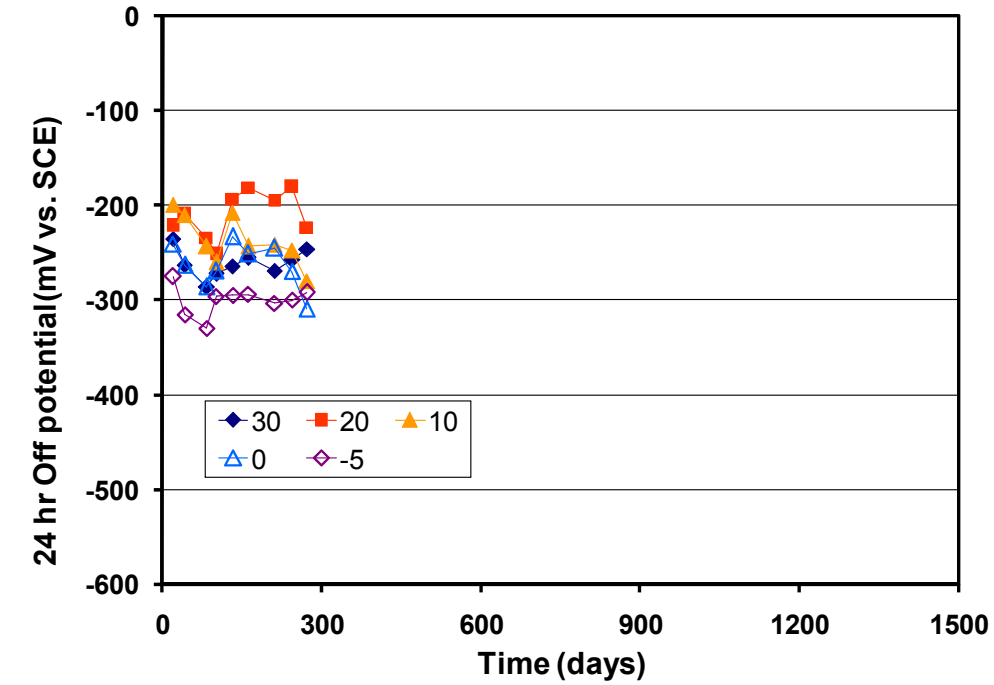

(a) 24 hr off potentials of left rebar in specimen N2

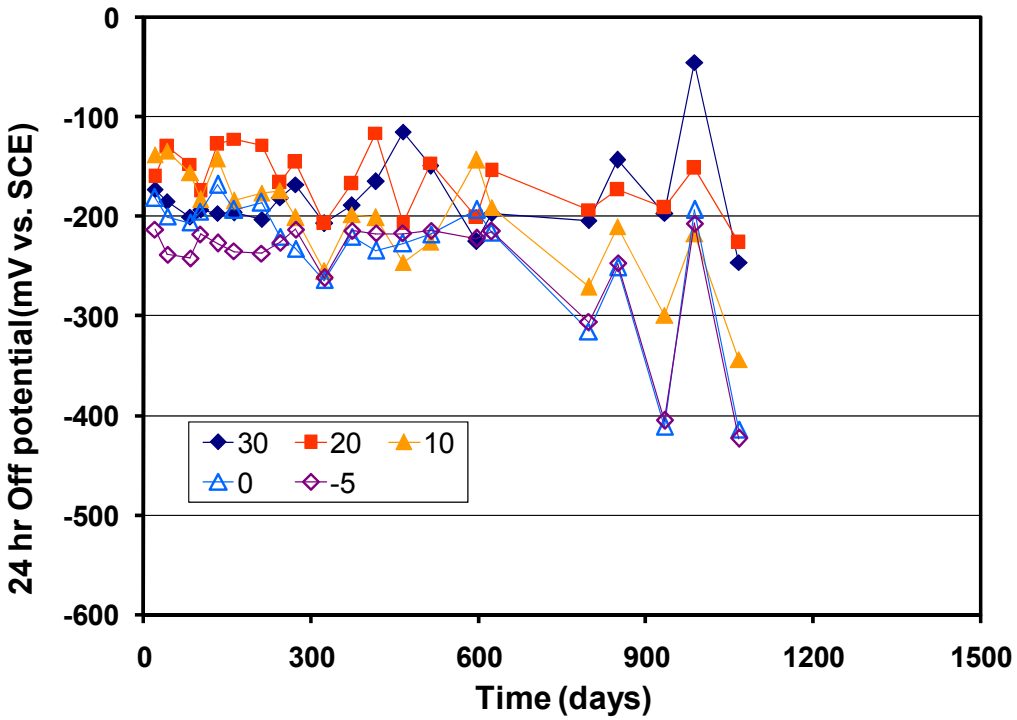

(b) 24 hr off potentials of right rebar in specimen N2

Figure F.8: 24-hr off potential plots of the N2 left bar and right bar at different elevations as a function of exposure time (measurement elevations in cm relative to the waterline)

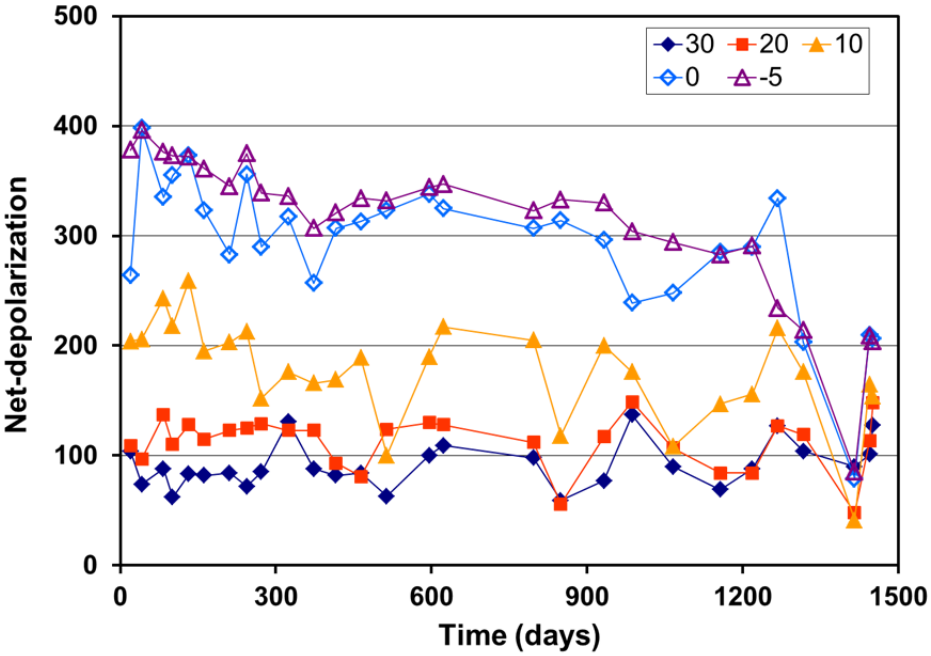

(a) Net depolarization (mV) after 24-hr plots of the M2 left bar

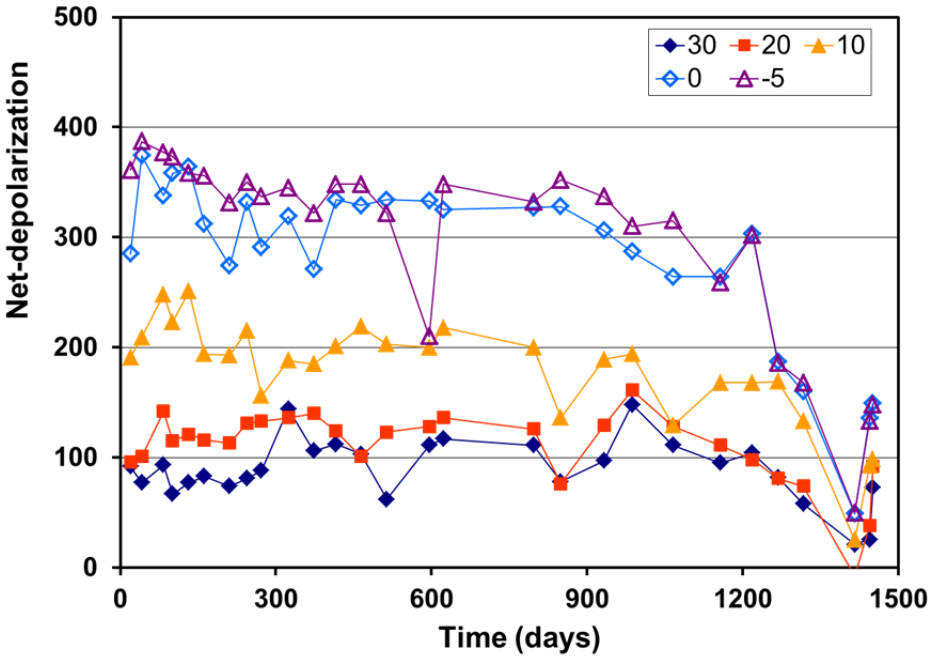

(b) Net depolarization (mV) after 24-hr plots of the M2 right bar

Figure F.9: Net depolarization (mV) after 24-hr plots of the M2 left bar and right bar at different elevations as a function of exposure time (measurement elevations in cm relative to the waterline).

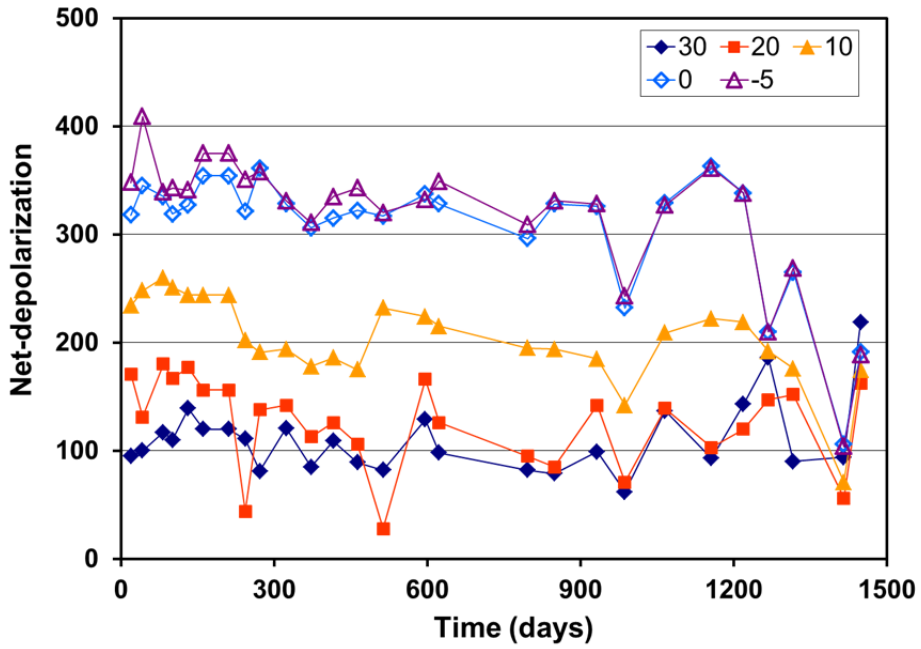

(a) Net depolarization (mV) after 24-hr plots of the K1 left bar

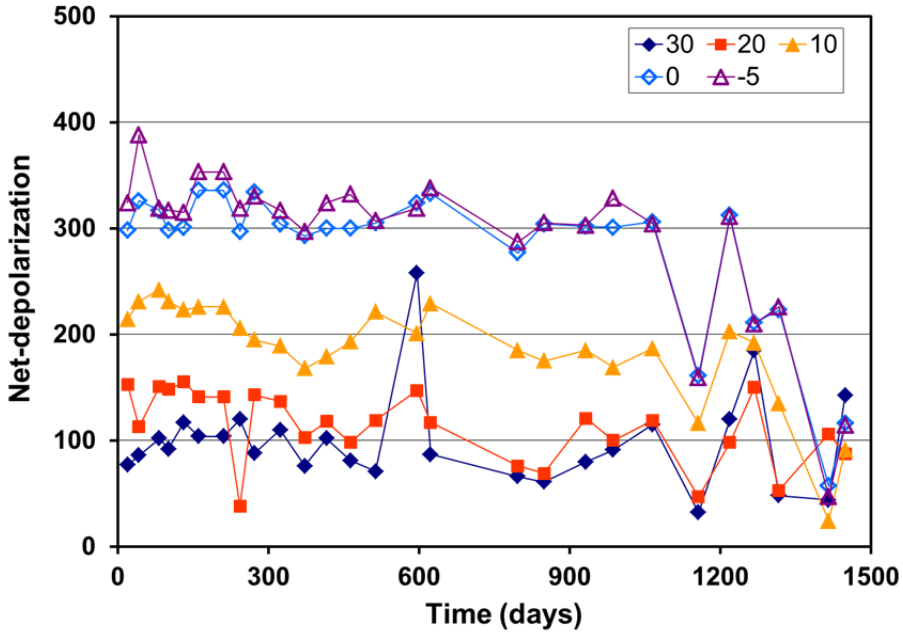

(b) Net depolarization (mV) after 24-hr plots of the K1 right bar

Figure F.10: Net depolarization (mV) after 24-hr plots of the K1 left bar and right bar at different elevations as a function of exposure time (measurement elevations in cm relative to the waterline).

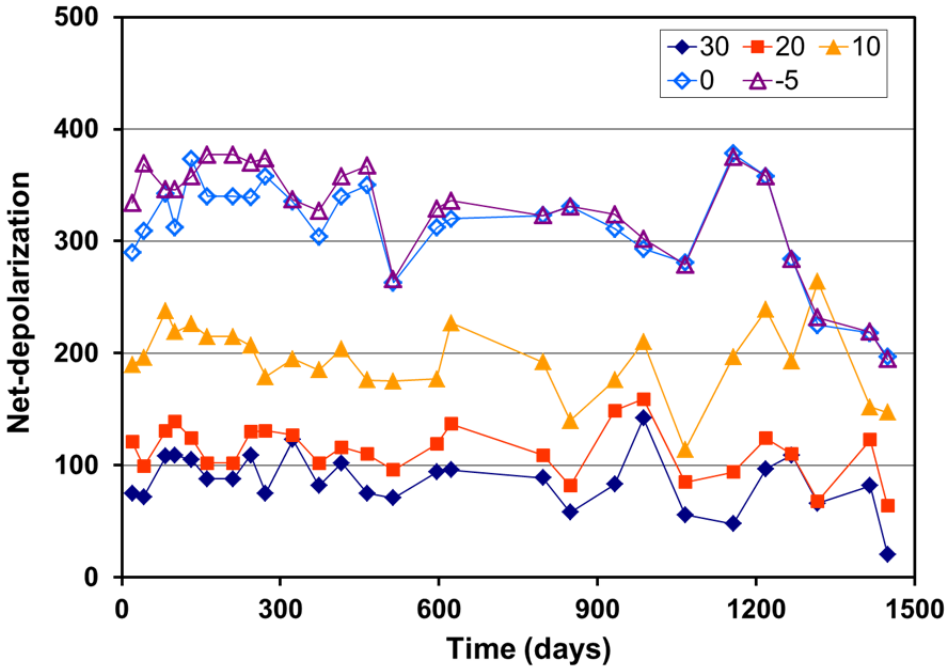

(a) Net depolarization (mV) after 24-hr plots of the K3 left bar

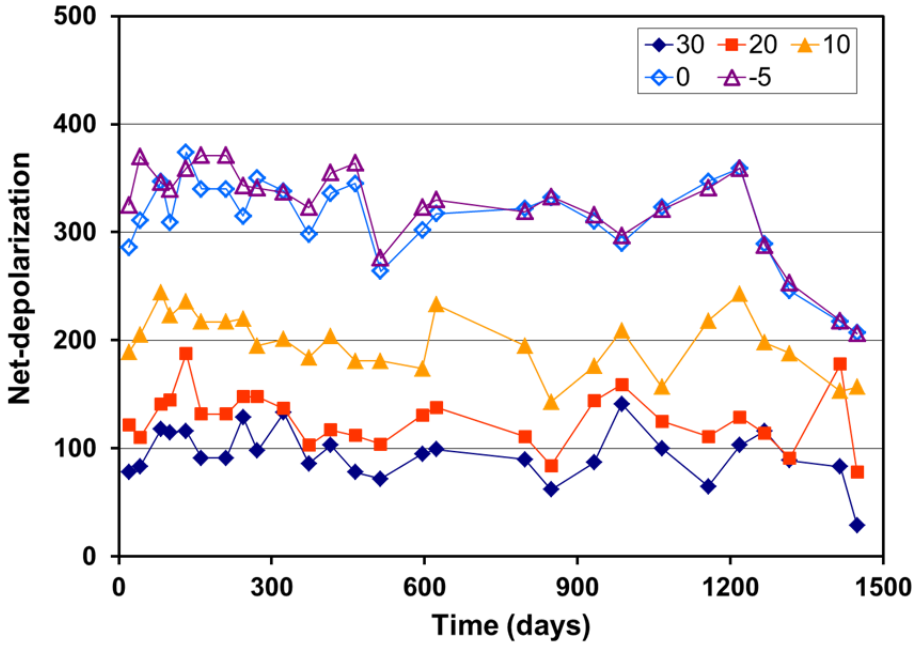

(b) Net depolarization (mV) after 24-hr plots of the K3 right bar

Figure F.11: Net depolarization (mV) after 24-hr plots of the K3 left bar and right bar at different elevations as a function of exposure time (measurement elevations in cm relative to the waterline).

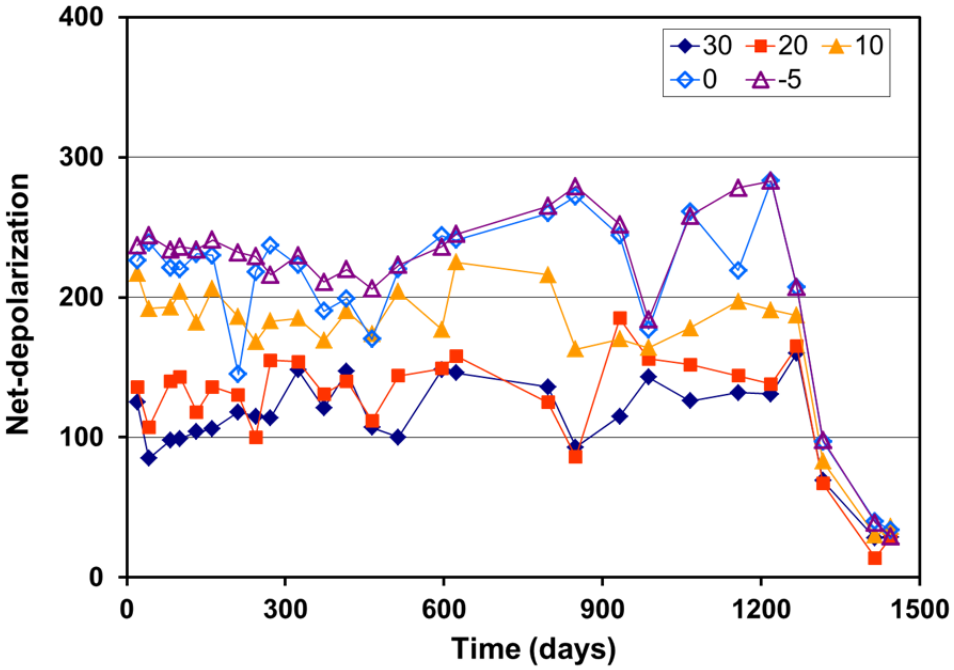

(a) Net depolarization (mV) after 24-hr plots of the N1 left bar

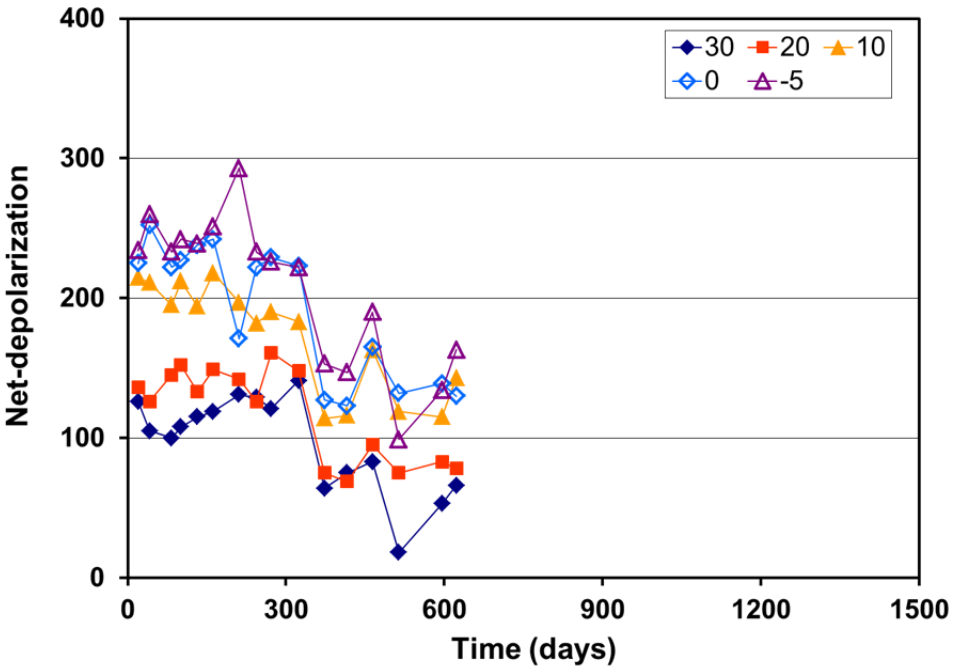

(b) Net depolarization (mV) after 24-hr plots of the N1 right bar

Figure F.12: Net depolarization (mV) after 24-hr plots of the N1 left bar and right bar at different elevations as a function of exposure time (measurement elevations in cm relative to the waterline).

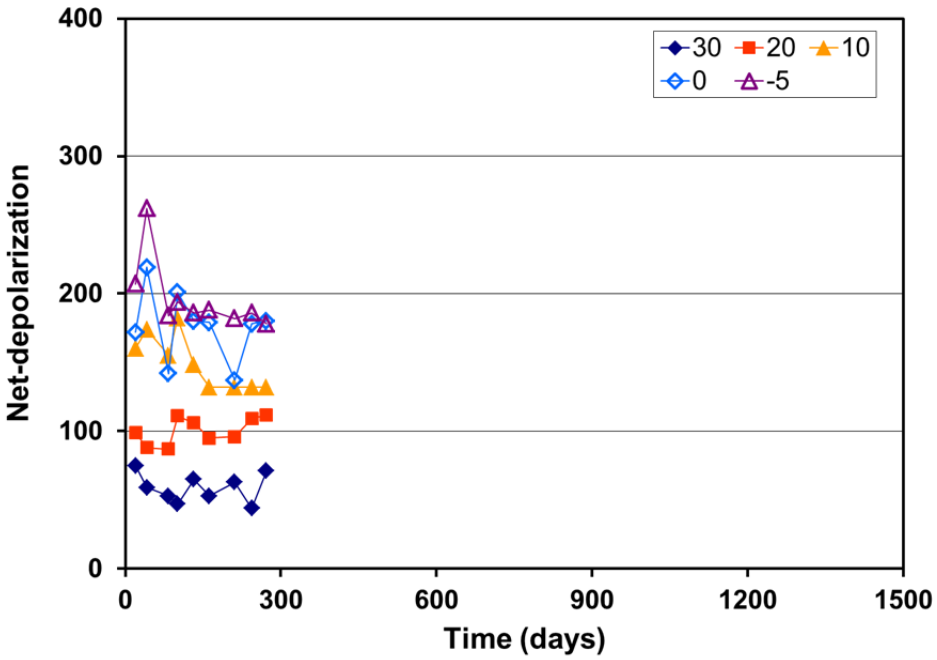

a) Net depolarization (mV) after 24-hr plots of the N2 left bar

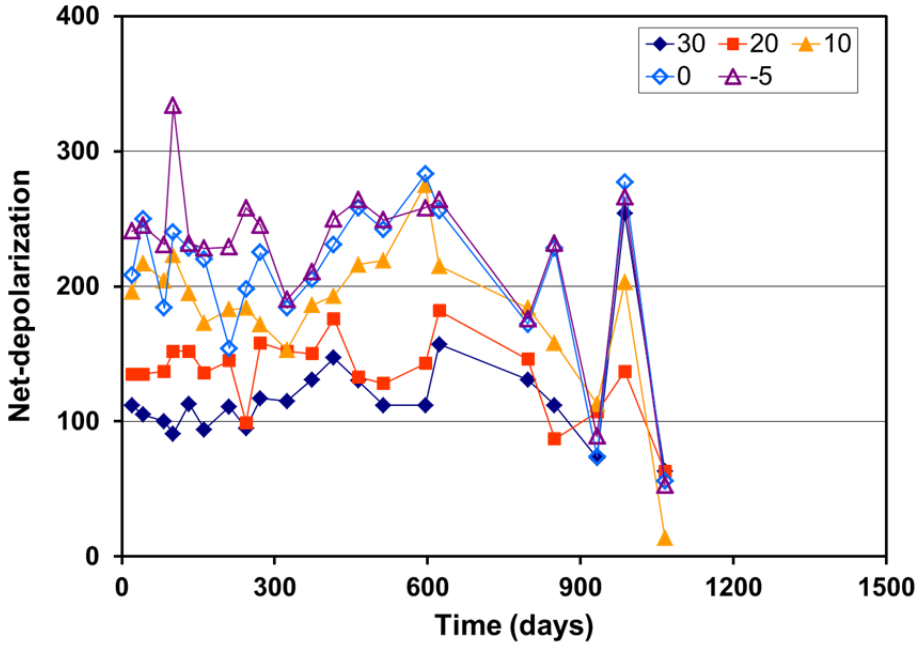

(b) Net depolarization (mV) after 24-hr plots of the N2 right bar

Figure F.13: Net depolarization (mV) after 24-hr plots of the N2 left bar and right bar at different elevations as a function of exposure time (measurement elevations in cm relative to the waterline).

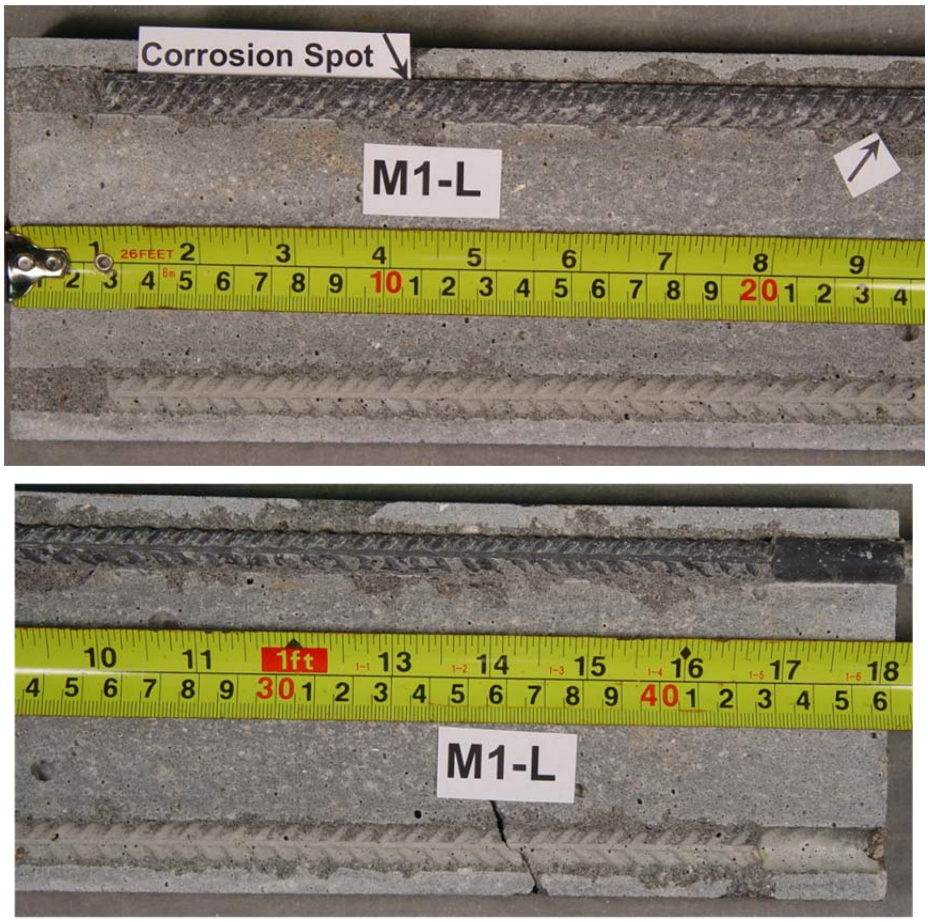

Figure F.14: M1 left rebar – corrosion spots on left rebar at 10.0 cm from the bottom of specimen (5.0 cm from the water line)

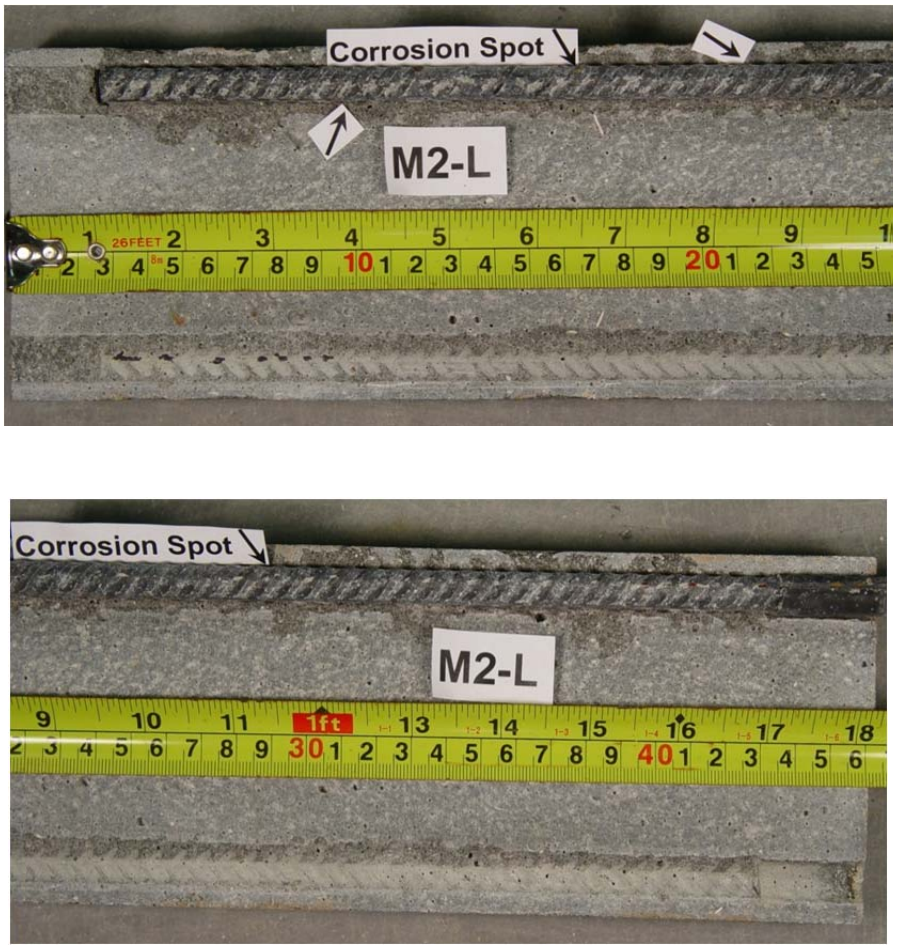

Figure F.15: M2 left rebar - corrosion spots on right rebar at 10 cm, 16.5cm, 21.5 cm and 29.0 cm from the bottom of specimen (5.0cm, 11.5cm, 16.5 cm and 24.0 from the water line)

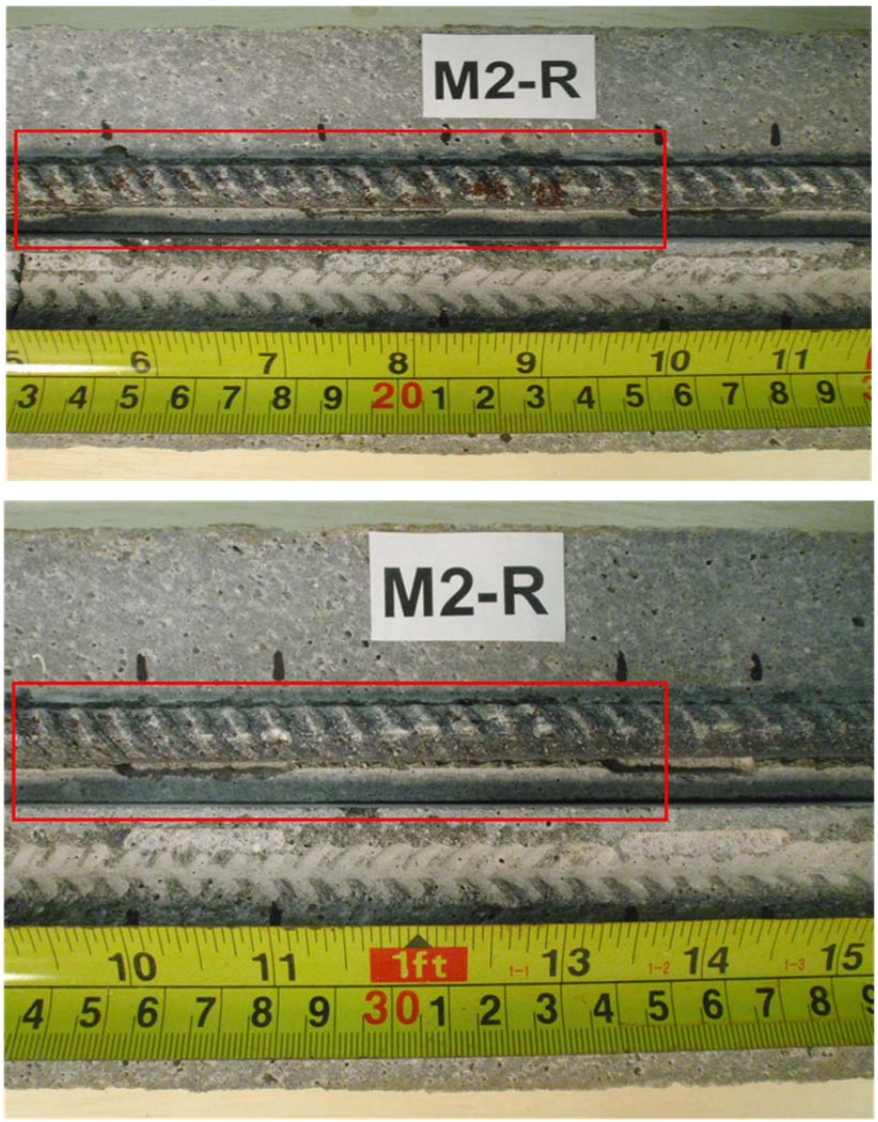

Figure F.16: M2 right rebar - corrosion spots on right rebar at 12.50 cm~35 cm from the bottom of specimen (7.50cm~30cm from the water line)

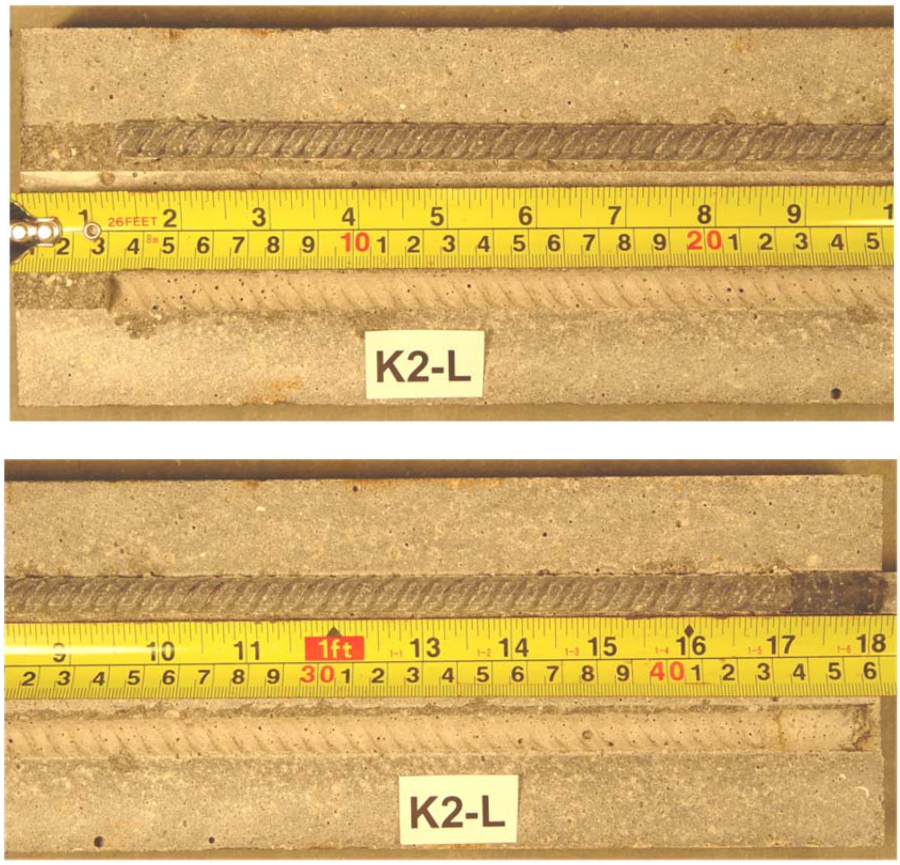

Figure F.17: K2 left rebar– no corrosion

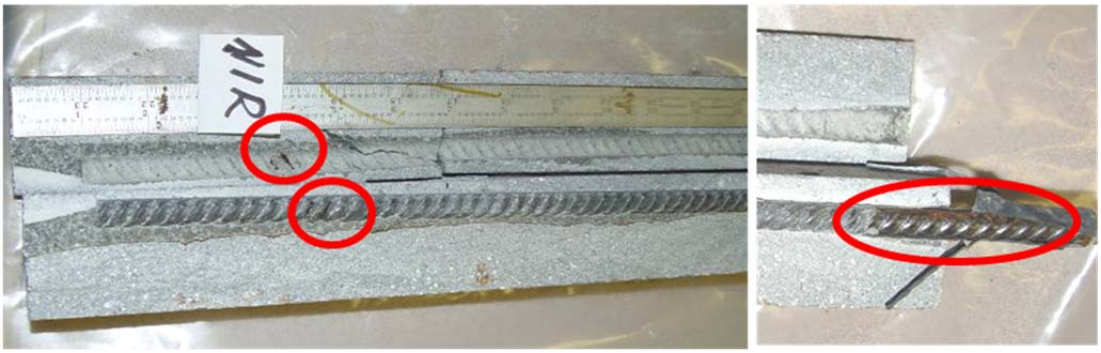

Figure F.18: N1 right rebar–corrosion spots at level 10.0 cm from the bottom of specimen(5.0cm from the water line) and underneath shrinkage tap

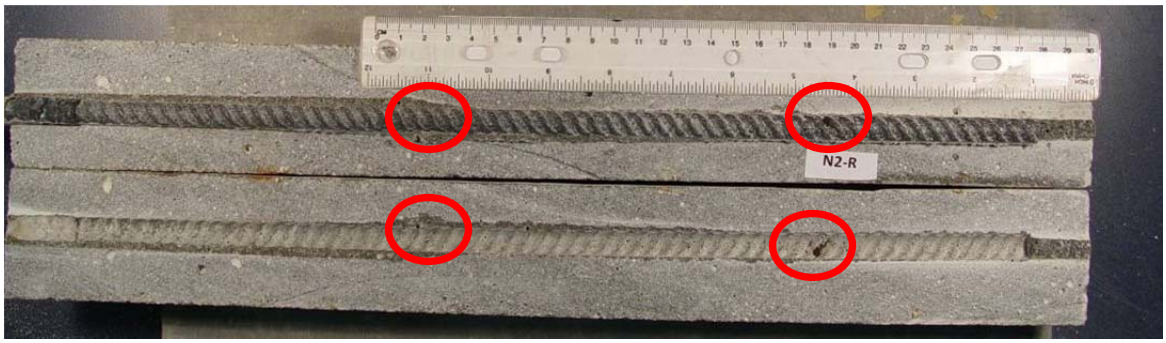

Figure F.19: N2 rebars–corrosion spot on left rebar underneath shrinkage tap and on right rebar at levels 11.35cm and 27.86cm from the bottom of specimen (6.35cm and 22.86cm from the water line)

Figure F.20: L1 rebars–corrosion spots on left rebar at levels 16.6 to 22.8cm from the bottom of specimen (11.6cm – 17.8cm from the water line) and on right rebar at level 30.0cm from the bottom of specimen (25.0cm from the water line)